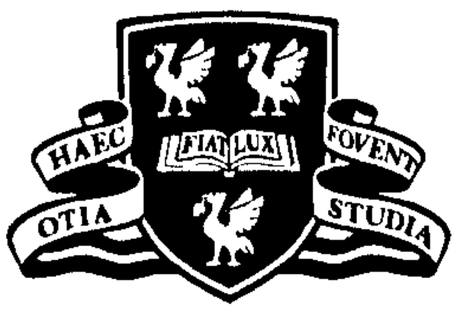

THE UNIVERSITY
of LIVERPOOL

THE INFLUENCE OF DENTS AND GOUGES ON THE LOAD CARRYING CAPACITY OF TRANSMISSION PIPELINES

Thesis submitted in accordance with the requirements
of the University of Liverpool for the
Degree of Doctor in Philosophy

by

Ibrahim Beleed Iflefel

May 2006

Acknowledgements

I would like to express my genuine gratitude to all those involved with making this research such an enjoyable and rewarding experience. I would like to thank my supervisor, Dr J. Blachut, whose guidance, encouragement and friendship has been the driving force for this research work.

I must thank Dr D.G. Moffat and Mr J. Mistry for their support and assistance during my first year. It has been a privilege to work with them.

Thanks must be extended to Mr S. Pennington for his advice and for his many hours spent for assistance in the experimental work. I would also like to thank Dr M. Lynch for his advice, particularly with regard to my early understanding of the FE modelling techniques.

My thanks are also due to the Libyan Secretary of Education and Libyan Culture Affairs Section for their assistance and financial support throughout this research work.

My heartfelt thanks are due to all my colleagues and friends with whom I shared the research experience. Their friendship has been greatly appreciated.

I am deeply indebted to my family for their support and encouragement, particulary my uncle Faraj for his continuing assistance and kindness. Without their love, encouragement and understanding throughout my years of study, this project and thesis would not have been possible.

Finally, my teachers who made their contribution throughout my life to reach this stage are gratefully acknowledged.

Statement of originality

This thesis is submitted for the degree of Doctor in Philosophy in the Faculty of Engineering at the University of Liverpool. The research project reported herein was carried out, unless otherwise stated, by the author in the Department of Engineering at the University of Liverpool between July 2001 and November 2005.

No part of this thesis has been submitted in support of an application for a degree or qualification of this or any other university or educational establishment. However, some parts of this thesis have been published in co-authorship with Dr D.G. Moffat, Mr J. Mistry, and Dr J. Blachut in the following papers:

- I.B. Iflefel, D.G. Moffat, J. Mistry, "The interaction of pressure and bending on a dented pipe", International Journal of Pressure Vessels & Piping, 2005, Vol. 82, 761-769.

- J. Blachut, I.B. Iflefel, "Analysis of steel pipelines with plain and gouged dents", Proceedings of the Tenth International Conference on Civil, Structural and Environmental Engineering Computing, (Editor) B.H.V. Topping, Rome, July 2005, (ISBN: 1-905088-02-7).

- I.B. Iflefel, J. Blachut, "Analysis of plain and gouged dents in pipes subjected to pressure and moment loading", in Proc. of joint ASME PVP/ICPVT-11 Conference, Vancouver, Canada, July 23-27, 2006.

I.B. Iflefel

March 2006

The Influence of Dents and Gouges on the Load Carrying Capacity of Transmission Pipelines

by Ibrahim Beleed IFLEFEL

Abstract

Damage to buried pipelines caused by mechanical digging equipment or by rock movement can lead to damage in the form of dents, gouges or cracks. This has been a recognised hazard and, as a result, there have been various research programmes aimed at (a) quantifying the behaviour of damaged pipelines, and (b) documenting procedures for minimising the likelihood of failure.

Practical needs have stimulated both experimental and numerical studies in this area in order to assess various aspects of structural integrity of damaged pipes. The presented work is concerned with the influence of dents, gouged dents, and cracked dents on pipelines. Investigation of distortion of the cross-section, dent propagation along the pipe length, residual dent depth, contact area between shell and rigid bodies, as well as bending of damaged pipes is investigated in this study.

This research work consist of two parts: (a) finite element analyses carried out for mild steel pipes, and (b) experimental programme on laboratory scale steel pipes. A finite element parameter study is detailed for dented, gouged and cracked dents in pipelines which are subjected to bending. Gouges were introduced at two different locations along the pipe length. The first location was at the mid-span of the pipe, i.e., underneath of the indenter, and the second was located off-centre. The gouges were modelled by removing part of the wall material. When gouges become very narrow they can be treated as cracks in the pipe wall. These are also studied here.

The objective of experimental study was to establish the validity of the finite element results. A total of six specimens have been manufactured and tested. The first three specimens were prepared without any surface defects whereas the second set of three had surface defects. All of these specimens were subjected to denting by hemispherical indenter, during which the pipe was supported along its length by a wooden saddle support. Dented pipes were subsequently subjected to bending followed by burst tests. The experimental results compare well with the corresponding finite element predictions. Recommendations for future work are presented in the final Chapter.

Nomenclature

English Symbols

a	radius of indenter
b	semi-axis of an ellipse
c	half length of crack or gouge
e	depth of crack or gouge
f	safety factor
k	spring stiffness
p	internal pressure
t	wall thickness of pipe
w	width of half gouge
A	the cross section area of pipe
CA	contact area
CA_o	projected contact area,
D	mean diameter of pipe
D_i	inner diameter of pipe
D_o	outer diameter of pipe
E	Young's modulus
F_{max}	maximum denting force
F_o	denting force for plain pipe
L	half length of pipe
L_D	axial length of dent propagation
M	bending moment
M_L	limit moment
M_{LP}	limit moment for plain pipe
M_{TES}	plastic moment (based on twice elastic slope method)
P_L	limit pressure
p_{LP}	limit pressure for plain pipe
P_{TES}	plastic pressure (based on twice elastic slope method)
R_i	inner radius of pipe
R_o	outer radius of pipe
U_2	displacement of a node in Y direction

Greek Symbols

δ	depth of dent
ϵ	general strain
σ_{yp}	yield stress
σ_{ϕ}	axial stress
σ_{θ}	hoop stress
σ_{UTS}	ultimate tensile stress
σ_t	the true stress
ϵ_t	the true strain
ϵ_{nom}	the nominal strain
σ_{nom}	the nominal stress
ϵ^{pl}	the plastic strain
ν	Poisson's ratio
θ	angle of rotation
ΔA	reduction of pipe's cross section area

Abbreviations

CNC	computer numerical control
CLOAD	concentrated load
DLOAD	distributed load
EDM	electrical discharge machine
D.O.F.	degree of freedom
FE	finite element
NLGEOM	non-linear geometric analysis
NMAP	technique for mapping nodes from one co-ordinate system to another
MPC	Multi Point Constraint

Contents

Chapter 1

Introduction

1.1 Background

Transmission pipelines are widely used for transporting oil and gas. This method of delivery represented, for example, 66 % of all oil transported in the United States in 2000, as can be seen in Figure (1.1). As a result of growing energy demand, there are thousands of kilometers of large diameter, high pressure transmission pipelines world wide. According to recent statistics, Europe and North America have the largest natural gas pipeline networks [1], Figure (1.2). It is likely that the need for additional pipelines will grow further.

1.2 The problem of mechanical damage

Damage to buried pipelines caused by mechanical digging equipment or by rock movement is a cause of concern to onshore and offshore transmission pipeline operators. The resulting damage in the form of dents and gouges, can affect the load carrying capacity and/or operating life of the pipeline. In addition, damage in the form of dents and gouges, or both, can result in failures at lower pressures than anticipated. Mechanical damage can also cause changes in the shape of the pipeline's cross section, changes in the wall thickness, and local changes in material properties.

Plain dents, plain gouges and combination of dents and gouges are regarded as

possible causes of pipelines failure. Dents in pipelines are usually defined as a change in pipe curvature but without reduction of the wall thickness. Dents are usually classified as local, short or long. Local dents could be caused by impact of sharp objects. Short and long defects are defined on the basis of the axial length which should be less than, or greater than, twice the circumferential breadth, respectively [2, 3]. Assessment procedures specify that dent's depth in a pipeline should not be greater than 8 % (Ref. [4]), and 6 % (Ref. [5]), of the pipe diameter. There is however evidence that dents of up to 24 %, and possibly up to 30 %, of the pipe diameter may not significantly affect pipe's burst pressure [2].

Plain gouges are usually defined as reduction in the wall thickness without any change in the pipe curvature. This type of defects has been studied extensively in the last few decades. However, there is a lack of comprehensive information on pipe behaviour once gouges appear in dents, and pipes are subjected to bending. One of the main objectives of the present study is investigation of pipes with gouged dents and of the load carrying capacity of these pipes.

The previous work on full and small size experiments on damaged pipes was carried out by various institutions, e.g., British Gas, Battelle Columbus Laboratories in the U.S.A., Metals Technology Laboratories CANMET in Canada, Metal Research Laboratories in the Netherlands, Cambridge University, and Centro Sviluppo Materiali in Italy. Despite these studies the effect of dents and gouges on pipe's structural integrity is not entirely understood. This is attributed to the complexity of the problem having a large number of variables which govern behaviour of damaged pipeline.

More recent activity in this area includes set-up of a data-base containing information about the influence of damage on pipeline performance. This has been carried out by UK Onshore Pipeline Association [6, 7]. Another data-base containing information on operational incidents is based on the European Gas-Pipeline Failures project [7].

1.3 Research motivation

Motivation for this work comes from frequent occurrence of external damage to the existing pipelines which are being caused by external forces, e.g., by excavation equipment, ship anchors, falling objects, etc.. The need for this type of work becomes obvious when one examines failure of pipelines as documented in various data-bases. One data-base that compiles the frequent occurrence of external damage to existing pipelines, is the United States Department of Transportation's database. It provides incident reports for years between 1970 and 1984, and from 1984 to 1997 (Figures (1.3) and (1.4)). Another one is by the Office of Pipeline Safety, USA, which contains compiled data on pipeline accidents for 2002-2003. It is clear from the latter data-base that for natural gas distribution pipelines, the largest portion of accidents was caused by outside force damage as can be seen in the Table (1.1).

The excavating equipment can accidentally damage a pipeline without any warning. Damage can cause the pipeline to leak or to rupture, resulting in an immediate loss of revenue, property damage or loss of human lives. Example of such catastrophic incident include an explosion on an El Paso Natural Gas Company pipeline near Carlsbad in August 2000, New Mexico. This accident killed 12 people and caused widespread property damage [8]. Moreover, damage to pipeline which did not appear to be serious, could weaken the pipeline causing a leak or rupture at a late stage as illustrated by an explosion of 0.914 m diameter Texas Eastern Gas Pipeline [9]. The latter accident was attributed to an unnoticed gouge caused by excavation equipment.

Understanding of the behavior of the above mentioned defects in pipes is vital to safe operation of pipeline systems. An improved understanding of the behaviour of defective pipes could also have significant benefits. There are two factors which give added urgency to the need for some additional work in this area. The first relates to the present plans by pipeline operators to increase, where possible, magnitude of basic design stress, and hence operating pressures, in transmission pipeline above the levels stipulated by current, published recommendations such as IGE/TD/1 [10, 11]. The second factor is related to new safety assessment procedures that are currently being developed and aim to deal with damaged pipelines [12, 13, 14], and [15].

1.4 Loading

In real situations the pipelines are subjected to various loading scenarios. Axial forces, moment loading and internal pressure are obvious and common types of load for most piping system. In addition, the piping system can be subjected to combined loading such as pressure and moment. One way of assessing structural integrity of a component is through its plastic load or limit load. In order to understand the effect of each load category on the plastic behaviour of a pipe it is necessary to apply these loads individually. In this study, the plastic loads of concern have been assessed individually for a dented pipe. Combination of both internal pressure and moment loading has then been studied. These are two, typical forms of loading and they frequently appear in practice. However, two loading sequences are possible here, e.g., applying moment first followed by the application of an increasing internal pressure or the other way around. This way, the interaction diagram between these two loads could be obtained. Other combination of loads are possible but they are not studied here.

1.5 The plastic load criteria

The limit and plastic load criteria adopted in the presented work are, as discussed by Gerdeen [16]. Plastic loads are often derived from FE or experimental load-displacement plots. There are a number of different criteria here. The twice, five times, and fifteen times elastic slope methods are recommended in ASME III Pressure Vessel Design Code [17] and Figure (1.5) shows a sketch illustrating fiften times elastic slope criterion. These criteria are arbitrary but they allow comparison of limit loads for similar components. Combined effect of two, simultaneously acting loads, is usually addressed through interaction diagrams. Figure (1.6) illustrates a case of simultaneously acting pressure and moment loading.

1.6 Finite element analysis

MSC/PATRAN [18] mesh generation program was used to create the FE models. The FE model was initially created as a flat plate with different sections in

places where dents and gouges were to be introduced. The aspect ratio of elements could be controlled easily with this approach. The file created by PATRAN was used as input file for the FE code ABAQUS [19]. The NMAP feature in ABAQUS was then used to convert the plate to a plain pipe. Solid brick element with 20-nodes, C3D20R, was used throughout the analysis. The FE analysis was carried out first on simple models in order to build confidence in the FE analyses prior to analyses of more complicated cases. Detailed descriptions of models, loading, boundary conditions, etc. are provided later.

1.7 Experimental work

Experimental studies have also been undertaken in addition to the FE analysis. Tests on laboratory scale pipes were conducted with the aim of validating the finite element results of dented pipes (with a number of them containing gouges). A special denting and four point bending test facilities were developed to carry out these tests. Six test pipes were manufactured and tested to destruction. Their diameter-to-wall-thickness ratio was, $\frac{D_o}{t} \cong 40.0$, specimen's length to outside diameter ratio was, $\frac{2L}{D_o} = 6.0$. All pipes were supported by a wooden saddle during denting. Test specimens were dented with a hemispherical indenter, for which the ratio of indenter's-diameter-to-pipe's-diameter was, $\frac{2a}{D_o} \cong 0.41$. Gouges were prepared using electrical discharge machine. The high speed milling machine was also used to prepare a wider slot gouge. Details about manufacture of models, thickness measurements, strain gauges, etc. are given in Chapters (6), (7) and in the Appendix (C).

1.8 Scope of the present work

Understanding the structural integrity of pipes with dents and gouges using full and small size tests have met with limited success. It appears that no work has been carried out for the bending of dented and gouged pipes (empty or pressurised). It is somewhat surprising that no work has been reported in this area despite its practical relevance. The main objectives of this study include the following tasks:

- Develop a procedure for the FE modelling of dents, gouges and combination of both. These procedures should be applicable to empty and to pressurised pipes.
- Determine the ultimate denting load, residual dent depth, distortion of pipe's cross section area at the dent's centre, and dent propagation along the pipe's length. Apply these analyses to empty and to pressurised pipes.
- Determine the interaction diagram for dented pipes. Determine the ultimate bending moment for combined surface defects (dents with gouges).
- Manufacture models and conduct experiments by denting laboratory scale pipes (both empty and pressurised ones). Introduce gouges into dents.
- Subject pipe specimens to a bending moment using the four point bending test facility with the presence of internal pressure.
- Determine the ultimate moment loading. Carry out burst tests on dented and then bent pipes.

It is hoped that the obtained results will contribute to a better assessment of pipelines with dents and pipelines with dents containing gouges.

1.9 Structure of the thesis

The presented work is divided into eight chapters. All tables and figures are presented at the end of each Chapter. A brief description of each Chapter is given below:

Chapter (1) Introduction and background to the research programme and the motivation behind it is outlined.

Chapter (2) A literature survey is given. It covers external damage to pipes caused by outside force (dents and gouges and combination of both).

Chapter (3) This Chapter covers numerical analyses of dents. For example, the contact area between indenter and shell and between shell and rigid support is computed and discussed. In addition, it quantifies propagation of the dent along the pipe's

length, distortion of pipe's cross section at the dent centre, as well as, determining the ultimate denting load and residual dent depth after removal of the indenter (spring back).

Chapter (4) This Chapter contains a preliminary finite element study into the denting and bending process of empty and of pressurised pipes. It is entirely numerical, i.e., based on the FE analyses. This Chapter deals with the interaction between internal pressure and bending moment for dented pipes. The Chapter is focussing on dented pipes without any surface defects, i.e., without cracks or gouges.

Chapter (5) This Chapter describes the results of the FE parameter study for plain dents and for gouged dents. Studied variables include gouge depth, length and its width. All studied gouges were axial and had two locations: at the centre, beneath the indenter, and off-centre. All models were subjected to denting followed by bending moment.

Chapter (6) Details about tests are presented here. This Chapter focusses on experimental denting process, corresponding finite element modelling and on strain gauge results.

Chapter (7) Details about experimental bending tests of dented pipes, and corresponding FE models, are presented in this Chapter. The Chapter contains comparison between experimental bending versus rotation curve, and the corresponding FE predictions. Comparison of experimental (strain gauge), and numerically generated (FE method) strains is also given in this Chapter.

Chapter (8) Conclusions and recommendations for future work are given here.

Natural Gas Distribution Pipeline Incident Summary by Cause 1/1/2002 - 12/31/2003						
Reported Cause	**Number of Incidents**	**% of Total Incidents**	**Property Damages**	**% of Total Damages**	**Fatalities**	**Injuries**
Construction/Operation	20	8.2	$3,086,000	6.7	0	16
Corrosion	2	0.8	-	0.0	1	8
Outside Force	153	62.4	$32,334,352	70.2	6	48
Other	70	28.6	$10,617,683	23.1	13	31
Total	245		$46,038,035		20	103

The failure data breakdown by cause may change as OPS receives supplemental information on accidents.

Table 1.1: Incidents in natural gas pipelines caused by outside force (adapted from the Office of Pipeline Safety; up-to-date information can be found at *http : //primis.rspa.dot.gov/pipelineinfo/stat − causes.htm*).

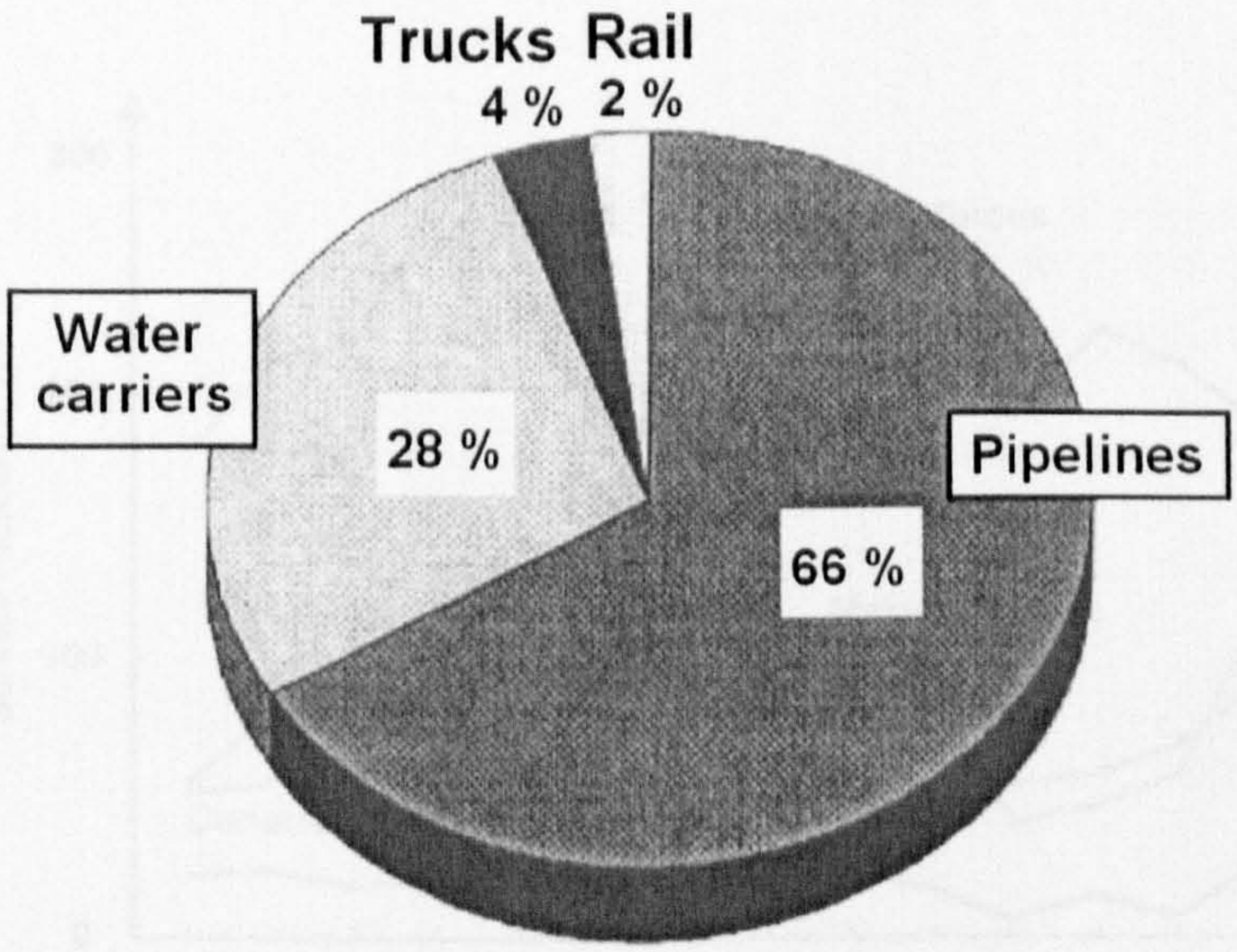

Source: Association of Oil Pipe Lines, *Shifts in Petroleum Transportation, 2002*

Figure 1.1: Modes of petroleum transportation in the USA. Total annual oil transport: 6.1×10^6 barrel miles (adapted from Ref. [20]).

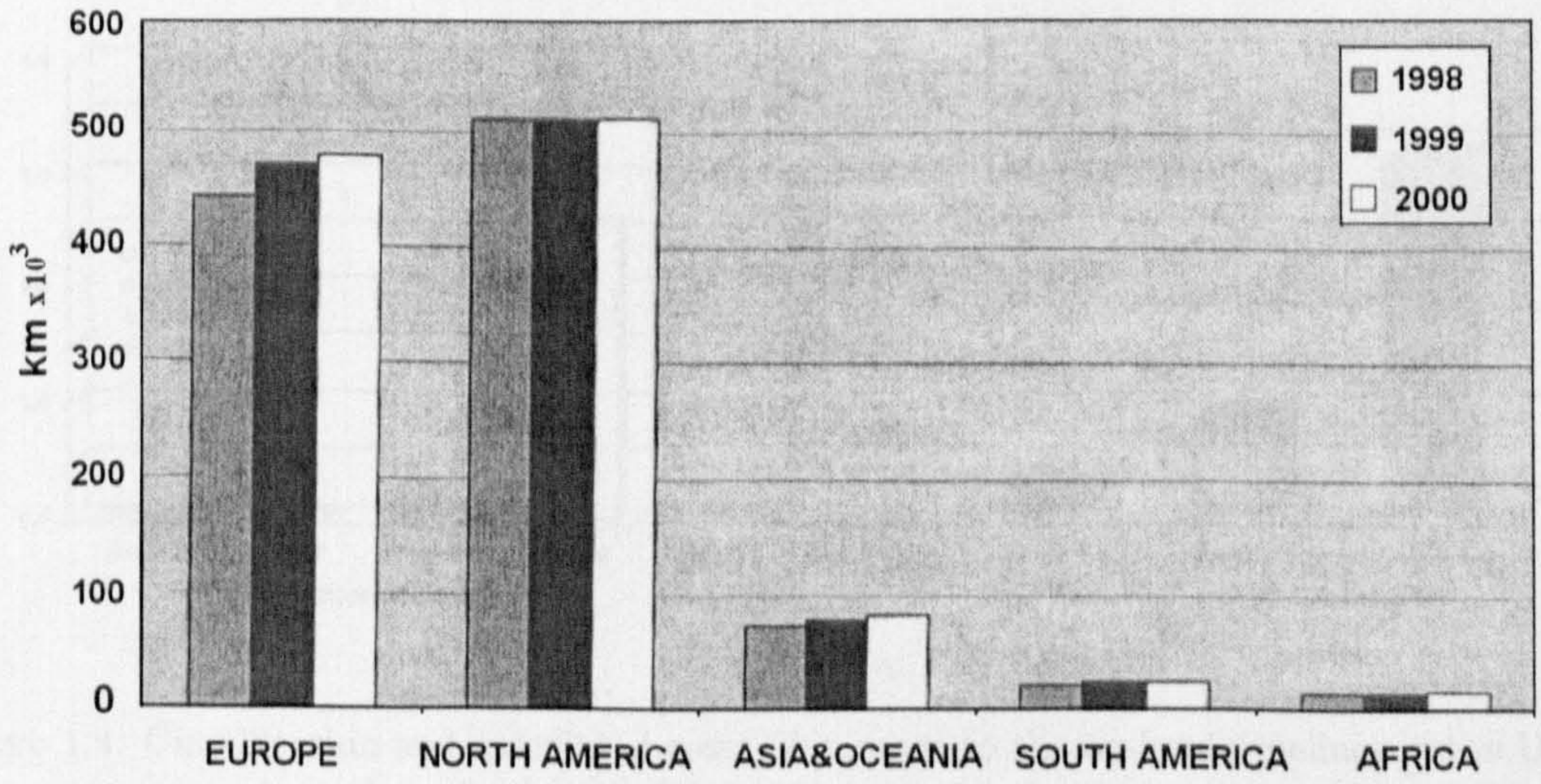

Figure 1.2: Length of world natural gas pipeline network (adapted from Ref. [1]).

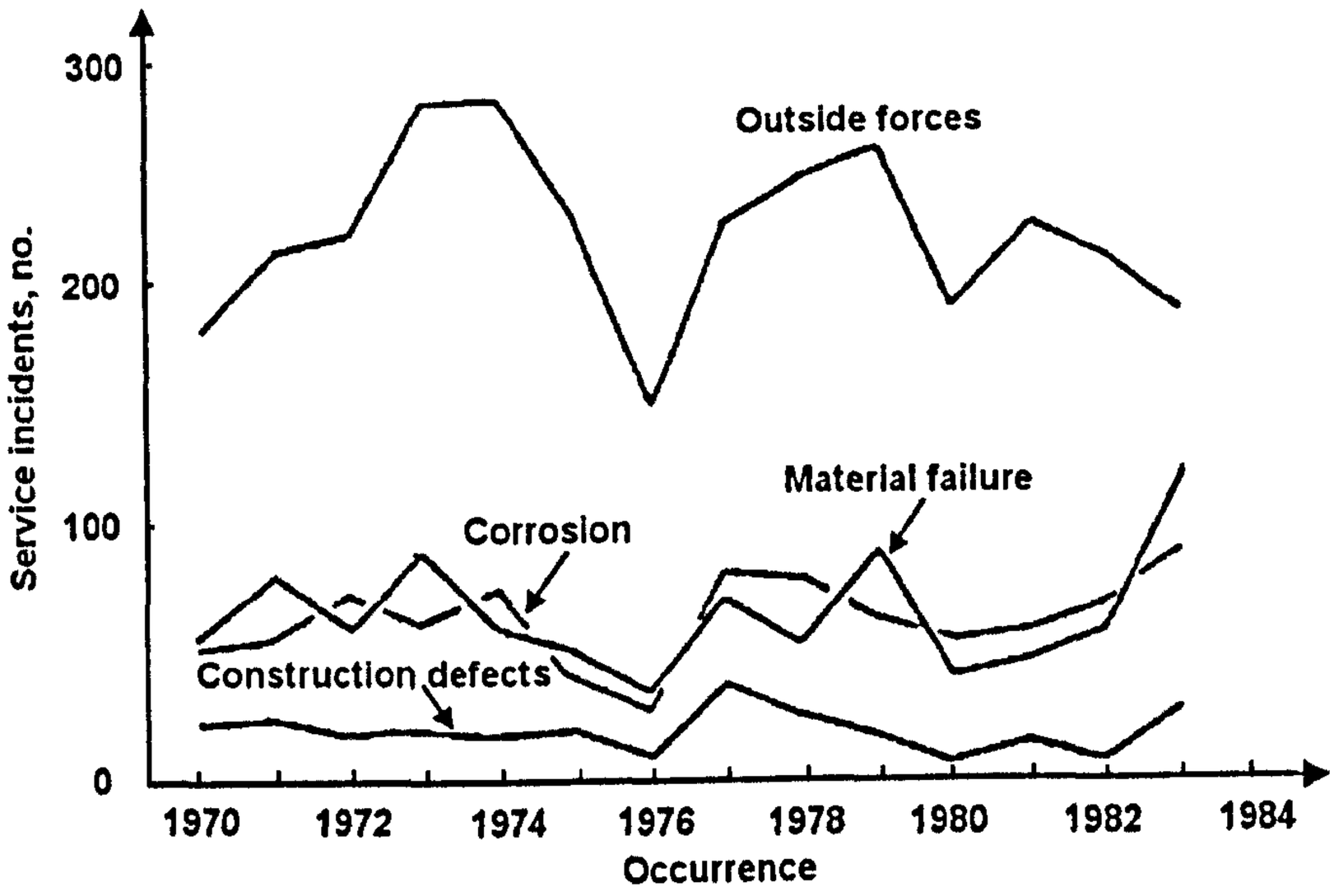

Figure 1.3: The pipeline incidents and their causes for years 1970 to 1984 in the USA (adapted from Ref. [21]).

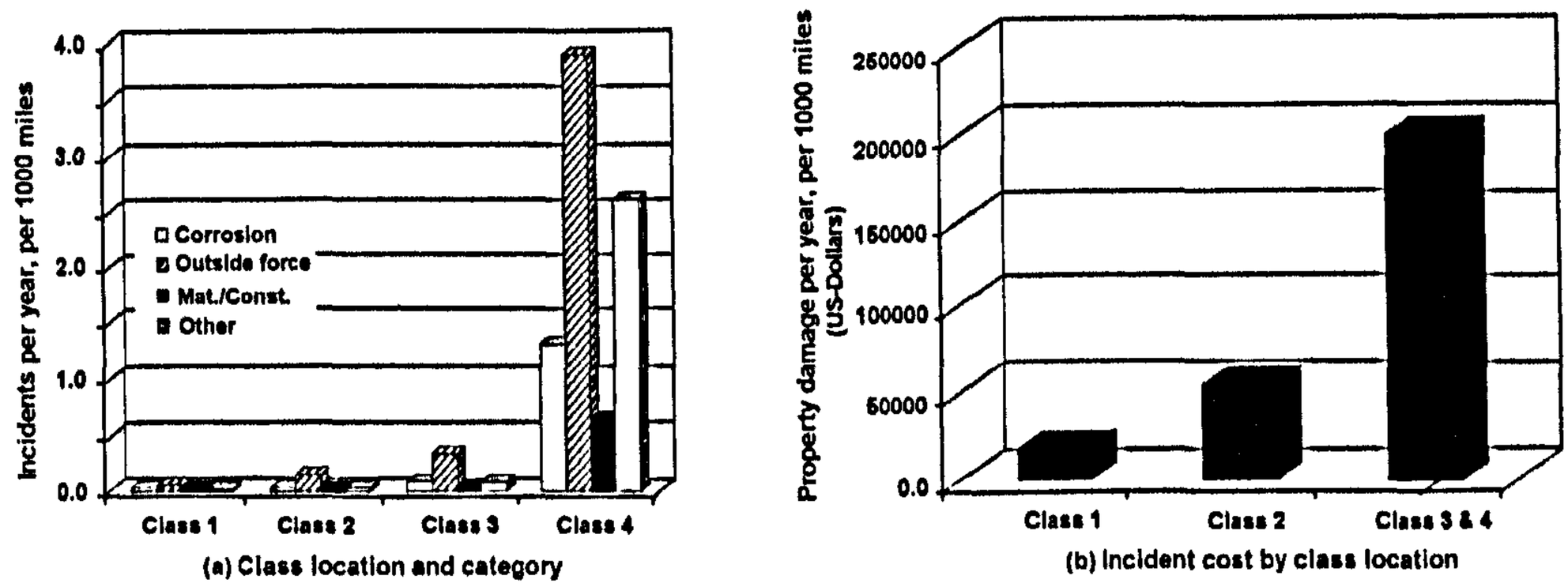

Figure 1.4: Classification and associated costs of damage to the on-land pipelines in the USA. Class 1 corresponds to low population density area, whilst Class 4 corresponds to highly urbanized locations (adapted from Ref. [22]).

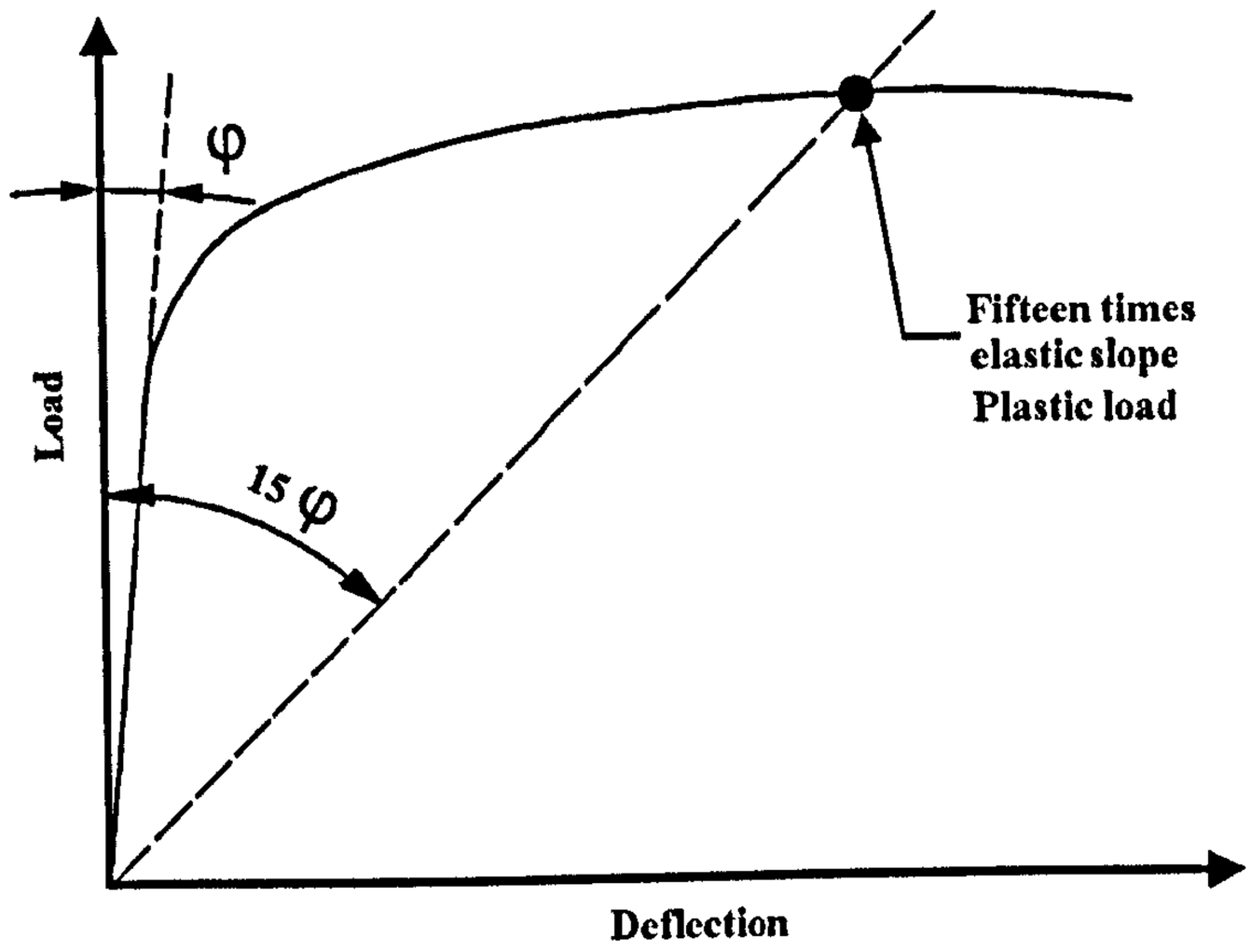

Figure 1.5: The fifteen times elastic slope method recommended in ASME III Pressure Vessel Design Code [17].

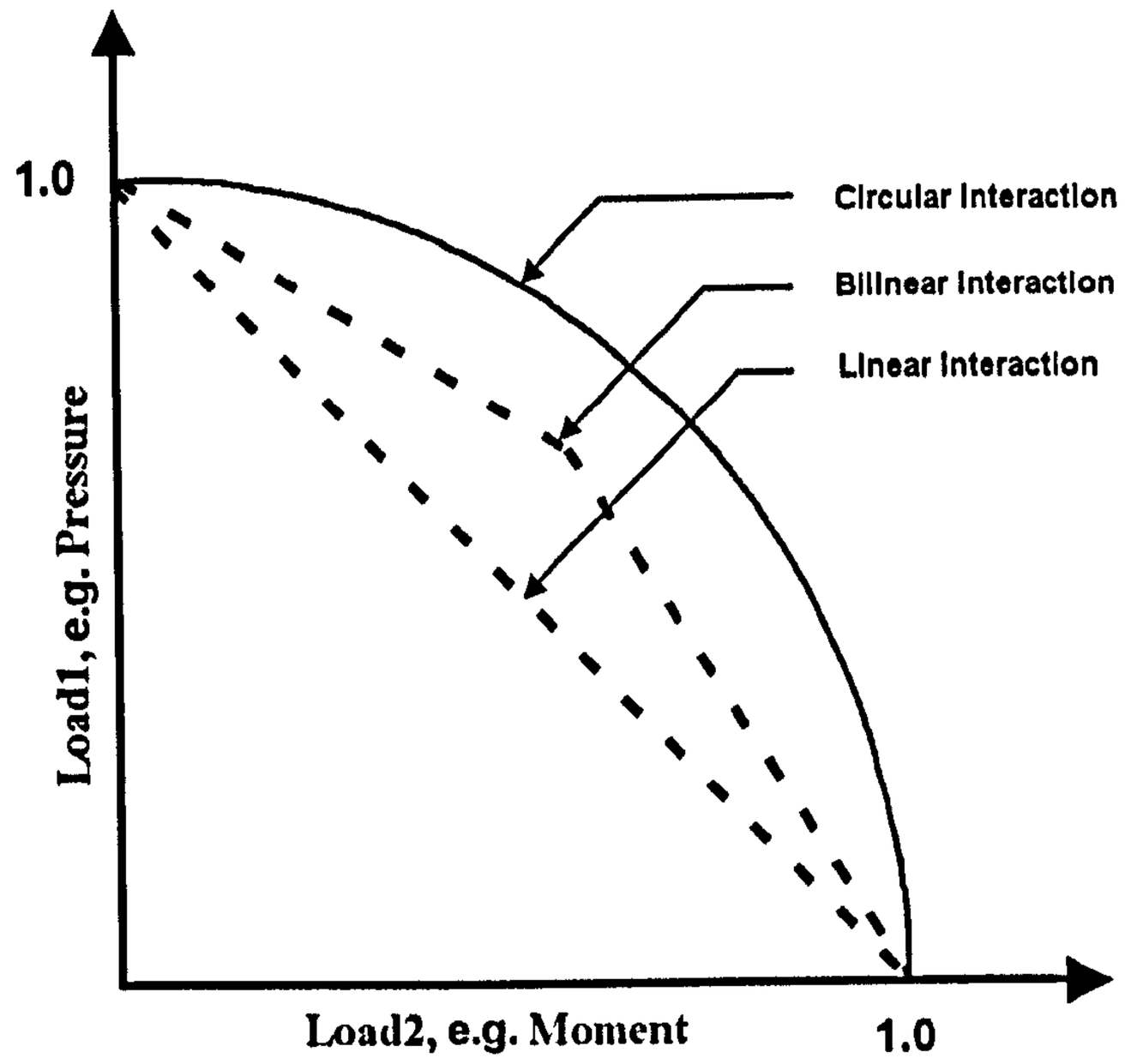

Figure 1.6: Format of the interaction diagram with three possible types of load interaction (only for positive loads).

Chapter 2

Literature review

2.1 General

This Chapter reviews literature available in the the public domain and which is associated with structural integrity of transmission pipelines. As has already been mentioned surface damage by outside forces remains the main focus of the review but some side issues are also mentioned. In order to maintain and improve safety record of pipelines, emphasis is being placed on the significance of defects and their role in structural integrity of pipelines.

2.2 Pipes with plain dents

Review of experimental and analytical investigations of dented pipelines was carried out by Alexander [23]. The author presents an overview of the current research related to constrained dent configurations such as those created by rocks. The author discusses several options for repairing damaged pipes. The principal aim was to assess defect severity in terms of future behaviour involving both static burst and cyclic pressure conditions.

Plain dent is defined as a change in curvature of the pipe wall without any reduction of its thickness [2]. Dents are usually classified as short/localised, long and continuous [2, 3]. Shallow and long dents can be removed completely by internal pres-

surisation. In this case, pipe regains complete circularity. Localised/short dents can be pushed out almost completely leaving only residual ripples or humps around dent regions. A parameter study was carried out by Rinehart et al. [24] to quantify the nature of dents which fall into transition region between the short and long dents. Their analysis was based on the existing full-scale data and on finite element analysis. The study showed that, unrestrained, longer dents experience centre cracking, re-rounding, and relatively short fatigue lives. Shorter dents experience cracking, little re-rounding, and also relatively short fatigue lives. Similar finding was also presented by Beller et al. [25] who used $3D$ finite element model.

Experimental and analytical work on dented pipes was presented by Alexander [26] and [27]. The analytical and experimental tests were carried out on $X52$ steel grade pipe with diameter to wall thickness ratio equal to, $\frac{D}{t} = 104.6$. The denting process for all cases was achieved under zero internal pressure. The author used two types of indenter to perform denting: dome cap and a long bar. The maximum depth of the dent to the pipe diameter was, $\frac{\delta}{D} = 18\%$. Forty-four different dent configurations were used in the course of testing. While the primary thrust of the work was experimental, analytical efforts were made to address dent mechanics using first-order quadrilateral shell, S4R5, elements. Soil interaction was modelled using spring elements with a trial and error approach.

Fifteen tests on pipeline ring specimens, made from steel $X52, X65$, and $X60$ grades, containing dented seam welds, are reported in Ref. [28]. The ring specimens were 75 mm wide slices of pipe, pressurised internally in a special test rig. Seven specimen were dented and then pressurised to failure. Three specimens achieved stresses exceeding yield and they did not fail. The other rings exhibited failure at stresses as low as 24% of the yield stress. Weld cracking was evident in some of the models after denting but prior to bursting.

Experimental tests on full scale steel pipe with diameter 508 mm, $X42$ grade, and 660 mm grade $X52$ were presented by Belonos et al. [29]. Two different dents were studied, long continuous dent and a localised dent. The results demonstrate that the metal adjacent to the dent contains some residual stresses even though the metal yields. The magnitude of this residual stress was obtained by the use of strain gauges.

Ong et al. [30] conducted 18 burst tests which revealed that the bursting strength of a pipe was generally insensitive to the existence of a local dent. The tests showed that the defect due to loss of thickness was the main factor governing the pipe failure. The finite element technique was used to model plain, local dent without any surface-defect. A shell element was used in this study. The strain-gauging results, and the finite element results, on plain local dent showed that the strain distribution in the local dent is different from strain distribution obtained for a long dent. The peak stress in a local dent occurred at the axial flank of the dent, while in a long dent it occurred at the dent's root. Also, the magnitude of the peak stress in a local dent was much smaller than that in the long dent. It is worth noting that results given in Ref. [30] are within the elastic range, only.

Eiber et al. [2], summaries research on burst tests which were conducted for temperatures ranging from $-31.1\ C°$ to $32.2\ C°$. There were 44 dents covering short and long plain dent configurations. The results show no effect of temperature on experimental results. The dents investigated had their depth of up to, $\frac{\delta}{D} = 8.2\%$ for 406 mm diameter pipe, and $\frac{\delta}{D} = 5.2\%$ for 762 mm diameter pipe. All dents were produced under zero internal pressure. Three different radii of indentors (solid bar) were used, i.e., 12.7 mm, 63.5 mm, and 140 mm. The solid bars were placed on the top of the pipe with their axis parallel, at 45°, and at 90° to the pipe axis. The most severe dent, from a stress magnification viewpoint, was found to be a long dent with its axis parallel to the pipe axis. It has been concluded that plain dents do not produce failures, unless they are near, or on the longitudinal weld.

Experiments on pressurised and dented pipe are reported in [31]. These experiments were on small scale pipes with diameter to wall thickness ratio, $\frac{D_o}{t} = 54.1$, and made from aluminum alloy. The indentation was caused by spherical rigid indenter resulting in a short dent. The denting process was carried out on empty pipes. Two crescent-shaped zones of high surface strain have been identified at the axial extremities of the dent. The location of these regions remained stationary as pressure was increased.

Collapse pressure tests of long cylinders which had local dents was carried out by Park et al. [32]. A number of stainless steel tubes type, SS-304, with diameter to wall thickness ratios of, $\frac{D}{t} = 33,\ 24$, and 19, were dented to various depths using

spherical indentors with diameters 0.4, and 1.6 of the tube diameter. The indentation was carried out in a standard, screw-type, electromechanical testing machine with the test specimen resting on a rigid flat plate. A thin, 1.6 mm, rubber pad was placed between the tube and the rigid plate to help prevent rotation of the tube during the early stage of indentation. The indentation was carried out for all specimens without internal pressure. Collapse was carried out by enclosing each tube in a stiff, 69 MPa capacity pressure vessel, and by applying external pressure. The results showed that tubes with relatively small dents had higher collapse pressures. Magnitude of collapse loads were found to be insensitive to the detailed geometry of a dent but they were dependent on the maximum of pipe ovalization (of its most deformed cross section).

Studies into plain dents produced on pressurised pipes can also be found in the literature. This type of defect usually occurs during service of a pipeline. In practice most of the damage is caused by digging and excavation equipment. Other damage is caused by natural events such as earthquakes, falling rocks, ice, etc.. A theoretical model describing the structural behaviour of dented pipe under pressure is given in Ref. [33]. It is reported that the model gave predictions for re-rounding that were in good agreement with results of tests. Tests also indicated that dent re-rounding is cycle-dependent.

2.3 Finite element simulation for the case of plain dent

It needs to be stressed that finite element analysis of dented pipes has not been undertaken to any great extent. The reason for this is unknown. One possibility is probably lack of large scale computing facilities. Available results are reviewed below.

Leis et al. [34] investigate dents on a pressurised pipe with a quarter model using 8-noded shell elements. The indenter and pipe support were modelled as rigid bodies. Additional analysis using a shell-to-solid approach was also conducted. This involved, 20-node solid brick element which was used in the indented region. Shell elements were used away from the dent region. The results obtained from the FE analysis in terms of a load displacement curve, were reasonable when comparison with experiment was made.

Other work has been presented by Pal et al. [35] who used a shell element with elastic-plastic material to simulate a severely dented pipe. The FE analysis was performed for two different grades of steel $X52$, and $X60$ in order to investigate the effect of SMYS (Specified Minimum Yield Stress) on the stress level, and on the magnitude of equivalent static load. The authors reported that the pipeline portion subjected to high stress, has yielded. Also, operating stresses after unloading, were high but did not exceed the SMYS.

Denting of pressurised pipelines under localised radial loading was modelled by Brooker [36]. He used a similar technique as Leis et al. [34], i.e., a shell-to-solid approach. It consisted of 8-noded full-integration solid elements in the dent region with five layers through wall thickness of the pipe, and 8-noded shell elements away from the dent region. The shape of the impacting excavator tooth was idealized as a truncated wedge. Contact between the pipeline and the indenter was modelled assuming frictionless behaviour. The tooth was modelled using a 4-node rigid element which was different when compared to the analytical rigid surface used by others, e.g., Leis et al. [34].

Dinovitzer et al. [37, 38, 39] have descried the finite element model which considered the dent's shape and line pressure history. The proposed nonlinear finite element analysis included fracture mechanics based crack growth.

Ref. [40] deals with a long radial indenting of pressurised pipes by finite element analysis and analytical methods. Several scenarios have been investigated such as different pressure levels, different support conditions, different material properties and different geometry of pipes. In addition to the FE, some analytical results are also provided. The elastic-plastic response of unpressurised pipes subjected to axially long radial indentation is given in Ref. [41]. A large FE study investigates deformations of indented rings.

2.4 Other cases

A closed-form solution for the evaluation of stresses associated with long axial dents in a pressurised pipe can be found in Ref. [42]. The author concludes that for

a long dent, the maximum bending stress always occurs at the root of the dent and its magnitude depends on both the dent's included angle and its profile. Sharp dent will induce a higher bending stress than a shallow dent. On the other hand, bending stresses induced in the local dent are smaller than those in the long dent.

2.5 Methods of denting and gouging

Different methods of producing dents and gouges can be found in the literature. Frequent approach uses a plain pipe which could be either pressure free or pressurised to a given level (usually to the design level). Next, a rigid object is pressed to deform pipe surface. This could be by static or by dynamic loading. Different indenters such as spherical, solid bar or plates are used.

Literature search shows that there are two approaches in which dents containing gouges/cracks could be manufactured for the purpose of experimental investigation. The first method is described in Ref. [43]. A sharp notch was machined into the exterior surface of the pipe and the entire area was indented with a hydraulic ram. The second method is described in References [3, 28]. The plain pipe was dented first and this was followed by the introduction of the mechanical damage (a narrow flaw machined in the base of the dent). The results obtained from both methods were compared by Maxey [44]. The second method proved to be less severe than the first method. Based on the results of 132 burst tests that involved rings and pipes, a method for prediction of failure was proposed.

Description of mechanical damage in pipelines which is based on 129 experiments involving rings and vessels made from dented pipe is presented by Jones [3]. It appears that dents of depth up to, $\frac{\delta}{D_o} = 24\%$, of the pipe diameter have no effect on pipeline integrity. Similar conclusion was reported by Hopkins et al. [28] for dents of up to, $\frac{\delta}{D} = 8\%$, and possibly up to, $\frac{\delta}{D} = 24\%$. Fowler et al. [45] present a full scale test on a pipe. Results indicate that dents are not a problem for normal pipeline service. In all experimental tests reported in the literature, the residual stresses due to denting and subsequent removal of the indenter are ignored.

2.6 Experimental and numerical work on dented and gouged pipes

Plain gouge defined by Eiber et al. [2] and by Jones [3] mean a reduction in the pipe wall thickness (without any change of the curvature of the pipe wall). This type of defect takes several forms such as V-notch or elliptic shape.

Mechanical damage can also cause changes to the material properties of the pipe material. These changes in material properties are rarely uniform, and anisotropy and non-homogeneity of the ligament below a gouge may result. Severely deformed area is usually located directly beneath the gouge. In 1991, Hope [46] carried out experiments on the effect of the mechanical damage on the pipe material properties. Mechanical damage in the form of dent-gouge was introduced into a full scale steel pipe. The investigation revealed a large deformation layer directly beneath the gouges with depth equal to $100 - 200\ \mu m$, and a large prestrain of up to 50%.

An estimate of the fatigue life of girth welds affected by dents is presented by Rosenfeld et al. [47]. The fatigue life is estimated by considering empirical dent stress factors, published weld fatigue data, prevailing minimum weld quality standards, and accepted fatigue analysis methods. Authors indicate that in many cases, a dent on a weld could remain in service without repair.

An experimental methodology for the evaluation of the resistance of gas pipeline being damaged by an excavator is presented by Mannucci et al. [48]. The test facility capable of carrying the experiment with and without internal pressure and other simulations is described.

Work on combined defects, i.e., on dents and gouges, and the corresponding failure pressure in a pipeline was reported by Maxey [43, 44]. The defect was produced for experimentation by machining a V-shaped notch in pipe wall and then pressing a round bar, laid over the notch, into the pipe to form a dent. The longer the notch-and-dent defect, the greater the difference in their severities. All of these notch-and-dent failures were leaks. Because the notch-and-dent defect is made under zero pressure conditions, relatively deep denting was accomplished. While this simulates damage done when the pipeline is being constructed or repaired, it does not reveal the nature

of denting and gouging when pipeline is under pressure.

Experiments on the effects of dents, gouges, and gouges in dents simulating external damage can also be found in Ref. [49]. Eight pipe sections were made from steel having diameters, $\frac{D}{t} = 24.5, 27.4, 33.4, 52.6$, and 91. The indenters used included cylinders and an actual tooth from an excavator. Gouges were introduced into dents the pipe was first dented with a cylindrical indenter to a depth, δ, a gouge of depth, e, was introduced into the bottom of the dent. This was done by a tool piece mounted at the end of a pendulum. The gouge produced by this method was U-shaped. It was 6.4 mm wide and with a radius of curvature equal to 6.4 mm at the bottom. After inserting the gouge to the dented pipe, the pipe was pressurised to failure. The result showed that a gouge in a dent is a more severe defect than either the gouge or the dent alone.

Lancaster et al. [50] conducted twelve tests on small scale pipes with diameter to wall thickness ratio, $\frac{D_o}{t} = 54.1$, and made from aluminum alloy 6063-TB. These tests contained axial gouges with four different depths and constant length. These pipes were dented under zero internal pressure to three different dent depths. Tested specimens were pressurised, using a specially designed burst rig, to the operating and failure pressure.

Another work by Lancaster et al. [51], describes small scale testing of pipes with combined dents and gouges. Results showed that dent size has little influence on failure pressure, which remains close to that of plain gouge of the same dimensions. It is reported that pipes with larger combined dents, $\frac{\delta}{D_o} = 15\%$, and gouges, $\frac{e}{t} = 45\%$, but without cracks may still be able to sustain normal pipeline operating pressures.

Analytical and finite element analysis was carried out by Spiekhout et al. [52] to evaluate the resistance against mechanical damage of pipelines. Two equations were proposed for assessment of the mechanical damage in elastic and plastic deformation region. The equations derived were for the relationship between dent depth and force. According to these relationships, the dent depth is proportional to the force for the elastic deformation. On the other hand, the force required to dent a pipeline with internal pressure is greater then one without internal pressure. The force/dent depth diagram which was obtained by means of finite element calculations closely matched

the force/dent depth curve resulting from tests. Additionally, an equation for burst pressure of notched dent was presented. Authors reported that for increasing diameter, the dent depth decreases and the burst pressure for the notched dent caused by the hydraulic excavator appears to increase, hence a better resistance to mechanical damage was obtained. Also, for increasing diameters the resistance to external forces appears to increase. The same conditions were applied to the pipe wall thickness. The higher internal pressure the remaining dent depth is smaller and the burst pressure rises.

2.7 Burst strength

Assessment of the burst strength of through and part-wall defects in pipelines has been obtained from experimental data as detailed below. Development of empirical equation was described by Kiefner et al. [53]. Equation given in Ref. [53], was validated against 92 through-wall defects and 48 part-wall defects. The experiments were carried out on full scale vessel burst tests containing axially oriented and machined V-notches.

Calculation of burst strength of dented pipes with cracks in dents is proposed by Ruxin et al. [54]. Comparisons of predicted burst strength based on the test results gives good agreement with numerical analysis. The burst reliability model of dented pipes is also given in this reference.

Burst test on small scale pipes with, $\frac{D}{t} = 95$, made from $X52$ steel and subjected to external loads are presented by Gresnigt et al. [55]. The external load (external pressure or two concentrated loads acting away from the dent region) were applied at zero internal pressure until deformations (ovalisation, curvature change and rotation) have become excessive. Subsequently specimens were used for the burst test. These tests have demonstrated that if ductility is good, even extremely deep dents do not affect burst pressures.

Work by Lancaster et al. [56] includes series of burst tests conducted on small scale pipes made from aluminum alloy 6063-TB and containing dents and smooth gouges. These results showed that gouges located near the axial extremity of a dent cause low-pressure failure, and indicate the presence of two regions of high strain at axial extremities of the initial dent. All specimens containing smooth gouges and which

were outside the high strain zones withstood pressures in excess of normal operating level. In 1993, Lancaster et al. [57], reviewed their experiments on pipes containing dents and gouges. Comparison of results on laboratory models with those of full-size tests, was made. Burst tests on ten pipe sections with external dent/notch combinations of damage while under pressure, are reported by Muntinga et al. [58].

2.8 Repairing gouges by grinding

Work on repairing shallow gouges in dents in pipelines by grinding out the gouge is described by Kiefner et al. [59]. A comparison between burst pressures and cyclic-pressure fatigue lives of pairs of pipe specimens, one of which was tested without being repaired while the other was tested after being repaired was demonstrated on pipe with diameter equal to 324 mm having axial gouges. The latter were machined into these specimens to the depths of, $\frac{e}{t} = 5\%$ to 10%. Indentation of the specimens was carried out with the pipes pressurised to a typical operating stress level. The maximum indentation as a percentage of the outside diameter ranged from, $\frac{\delta}{D} = 5\%$ to $\frac{\delta}{D} = 20\%$. After the pressurisation, one specimen of each pair was repaired by grinding out the notch and any associated cracked material. The specimens were then subjected either to burst testing or pressure-cycles fatigue testing to failure. The results showed that the specimens with gouges removed by grinding uniformly exhibited burst pressures in excess of the 100% SMYS pressure. In contrast, the unrepaired specimens exhibited failure pressures which decreased with increasing dent depths to levels as low as 41% of SMYS. The specimens with gouges removed by grinding exhibited pressure-cycle fatigue lives at least four times as long as those of the unrepaired specimens.

2.9 Resistance of pipe to puncture

Four experiments on the resistance of the pipe to puncture were conducted by Maxey [44]. The penetration experiments were conducted by pressurising the specimen to the desired pressure level and then slowly pressing a wedge into the specimen by means of a hydraulic jack. Special monitoring equipment was used to record continuously the wedge and depth of the penetration. The wedge used was a 25.4 mm

long round bar with 45° machined wedge oriented parallel to the axis of the pipe. It was pressed to the pressurised vessel. The results showed that, thicker pipes exhibited the greatest resistance to penetration. Work on the design of pipelines to resist puncture caused by accidental impact from an excavator bucket tooth was presented by Driver and Zimmerman [60]. They developed a formula for determining the puncture resistance of a pipe to concentrated outside forces.

A series of 14 experiments on steel pipelines, with two diameters equal to, 273 mm, and 355.6 mm, and wall thickness varied between 4.8 mm to 6.9 mm is described in Ref. [61]. The indenter used was the excavator bucket teeth with different tooth geometries. The indentation was to cause puncture. The experimental models were simulated using a shell-solid sub-model finite element as described in References [62] and [63].

2.9.1 Finite element simulation of puncture

Recent work on the pipeline puncture under excavator loading, using finite element techniques, is due to Brooker [62]. The author modelled a quarter model with a shell-to-solid sub-model techniques. Eight - node, hexahedral elements in the contact regions were used. Shell elements were used in an area away from the penetration regions. Multi-Point Constraints were used to define the shell-to-solid transition. The results obtained from this model include: puncture loads and residual dent depths. They agreed well with experimental results published by European pipeline research group.

Brooker [63], published work on the puncture which is a parameter study and examines a wide range of pipeline diameters, wall thicknesses and excavator tooth dimensions. An equation for the puncture resistance load was derived, and it was compared with the derived equations by Zimmerman [60] and Spiekhout [52].

2.10 Codes and guidelines

Several codes are available for assessment of defect in the transmission pipelines. British Standard, $PD6493$, is widely used for assessing damaged pipelines. It has three

levels. The lowest level accounts for linear elastic fracture mechanics. The second level is based on R-curve which is used when failure is likely to occur. This level takes into the account the effects of plasticity. The third level is based on J-integral which accounts for crack arrest. ASME Code, B31.8, and B31.4, are used for assessment of dents and gouges in pipelines. Both codes are conservative in their assessment of dents with gouges. B31.8 Code permits the removal of gouges using approved repair methods, but B31.8 does not permit any repair.

2.11 The European pipeline research group

The European pipeline research group has conducted a test programme for 15 years to address the issue of external damage. This has resulted in database consisting of a large number of test results. A summary of the assessment is presented by Roovers et al. [64]. Some of the methods described in this document have been used by companies for many years and where necessary they have been revised in the light of operating experience. Other methods have been developed more recently, in response to newly emerging requirements [12, 14]. The types of damage addressed in the document include dents, gouges and dent/gouge combinations.

2.12 Tabulation of known experiments

The literature survey has revealed that experimental data is very fragmented and scattered. Also, different approaches have been used to assess surface damage. Some experiments simulated realistic cases whilst reasoning behind some of them is unclear. It was felt that it would be beneficial to collect all available experimental data and present it in a single Table. This Table forms Appendix (A), as Table (A.1). It contains details about 420 experiments conducted by various institutions. It also gives basic information about the experiments, i.e., geometry of pipe, dent, gouge, material data, type of test, etc. Figure (2.1) shows typical forms of indenting a horizontal pipe - ranging from hemispherical rigid indenter to another cylinder acting as an indenter.

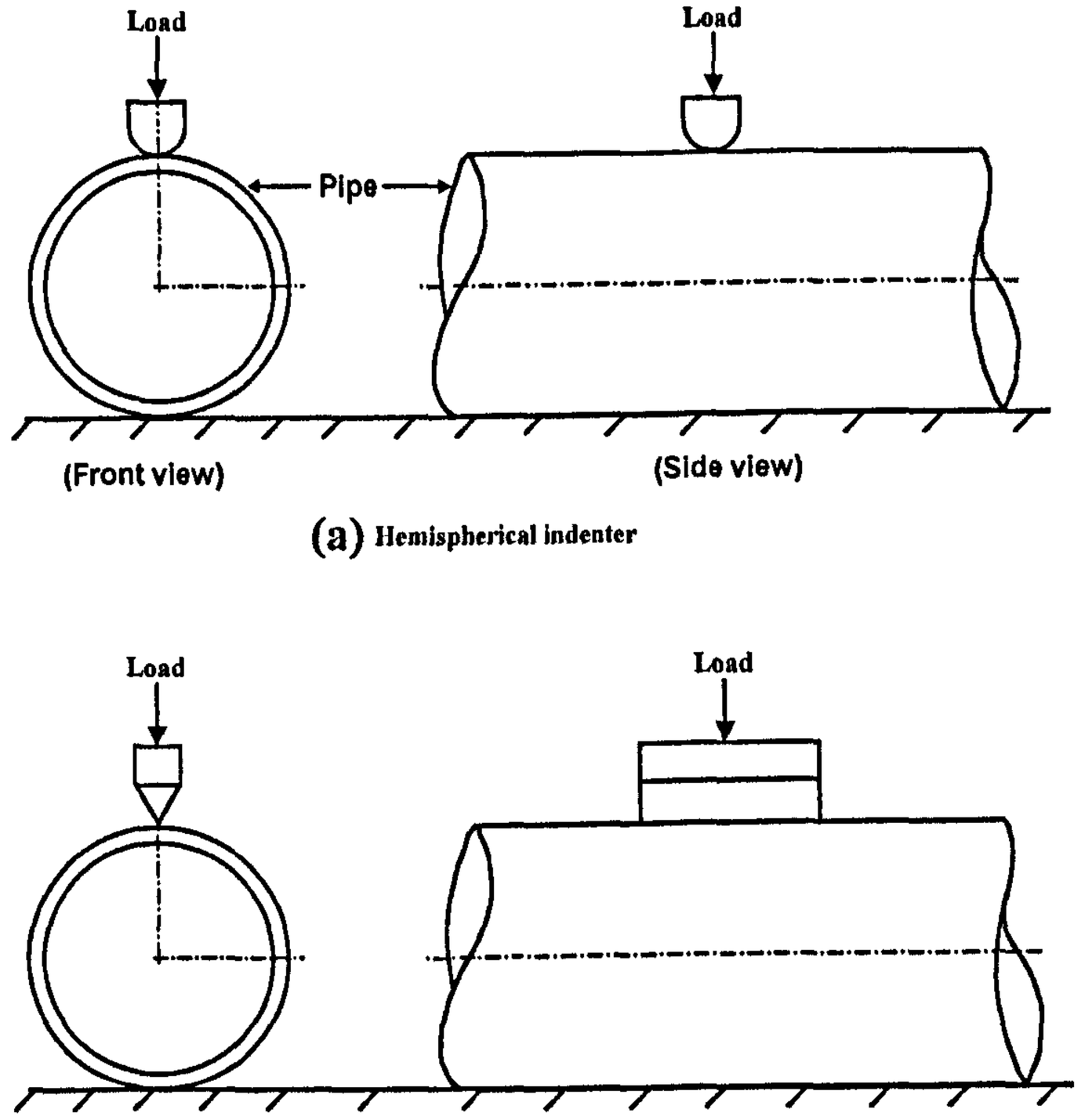

Figure 2.1: Different methods of denting of pipes. Different indenters are used, i.e., hemispherical, V-notch, solid bar or cylinder. Usually the indentation is carried out at the pipe's mid-span. Also, for empty and not pressurised pipes.

Chapter 3

Analysis of plain dents in steel pipeline

3.1 Finite Element modelling

Recent advances in computer technology have led to progress in understanding of many complex engineering problems. Structural integrity of pressure vessels and piping is an example of one of them. Many engineering software tools such as PATRAN, ANSYS, and ABAQUS were developed to facilitate this progress.

The finite element code used in this study is ABAQUS/Standard 6.3 [19]. Geometry of the pipe was created using PATRAN 2001 r2a [18]. The output file obtained from PATRAN was transferred to ABAQUS/Standard 6.3. Additional analysis options were added to this file before any computing was performed. This includes creation of a rigid indenter, rigid pipe support, the use of NMAP parameter, description of contact surfaces, ect. The analyses were performed on both the whole model and on a quarter model to ensure that a quarter model predicted the same results as the whole model. General view of the model which was used is shown in Figure (3.1).

3.1.1 Pipe geometry

Numerical analyses are based on a single geometry of the pipe for which the ratio of outside diameter-to-the-wall-thickness is, $\frac{D_o}{t} \cong 40.0$. Diameter of indenter was

such that, $\frac{2a}{D_o} = 0.41$, (see Table 3.1 and Fig.3.2). It is seen from Table (3.1) that the adopted model can be classed as small scale model. These dimensions are close to experimental models to be tested and analysed later in Chapters (6) and (7).

Let us consider a horizontal circular pipe with outside diameter, D_o, of uniform wall thickness, t, with total length, $2L$, subjected to uniform internal pressure, p, and being dented in the mid-span by a vertical, rigid indenter. These arrangements are sketched in Figure (3.1). Whenever the internal pressure is applied, the resulting axial stress is always taken into consideration. The above pipe is to be supported either by a rigid saddle, or by a rigid horizontal plate. In addition, a set of elastic spring elements is to be used as a possible support for the pipe. Sections through the pipe showing indentor, pipe, and three different types of support are illustrated in Figure (3.2). Figure (3.2a) shows a section through the pipe and the indentor, as well as through the rigid saddle support extending by 120° in the hoop direction. Three typical meridional profiles for the indenter are considered in the current study, and they are prolate elliptical, circular and oblate elliptical. The range of indenter's shapes considered in this study varied between $\frac{a}{b} = 0.25$, and $\frac{a}{b} = 4.0$. Shapes of the latter two together with hemispherical indenter are sketched in Figure (3.3).

3.2 Boundary conditions

As mentioned previously due to the symmetry of the problem, a quarter FE model was used throughout this study. The FE model which has finally been adopted can be seen in Figure (3.4). The boundary conditions were applied along lines 1, 2, 3, and 4 (depicted in Figure 3.5). List of variables which were constrained is explicitly stated in Table (3.2). Rigid body motion is prevented by taking a single node, NC, shown in Figure (3.5), and applying to it boundary conditions given in Table (3.2). Restraints were also applied to the rigid indenter allowing it to move only in one direction, i.e., vertically along Y-axis. Indentor was not allowed to rotate. The rigid saddle support was fully restrained in all directions.

3.3 Friction between pipe and rigid surface

It is seen from the arrangements which have been described so far that there is going to be contact interaction between indenter and pipe and between pipe and its support. Friction needs to be considered between both of these interfaces. Contacting surfaces transmit shear as well as normal forces across their interface. ABAQUS includes the friction model as a part of surface interaction definition. Several values of friction coefficients were used to determine the most suitable value. Results have showed that the friction coefficient had little effect on the dent profile, on residual depth of the dent, and on the ultimate denting load as can be seen in Table (3.3). As a result of these analyses a value of 0.35 for the coefficient of friction, (between the indenter and pipe, and between pipe and its rigid support), was used throughout all of the remaining analyses.

3.4 Application of bending

Once the pipe was dented it was subjected to bending. The aim here was to obtain the maximum values of moment which could be applied to a dented, i.e., damaged component. More detailed description of bending is given later. The way in which bending was applied is briefly outlined here. For moment loading, the nodes at the end of the pipe were tied to a master node at the pipe center. The "Multi-Point Constraint", *MPC* option in ABAQUS was used to apply moment loading via rotation of the master node. For cases of combined loading, where bending moment was applied first, the moment was kept constant using the ABAQUS's "Concentrated Load", *CLOAD* parameter followed by the application of increasing internal pressure. Again, details are given later.

3.5 Material properties

Prior to the FE calculations, uni-axial tensile tests were carried out on flat steel specimens in order to obtain material properties. Details about machining flat tensile coupons, their dimensions, ect. is given in Chapter (6). A typical engineering stress-

strain curve obtained from tensile test is plotted in Figure (3.6). This response curve has been converted to the true-stress, true-strain curve according to Equations (3.1) and (3.2), respectively. Result of this conversion is Figure (3.7a). The yield stress, σ_{yp}, taken as an average value of all tests, was found to be, $\sigma_{yp} = 316\ MPa$. Other average values are Young's modulus, $E = 210\ GPa$, and Poisson's ratio, $\nu = 0.3$. It is worth nothing here that most of the calculations are based on the full true stress-strain curve. The curve shown in Figure (3.7a) has been approximated by a set of 26 linear segments, as shown in Figure (3.7b). This 26 segment curve was entered into the ABAQUS input file.

$$\sigma_t = \sigma_{nom}(1 + \varepsilon_{nom}) \tag{3.1}$$

$$\varepsilon_t = ln(1 + \varepsilon_{nom}) \tag{3.2}$$

3.5.1 Additional details about the FE modelling

- Indenters, and pipe's support were modelled using an analytical rigid surface option in ABAQUS.

- The quarter FE model as seen in Figure (3.4) was constructed first as a flat plate in rectangular co-ordinate system using PATRAN, (see Fig. 3.8a). The mesh in the area where the dent is to occur needed to be refined (the top left corner). The flat plate was divided into a number of 'solids' with each solid having four edges as illustrated in Figure (3.8a). This method easily controls the aspect ratio of the element size. It allows the introduction of the defect to plate and subsequently to the pipe. Solid section could be divided much easily in plates then in pipes. Next, meshing was applied to these solids. Twenty node solid brick elements with reduced integration, $C3D20R$, were used. The resulting model is shown in Figure (3.8b).

- Once the meshing procedure is complete in PATRAN, the flat plate is rotated to a quarter pipe using NMAP option in ABAQUS, and result of this transformation is shown in Figure (3.8c).

As can be seen from Figure (3.9), several types of elements were tried to identify the most convenient element type for the FE model. These included shell elements, $S4R$, $S8R5$, solid brick elements, $C3D8R$, and $C3D20R$. Combination of solid-shell elements was also tried. Within the element library in ABAQUS there are two types of brick elements, i.e., C3D20R and C3D20. The reduced integration elements $C3D20R$ have 8 integration points whereas $C3D20$ have 27 integration points. The element type, $C3D20R$, requires less computer time especially for $3D$ models whereas element type $C3D20$ is more time consuming.

Shell elements, $S4R$, and $S8R5$, are usually used for arbitrarily large rotations but only for small strain. The change in thickness with deformation is ignored in these elements. In contact problems the shell element uses its mid surface for contact, which can give inaccurate results.

Previous FE studies at the University of Liverpool [65, 66], show that the C3D20R element was the most suitable element for linear and nonlinear problems and it was used successfully for a variety of non-linear applications. This type of element is also recommended by ABAQUS, specially for complex problems involving contact and large deformations. Model based on shell elements, and model based on shell-solid sub-model were therefore, excluded. In addition, it has been decided to avoid wedge elements such as, C3D15R, since they tend to introduce high stress regions.

3.6 Convergency tests of FE models

Convergency tests were carried out on a quarter model. This includes variable number of elements through the thickness, different type of the elements, different mesh density in the dented area, and also different length of the pipe. The effect of the number of elements through the thickness was investigated using a quarter model with length, $\frac{2L}{D_o} = 6.0$. These models were dented to $(\frac{\delta}{D_o})_{max} = 0.36$, with $p = 0.0$ and $p = 11.2MPa$. The results obtained are presented in Table (3.4) for denting with internal pressure and in Table (3.5) for empty pipe. Results indicate that the model with two elements through the pipe's wall thickness are adequate for carrying denting process for both empty and for pressurised pipe. Therefore, two elements through the

thickness were applied in all future modelling of dents.

3.6.1 Effect of pipe length

In order to optimize the computing time, four different total lengths of pipes were tried, i.e., $2L = 3D_o$, $6D_o$, $9D_o$, and $12D_o$. These models were dented to the depth, $(\frac{\delta}{D_o})_{max} = 0.36$. The results of these analyses are presented in Tables (3.6) and (3.7). These tables show that models with lengths: $2L = 6D_o$, $2L = 9D_o$, and $2L = 12D_o$ gave the same values of ultimate denting load and the same magnitude of ultimate bending moment. A slight change in the residual dent depths was noticed. The presence of internal pressure during denting reduced the dent propagation.

The parameter study also included the effect of bending moment on the pipe length. This was carried out for empty and for pressurised cases. Results are presented in Tables (3.6) and (3.7). These tables show that the bending moment has effect on pipe length but only for length $2L = 3D_o$, i.e., for the shortest case studied here. It can be concluded, that the most convenient total length, 2L, of finite element model could be, $6D_o$.

3.7 Denting of plain pipes

3.7.1 Pressure loading

Before commencing FE analysis one should decide on the level of internal pressure applied to the pipe. One possibility is to adopt an equation introduced by Zimmerman et al. [11]. According to this reference the design pressure with safety factor, $f = 0.72$, can be written as:

$$p = \frac{2tf\sigma_{yp}}{D_o} \tag{3.3}$$

This pressure will lead to the axial, σ_φ, and hoop stress, σ_θ. The axial stress, σ_φ, was applied to simulate the end cap. It was applied as a tensile pressure on the pipe end face:

$$\sigma_{\varphi} = \frac{pD_i^2}{(D_o^2 - D_i^2)} \tag{3.4}$$

The hoop stress, σ_θ was calculated using Lame's equation. The corresponding equation has the following form:

$$\sigma_\theta = \frac{2p}{\left(\frac{B}{A}\right)^2 - 1} \tag{3.5}$$

Values of the radial stress, σ_r, were checked using Lame's equation. The radial expansion of the cylinder was checked using the the following equation:

$$\Delta R = \frac{R}{E}[\sigma_\theta - \nu\sigma_\varphi] \tag{3.6}$$

3.7.2 Denting process for pressurised pipe

The plain pipe was pressurised to the required pressure using Equations (3.3) and (3.4). The denting process started as follows:

- Bring the rigid support and indenter's surface to the pipe by using "Model Change Option" in ABAQUS. This is done by executing two steps in ABAQUS.
- Remove the fixed node, NC, which was used previously during the pressurisation step. Now, the pipe is lying between both rigid surfaces which prevent any rigid body motion. Hence, NC is not needed anymore.
- Additional steps are needed to adjust position of rigid surfaces and that of deformable shell to ensure fine contact of all three components (indenter-pipe-support).
- The rigid indenter is now moved downwards in vertical direction, at prescribed steps. This is done by applying displacement steps to the reference node of the rigid indenter.
- Continue denting of the pipe to the prescribed depth, $(\frac{\delta}{D_o})_{max}$, as sketched in Figure (3.10).

- Remove the rigid indenter by applying negative displacement to the reference node of the rigid indenter. Obtain the residual dent depth due to elastic spring back.

- Release the internal pressure. This results in an increase of the residual dent depth, i.e., due to elastic spring back.

3.7.3 Denting process for empty pipe

The following steps were applied to the plain pipe without internal pressure in order to dent it to a prescribed depth:

- Node, NC, is being fixed to prevent rigid body motion. Adjust position of rigid surfaces and deformable shell in order to ensure their fine contact.

- Release the fixed node, NC.

- Move down the indenter in vertical direction by applying displacement to the reference node on the rigid indenter.

- Continue until the required depth, $(\frac{\delta}{D_o})_{max}$, is attained.

- Remove the rigid indenter by applying negative displacement to the reference node on the rigid indenter. Obtain the residual dent depth due to elastic spring back.

Figure (3.11) shows typical mesh adopted for denting a pipe without any surface damage (gouges).

3.8 Results

3.8.1 Support of pipe by saddle

A typical loading-unloading curve for different dent depths is presented in Figure (3.12). The load required for denting the empty pipe is smaller than that required for pressurised one, see Figure (3.13) for comparison. Examples of the profile

of the residual dent along the pipe axis, and at the mid-span of the pipe, are presented in Figures (3.14), (3.15), (3.16), and (3.17).

A set of typical results which were obtained for a circular pipe being dented by prolate, $\frac{a}{b} = 0.25$, hemispherical, $\frac{a}{b} = 1.0$ and oblate, $\frac{a}{b} = 4.0$, indenters is depicted in Figure (3.18). This figure consists of two sets of load-deflection curves. The first set was obtained with zero internal pressure. The second set of curves was obtained once pipe was subjected to constant internal pressure equal to the design pressure, which for this case is, 11.2 MPa. The maximum depth of the indentation in all of these calculations was arbitrarily set to, $(\frac{\delta}{D_o})_{max} = 0.36$. After reaching the prescribed depth, and the maximum denting force, the unloading followed. It is seen from Figure (3.18) that permanent, non-zero indentation depth is obtained after complete unloading and the indenter's separation from the pipe.

For the case of $p = 0.0$ and $\frac{a}{b} = 1.0$ (hemispherical indenter), the permanent depth at the center of the dent is, $(\frac{\delta}{D_o})_R = 0.338$. This means that there has been an elastic spring-back from, $(\frac{\delta}{D_o})_{max} = 0.36$ to $(\frac{\delta}{D_o})_R = 0.338$, i.e., 6 % of the maximum depth at the centre has been recovered during unloading. In this case, the maximum denting force corresponding to the prescribed depth of, $(\frac{\delta}{D_o})_{max} = 0.36$ was recorded as 26.5 kN. For the case of $p = 11.2\ MPa$, and $\frac{a}{b} = 1.0$ (hemispherical indenter) the permanent depth after unloading, at the dent's centre is, $(\frac{\delta}{D_o})_R = 0.228$. In this case the spring back amounts to about 37.0 %.

Permanent dent reduces the area of the pipe's cross-section and the largest reduction of the cross-section occurs at the mid-span of pipe, i.e., at the centre of indenter's application. In the current calculations, the loss of the circular cross-section area has been estimated by the ratio, $(\frac{\Delta A}{A_o}) \times 100$ %, where A_o is the area of the initial-circular cross-section and $\Delta A = A - A_o$ (with A being the area at the pipe's mid-span cross-section at the end of denting process). Values of the $(\frac{\Delta A}{A_o})$ ratio for the above two cases can be found in Table (3.8), and they are 18.3 % for $p = 0.0$, and 7.5 % for $p = 11.2\ MPa$.

In the process of denting, the pipe's circular cross-section is being distorted not only around the application of the indenter but the distortion also spreads along length of the pipe. It is of interest to know how far from centre of the dent the pipe

re-gains its circular cross-section. Let the length L_D, indicate portion of the pipe where its cross-section is not circular due to the existence of permanent dent at the mid-span, see Figure (3.19) for clear explanation. For both cases discussed above, magnitudes of the $\frac{L_D}{D_o}$-ratio are 4.6 for $p = 0.0$, and 3.3 for $p = 11.2\ MPa$ (results of other cases can be found in Table (3.8)).

Additional calculations were carried out for three other values of prescribed dent's depth, i.e., for $(\frac{\delta}{D_o})_{max} = 0.06, 0.12$, and 0.24 (assuming hemispherical indenter). Results which were obtained, for both pressure free and pressurised pipe, are given in Table (3.8). The resulting plots of denting force versus depth of the dent are similar to those shown in Figure (3.18). In addition to the hemispherical indenter, calculations were also carried out for prolate and oblate shapes of the indenter. A sample of results for numerical models of length $\frac{2L}{D_o} = 12.0$ is depicted in Figure (3.18) for both pressure free and for pressurised pipe. It is seen here that the trend in denting load versus deflection curves, is similar to results obtained for hemispherical indenters. Table (3.8) provides values of the maximum denting force and the magnitude of $(\frac{\delta}{D_o})_R$ after unloading. For the case of pressurised pipe, the pipe remains pressurised during the whole unloading path. Results of additional calculations for elliptic indentors, are provided in Tables (3.9) and (3.10)

3.8.2 Ultimate denting load

It is worth noting here that numerically simulated denting process can continue for much larger magnitudes of dent's depth then these which were considered previously. For example, when the pipe is subjected to internal pressure, $p = 11.2\ MPa$, the load carrying capacity can reach the maximum of 107.6 kN at $(\frac{\delta}{D_o})_{max} = 0.67$. At the peak load, pipe's structural integrity however ends with a sudden wall thinning and gross plastic flow around the dent's perimeter. As a result, the indenter plunges through the wall. When the pipe is not pressurised, the denting process can continue until the pipe is entirely squashed by the indenter. Figure (3.20) illustrates the full loading paths for indenters $\frac{a}{b} = 0.25,\ 1.0$, and 4.0. The lower set of curves corresponds to the internal pressure, $p = 0.0$. The top set of curves was obtained for internally pressurised pipe (at the design level, $p = 11.2\ MPa$). It is seen here that in all cases the load carrying

capacity reaches the maximum, and there is no loss of pipe's structural integrity from a numerical point of view. The corresponding values of F_{max}, and $(\frac{\delta}{D_o})_{max}$ are provided in Table (3.11). Plots of deformed cross-section show that, from a practical point of view, some of these results are spurious since the indenter penetrates the bottom portion of the pipe (and this has not been included in the current FE modelling). Hence, in Table (3.11), these values are in brackets. Deformed cross-sections with nearly-squashed configurations were identified visually as meaningful through the post-processing, and the corresponding values of denting load and denting depth are given in Table (3.11).

Plot showing a typical cross-section which has been squashed by circular indenter, for the case of empty pipe, is depicted in Figure (3.21a). It is seen here that the upper portion of the pipe nears the rigid saddle support (which extends by 120°). On the other hand, Figure (3.21b), shows the deformed cross-section at the ultimate magnitude of denting force in the case of pipe being internally pressurised to $p = 11.2\ MPa$. At peak load the growth of large plastic deformations occurs and leads to the ultimate loss of structural integrity (see large plastic deformations indicated in Figure (3.21b) by points $N1$ and $N2$, and also shown in Figure (3.22b).

Deformed portions of the pipe at the maximum load, and corresponding to the mid-span cross-section depicted in Figure (3.21), are shown in Figures (3.22a) and (3.22b). It is seen here that there is a severe distortion of the cross-section at the pipe's mid-span, just underneath of the indenter. Values of the $(\frac{\Delta A}{A_o})$ ratio are also provided in Table (3.11) where it is seen that they vary from 25.0 % to 84.0 %. Calculations show that for the current case the length, L_D, varies from $4.5D_o$ to $5.5D_o$, and Table (3.11) contains the remaining results.

3.9 Support of pipe by flat plate

So far, the main focus of numerical calculations was on pipes supported by a saddle. Limited calculations were also performed for a pipe placed on flat, horizontal, and rigid plane. A set of loading and unloading curves has been generated for prolate $\frac{a}{b} = 0.25$, hemispherical $\frac{a}{b} = 1.0$, and oblate $\frac{a}{b} = 4.0$ indenters. The total length of the pipe was, $\frac{2L}{D_o} = 12.0$, and only one depth of the dent was considered, i.e.,

$(\frac{\delta}{D_o})_{max} = 0.36$. Results which were obtained can be found in Table (3.12). Typical loading and unloading plots, for a hemispherical indenter, are shown in Figure (3.23). Results showed that the trend of loading / unloading curves is similar to those obtained for a pipe supported by a saddle. Magnitude of forces, at a given dent's depth, are smaller for pipes supported by a rigid plate than for pipes supported by a saddle. The same dent's depth can be reached using forces which are 20.0 % to 30.0 % smaller than in the case of support by saddle. Distortion of the circular cross-section, at the mid-span, varies from 13.0 % to 16.0 % for support by flat plate whilst the same ratio, for support by a saddle, is larger and it varies from 15.0 % to 20.0 %. The same observation remains true for the case of pipe being internally pressurised and then dented. Propagation of pipe's cross-section distortion is also larger for a support by saddle than for a pipe support by a rigid, flat plate.

3.10 Support of dented pipe by elastic springs

This section considers pipe being supported by a set of elastic springs. Each node, within the range $0° \leq \Theta \geq 120°$ is being supported by two elastic springs : one vertical and the second acting horizontally as sketched in Figure (3.2c). Calculations were performed for linear elastic springs with the stiffness coefficient $K = 80\ MN/m$. This value of K corresponds to saturated sand or stiff clay [67]. Typical load deflection curves are provided in Figure (3.23), where it is seen that Winkler's foundation provides slightly stiffer response than both rigid plate and rigid saddle. Table (3.12) provides direct comparison of results obtained for three different types of pipe support, i.e. for rigid saddle, rigid flat plate and linear springs. In addition to hemispherical indenter calculations were also performed for prolate and oblate elliptical shapes of indenter. In general there is not much difference between results obtained for the above mentioned modes of pipe support. One interesting observation is that the largest distortion of pipe's cross-section occurs for a support by springs. In view of results given in this section it was decided to adopt only one mode of pipe support, i.e., by saddle support.

3.11 Modelling of contact

In this study the contact problem was solved numerically using an algorithm which is an internal part of ABAQUS. This algorithm is formulated as an interaction between master and slave surfaces. Rigid components, i.e., indenter serves as 'master' whilst deformable pipe remains a 'slave' surface. Similar algorithm is applied to pipe-rigid support interface.

3.11.1 Contact area at indenter-pipe and pipe-support interfaces

Numerically simulated process of denting shows that contact between rigid indenter and deformable pipe changes not only in size but also in shape. During loading process gap between two surfaces not only closes but it can also open. As a result contact pressure between the two surfaces changes along the primary loading path. Typical results for hemispherical indenter are shown in Figure (3.24) for two cases, i.e., for pressure free pipe, and for pressurised pipe to the design level $p = 11.2\ MPa$. Top four sketches in Figure (3.24) show how the contact area changes its magnitude and shape for four values of dent's depth, i.e., for $(\frac{\delta}{D_o})_{max} = 0.027,\ 0.097,\ 0.180$, and 0.36. Contact pressure is not uniform along the contact surface. Points having the highest pressure are marked in this figure by full circles. It is also seen here that the maximum pressure changes its position as the denting depth increases. The growth of contact area is nearly linear for both pressure free pipe and for internally pressurised case - as shown in Figure (3.25). Magnitude of contact is, as expected, larger for pressurised pipe. It is worth noting that the contact area splits into concentric rings at some value of dent's depth as shown in Figure (3.24) (for hemispherical indenter), and in Figure (3.26) (for elliptical indenter). Results of calculations carried out for prolate and oblate elliptical profile of the indenter and results are summarized in Table (3.13). One characteristic feature of the contact for both prolate and elliptical profiles was the fact that the maximum contact pressure often was not confined to a single point but it was spread over a single or over several patches. This is illustrated in Figure (3.26) for the case of $\frac{a}{b} = 0.25$ indenter, and in Figure (3.27) for case of $\frac{a}{b} = 4.0$. It has already been mentioned, that pipe considered in this section is supported by a rigid saddle spanning 120° in the hoop direction. Contact area at the interface between

pipe and rigid support by a saddle has also been recorded for different magnitudes of dent's depth. The contact area is confined to hatched patches showed in Figure (3.28) (showing only a quarter model). It is seen that contact patches appear away from pipe mid-span for $\frac{\delta}{D_o} = 0.027,\ 0.097$, and 0.18. Contact patches appear to drift towards pipe's mid-span for large or deep values of $(\frac{\delta}{D_o})_{max}$, e.g., $(\frac{\delta}{D_o})_{max} = 0.36$.

3.12 Summary

- A number of observations can be made as a result of this numerical study of a single geometry pipe made from mild steel. Within the studied range of parameters, magnitude of denting force increases nearly linearly with depth of dent. For a pressure free pipe there is not much difference in its magnitude for different shapes of indenters (hemispherical or elliptical). For pressurised pipe, the magnitude of denting force can not only be several times higher but its actual value is strongly affected by shape of the indenter, i.e., whether it is of prolate or of oblate elliptical profile.

- Pipes of studied geometry are likely to withstand deeper dents when they remain pressure free. On the other hand, depth of dents can be about 50.0 % smaller when the internal pressure is kept equal to the design level.

- Permanent distortion of pipe's circular cross-section will propagate along pipe's length. Within the studied range of indenter's shapes and denting depths this distance can be as high as ten times pipe diameter. At the same time the cross-section area underneath the indenter can be reduced by as much as 18.0 %.

- Growth of contact area between rigid indenter and pipe varies linearly with dent's depth. Contact area can change shape and some parts which were in contact may become contact free during denting. Contact area between pipe and rigid saddle support not only changes its shape but drifts axially during denting process.

D_o (mm)	t (mm)	a (mm)	$\frac{2L}{D_o}$	$\frac{a}{b}$
84.20	2.07	13.35	6.0, 12.0	4.0, 2.0, 1.0, 0.5, 0.25

Table 3.1: Dimensions of pipe and indenter. Also, profiles of indenters to be considered: oblate elliptical $\frac{a}{b} = 4.0$, and 2.0; hemispherical, $\frac{a}{b} = 1.0$; and prolate elliptical $\frac{a}{b} = 0.5$, and 0.25.

D.O.F	*Line* 1	*Line* 2	*Line* 3	*Line* 4
u_x	Free	Constrained	Free	Constrained
u_y	Free	Free	Free	Free
u_z	Constrained	Free	Free	Free
Φ_x	Free	Free	Free	Free
Φ_y	Free	Free	Free	Free
Φ_z	Free	Free	Free	Free

Note: For the node NC the following constrains were used: $u_x = u_z = 0.0$; $u_y \neq 0.0$;

$$\Phi_x = \Phi_y = \Phi_z = 0.0 \ .$$

Table 3.2: Constraints imposed on three displacements, u, and on three rotations, Φ, along the four edges of the quarter Finite Element depicted in Figure (3.5).

Friction Coef.	0.06	0.2	0.35	0.6	0.8	1.0
$(\frac{\delta}{D_o})_{max}$	0.154	0.154	0.154	0.154	0.154	0.154
F_{max}	12.0	12.0	12.0	12.0	12.0	12.0
$(\frac{\delta}{D_o})_R$	0.134	0.134	0.135	0.135	0.135	0.135

Table 3.3: The maximum depth of the dent, $(\frac{\delta}{D_o})_{max}$; maximum denting force, F_{max}; and residual dent depth, $(\frac{\delta}{D_o})_R$, obtained for six different values of the coefficient of friction. Also, p = 0.0, and $\frac{2L}{D_o} = 6.0$.

No. of elements	'1'	'2'	'3'	'4'
F_{max} (kN)	69.0	70.43	70.43	70.43
$(\frac{\delta}{D_o})_{max}$	0.36	0.36	0.36	0.36
$(\frac{\delta}{D_o})_R$	0.251	0.228	0.228	0.228

Note: '1' ≡ single layer of elements; '2' ≡ two layers of elements through thickness, etc.

Table 3.4: The effect of the number of elements through the wall thickness on the ultimate denting load, F_{max}, and on residual dent's depth, $(\frac{\delta}{D_o})_R$. Results were obtained for p = 11.2 MPa, $\frac{a}{b} = 1.0$, and $\frac{2L}{D_o} = 6.0$.

No. of elements	*'1'*	*'2'*	*'3'*	*'4'*
F_{max} (kN)	26.93	26.5	26.5	26.5
$(\frac{\delta}{D_o})_{max}$	0.36	0.36	0.36	0.36
$(\frac{\delta}{D_o})_R$	0.338	0.338	0.338	0.338

Note: '1' ≡ single layer of elements; '2' ≡ two layers of elements through thickness, etc.

Table 3.5: The effect of number of element through the wall thickness on the ultimate denting load, F_{max}, and on residual dent's depth, $(\frac{\delta}{D_o})_R$. Results were obtained for p = 0.0, $\frac{a}{b} = 1.0$, and $\frac{2L}{D_o} = 6.0$.

Length, 2L	*'3D_o'*	*'6D_o'*	*'9D_o'*	*'12D_o'*
F_{max} (kN)	69.08	70.43	70.43	70.43
$(\frac{\delta}{D_o})_{max}$	0.36	0.36	0.36	0.36
$(\frac{\delta}{D_o})_R$	0.219	0.228	0.228	0.228
$(CBM)_{max}$ (kNm)	4.57	4.51	4.51	4.52
$(OBM)_{max}$ (kNm)	3.81	3.7	3.7	3.7

Table 3.6: The effect of the pipe length, $2L$, on the ultimate denting load, F_{max}, maximum dent depth, $(\frac{\delta}{D_o})_{max}$, residual dent depth, $(\frac{\delta}{D_o})_R$, and on ultimate 'Closing' and 'Opening' bending moments. Also, $p = 11.2\ MPa$, and two layers of elements through the wall.

Length, 2L	*'3D_o'*	*'6D_o'*	*'9D_o'*	*'12D_o'*
F_{max} (kN)	24.41	26.5	26.5	26.5
$(\frac{\delta}{D_o})_{max}$	0.36	0.36	0.36	0.36
$(\frac{\delta}{D_o})_R$	0.338	0.338	0.338	0.338
$(CBM)_{max}$ (kNm)	2.63	2.93	2.93	2.93
$(OBM)_{max}$ (kNm)	4.51	4.2	4.2	4.2

Table 3.7: The effect of the pipe length, $2L$, on the ultimate denting load, F_{max}, maximum dent depth, $(\frac{\delta}{D_o})_{max}$, residual dent depth, $(\frac{\delta}{D_o})_R$, and ultimate bending moment. Also, $p = 0.0$, and two layers of elements through the wall.

$p\ (MPa)$	$(\frac{\delta}{D_o})_{max}$	$(\frac{\delta}{D_o})_R$	$F_{max}\ (kN)$	$\frac{\Delta A}{A_o}\ (\%)$	$(\frac{L_D}{D_o})$
0.0	0.06	0.048	7.1	1.10	0.7
	0.12	0.105	11.1	3.1	1.5
	0.24	0.220	19.1	9.4	3.0
	0.36	0.338	26.5	18.3	4.6
11.2	0.06	0.045	12.5	0.7	1.1
	0.12	0.086	23.9	1.8	1.7
	0.24	0.157	47.5	4.3	2.2
	0.36	0.228	70.43	7.5	3.3

Table 3.8: Results for four dents in pressure-free pipe, $p = 0.0$. Results for further four dents in the case of internally pressurised pipe, $p = 11.2MPa$ (equivalent to the design pressure), are given in rows 6-9. Total length, $\frac{2L}{D_o} = 12.0$, and $\frac{a}{b} = 1.0$.

$\frac{a}{b}$	$p\ (MPa)$	$(\frac{\delta}{D_o})_{max}$	$(\frac{\delta}{D_o})_R$	$F_{max}\ (kN)$	$\frac{\Delta A}{A_o}\ (\%)$	$(\frac{L_D}{D_o})$
0.5	**0.0**	0.06	0.0480	6.57	1.1	0.6
		0.12	0.1041	10.5	2.9	1.8
		0.24	0.220	18.25	8.8	3.0
		0.36	0.338	25.51	17.1	5.0
	11.2	0.06	0.046	11.35	0.8	0.5
		0.12	0.091	20.97	1.9	1.1
		0.24	0.171	40.6	4.4	2.0
		0.36	0.247	59.6	7.6	3.0
0.25	**0.0**	0.06	0.0475	6.17	1.34	0.6
		0.12	0.1027	9.86	2.60	1.8
		0.24	0.2180	17.10	8.0	3.0
		0.36	0.3350	23.73	15.4	5.3
	11.2	0.06	0.0464	9.91	0.70	0.5
		0.12	0.0955	17.74	1.76	1.1
		0.24	0.1829	33.4	4.27	2.0
		0.36	0.2690	48.5	7.60	3.0

Table 3.9: Results for prolate elliptical indenters, $\frac{a}{b} = 0.5$, and $\frac{a}{b} = 0.25$. Residual depth of the dent was recorded once the pressure was released to zero. Total length of the model, $\frac{2L}{D_o} = 12.0$.

$\frac{a}{b}$	$p\ (MPa)$	$(\frac{\delta}{D_o})_{max}$	$(\frac{\delta}{D_o})_R$	$F_{max}\ (kN)$	$\frac{\Delta A}{A_o}\ (\%)$	$(\frac{L_p}{D_o})$
4.0	0.0	0.06	0.0476	8.91	1.1	0.6
		0.12	0.106	12.85	3.5	1.7
		0.24	0.224	21.19	10.7	3.0
		0.36	0.39	28.5	20.5	5.0
	11.2	0.06	0.0344	17.93	0.40	1.1
		0.12	0.052	31.6	0.45	1.5
		0.24	0.119	59.5	2.6	2.0
		0.36	0.194	78.4	6.8	4.4
2.0	0.0	0.06	0.048	7.90	1.1	0.7
		0.12	0.105	11.8	3.3	1.5
		0.24	0.222	20.1	10.1	3.0
		0.36	0.340	27.5	19.4	5.0
	11.2	0.06	0.041	13.6	0.6	1.1
		0.12	0.074	27.5	1.3	1.7
		0.24	0.140	53.6	3.6	1.9
		0.36	0.205	77.4	6.9	4.2

Table 3.10: Results for oblate elliptical indenters $\frac{a}{b} = 4.0$, and $\frac{a}{b} = 2.0$. Residual depth of the dent was recorded once the pressure was released to zero. Total length of the model, $\frac{2L}{D_o} = 12.0$.

$p\ (MPa)$	$\frac{a}{b}$	$F_{max}\ (kN)$	$(\frac{\delta}{D_o})_{max}$	$\frac{\Delta A}{A_o}\ (\%)$	$(\frac{L_D}{D_o})$
0.0	0.25	38.4 (58.2)	0.61 (1.59)	69.5	5.5
	1.0	49.6 (58.7)	0.88 (1.19)	84.4	5.5
	4.0	50.2 (64.0)	0.81 (1.20)	81.4	5.5
11.2	0.25	106.5	0.87	58.0	5.0
	1.0	107.6	0.67	48.0	4.5
	4.0	81.2	0.41	25	4.5

Table 3.11: Values of the maximum denting force and corresponding dent's depth for three shapes of indenters. Ultimate values of the force and dent's depth are given in brackets, the total length, $\frac{2L}{D_o} = 12.0$.

		Saddle Support			*Flat Plate*			*Springs*		
		$\frac{a}{b}$			$\frac{a}{b}$			$\frac{a}{b}$		
		4.0	**1.0**	**0.25**	**4.0**	**1.0**	**0.25**	**4.0**	**1.0**	**0.25**
0.0	F_{max} (kN)	28.5	26.5	23.7	21.9	21.1	19.9	34.5	31.5	27.0
	$(\frac{\delta}{D_o})_{max}$	0.36	0.36	0.36	0.36	0.36	0.36	0.36	0.36	0.36
	$(\frac{\delta}{D_o})_R$	0.34	0.338	0.34	0.33	0.33	0.33	0.34	0.34	0.34
	$(\frac{\Delta A}{A_o})$ (%)	20.5	18.3	15.4	16.3	15.0	13.4	21.3	18.8	15.9
	$(\frac{L_D}{D_o})$	5.0	4.6	5.3	5.2	4.2	4.5	4.5	4.5	4.5
11.2	F_{max} (kN)	78.4	70.43	48.5	67.8	59.0	44.5	78.5	71.8	50.6
	$(\frac{\delta}{D_o})_{max}$	0.36	0.36	0.36	0.36	0.36	0.36	0.36	0.36	0.36
	$(\frac{\delta}{D_o})_R$	0.19	0.228	0.27	0.18	0.20	0.26	0.21	0.25	0.28
	$(\frac{\Delta A}{A_o})$ (%)	6.8	7.5	7.6	3.1	5.0	6.0	9.3	9.7	8.6
	$(\frac{L_D}{D_o})$	4.4	3.3	3.0	3.0	3.0	3.0	3.0	3.0	3.0

Table 3.12: Comparison of results for three different types of pipe support, i.e., by saddle, by flat plate, and by a set of linear elastic springs (Winkler's foundation). The total length of pipe, $\frac{2L}{D_o} = 12.0$.

		$\frac{a}{b} = 0.25$		$\frac{a}{b} = 1.0$		$\frac{a}{b} = 4.0$	
p (MPa)	$(\frac{\delta}{D_o})_{max}$	F_{max} (kN)	$\frac{CA}{CA_o}$	F_{max} (kN)	$\frac{CA}{CA_o}$	F_{max} (kN)	$\frac{CA}{CA_o}$
0.0	0.027	4.05	0.006	5.33	0.019	6.50	0.033
	0.097	8.50	0.022	9.60	0.054	11.4	0.080
	0.18	13.73	0.044	15.28	0.085	17.7	0.195
	0.36	23.73	0.087	26.5	0.166	28.5	0.310
11.2	0.027	6.80	0.008	7.93	0.0167	10.4	0.042
	0.097	15.0	0.046	19.71	0.115	27.9	0.211
	0.18	26.9	0.093	36.18	0.233	47.9	0.550
	0.36	48.5	0.181	70.43	0.446	78.4	0.550

Table 3.13: Contact area, CA, between indenter and pipe. Results for four different depths of the indenter are provided. The initial, projected area is, $CA_o = \pi a^2$.

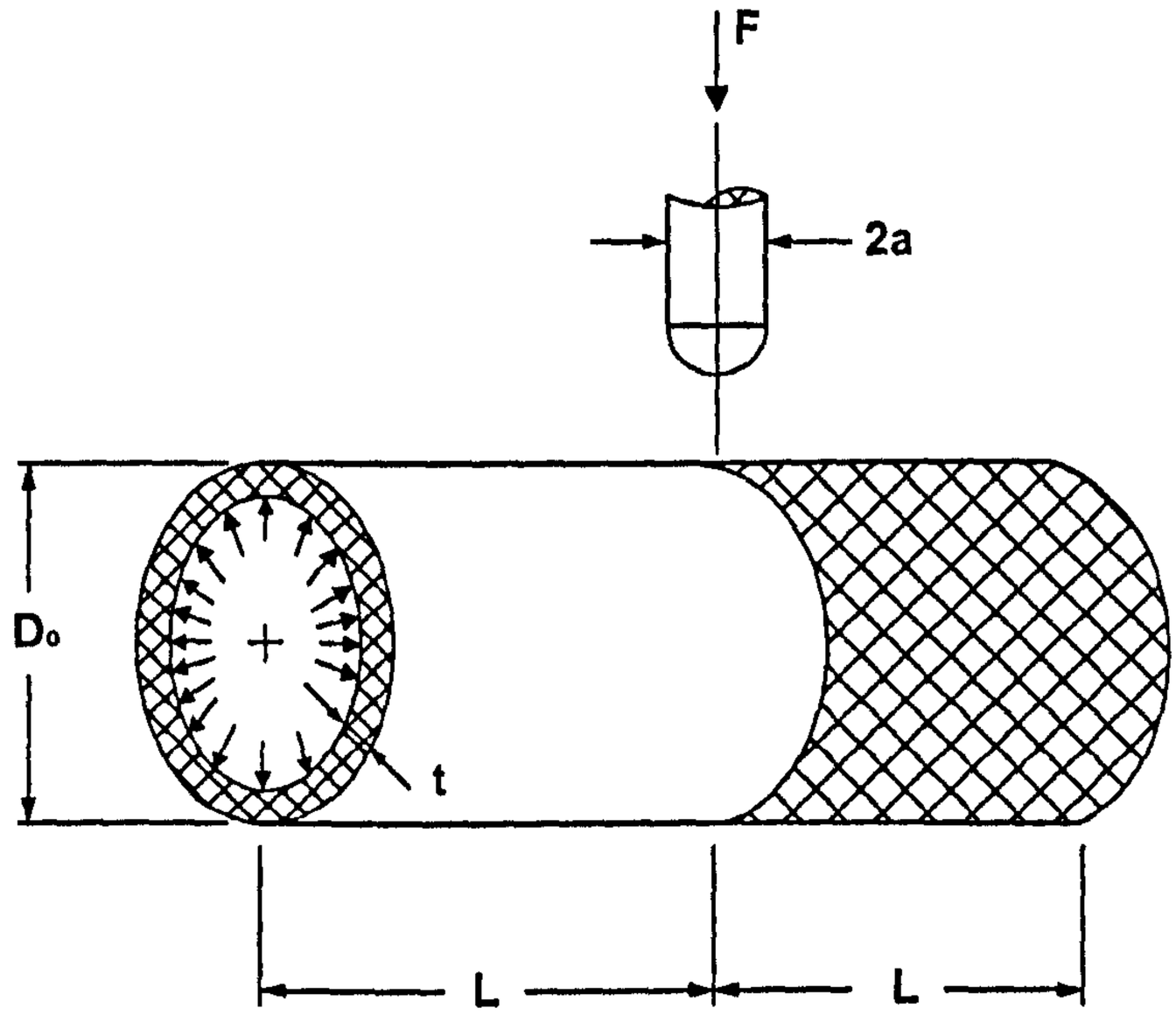

Figure 3.1: Geometry of deformable pipe and rigid indenter, with its parameters (pipe's support is not shown).

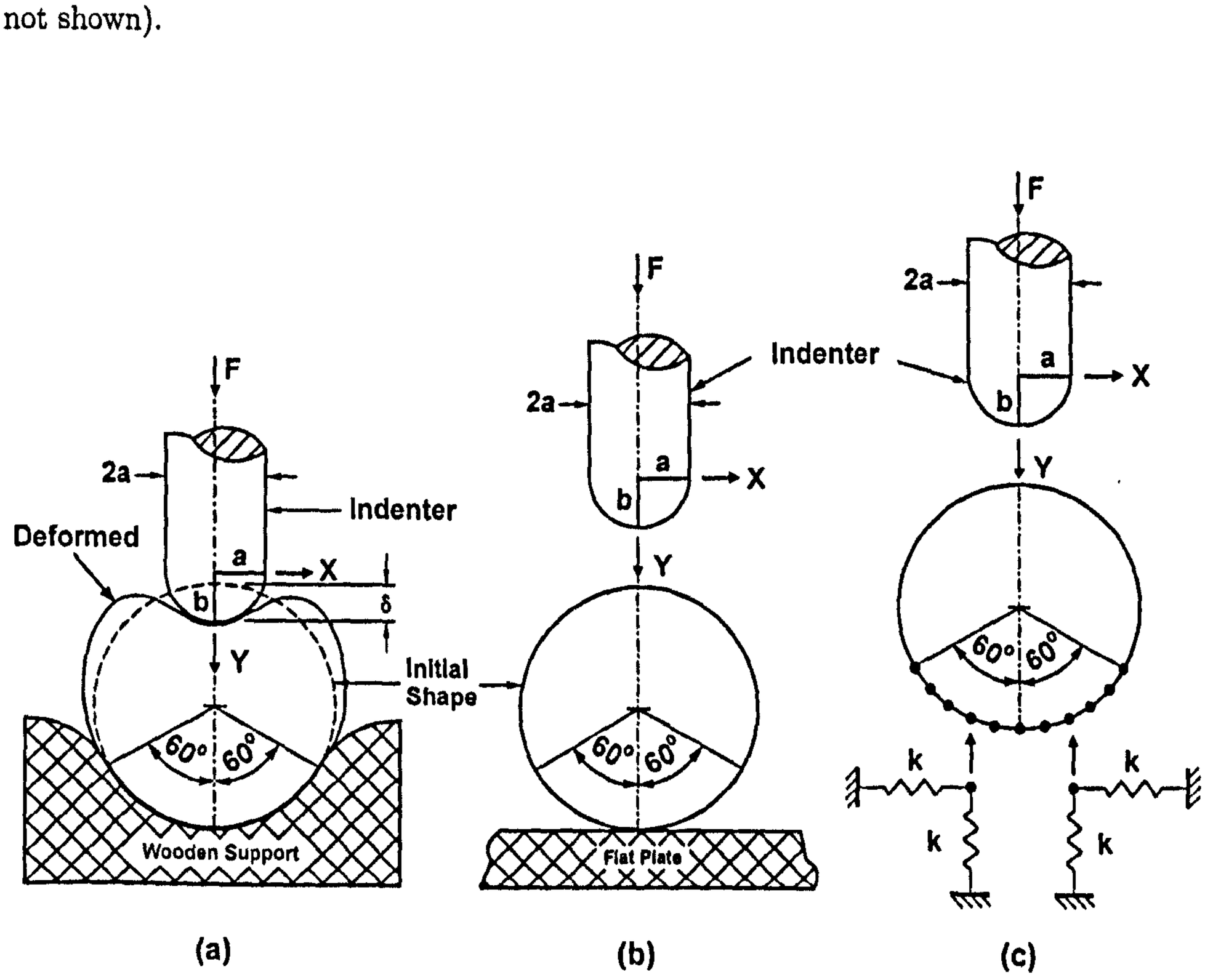

Figure 3.2: Illustration of three different forms of pipe support, i.e., by saddle - Fig. 3.2a, by flat plate - Fig. 3.2b, and by linear springs - Fig. 3.2c.

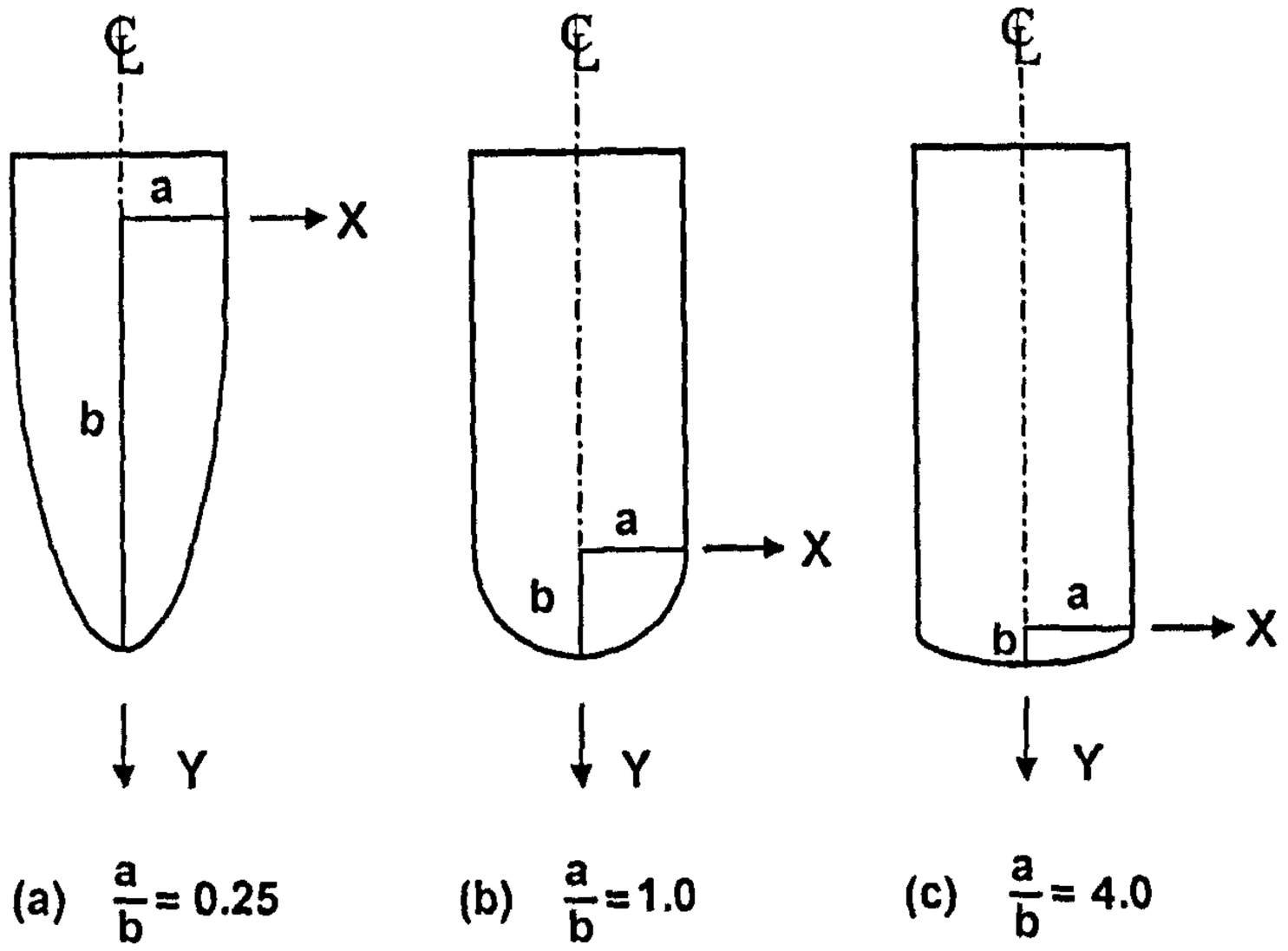

Figure 3.3: Illustration of three shapes of the indenter used in the current study, i.e., prolate elliptical profile, $\frac{a}{b} = 0.25$ - Fig. 3.3a; hemispherical profile, $\frac{a}{b} = 1.0$ - Fig. 3.3b; and oblate elliptical profile, $\frac{a}{b} = 4.0$ - Fig. 3.3c.

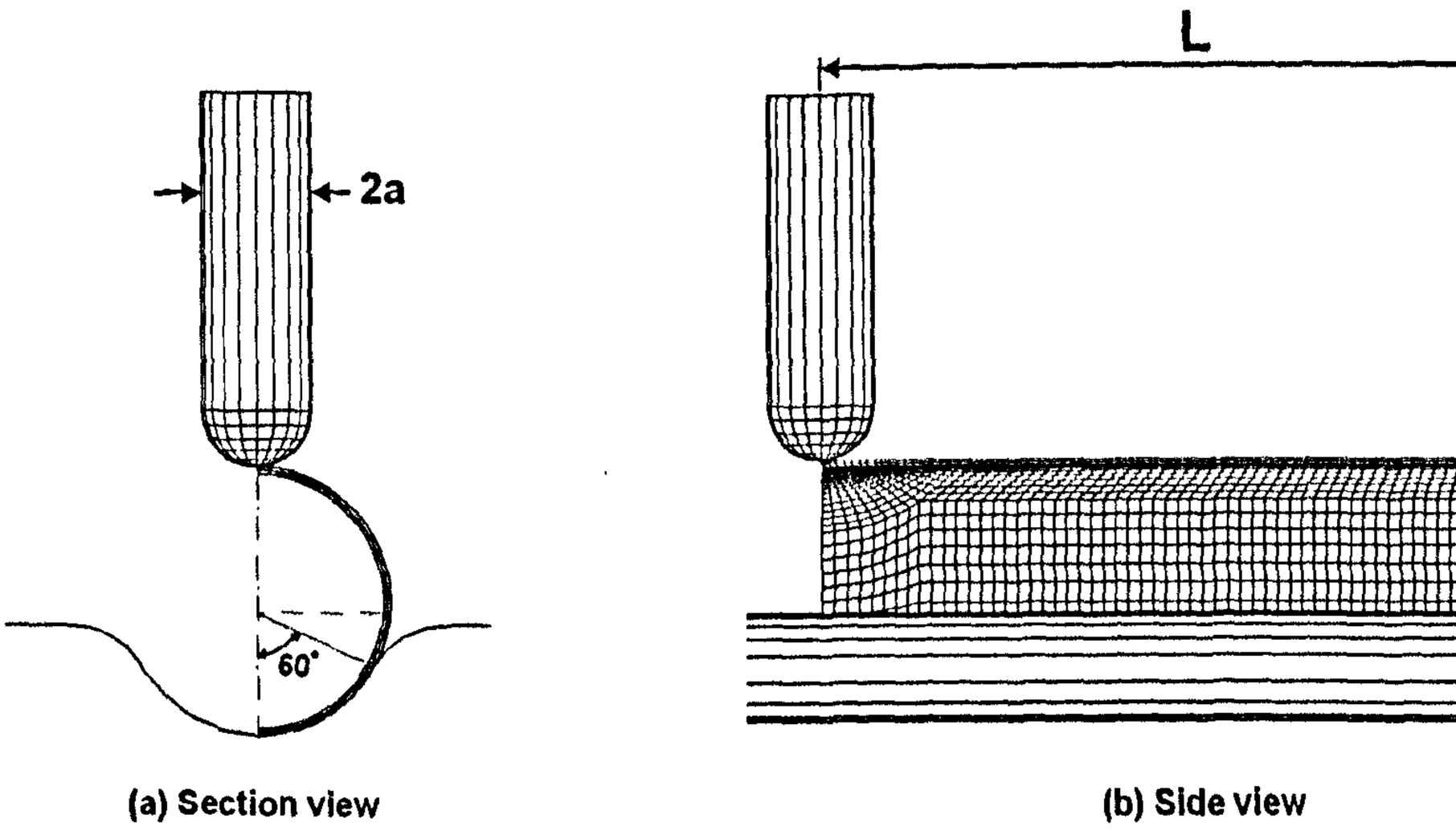

Figure 3.4: A general view of a quarter FE model. Hemispherical rigid indenter, $\frac{a}{b} = 1.0$, and rigid saddle support are also shown.

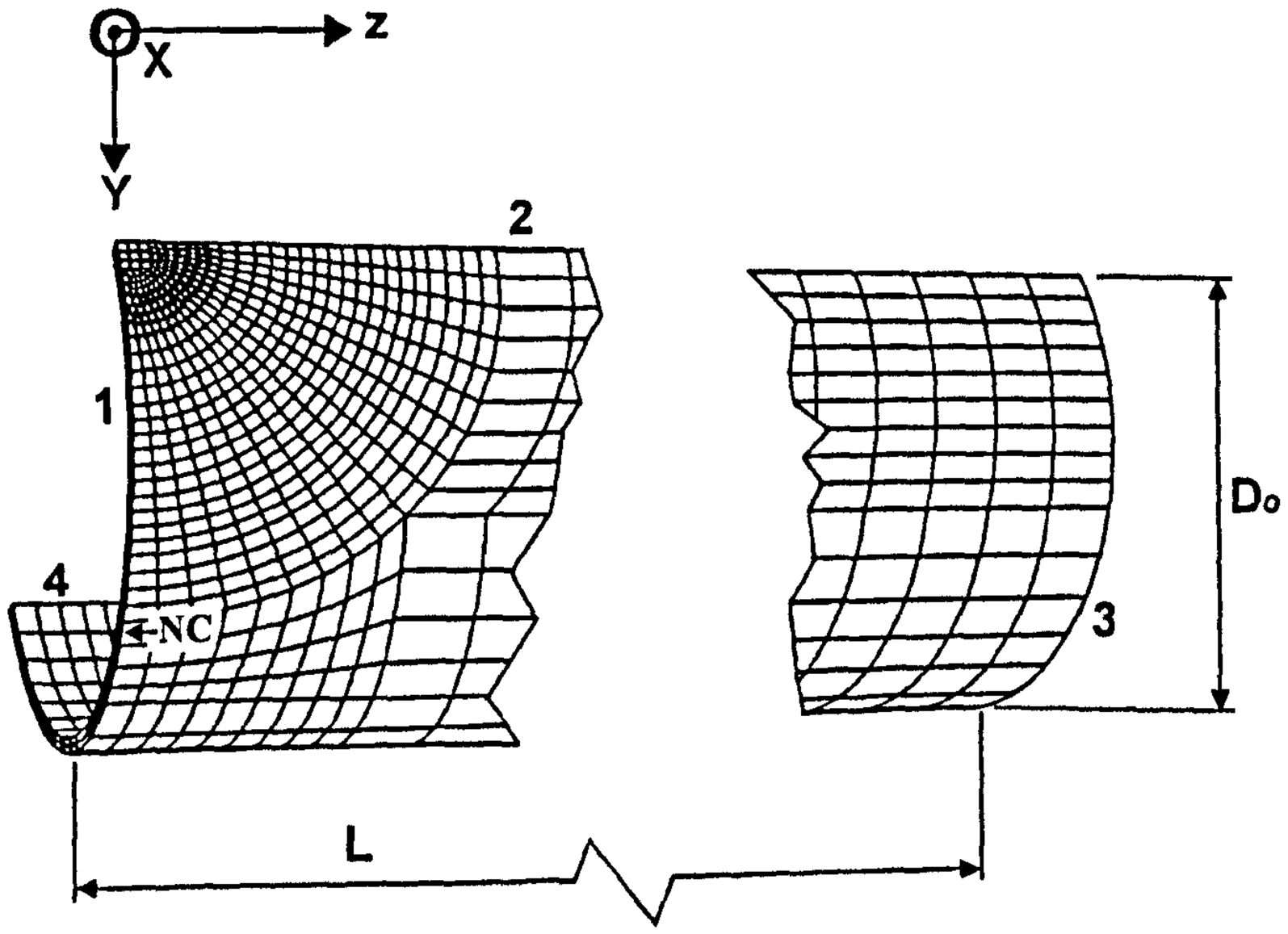

Figure 3.5: Quarter model used in the FE analyses (D_o is outside diameter). Also, edges 1, 2, 3 and 4 along which boundary conditions have been applied (see Table 3.2). NC is the node at which constraints were applied to prevent rigid body motion.

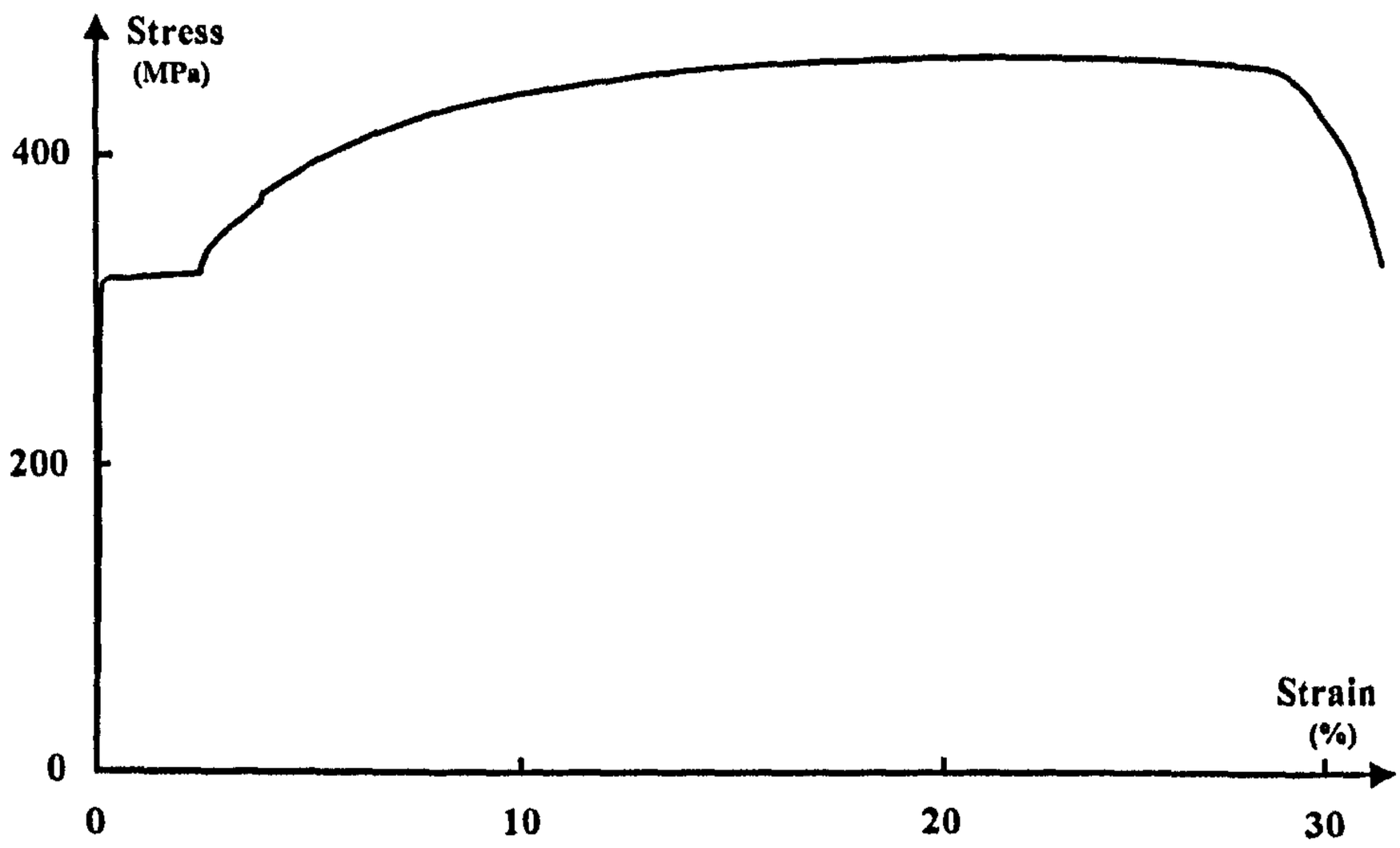

Figure 3.6: Typical uni-axial stress-strain curve for mild steel pipe ASTME A/A5 53B SCH80 (engineering stress-strain curve, flat coupon, tensile test).

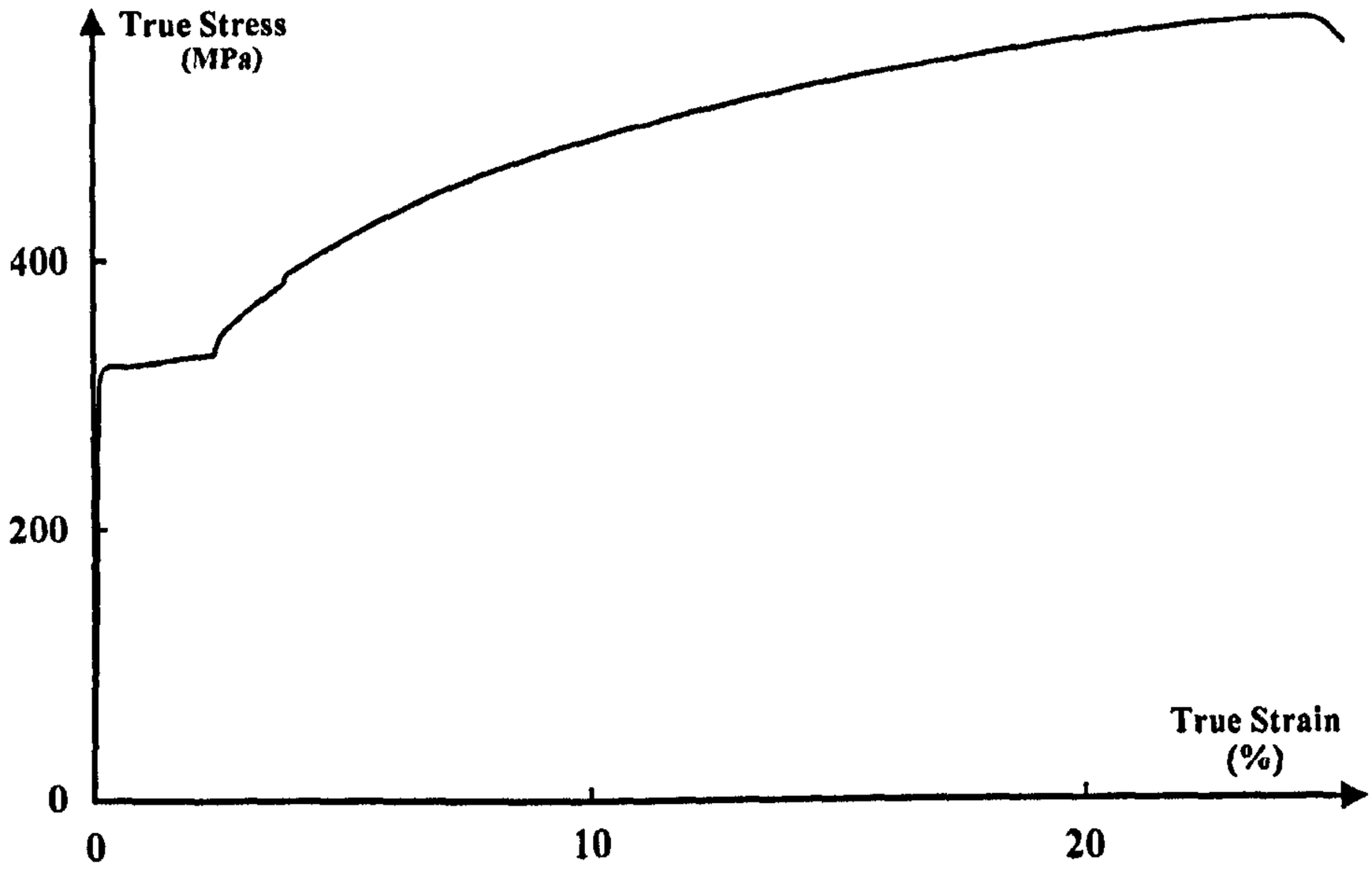

(a) True stress-strain curve.

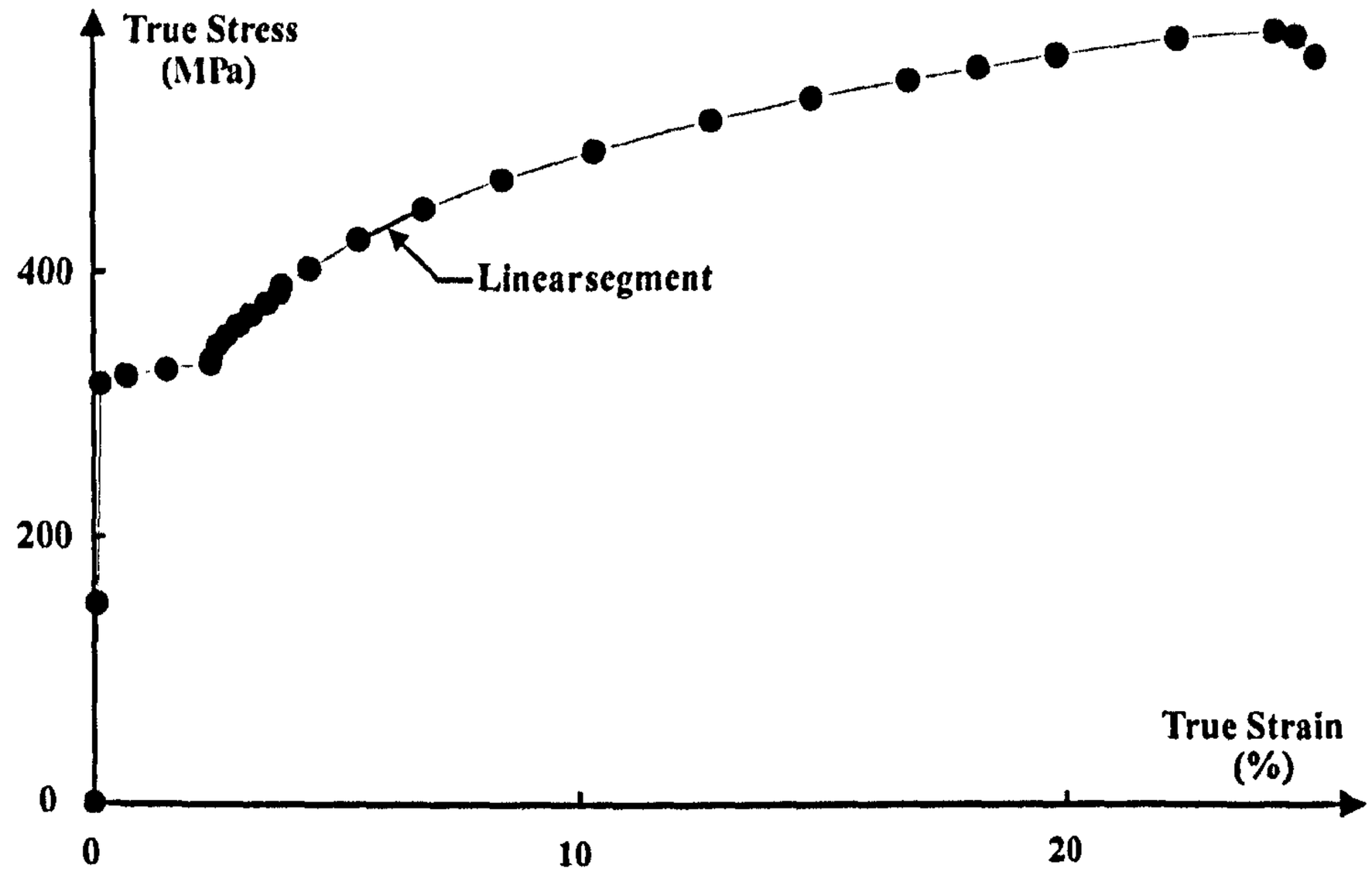

(b) Twenty six line segments of true stress-strain curve which were input to ABAQUS.

Figure 3.7: The true stress-strain curve data used in the FE models.

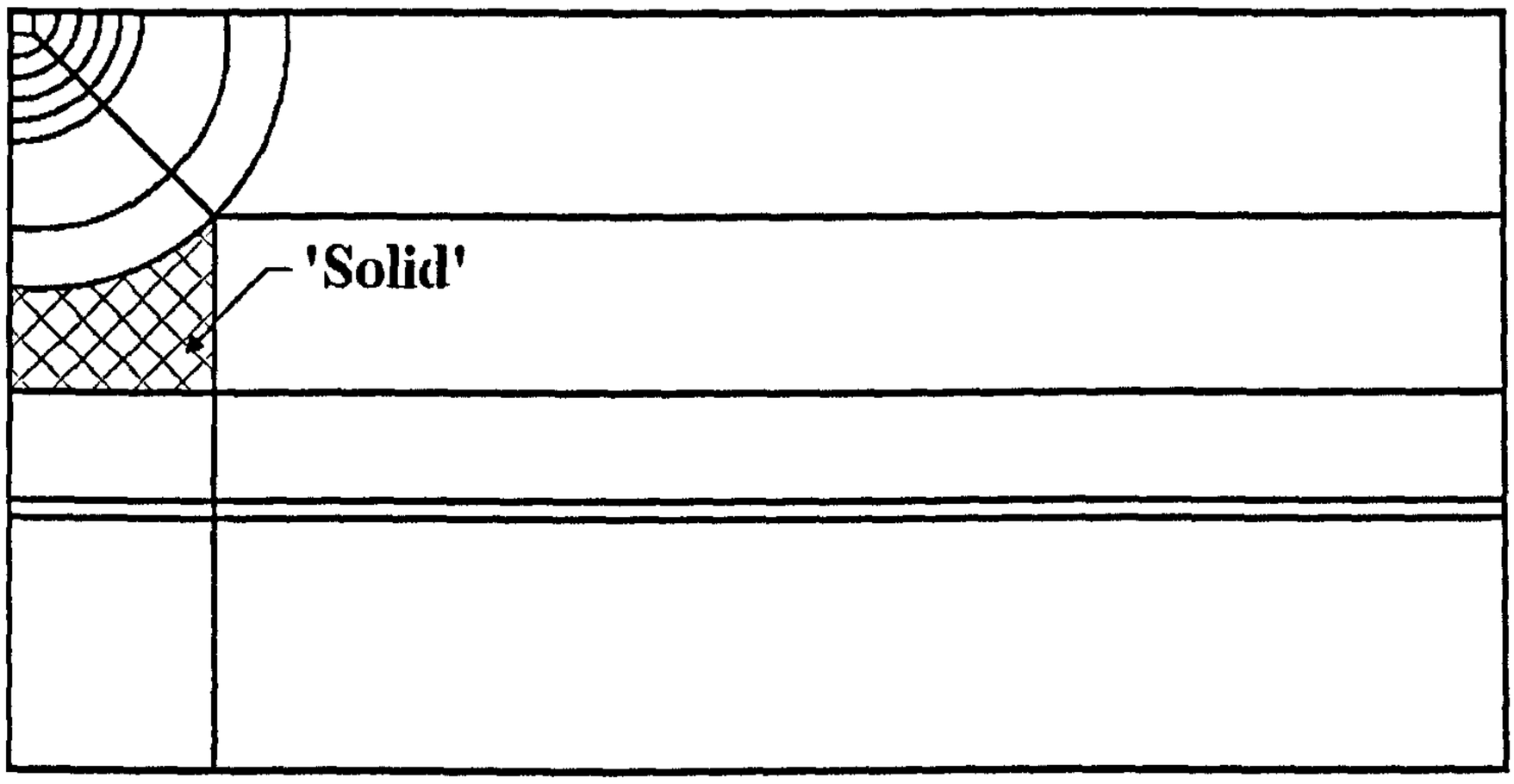

(a) The solid sections in flat plate - view from above (PATRAN).

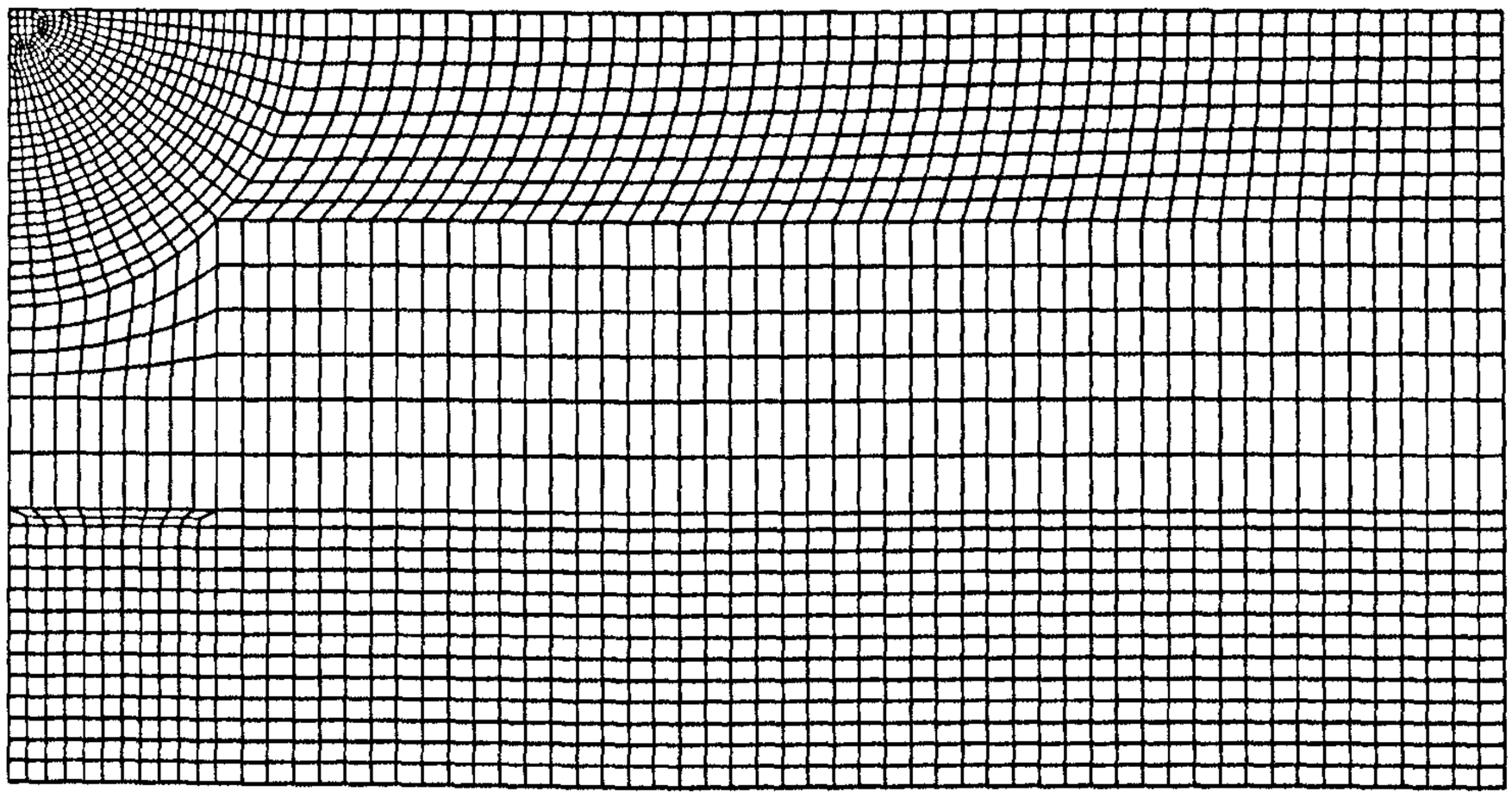

(b) Meshing of the flat plate using NMAP parameter - view from above (PATRAN).

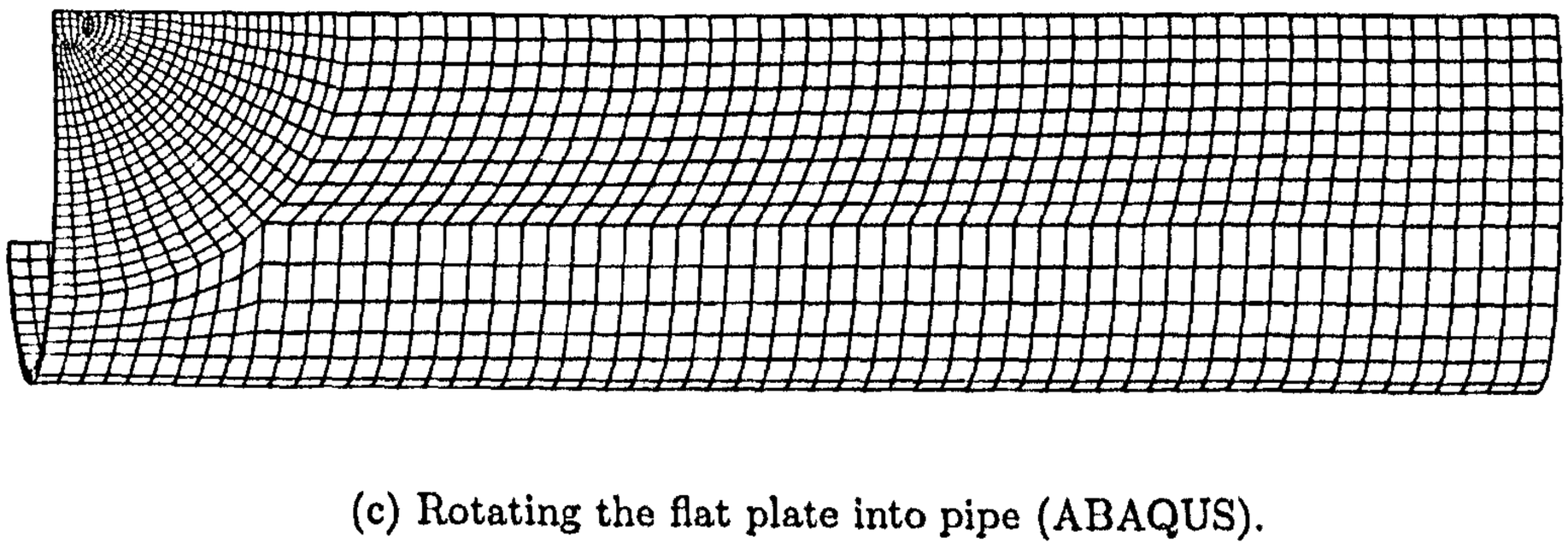

(c) Rotating the flat plate into pipe (ABAQUS).

Figure 3.8: Sequence of steps leading from flat plate in PATRAN to a quarter FE model in ABAQUS.

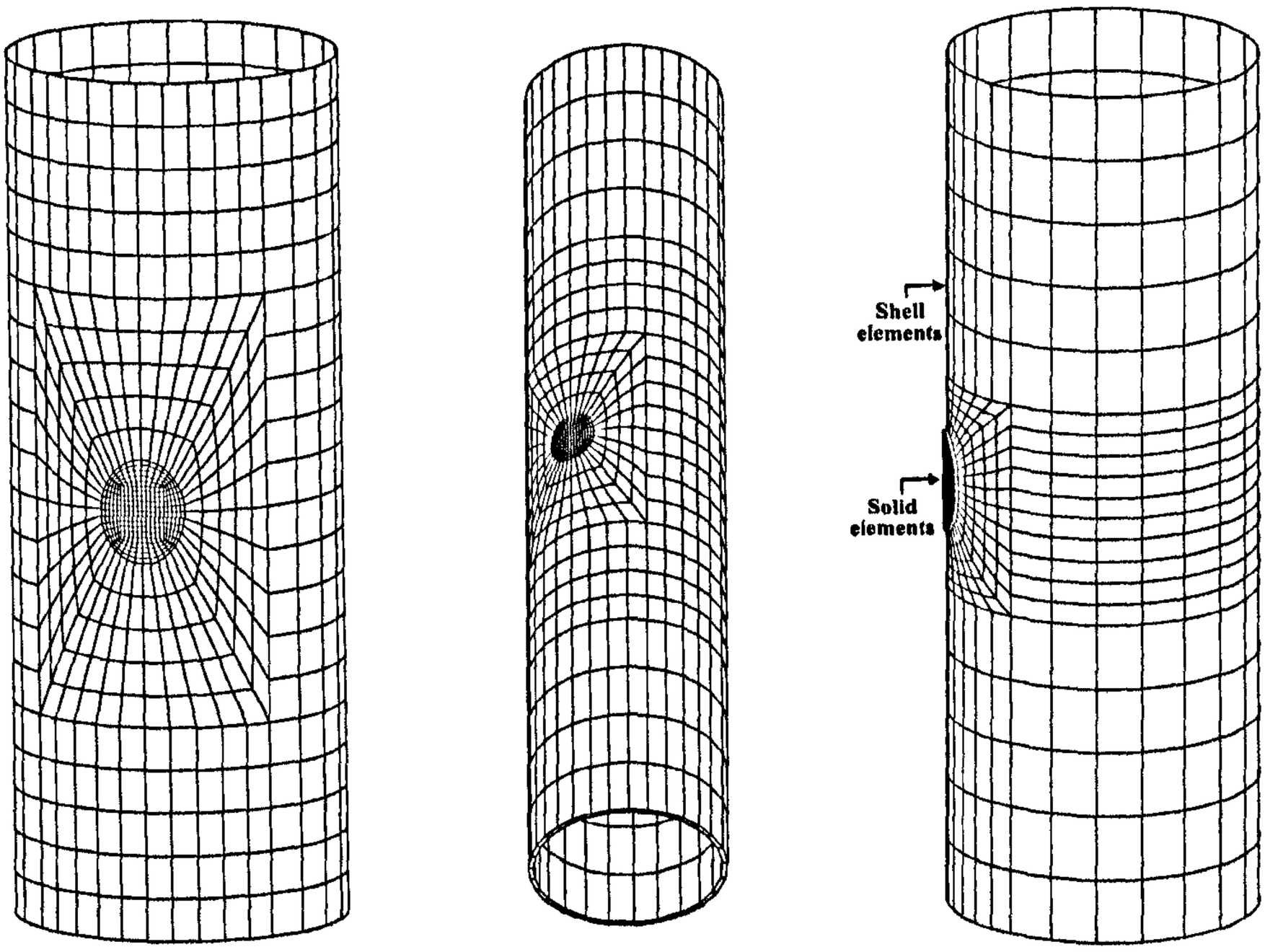

(a) Shell elements. (b) Solid elements. (c) Combined elements.

Figure 3.9: Finite element verification models; pure shell elements, Fig. 3.9a; pure solid elements, Fig. 3.9b; and combination of shell and solid elements, Fig. 3.9c.

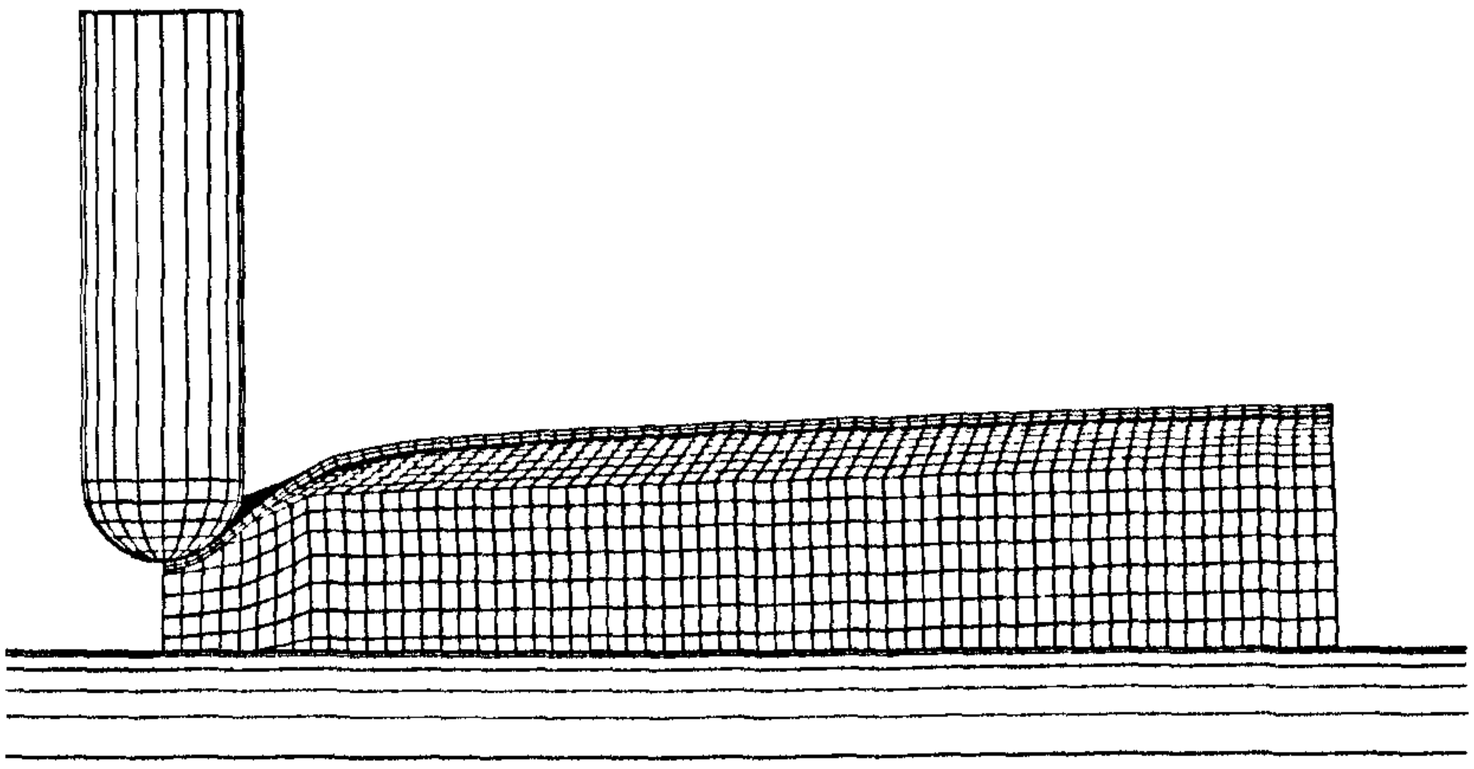

(a) Side view of the dented pipe model (quarter model).

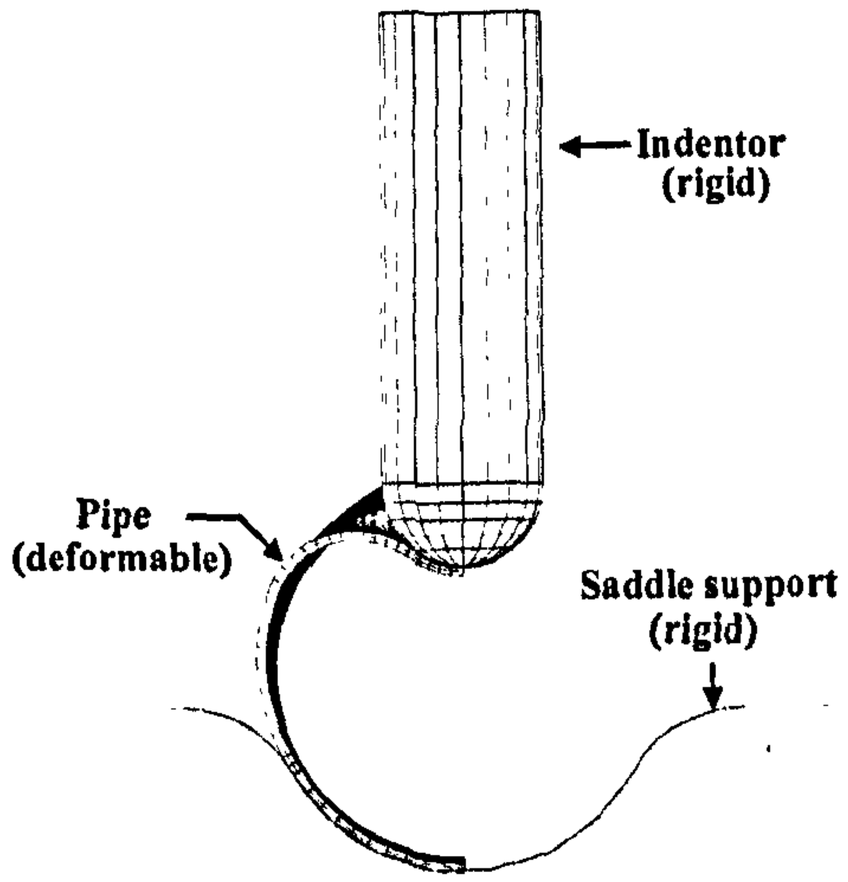

(b) Cross-section view of dented pipe.

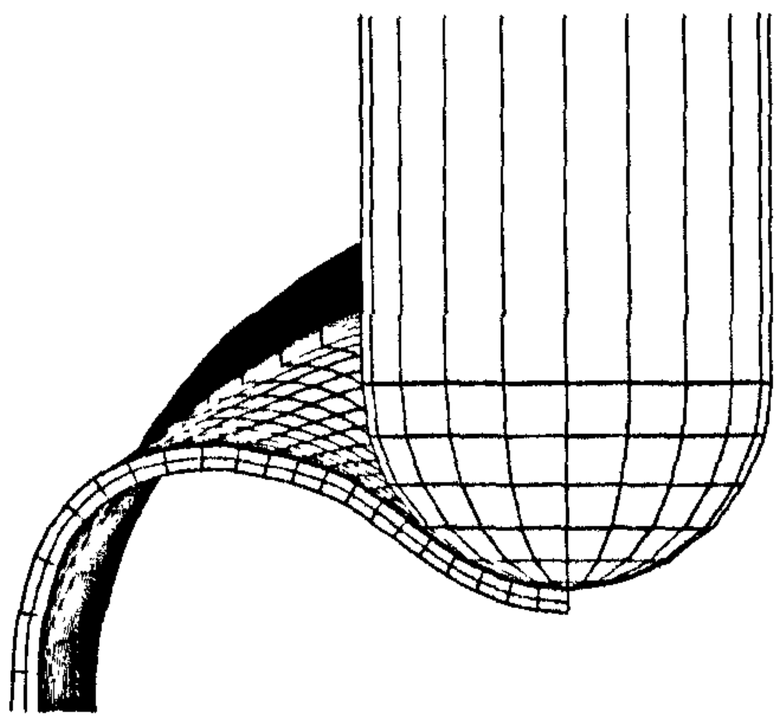

(c) Close view of the indented area.

Figure 3.10: Different views of denting process by a hemispherical indenter. Note that pipe wall is modelled by two layers of brick elements.

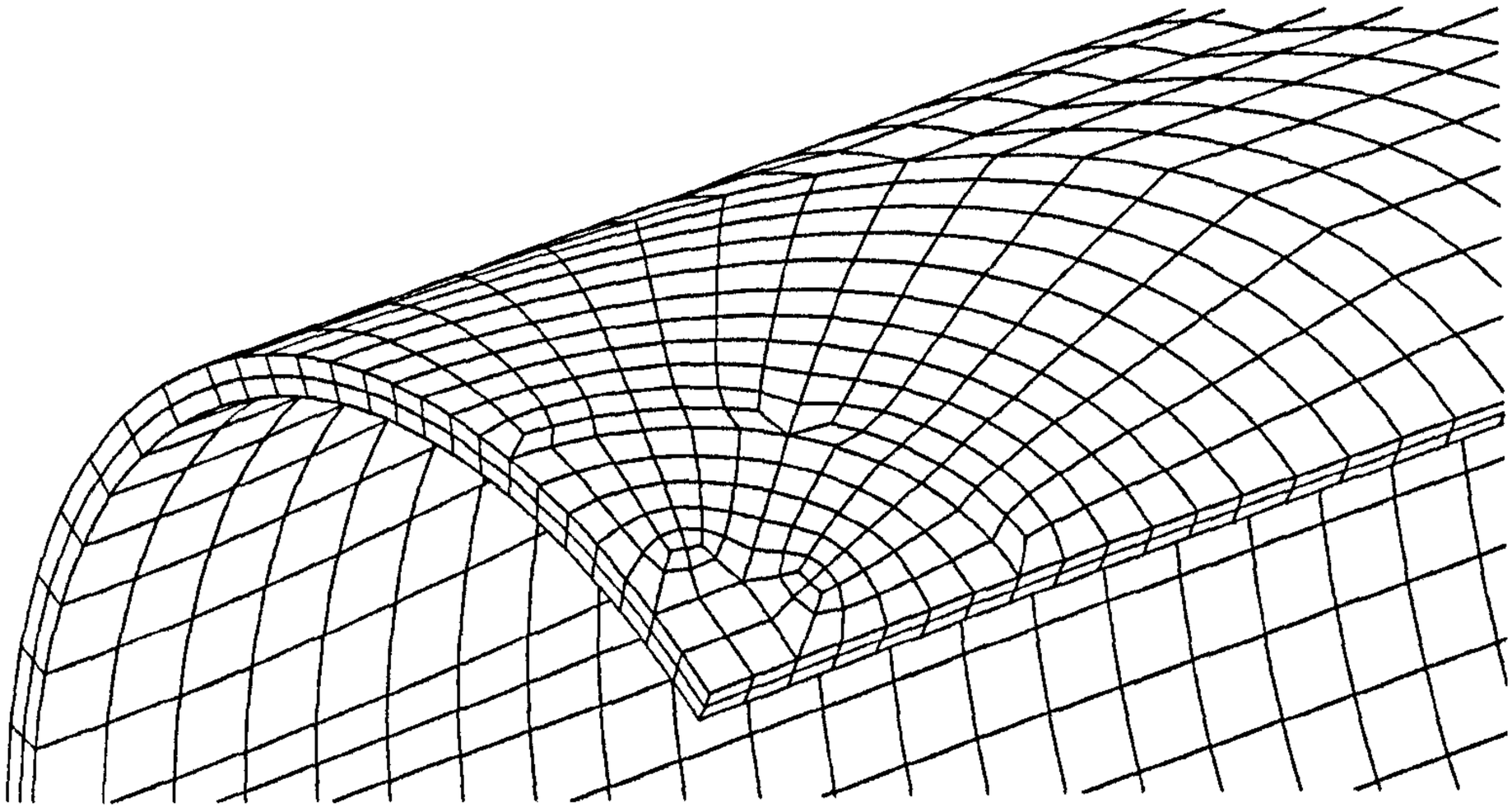

(a) Plain pipe, i.e., without any gouging, before denting.

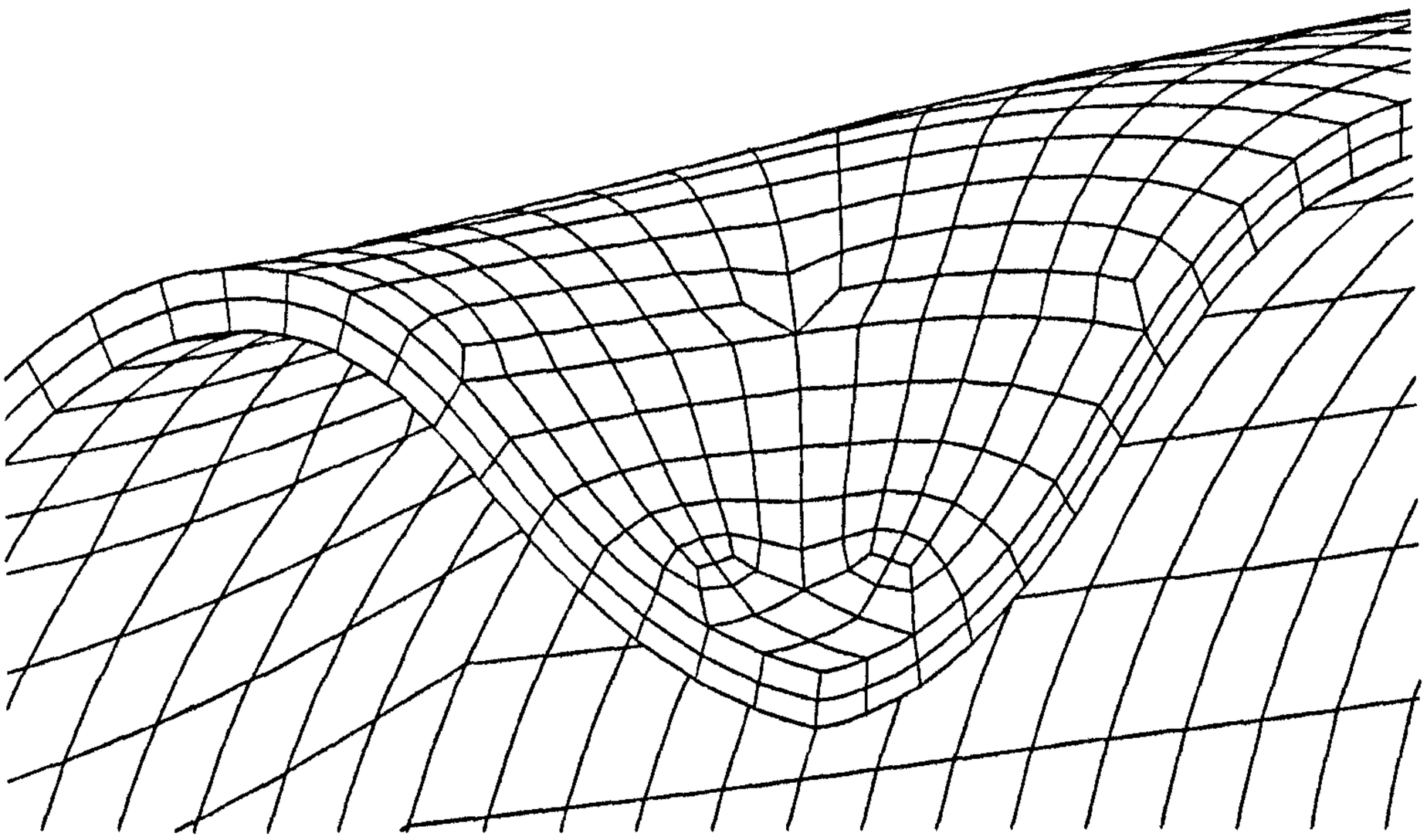

(b) Plain pipe after denting (no internal pressure).

Figure 3.11: Close view of a pipe before and after denting. Illustration of adopted meshing.

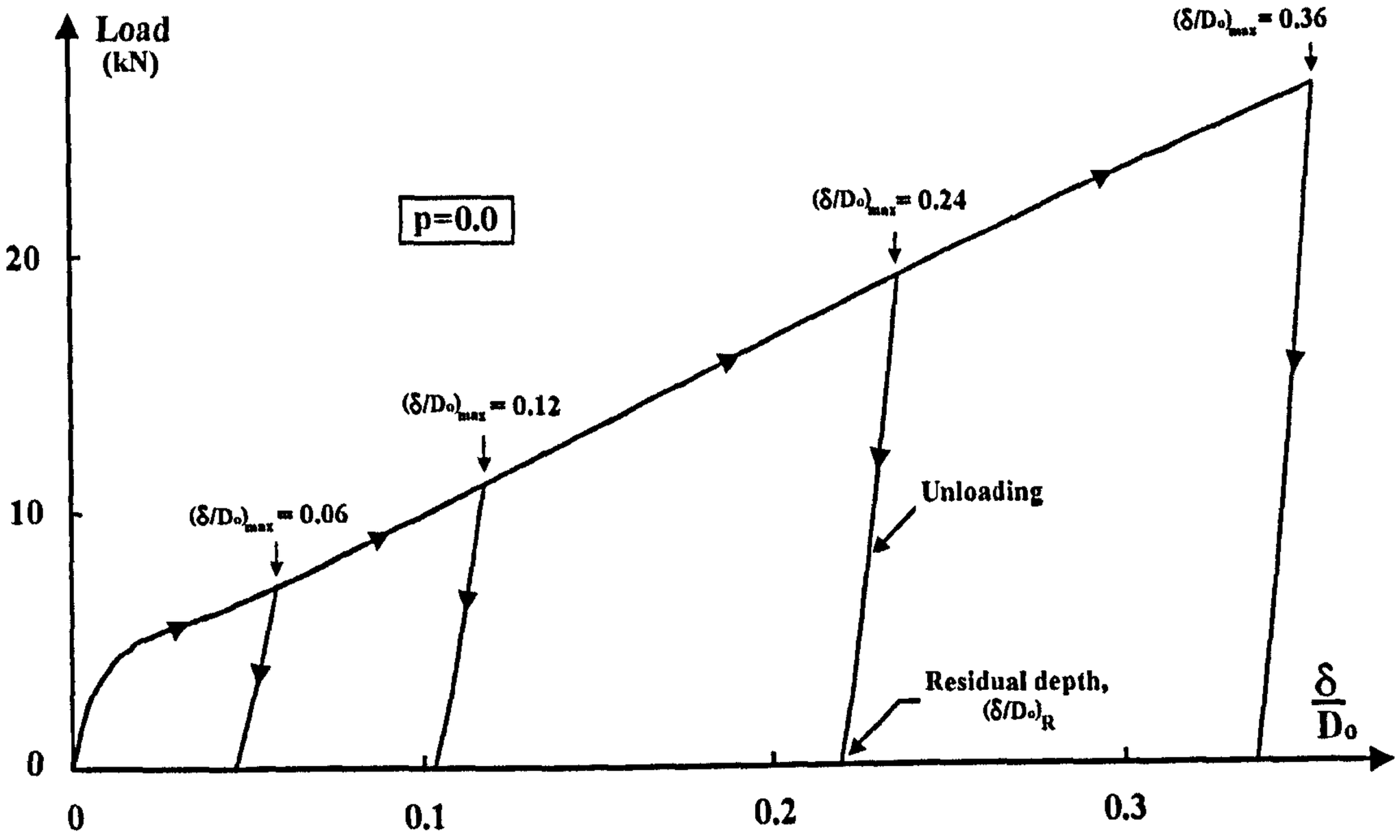

Figure 3.12: Plots of denting load versus displacement of centre node. Both loading and unloading are shown for four dent depths, $(\frac{\delta}{D_o})_{max}$ = 0.06, 0.12, 0.24, and 0.36 with the corresponding residual dent depths. Also, $\frac{a}{b} = 1.0$, and $\frac{2L}{D_o} = 12.0$.

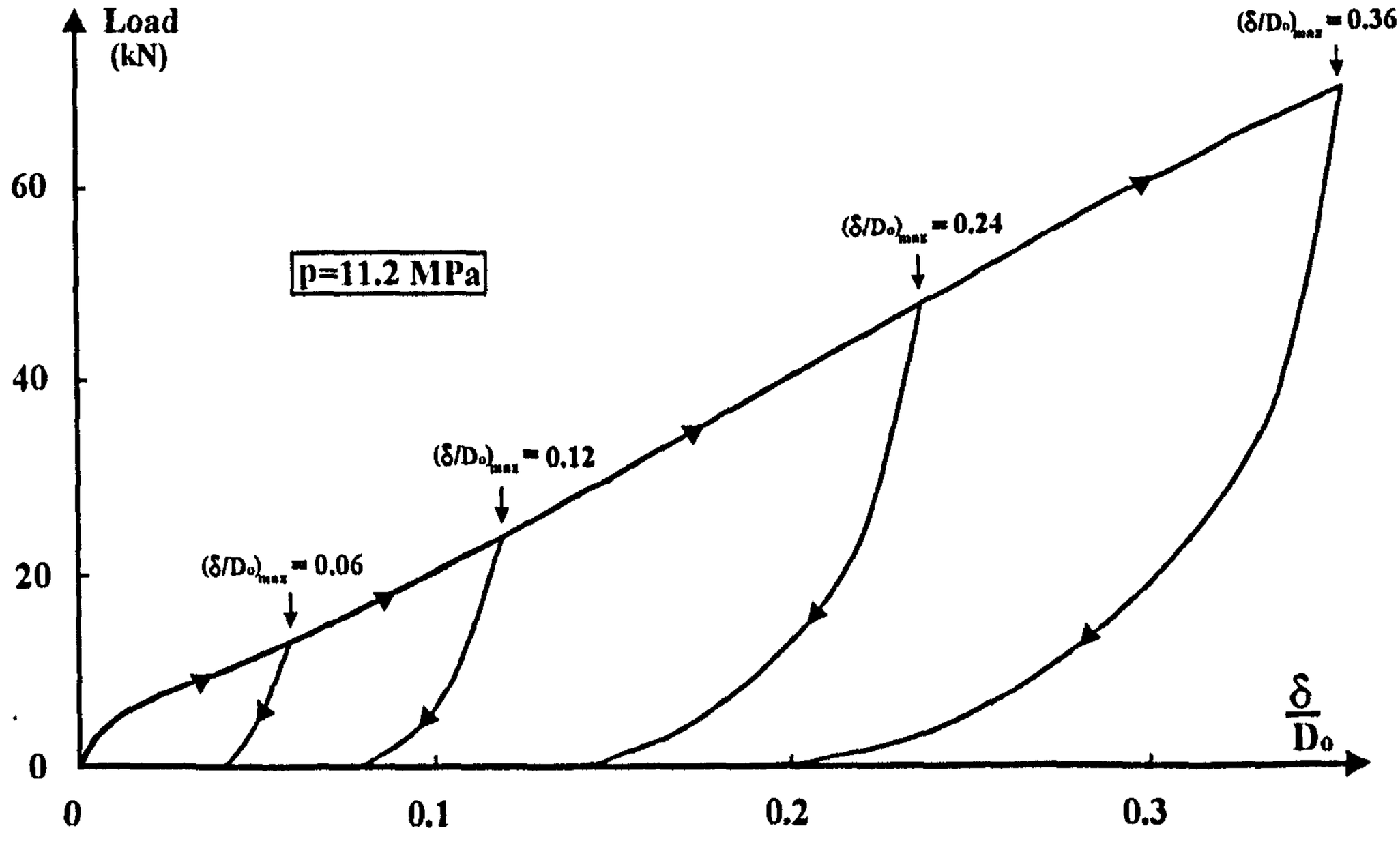

Figure 3.13: Plots of denting load versus displacement of mid-span node in the case of pressurised pipe. Both loading and unloading are shown for four dent depths, $(\frac{\delta}{D_o})_{max}$ = 0.06, 0.12, 0.24, and 0.36 with the corresponding residual dent depths. Also, $\frac{a}{b} = 1.0$, and $\frac{2L}{D_o} = 12.0$.

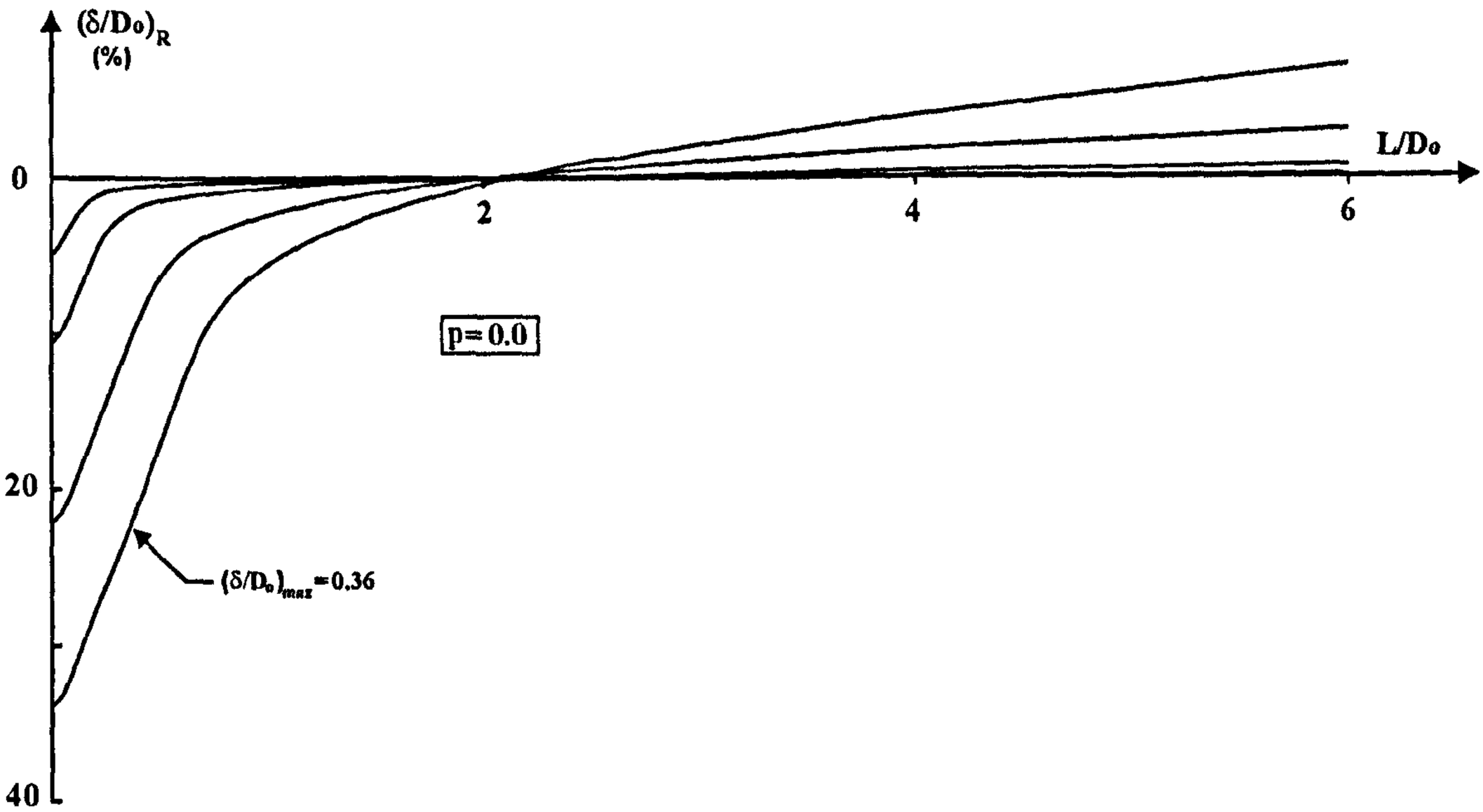

Figure 3.14: Profile of residual dent along pipe axis for different dent depth, i.e., for $(\frac{\delta}{D_o})_{max} =$ 0.06, 0.12, 0.24, and 0.36. Also, $p = 0.0$, $\frac{a}{b} = 1.0$, and $\frac{2L}{D_o} = 12.0$.

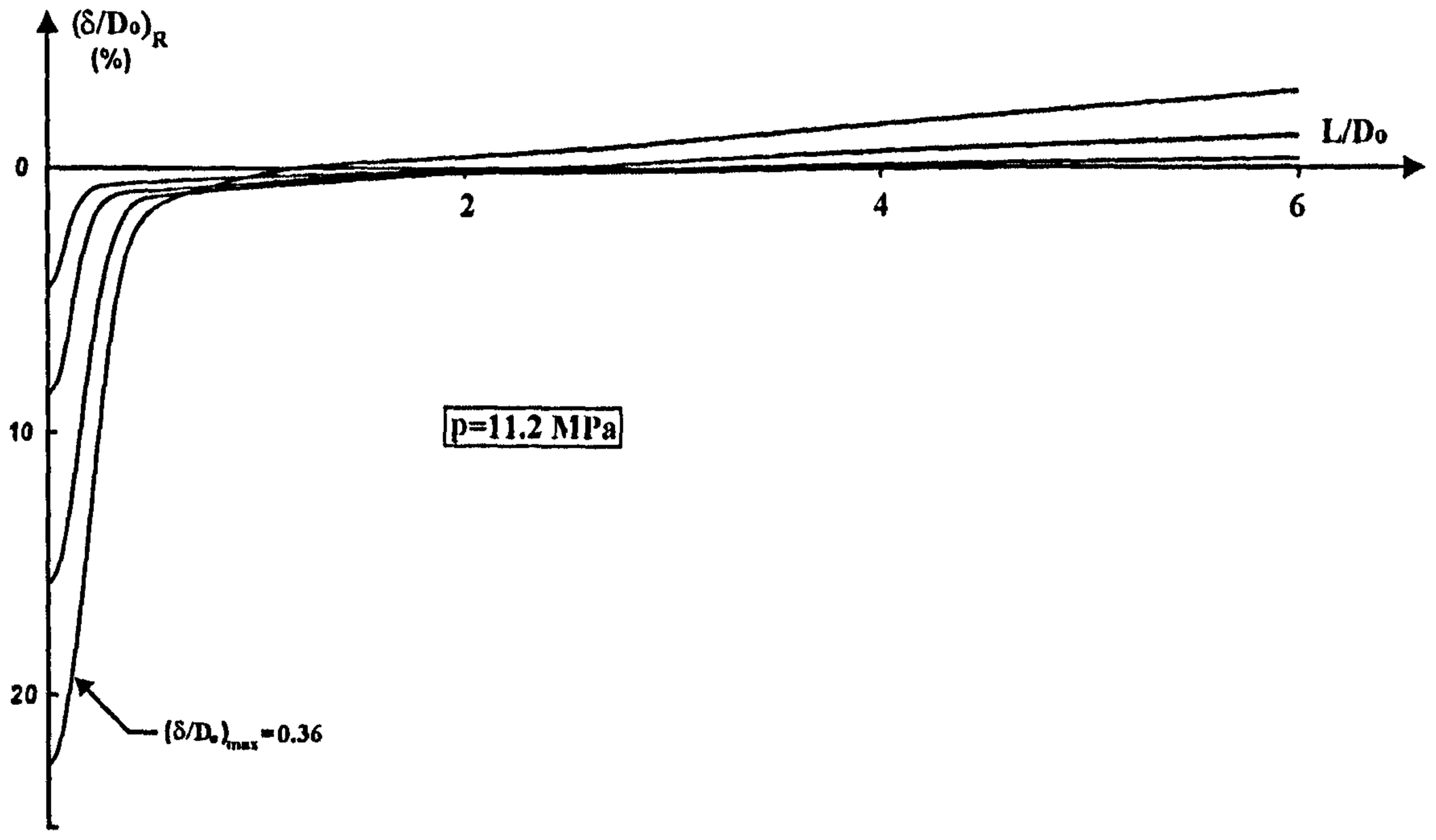

Figure 3.15: Profile of residual dent along pipe length for different dent depth, i.e., for $(\frac{\delta}{D_o})_{max}$ = 0.06, 0.12, 0.24, and 0.36. Also, $p = 11.2\ MPa$, $\frac{a}{b} = 1.0$, and $\frac{2L}{D_o} = 12.0$.

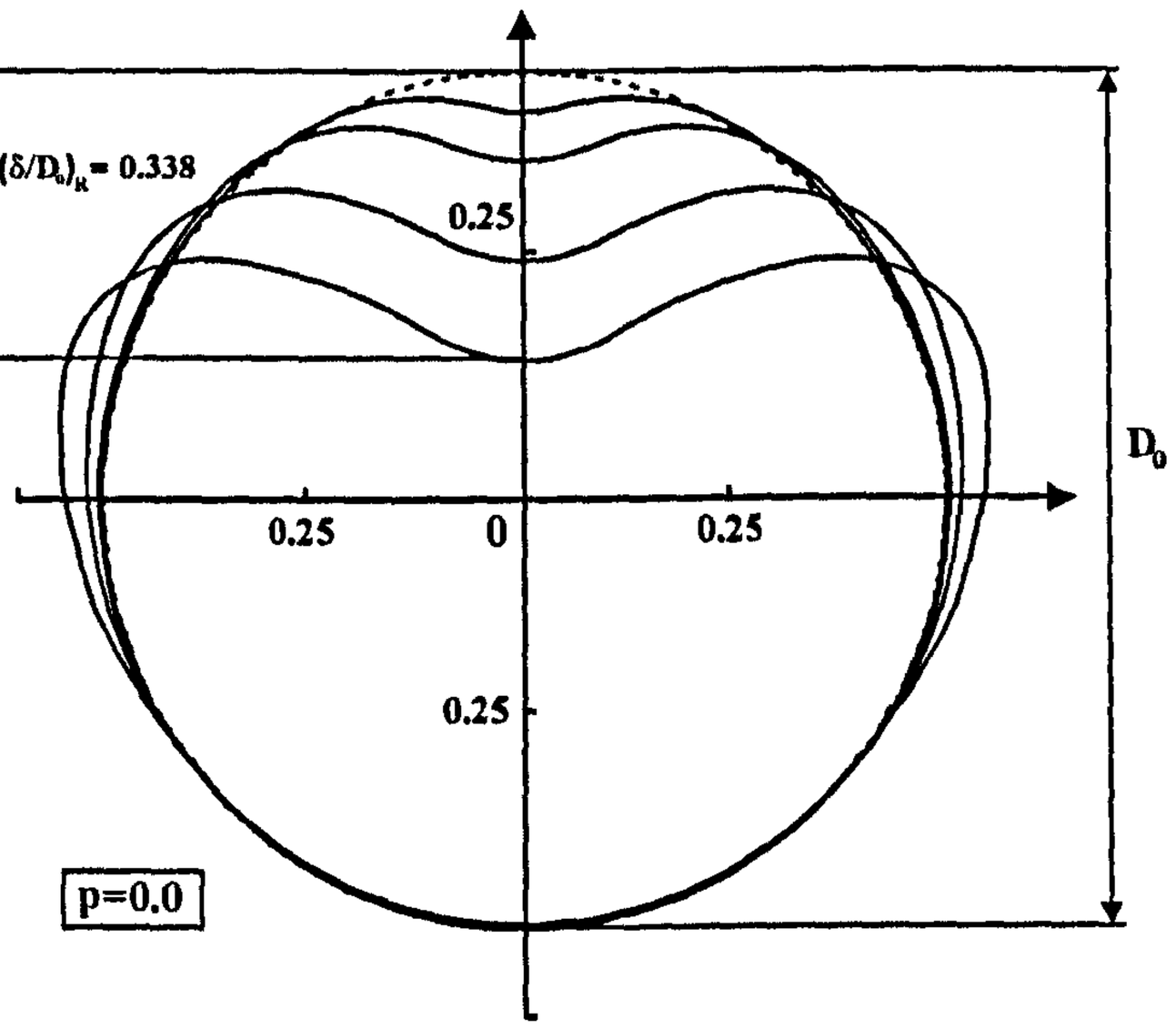

Figure 3.16: Profiles of residual dent at the mid-span for different dent depths, i.e., for $(\frac{\delta}{D_o})_{max} = 0.06,\ 0.12,\ 0.24$, and 0.36. Also, $p = 0.0$, $\frac{a}{b} = 1.0$ and $\frac{2L}{D_o} = 12.0$.

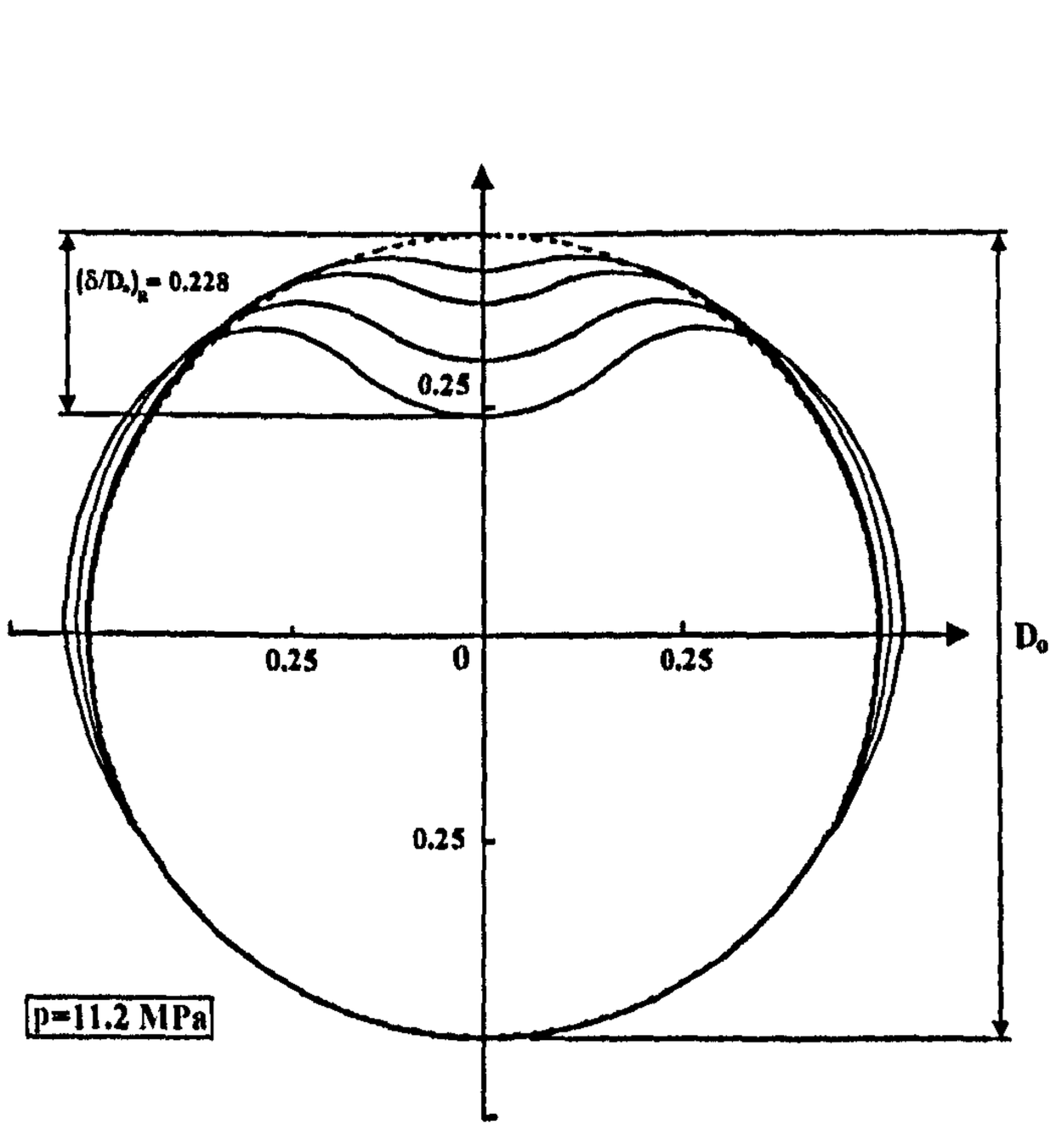

Figure 3.17: Profile of residual dent at the mid-span for different dent depth, i.e., for $(\frac{\delta}{D_o})_{max} = 0.06,\ 0.12,\ 0.24$, and 0.36. Also, $p = 11.2\ MPa$, $\frac{a}{b} = 1.0$, and $\frac{2L}{D_o} = 12.0$.

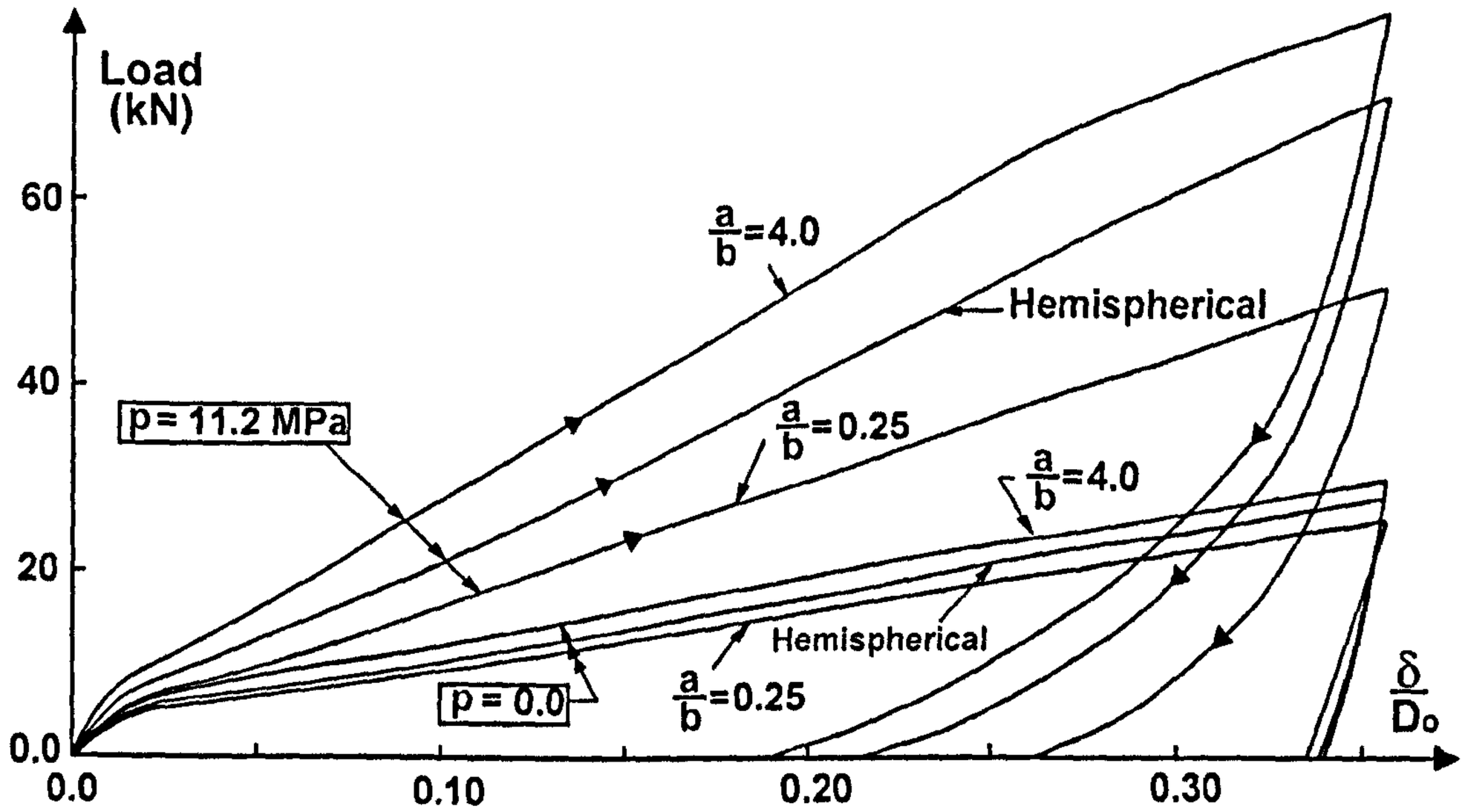

Figure 3.18: Denting force versus vertical displacement of a node underneath of the indenter. Results are shown for a non-pressurised pipe and for the pressurised pipe to $p = 11.2MPa$. Three shapes of the indenter were used. Also, $\frac{2L}{D_o} = 12.0$.

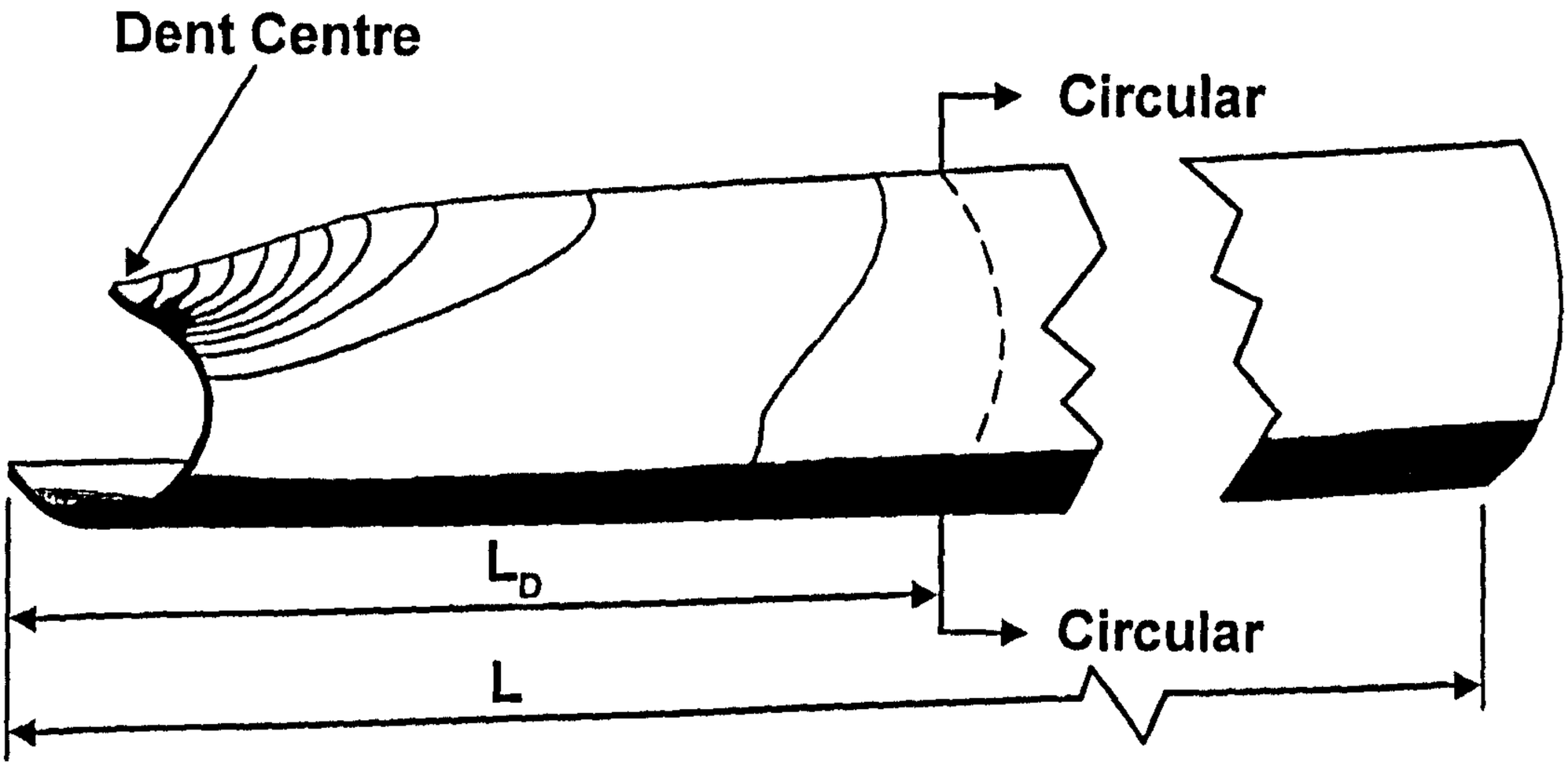

Figure 3.19: Sketch showing the length, L_D, along which pipe cross-section is not circular due to propagation of distortion caused by indenter being applied at pipe's mid-length.

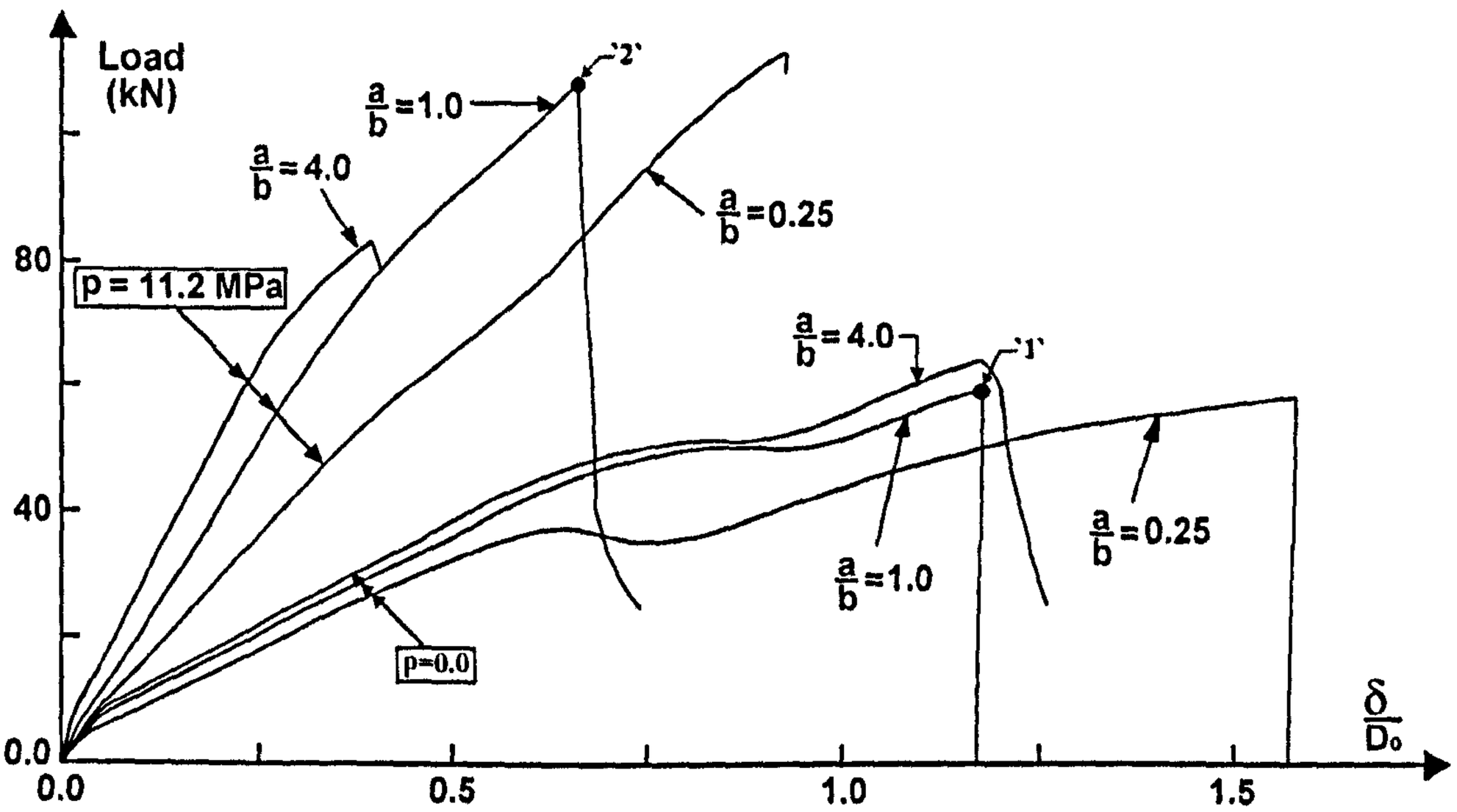

Figure 3.20: Plots of denting load versus depth of the dent for empty pipe, $p = 0.0$, and for pressurised pipe, $p = 11.2\ MPa$. Results for three different shapes of the indenter are shown.

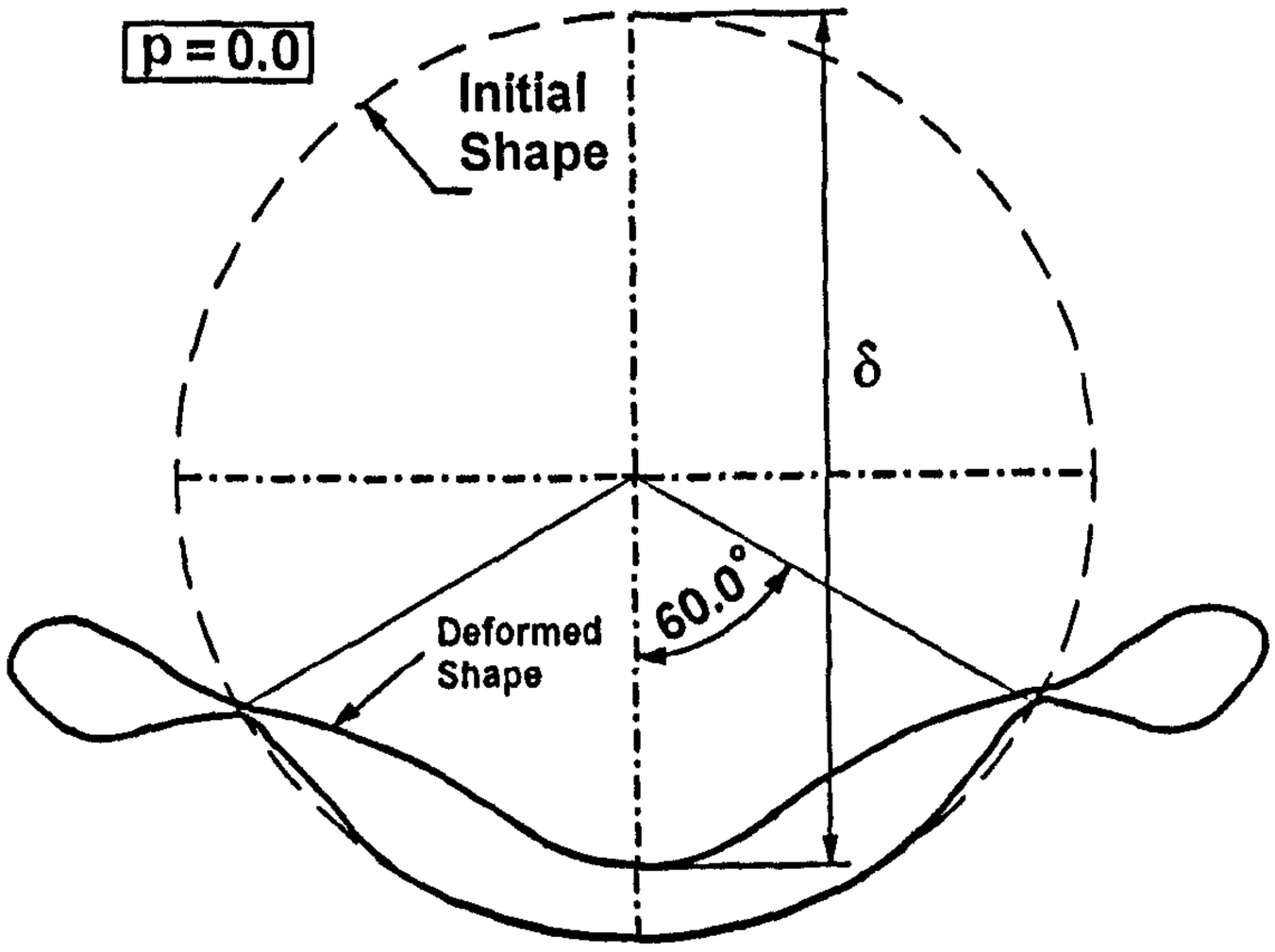

(a) Section through the pipe at collapse (point '1' in Fig. 3.20, $F_{max} = 54.0\ kN$, and $\frac{a}{b} = 1.0$).

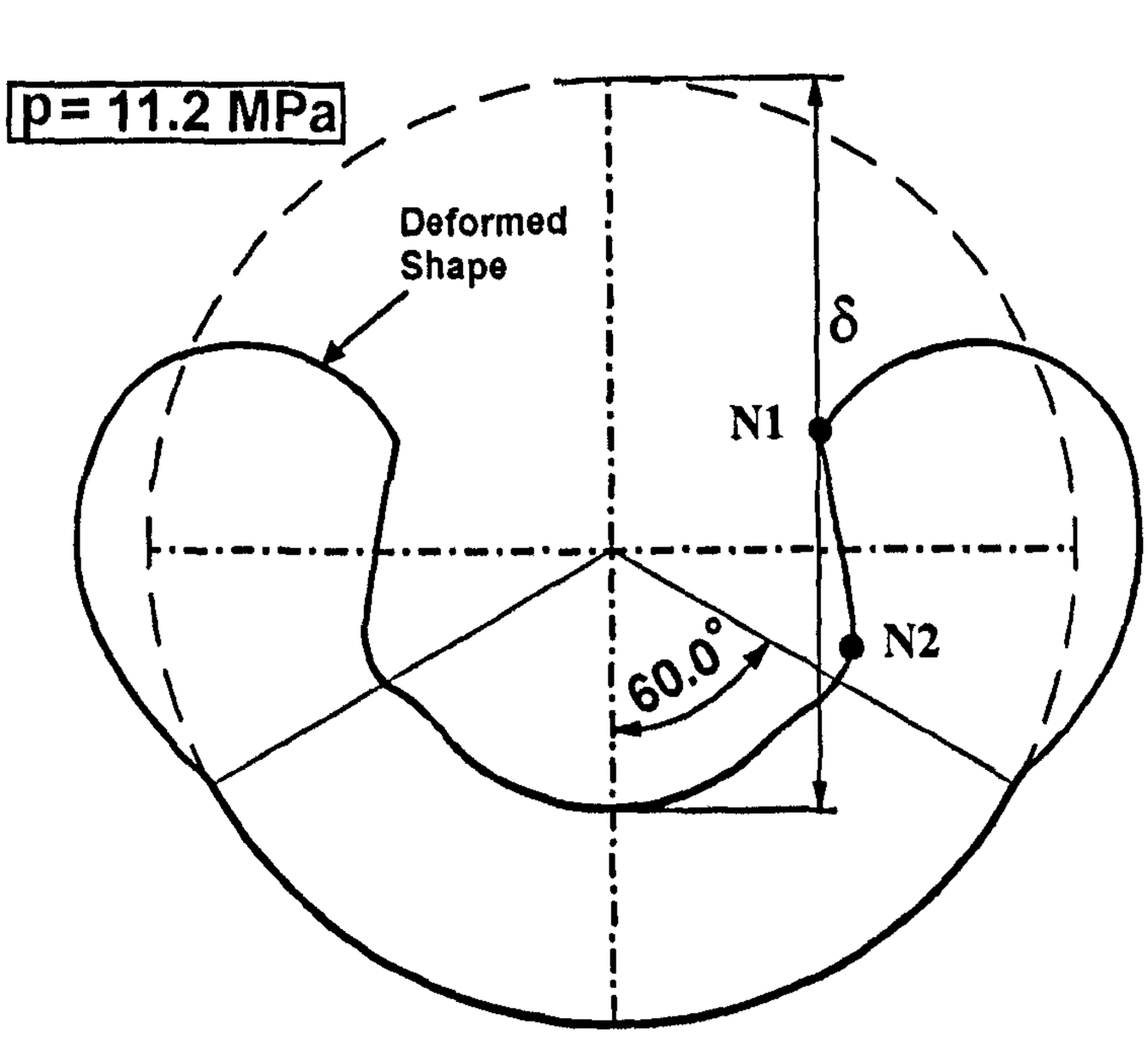

(b) Section through the pipe at collapse (point '2' in Fig. 3.20, $F_{max} = 107.6\ kN$, and $\frac{a}{b} = 1.0$).

Figure 3.21: View of typical deformation of the cross-section, for empty and for pressurised pipe at the maximum, i.e., collapse load (for hemispherical indenter, and at mid-span).

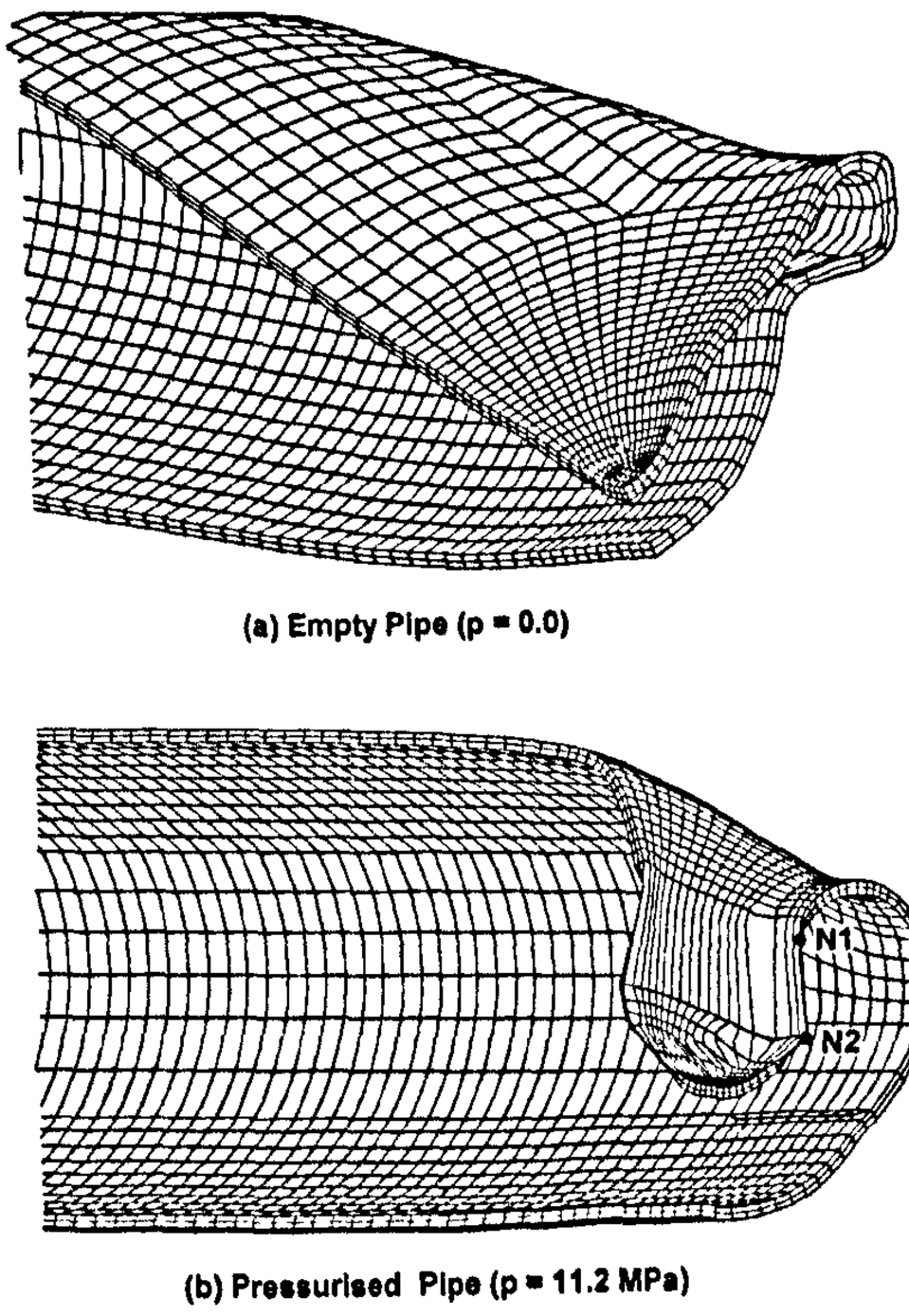

Figure 3.22: Close view at collapse for the case of, empty pipe ($p = 0.0$), and for pressurised pipe ($p = 11.2\ MPa$). Also, $\frac{a}{b} = 1.0$, and $\frac{2L}{Do} = 12.0$.

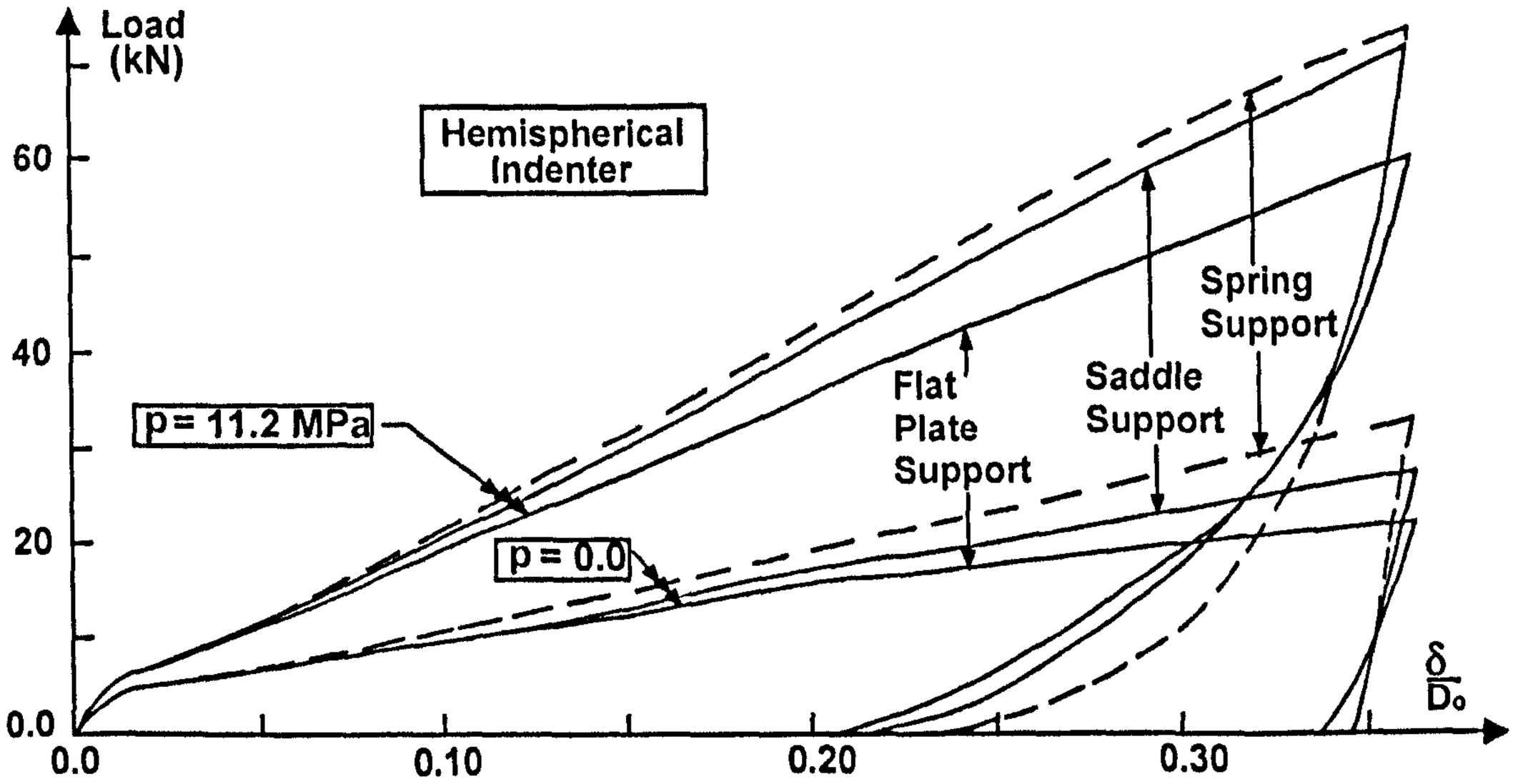

Figure 3.23: Denting load versus dent's depth curves for a pipe being supported by a saddle, by flat plate, and by springs. Also, $\frac{a}{b} = 1.0$, and $\frac{2L}{D_o} = 12.0$.

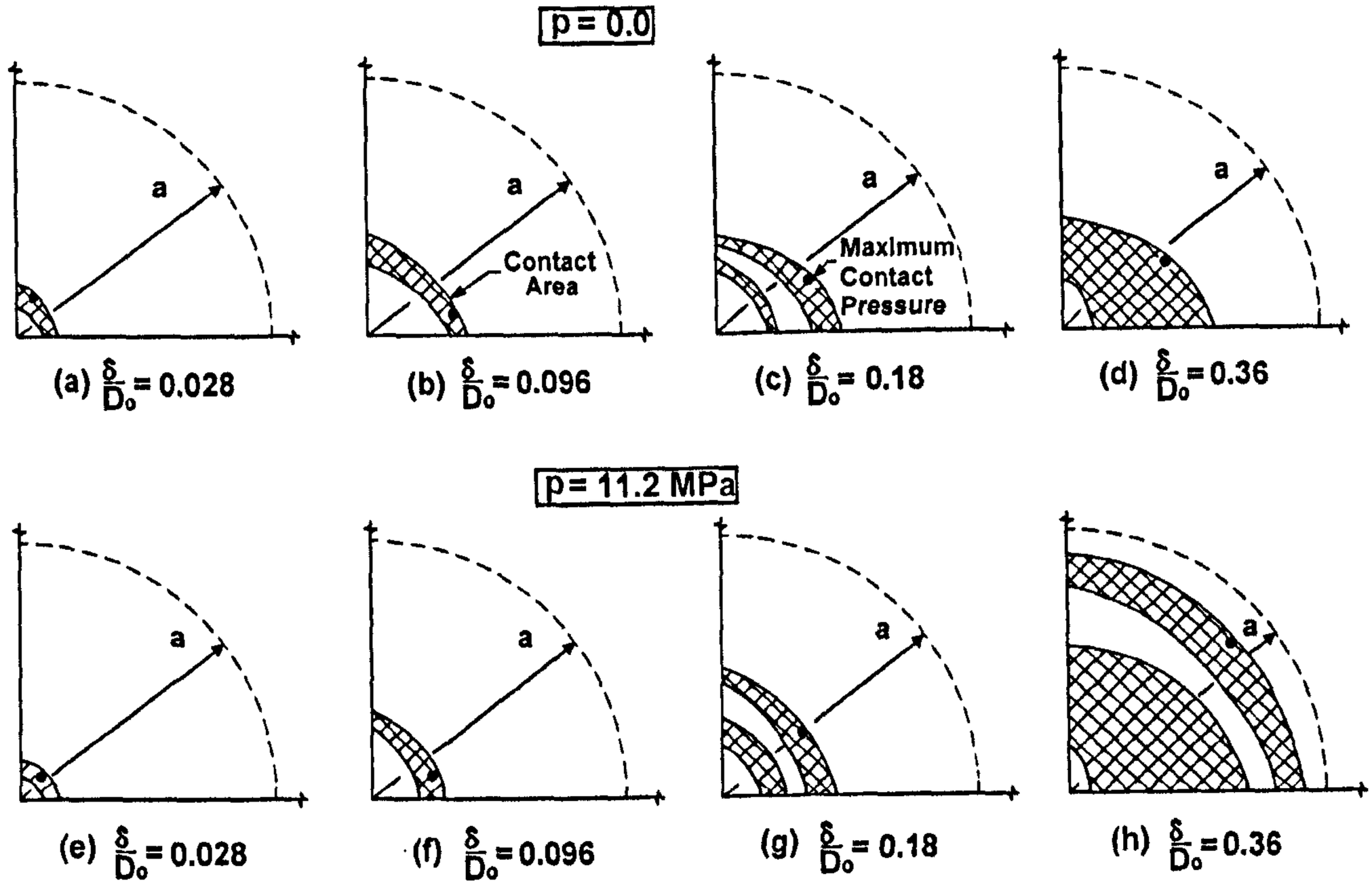

Figure 3.24: Spread of contact area between hemispherical indenter and pipe for pressure free pipe sub - figures 3.24a, b, c, d and for pressurised pipe Figs 3.24e, f, g, h. Also, $\frac{a}{b} = 1.0$, and $\frac{2L}{Do} = 12.0$.

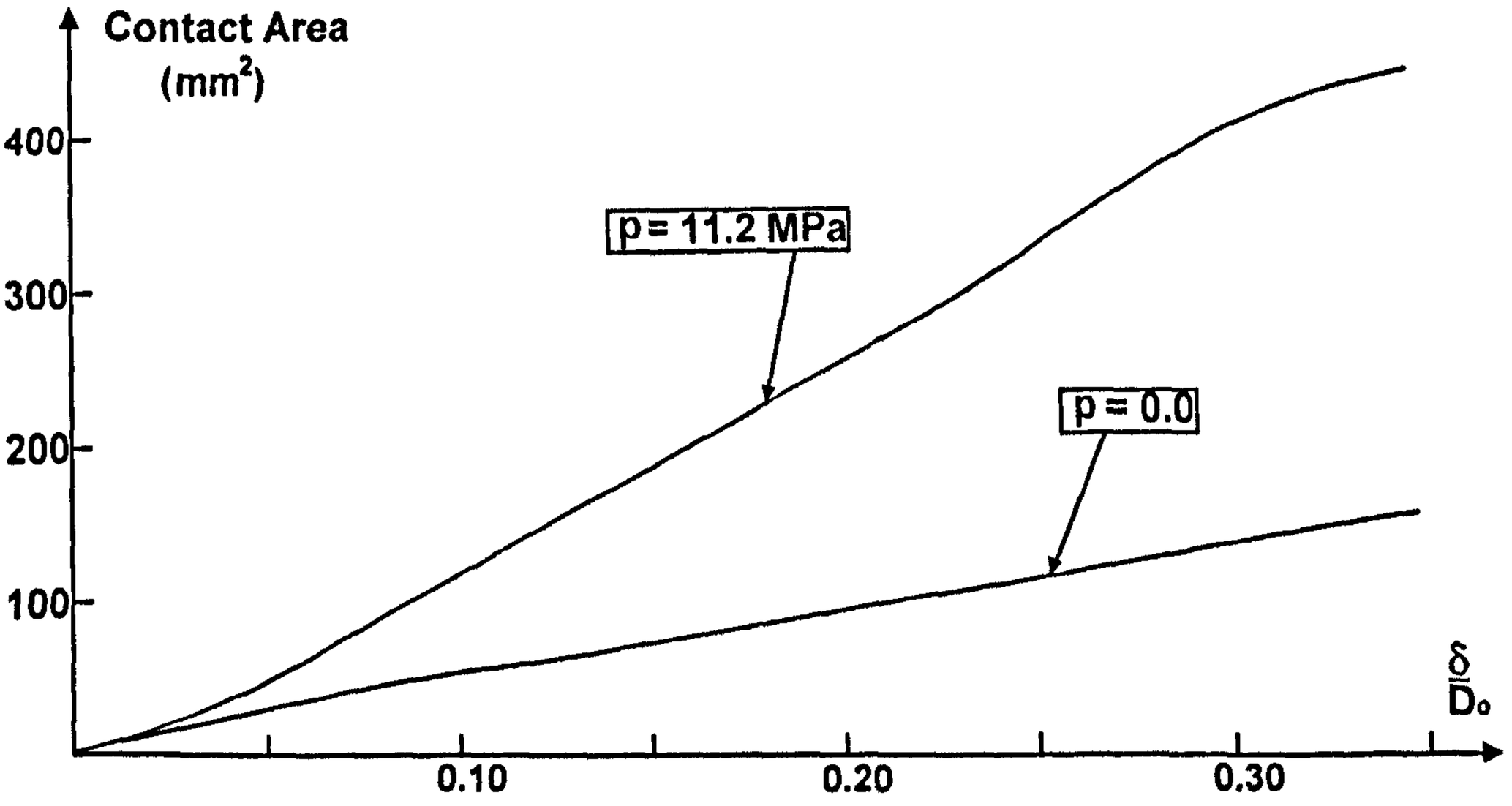

Figure 3.25: Growth of contact area between hemispherical indenter and the pipe as a function of dent's depth. Two cases are shown, i.e., for pressure free pipe and for a pipe being pressurised to the design pressure, $p = 11.2\ MPa$. Also, $\frac{2L}{D_o} = 12.0$, and $\frac{a}{b} = 1.0$.

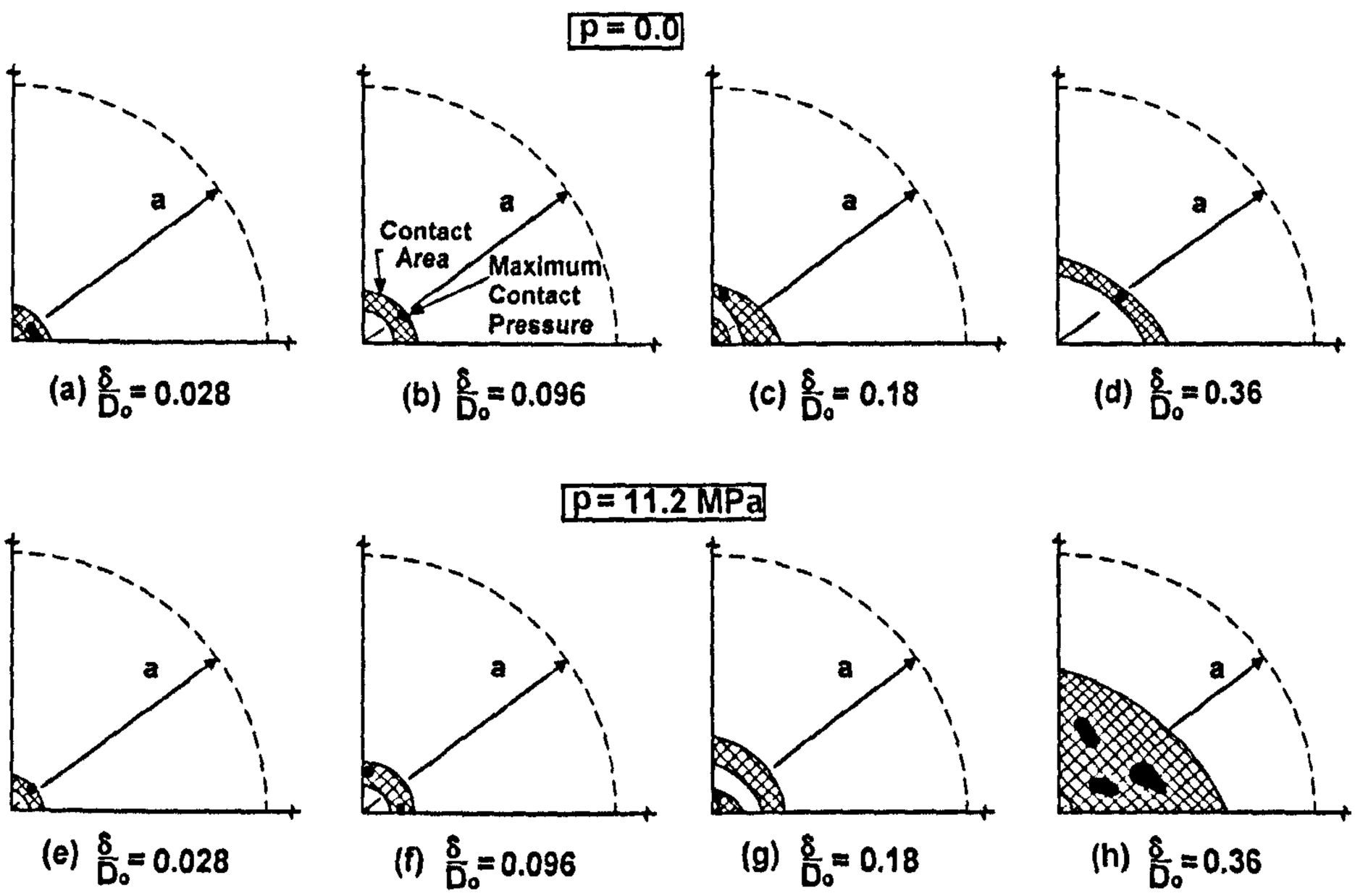

Figure 3.26: Spread of contact area between elliptical indenter, $\frac{a}{b} = 0.25$ and the pipe surface. Two cases are shown, i.e., empty and pressurised pipe. Also, $\frac{2L}{D_o} = 12.0$.

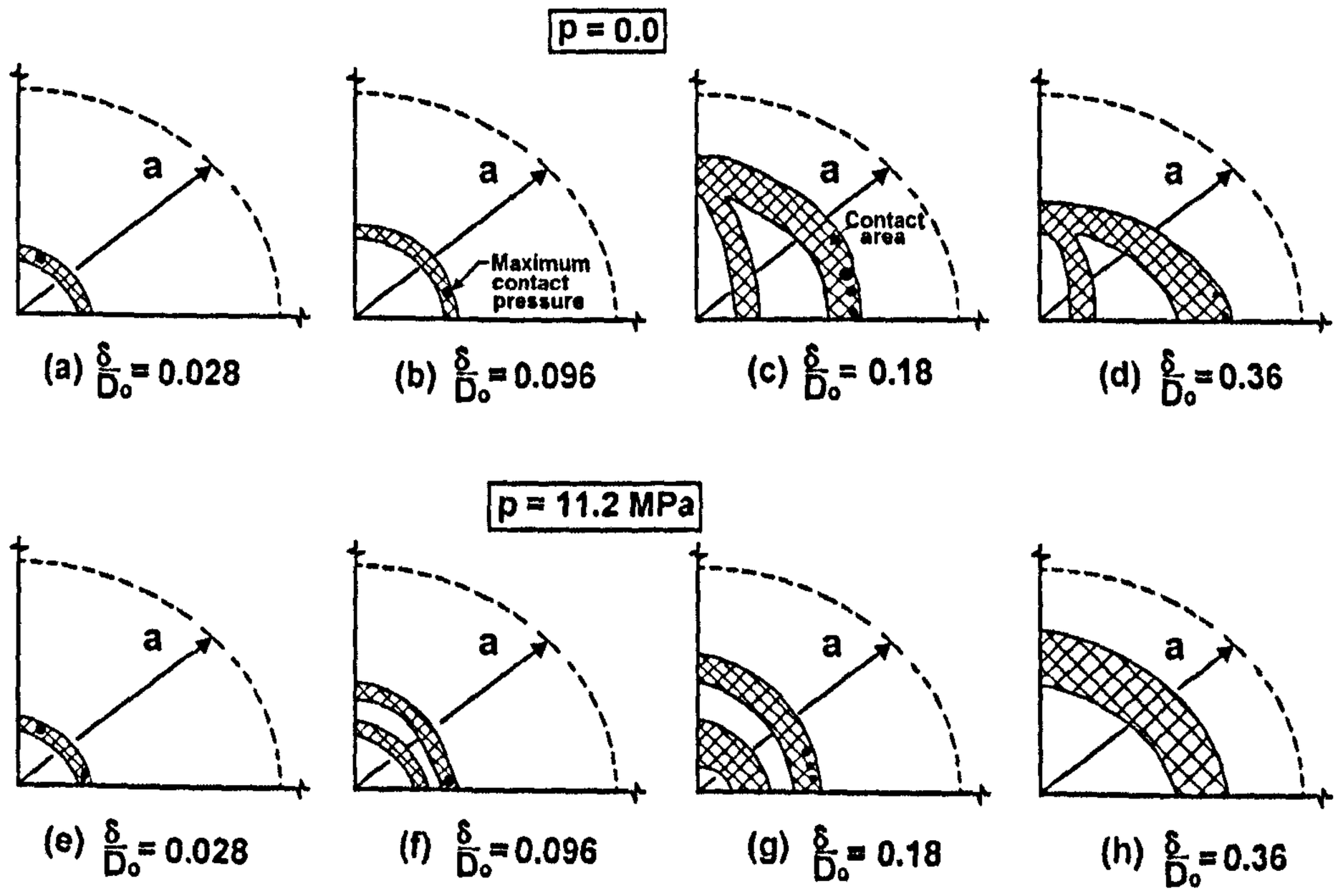

Figure 3.27: Spread of contact area between elliptical indenter, $\frac{a}{b} = 4.0$ and the pipe surface. Two cases are shown, i.e., empty and pressurised pipe. Also, $\frac{2L}{D_o} = 12.0$.

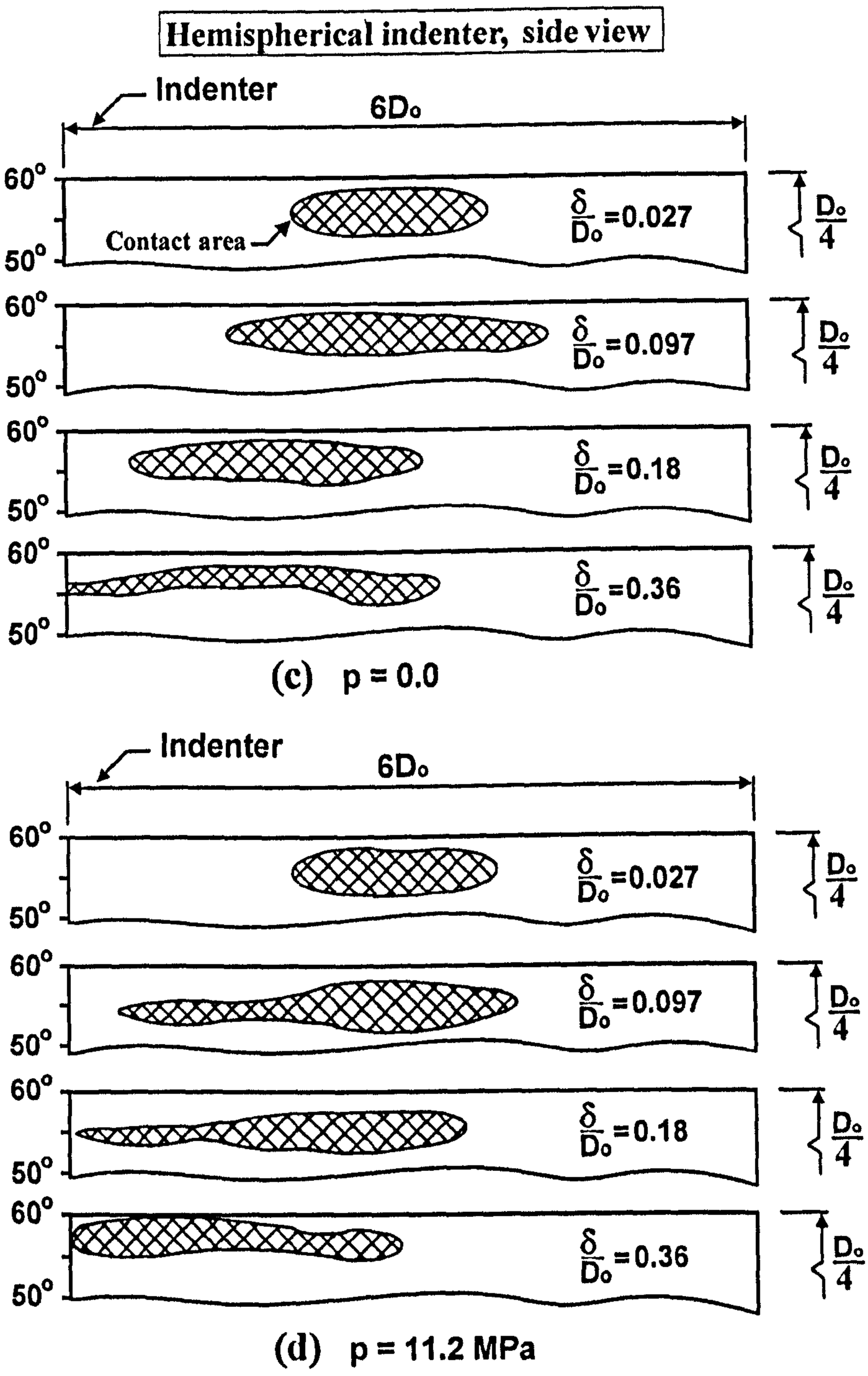

Figure 3.28: Shape and location of contact area between pipe and rigid, saddle support. Only, a quarter model is shown. Note how contact patches drift towards mid-span of the pipe for deeper dents. Also, $\frac{a}{b} = 1.0$, and $\frac{2L}{D_o} = 12.0$.

Chapter 4

The interaction of pressure and bending on a dented pipe

4.1 Introduction

This Chapter addresses the behaviour of dented pipe under given pressure, moment loading or combination of both of them. The strength of the dented pipe is first assessed under pure bending, applied in such a way that the dent is either on the tension side or on the compression side as it can be seen in the Figure (4.1). If the dent occurs on the compression side of the pipe during bending, the moment is referred to as closing bending moment, and if it occurs on the tension side of the pipe, the moment is referred to as opening bending moment. The strength of the dented pipe is assessed under internal pressure loading. Finally the behaviour of the dented pipe under simultaneously acting bending and pressure loading is assessed, and interaction diagrams are discussed.

4.2 Finite element modelling

The pipe dimensions used in this Chapter were selected to be close to those of an experimental component, the results of which are given in Chapter (6). The dimensions are given in Table (3.1). Only one indenter is being used here, i.e., hemispherical

with, $\frac{a}{b} = 1.0$. The plain pipe is modelled using PATRAN [18] and the stress analysis is conducted using ABAQUS [19]. A quarter model is used in which length is taken as, $\frac{2L}{D_o} = 6.0$. Boundary conditions remained the same as in Chapter (3), (see Figure (3.5) for details). For pressure loading, the inner pipe wall was subjected to pressure p. A tensile stress of magnitude, $\frac{pD_i^2}{D_o^2 - D_i^2}$, was applied to the pipe's end.

4.3 The interaction diagram theory for plain pipe

The general concept for load interaction is defined as the effect of combining two loads that cause the effective stress, e.g., Huber-Mises-Hencky, to reach yield stress. This is referred to as first yield load interaction. Different possibilities of interaction format can be obtained as illustrated in Figure (1.6). The circular interaction, in the form $A^2 + B^2 = 1$, where A and B are two non-dimensional loads. The Huber-Mises-Hencky biaxial effective stress is given by the following expression:

$$\sigma_{yp}^2 = \sigma_\theta^2 - \sigma_\theta \sigma_\phi + \sigma_\phi^2 \tag{4.1}$$

From which:

$$\sigma_\phi = \frac{\sigma_\theta \pm \sqrt{\sigma_\theta^2 - 4(\sigma_\theta^2 - \sigma_{yp}^2)}}{2} \tag{4.2}$$

After re-arranging one obtains:

$$\sigma_\phi = \frac{\sigma_\theta}{2} \pm \sqrt{\sigma_{yp}^2 - \frac{3}{4}\sigma_\theta^2} \tag{4.3}$$

The axial stress due to combined pressure and moment is obtained as follows:

$$\sigma_\phi = \frac{pr}{2t} \pm \frac{M}{\pi r^2 t} \tag{4.4}$$

Taking the hoop stress as:

$$\sigma_\theta = \frac{pr}{t} \tag{4.5}$$

one obtains from Eq. (4.3):

$$\frac{pr}{2t} \pm \frac{M}{\pi r^2 t} = \frac{pr}{2t} \pm \sqrt{\sigma_{yp}^2 - \frac{3}{4}(\frac{pr}{t})^2} \tag{4.6}$$

Non dimentionalising can be carried out, using the following yield moment and pressure equations:

$$M_y = \pi r^2 t \sigma_{yp} \quad and \quad p_y = \frac{2}{\sqrt{3}}(\frac{t}{r})\sigma_{yp} \tag{4.7}$$

Equation (4.6) then becomes:

$$\frac{M}{\pi r^2 t}(\frac{\pi r^2 t \sigma_{yp}}{M_y}) = \sqrt{[\sigma_{yp}^2 - \frac{3}{4}(\frac{pr}{t})^2(\frac{\frac{4}{3}(\frac{t}{r})^2\sigma_{yp}^2}{p_y^2})]} \tag{4.8}$$

After re-arranging:

$$(\frac{M}{M_y})^2\sigma_{yp}^2 = \sigma_{yp}^2 - (\frac{p}{p_y})^2\sigma_{yp}^2, \tag{4.9}$$

Finally:

$$[\frac{M}{M_y}]^2 + [\frac{p}{p_y}]^2 = 1 \tag{4.10}$$

4.4 Limit pressure and moment for plain pipe.

4.4.1 Limit pressure for plain pipe

The RIKS method was used to facilitate obtaining of the limit pressure for the plain pipe by using ABAQUS. The material used in the FE was modelled as elastic/perfectly plastic. The value of the yield point of material, σ_{yp}, was assumed as $\sigma_{yp} = 316.0\ MPa$. Figure (4.2) shows the plot of pressure versus node radial displacement, U_2, for the plain pipe. As it can be seen from this figure the maximum pressure obtained from ABAQUS is $P_{max} = 18.4\ MPa$. ABAQUS was not capable of producing the horizontal line of pressure versus radial displacement. The maximum pressure value obtained from the FE analyses was the same as the calculated value using the Huber-Mises-Hencky criterion, i.e.,:

$$P_L = \frac{2}{\sqrt{3}}(\sigma_{yp})\ln(\frac{R_0}{R_i}), \tag{4.11}$$

Which gives the following value: $P_L = \frac{2}{\sqrt{3}}(316.0)\ln(\frac{42.1}{40.03}) = 18.4\ MPa$.

4.4.2 Limit moment for plain pipe

Limit moment for plain pipe was obtained from load-rotation curve generated by ABAQUS. Figure (4.3) shows typical moment versus rotation curve for plain pipe with elastic-perfectly plastic material and at zero internal pressure. The plain pipe was subjected to bending moment by applying rotation to the master node. The nodes at the end edge of the pipe were tied to the center *MASTER* node using the *ABAQUS* beam Multi Point Constraint. The FE limit moment value was closer to the calculated value obtained using the following equation:

$$M_L = D_m^2 t \sigma_{yp}, \tag{4.12}$$

Which gives:

$M_L = 0.08213^2 \times 0.00207 \times 316.0 \times 10^6 = 4412\ Nm.$

4.5 Denting process

Prior to bending the pipe had to be dented. The denting process has already been described in Chapter (3). The dimension of the model pipe used here is the same as in Chapter (3), see Table (3.1). The solid indentor used to produce the dent was of hemispherical shape, $\frac{a}{b} = 1.0$. The ground support, of saddle shape, was assumed to be rigid and continuous along the model length. The "saddle" angle was chosen to be 120°. In the analysis, both the ground support and the spherical indentor were simulated by analytical rigid surfaces available in ABAQUS.

4.6 Bending process

Once the denting had been completed, the denting results were stored for the next phase of the analysis. This part of the analysis was re-started from the previous analysis using *RESTART* option in ABAQUS. This was done to ensure that the residual stresses introduced as a result of the denting process were carried forward into the second phase of analysis, i.e., loading by a bending moment. The restart input

file contains four steps and these can be summarized as follows:

1. Remove the rigid support surface and the indenter support using, MODEL CHANGE parameter.

2. Fix one node, i.e, NC (see Fig.(3.5)), to prevent any rigid body motion.

3. Apply either moment or pressure (M or p), or a combination of two.

4. Apply Riks method for nonlinear analysis to determine the corresponding plastic loads.

For combined loading, plastic loads, for either pressure or moment, are used to plot the interaction diagrams. Figure (4.4) shows plot of load versus centre node displacement for two models of material properties, i.e., for elastic-perfectly plastic model of material and for full stress-strain model of material. There is not a great deal of variation between these two curves for the loading parts. However, there is a large difference in the unloading part, and, in particular, in the residual dent depth. The Huber-Mises-Hencky yield criterion was used throughout the cycle and, for the unloading path, isotropic hardening was assumed for the full stress strain model. In the latter case, the non-linear geometry *NLGEOM* option in ABAQUS has been used. Figure (4.5) shows the load versus dent depth curves for three different residual dent depth ratios, $(\delta/\mathrm{D}_o)_R = 0.053,\ 0.1$ and 0.14 using full stress strain curve. Additional computing for denting pressurised pipes has also been performed. These values of maximum depth of dents was considered, i.e., $(\frac{\delta}{D_o})_{max} = 0.078,\ 0.155$, and 0.23. After removal of the indenter and release of internal pressure, the residual depths were, $(\frac{\delta}{D_o})_R = 0.06,\ 0.11$, and 0.15. These configurations are to be used for bending. Once the indentor and the rigid support surface had been removed using the MODEL CHANGE parameter in ABAQUS, the design pressure was released. Table (4.1) shows the residual dent depths for both elastic-perfectly plastic material, and for full stress strain curve, prior to and after the release of pressure. Figure (4.6) shows the profile of the residual dent (after pressure release) along its length for both material options. Figures (4.7) and (4.8) illustrate the residual dent profiles for materials given by, full stress strain curve and by, elastic-perfectly plastic material, respectively. It will be seen that the

two dent profiles are significantly different. Thus, from here on the full stress-strain curve will be used in the analysis.

4.7 Moment and pressure loading

4.7.1 Opening and closing bending moment

The dented pipe was subjected to bending moment with zero pressure using the full stress-strain material model and *NLGEOM* option. Bending could be applied in either direction, referred to here as "closing" bending moment or "opening" bending moment, the former being applied such that the dent was on the compression side of the pipe and the latter such that the dent was on the tensile side. Figures (4.9) and (4.10) illustrate the deformation modes for the two bending directions at the last increment of the analysis for, $(\frac{\delta}{D_o})_R = 0.15$. It is clear from Figure (4.9) that closing bending moment tends to magnify the dent depth, thus reducing the strength. For the opening bending moment case, Figure (4.10), plastic buckling/bulging can be seen to have occurred on the compression side.

The results of the previous analysis are plotted in Figure (4.11) which shows bending moment versus rotation for both opening and closing bending moment, for three different dent depths. As can be seen from this figure, the maximum bending moments required for opening are greater than those for closing bending moment and, for both sets of curves, the moment tends thereafter to reduce as the rotation increases. The opening curves plateau and then drop as buckling/bulging occurs at the bottom surfaces. This latter behaviour is almost identical to that of the undented pipe, the latter buckling/bulging at a slightly higher rotation.

Figure (4.12) shows bending moment versus rotation for a dented pipe with internal pressure, $p = 11.2\ MPa$, for three dent depths. These residual dent depths were the values obtained following springback on removal of the indentor and the design pressure. It can be seen by comparing Figures (4.11) and (4.12) that the presence of the design pressure decreases the bending yield strength but increases the ultimate moment carrying capacity of the dented pipe. The opening bending moment and closing bending moment curves in Figure (4.12) are essentially identical and indeed are identical to the

curve for the undented pipe.

4.7.2 Pressure loading

Figure (4.13) shows pressure versus radial displacement, U_2, at the centre of the dent, $(\frac{\delta}{D_o})_R = 0.15$. The ABAQUS analysis was unable to proceed beyond pressure $p = 18.4\ MPa$ due to convergence problems. The Huber-Mises-Hencky limit pressure for an undented pipe is

$$P_{LP} = \frac{2}{\sqrt{3}}\sigma_{yp}\ell n\left(\frac{D_o}{D_i}\right) \tag{4.13}$$

Using the yield and diameter values quoted previously gives a limit pressure of 18.40 MPa, i.e., virtually the same value as the maximum pressure achieved in Figure (4.13). This is not surprising since it is well known that smooth plain dents do not generally reduce the pressure load carrying capacity. What happens is that the pressure tends to push the dent out, thus cancelling its weakening effect. The deformed shape of the dent at, $p = 18.40\ MPa$ is shown in Figure (4.14) and a comparison with Figure (4.7) will show that the dent has recovered significantly but without the pipe regaining complete circularity.

The behaviour of the dented pipe during pressurisation was investigated further. This was carried out by checking the spread of plastic strain in dented pipe. The plastic stain was investigated at points 'A', 'B', 'C', and 'D' as shown in Figure (4.13). The results show that increasing internal pressure increases, the plastic strain as can be seen in Figure (4.15). The maximum plastic strain obtained was, 42%, at the maximum pressure of 18.4 MPa. It is seen that the dent's rim is the weakest point in dent (this observation agrees with finding given in Ref. [68].

4.8 Moment-pressure interaction

Combined loading has been investigated using a residual dent depth of, $(\frac{\delta}{D_o})_R = 0.15$, and the analysis has again used the full stress-strain curve material and the *NLGEOM* option.

4.8.1 Combined opening bending and pressure loading

The dented pipe was subjected to opening bending moment where the surface of the dent was pushed out as a result of both the pressure and opening moment. In Figure (4.16), opening bending moment was applied to the dented pipe at different internal pressure levels, i.e., 0.0 P_{LP}, 0.2 P_{LP}, 0.4 P_{LP}, 0.6 P_{LP}, 0.8 P_{LP}, and 0.97 P_{LP} where P_{LP} = 18.4 MPa is the plain pipe, Huber-Mises-Hencky, limit pressure given by equation (4.13).

The procedure was first to pressurise the dented pipe to the required internal pressure and then to apply a bending moment. The dented shape with no internal pressure (as in Figure (4.11)) showed increasing strength as the bending rotation increased up to 6° (0.1 rad) and after that it started to drop off due to buckling/bulging as discussed above. The dented pipe with different internal pressure levels shows a continuing increase in the pipe strength up to 14° (0.25 rad) in all cases as the bending rotation increases, see Figure (4.16).

Figure (4.17) shows pressure versus centre displacement, U_2, for different bending moment values, i.e., 0.0 M_{LP}, 0.2 M_{LP}, 0.4 M_{LP} 0.6 M_{LP}, 0.8 M_{LP}, 0.9 M_{LP}, and 0.97 M_{LP}, where M_{LP} = 4.412 kNm which is the plain pipe limit moment given by: $M_{LP} = D_m^2\ t\ \sigma_{yp}$.

The bending moment was applied first as a constant moment and in the second step the pressure was applied to the dented pipe. All nonlinear analyses were performed using the *RIKS* method. Figure (4.17) shows that the dent depths are reduced as the pressure increases. All curves tend to converge towards the same path, in some cases the dent depth has completely recovered although there is some residual deformation. Note that all of these curves started from different points due to the fact that the applied moment at the first step, had different magnitudes.

The main criterion employed here in assessing plastic loads from Figures (4.16) and (4.17) for constructing interaction diagrams was the well-known *ASME* [5] twice elastic slope method (see Figure (1.5)). However, in some load/deformation plots where there is a plateau, e.g., Figure (4.16) the five times elastic slope criterion has also been used to ensure that the plastic load is reasonably on the plateau region. The twice

elastic slop and five times elastic slope criteria are considered to be useful in providing plastic load levels beyond which deformations become excessive. Both plastic pressure and moment (based on twice elastic, and five times elastic slope values), have been normalised using the relevant limit loads P_{LP} and M_{LP} for plain, undented pipe.

The interaction diagrams are presented in Figure (4.18). This figure shows that the interaction is essentially circular in form for both criteria when pressure loading is applied first. However, when moment is applied first, the twice elastic slope criterion results in an almost linear relationship up to $\frac{M}{M_{LP}} = 0.8$. The equation of the best-fit straight line for these five points is;

$$\frac{p}{P_{LP}} = 0.685 - 0.194\left(\frac{M}{M_{LP}}\right) \tag{4.14}$$

Two additional levels of moment beyond $\frac{M}{M_{LP}} = 0.8$ were run, i.e., $\frac{M}{M_{LP}} = 0.9$, and $\frac{M}{M_{LP}} = 0.97$, and the results are given in Figure (4.17). However, it was not possible to use either of the elastic slope method on these curves to obtain plastic loads since the twice elastic slope and five times elastic slope lines do not intersect the response curves obtained from ABAQUS. The points are thus not presented in Figure (4.18).

4.8.2 Combined closing bending and pressure loading

Closing bending moment was applied to the dented pipe with different pressure levels, i.e., 0.0 P_{LP}, 0.2 P_{LP}, 0.4 P_{LP}, 0.6 P_{LP}, 0.8 P_{LP}, and 0.97 P_{LP}, where P_{LP} = 18.40 MPa as before. The moment versus rotation curves are presented in Figure (4.19). As before, the procedure was to pressurise the dented pipe to the required internal pressure and then to apply an increasing bending moment until gross deformation occurred. The dented shape with internal pressure in the cases of 0.4 P_{LP}, 0.6 P_{LP}, 0.8 P_{LP}, and 0.97P_{LP} show an increasing bending strength as the bending rotation increases whereas cases 0.2 P_{LP}, and 0.0P_{LP} show a sharp drop beyond maximum bending moment as the bending rotation increases.

Figure (4.20) depicts pressure versus centre node displacement, U_2, for different bending moment levels, i.e., for 0.0 M_{LP}, 0.2 M_{LP}, 0.4 M_{LP}, 0.6 M_{LP}, 0.8 M_{LP}, and 0.825 M_{LP}. In this case the closing bending moment was applied first and kept constant and then the dented pipe was pressurised incrementally using the $RIKS$ method. The

figure shows that the dent started to recover as the pressure increased and all curves tend towards the same path. In some cases the dent depth has completely recovered. As before, all of these curves started from different points due to the moment of different magnitudes being applied at the first step. In conclusion, the closing bending moment has little influence on the pressure loading, the twice elastic slope or five times elastic slope methods gave essentially the same values for all the curves.

The twice elastic slope criterion has been applied to the response curve shown in Figure (4.19) and the resulting interaction diagram for the situation where pressure is applied first, is given in Figure (4.21). The moment-applied-first points from Figure (4.20) are also included. The best fit line for the five points between $(\frac{M}{M_{LP}}) = 0.0$, and 0.8 was found to be horizontal at a level of, $(\frac{P}{P_{LP}}) = 0.675$.

4.9 Discussion

To some extent, the results have been discussed as they have been presented. However an attempt will be made here to emphases the more important outcomes of the work.

Firstly, the load versus dent depth curves in Figures (4.4) and (4.5) are typical of those produced by other investigators. The present results have indicated that the use of elastic-perfectly plastic material properties will not produce a representative residual dent and thus the full stress-strain curve should be used in this type of analyses.

The results for bending of dented pipes without internal pressure are presented in Figure (4.11). For opening bending moment, the maximum moment for all dent depths was of the same order as the limit moment of an undented pipe (4.412 kNm). In each of the three opening bending moment models, buckling occurred on the compression side, but only after the plastic load had been established. The strength of dented pipes under closing bending moment is significantly influenced by the presence of the dents. The maximum moment for the, $(\frac{\delta}{D_o})_R = 0.15$, case being about, 15%, lower than the limit moment for an undented pipe. Also, the situation is unstable, since the moment levels drop off quickly as the dents collapse inwards.

The influence of the presence of design pressure on the moment carrying ca-

pacity of dented pipes is interesting. Figure (4.12) shows that the behaviour was not dependent either on dent depth or whether opening bending moment or closing bending moment were applied. In each case, the curves reached a plateau at about, 15%, below the undented pipe limit moment (4.412 kNm), and before eventually achieving moment levels of about the same magnitude as that of the plain pipe value.

The pressure versus dent-centre radial displacement is shown in Figure (4.13). As explained previously, the ABAQUS analysis could not proceed beyond the limit pressure for undented pipes due to convergence problems. This means that the strain-hardening section of the stress-strain curve, Figure (3.7), has not been utilized. By excluding the *NLGEOM* feature, the maximum pressure achieved was, 33.0 MPa, which is a better representation of pressure carrying capacity. However, Figure (4.13) is sufficient to provide the ASME's twice elastic slope and five times elastic slope pressures.

From Figure (4.16), the opening bending moment carrying capacity of, $(\frac{\delta}{D_o})_R = 0.15$, pipe is considerably influenced by the level of internal pressure. The curves are such that either the twice elastic slope or five times elastic slope criteria can be used to establish plastic loads. The latter perhaps being more relevant since the plastic loads are then on the plateaus of the curves. The twice elastic slope and five times elastic slope plastic moments from Figure (4.16) are used to plot the interaction diagrams in Figure (4.18). Both criteria, with pressure applied first, give essentially circular interaction, i.e.

$$(\frac{p}{P_{PL}})^2 + (\frac{M}{M_{LP}})^2 = 1.0 \tag{4.15}$$

With moment applied first, the opening bending moment results are as in Figure (4.17) with an interaction diagram in Figure (4.18) that is no longer circular, but linear in form, at least up to, $\frac{M}{M_{LP}} = 0.8$. The equation of this line was given before as Equation (4.14).

For closing bending moment, the moment versus rotation curves for different pressure levels are given in Figure (4.19). For this data, only the twice elastic slope criterion is used for plastic loads. For the p = $0.0P_{LP}$, and $0.2P_{LP}$ curves, the twice elastic slope plastic moments are not much different from the peak moments achieved.

The interaction diagram in Figure (4.21), for pressure applied first, again tends towards circular but with the moment only value of, M/M_{LP}, being significantly less than unity. For moment loading applied first, the pressure carrying capacity is unaffected, at least for up to, $M/M_{LP} = 0.8$.

4.10 Summary

The following conclusions on the behaviour of dented pipes under pressure and / or moment loading are listed:

- In the FE modelling of the behaviour of dented pipes, it is essential to use the full stress-strain material model.
- The results confirm that the behaviour of dented pipes under moment loading only is dependent on whether the dent is on the compression (closing bending moment) or tension (opening bending moment) side of the pipe. Dented pipes are stronger under opening bending than under closing bending. For opening bending, plastic buckling/bulging occurs on the compression side of the pipe as gross deformation develops.
- For opening bending, the presence of internal pressure decreases the yield moment but increases the ultimate moment carrying capacity by preventing buckling/bulging from occurring opposite the dent. For closing bending, the presence of pressure is more complex in that, for low pressure levels both the yield and ultimate moment capacities are increased, whereas for higher pressures, yield moments are significantly reduced while ultimate moments are significantly increased.
- Plastic load interaction diagrams for combined internal pressure and moment loading have been presented for both opening and closing bending applications. When pressure was applied first, the interaction diagrams were of essentially circular form whereas, when bending moment was applied first, the interactions were linear in form. It appears that damage assessment guidelines would need to take both of these results into account.

Material model	$(\frac{\delta}{D_o})_R$, $p = 0.0$	$(\frac{\delta}{D_o})_R$, $p = 11.2\ MPa$
Full stress – strain curve	0.150	0.142
Elastic/perfectly plastic material	0.055	0.050

Table 4.1: The influence of material modelling and pressure on the residual depth of a dent, $(\frac{\delta}{D_o})_R$.

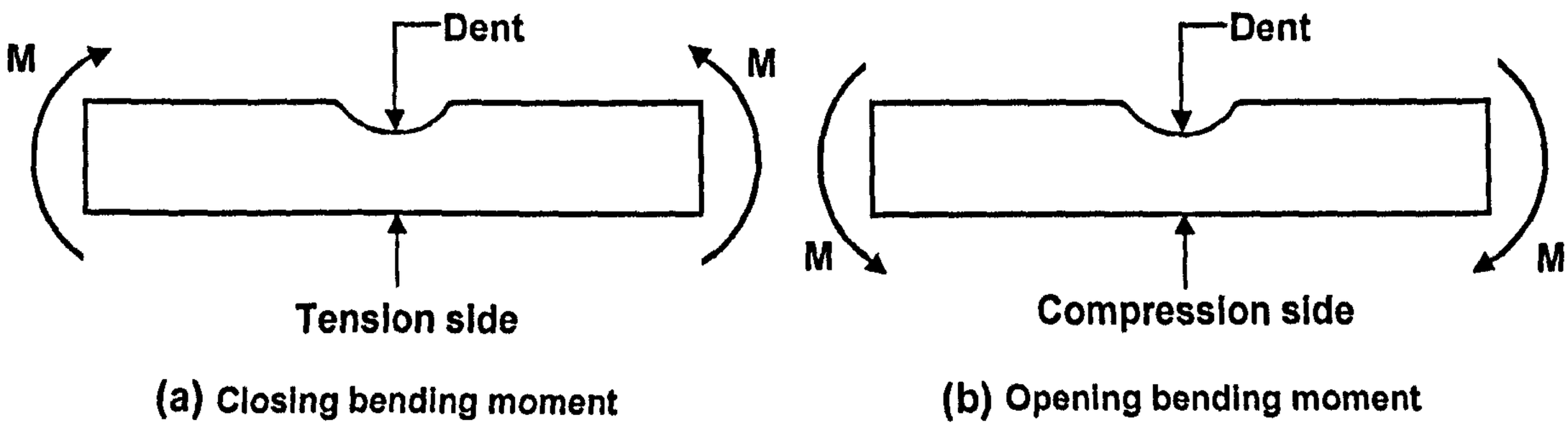

Figure 4.1: Direction of bending moment: the left figure illustrates closing bending moment, and the right sketch illustrates opening bending moment.

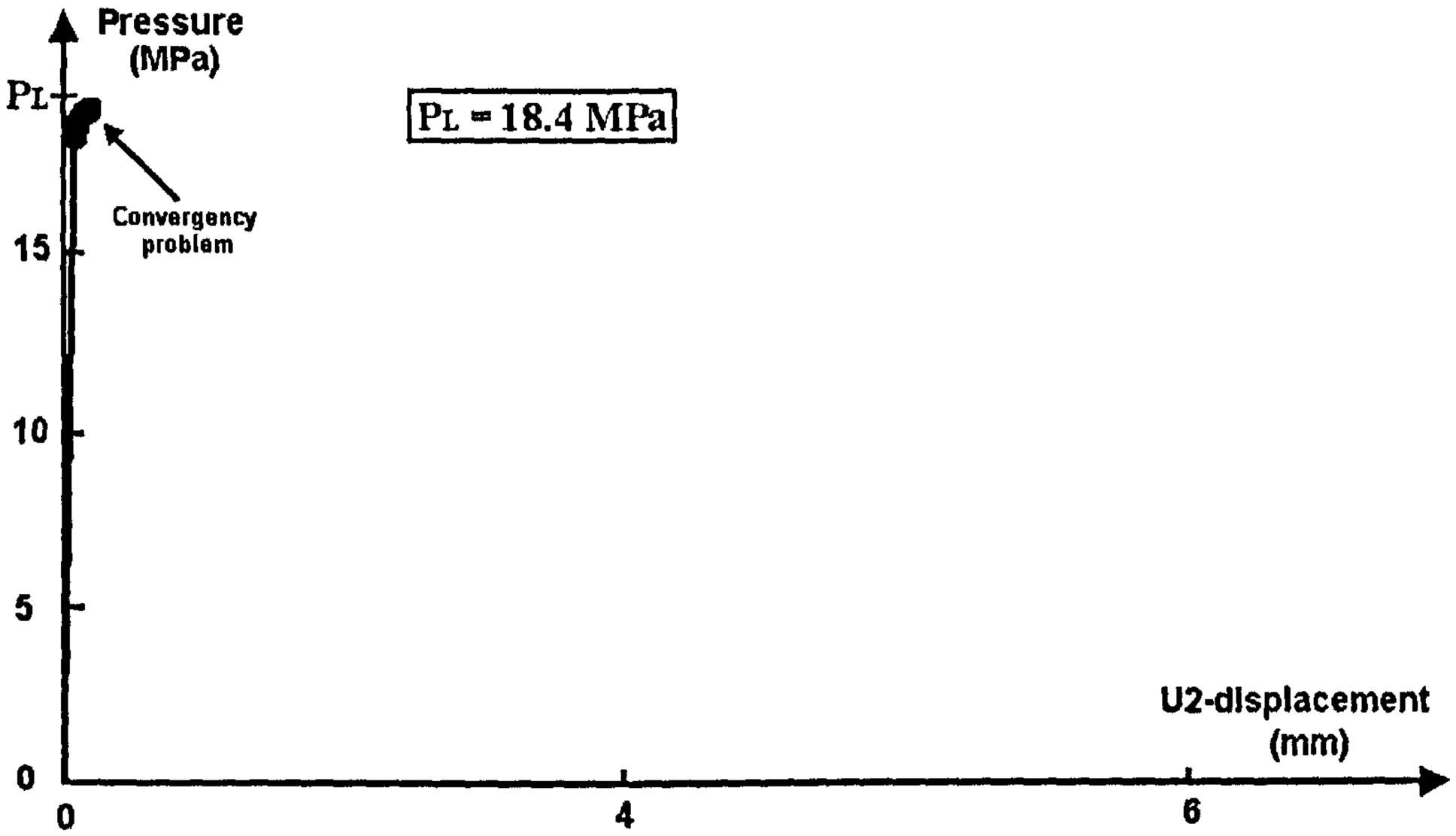

Figure 4.2: Plot of pressure versus centre node displacement using *Riks* method, for $\frac{2L}{D_o} = 6.0$, and $\frac{a}{b} = 1.0$.

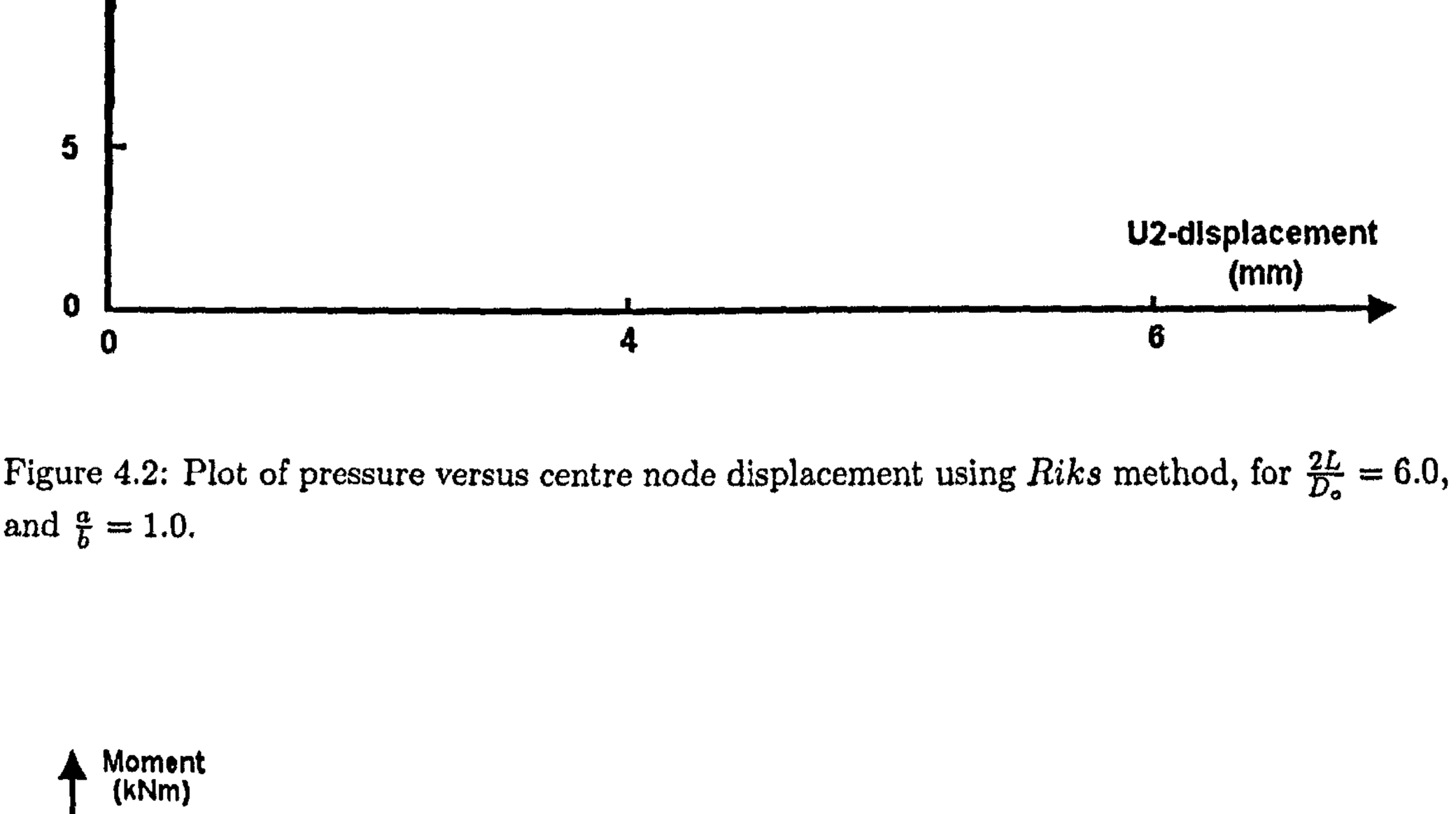

Figure 4.3: Plot of moment versus angular rotation using *Riks* and Multi-Point Constraint option in ABAQUS. Also, $\frac{2L}{D_o} = 6.0$, and $p = 0.0$.

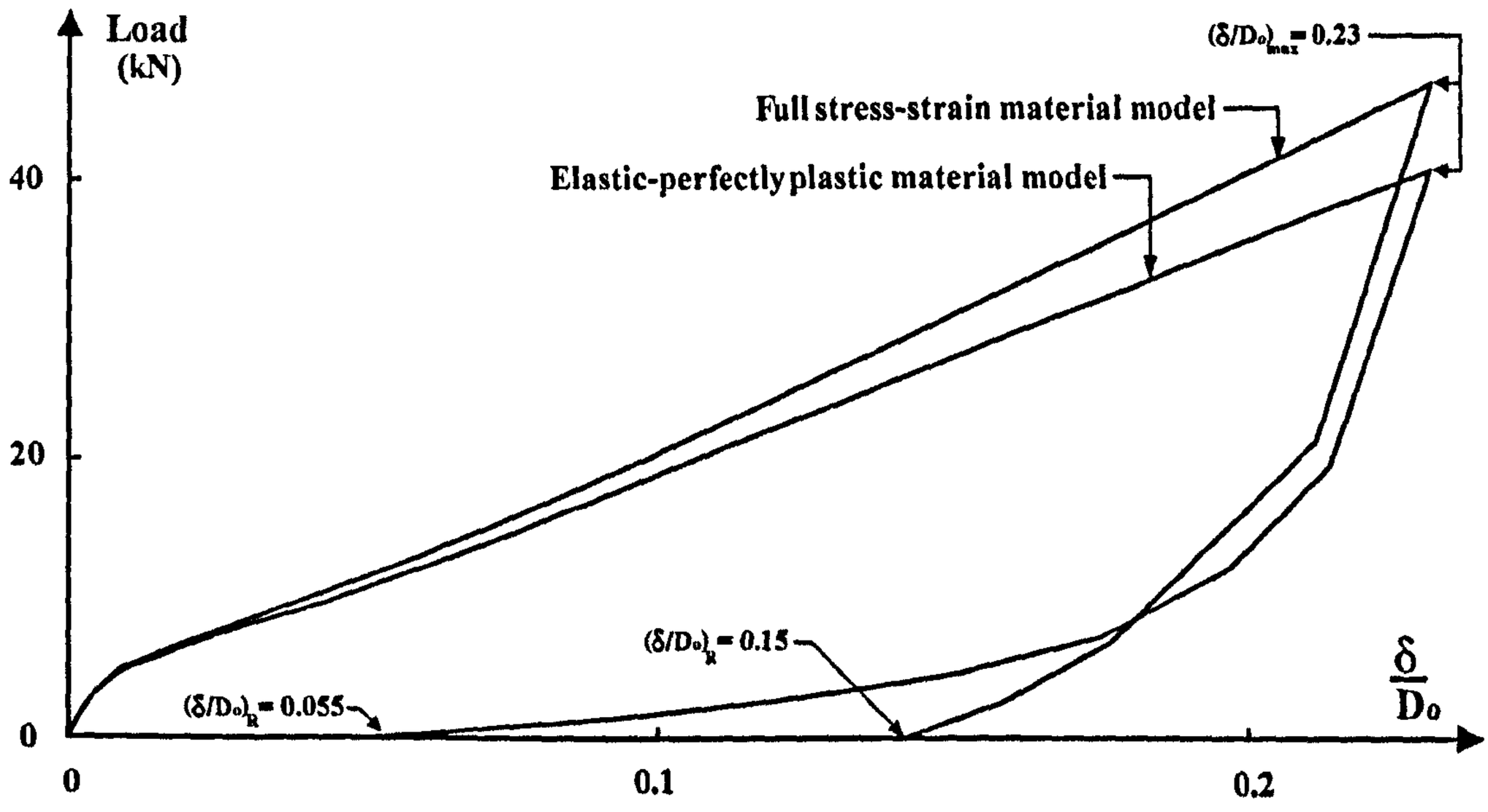

Figure 4.4: Plot of denting load versus dent depth for two types of material modelling, i.e., for elastic/perfectly plastic and for full stress strain curve. Also, $\frac{a}{b} = 1.0$, $\frac{2L}{D_o} = 6.0$, and $p = 11.2\ MPa$.

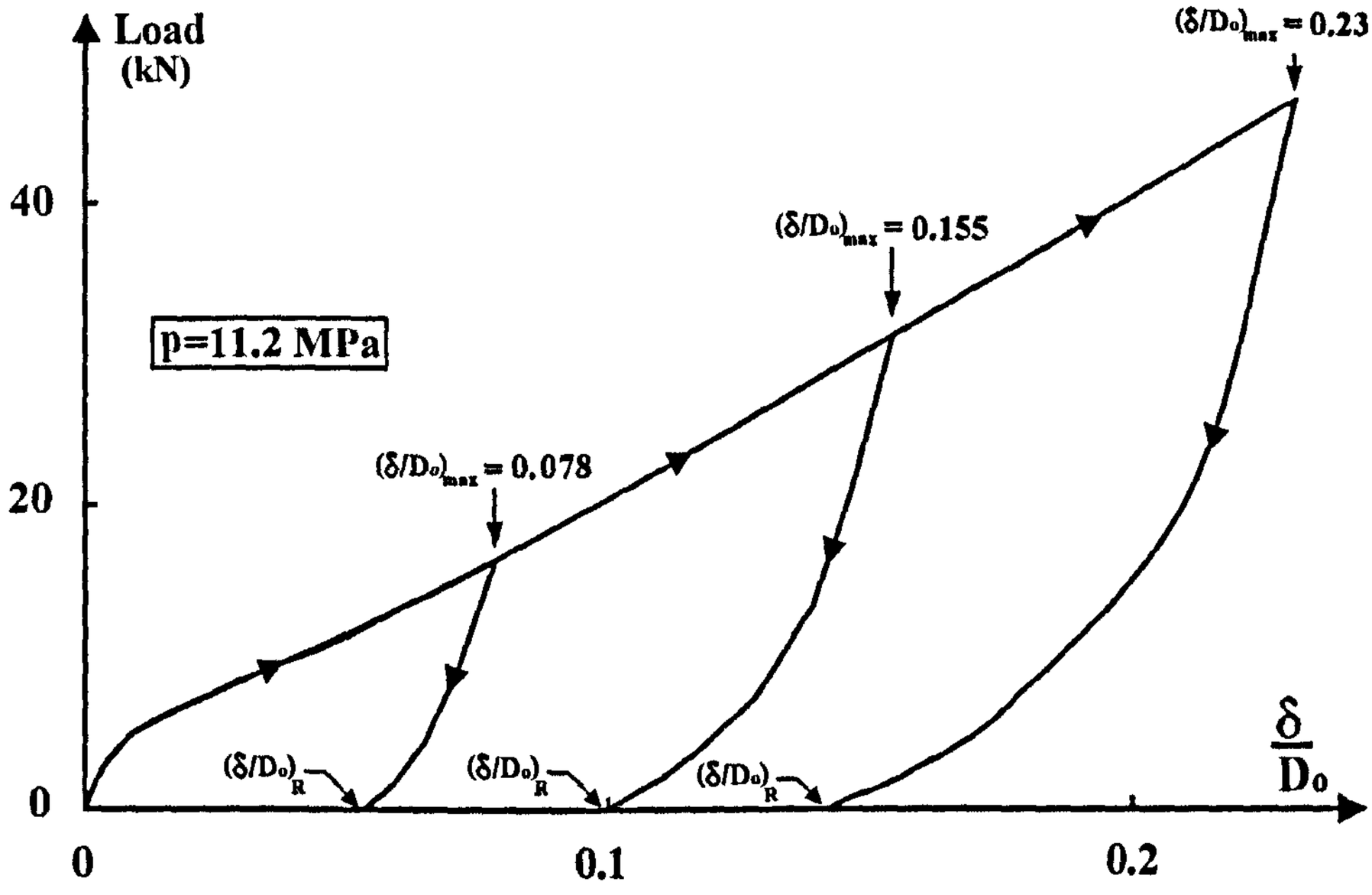

Figure 4.5: Different residual dent depths, $\left(\frac{\delta}{Do}\right)_R$, obtained for full stress-strain modelling of material. Also, $\frac{a}{b} = 1.0$, $\frac{2L}{D_o} = 6.0$, and $p = 11.2\ MPa$.

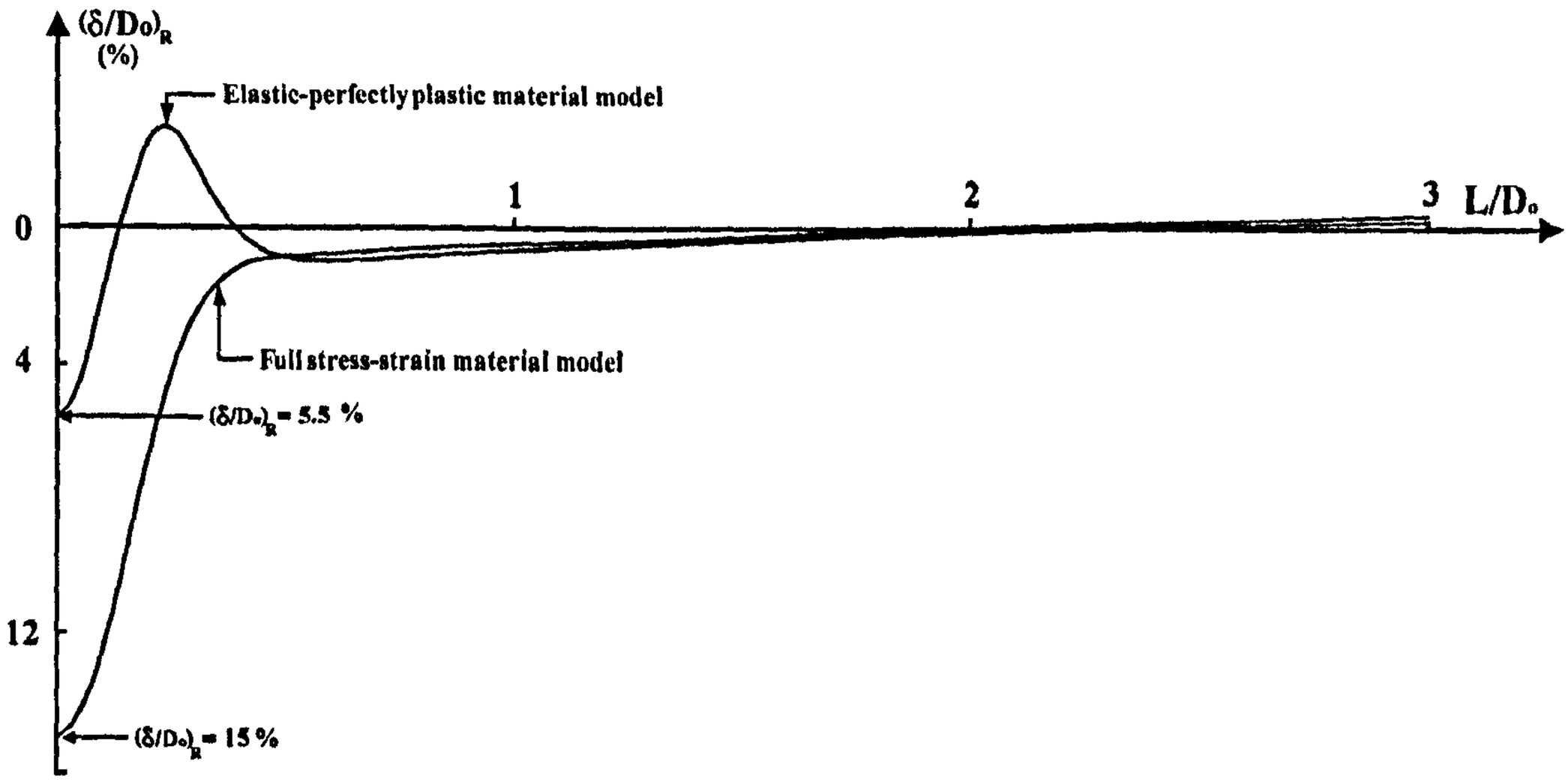

Figure 4.6: Residual dent profile in axial direction after release of internal pressure for both elastic/perfectly plastic and for full stress-strain curve. Also, $\frac{2L}{D_o} = 6.0$, and $p = 11.2\ MPa$.

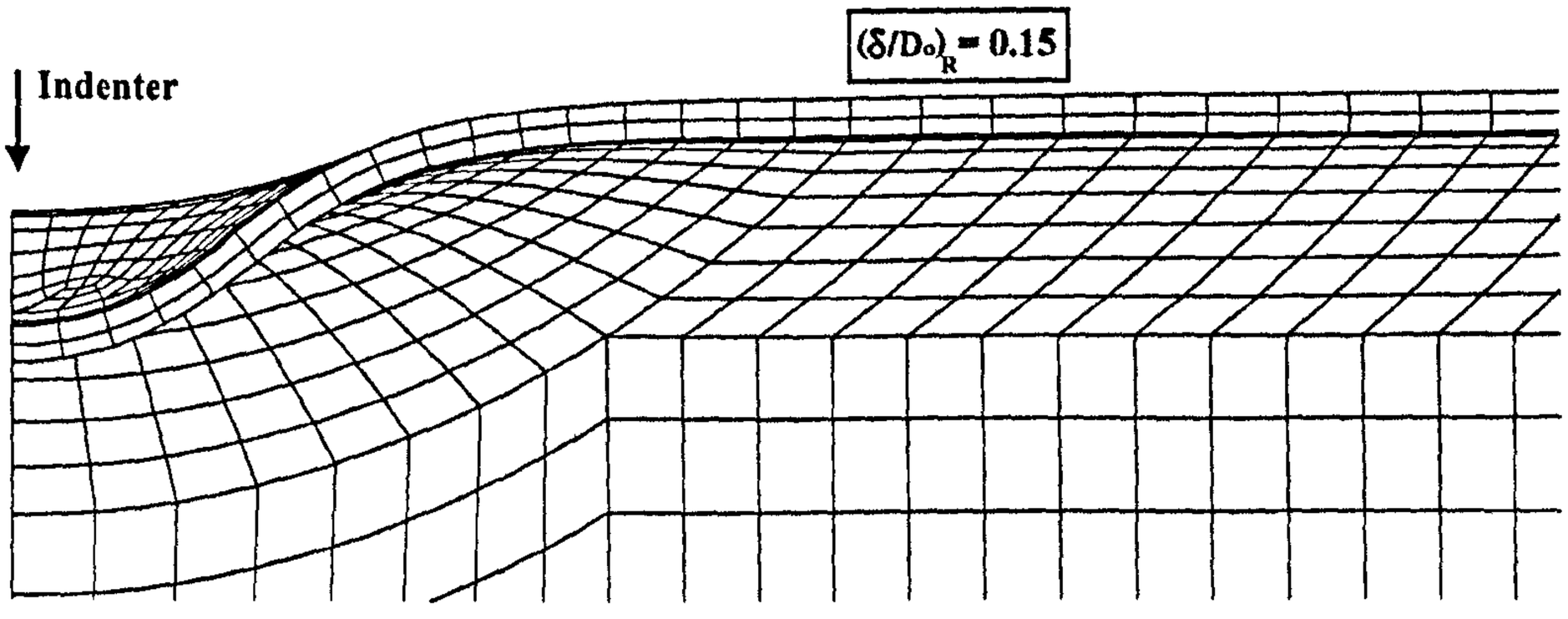

Figure 4.7: View of the residual dent shape after denting with full stress-strain material. Also, $p = 11.2\ MPa$, $\frac{2L}{D_o} = 6.0$, and $\frac{a}{b} = 1.0$.

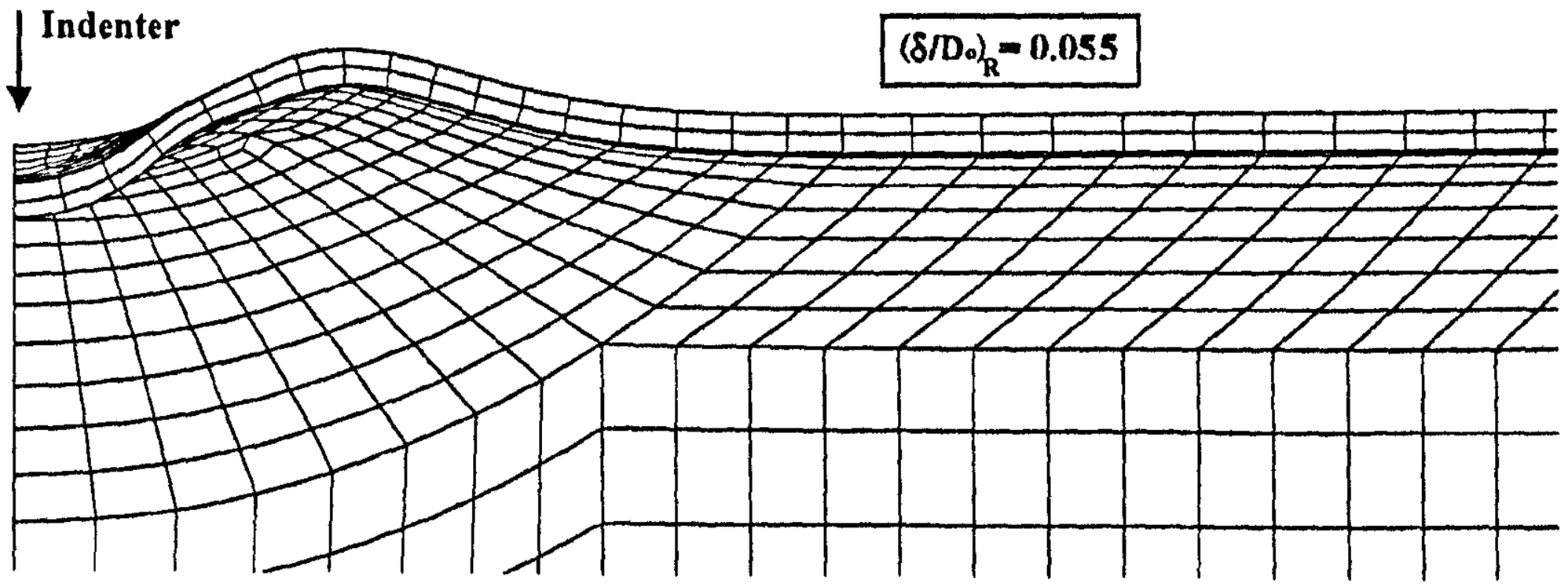

Figure 4.8: Zoomed area of the residual dent shape after denting with elastic/perfectly plastic material. Also, $p = 11.2\ MPa$, $\frac{2L}{D_o} = 6.0$, and $\frac{a}{b} = 1.0$.

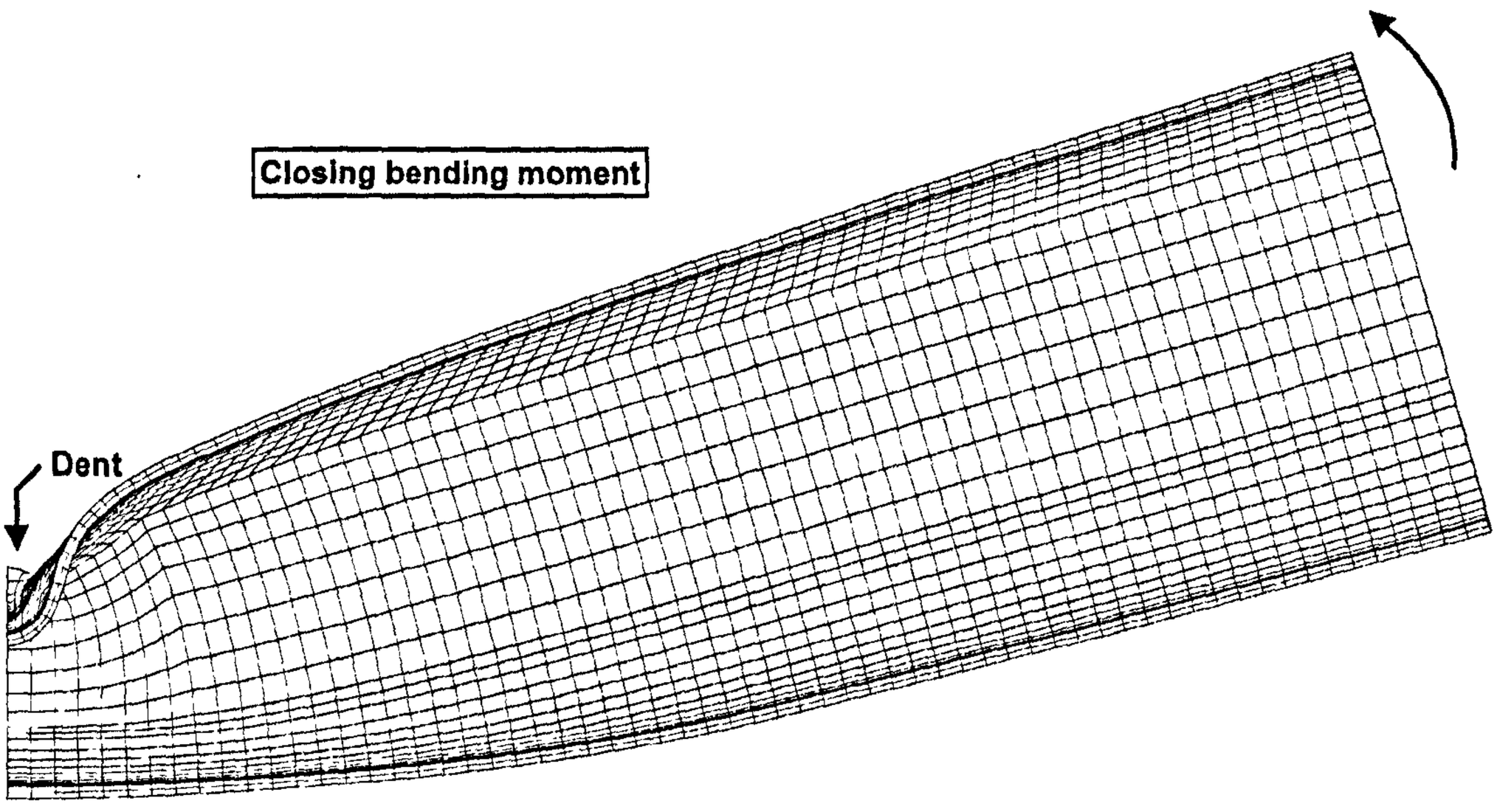

Figure 4.9: Influence of bending on dented pipe with, $(\frac{\delta}{D_o})_R = 0.15$, $\frac{2L}{D_o} = 6.0$. Results are shown for closing bending mode (see sketch in Figure 4.1a for description of moment).

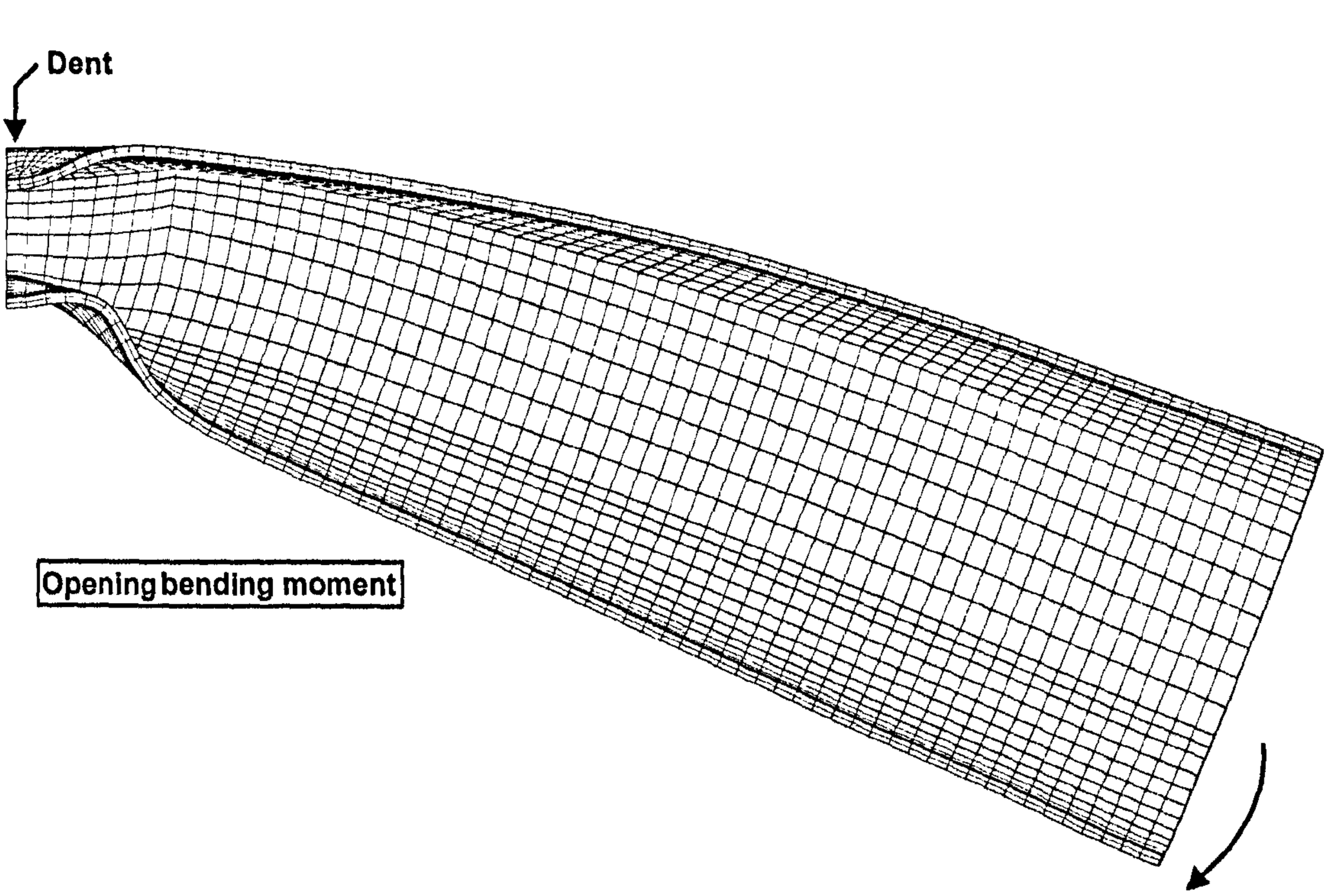

Figure 4.10: Influence of bending on dented pipe with, $(\frac{\delta}{D_o})_R = 0.15$, $\frac{2L}{D_o} = 6.0$. Results shown are for the opening bending mode (see sketch in Figure 4.1b for description of moment).

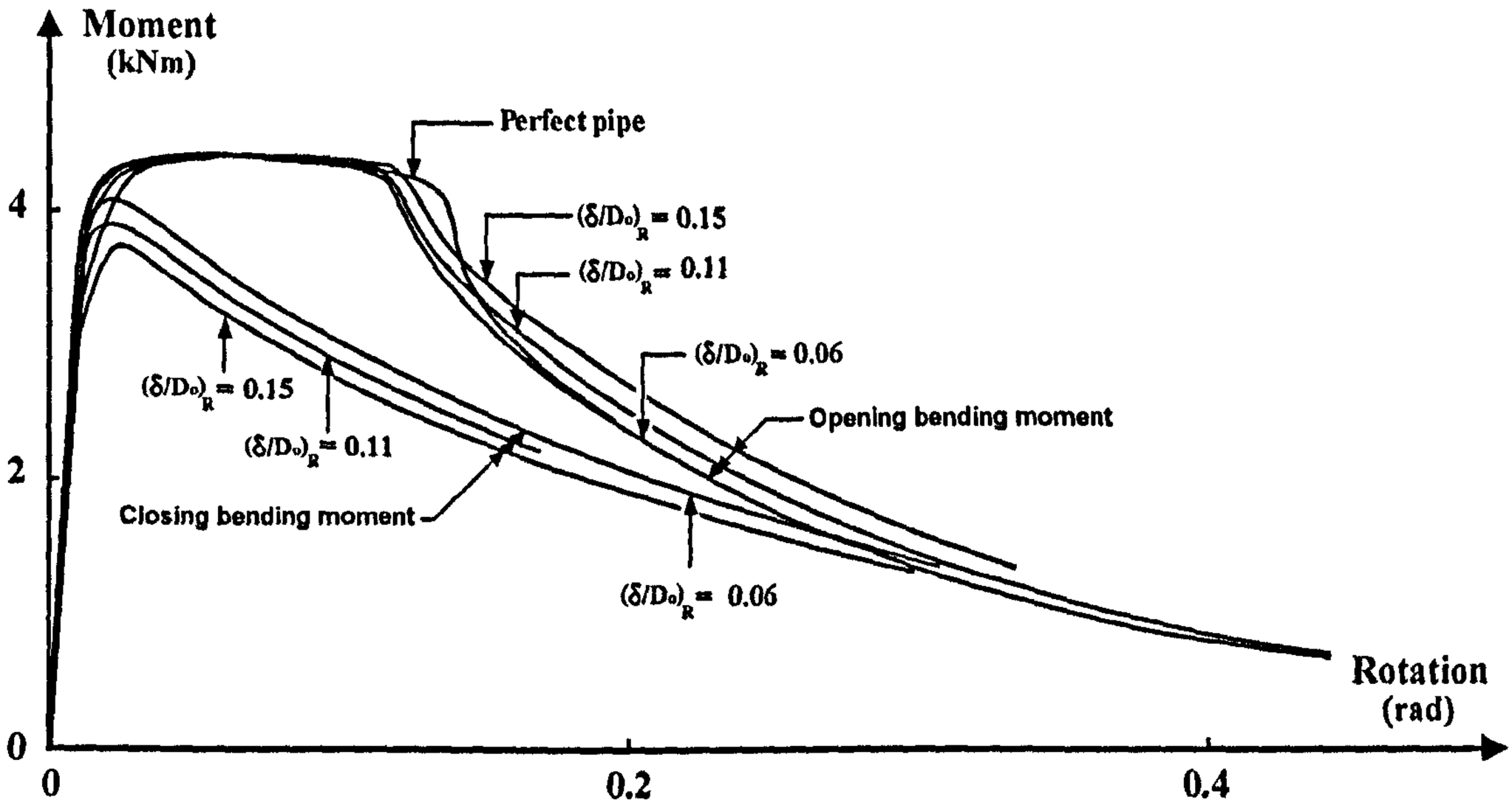

Figure 4.11: Opening and closing moments versus pipe rotation for different dent depths. Also, $p = 0.0$, and $\frac{2L}{D_o} = 6.0$.

Figure 4.12: Opening and closing moments versus pipe rotation for different dent depths. Also, $p = 11.2\ MPa$, and $\frac{2L}{D_o} = 6.0$.

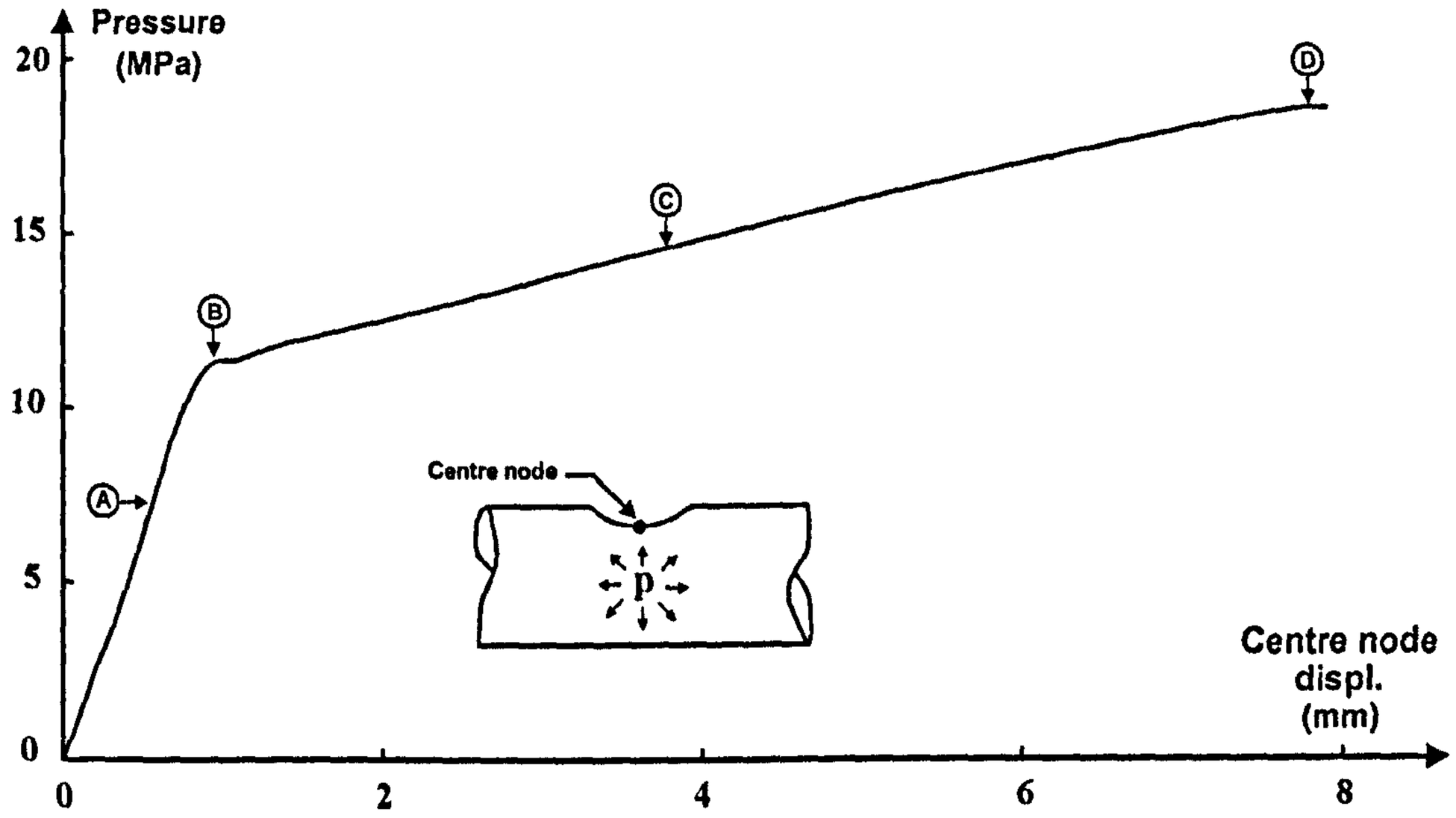

Figure 4.13: Pressure versus centre node displacement for dented pipe. Also, $\frac{2L}{D_o} = 6.0$. Pipe was initially dented to, $\left(\frac{\delta}{D_o}\right)_R = 0.15$. Points 'A', 'B', 'C', and 'D' were used for checking the plastic strain - see Figure (4.15).

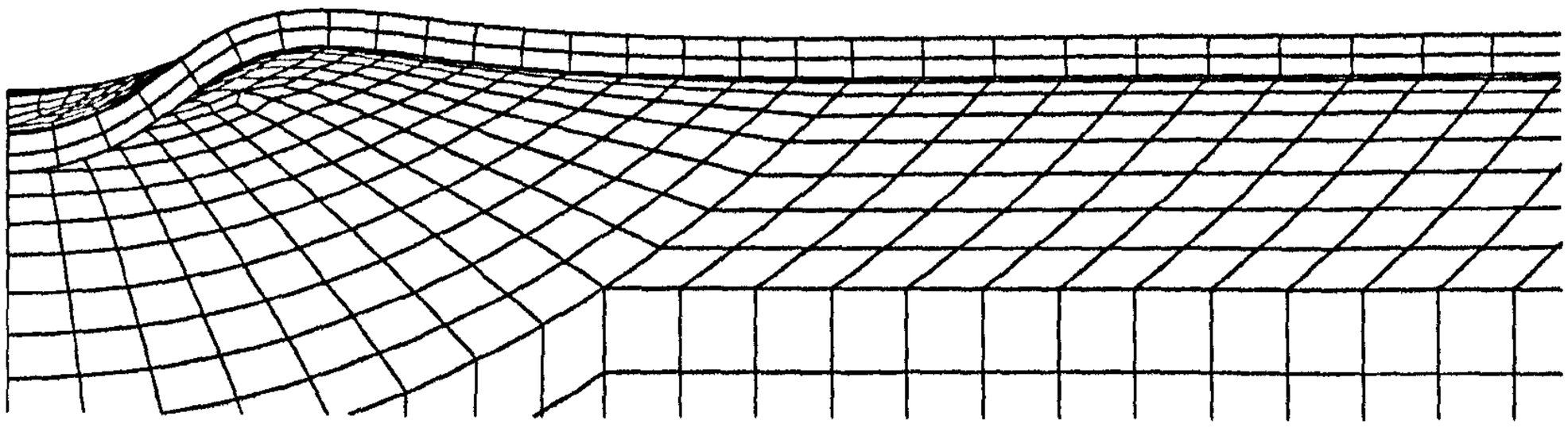

Figure 4.14: Closer view of the dented area once the limit pressure, $P_L = 18.4\ MPa$, was applied to residual dent shape. Also, $\frac{2L}{D_o} = 6.0$, and $\left(\frac{\delta}{D_o}\right)_R = 0.15$.

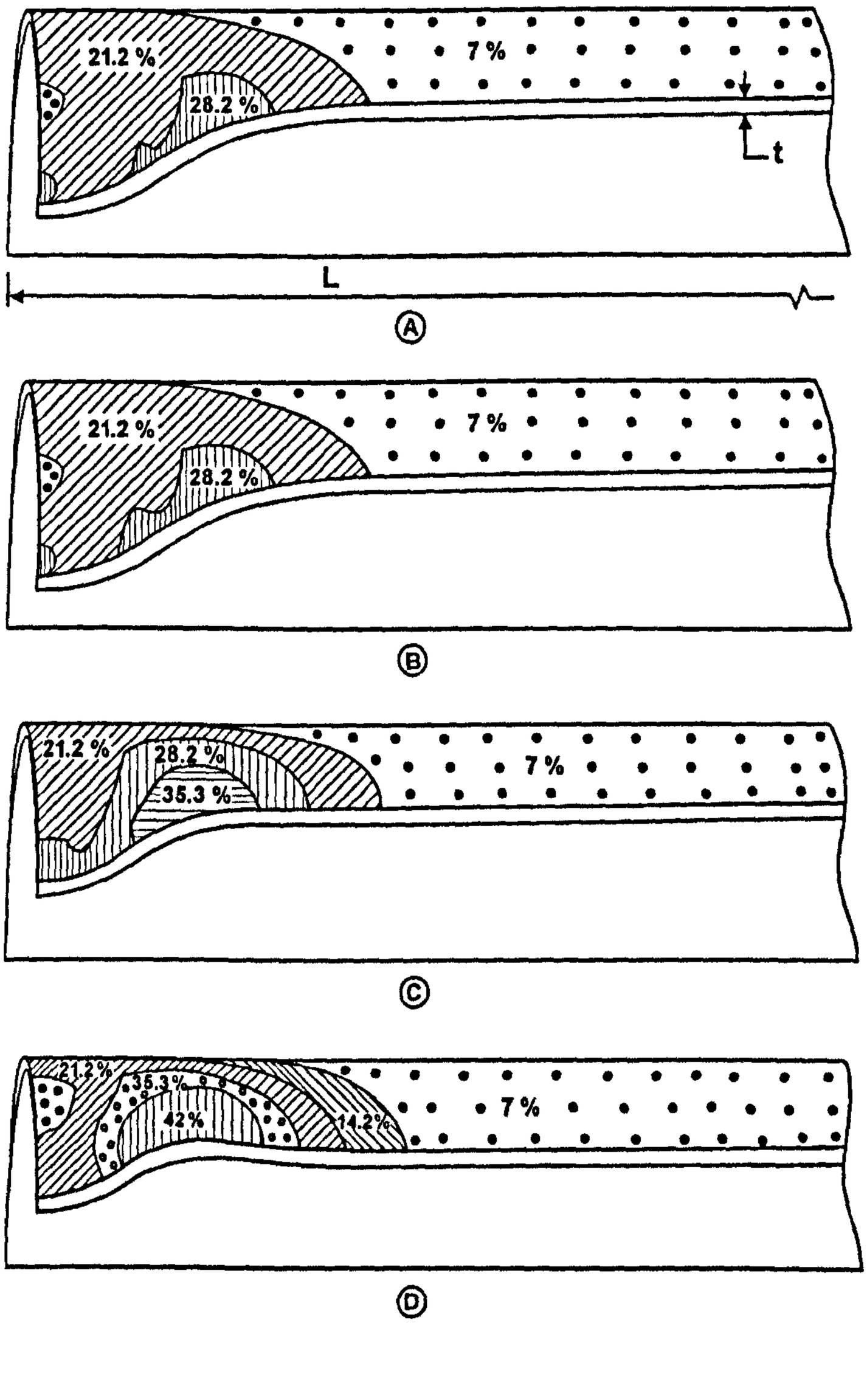

Figure 4.15: Closer view of the dented area showing spread of plastic strain at different stages of pressurisation. Also, the limit pressure was, $P_L = 18.4\ MPa$, $\frac{2L}{D_o} = 6.0$, and $\left(\frac{\delta}{Do}\right)_R = 0.15$. Points 'A', 'B', 'C', and 'D' correspond to points on Figure (4.13).

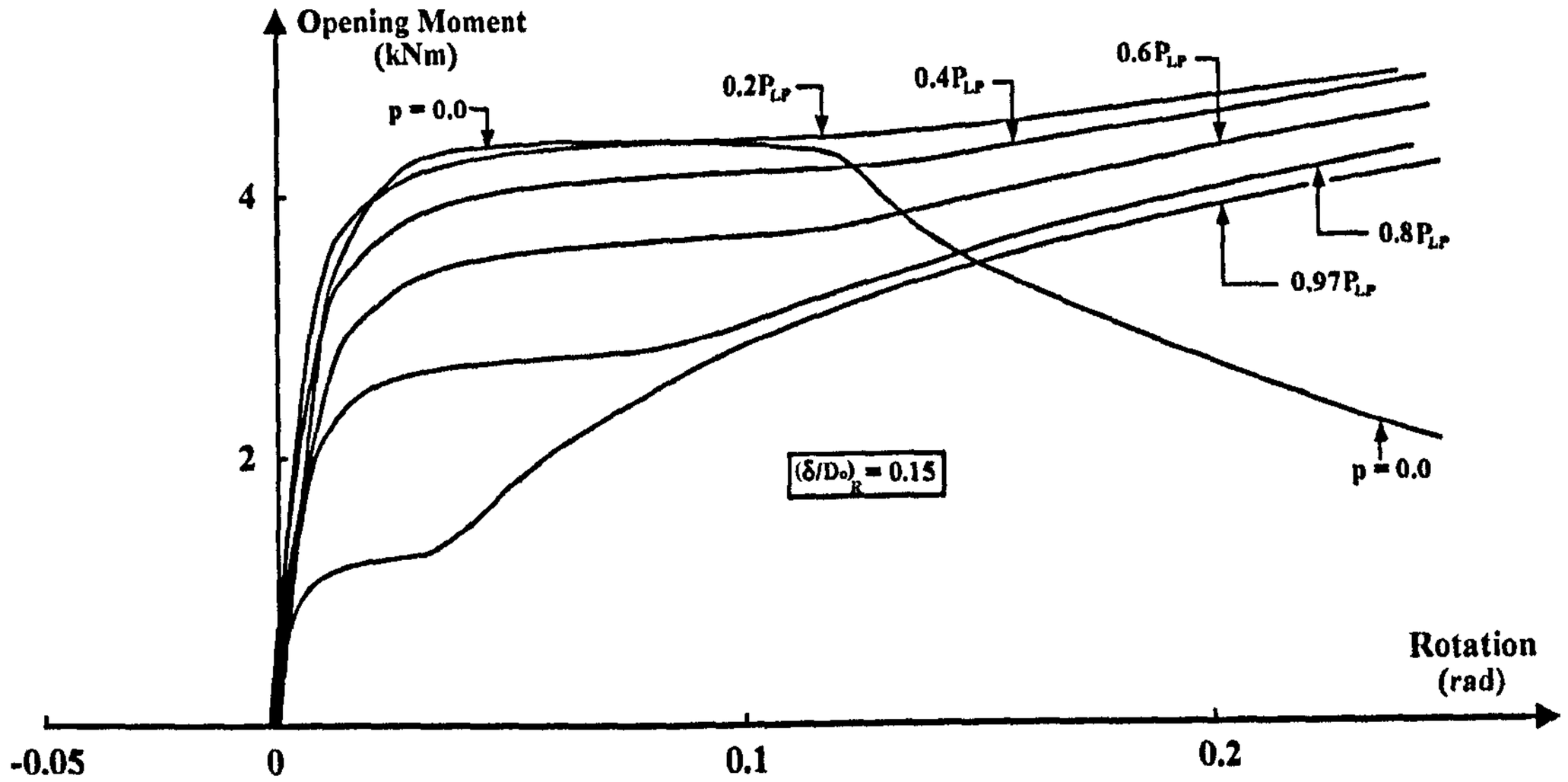

Figure 4.16: Opening bending moment versus rotation for different initial pressure levels of P_{LP}, ($P_{LP} = 18.4\ MPa$). Also, $\frac{2L}{D_o} = 6.0$.

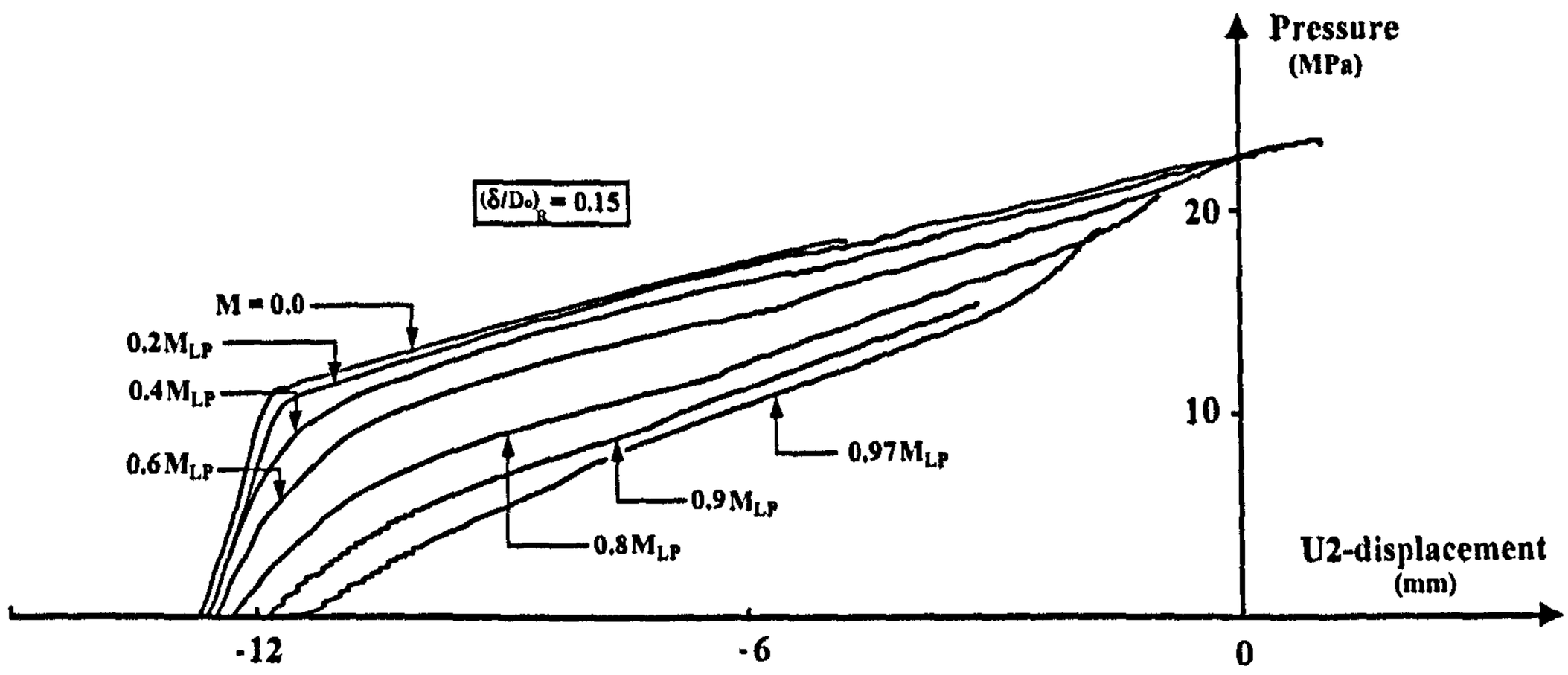

Figure 4.17: Pressure versus centre node displacement for different initial levels of open bending loading ($M_{LP} = 4412\ Nm$). Also, $\frac{2L}{D_o} = 6.0$.

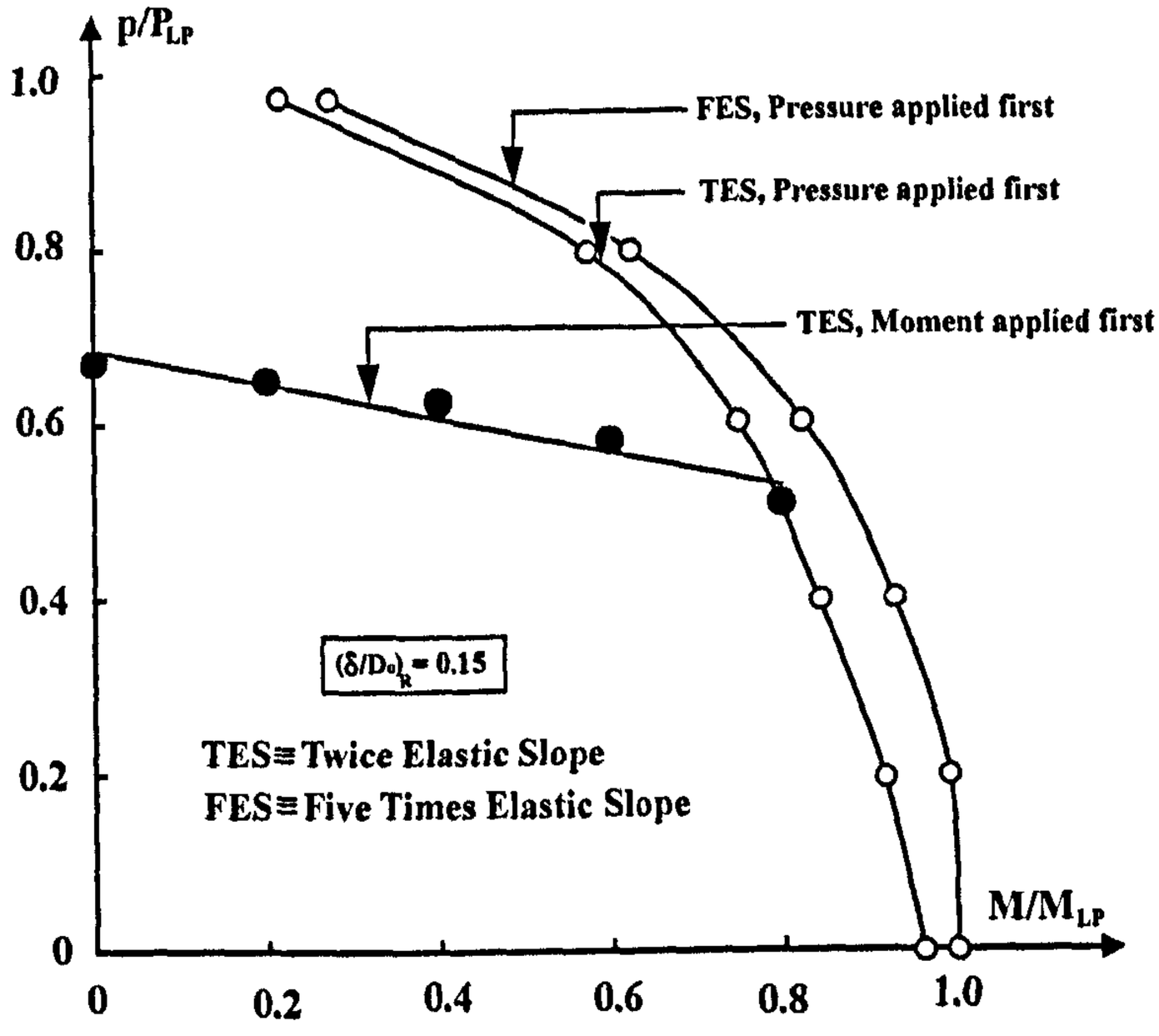

Figure 4.18: Interaction diagrams for pressure and open bending loading for dented pipe. Also, $\frac{2L}{D_o} = 6.0$.

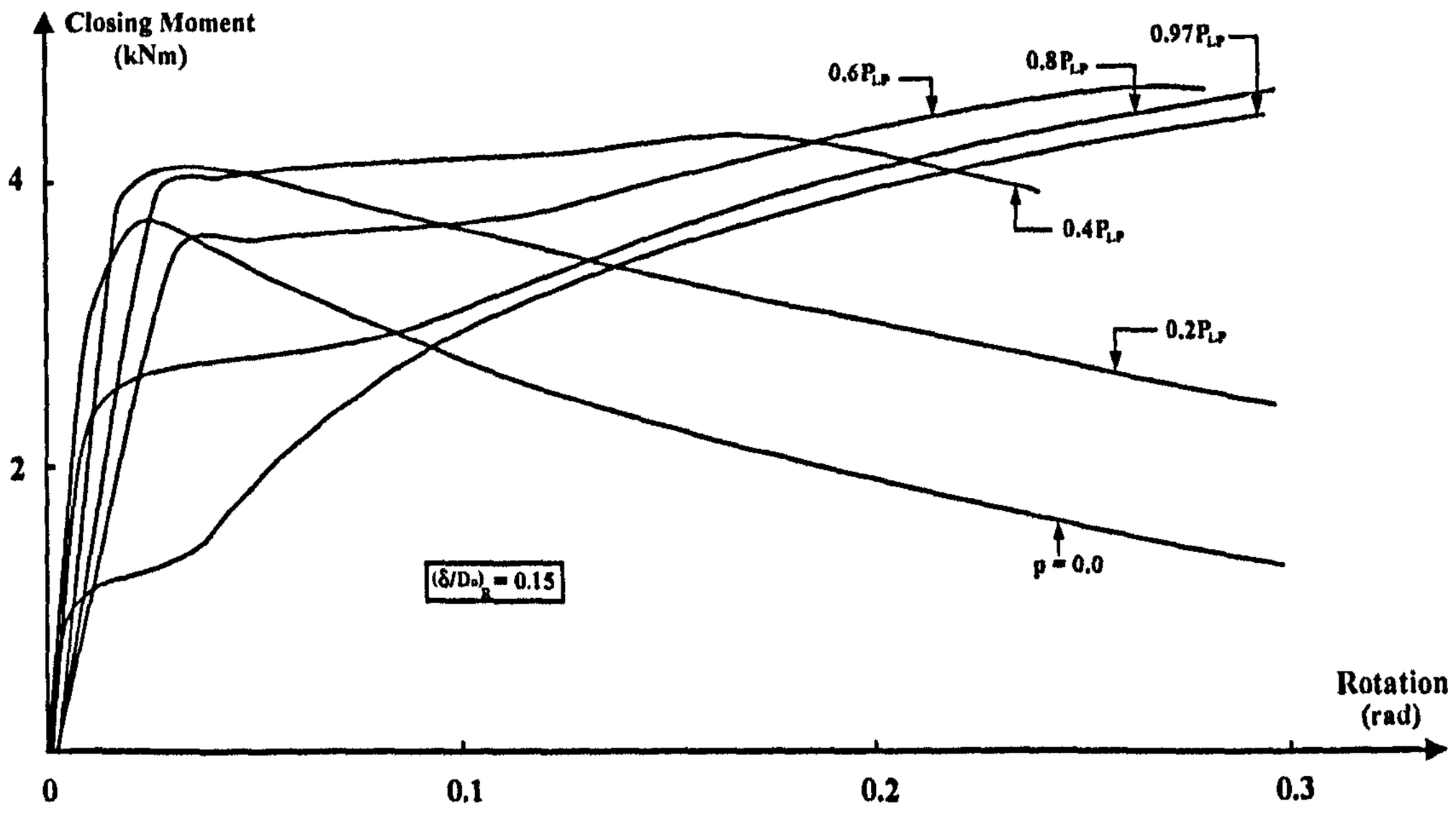

Figure 4.19: Closing bending moment versus pipe rotation for different initial pressure levels ($P_{LP} = 18.4\ MPa$). Also, $(\frac{\delta}{D_o})_R = 0.15$, and $\frac{2L}{D_o} = 6.0$.

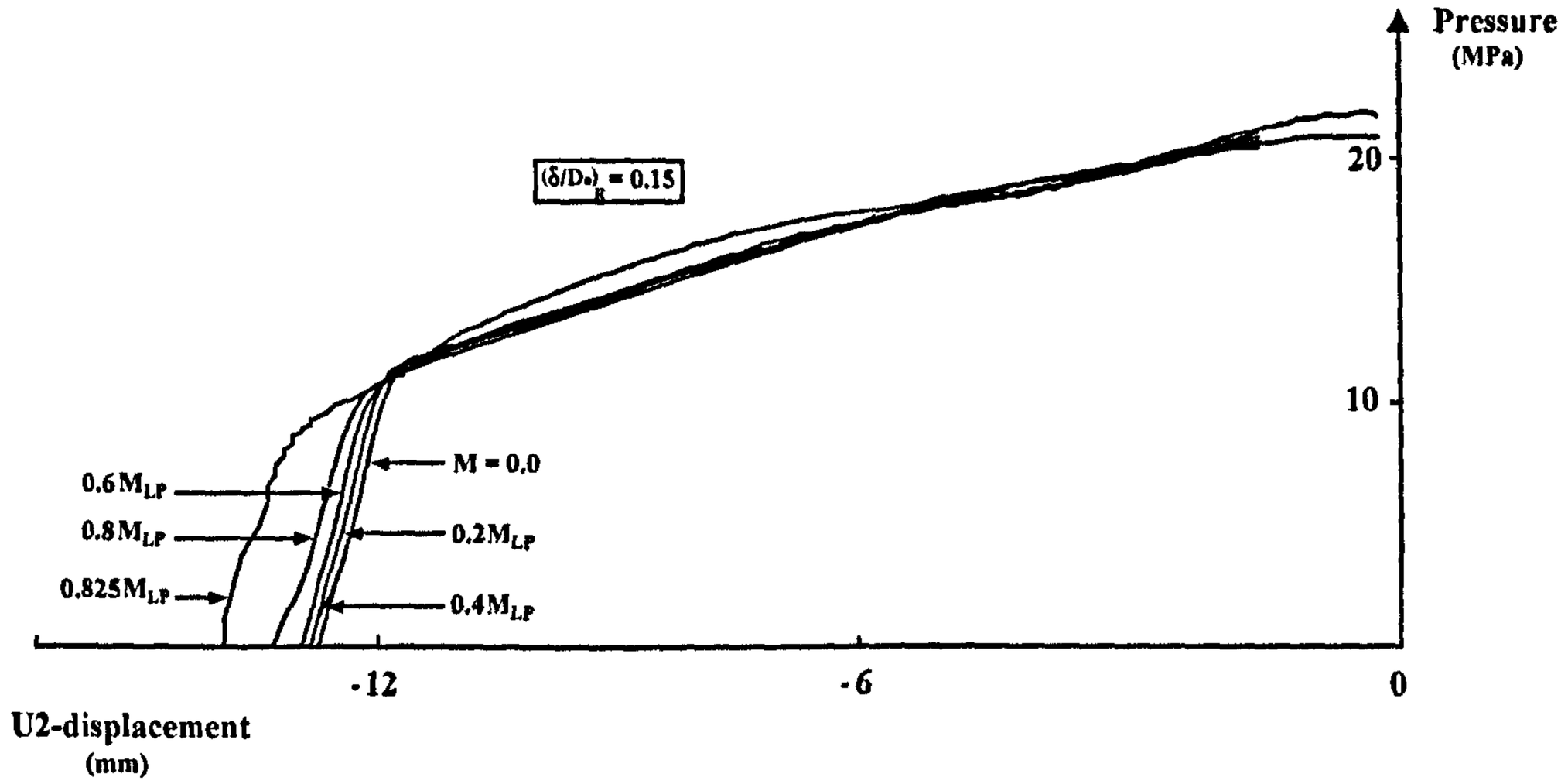

Figure 4.20: Pressure versus centre node displacement for different levels of closing bending moment loading. Also, $\frac{2L}{D_o} = 6.0$.

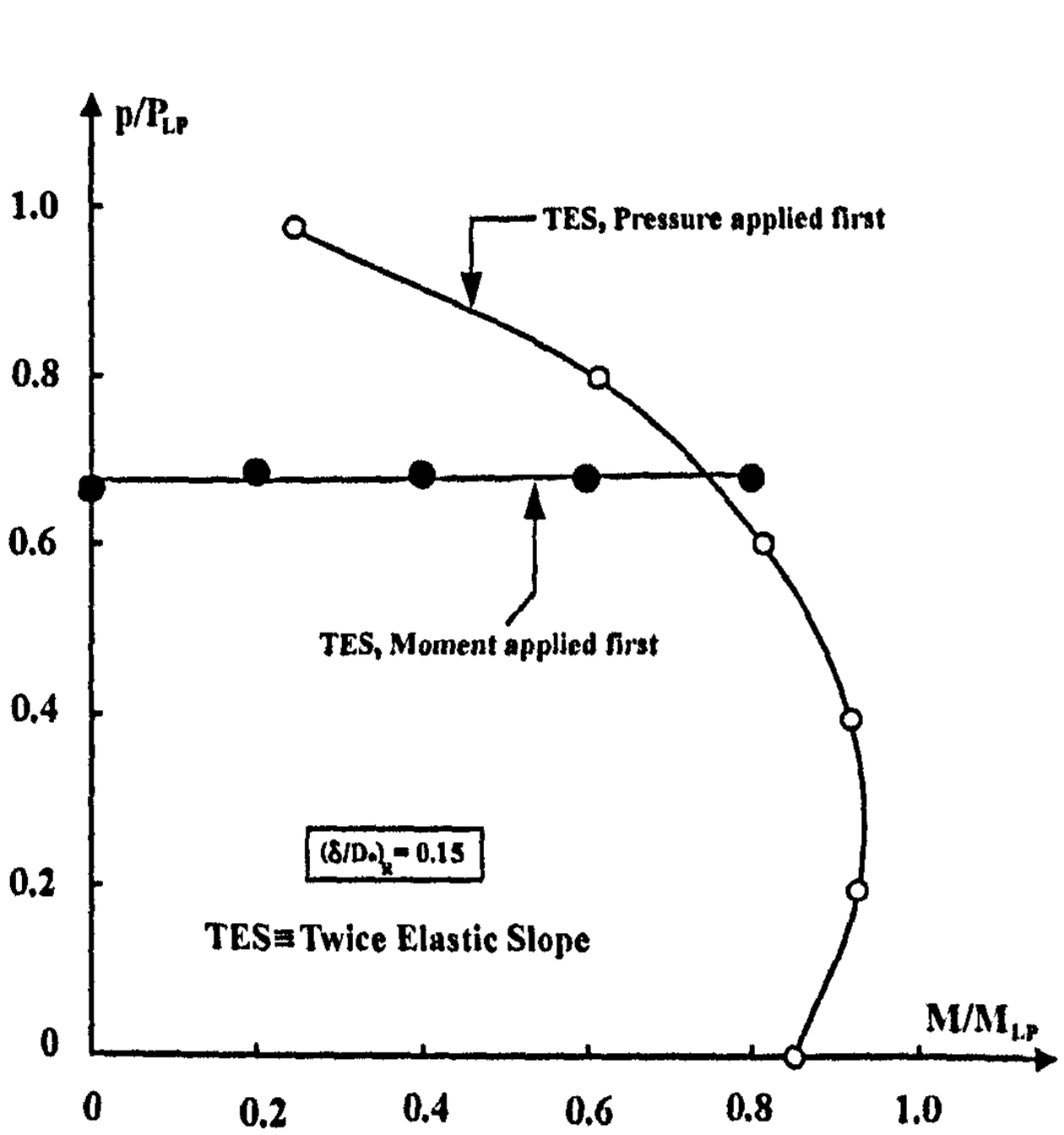

Figure 4.21: Interaction diagram for pressure and closing bending moment loading. Also, $\frac{2L}{D_o} = 6.0$.

Chapter 5

Numerical analysis of gouged dents in steel pipelines

5.1 Introduction

This chapter is focusing on gouged dents in mild steel pipelines. This type of defect has been identified as the most severe type causing most pipelines to fail [21, 22]. Only axial gouges are to be considered. They are introduced onto the outer surface of the pipe. Gouges are introduced to pipe surface by removal of material. Once a gouge is modelled, denting and bending moment are applied in two consecutive steps. Both closing and opening bending moment are to be examined. This Chapter focuses on the finite element modelling of gouges within the indented area. The following parameters describing a gouge are to be included: width, length and depth. Cracks within dented area are also to be modelled (by Node Release Method). As in previous Chapters this numerical work is carried out by using PATRAN and ABAQUS codes.

Gouges are to be introduced into the quarter model. Geometry of a quarter FE model with all surfaces, solids, and elements is created in *PATRAN*. History of model generation is stored in the journal file, *.jou. The journal file, *.jou, has a small size, and it can be stored for future needs or modifications of the model. A sample of journal file is attached, as an illustration, in Appendix (B). The input file, *.inp, generated by PATRAN is used as an input file to *ABAQUS*. The input file generated

by PATRAN contains data describing the model with node sets, and elements to which the loading and boundary conditions need to be applied - (see the sequence of FE modelling and analysis steps in Figure (B.1). A sample of the input file is also attached in Appendix (B).

5.1.1 Defect parameters and their location

Gouges are introduced to the plain pipe's wall which is to be subsequently dented. Due to the symmetry conditions only a quarter model of the pipe is to be modelled. Geometry of a quarter gouge is depicted in Figure (5.1). Its depth is denoted by, e, whilst half-width and half length are denoted by, w, and, c, respectively. Two gouges, placed on both sides of the dent, are also considered. Both cases are shown in Figure (5.2).

It is worth noting that two gouges, on both sides of dent centre are introduced because the level of stress there has been identified as very high (experimental work reported in [50]). Another type of damage considered in this Chapter is an axial crack. Cracks are to be modelled by Node Release Method - see Figure (5.3) for the illustration.

5.1.2 Modelling of 'Solids' in PATRAN

Three types of 'solid models' were prepared in PATRAN in order to handle: gouged pipes and the Node Release Method. These can be seen in Figures (5.4), (5.5), and (5.6), respectively. It is seen from Figure (5.4) and from Figure (5.5) that denser meshing was introduced in the area of perceived gouges. In particular the number of elements through the thickness had to be adjusted. Also, this number had to dissipate to two layers through the thickness away from gouges. The pipe dimensions used in this Chapter are the same as used in Chapters (3) and (4), i.e., the ratio of the outside-diameter-to-the-wall-thickness is, $\frac{D_o}{t} \cong 40.0$, with pipe's total length being such that, $\frac{2L}{D_o} = 6.0$.

5.1.3 Mesh generation

Shell and solid elements are commonly used for modelling of pressurised components such as vessels, pipes etc. However, for complex problems with nonlinear geometries such as a pipe containing dents and gouges, shell elements are not suitable. The element type used in this Chapter is 20-noded, isoparametric, quadratic brick element with reduced integration points, and three translatory degrees of freedom per node, $C3D20R$. This type of element has a quadratic shape function which describes the geometry and deformation profile more accurately when compared to the first order elements, e.g., $C3D8$. It is worth reporting work of Lynch [65] on comparative performance of elements $C3D20$, $C3D20R$, and $C3D8$.

The author reported that, the limit pressure improved by 7.0 % when $C3D20R$ rather than $C3D8$ elements where employed. Another investigation was carried out by Hsieh et al. [69]. They modelled axisymmetric case with, $C3D8$, 8-noded brick elements as well as with $C3D20R$, 20-node elements. For moment loading, the results showed that 8-noded model overestimated the limit load obtained from 20-node model by about, 20 %. Similar results for pressure loading were also reported. Limit pressure based on elements, $C3D8$, was 29 % higher than the limit pressure based on the 20-node elements. Wedge elements $C3D15$ were avoided as these produced poor results in structural analyses (especially when they were used in the critical regions).

5.1.4 Pressure loading and boundary conditions

The pressure loading applied to models is the same as described in Chapters (3) and (4). The axial stress due to internal pressure of magnitude, $\frac{pR_i^2}{(R_o^2-R_i^2)}$, is applied on the pipe end face. The end effect has no influence on the denting load because the pipe end is located away from the dent centre. In this study, the analyses were carried out for two pressure levels, i.e., for the design level and for 25 % of the design level. The boundary conditions used in this Chapter are the same as those in Chapters (3) and (4), (see Figure (3.5) and Table (3.2)). In the presence of cracks, some of the constrains were left free on the crack face.

5.1.5 Analysis type and post processing

The stress analysis of FE models was carried out using ABAQUS 6.3. The denting procedure was carried out on a pipe described by the full stress-strain material model. The maximum bending moment was obtained from the ABAQUS FE analysis by using the *Riks* algorithm. The ABAQUS Viewer was used for visualization of FE models and of obtained results. The Microsoft Excel was also used to process some of the data obtained from ABAQUS.

5.2 Modelling of a gouge

A quarter model of the pipe was initially modelled as a flat plate. The plain gouges were introduced to that flat plate by taking off part of the wall thickness as required for each individual case. This was done in PATRAN using Geometry parameter. A sample of two solid models are shown in Figures (5.5) for centre gouges, and in Figure (5.6) for an off-centre case. It is seen from Figures (5.5) and (5.6) that gouges were introduced to the plain pipe before denting process took place.

Once modelling of solids in PATRAN was completed, boundary and loading conditions were added to the model. Then, the solid sections were meshed using brick solid elements, $C3D20R$. The 'gouged area' was modelled with eight elements through the wall thickness. The number of elements through the wall thickness was reduced to four elements through the thickness and finally it was reduced to two elements through wall thickness away from the gouge and dent centre - see Figure (5.7). The ligaments were modelled using six elements for, $\frac{e}{t} = 0.25$. Four elements were used for, $\frac{e}{t} = 0.50$, and two elements for, $\frac{e}{t} = 0.75$. A view of the gouged area before using, NMAP, parameter is shown in Figure (5.8). Figures (5.9) and (5.10), show a closer view of axial gouge at the centre after the NMAP parameter was used.

5.2.1 Shape of gouges

Shape of gouges was chosen to be rectangular. This shape of a defect was chosen because:

- Defects taking a rectangular shapes are easier to model, and they are likely to be less troublesome when running. Also, they are easier to manufacture, and hence they can be used to compare FE results with experimental results.

- Electrical discharge machine can be readily used to manufacture an axial slot gouge of a rectangular shape, with fine dimensions.

5.3 Analysis of cracked/dented pipes through Node Release Method

Cracks were introduced either at the mid-span of the pipe or at a distance, $\frac{D_o}{2}$, from the indenter's centre - as sketched in Figures (5.2a) and (5.2b), respectively. Cracks were introduced into the FE model before denting has started. A range of axial plain cracks were created with different dimensions. The following cases were prepared and analysed: $\frac{2c}{D_o} = 0.25, 0.50, 0.75$, and 1.0 (where $2c \equiv$ crack length). The crack depths, $\frac{e}{t}$ were assumed as: $\frac{e}{t} = 0.25, 0.50$, and 0.75. The cracks had no width, i.e., $\frac{2w}{t} \equiv 0.0$ (since the cracks were modelled using the Node Release Method). Table (5.1) lists the FE models which were analysed.

Calculation of the ultimate denting load, distortion of the cross section area, and the residual dent depth in pipe with, and without, internal pressure were investigated for both crack locations. A sample of results, for pressure free pipe, is given in Table (5.2), for both mid-span and for off-centre positions of cracks. Only hemispherical indenter was used with a single denting depth, $(\frac{\delta}{D_o})_{max} = 0.36$. As mentioned previously, after reaching the depth of, $(\frac{\delta}{D_o})_{max} = 0.36$, the pipe was unloaded and final depth after any spring back, $(\frac{\delta}{D_o})_R$, was recorded. When the crack depth was, $\frac{e}{t} = 0.5$, the length of the crack had no effect on the magnitude of the denting force. For through the thickness cracks the magnitude of the denting force dropped by 16 % (for crack length, $\frac{2c}{D_o}$, varying from 0.25 to 1.0). The amount of spring back and distortion of the pipe's circular cross section remained practically unaffected by variations of crack depth and by variation of their axial length (when compared to non-cracked pipes). Off-centre cracks influenced the magnitude of the denting force by a larger amount but only in the case of through the thickness crack, $\frac{e}{t} = 1.0$. Here, the magnitude of

denting force dropped by 50% when the axial length of the crack grew from, $\frac{2c}{D_o} = 0.25$ to $\frac{2c}{D_o} = 1.0$.

Generally, the magnitude of denting force needed to produce the same depth of a central dent, in a cracked pipe, is smaller than in the case of non-cracked pipes. In the case of, $(\frac{\delta}{D_o})_{max} = 0.36$, this is in order of, 9 % to 18 % (compared with results in Table (3.8) and Table (5.2)). It is worth noting that the spring back and distortion of the cross section, $\frac{A}{A_o}$, are nearly the same for cracked and for non-cracked pipes.

For a pressurised pipe (to the design level, $p = 11.2\ MPa$), it was impossible to consider cracks deeper than half of the wall thickness due to the lack of FE convergence. Hence, only, $\frac{e}{t} = 0.25$, and $\frac{e}{t} = 0.5$ were analysed. Corresponding results are given in Table (5.3). Cracked pipes with internal pressure show different behaviour to cracked but pressure free pipes. Firstly, as mentioned earlier, cracks deeper than 50% of the wall thickness cannot sustain denting process to the depth of, $(\frac{\delta}{D_o})_{max} = 0.36$ (lack of convergence of the FE analysis). For the remaining crack depths the magnitude of the denting force is nearly the same as for non-cracked pipes (again, comparing results of Table (3.8) and Table (5.3). Changes in distortion of circular cross-section, $\frac{A}{A_o}$, are very small. The largest spring back after removal of the indenter amounts to about, 12% of the prescribed dent's depth, $(\frac{\delta}{D_o})_{max} = 0.36$. These observations apply equally to cracks directly underneath of the indenter as well as to their off-centre positioning.

5.4 Analysis of gouged and dented pipes

Seventy two FE models were prepared with different variables such as gouge depth, width, and length. Tables (5.4), (5.5), and (5.6) show these FE models. It is seen that each Table consists of 12 models (4 gouge lengths, and each having 3 gouge depths). Length of a gouge, $2c$, is normalised by, D_o, and the following values were used: $\frac{2c}{D_o} = 0.25, 0.50, 0.75$, and 1.0. At the same time width of the gouge was normalised by wall thickness, t, and the following values were used: $\frac{2w}{t} = 0.0, 0.483, 1.45$, and 2.415. It is seen from Tables (5.4), (5.5), and (5.6) that, the ratio of the gouge depth to the wall thickness, $\frac{e}{t}$, had the following values: $\frac{e}{t} = 0.25, 0.50$, and 0.75. All of the gouged FE models were to be dented with and without internal pressure in the pipe.

The dented models were then used for second stage of the analysis, i.e., for the case of loading by bending moment.

The denting procedure for empty and for pressurised perfect pipes, i.e., without gouges or cracks, was described in Chapter (3) where typical plots of loading and unloading paths were obtained. The same procedure is applied here, initially for empty plain pipes with axial slot gouges having different width, length, and depth.

The results obtained for mid-span gouge are plotted in Figure (5.11), and for off-centre gouges they are plotted in Figure (5.12). The denting load for gouged or cracked dents was normalised using, F_o (denting load for a plain pipe). As it can be seen from Figure (5.11), the denting load decreases as the gouge length increases from $\frac{2c}{D_o} = 0.25$ to $\frac{2c}{D_o} = 1.0$. In addition, the denting load decreases as the gouge depth increases and it reaches minimum for deeper gouge, $\frac{e}{t} = 0.75$. This decrease in denting load is due to the partial removal of the wall material which makes the structure weaker. At the same time the magnitude of denting load remains nearly constant for cracked pipes (results based on Node Release Method – Fig. (5.11)).

For off-centre gouges, Figure (5.12) shows the denting load versus the gouge and crack depth. It is seen here that the denting load decreases as the gouge depth increases. Besides, the denting load decreases as the gouge length increases, from $\frac{2c}{D_o} = 0.25$ to $\frac{2c}{D_o} = 1.0$. The gouge width has small effect on denting load but in one case there was a large drop of the denting load (for wider gouge, Figure (5.12b)). For cracked pipes the denting load is constant except for longer cracks - Figure (5.12d) where there is a small drop in magnitude of denting load. The denting load was constant for cracked pipes because there is no removal of material from pipe's wall.

As mentioned previously as the indenter is removed, the dented area is pushed out slightly due to the remaining residual stress in the deformed shape. Table (5.7) shows the residual dent depth, $(\frac{\delta}{D_o})_R$, for different gouge's dimensions. As it can be seen the residual dent depths decreases as the gouge depth increases. For off-centre gouges, the residual dent depth is nearly the same in most cases - see Table (5.8).

5.4.1 Reduction of thickness in ligaments

The reduction of the ligament thickness, for gouges at the mid-span, increases as the gouge depth increases - see Table (5.9). For deeper gouge, $\frac{e}{t} = 0.75$, there was a significant reduction of the wall thickness. Table (5.10) shows that for off-centre gouges the reduction of the wall thickness is not as large as that in mid-span gouges.

5.4.2 Gouged and dented pipes, ($p = 2.8\ MPa$)

Numerical results show that the presence of the internal pressure increases the strength of pipes. The ultimate denting load, for example, becomes larger than for empty pipes. The results obtained for mid-span gouges are plotted in Figure (5.13). They show decrease in denting load as the gouge length and gouge depth increase. The gouge's width is becoming another important variable. As the gouge width increases the denting load decreases. For off-centre gouges, Figure (5.14) shows similar trends in the denting load as for mid-span cases. The denting load decreases as the gouge width and depth increase. This decrease in the denting load is due to the long running cracks or gouges, which make the structure weaker. Convergency problem for deeper and larger gouges occurred as can be seen in Figure (5.14c) and in Figure (5.14d).

The presence of the internal pressure during the denting process stiffens the pipe and it increases the spring back after indenter is removed. Magnitude of the spring back, in the case of pressurised pipes, was larger than for non pressurised pipes (since the internal pressure pushed the indented area out). Table (5.11) shows the residual dent depths after removal of the indenter and release of the internal pressure. For off-centre gouges, similar conclusion can be applied to the residual dent depth which increases as the gouge depths increases – see Table (5.12). The reduction of the ligament thickness for mid-span gouges, underneath the indentor is larger when compared with the reduction in off-centre gouges. The results obtained for mid-span gouges are presented in Table (5.13), and for off-centre gouges they are presented in Table (5.14).

5.4.3 Changing shape of a gouge

During numerical analysis a convergency problem occurred during pressurisation and denting of a pipe having larger and deeper gouges. This problem was investigated further. Instead of having a flat bottom, some additional material was added these - see Figure (5.15) for different profiles of the ligament.

These models had axial slot gouges with a constant length, $\frac{2c}{D_o} = 0.50$. Different cross-section shapes of gouges were used in computations and they are sketched in Figure (5.15). The figure shows gouge ligament with the following, different thickness profiles: model (a) has a rectangular defect with, $\frac{e}{t} = 0.625$; model (b) has rectangular defect with, $\frac{e}{t} = 0.75$; models (c) and (d) have rectangular defect with, $\frac{e}{t} = 0.75$ and their bottom is reinforced with additional material; model (e) simulates a V-notch defect (with maximum gouge depth, $\frac{e}{t} = 0.75$).

The above models were dented to, $(\frac{\delta}{D_o})_{max} = 0.36$, with $p = 0.0$ and with $p = 2.8$ MPa. Figure (5.16) shows top view of the gouge before and after denting procedure. The rectangular slot gouge was expanding in both directions as the the denting load increased. The maximum width, WE, and length, LE, of bulges are given in Tables (5.15) and (5.16). Figure (5.17) shows the FE model, in which the gouge has the V-notch shape. The deformed V-notch model is plotted in Figure (5.18). It is worth noting the following:

- The bottom of gouges expands in hoop and axial directions due to the denting load. This expansion is maximum at the dent centre. As the denting load increases these expansions increase until puncture occurs. The largest extension was recorded for the model simulating the V-notch.

- The largest reduction of the ligament's thickness was recorded in the dent having a mid-span gouge. For, $p = 2.8\ MPa$, the maximum reduction of the thickness of ligament was 79.4%. For, $p = 0.0$, the maximum reduction of thickness of ligament was 74.0%. As the ligament width decreases, the reduction of the wall thickness increases specially for larger $\frac{e}{t}$. The weakest of analysed FE models were models with gouges having V-notch shape.

5.5 Analysis of dented and gouged pipes subjected to bending

The bending moment is to be applied to gouged plain, and gouged dented pipes with and without internal pressure. Also, the bending moment will be of opening or closing type - as sketched in Figure (4.1). Due to the large amount of results from the parameter study, only a sample of them is presented in graphical format. The remaining results are given in tabular format.

It has been shown in Chapter (4), for example in Figure (4.11), that plastic bending moment can only be obtained for the opening bending moment. It is immaterial whether this is based on two or five times elastic slope approach. But for the closing moment acting on a dented pipe it was impossible to adopt any of these two criteria. Therefore, in this Chapter, it was decided to use the ultimate bending moment values instead of plastic loads used previously. Two typical graphs showing bending moment versus pipe end rotation are shown in Figure (5.19). This figure illustrates two limit loads, i.e., 'P1' and 'P2', obtained through the application of the *Riks* method to the opening and closing bending moment, respectively. It is seen here that failure at 'P1' and at 'P2' corresponds to two different modes of failure. These modes can be seen in Figure (4.9) and in Figure (4.10) where it is seen that buckling/bulging is the failure mode associated with 'P1'. The buckle occurs on the other side of the dent. Growth of the dent and squashing of the mid-span cross-section corresponds to the mode, 'P2'.

Bending moment can cause failure growth of 'a buckle' near the pipe's end. This is illustrated here by plotting magnitude of bending moment versus pipe end rotation for pressurised pipe, - see Figure (5.20), and examing the deformed shape at the ultimate bending moment, 'P1', – see Figure (5.21b). When pipe remains empty its shape at failure, corresponding to 'P2' – see Figure (5.21b), is depicted in Figure (5.21a).

Figure (5.22) shows a sample of results for the opening bending moment and for closing bending moment when plain pipe had axial gouges but it remained not dented. Figure (5.22a) depicts results for mid-span gouge whilst Figure (5.22b) for an off-centre gouge. Additional results are provided in this figure for dented pipe, to

$(\frac{\delta}{D_o})_{max} = 0.36$, and having gouges. Figure (5.22c) shows results for mid-span gouge, and Figure (5.22d) is for an off-centre gouge. The denting procedure was carried out for both empty and for pressurised pipe, $p = 2.8\ MPa$. The objective of this task was to compare the results for dented and gouged pipe with results for plain pipe without defects. The results show that the presence of internal pressure strengthens the structure (especially for opening bending moment). The value of angular rotation, for opening moment at failure is larger than the corresponding value for closing moment loading. Also, there is not much difference between the ultimate bending moments for plain pipes with axial slot gouges at both locations, i.e., mid-span and off-centre. The remaining results of the ultimate moment values for both opening and closing moment for empty and for pressurised pipes are tabulated and they are as follows:

- For mid-span gouges, values of the ultimate opening and closing moments (from Node Release Method) are given in Tables (5.17) - (5.20). Values of the ultimate opening and closing moments (using removal of material) are given in Tables (5.21) - (5.32).

- For off-centre gouges, values of the opening and closing moments (from Node Release Method) are given in Tables (5.33) - (5.36). Values of the ultimate opening and closing moments (using removal of material) are given in Tables (5.37) - (5.48).

Results for gouged pipes can be compared with results for gouges free pipe given in Table (5.49). The latter Table has relevant results for internal pressure, p = 2.8 MPa, and p = 5.6 MPa. Samples of deformed shapes of gouged plain pipes at the ultimate bending moment are shown in Figure (5.23), and in Figure (5.24) for mid-span gouges. Figure (5.25), and Figure (5.26) show similar results for off-centre gouges. Deformed pipes, which contained mid-span gouges and dents, at the ultimate bending moments, are depicted in Figure (5.27) for closing moment, and in Figure (5.28) for opening bending moment. Similar results are plotted in Figure (5.29) and in Figure (5.30).

5.6 Closure

It is worth noting the following:

- Cracks deeper than 50% of the wall thickness could not sustain denting to the depth of, $(\frac{\delta}{D_o})_{max} = 0.36$, in pipes subjected to pressure equal to the design level (due to the lack of convergence of the FE analysis).

- The amount of spring back and distortion of the pipe's circular cross section remained practically unaffected by variation of crack depth and crack axial length.

- During denting the reduction of the wall, or ligament, thickness increases as the gouge depth becomes larger.

- The magnitude of the ultimate closing bending moment increases in presence of internal pressure. Presence of dents weakens the structure and buckling/bulging or collapse occurs faster when compared to non dented pipes.

Variable	$\left(\frac{2c}{D_o}\right) = 0.25$	$\left(\frac{2c}{D_o}\right) = 0.50$	$\left(\frac{2c}{D_o}\right) = 0.75$	$\left(\frac{2c}{D_o}\right) = 1.0$
$\left(\frac{e}{t}\right) = 0.25$	Yes	Yes	Yes	Yes
$\left(\frac{e}{t}\right) = 0.50$	Yes	Yes	Yes	Yes
$\left(\frac{e}{t}\right) = 0.75$	Yes	Yes	Yes	Yes
$\left(\frac{e}{t}\right) = 1.0$	Yes	Yes	Yes	Yes

Table 5.1: List of Finite Element models to be analysed using Node Release Method (zero 'width' cracks). Also, $\frac{2L}{D_o} = 6.0$, and $\frac{2w}{t} = 0.0$.

	$\left(\frac{e}{t}\right) \downarrow$	$\left(\frac{2c}{D_o}\right) \rightarrow$	0.25	0.50	0.75	1.0
Centre	0.5	F_{max} (kN)	24.2	24.2	24.2	24.3
		$\left(\frac{\delta}{D_o}\right)_R$	0.340	0.340	0.340	0.339
		$\left(\frac{A}{A_o}\right)$ (%)	18.2	18.2	18.1	19.7
	1.0	F_{max} (kN)	23.6	22.6	21.5	20.3
		$\left(\frac{\delta}{D_o}\right)_R$	0.348	0.347	0.345	0.334
		$\left(\frac{A}{A_o}\right)$ (%)	18.3	18.5	19.2	19.5
Offcentre	0.5	F_{max} (kN)	24.4	24.3	24.1	23.9
		$\left(\frac{\delta}{D_o}\right)_R$	0.339	0.338	0.338	0.338
		$\left(\frac{A}{A_o}\right)$ (%)	18.1	18.0	18.0	18.0
	1.0	F_{max} (kN)	25.5	24.3	23.6	16.9
		$\left(\frac{\delta}{D_o}\right)_R$	0.338	0.338	0.338	0.329
		$\left(\frac{A}{A_o}\right)$ (%)	17.9	18.8	19.5	19.2

Table 5.2: Results for cracked pipe subjected to denting depth, $(\frac{\delta}{D_o})_{max} = 0.36$, and for mid-span and off-centre positions of cracks. All results are for pressure free pipe, $p = 0.0$. Node Release Modelling was used and model length was $\frac{2L}{D_o} = 6.0$.

	$\left(\frac{e}{t}\right)\downarrow$	$\left(\frac{2c}{D_o}\right)\rightarrow$	**0.25**	**0.50**	**0.75**	**1.0**
Centre	**0.25**	F_{max} (kN)	70.2	70.2	70.0	70.0
		$\left(\frac{\delta}{D_o}\right)_R$	0.219	0.217	0.216	0.216
		$\left(\frac{A}{A_o}\right)$ (%)	6.9	6.9	6.8	6.8
	0.50	F_{max} (kN)	70.3	70.2	69.9	69.9
		$\left(\frac{\delta}{D_o}\right)_R$	0.218	0.215	0.210	0.210
		$\left(\frac{A}{A_o}\right)$ (%)	6.9	6.7	6.5	6.3
Offcentre	**0.25**	F_{max} (kN)	69.6	69.6	69.5	69.5
		$\left(\frac{\delta}{D_o}\right)_R$	0.209	0.209	0.208	0.209
		$\left(\frac{A}{A_o}\right)$ (%)	6.3	6.3	6.3	6.3
	0.50	F_{max} (kN)	69.6	69.5	69.4	69.3
		$\left(\frac{\delta}{D_o}\right)_R$	0.209	0.207	0.204	0.202
		$\left(\frac{A}{A_o}\right)$ (%)	6.3	6.2	6.4	5.8

Table 5.3: Results for cracked pipe subjected to denting depth, $(\frac{\delta}{D_o})_{max} = 0.36$, and for mid-span and off-centre positions of cracks. All results are for pressurised pipe, $p = 11.2\ MPa$. Node Release Modelling was used and model length was $\frac{2L}{D_o} = 6.0$.

Variable	$\left(\frac{2c}{D_o}\right) = 0.25$	$\left(\frac{2c}{D_o}\right) = 0.50$	$\left(\frac{2c}{D_o}\right) = 0.75$	$\left(\frac{2c}{D_o}\right) = 1.0$
$\left(\frac{e}{t}\right) = 0.25$	Yes	Yes	Yes	Yes
$\left(\frac{e}{t}\right) = 0.50$	Yes	Yes	Yes	Yes
$\left(\frac{e}{t}\right) = 0.75$	Yes	Yes	Yes	Yes

Table 5.4: List of Finite Element models to be analysed. Also, $\frac{2c}{D_o} = 6.0$, and $\frac{2w}{t} = 0.483$.

Variable	$\left(\frac{2c}{D_o}\right) = 0.25$	$\left(\frac{2c}{D_o}\right) = 0.50$	$\left(\frac{2c}{D_o}\right) = 0.75$	$\left(\frac{2c}{D_o}\right) = 1.0$
$\left(\frac{e}{t}\right) = 0.25$	Yes	Yes	Yes	Yes
$\left(\frac{e}{t}\right) = 0.50$	Yes	Yes	Yes	Yes
$\left(\frac{e}{t}\right) = 0.75$	Yes	Yes	Yes	Yes

Table 5.5: List of Finite Element models to be analysed. Also, $\frac{2L}{D_o} = 6.0$, and $\frac{2w}{t} = 1.449$.

Variable	$\left(\frac{2c}{D_o}\right) = 0.25$	$\left(\frac{2c}{D_o}\right) = 0.50$	$\left(\frac{2c}{D_o}\right) = 0.75$	$\left(\frac{2c}{D_o}\right) = 1.0$
$\left(\frac{e}{t}\right) = 0.25$	Yes	Yes	Yes	Yes
$\left(\frac{e}{t}\right) = 0.50$	Yes	Yes	Yes	Yes
$\left(\frac{e}{t}\right) = 0.75$	Yes	Yes	Yes	Yes

Table 5.6: List of Finite Element models to be analysed. Also, $\frac{2L}{D_o} = 6.0$, and $\frac{2w}{t} = 2.415$.

variable	$\left(\frac{2c}{D_o}\right)$	$\frac{e}{t} = 0.25$	$\frac{e}{t} = 0.50$	$\frac{e}{t} = 0.75$
$\frac{2w}{t} = 0.50$	0.25	0.342	0.341	0.341
	0.50	0.342	0.341	0.341
	0.75	0.341	0.341	0.341
	1.0	0.341	0.341	0.341
$\frac{2w}{t} = 1.45$	0.25	0.341	0.34	0.34
	0.50	0.34	0.34	0.27
	0.75	0.34	0.34	0.27
	1.0	0.34	0.34	0.27
$\frac{2w}{t} = 2.42$	0.25	0.34	0.34	0.32
	0.50	0.34	0.33	0.32
	0.75	0.34	0.33	0.32
	1.0	0.34	0.33	0.32

Table 5.7: The residual dent depth, $(\frac{\delta}{D_o})_R$, after removal of the indenter. Pipe had mid-span gouge and it was dented to: $(\frac{\delta}{D_o})_{max} = 0.36$. Also, $p = 0.0$, $\frac{2L}{D_o} = 6.0$, and $\frac{a}{b} = 1.0$.

variable	$\left(\frac{2c}{D_o}\right)$	$\frac{e}{t} = 0.25$	$\frac{e}{t} = 0.50$	$\frac{e}{t} = 0.75$
$\frac{2w}{t} = 0.50$	0.25	0.342	0.342	0.342
	0.50	0.342	0.342	0.342
	0.75	0.342	0.342	0.342
	1.0	0.342	0.342	0.342
$\frac{2w}{t} = 1.45$	0.25	0.342	0.342	0.342
	0.50	0.342	0.342	0.342
	0.75	0.342	0.342	0.343
	1.0	0.341	0.340	0.34
$\frac{2w}{t} = 2.42$	0.25	0.342	0.342	0.342
	0.50	0.342	0.342	0.346
	0.75	0.342	0.342	0.343
	1.0	0.340	0.340	0.34

Table 5.8: The residual dent depth, $(\frac{\delta}{D_o})_R$, for the off-centre gouge. Pipe was dented to: $(\frac{\delta}{D_o})_{max} = 0.36$. Also, $p = 0.0$, $\frac{2L}{D_o} = 6.0$, and $\frac{a}{b} = 1.0$.

variable	$\left(\frac{2c}{D_o}\right)$	$\frac{e}{t} = 0.25$	$\frac{e}{t} = 0.50$	$\frac{e}{t} = 0.75$
$\frac{2w}{t} = 0.50$	0.25	5.4	10.3	10.0
	0.50	5.3	11.0	10.0
	0.75	5.5	11.0	11.0
	1.0	5.6	11.0	12.0
$\frac{2w}{t} = 1.45$	0.25	4.85	9.4	12.0
	0.50	5.1	9.3	11.0
	0.75	5.0	9.3	13.0
	1.0	5.0	9.0	13.0
$\frac{2w}{t} = 2.42$	0.25	4.7	8.0	10.0
	0.50	4.7	7.0	10.0
	0.75	4.8	8.0	10.0
	1.0	4.8	9.0	11.0

Table 5.9: The reduction of the ligament thickness at the centre of the gouge; mid-span gouge, $(\frac{\delta}{D_o})_{max} = 0.36$, $p = 0.0$, $\frac{2L}{D_o} = 6.0$, and $\frac{a}{b} = 1.0$. Results are given as $\frac{t_i}{t} \times 100$ %.

variable	$\left(\frac{2c}{D_o}\right)$	$\frac{e}{t} = 0.25$	$\frac{e}{t} = 0.50$	$\frac{e}{t} = 0.75$
$\frac{2w}{t} = 0.50$	0.25	3.5	3.58	3.5
	0.50	3.56	3.43	3.33
	0.75	3.7	3.50	3.3
	1.0	5.27	3.50	3.3
$\frac{2w}{t} = 1.45$	0.25	3.55	3.6	3.4
	0.50	3.6	3.5	3.3
	0.75	3.41	3.20	3.0
	1.0	5.0	3.20	3.0
$\frac{2w}{t} = 2.42$	0.25	3.50	3.50	3.40
	0.50	3.60	3.40	4.44
	0.75	3.40	3.0	3.0
	1.0	4.67	3.0	3.5

Table 5.10: The reduction of the ligament thickness at the centre of the gouge; Off-centre gouge, $(\frac{\delta}{D_o})_{max} = 0.36$, $p = 0.0$, $\frac{2L}{D_o} = 6.0$, and $\frac{a}{b} = 1.0$. Results are in: %.

variable	$\left(\frac{2c}{D_o}\right)$	$\frac{e}{t} = 0.25$	$\frac{e}{t} = 0.50$	$\frac{e}{t} = 0.75$
$\frac{2w}{t} = 0.50$	0.25	0.323	0.320	0.313
	0.50	0.324	0.318	0.316
	0.75	0.324	0.320	0.316
	1.0	0.324	0.325	0.317
$\frac{2w}{t} = 1.45$	0.25	0.323	0.321	0.31
	0.50	0.322	0.318	0.30
	0.75	0.353	0.321	0.30
	1.0	0.323	0.322	0.27
$\frac{2w}{t} = 2.42$	0.25	0.32	0.31	0.30
	0.50	0.32	0.31	0.30
	0.75	0.32	0.31	0.27
	1.0	0.34	0.32	0.30

Table 5.11: The residual dent depth, $(\frac{\delta}{D_o})_R$, after releasing of the internal pressure; mid-span gouge, $(\frac{\delta}{D_o})_{max} = 0.36$, $p = 2.8\ MPa$. Also, $\frac{2L}{D_o} = 6.0$, and $\frac{a}{b} = 1.0$.

variable	$\left(\frac{2c}{D_o}\right)$	$\frac{e}{t} = 0.25$	$\frac{e}{t} = 0.50$	$\frac{e}{t} = 0.75$
$\frac{2w}{t} = 0.50$	0.25	0.323	0.323	0.323
	0.50	0.324	0.321	0.318
	0.75	0.324	0.320	$\star$
	1.0	0.324	0.318	$\star$
$\frac{2w}{t} = 1.45$	0.25	0.324	0.323	0.323
	0.50	0.324	0.321	0.318
	0.75	0.324	0.320	$\star$
	1.0	0.322	0.316	$\star$
$\frac{2w}{t} = 2.42$	0.25	0.324	0.323	0.323
	0.50	0.323	0.322	0.318
	0.75	0.324	0.321	$\star$
	1.0	0.320	0.310	$\star$

$\star \equiv$ no convergency during denting

Table 5.12: The residual dent depth, $(\frac{\delta}{D_o})_R$, after releasing of the internal pressure; off-centre gouge, $(\frac{\delta}{D_o})_{max} = 0.36$, $p = 2.8\ MPa$. Also, $\frac{2L}{D_o} = 6.0$, and $\frac{a}{b} = 1.0$.

variable	$\left(\frac{2c}{D_o}\right)$	$\frac{e}{t} = 0.25$	$\frac{e}{t} = 0.50$	$\frac{e}{t} = 0.75$
$\frac{2w}{t} = 0.50$	0.25	7.0	12.1	12.0
	0.50	7.0	12.0	12.1
	0.75	7.0	12.0	12.1
	1.0	7.0	11.0	12.0
$\frac{2w}{t} = 1.45$	0.25	7.0	12.0	12.0
	0.50	8.0	11.0	11.0
	0.75	7.0	12.0	9.4
	1.0	7.0	12.0	9.0
$\frac{2w}{t} = 2.42$	0.25	7.0	8.3	9.0
	0.50	7.0	7.4	9.0
	0.75	7.0	8.4	9.0
	1.0	7.0	10.0	12.0

Table 5.13: The reduction of the ligament thickness at the centre of the gouge; mid-span gouge, $(\frac{\delta}{D_o})_{max} = 0.36$, $p = 2.8\ MPa$, $\frac{2L}{D_o} = 6.0$, and $\frac{a}{b} = 1.0$. Results are in: %.

variable	$\left(\frac{2c}{D_o}\right)$	$\frac{e}{t} = 0.25$	$\frac{e}{t} = 0.50$	$\frac{e}{t} = 0.75$
$\frac{2w}{t} = 0.50$	0.25	4.8	10.0	4.4
	0.50	4.8	4.62	4.5
	0.75	4.8	4.43	$\star$
	1.0	7.0	16.0	$\star$
$\frac{2w}{t} = 1.45$	0.25	4.8	4.8	0.342
	0.50	4.8	4.6	0.342
	0.75	4.6	4.0	$\star$
	1.0	7.0	12.0	$\star$
$\frac{2w}{t} = 2.42$	0.25	4.9	4.9	4.8
	0.50	4.8	4.5	4.3
	0.75	4.3	3.7	$\star$
	1.0	7.0	10.0	$\star$

$\star \equiv$ no convergency during denting

Table 5.14: The reduction of the ligament thickness at the centre of the gouge; Off-centre gouge, $(\frac{\delta}{D_o})_{max} = 0.36$, $p = 2.8\ MPa$, $\frac{2L}{D_o} = 6.0$, and $\frac{a}{b} = 1.0$. Results are in: %.

Model	F_{max} (kN)	$\left(\frac{\delta}{D_o}\right)_R$	$\left(\frac{t_o-t}{t_o}\right) \times 100$	LE (%)	WE (%)
model (a)	37.2	0.312	11.3	33	78
model (b)	34.9	0.226	12.2	24	62
model (c)	35.7	0.302	16.4	4.7	50
model (d)	35.4	0.296	79.4	4.7	56
model (e)	35.0	0.295	71.0	19	50

LE: Growth of gouge bulging in axial direction, WE: Growth of gouge width

Table 5.15: Summary of FE results for different gouge shapes; p=2.8 MPa, $\frac{2w}{D_o} = 0.0594$, $\frac{2c}{D_o} = 1.0$, $\frac{a}{b} = 1.0$, $(\frac{\delta}{D_o})_{max} = 0.36$, and $\frac{2L}{D_o} = 6.0$.

Model	F_{max} (kN)	$\left(\frac{\delta}{D_o}\right)_R$	$\left(\frac{t_o-t}{t_o}\right) \times 100$	LE (%)	WE (%)
model (a)	24.7	0.332	10.6	8.5	10
model (b)	22.7	0.320	11.10	9.5	68
model (c)	23.5	0.328	15.9	12	76
model (d)	23.2	0.333	74.0	33	74
model (e)	22.5	0.335	71.3	19	62

LE: Growth of gouge bulging in axial direction, WE: Growth of gouge width

Table 5.16: Summary of FE results for different gouge shapes; p=0.0, $\frac{2w}{D_o} = 0.0594$, $\frac{2c}{D_o} = 1.0$, $\frac{a}{b} = 1.0$, $(\frac{\delta}{D_o})_{max} = 0.36$, and $\frac{2L}{D_o} = 6.0$.

Model type	$\frac{e}{t}\downarrow$	$\left(\frac{2c}{D_o}\right) = 0.25$	$\left(\frac{2c}{D_o}\right) = 0.50$	$\left(\frac{2c}{D_o}\right) = 0.75$	$\left(\frac{2c}{D_o}\right) = 1.0$
Plain pipe	**0.25**	5.09	5.09	5.09	5.09
	0.50	5.09	5.09	5.09	5.09
	0.75	5.09	5.09	5.09	5.09
Dented pipe	**0.25**	4.80	4.50	4.80	4.80
	0.50	4.80	4.80	4.80	4.80
	0.75	4.81	4.81	4.80	4.83

Table 5.17: Values of the ultimate opening bending moment for plain pipe, and for dented pipe, $(\frac{\delta}{D_o})_{max} = 0.36$, $p = 2.8\ MPa$, and $\frac{2L}{D_o} = 6.0$. Node Release Method, $\frac{2w}{t} = 0.0$. Results are in: kNm.

Model type	$\frac{e}{t}\downarrow$	$\left(\frac{2c}{D_o}\right) = 0.25$	$\left(\frac{2c}{D_o}\right) = 0.50$	$\left(\frac{2c}{D_o}\right) = 0.75$	$\left(\frac{2c}{D_o}\right) = 1.0$
Plain pipe	**0.25**	5.07	5.09	5.07	5.08
	0.50	4.90	5.06	4.93	5.0
	0.75	4.55	4.64	4.64	4.64
Dented pipe	**0.25**	3.51	3.51	3.51	3.51
	0.50	3.51	3.51	3.51	3.51
	0.75	3.52	3.52	3.52	3.50

Table 5.18: Values of the ultimate closing bending moment for plain pipe, and for dented pipe, $(\frac{\delta}{D_o})_{max} = 0.36$, $p = 2.8\ MPa$, and $\frac{2L}{D_o} = 6.0$. Node Release Method, $\frac{2w}{t} = 0.0$. Results are in: kNm.

Model type	$\frac{e}{t}\downarrow$	$\left(\frac{2c}{D_o}\right) = 0.25$	$\left(\frac{2c}{D_o}\right) = 0.50$	$\left(\frac{2c}{D_o}\right) = 0.75$	$\left(\frac{2c}{D_o}\right) = 1.0$
Plain pipe	**0.25**	4.47	4.47	4.47	4.47
	0.50	4.47	4.47	4.47	4.47
	0.75	4.47	4.47	4.47	4.47
Dented pipe	**0.25**	4.22	4.22	4.22	4.22
	0.50	4.22	4.22	4.22	4.23
	0.75	4.20	4.21	4.23	4.24

Table 5.19: Values of the ultimate opening bending moment for plain pipe, and for dented pipe, $(\frac{\delta}{D_o})_{max} = 0.36$, $p = 0.0$, and $\frac{2L}{D_o} = 6.0$. Node Release Method, $\frac{2w}{t} = 0.0$. Results are in: kNm.

Model type	$\frac{e}{t}\downarrow$	$\left(\frac{2c}{D_o}\right) = 0.25$	$\left(\frac{2c}{D_o}\right) = 0.50$	$\left(\frac{2c}{D_o}\right) = 0.75$	$\left(\frac{2c}{D_o}\right) = 1.0$
Plain pipe	**0.25**	4.47	4.47	4.47	4.47
	0.50	4.47	4.47	4.47	4.47
	0.75	4.47	4.47	4.47	4.47
Dented pipe	**0.25**	2.93	2.93	2.93	2.93
	0.50	2.93	2.93	2.93	2.95
	0.75	2.92	2.92	2.92	2.94

Table 5.20: Values of the ultimate closing bending moment for plain pipe, and for dented pipe, $(\frac{\delta}{D_o})_{max} = 0.36$, $p = 0.0$, and $\frac{2L}{D_o} = 6.0$. Node Release Method, $\frac{2w}{t} = 0.0$. Results are in: kNm.

Model type	$\frac{e}{t}\downarrow$	$\left(\frac{2c}{D_o}\right) = 0.25$	$\left(\frac{2c}{D_o}\right) = 0.50$	$\left(\frac{2c}{D_o}\right) = 0.75$	$\left(\frac{2c}{D_o}\right) = 1.0$
Plain pipe	**0.25**	5.04	5.03	5.03	5.03
	0.50	5.04	5.04	5.03	5.04
	0.75	5.04	5.04	5.03	5.04
Dented pipe	**0.25**	4.75	4.73	4.74	4.72
	0.50	4.73	4.71	4.74	4.75
	0.75	4.64	4.11	4.74	4.76

Table 5.21: Values of the ultimate opening bending moment for plain pipe, and for dented pipe, $(\frac{\delta}{D_o})_{max} = 0.36$, $\frac{2w}{t} = 0.5$, $p = 2.8\ MPa$, and $\frac{2L}{D_o} = 6.0$. Results are in: kNm.

Model type	$\frac{e}{t}\downarrow$	$\left(\frac{2c}{D_o}\right) = 0.25$	$\left(\frac{2c}{D_o}\right) = 0.50$	$\left(\frac{2c}{D_o}\right) = 0.75$	$\left(\frac{2c}{D_o}\right) = 1.0$
Plain pipe	**0.25**	4.82	4.91	4.86	4.88
	0.50	4.53	4.69	4.86	4.62
	0.75	4.40	4.27	4.38	4.31
Dented pipe	**0.25**	3.46	3.19	3.45	3.46
	0.50	3.46	3.50	3.48	3.46
	0.75	3.44	3.50	3.48	3.45

Table 5.22: Values of the ultimate closing bending moment for plain pipe, and for dented pipe, $(\frac{\delta}{D_o})_{max} = 0.36$, $\frac{2w}{t} = 0.5$, $p = 2.8\ MPa$, and $\frac{2L}{D_o} = 6.0$. Results are in: kNm.

Model type	$\frac{e}{t}\downarrow$	$\left(\frac{2c}{D_o}\right) = 0.25$	$\left(\frac{2c}{D_o}\right) = 0.50$	$\left(\frac{2c}{D_o}\right) = 0.75$	$\left(\frac{2c}{D_o}\right) = 1.0$
Plain pipe	**0.25**	4.42	4.42	4.42	4.42
	0.50	4.42	4.42	4.41	4.41
	0.75	4.42	4.42	4.41	4.41
Dented pipe	**0.25**	4.14	4.15	4.14	4.16
	0.50	4.15	4.16	4.15	4.17
	0.75	4.17	4.19	4.15	4.18

Table 5.23: Values of the ultimate opening bending moment for plain pipe, and for dented pipe, $(\frac{\delta}{D_o})_{max} = 0.36$, $\frac{2w}{t} = 0.5$, $p = 0.0$, and $\frac{2L}{D_o} = 6.0$. Results are in: kNm.

Model type	$\frac{e}{t}\downarrow$	$\left(\frac{2c}{D_o}\right) = 0.25$	$\left(\frac{2c}{D_o}\right) = 0.50$	$\left(\frac{2c}{D_o}\right) = 0.75$	$\left(\frac{2c}{D_o}\right) = 1.0$
Plain pipe	**0.25**	4.42	4.42	4.42	4.42
	0.50	4.42	4.41	4.41	4.41
	0.75	4.41	4.40	4.40	4.40
Dented pipe	**0.25**	2.86	2.87	2.87	2.88
	0.50	2.87	2.87	2.86	2.89
	0.75	2.94	3.10	2.85	2.92

Table 5.24: Values of the ultimate closing bending moment for plain pipe, and for dented pipe, $(\frac{\delta}{D_o})_{max} = 0.36$, $\frac{2w}{t} = 0.5$, $p = 0.0$, and $\frac{2L}{D_o} = 6.0$. Results are in: kNm.

Model type	$\frac{e}{t}\downarrow$	$\left(\frac{2c}{D_o}\right) = 0.25$	$\left(\frac{2c}{D_o}\right) = 0.50$	$\left(\frac{2c}{D_o}\right) = 0.75$	$\left(\frac{2c}{D_o}\right) = 1.0$
Plain pipe	0.25	5.04	5.03	5.04	5.03
	0.50	5.04	5.04	5.02	5.02
	0.75	4.70	5.04	5.01	5.02
Dented pipe	0.25	4.54	4.73	4.73	4.73
	0.50	4.74	4.70	4.71	4.73
	0.75	4.74	4.67	4.74	4.72

Table 5.25: Values of the ultimate opening bending moment for plain pipe, and for dented pipe, $(\frac{\delta}{D_o})_{max} = 0.36$, $\frac{2w}{t} = 1.45$, $p = 2.8\ MPa$, and $\frac{2L}{D_o} = 6.0$. Results are in: kNm.

Model type	$\frac{e}{t}\downarrow$	$\left(\frac{2c}{D_o}\right) = 0.25$	$\left(\frac{2c}{D_o}\right) = 0.50$	$\left(\frac{2c}{D_o}\right) = 0.75$	$\left(\frac{2c}{D_o}\right) = 1.0$
Plain pipe	0.25	4.92	4.62	4.71	4.69
	0.50	4.65	4.46	4.42	4.44
	0.75	4.54	4.40	4.34	4.33
Dented pipe	0.25	3.59	3.45	3.45	3.46
	0.50	3.59	3.46	3.45	3.45
	0.75	3.70	3.60	3.57	3.55

Table 5.26: Values of the ultimate closing bending moment for plain pipe, and for dented pipe, $(\frac{\delta}{D_o})_{max} = 0.36$, $\frac{2w}{t} = 1.45$, $p = 2.8\ MPa$, and $\frac{2L}{D_o} = 6.0$. Results are in: kNm.

Model type	$\frac{e}{t}\downarrow$	$\left(\frac{2c}{D_o}\right) = 0.25$	$\left(\frac{2c}{D_o}\right) = 0.50$	$\left(\frac{2c}{D_o}\right) = 0.75$	$\left(\frac{2c}{D_o}\right) = 1.0$
Plain pipe	0.25	4.41	4.42	4.41	4.41
	0.50	4.42	4.41	4.41	4.41
	0.75	4.42	4.41	4.40	4.40
Dented pipe	0.25	4.14	4.16	4.16	4.15
	0.50	4.15	4.17	4.15	4.18
	0.75	4.18	4.19	4.20	4.20

Table 5.27: Values of the ultimate opening bending moment for plain pipe, and for dented pipe, $(\frac{\delta}{D_o})_{max} = 0.36$, $\frac{2w}{t} = 1.45$, $p = 0.0$, and $\frac{2L}{D_o} = 6.0$. Results are in: kNm.

Model type	$\frac{e}{t}\downarrow$	$\left(\frac{2c}{D_o}\right) = 0.25$	$\left(\frac{2c}{D_o}\right) = 0.50$	$\left(\frac{2c}{D_o}\right) = 0.75$	$\left(\frac{2c}{D_o}\right) = 1.0$
Plain pipe	0.25	4.41	4.40	4.40	4.40
	0.50	4.41	4.38	4.36	4.37
	0.75	4.38	4.37	4.30	4.32
Dented pipe	0.25	2.86	2.86	2.87	2.88
	0.50	2.86	2.86	2.86	2.89
	0.75	2.79	3.04	3.06	3.04

Table 5.28: Values of the ultimate closing bending moment for plain pipe, and for dented pipe, $(\frac{\delta}{D_o})_{max} = 0.36$, $\frac{2w}{t} = 1.45$, $p = 0.0$, and $\frac{2L}{D_o} = 6.0$. Results are in: kNm.

Model type	$\frac{e}{t}\downarrow$	$\left(\frac{2c}{D_o}\right) = 0.25$	$\left(\frac{2c}{D_o}\right) = 0.50$	$\left(\frac{2c}{D_o}\right) = 0.75$	$\left(\frac{2c}{D_o}\right) = 1.0$
Plain pipe	**0.25**	5.04	5.04	5.02	5.03
	0.50	5.02	5.036	5.01	5.01
	0.75	5.01	5.03	5.0	5.0
Dented pipe	**0.25**	4.72	4.72	4.72	4.72
	0.50	4.72	4.71	4.69	4.74
	0.75	4.61	4.77	4.71	4.72

Table 5.29: Values of the ultimate opening bending moment for plain pipe, and for dented pipe, $(\frac{\delta}{D_o})_{max} = 0.36$, $\frac{2w}{t} = 2.42$, $p = 2.8\ MPa$, and $\frac{2L}{D_o} = 6.0$. Results are in: kNm.

Model type	$\frac{e}{t}\downarrow$	$\left(\frac{2c}{D_o}\right) = 0.25$	$\left(\frac{2c}{D_o}\right) = 0.50$	$\left(\frac{2c}{D_o}\right) = 0.75$	$\left(\frac{2c}{D_o}\right) = 1.0$
Plain pipe	**0.25**	4.55	4.58	4.43	4.57
	0.50	4.40	4.40	4.38	4.39
	0.75	4.30	4.28	4.30	4.29
Dented pipe	**0.25**	3.45	3.45	3.45	3.45
	0.50	3.50	3.50	3.12	3.46
	0.75	3.55	3.59	3.10	3.55

Table 5.30: Values of the ultimate closing bending moment for plain pipe, and for dented pipe, $(\frac{\delta}{D_o})_{max} = 0.36$, $\frac{2w}{t} = 2.42$, $p = 2.8\ MPa$, and $\frac{2L}{D_o} = 6.0$. Results are in: kNm.

Model type	$\frac{e}{t}\downarrow$	$\left(\frac{2c}{D_o}\right) = 0.25$	$\left(\frac{2c}{D_o}\right) = 0.50$	$\left(\frac{2c}{D_o}\right) = 0.75$	$\left(\frac{2c}{D_o}\right) = 1.0$
Plain pipe	**0.25**	4.42	4.42	4.41	4.41
	0.50	4.42	4.41	4.40	4.40
	0.75	4.41	4.41	4.39	4.38
Dented pipe	**0.25**	4.15	4.16	4.16	4.17
	0.50	4.12	4.17	4.18	4.18
	0.75	4.28	4.17	4.20	4.20

Table 5.31: Values of the ultimate opening bending moment for plain pipe, and for dented pipe, $(\frac{\delta}{D_o})_{max} = 0.36$, $\frac{2w}{t} = 2.42$, $p = 0.0$, and $\frac{2L}{D_o} = 6.0$. Results are in: kNm.

Model type	$\frac{e}{t}\downarrow$	$\left(\frac{2c}{D_o}\right) = 0.25$	$\left(\frac{2c}{D_o}\right) = 0.50$	$\left(\frac{2c}{D_o}\right) = 0.75$	$\left(\frac{2c}{D_o}\right) = 1.0$
Plain pipe	**0.25**	4.41	4.39	4.38	4.38
	0.50	4.37	4.35	4.31	4.33
	0.75	4.32	4.32	4.23	4.26
Dented pipe	**0.25**	2.86	2.86	2.87	2.89
	0.50	2.87	2.86	2.87	2.89
	0.75	3.01	3.06	3.06	3.0

Table 5.32: Values of the ultimate closing bending moment for plain pipe, and for dented pipe, $(\frac{\delta}{D_o})_{max} = 0.36$, $\frac{2w}{t} = 2.42$, $p = 0.0$, and $\frac{2L}{D_o} = 6.0$. Results are in: kNm.

Model type	$\frac{e}{t}\downarrow$	$\left(\frac{2c}{D_o}\right) = 0.25$	$\left(\frac{2c}{D_o}\right) = 0.50$	$\left(\frac{2c}{D_o}\right) = 0.75$	$\left(\frac{2c}{D_o}\right) = 1.0$
Plain pipe	**0.25**	5.09	5.09	5.09	5.09
	0.50	5.09	5.09	5.09	5.09
	0.75	5.09	5.09	5.09	5.09
Dented pipe	**0.25**	4.83	4.80	4.83	4.83
	0.50	4.86	4.80	4.80	4.81
	0.75	4.79	4.81	4.83	4.83

Table 5.33: Values of the ultimate opening bending moment for plain pipe, and for dented pipe, $(\frac{\delta}{D_o})_{max} = 0.36$, $p = 2.8\ MPa$, off-centre gouges. Node Release Method, $\frac{2w}{t} = 0.0$. Results are in: kNm.

Model type	$\frac{e}{t}\downarrow$	$\left(\frac{2c}{D_o}\right) = 0.25$	$\left(\frac{2c}{D_o}\right) = 0.50$	$\left(\frac{2c}{D_o}\right) = 0.75$	$\left(\frac{2c}{D_o}\right) = 1.0$
Plain pipe	**0.25**	5.07	5.09	5.07	5.08
	0.50	5.09	5.09	4.93	5.0
	0.75	4.55	4.64	4.64	4.65
Dented pipe	**0.25**	3.51	3.51	3.51	3.51
	0.50	3.53	3.52	3.51	3.51
	0.75	3.52	3.53	3.52	3.52

Table 5.34: Values of the ultimate closing bending moment for plain pipe, and for dented pipe, $(\frac{\delta}{D_o})_{max} = 0.36$, $p = 2.8\ MPa$, off-centre gouges. Node Release Method, $\frac{2w}{t} = 0.0$. Results are in: kNm.

Model type	$\frac{e}{t}\downarrow$	$\left(\frac{2c}{D_o}\right) = 0.25$	$\left(\frac{2c}{D_o}\right) = 0.50$	$\left(\frac{2c}{D_o}\right) = 0.75$	$\left(\frac{2c}{D_o}\right) = 1.0$
Plain pipe	**0.25**	4.47	4.47	4.47	4.47
	0.50	4.47	4.42	4.47	4.47
	0.75	4.47	4.47	4.47	4.47
Dented pipe	**0.25**	4.21	4.21	4.21	4.21
	0.50	4.22	4.22	4.23	4.23
	0.75	4.22	4.25	4.26	4.26

Table 5.35: Values of the ultimate opening bending moment for plain pipe, and for dented pipe, $(\frac{\delta}{D_o})_{max} = 0.36$, $p = 0.0$, off-centre gouges. Node Release Method, $\frac{2w}{t} = 0.0$. Results are in: kNm.

Model type	$\frac{e}{t}\downarrow$	$\left(\frac{2c}{D_o}\right) = 0.25$	$\left(\frac{2c}{D_o}\right) = 0.50$	$\left(\frac{2c}{D_o}\right) = 0.75$	$\left(\frac{2c}{D_o}\right) = 1.0$
Plain pipe	**0.25**	4.47	4.47	4.47	4.47
	0.50	4.47	4.47	4.47	4.47
	0.75	4.47	4.47	4.47	4.47
Dented pipe	**0.25**	2.93	2.94	2.94	2.93
	0.50	3.0	3.0	3.0	3.0
	0.75	3.0	3.0	3.0	3.0

Table 5.36: Values of the ultimate closing bending moment for plain pipe, and for dented pipe, $(\frac{\delta}{D_o})_{max} = 0.36$, $p = 0.0$, off-centre gouges. Node Release Method, $\frac{2w}{t} = 0.0$. Results are in: kNm.

Model type	$\frac{e}{t}\downarrow$	$\left(\frac{2c}{D_o}\right) = 0.25$	$\left(\frac{2c}{D_o}\right) = 0.50$	$\left(\frac{2c}{D_o}\right) = 0.75$	$\left(\frac{2c}{D_o}\right) = 1.0$
Plain pipe	0.25	5.04	5.04	5.02	5.04
	0.50	5.04	5.04	5.03	5.03
	0.75	5.04	5.04	5.02	5.04
Dented pipe	0.25	4.80	4.80	4.73	4.78
	0.50	4.77	4.82	4.73	4.80
	0.75	4.77	4.81	$\star$	$\star$

$\star \equiv$ convergency problem during denting

Table 5.37: Values of the ultimate opening bending moment for plain pipe, and for dented pipe, $(\frac{\delta}{D_o})_{max} = 0.36$, $\frac{2w}{t} = 0.5$, $p = 2.8\ MPa$, off-centre gouges. Results are in: kNm.

Model type	$\frac{e}{t}\downarrow$	$\left(\frac{2c}{D_o}\right) = 0.25$	$\left(\frac{2c}{D_o}\right) = 0.50$	$\left(\frac{2c}{D_o}\right) = 0.75$	$\left(\frac{2c}{D_o}\right) = 1.0$
Plain pipe	0.25	4.82	4.89	4.85	4.90
	0.50	4.60	4.64	4.55	4.61
	0.75	4.40	4.41	4.38	4.41
Dented pipe	0.25	3.46	3.47	3.46	3.46
	0.50	3.47	3.48	3.47	3.46
	0.75	3.47	3.47	$\star$	$\star$

$\star \equiv$ convergency problem during denting

Table 5.38: Values of the ultimate closing bending moment for plain pipe, and for dented pipe, $(\frac{\delta}{D_o})_{max} = 0.36$, $\frac{2w}{t} = 0.5$, $p = 2.8\ MPa$, off-centre gouges. Results are in: kNm.

Model type	$\frac{e}{t}\downarrow$	$\left(\frac{2c}{D_o}\right) = 0.25$	$\left(\frac{2c}{D_o}\right) = 0.50$	$\left(\frac{2c}{D_o}\right) = 0.75$	$\left(\frac{2c}{D_o}\right) = 1.0$
Plain pipe	0.25	4.42	4.42	4.42	4.42
	0.50	4.42	4.41	4.41	4.41
	0.75	4.42	4.41	4.41	4.40
Dented pipe	0.25	4.17	4.17	4.17	4.17
	0.50	4.16	4.19	4.19	4.16
	0.75	4.16	4.18	4.19	$\star$

$\star \equiv$ convergency problem during denting

Table 5.39: Values of the ultimate opening bending moment for plain pipe, and for dented pipe, $(\frac{\delta}{D_o})_{max} = 0.36$, $\frac{2w}{t} = 0.5$, $p = 0.0$, off-centre gouges. Results are in: kNm.

Model type	$\frac{e}{t}\downarrow$	$\left(\frac{2c}{D_o}\right) = 0.25$	$\left(\frac{2c}{D_o}\right) = 0.50$	$\left(\frac{2c}{D_o}\right) = 0.75$	$\left(\frac{2c}{D_o}\right) = 1.0$
Plain pipe	0.25	4.42	4.42	4.41	4.41
	0.50	4.42	4.41	4.41	4.40
	0.75	4.41	4.40	4.40	4.38
Dented pipe	0.25	2.91	2.92	2.91	2.91
	0.50	2.93	2.97	3.0	2.90
	0.75	2.93	3.0	3.0	$\star$

$\star \equiv$ convergency problem during denting

Table 5.40: Values of the ultimate closing bending moment for plain pipe, and for dented pipe, $(\frac{\delta}{D_o})_{max} = 0.36$, $\frac{2w}{t} = 0.5$, $p = 0.0$, off-centre gouges. Results are in: kNm.

Model type	$\frac{e}{t}\downarrow$	$\left(\frac{2c}{D_o}\right) = 0.25$	$\left(\frac{2c}{D_o}\right) = 0.50$	$\left(\frac{2c}{D_o}\right) = 0.75$	$\left(\frac{2c}{D_o}\right) = 1.0$
Plain pipe	0.25	5.03	5.04	5.04	5.03
	0.50	5.02	5.03	5.02	5.02
	0.75	5.0	5.02	5.0	5.0
Dented pipe	0.25	4.75	4.73	4.73	4.73
	0.50	4.75	4.78	4.79	4.72
	0.75	4.75	4.81	⋆	⋆

⋆ ≡ convergency problem during denting

Table 5.41: Values of the ultimate opening bending moment for plain pipe, and for dented pipe, $(\frac{\delta}{D_o})_{max} = 0.36$, $\frac{2w}{t} = 1.45$, $p = 2.8\ MPa$, off-centre gouges. Results are in: kNm.

Model type	$\frac{e}{t}\downarrow$	$\left(\frac{2c}{D_o}\right) = 0.25$	$\left(\frac{2c}{D_o}\right) = 0.50$	$\left(\frac{2c}{D_o}\right) = 0.75$	$\left(\frac{2c}{D_o}\right) = 1.0$
Plain pipe	0.25	4.65	4.66	4.78	4.75
	0.50	4.41	4.46	4.46	4.44
	0.75	4.36	4.34	4.33	4.35
Dented pipe	0.25	3.47	3.47	3.46	3.45
	0.50	3.47	3.48	3.46	3.44
	0.75	3.47	3.49	⋆	⋆

⋆ ≡ convergency problem during denting

Table 5.42: Values of the ultimate closing bending moment for plain pipe, and for dented pipe, $(\frac{\delta}{D_o})_{max} = 0.36$, $\frac{2w}{t} = 1.45$, $p = 2.8\ MPa$, off-centre gouges. Results are in: kNm.

Model type	$\frac{e}{t}\downarrow$	$\left(\frac{2c}{D_o}\right) = 0.25$	$\left(\frac{2c}{D_o}\right) = 0.50$	$\left(\frac{2c}{D_o}\right) = 0.75$	$\left(\frac{2c}{D_o}\right) = 1.0$
Plain pipe	0.25	4.42	4.41	4.41	4.41
	0.50	4.41	4.40	4.40	4.40
	0.75	4.41	4.40	4.39	4.38
Dented pipe	0.25	4.17	4.17	4.16	4.17
	0.50	4.16	4.18	4.19	4.20
	0.75	4.17	4.18	4.19	4.20

Table 5.43: Values of the ultimate opening bending moment for plain pipe, and for dented pipe, $(\frac{\delta}{D_o})_{max} = 0.36$, $\frac{2w}{t} = 1.45$, $p = 0.0$, off-centre gouges. Results are in: kNm.

Model type	$\frac{e}{t}\downarrow$	$\left(\frac{2c}{D_o}\right) = 0.25$	$\left(\frac{2c}{D_o}\right) = 0.50$	$\left(\frac{2c}{D_o}\right) = 0.75$	$\left(\frac{2c}{D_o}\right) = 1.0$
Plain pipe	0.25	4.41	4.40	4.40	4.40
	0.50	4.40	4.38	4.37	4.37
	0.75	4.38	4.34	4.33	4.31
Dented pipe	0.25	2.90	2.92	2.92	2.91
	0.50	2.92	3.0	3.0	3.0
	0.75	2.94	3.0	3.0	3.0

Table 5.44: Values of the ultimate closing bending moment for plain pipe, and for dented pipe, $(\frac{\delta}{D_o})_{max} = 0.36$, $\frac{2w}{t} = 1.45$, $p = 0.0$, off-centre gouges. Results are in: kNm.

Model type	$\frac{e}{t}\downarrow$	$\left(\frac{2c}{D_o}\right) = 0.25$	$\left(\frac{2c}{D_o}\right) = 0.50$	$\left(\frac{2c}{D_o}\right) = 0.75$	$\left(\frac{2c}{D_o}\right) = 1.0$
Plain pipe	**0.25**	5.02	5.04	5.01	5.02
	0.50	5.0	5.02	5.0	5.03
	0.75	5.0	5.0	4.96	5.0
Dented pipe	**0.25**	4.75	4.75	4.78	4.73
	0.50	4.74	4.75	4.79	4.75
	0.75	4.75	4.74	$\star$	$\star$

$\star \equiv$ convergency problem during denting

Table 5.45: Values of the ultimate opening bending moment for plain pipe, and for dented pipe, $(\frac{\delta}{D_o})_{max} = 0.36$, $\frac{2w}{t} = 2.42$, $p = 2.8\ MPa$, off-centre gouges. Results are in: kNm.

Model type	$\frac{e}{t}\downarrow$	$\left(\frac{2c}{D_o}\right) = 0.25$	$\left(\frac{2c}{D_o}\right) = 0.50$	$\left(\frac{2c}{D_o}\right) = 0.75$	$\left(\frac{2c}{D_o}\right) = 1.0$
Plain pipe	**0.25**	4.56	4.58	4.71	4.64
	0.50	4.40	4.39	4.38	4.40
	0.75	4.30	4.30	4.30	4.27
Dented pipe	**0.25**	3.47	3.47	3.46	3.45
	0.50	3.47	3.48	3.46	3.45
	0.75	3.47	3.49	$\star$	$\star$

$\star \equiv$ convergency problem during denting

Table 5.46: Values of the ultimate closing bending moment for plain pipe, and for dented pipe, $(\frac{\delta}{D_o})_{max} = 0.36$, $\frac{2w}{t} = 2.42$, $p = 2.8\ MPa$, off-centre gouges. Results are in: kNm.

Model type	$\frac{e}{t}\downarrow$	$\left(\frac{2c}{D_o}\right) = 0.25$	$\left(\frac{2c}{D_o}\right) = 0.50$	$\left(\frac{2c}{D_o}\right) = 0.75$	$\left(\frac{2c}{D_o}\right) = 1.0$
Plain pipe	**0.25**	4.41	4.41	4.40	4.40
	0.50	4.41	4.39	4.38	4.38
	0.75	4.40	4.26	4.36	4.36
Dented pipe	**0.25**	4.17	4.18	4.16	4.18
	0.50	4.17	4.18	4.20	4.20
	0.75	4.17	3.35	4.20	4.19

Table 5.47: Values of the ultimate opening bending moment for plain pipe, and for dented pipe, $(\frac{\delta}{D_o})_{max} = 0.36$, $\frac{2w}{t} = 2.42$, $p = 0.0$, off-centre gouges. Results are in: kNm.

Model type	$\frac{e}{t}\downarrow$	$\left(\frac{2c}{D_o}\right) = 0.25$	$\left(\frac{2c}{D_o}\right) = 0.50$	$\left(\frac{2c}{D_o}\right) = 0.75$	$\left(\frac{2c}{D_o}\right) = 1.0$
Plain pipe	**0.25**	4.40	4.39	4.39	4.38
	0.50	4.37	4.34	4.33	4.33
	0.75	4.33	4.17	4.27	4.30
Dented pipe	**0.25**	2.91	2.94	2.94	2.92
	0.50	2.91	3.0	3.0	3.0
	0.75	2.94	2.80	3.0	3.0

Table 5.48: Values of the ultimate closing bending moment for plain pipe, and for dented pipe, $(\frac{\delta}{D_o})_{max} = 0.36$, $\frac{2w}{t} = 2.42$, $p = 0.0$, off-centre gouges. Results are in: kNm.

p (MPa) $\downarrow$	F_{max} (kN)	$\left(\frac{\delta}{D_o}\right)_{max}$	$\left(\frac{\delta}{D_o}\right)_R$	$\frac{\Delta A}{A_o}$ (%)
2.8	40.57	0.36	0.327	14.8
5.6	52.85	0.36	0.290	12.0

Table 5.49: Results for dents in gouge free pipe for two value of pressure. Also, $\frac{a}{b} = 1.0$, $(\frac{\delta}{D_o})_{max} = 0.36$, and $\frac{2L}{D_o} = 6.0$.

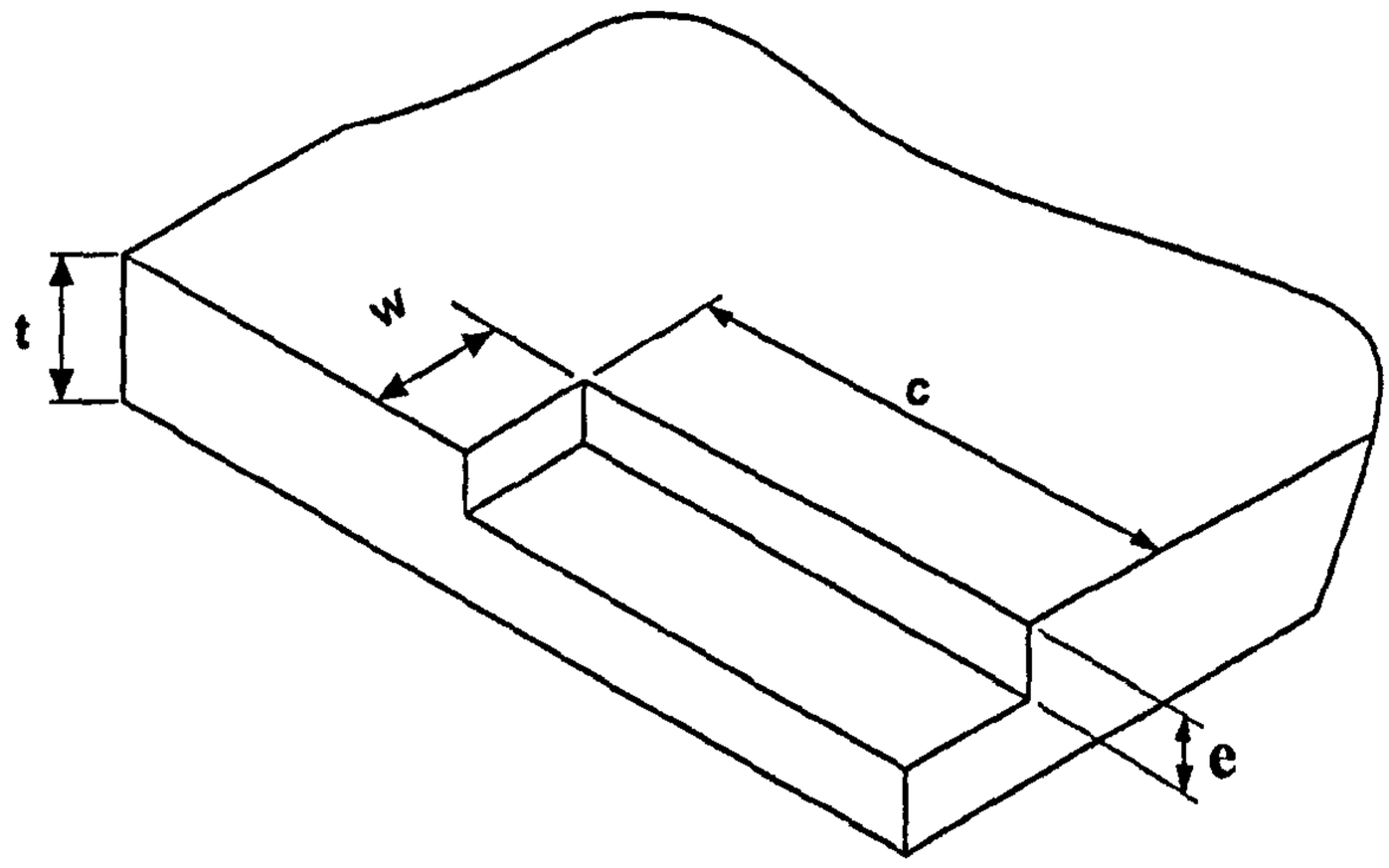

Figure 5.1: Geometry of axial gouge with its parameters, e, w, and c.

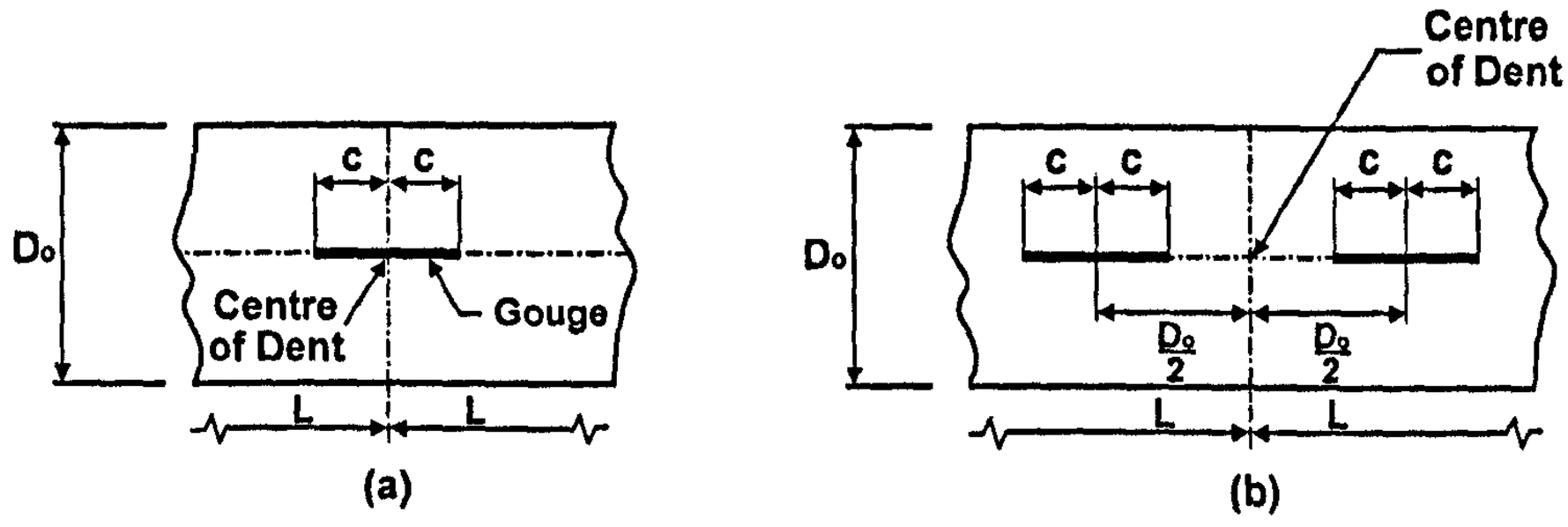

Figure 5.2: Sketch showing size and location of a single, axial gouge - Fig. 5.2a. Two axial gouges placed symmetrically around the mid-length are shown in Fig. 5.2b.

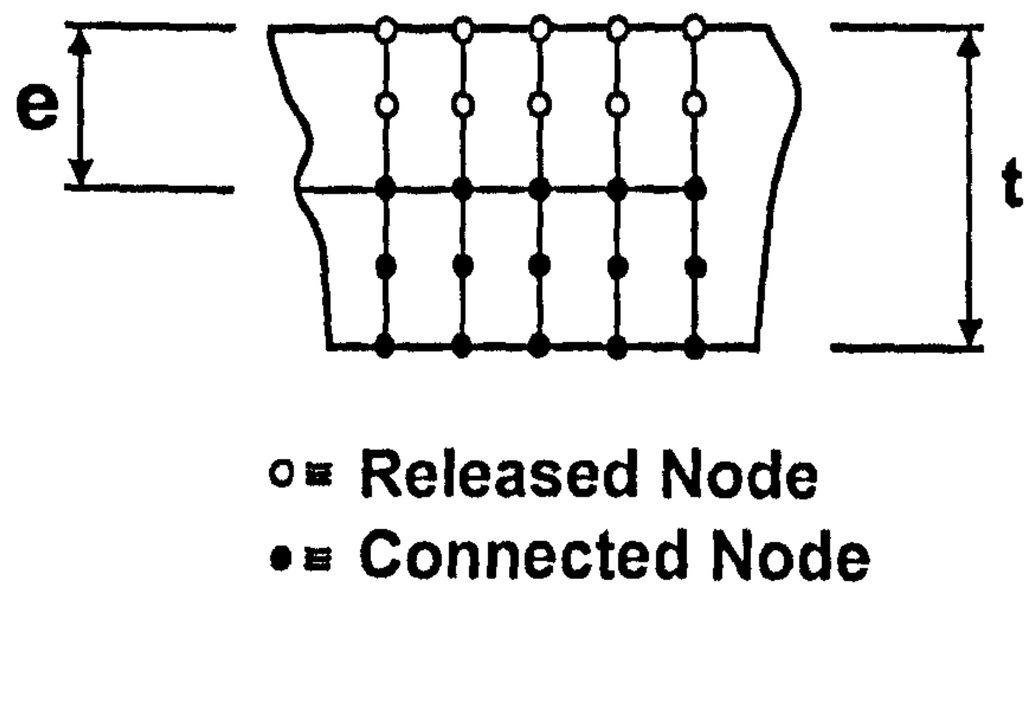

Figure 5.3: Sketch showing section through the pipe wall illustrating the node release method for $\frac{e}{t} = 0.5$.

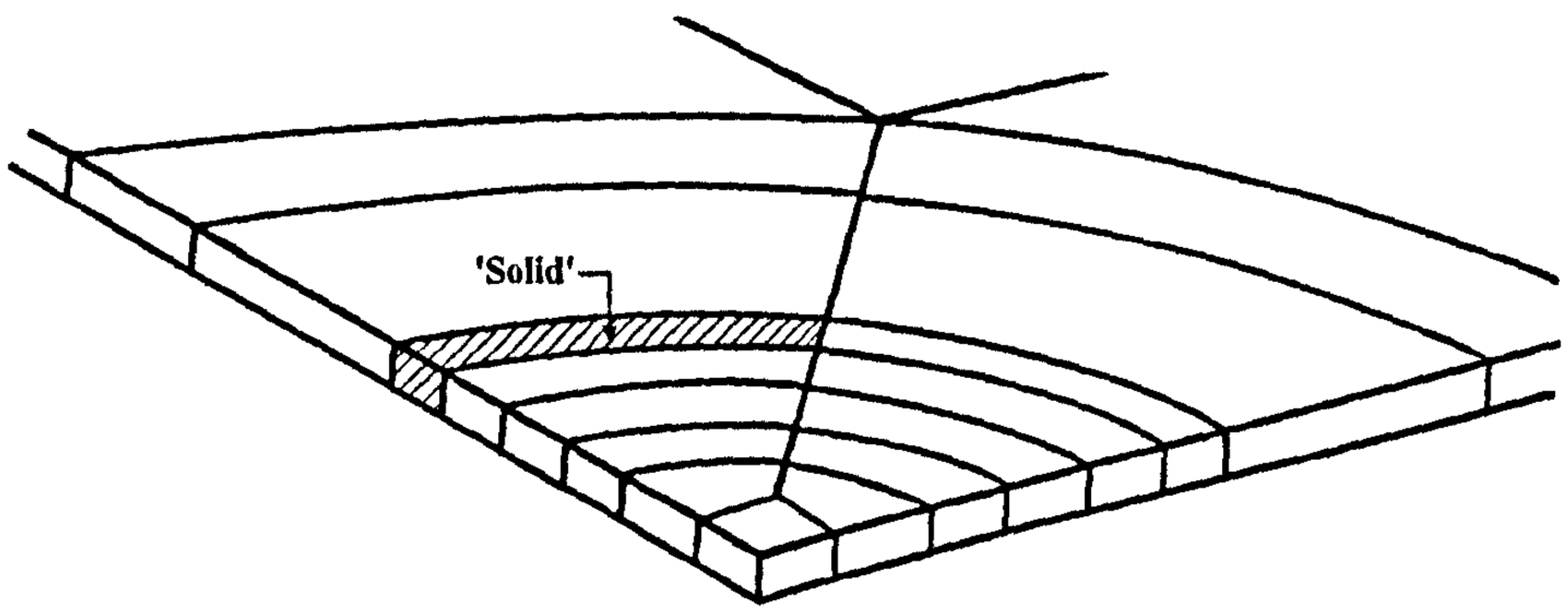

Figure 5.4: Closer view of a quarter solid FE model without defect (PATRAN).

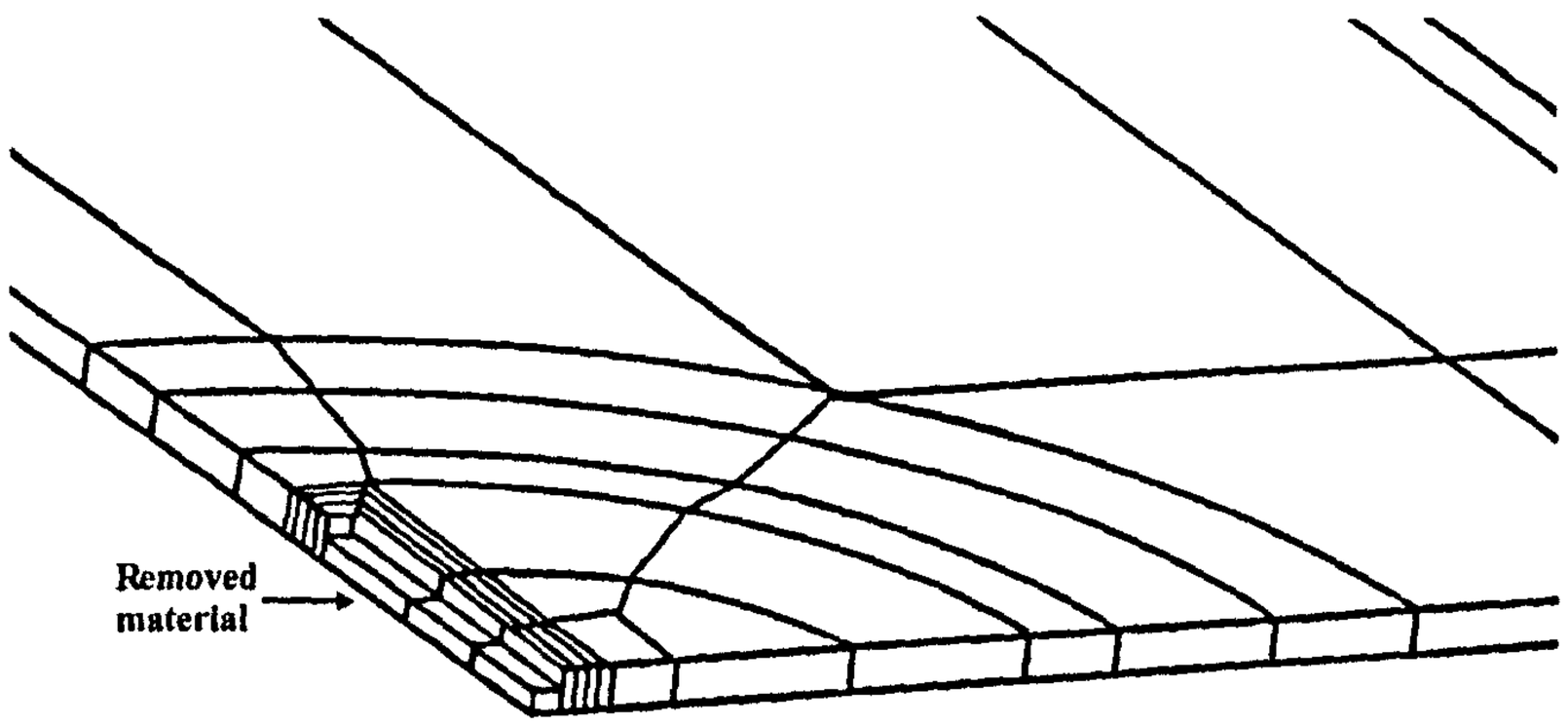

Figure 5.5: Closer view of a quarter solid FE model (PATRAN). Note how material has been removed in order to create a gouge at pipe's mid-span.

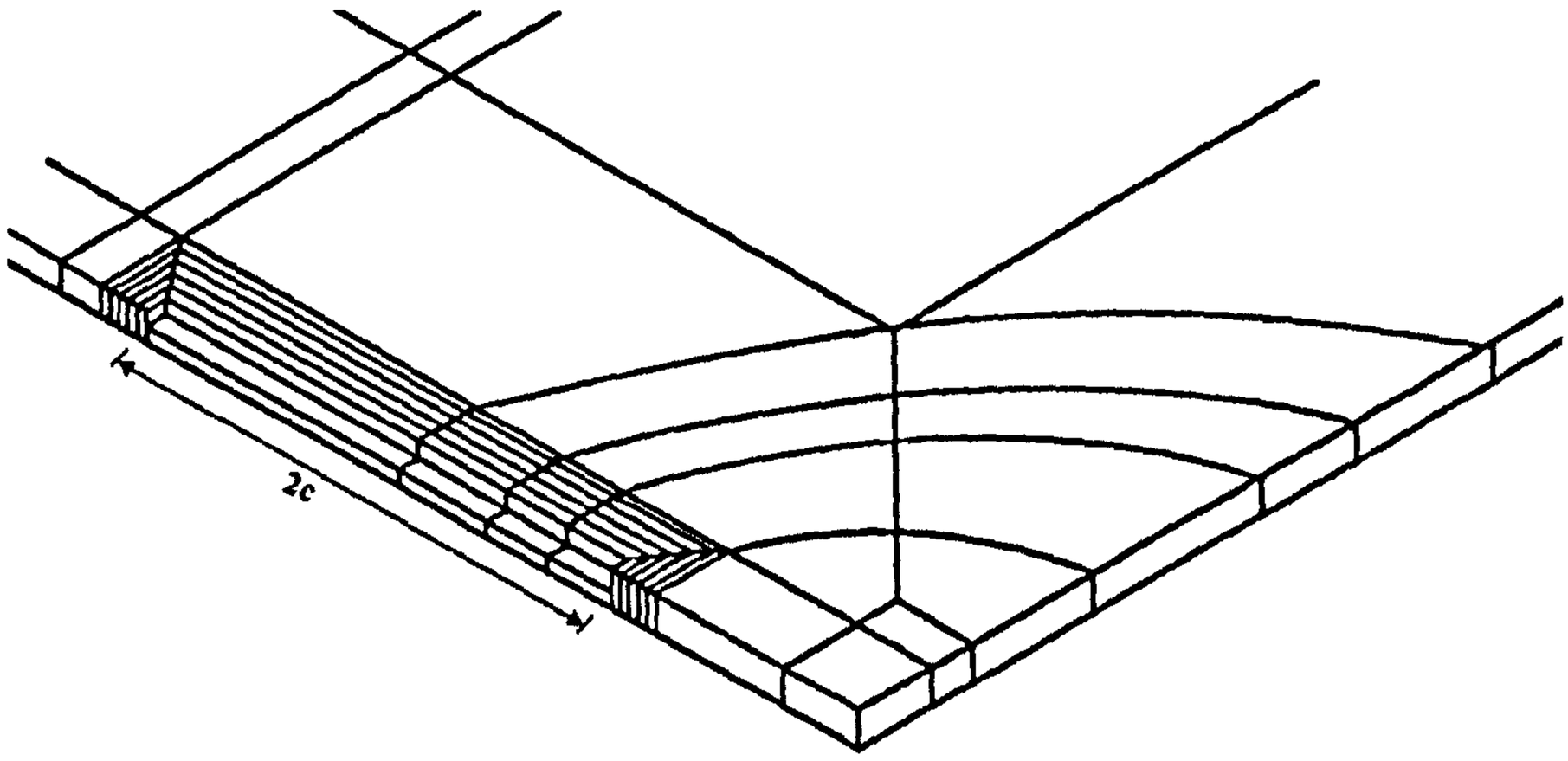

Figure 5.6: Closer view of a quarter solid FE model (PATRAN). Note how material has been removed to create an off-centre gouge. Gouge of length is, 2c. Also, illustration of denser meshing of solids.

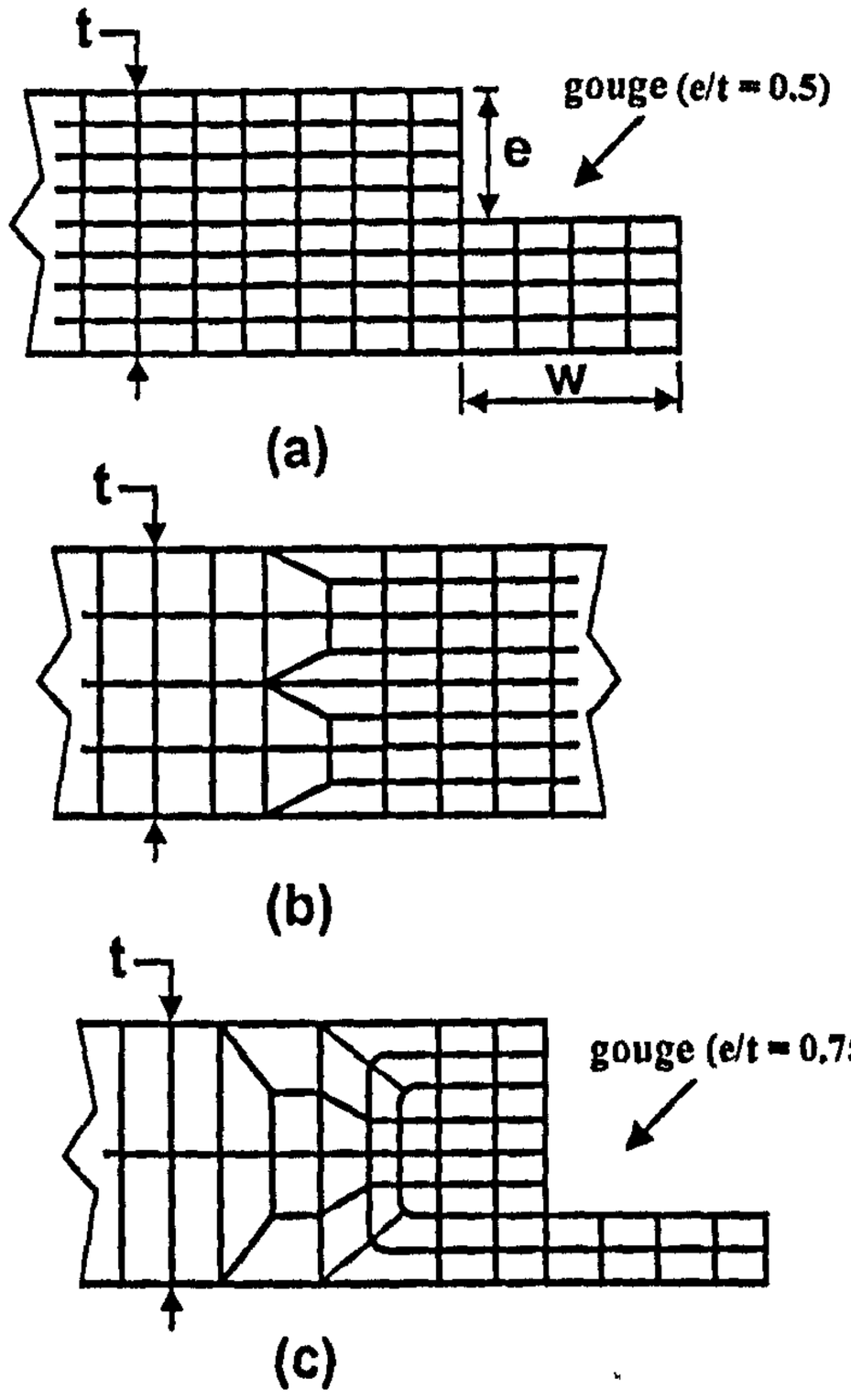

Figure 5.7: Illustration of mesh arrangements for transition of number of elements through the wall thickness; Fig. 5.7a illustrates transition from 4 to 8 elements through thickness; Fig. 5.7b shows transition from 8 to 4 layers through thickness, and Fig. 5.7c shows transition from 2 layers in ligament to 8 layers, and then from 8 layers, to 2 layers through thickness.

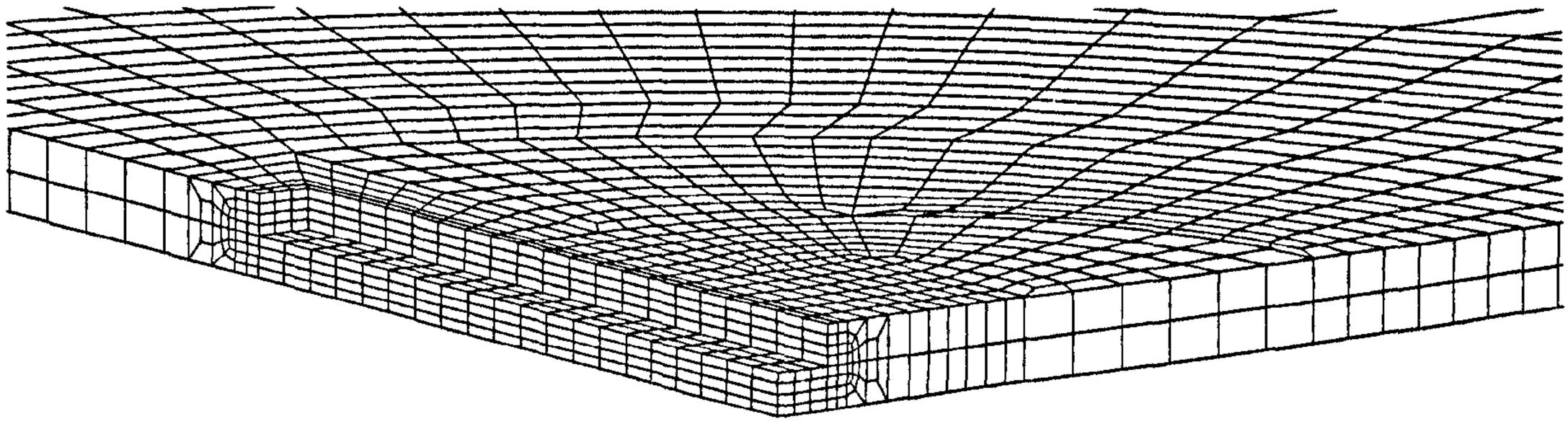

Figure 5.8: Close view of FE model with an axial gouge at the mid-span after meshing solids in PATRAN. Note that there are 8 brick elements through the wall thickness in gouge vicinity, and four layers of brick elements at the bottom (ligament) of the gouge.

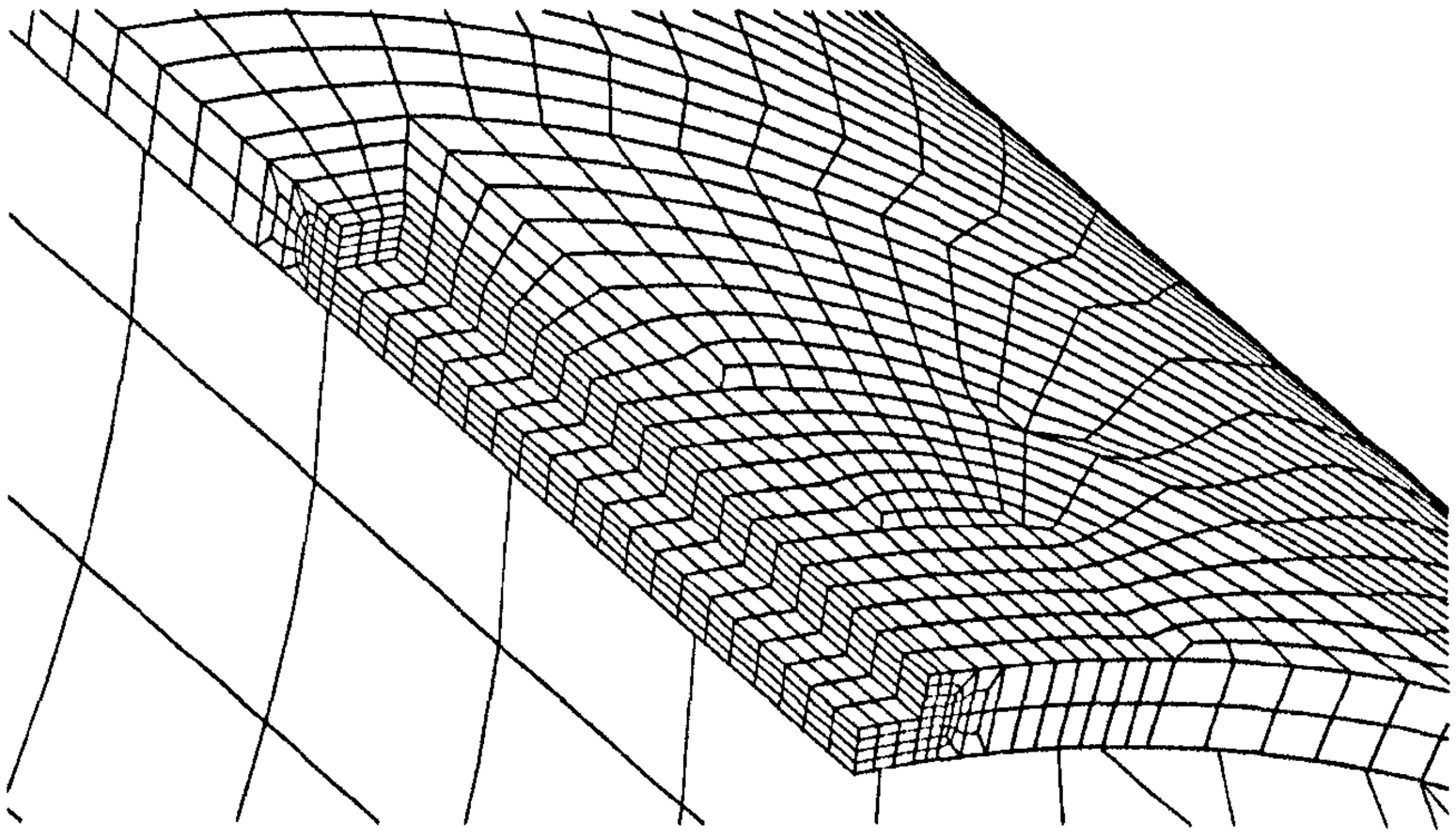

Figure 5.9: Close view of FE model with axial gouge at the centre after flat model was transformed into pipe (through the application of NMAP parameter).

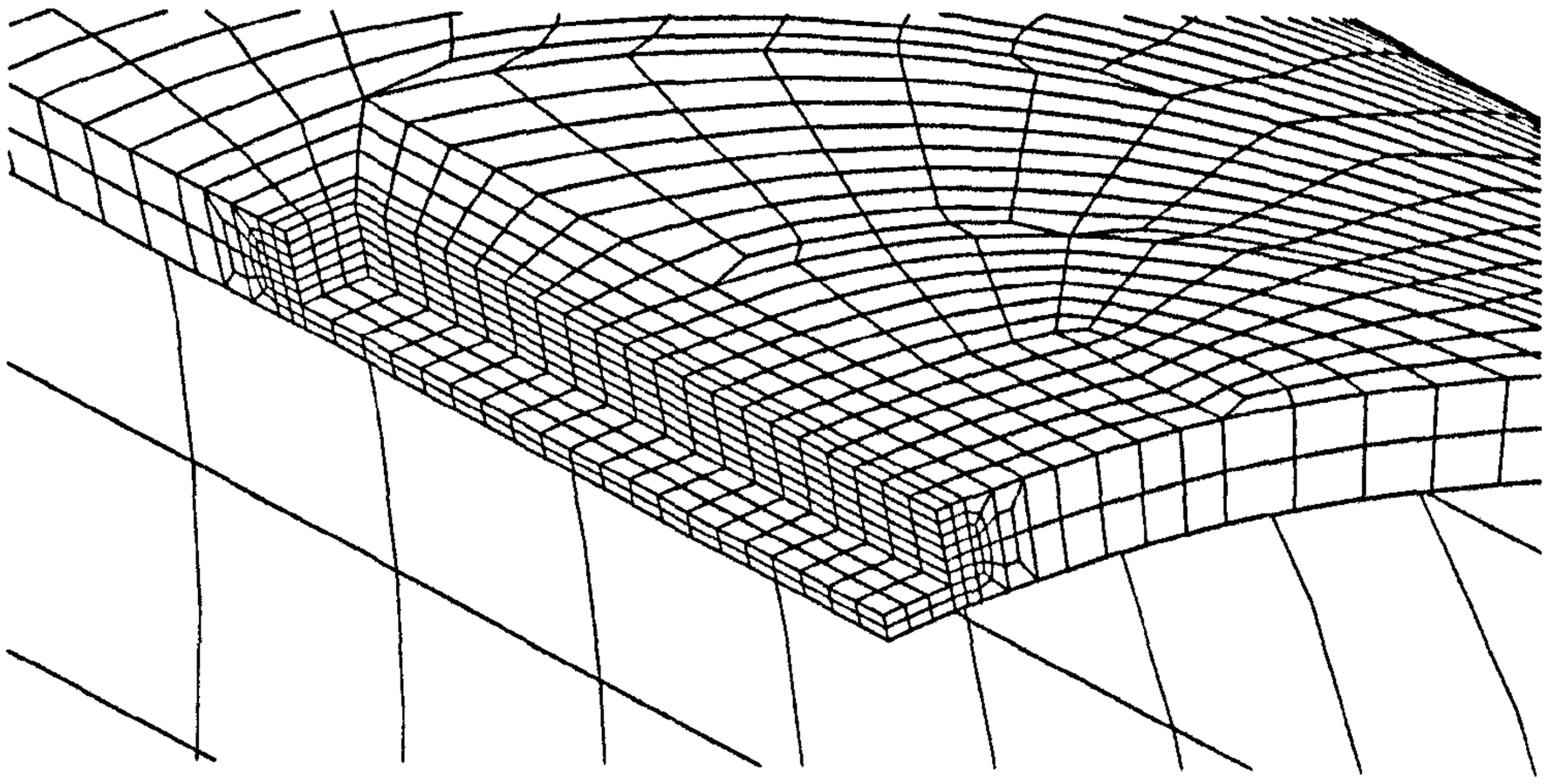

Figure 5.10: View of another gouge having two layers at the bottom (ligament). Note how layers of brick elements were reduced to two layers away from the gouge.

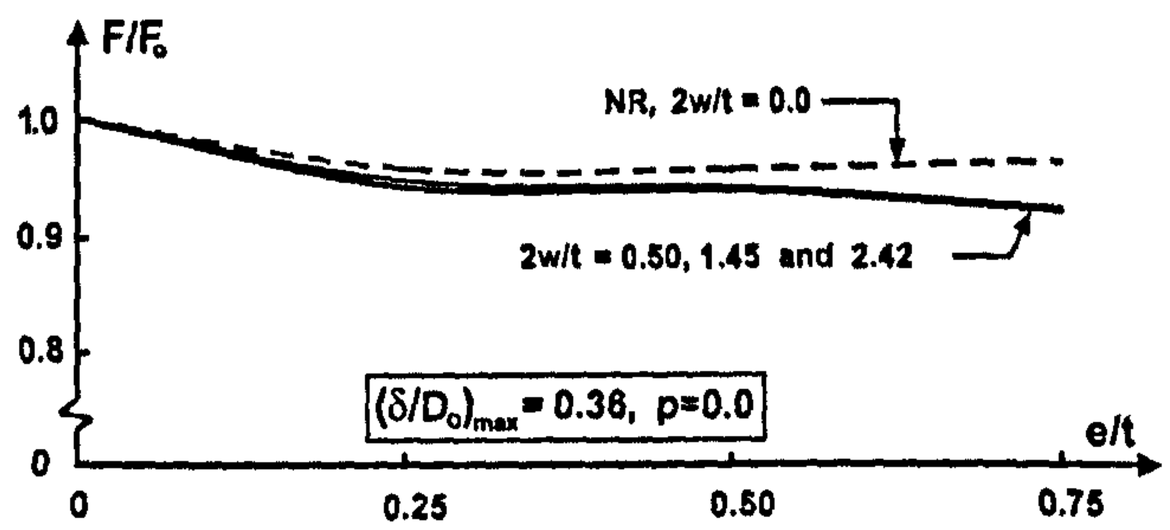

(a) $\frac{2c}{D_o} = 0.25$

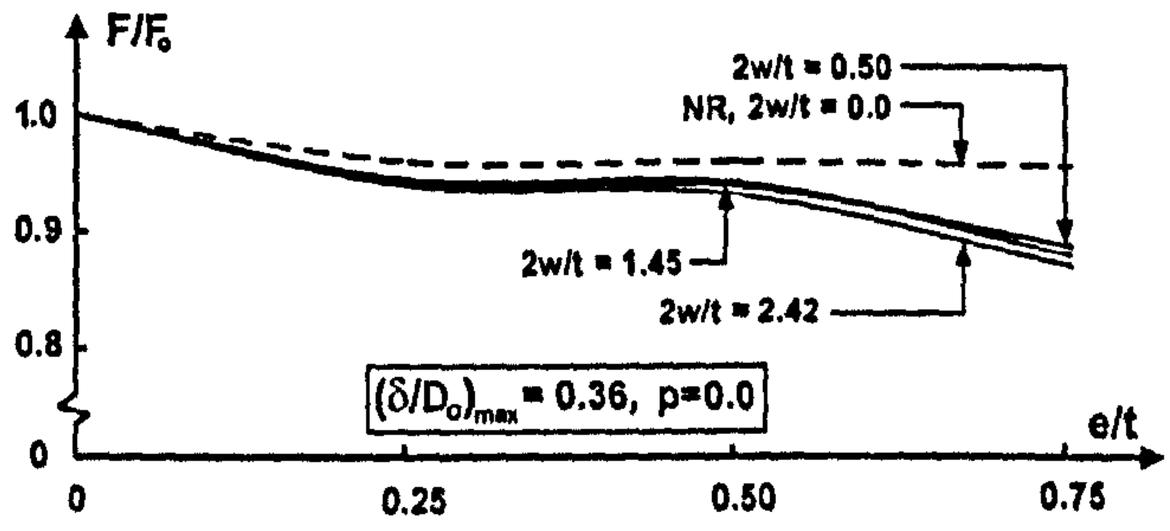

(b) $\frac{2c}{D_o} = 0.50$

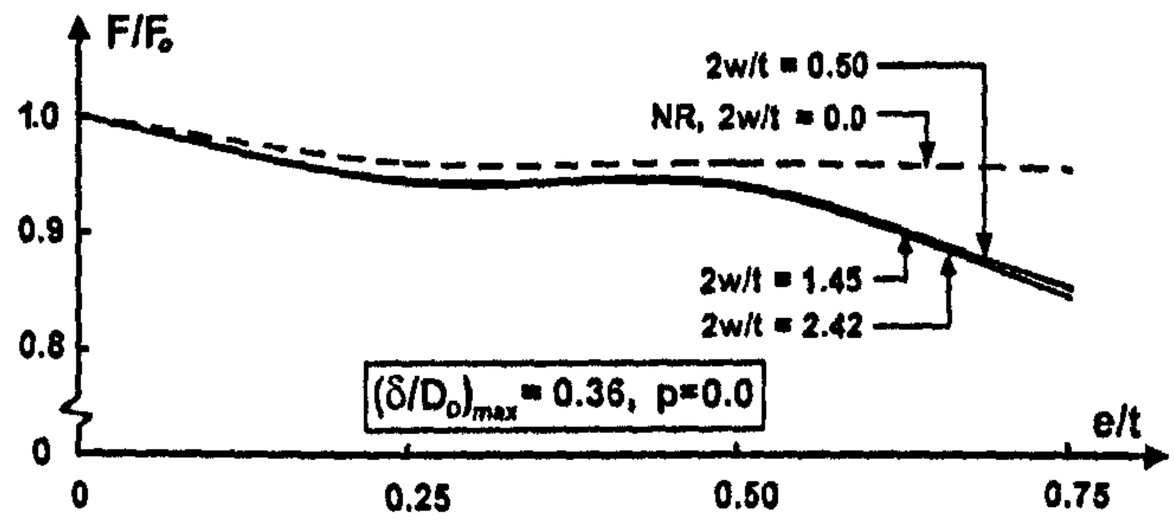

(c) $\frac{2c}{D_o} = 0.75$

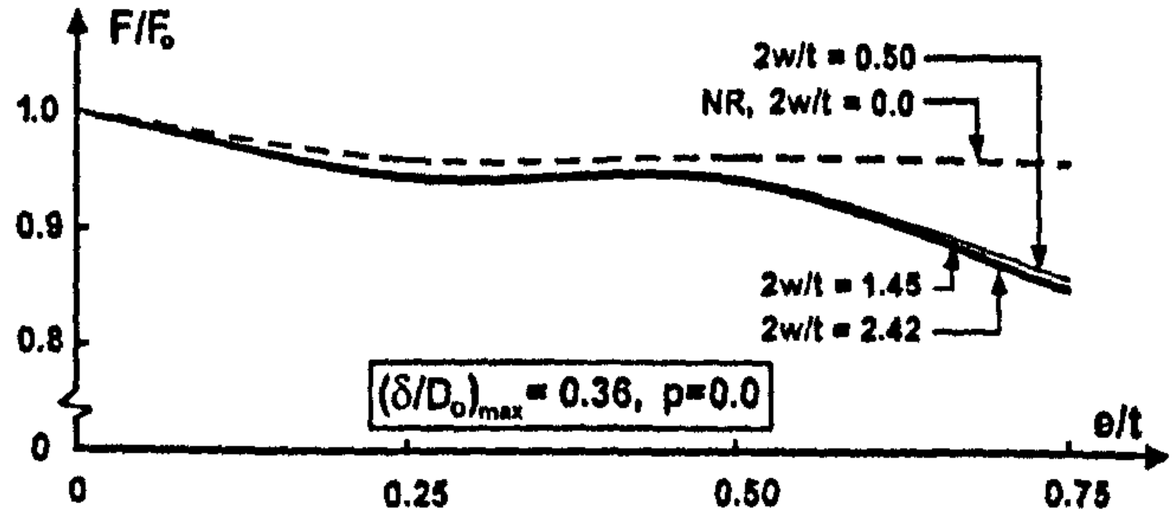

(d) $\frac{2c}{D_o} = 1.0$

Figure 5.11: Plot of dimensionless denting force, $\frac{F}{F_o}$, versus depths of gouges, $\frac{e}{t}$. Results for four widths of gouges: $\frac{2w}{t} = 0.0, 0.5, 1.45$, and 2.42 are shown. Also, $\frac{a}{b} = 1.0$, and $\frac{2L}{D_o} = 6.0$. Gouges are placed at mid-span, underneath the indenter. F_o: is denting load for plain pipe without gouge ($F_o = 26.5\ kN$). NR $\equiv$ Node Release Method.

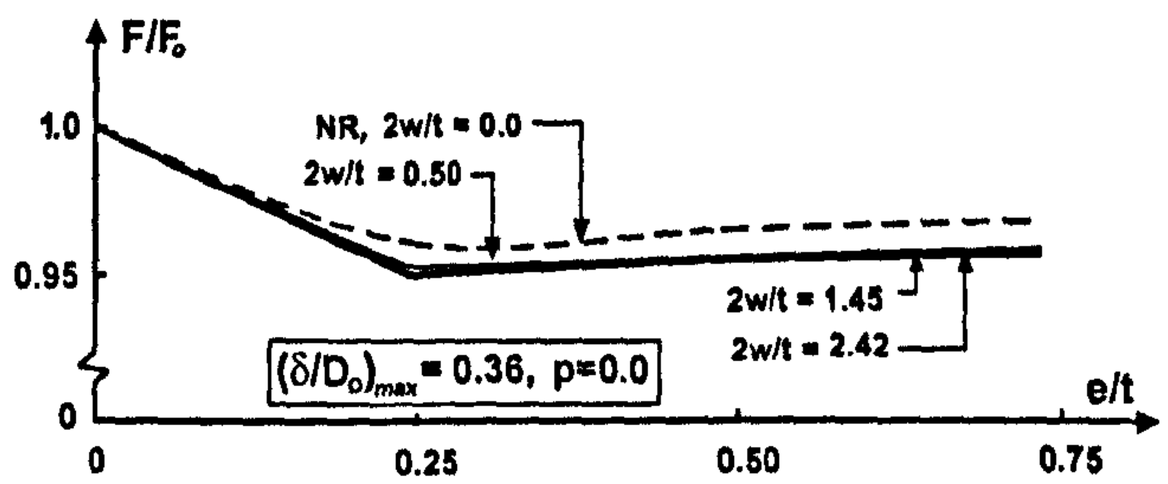

(a) $\frac{2c}{D_o} = 0.25$

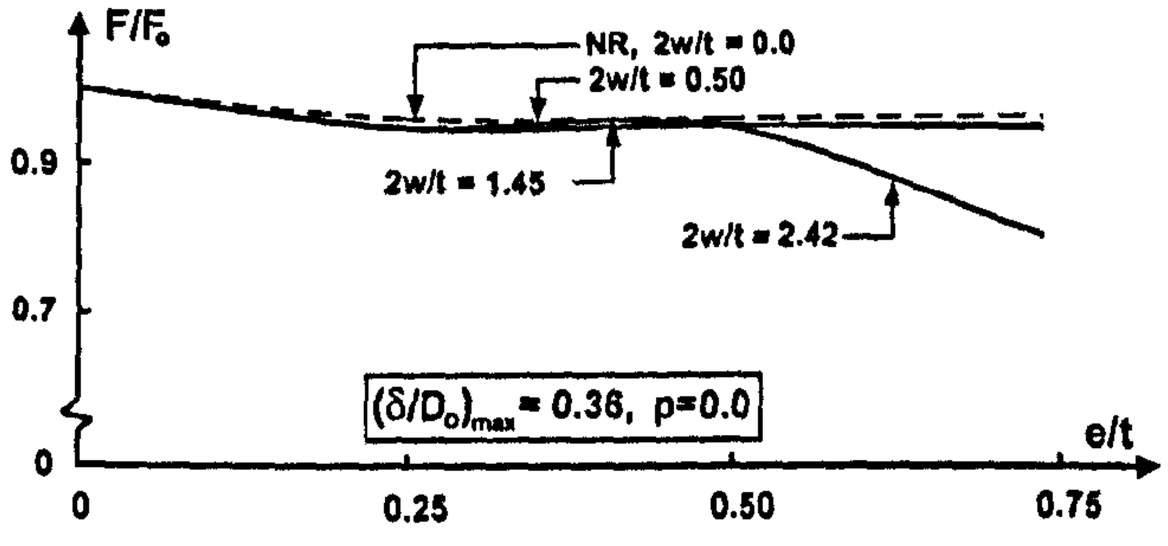

(b) $\frac{2c}{D_o} = 0.50$

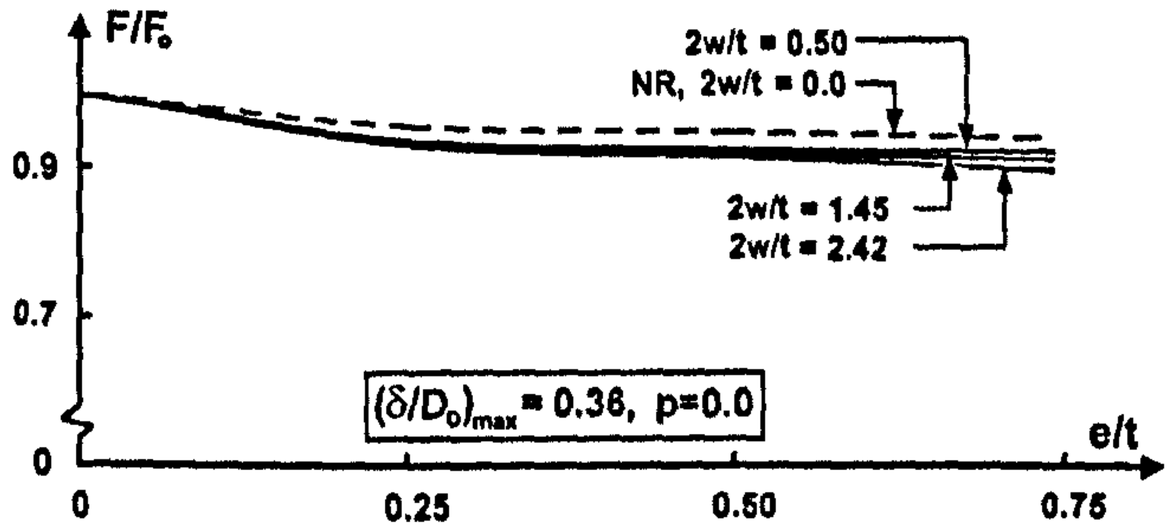

(c) $\frac{2c}{D_o} = 0.75$

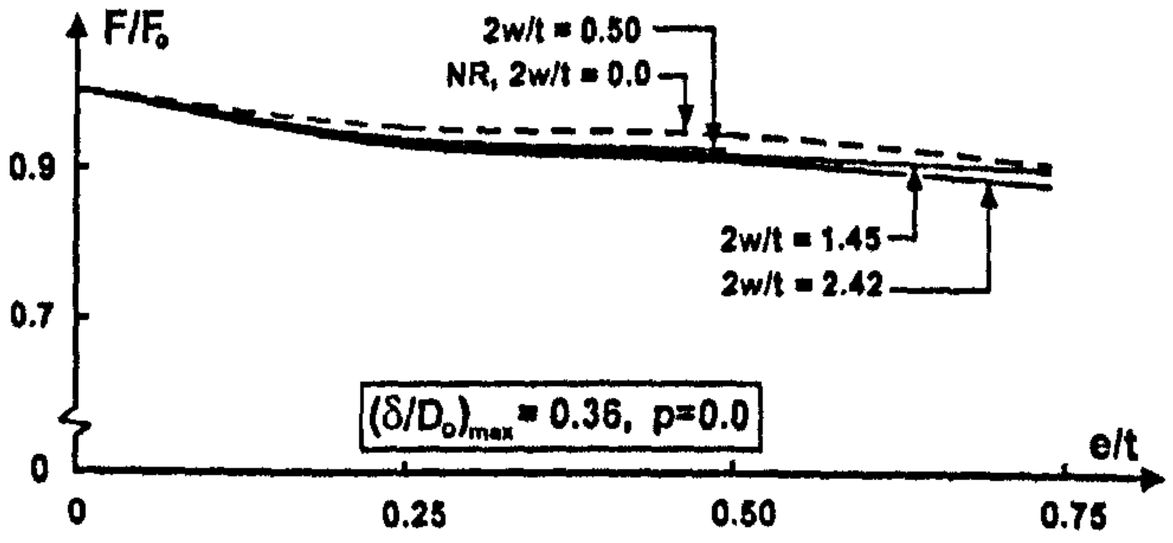

(d) $\frac{2c}{D_o} = 1.0$

Figure 5.12: Plot of dimensionless denting force, $\frac{F}{F_o}$, versus depths of gouges, $\frac{e}{t}$. Results for four widths of gouges: $\frac{2w}{t} = 0.0, 0.5, 1.45$, and 2.42 are shown. Also, $\frac{a}{b} = 1.0$, and $\frac{2L}{D_o} = 6.0$. Gouges are placed off-centre by $\frac{D_o}{2}$. F_o: is denting load for plain pipe without gouge ($F_o = 26.5\ kN$). NR $\equiv$ Node Release Method.

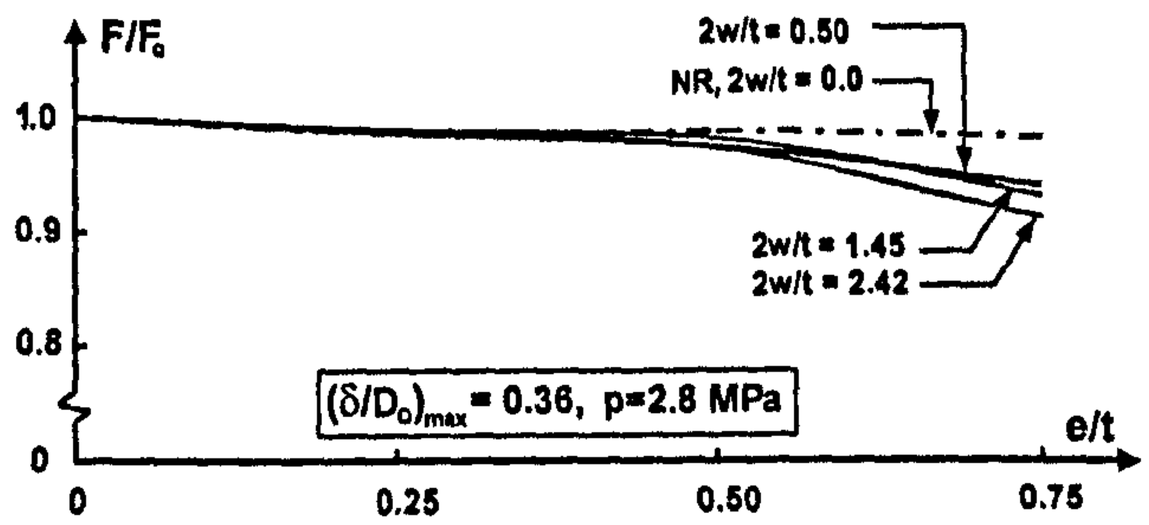

(a) $\frac{2c}{D_o} = 0.25$

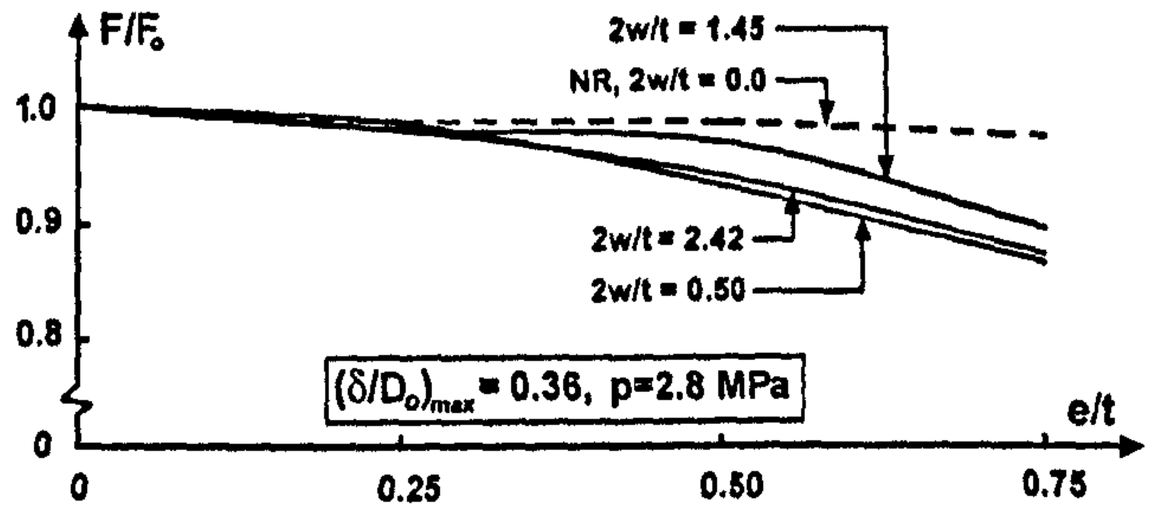

(b) $\frac{2c}{D_o} = 0.50$

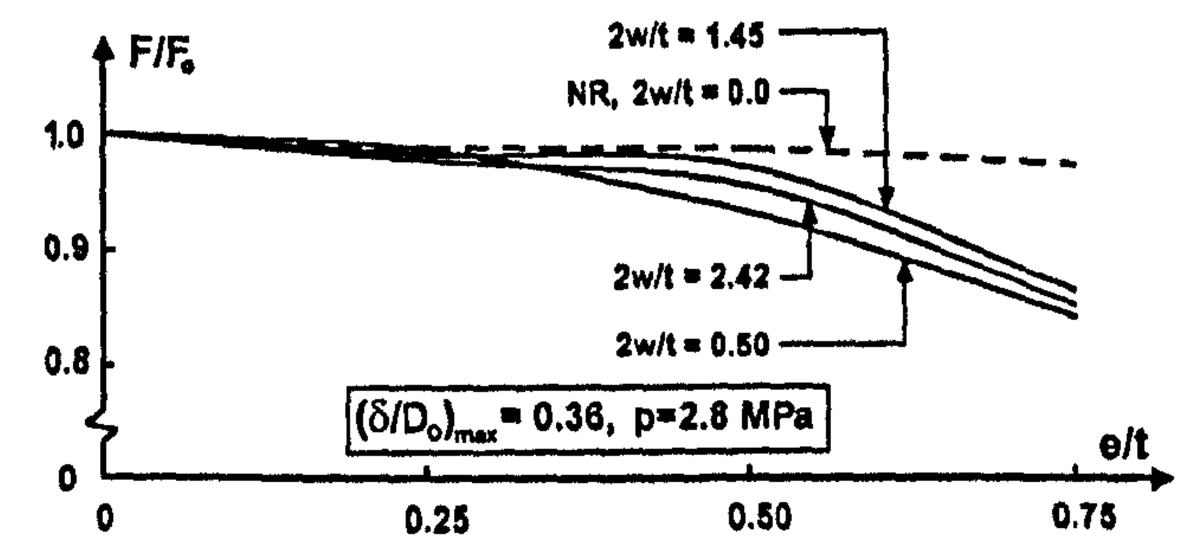

(c) $\frac{2c}{D_o} = 0.75$

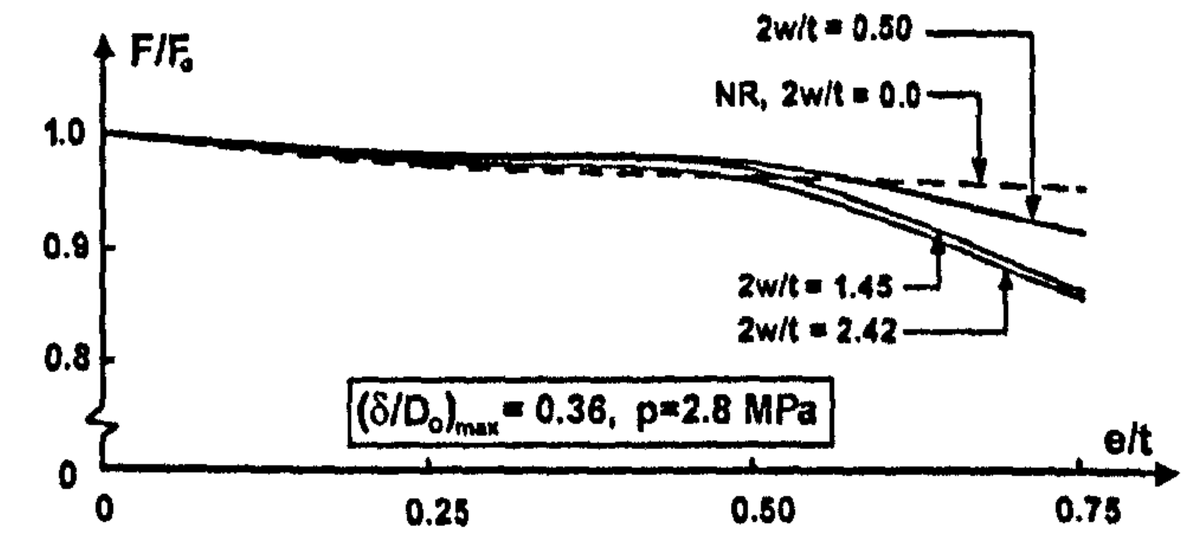

(d) $\frac{2c}{D_o} = 1.0$

Figure 5.13: Plot of dimensionless denting force, $\frac{F}{F_o}$, versus depths of gouges, $\frac{e}{t}$. Results for four width of gouges, $\frac{2w}{t} = 0.0, 0.5, 1.45$, and 2.42 are shown. Also, $\frac{a}{b} = 1.0$, and $\frac{2L}{D_o} = 6.0$. Gouges are placed at mid-span, underneath the indenter. F_o: is denting load for plain pipe without gouge ($F_o = 40.57\ kN$). NR $\equiv$ Node Release Method.

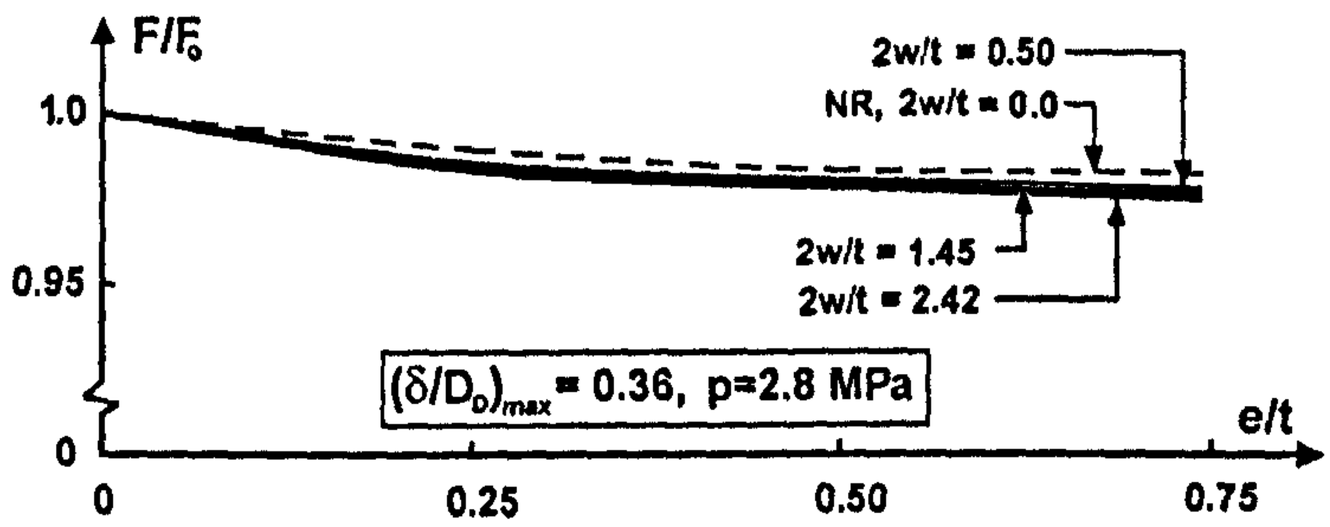

(a) $\frac{2c}{D_o} = 0.25$

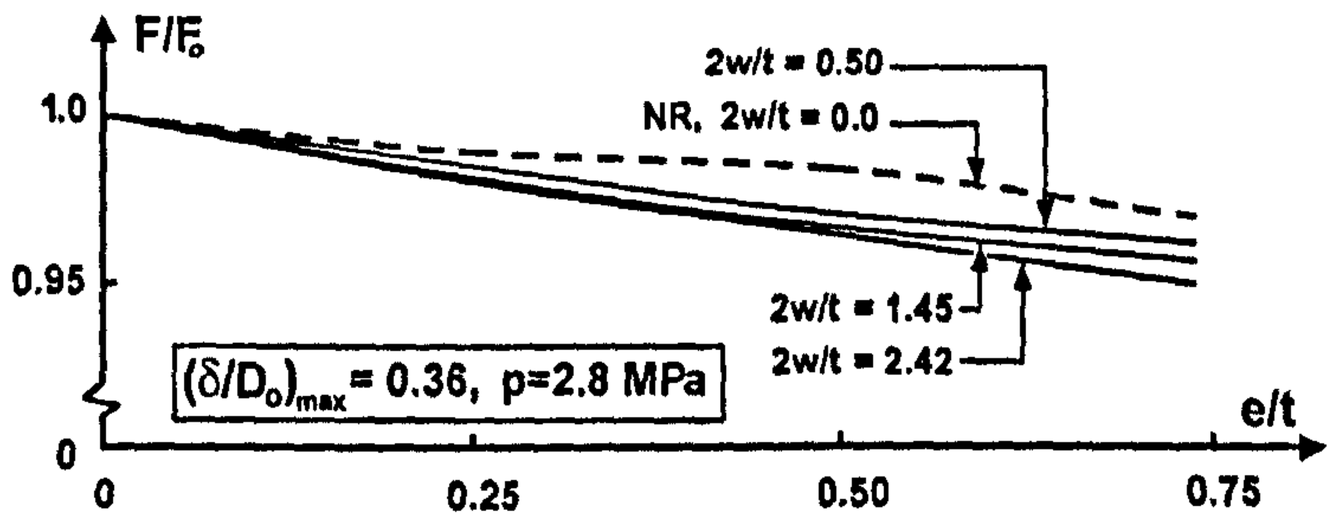

(b) $\frac{2c}{D_o} = 0.50$

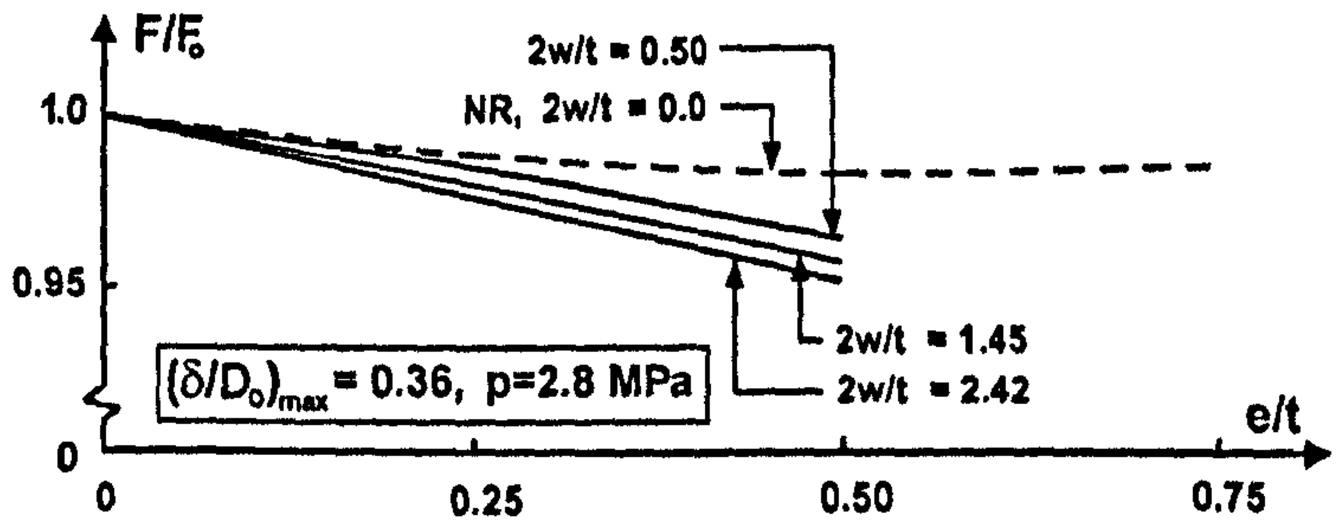

(c) $\frac{2c}{D_o} = 0.75$

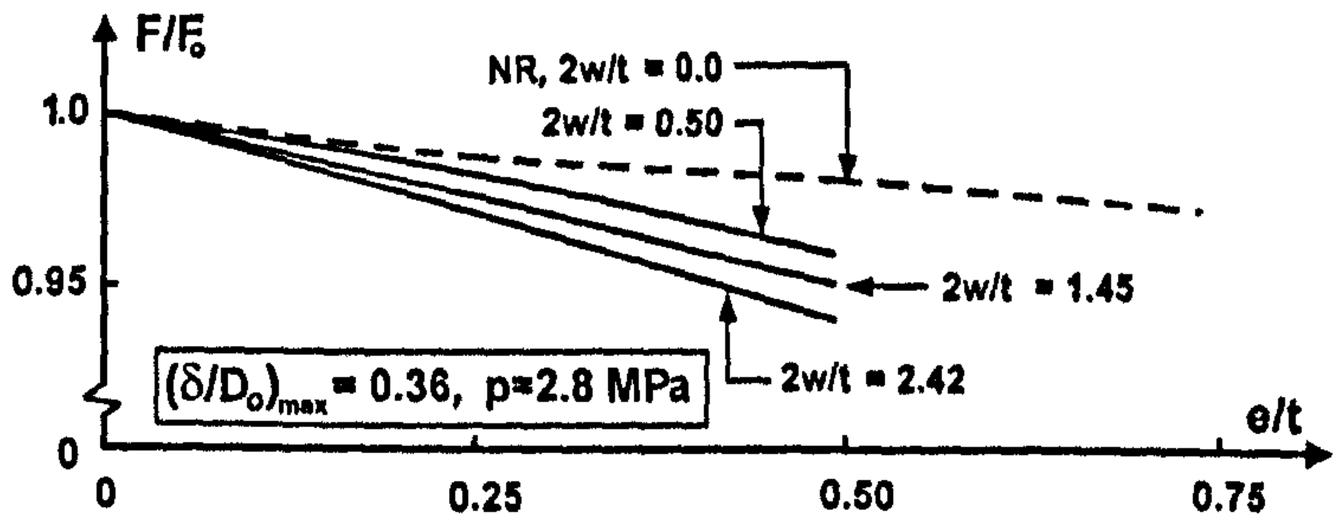

(d) $\frac{2c}{D_o} = 1.0$

Figure 5.14: Plot of dimensionless denting force, $\frac{F}{F_o}$, versus the depths of gouges, $\frac{e}{t}$. Results for four width of gouges $\frac{2w}{t} = 0.0, 0.5, 1.45$, and 2.42 are shown. Also, $\frac{a}{b} = 1.0$, and $\frac{2L}{D_o} = 6.0$. Gouge are placed at off-centre by $\frac{D_o}{2}$. F_o: denting load for plain pipe without gouge ($F_o = 40.57\ kN$). NR $\equiv$ Node Release Method.

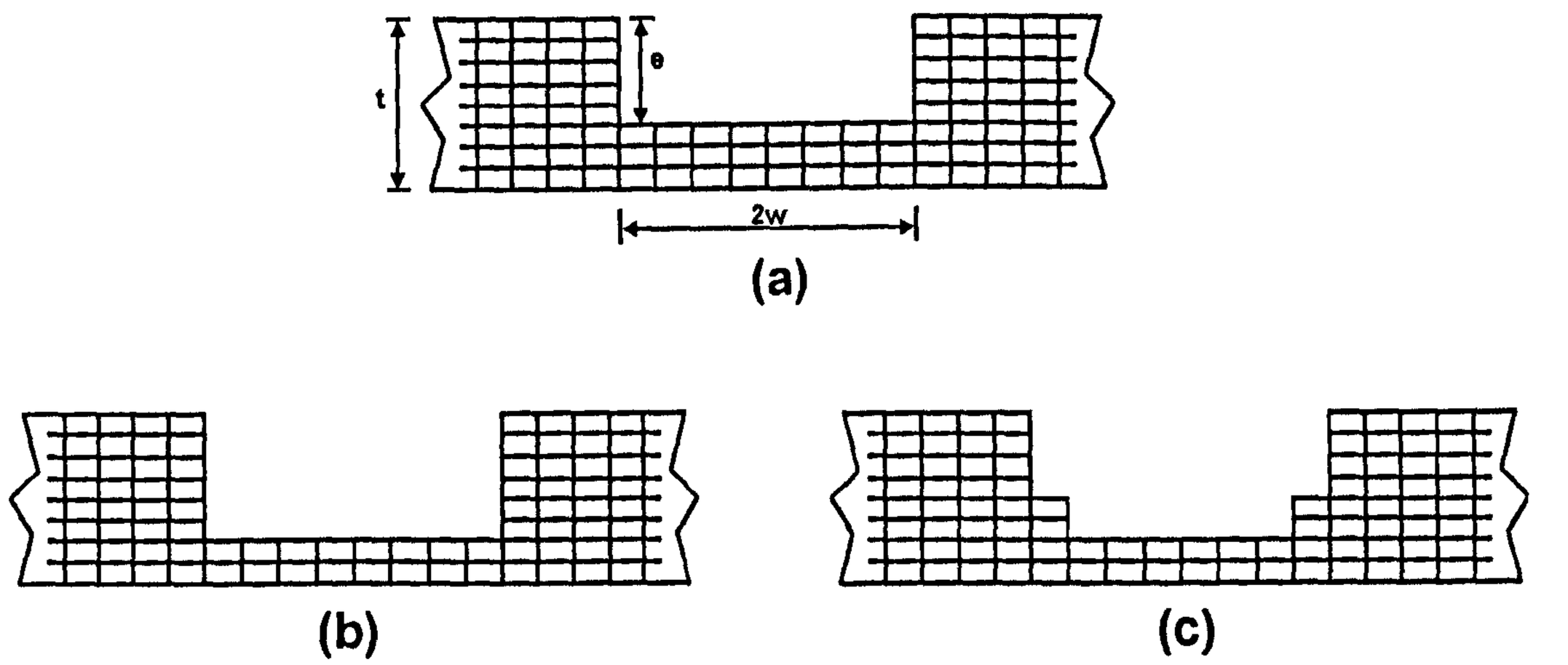

Figure 5.15: Sketch showing a cross-section of axial slot gouges having different shapes, (a) a rectangular surface defect with 3 layers of elements in ligament, $\frac{e}{t} = 0.625$; (b) a rectangular surface defect with 2 elements in ligament $\frac{e}{t} = 0.75$; (c) a rectangular surface defect with 2 layers of elements in ligament; (d), and (f) are similar to case (b), and case (e) represents a notch defect with 2 elements in ligament, $\frac{e}{t} = 0.75$.

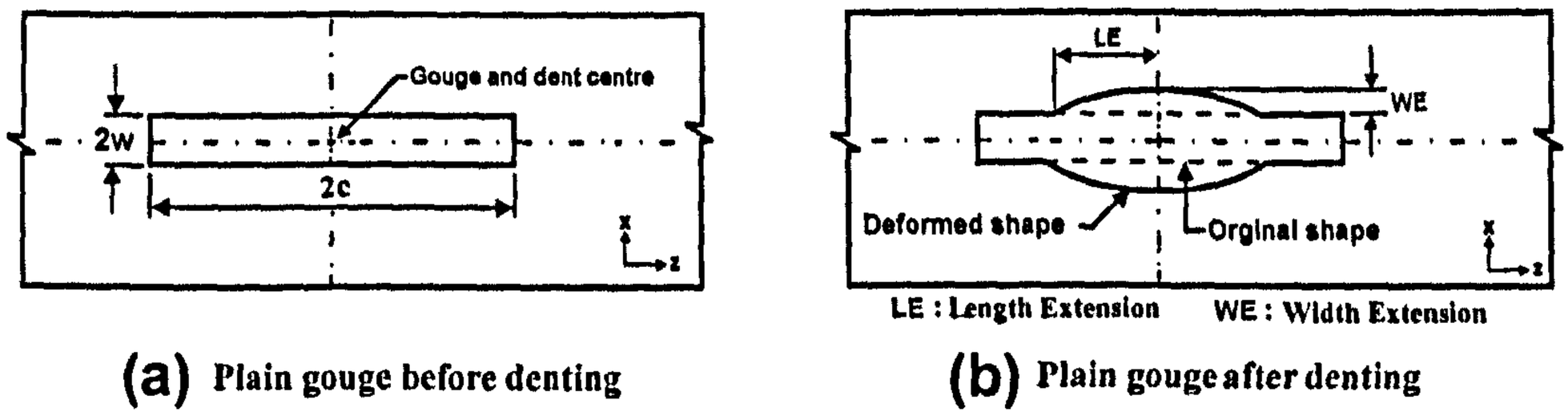

Figure 5.16: Axial, mid-span gouge Fig. (5.16a). Growth of width, WE, and its axial length, LE, Fig. (5.16b).

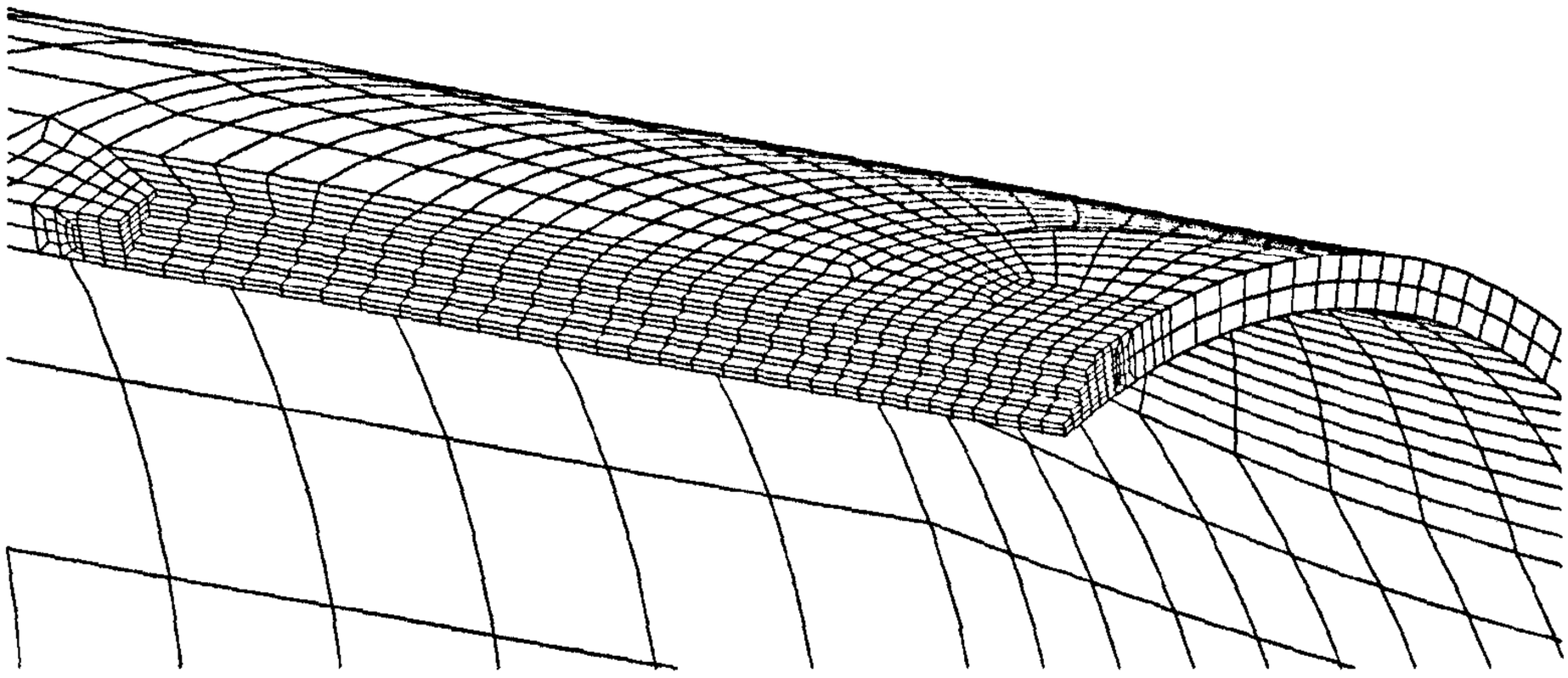

Figure 5.17: FE model with axial slot gouge illustrating the V notch geometry with two elements through thickness (as modelled). Also, $\frac{a}{b} = 1.0$, and $\frac{2L}{D_o} = 6.0$.

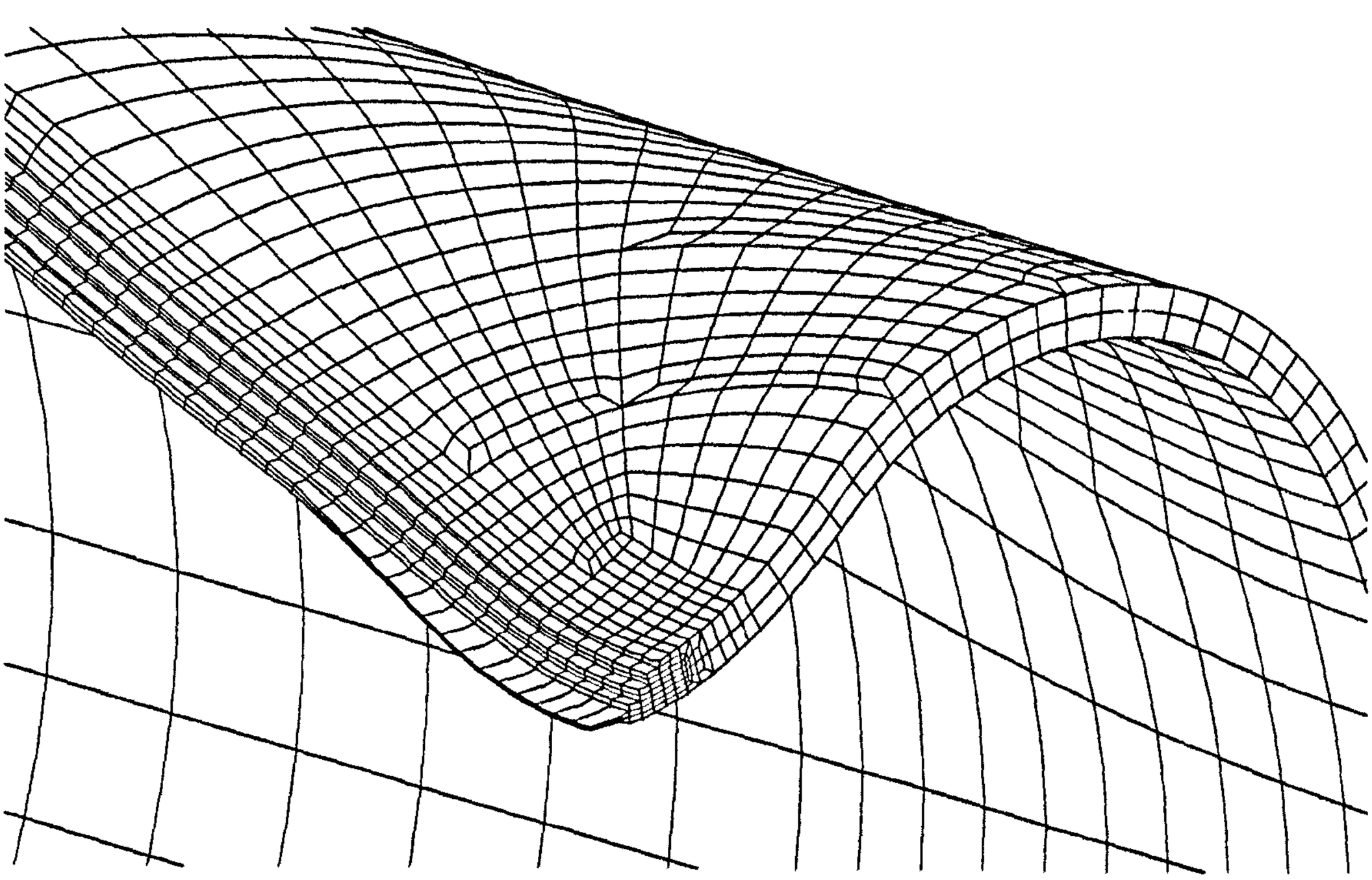

Figure 5.18: FE model with axial slot gouge after denting. Note how the bottom surface of the gouge is extended in hoop direction ($(\frac{\delta}{D_o})_{max} = 0.36$, $p = 2.8\ MPa$, and $\frac{2L}{D_o} = 6.0$).

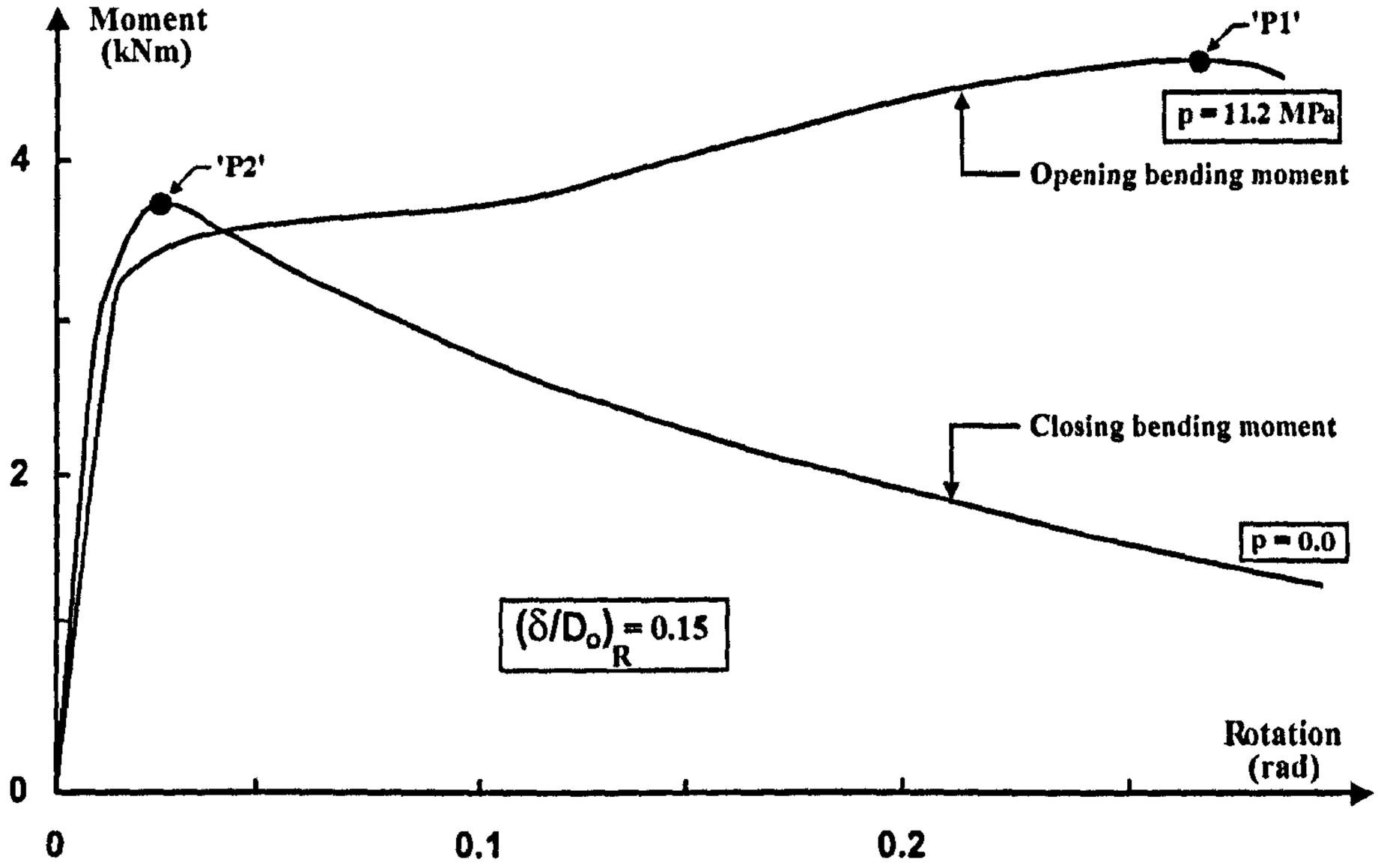

Figure 5.19: Plot of bending moment versus pipe's end rotation for empty, and for pressurised pipe, $p = 2.8\ MPa$. Pipe has a dent but it has no gouge. Also, $\frac{2L}{D_o} = 6.0$. Points 'P1', and 'P2' denote the ultimate moment values.

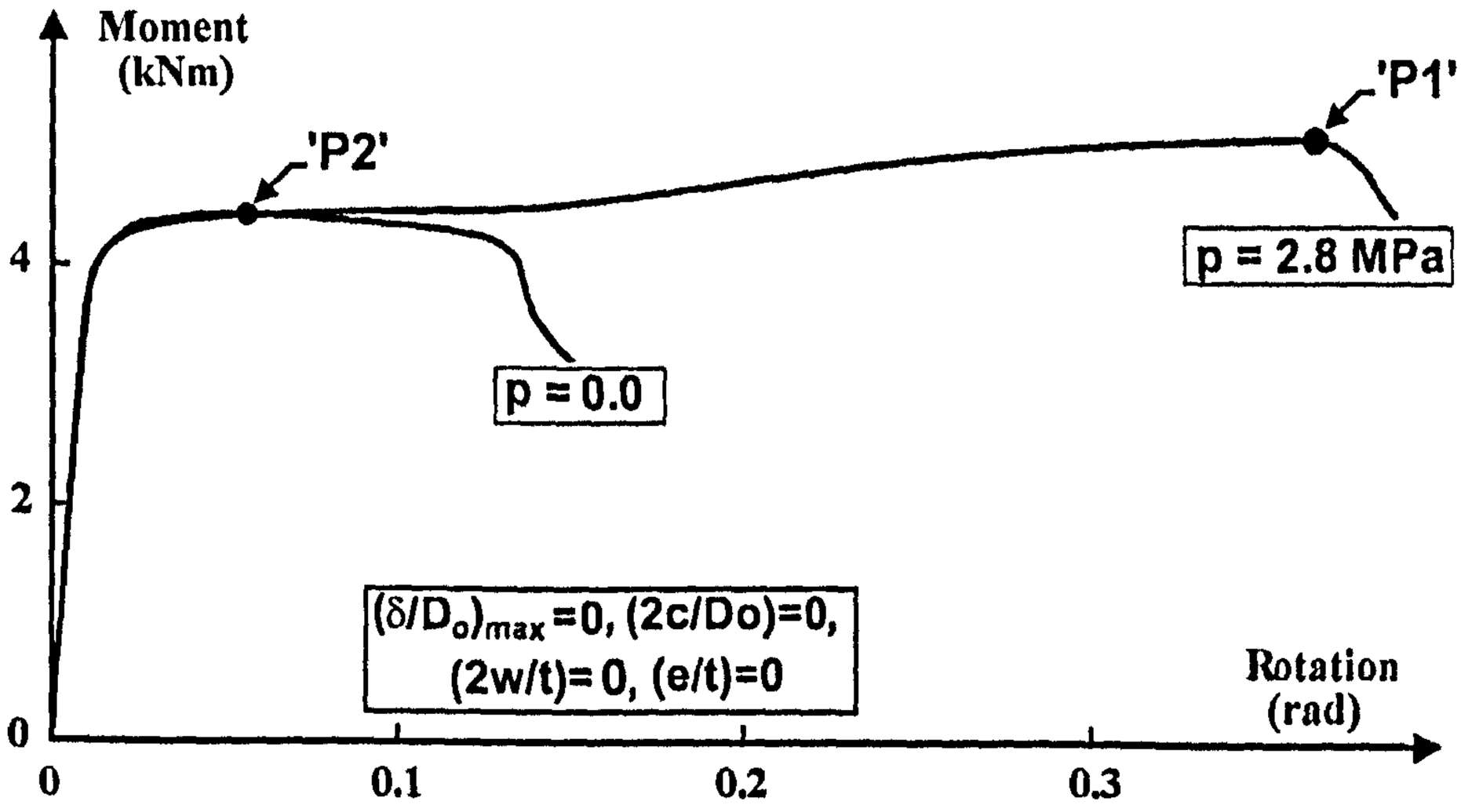

Figure 5.20: Plot of bending moment plot versus pipe's end rotation for empty, and for pressurised pipe, $p = 2.8\ MPa$. Perfect pipe. Also, $\frac{2L}{D_o} = 6.0$. Points 'P1' and 'P2', denote the ultimate moment values.

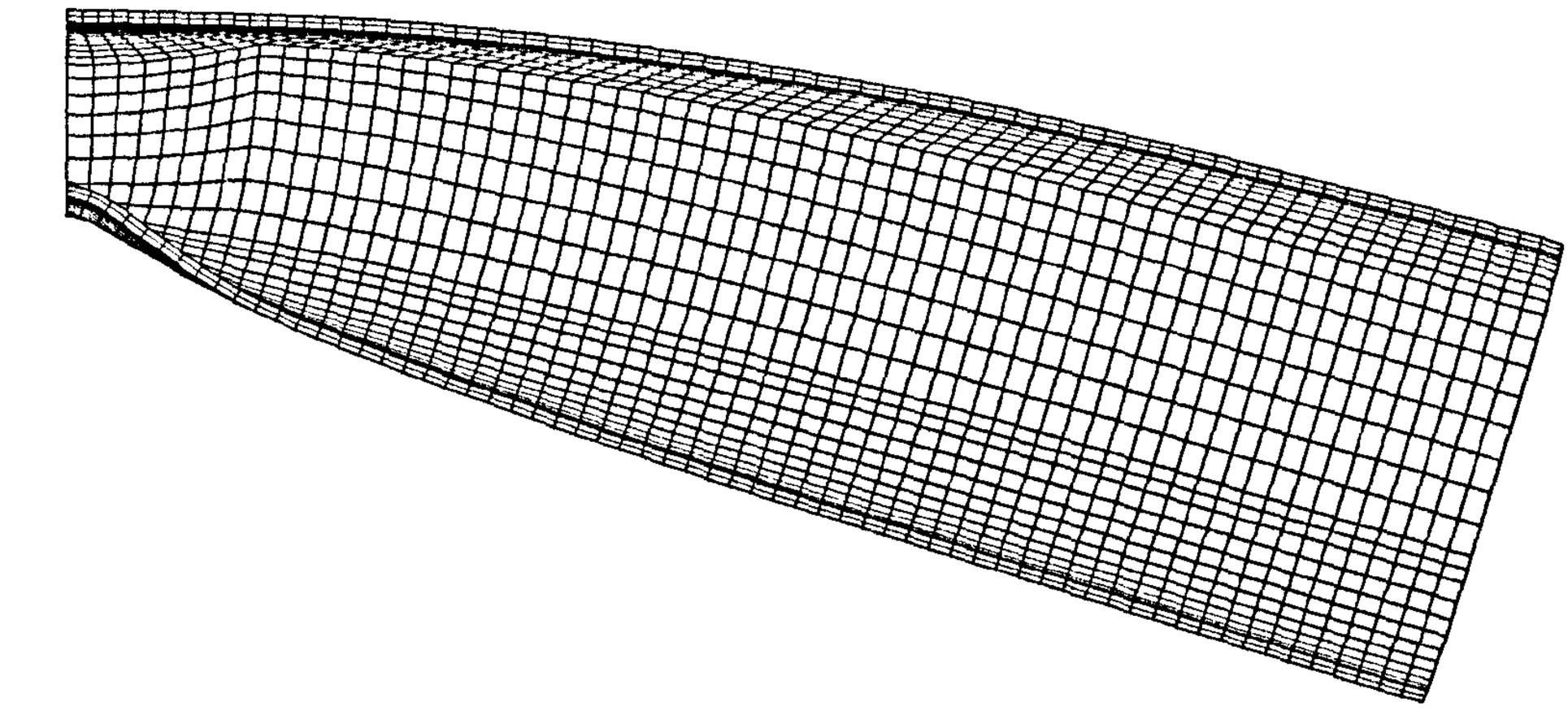

(a) p = 0.0; Point 'P2' - Fig. (5.20).

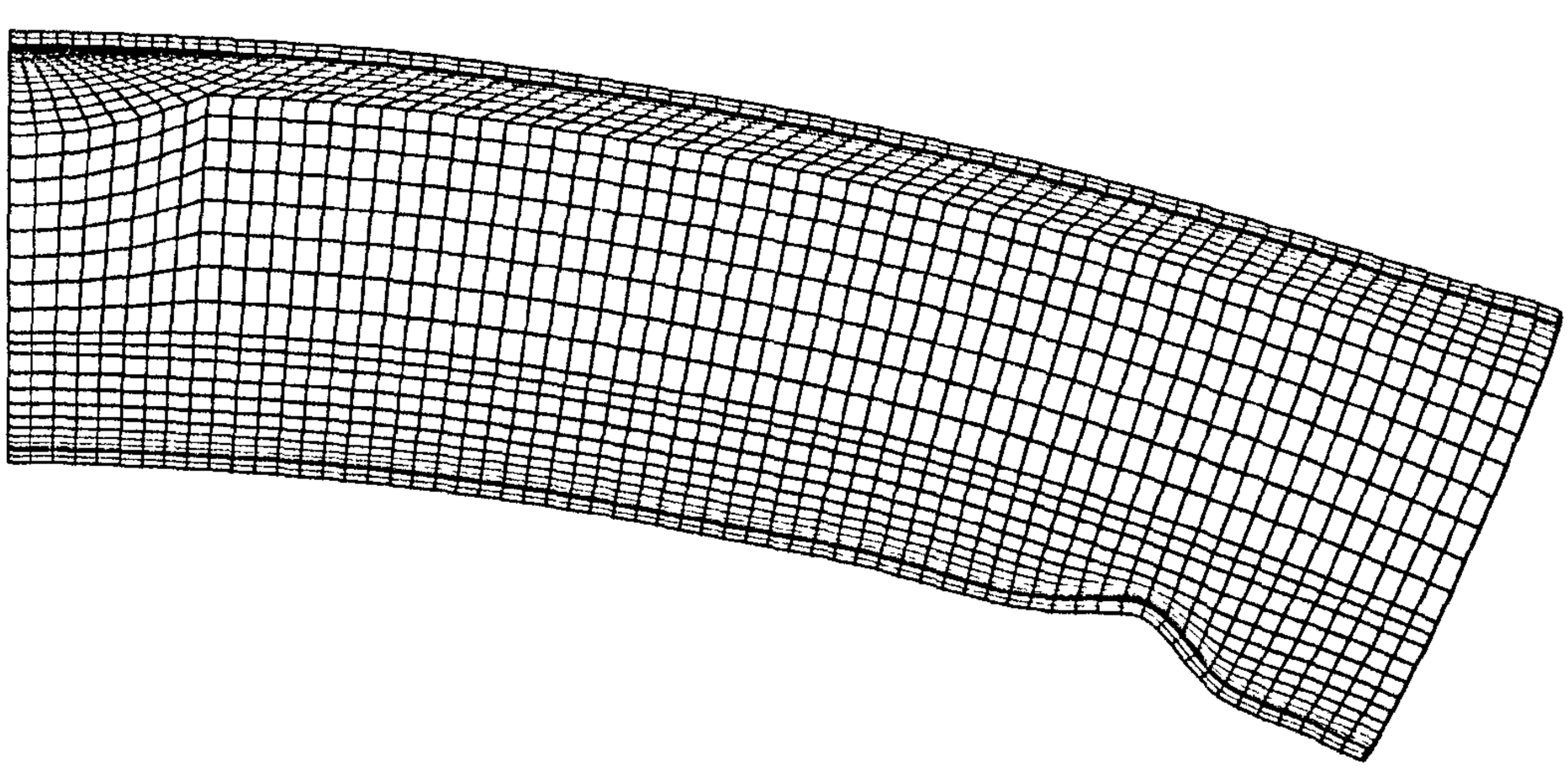

(b) p = 2.8 MPa; Point 'P1' - Fig. (5.20).

Figure 5.21: View of bent pipe at the collapse bending moment. Fig. 5.21a corresponds to point 'P2' in Fig. 5.20. Fig. 5.21b corresponds to point 'P1' in Fig. 5.20. Also, no gouge, and no dent were present in the pipe.

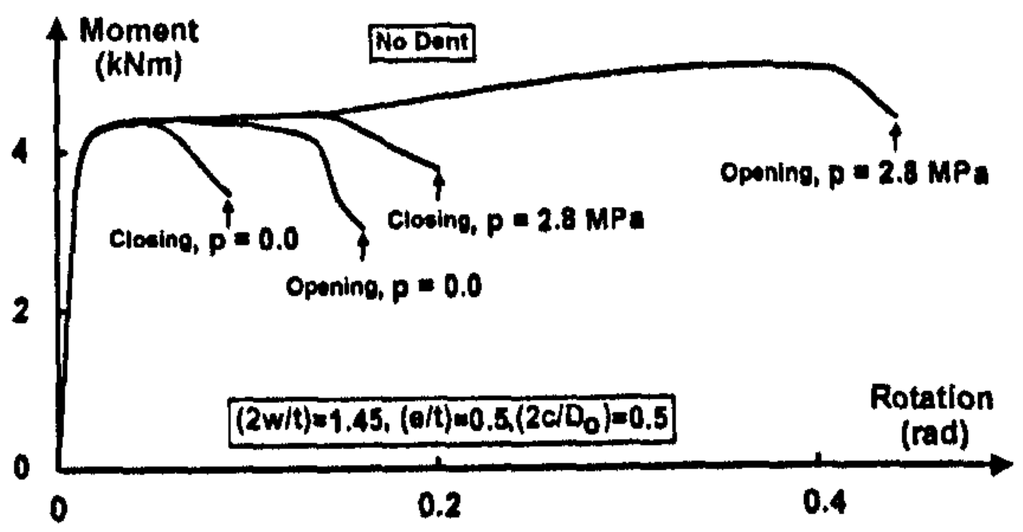

(a) Gouged pipe at mid-span.

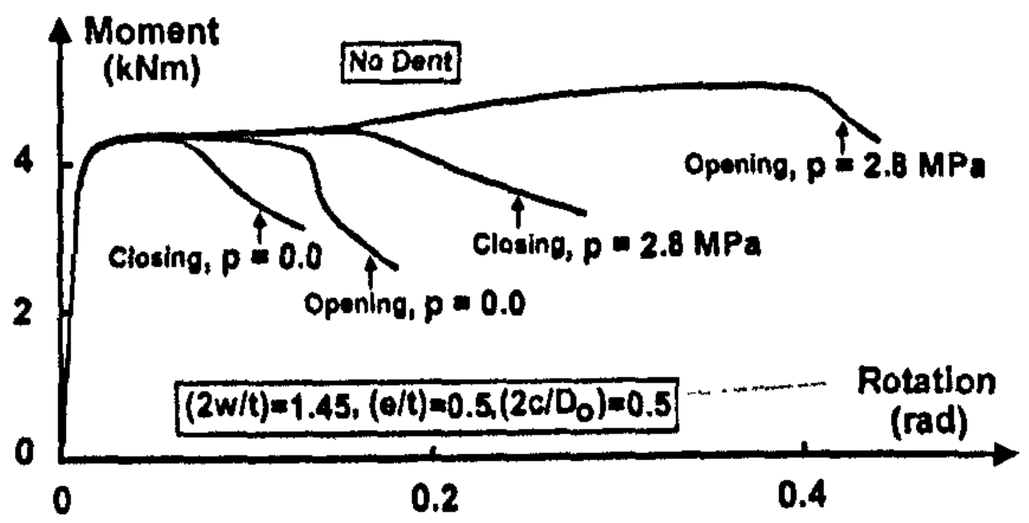

(b) Gouged pipe at off-centre (as in Fig. 5.2b).

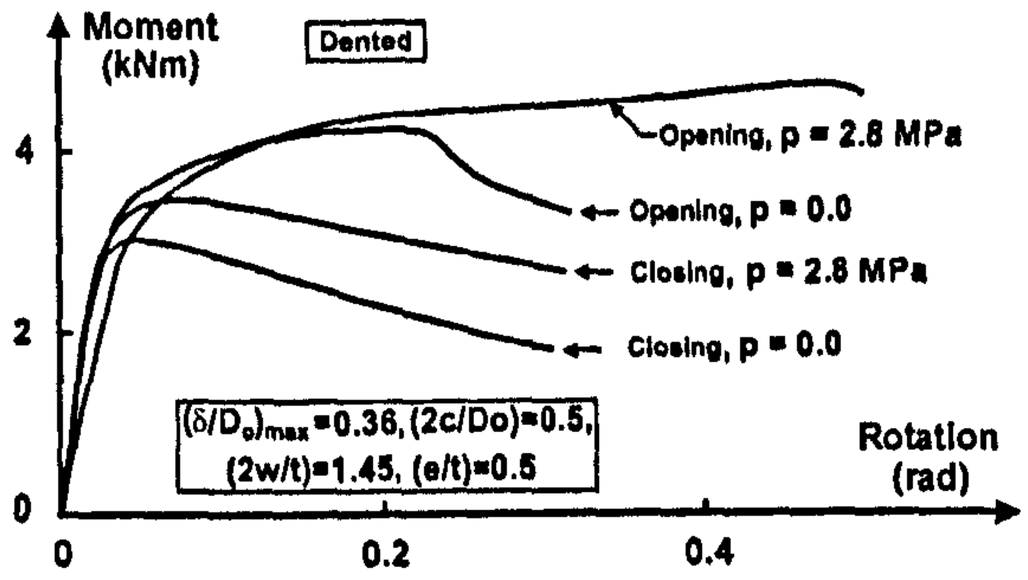

(c) Gouged pipe at mid-span.

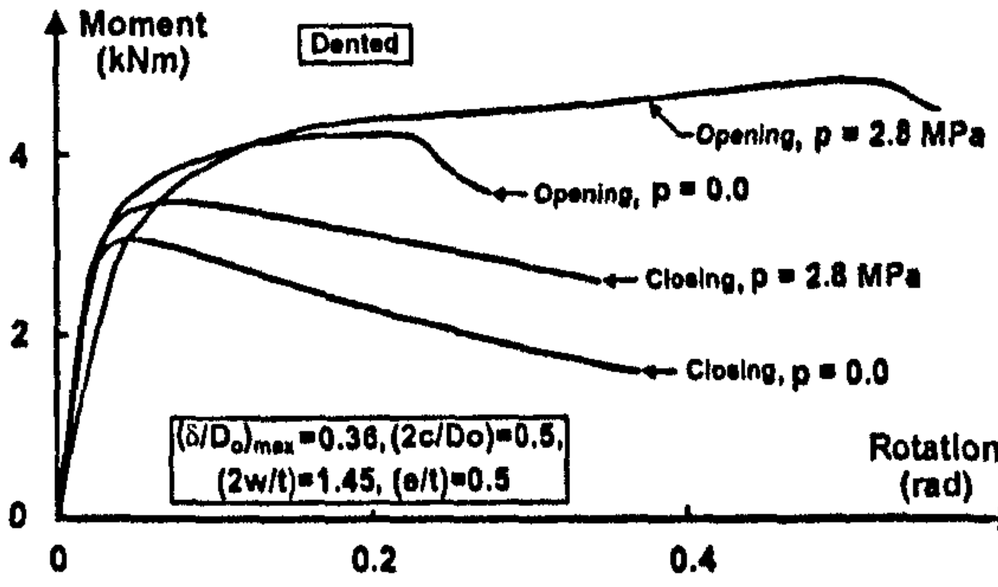

(d) Gouged pipe at off-centre (as in Fig. 5.2b).

Figure 5.22: Comparison of results for opening and for closing bending moments (undented and dented pipes). Results for two locations of gouges are shown. Also, $(\frac{\delta}{D_o})_{max} = 0.36$, and $\frac{2L}{D_o} = 6.0$.

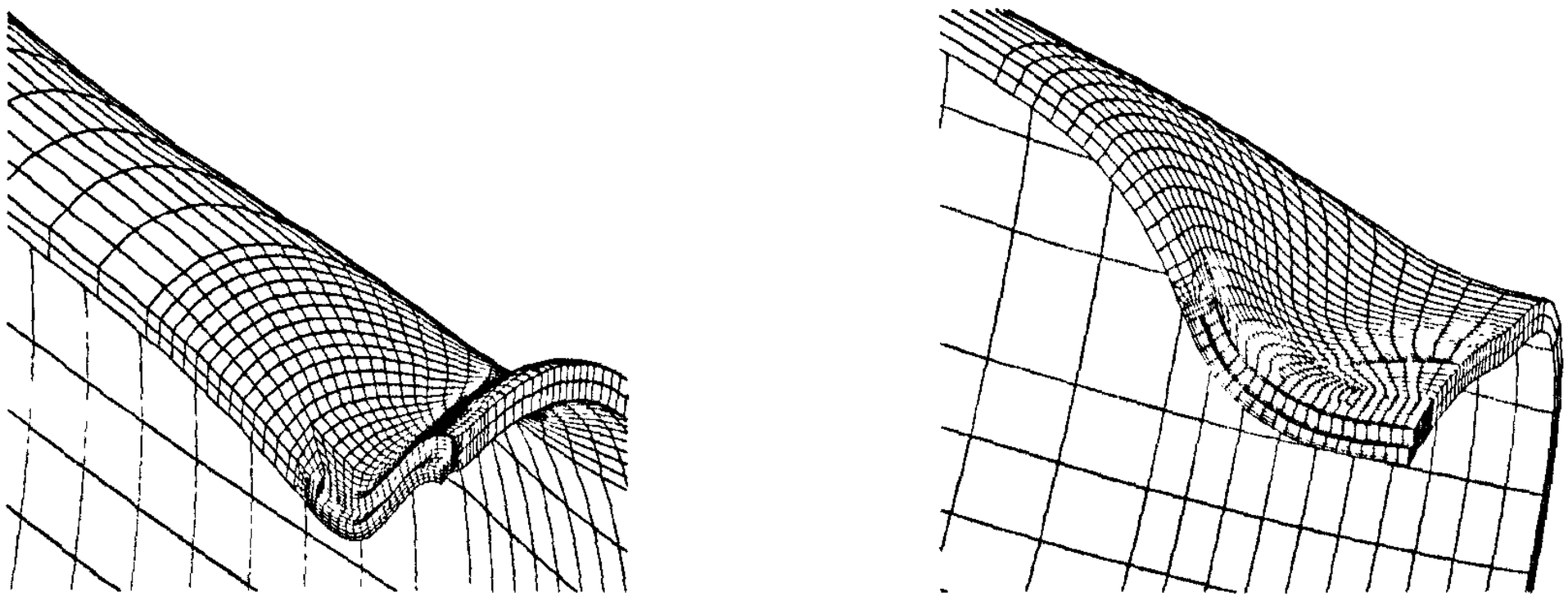

(a) Closing bending moment, p = 2.8 MPa. (b) Closing bending moment, p = 0.0.

Figure 5.23: Close view of deformed pipe when subjected to the ultimate closing bending moment, mid-span gouges ($\frac{2w}{t} = 1.45$, $\frac{e}{t} = 0.5$, $\frac{2c}{D_o} = 0.5$, and $\frac{2L}{D_o} = 6.0$).

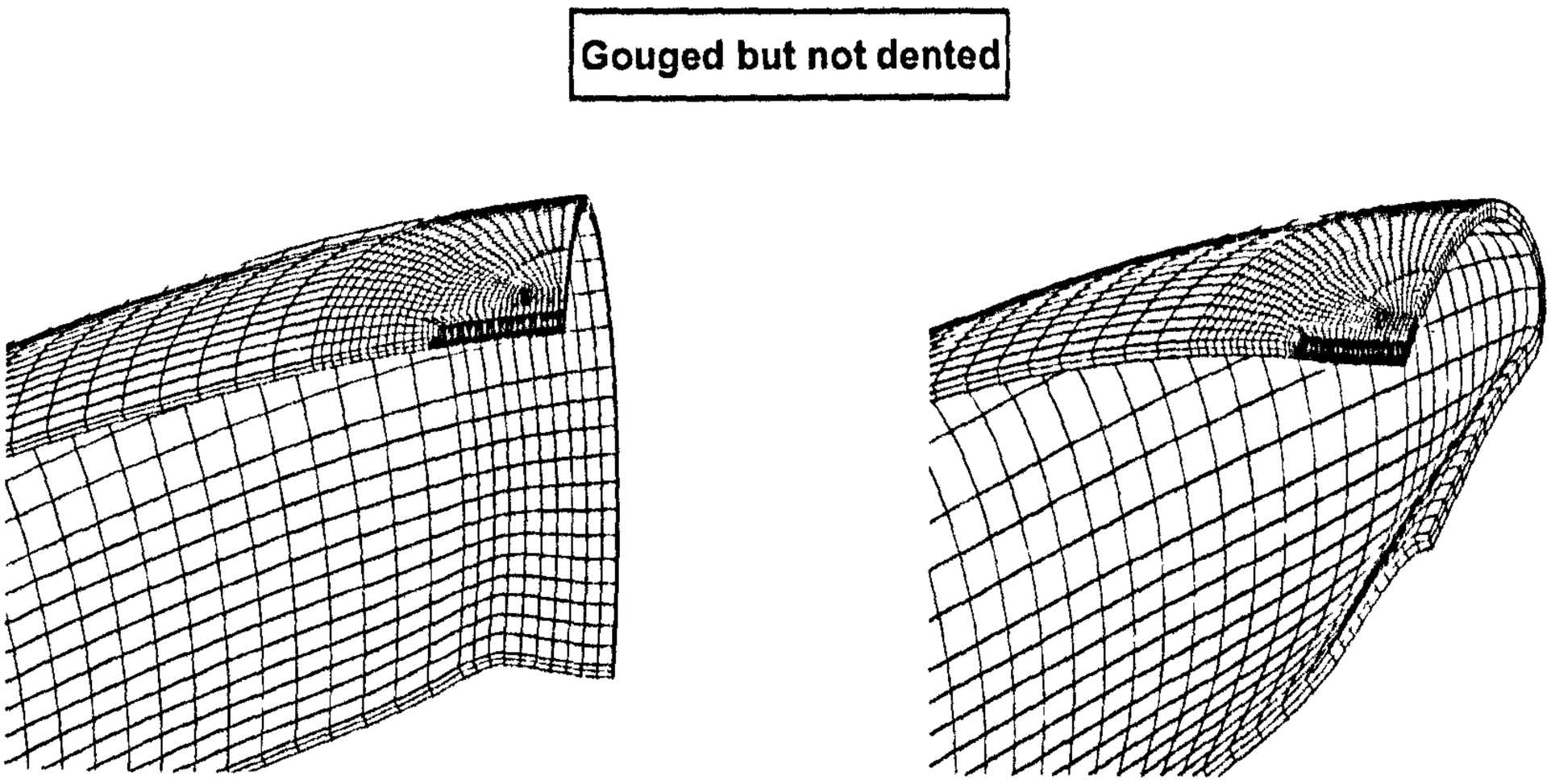

(a) Opening bending moment, p = 2.8 MPa. (b) Opening bending moment, p = 0.0.

Figure 5.24: Close view of deformed geometry when subjected to the ultimate opening bending moment, mid-span gouges ($\frac{2w}{t} = 1.45$, $\frac{e}{t} = 0.5$, $\frac{2c}{D_o} = 0.5$, and $\frac{2L}{D_o} = 6.0$).

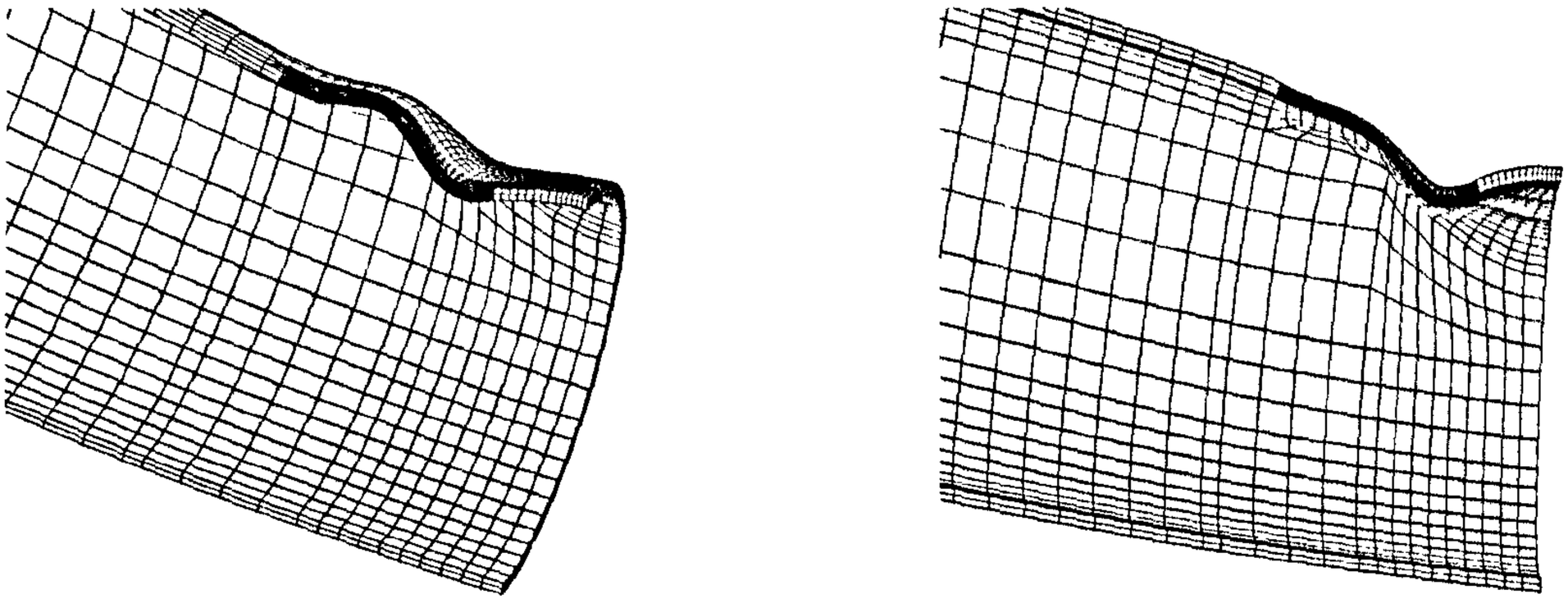

(a) Closing bending moment, p = 2.8 MPa. (b) Closing bending moment, p = 0.0.

Figure 5.25: Close view of deformed geometry at the ultimate closing bending moment for off-centre gouges ($\frac{2w}{t} = 1.45$, $\frac{e}{t} = 0.5$, $\frac{2c}{D_o} = 0.5$, and $\frac{2L}{D_o} = 6.0$).

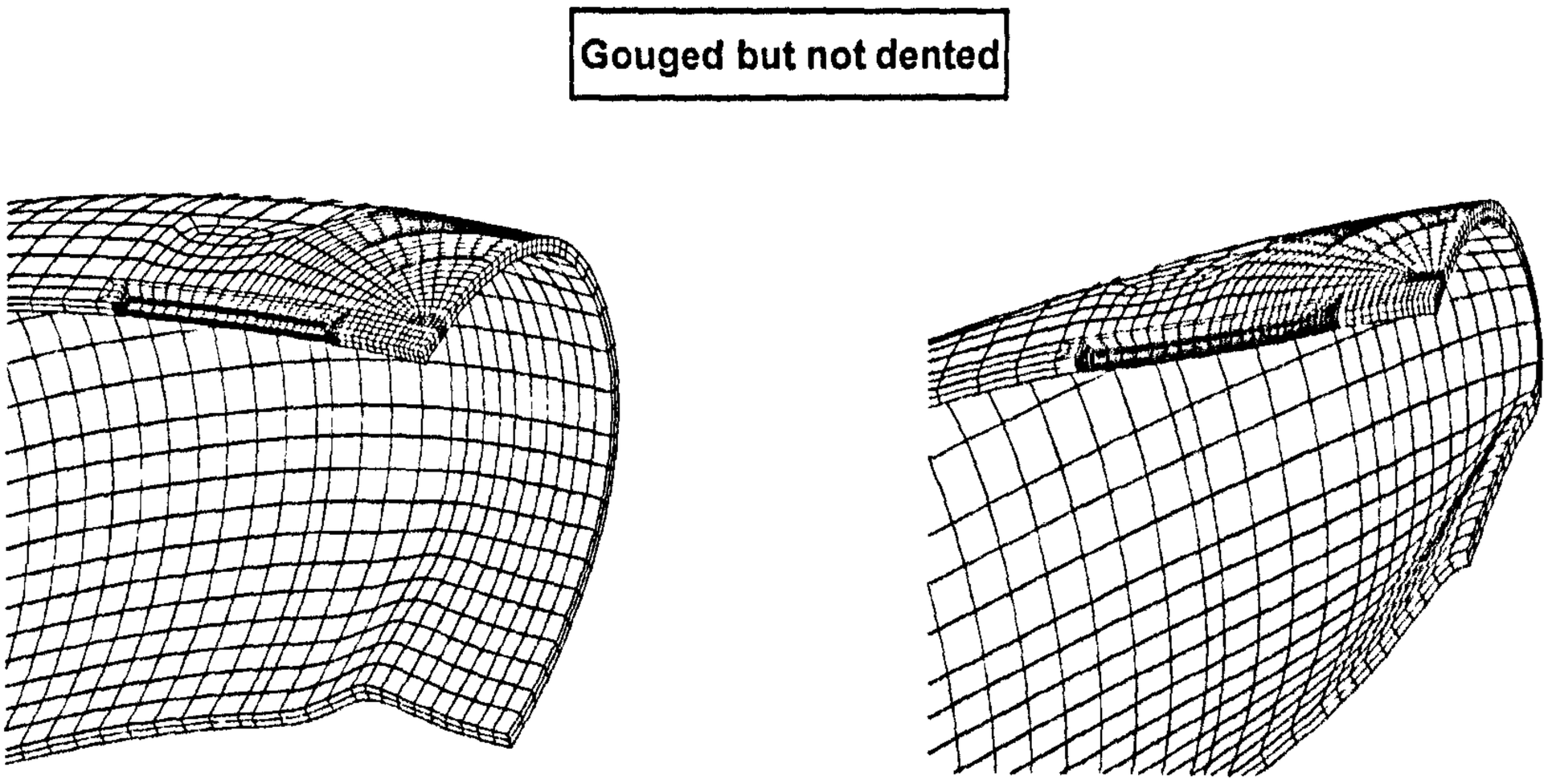

(a) Opening bending moment, p = 2.8 MPa. (b) Opening bending moment, p = 0.0.

Figure 5.26: Close view of deformed geometry at the ultimate opening bending moment for off-centre gouges ($\frac{2w}{t} = 1.45$, $\frac{e}{t} = 0.5$, $\frac{2c}{D_o} = 0.5$, and $\frac{2L}{D_o} = 6.0$).

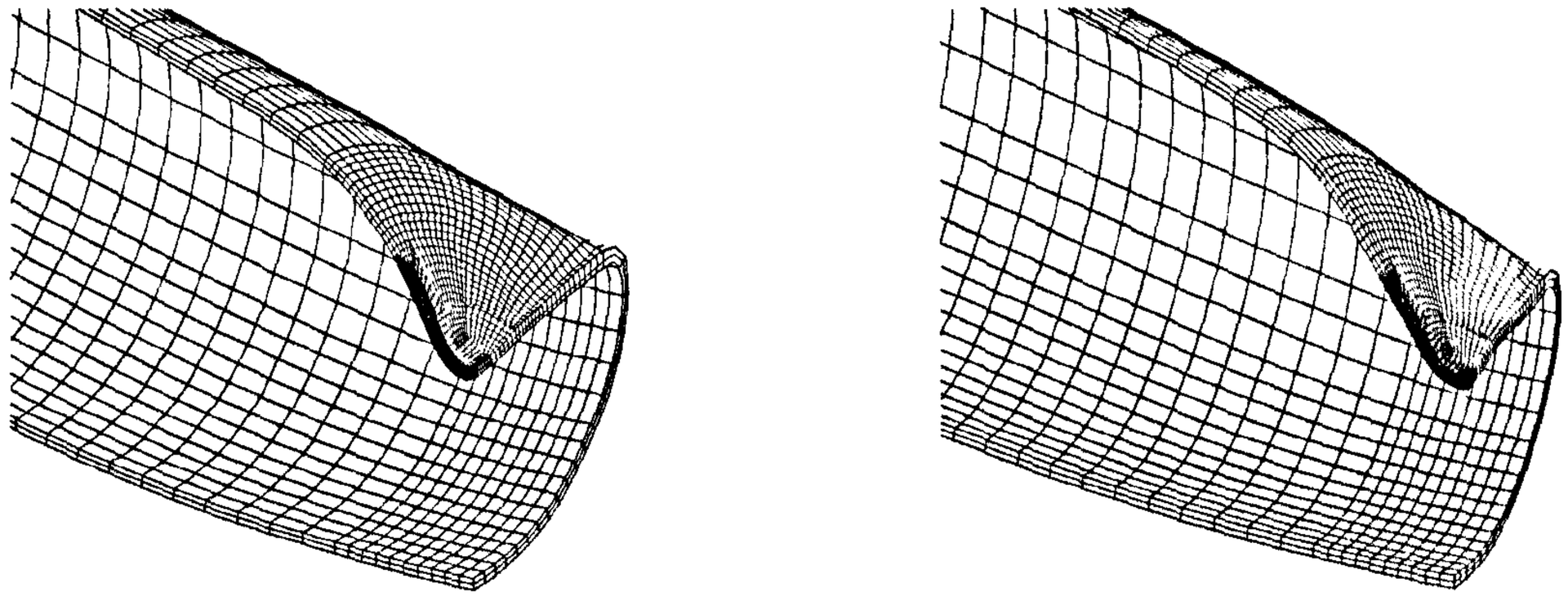

(a) Closing bending moment, p = 2.8 MPa. (b) Closing bending moment, p = 0.0.

Figure 5.27: Close view of deformed pipe when subjected to the ultimate closing bending moment, mid-span gouges ($\frac{2w}{t} = 1.45$, $\frac{e}{t} = 0.5$, $\frac{2c}{D_o} = 0.5$, and $\frac{2L}{D_o} = 6.0$).

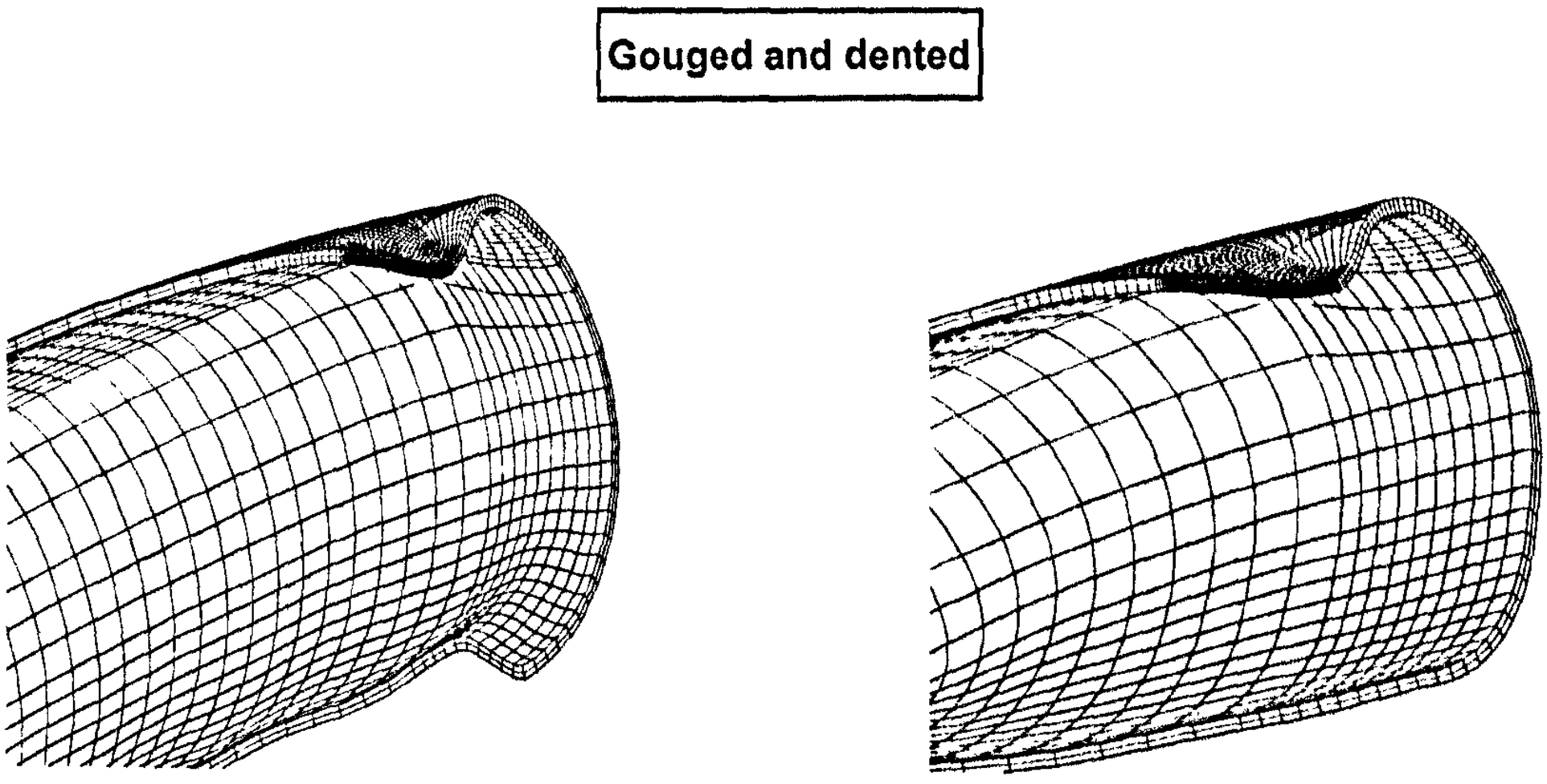

(a) Opening bending moment, p = 2.8 MPa. (b) Opening bending moment, p = 0.0.

Figure 5.28: Close view of deformed geometry when subjected to the ultimate opening bending moment, mid-span gouges ($\frac{2w}{t} = 1.45$, $\frac{e}{t} = 0.5$, $\frac{2c}{D_o} = 0.5$, and $\frac{2L}{D_o} = 6.0$).

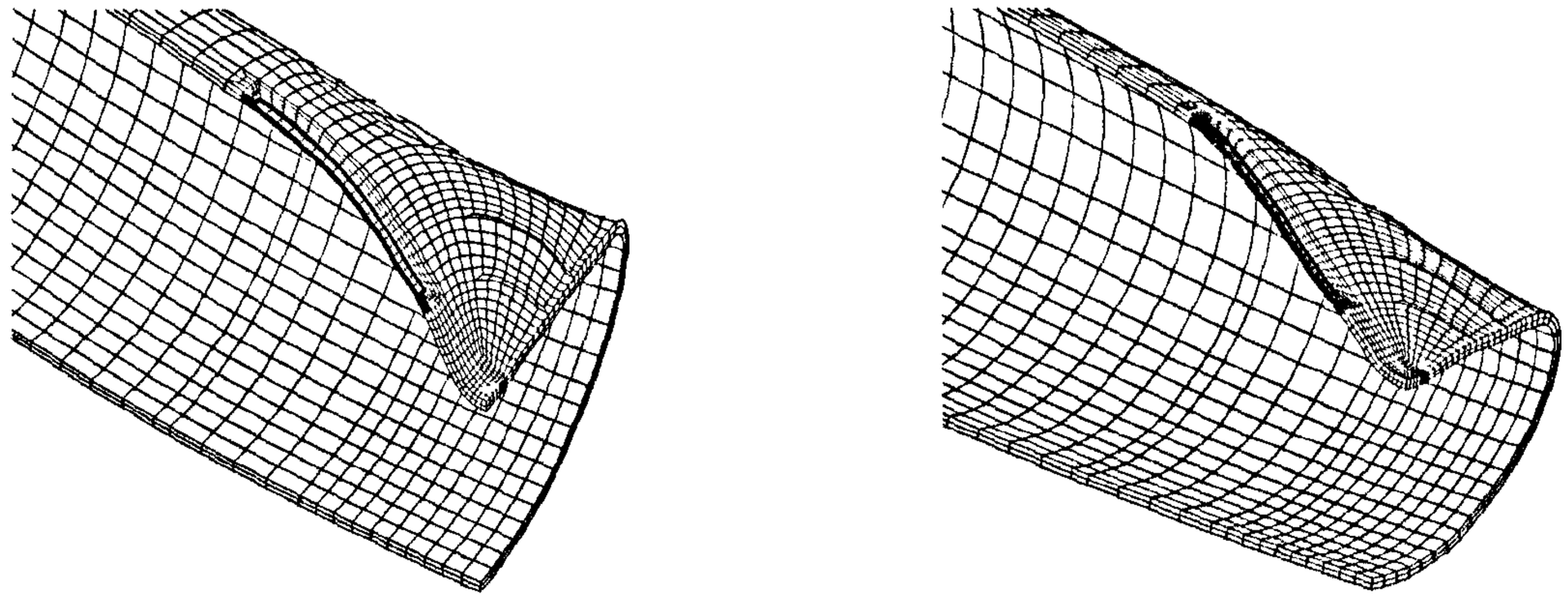

(a) Closing bending moment, p = 2.8 MPa. (b) Closing bending moment, p = 0.0.

Figure 5.29: Close view of deformed geometry of the FE model when subjected to the ultimate closing bending moment for off-centre gouge ($\frac{2w}{t} = 1.45$, $\frac{e}{t} = 0.5$, $\frac{2c}{D_o} = 0.5$, and $\frac{2L}{D_o} = 6.0$).

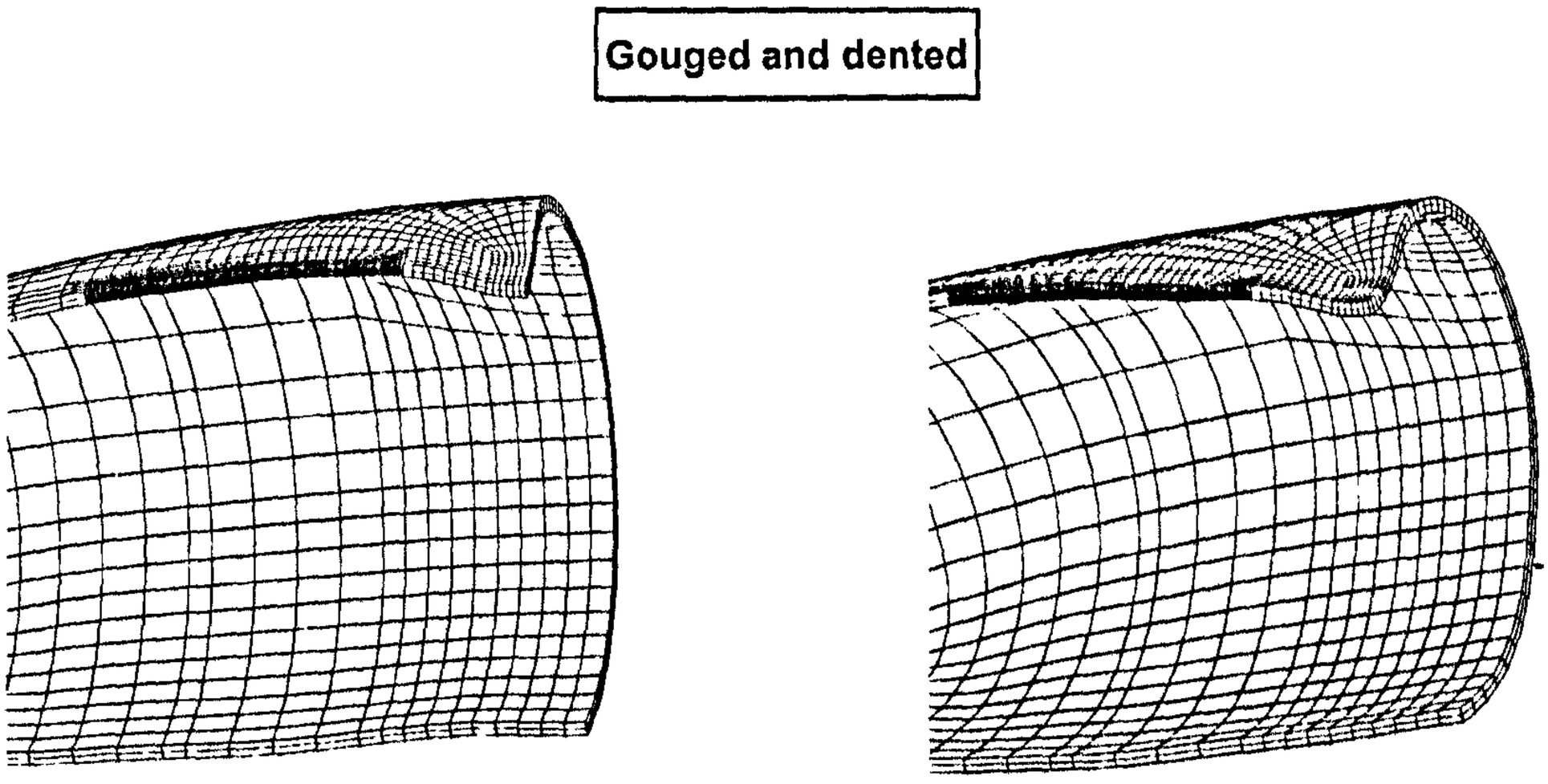

(a) Opening bending moment, p = 2.8 MPa. (b) Opening bending moment, p = 0.0.

Figure 5.30: Close view of deformed geometry of the FE model when subjected to the ultimate opening bending moment for off-centre gouges ($\frac{2w}{t} = 1.45$, $\frac{e}{t} = 0.5$, $\frac{2c}{D_o} = 0.5$, and $\frac{2L}{D_o} = 6.0$).

Chapter 6

Experimental programme: Denting of pipes

6.1 Introduction

This Chapter contains information on a number of tests in order to benchmark the FE results. Details are provided about obtaining tensile properties, manufacturing of test specimens, their pre-experiment measurements and testing.

6.2 Pre-experimental arrangements

6.2.1 Manufacturing of experimental models

All models were made by machining mild steel pipe from inside and from outside to secure the outside diameter-to-wall thickness ratio, $\frac{D_o}{t} \cong 40$. The initial length of pipe was about 610 mm, and it was cut into three pieces, P1, P2, and P3 - as shown in Figure (6.1a). This was done in order to minimise the pipe's vibrations during CNC machining. Length of the middle portion was nominally, $3D_o$, with the other two parts having equal length of, $1.5D_o$. Nominal wall thickness of all three parts was the same, i.e., $t = 2.1$ mm. All three parts were subsequently welded and two additional extensions, 250 mm long and 6.75 mm thick, were added at both ends. The

above arrangements are shown in Figure (6.1b). Six such pipe models were prepared and they are designated here as SP1, SP2, .., SP6. Sketches illustrating geometry of gouges, and location of gouges are depicted in Figure (5.1) and in Figure (5.2).

The first three specimens were machined without surface gouges whereas the remaining three pipes were manufactured with surface gouges running axially. A single axial gouge was introduced at the centre of anticipated dent in the fourth model, SP4. Two gouges, of the same dimensions were introduced on peripheries of anticipated dent in the fifth pipe specimen, SP5. Electrical discharge machine was used to create gouges in SP4, and SP5. The sixth pipe, SP6, had a large axial defect introduced at the centre. The latter was introduced by standard machining.

Once the machining was completed, the test specimens were grided with permanent lines which were used for measuring the wall thickness and pipe's diameter. A sample of this survey is presented in Table (6.1) for thickness measurements, and in Table (6.2) for outside diameter measurements. As it can be seen from both Tables, fifteen points in the longitudinal direction × eight points in the circumferential direction were taken giving a total of 120 points for thickness and 60 points for diameter measurements. Table (6.3) shows all test sections P1, P2, and P3 with their dimensions before welding. The standard deviation equation (6.1) was used for both thickness and diameter measurements, i.e.

$$\Delta t = \left(\sum_{i=1}^{N} (t_{average} - t_i)^2 / (N-1) \right)^{0.5} \tag{6.1}$$

where N is number of measurements. The same procedure was adopted for all test pipes. The results which were obtained are given in Table (6.4). The thickness measurements were obtained by using either Teledictor ultrasound probe or by using Mitutoyo linear gauge. The outside diameter was measured using Vernier callipers and micro-meter tools. The highest coefficients of variance obtained were 0.20 % and 0.14 % for thickness and for outside diameter, respectively. The above dimensions were used in the FE modelling of experiments.

Pipes were also checked for straightness and for any ovalisation once surface gouges were introduced and welding took place. More details about dimensions of

defects and their location, dimensions of models, and welding details can be found in the attached technical drawings, in Appendix (C). Other experimental details are as follows:

- The test specimens were machined using either Computer Numerical Control machine ($CNC-Anilam\ 4200T$), or by using Binns & Berry centre lathe machine.
- The welding of parts P1, P2, P3, and extensions was conducted using Tungsten Inert Gas technique with weld prep made according to BS 5500 [70].
- The surface defects were introduced using electric discharge machine. In one case, SP6, a high speed milling machine was used (Bridgeport machine).

6.2.2 Machining of electrodes and introduction of gouges

Nominal dimensions of defects introduced by the electrical discharge machine were chosen to have the dent-to-wall-thickness ratio, $\frac{e}{t} \cong 0.47$, the length-to-outside-diameter ratio, $\frac{2c}{D_o} \cong 0.25$, and the width-to-wall-thickness ratio, $\frac{2w}{t} \cong 0.50$. Nominal dimensions of the machined gouge had these ratios given by: $\frac{e}{t} \cong 0.23$, $\frac{2c}{D_o} \cong 0.81$, and $\frac{2w}{t} \cong 1.20$. All gouges were to be introduced to part P2 prior to welding, i.e., gouges were introduced into the near perfect pipe's geometry.

Manufacturing of gouges in the pipe's outer surface is a complicated procedure. It is difficult to manufacture very thin cracks or gouges with a width of less than 1.0 mm using high speed milling machine or CNC machine. Therefore, the first step was to devise a method which would allow manufacturing of a narrow gouge. This was done by using electrical discharge machine which uses an electrode to create damage of a given profile. The material used for the electrical discharge machine was Erodex (purchased from Erodex UK limited, Park Road, Halesowen, West Midlands, B63 2RH), in the form of 1.0 mm thick sheet.

Profile of an electrode was cut using a three axis milling machine (Bridgeport machine). Figure (C.1), in Appendix (C), shows the drawing detailing the Erodex template which in turn defines dimensions of the surface defect. Slot-type gouges were manufactured by an outside firm (OMEGA Tooling, Toolmakers and Precision

Engineers, 15 Cornhill, Liverpool, L1 8DZ). Each gouge required a new electrode. Figure (6.2) shows the electrode machined from Erodex.

The electrical discharge machine, (*AGIG, A GICTRON 3U*), was used to create a single axial slot gouge in SP4, at mid-span. Two axial gouges were created in SP5 and these gouges were at off-centre by distance, $\frac{D_o}{2}$, as detailed in the drawing shown in Figure (C.2) and in Figure (C.3), in Appendix (C). The specimen was placed horizontally and covered with dielectric fluid, (Dielectric 200T, BP OIL), in electro-discharge machine. The Erodex electrode was mounted in the machine holder as can be seen in the sketch shown in Figure (6.3).

The spark erosion generated the slot gouge which can be seen in Figure (6.4). This procedure is very accurate and it gives a high quality of finished surface in the slots. The high speed milling machine (Bridgeport) was used to create a wider axial gouge in SP6 - see Figure (C.4) in Appendix (C), for more details of this gouge. The ends of this slot had circular shape with radius equal to 1.0 *mm* due to the bull radius used during machining. Further pieces of relevant information are as follows:

- The axial slot gouges were introduced to the pipe's surface under zero internal pressure.
- All gouges produced by electrical discharge machine had rectangular shape and they had nearly the same dimensions.
- Gouges were at the centre or off-centre (off-set distance was equal to, $\frac{D_o}{2}$).
- All gouged pipes were later subjected to denting with presence of internal pressure.

6.2.3 Dimensional survey of gouges

Once the preparation of gouges was completed, their dimensional survey was carried out. Acrylic casting - see Figure (6.5a) was used to check dimensions of defects. Liquid acrylic was used to obtain mould of a gouge. This male mould was then measured (width, depth, and length), at points shown in Figure (6.5b). Results of these measurement are given in Table (6.5) for SP4. It is seen from Table (6.5) that

width varied by less than 2% and variation in gouge's depth was less than 4%. In addition, the electrode itself was measured before and after being used. The results are given in Table (6.6). They show a small reduction in electrode's wall thickness and this reduction was of about 4 %. As a result the electrode could not be used twice.

Similar measurements were carried out for two gouges in model, SP5. Results are given in Table (6.7) and in Table (6.8). The results show small variation in depth and width of both gouges. The average depth was 0.95 *mm* for slot (A) and 0.98 *mm* for slot (B). The electrode itself was measured before and after being used and the results are given in Table (6.9) for slot (A), and in Table (6.10) for slot (B).

Table (6.11) shows measurements of gouge width and depth at eight points along the gouge length, for model SP6. The results show small variation in depth and in width. The average values were 2.50 *mm* for the width, and 0.48 *mm* for the depth of the gouge. Finally, the average values were normalised using the pipe's wall thickness and pipe's outside diameter. These values for gouges in SP4, SP5, and in SP6 are given in Table (6.12).

6.2.4 Welding of the test specimens

Parts P1, P2, and P3 were weld preped according to the BS 5500 [70], and as detailed in Figure (C.5), in Appendix (C). Two extensions were machined to fit the P1+P2+P3 specimens and they had similar welding prep. Details about one of the ends are sketched in Figure (C.6), in Appendix (C). The welding of all components was carried out using Tungsten Inert Gas at Central Steel Fabrications Ltd, (39-41 Speakland Road, Liverpool, L7 6HY). The final shape of a welded test specimen with extensions can be seen in Figure (6.1a). The details of all dimensions, including gouges are summarised in Table (6.13).

6.2.5 Machining pipe's support and indenter

The ground support was made in a form of saddle made from a piece of wood - for more details see Figure (C.7) in Appendix (C). The saddle has a span angle of 120°, and it was machined to support full length of the pipe during denting. Details

of the wood support and its dimensions are provided in Figure (C.7). The indenter, hemispherical, was machined from steel. It had the diameter $D_{indenter} = 34.7\ mm$, and hight equal to $H_{indenter} = 80.0\ mm$ - see Figure (6.6). The indenter was smoothed and polished so that the contact between the indenter and pipe's surface was as smooth as possible.

6.2.6 Material properties of pipe models

The material properties of tested pipes were obtained from tensile tests. The tensile test specimens were designed according to the $BS\ EN\ 10002 - 1 : 1990$ [71]. A section of 400 mm pipe length was cut for this purpose. This pipe was initially machined from outside surface to facilitate extraction of flat test coupons - see Figure (C.8). Four axial tensile test specimens were then cut from this section as sketched in Figure (C.8). Next, pipe pieces were machined flat from both sides as can be seen in Figure (6.7). Figure (6.8) shows a sample of the tensile test specimen before and after being tested. The tensile test specimens were measured for their thickness and width before testing. Results of these measurements are summarised in Table (6.14).

Two of tensile specimens (coupon number 1 and 3) were tested with strain gauges (four strain gauges for each specimen, two gauges for each side). Strain gauges measured longitudinal and transverse strain so that any bending could be taken into account. The strain gauges were placed at 90° to each other. The tensile specimens with strain gauges were tested twice. First, to obtain elastic constants of the material. The second test was carried out until neck was formed and fracture occurred. The other two tensile specimens (coupons number 2 and 4) were equipped with an extensometer allowing calculation of the strain values. Displacement rate of 2.0 mm/min (equivalent to a strain rate of 220 $\mu\varepsilon/s$) was used for tensile specimens number 1 and 3. Displacement rate of 0.5 mm/min (equivalent to a strain rate of 20 $\mu\varepsilon/s$) was applied to tensile specimens number 2 and 4.

The results showed that there were no significant differences between the results for these three tests, as shown in Figure (6.9), i.e., for tensile tests 1, 2, and 3. The tensile test number 4 showed a reduction, approximately 15%, in the lower yield stress. A reduction of the yield stress would be expected for mild steel with a reduced

strain rate, as explained by Lynch et al. [65]. Therefore, it was decided to exclude the tensile test specimens number 4 and the average results for the other three specimens are shown in Figure (6.10). The nominal stress-strain curve was converted to true stress-strain curve as described in Chapter (3). This conversion was explained in details by Dieter [72] using two equations, i.e., (6.2) for the stress, and the equation (6.3) for strain:

$$\sigma_t = \sigma_{nom}(1 + \varepsilon_{nom}) \tag{6.2}$$

$$\varepsilon_t = ln(1 + \varepsilon_{nom}) \tag{6.3}$$

where σ_{nom}, ε_{nom} are nominal stress and nominal strain, respectively; σ_t, and ε_t are true-stress and true-strain, respectively. The results of this conversion are plotted in Figure (6.11). The latter figure was used in ABAQUS input file through a set of 19 line segments, as shown in Figure (6.12). This material properties are applicable to pipes SP3, SP4, SP5, and SP6. Results shown in Figure (3.7b) are applicable to pipes SP1, and SP2. A summary of both materials is given in Table (6.15).

6.3 Instrumentation

6.3.1 Strain gauges

A number of strain readings were carried out during different phases of this study. The strain gauges used were "EA-06-062AP-120", manufactured by MM (Micro-Measurements Group, Inc., USA). The strain gauges were bonded to pipe surface, and oriented in both hoop and longitudinal directions at selected points. Details about their location, for each individual experiment, are plotted in Figures (C.9), (C.10), (C.11), (C.12), and in Figure (C.13). In addition, all gauges were coated after installation using strain gauge protective epoxy coatings.

6.3.2 Displacement and pressure transducers

During pressurisation, denting of pipes, and their bending, displacement transducer was used to measure the diameter change. The displacement transducer (WSM type: HS 10) with a range of displacement $(0 - 11.2)\ mm$ was used for this purpose. The linear calibration, to give an output of 1000 $\mu\varepsilon/mm$, was conducted with the assistance of a barrel-micrometer (resolution = 0.00254 mm) and the Brüel Kjaer ($B\&K$) strain indicator. A dead weight testing machine, and a ($B\&K$) strain indicator, were used to calibrate the pressure transducer with an output of 145 $\mu\varepsilon/MPa$.

6.3.3 Pressure accumulator

Pressure accumulator manufactured by Fawcett Engineering Ltd, UK was used throughout experimental tests when pipes were pressurised. The pressure accumulator was used to compensate for any change of the pressure inside the pipe. This was needed during denting and bending procedures. The accumulator was connected to the pipe, pressure transducer and to hand pump to monitor any change in the pressure. The medium used in the accumulator was nitrogen and oil whilst medium inside the pipe was oil.

6.3.4 Recording instruments

The strain gauge, and pressure transducer data were displayed, collected and stored using data acquisition system which was developed at the University of Liverpool. A quarter bridge arrangement was used for strain gauges and full bridge arrangement for displacement and for pressure transducer. The Dartec load and displacement were also stored for the whole test. The results were stored in columns and each column represented a separate type of input. This file could be easily transferred to any outside software for post-processing.

6.4 Test arrangements

6.4.1 Checking test specimens before pressurisation

All test specimens were checked for any cracks caused by machining, by denting process, or during springback. None of specimens have shown any external signs of cracking. Some dented specimens had signs of wall thinning at the centre of the gouge.

6.4.2 Denting of empty pipe, SP1, without surface defect, $p = 0.0$

Specimen, SP1, has been dented under zero internal pressure. It was supported along its full horizontal length by saddle support made from pine wood as described in Section (6.2.5). Hemispherical indenter made from steel was placed on the top, at mid-span of the pipe, and pushed down in vertical direction into the pipe. This was achieved by using compression machine (Dartec). Denting load and the corresponding displacements were monitored during the test and the relevant results were stored. The denting speed was 0.1 mm/min. Once the denting process was completed, the indenter was removed and springback occurred. The results obtained were analysed and they are compared with the FE predictions in Table (6.16). Other measurements, e.g., residual dent depth, were stored in a column format during each load step. Post-processed results are summarised as follows:

- Figure (6.13) shows loading-unloading curve for denting of, SP1. The maximum denting depth was $(\frac{\delta}{D_o})_{max} = 0.16$. It is seen that a good agreement was obtained between FE and the experiment. The maximum difference in load magnitude was 0.41 kN, i.e., $(\frac{12.11-11.70}{12.11} \times 100) = 3.38$ %. The difference in residual dent depth after springback was less than 0.5 mm. This figure also shows small difference in loading paths at the beginning of the denting. This is attributed to the fact that in the experiment the support was made from wood. In the FE analyses it was assumed that the wood was rigid. Section (6.5.3) addresses this problem in a greater detail.

- Figure (6.14) shows profile of residual dent along the the pipe length. The experimental profile of the dent was obtained by measuring the deformed specimen

using linear transducer gauge (shown in Figure (6.15), and in Figure (6.16)). It is seen from Figure (6.14) that good agreement between experiment and FE was obtained.

6.5 Denting of pressurised pipes, $p = 5.6\ MPa$, and $p = 11.2\ MPa$

Experimental arrangement for a pressurised pipe is sketched in Figure (6.17). The test specimen was filed with oil. In order to keep the pressure inside of the pipe constant during denting, the test specimen was connected to pressure accumulator. Three displacement transducers were used to monitor the surface behaviour during denting. Figure (6.18) shows the experimental arrangement for denting a pressurised pipe. The control unit of Dartec was connected to the computer controller for storing the loading data. Strain gauges, and pressure transducer were connected to *B&K* strain indicator which in turn was connected to the computer controller.

6.5.1 Pipes without surface defect

Two test specimens, SP2, and SP3, i.e., without surface defects were filled with oil and they were pressurised to the design level, $p = 11.2\ MPa$, using a hand pump. The internal pressure was kept constant during the denting test by using the pressure accumulator. If necessary pressure was increased using hand pump. Lowering of the pressure was also possible. The test specimens were supported by wooden saddle support along their length, $6D_o$. The test specimens were placed horizontally, and the hemispherical indenter moved vertically. Arrangements for testing are shown in Figure (6.18). The denting procedure was quasi-static, the hemispherical indenter moved with speed, 0.1 *mm/min*. Figure (6.19) shows a close view of the contact between indenter and pipe surface. The indenter pushed the surface into the required displacement through Dartec control unit of the cross-head displacement. The results of the test can be seen in Figure (6.20) for SP2. Closer view of the dent is shown in Figure (6.21) for SP3.

Experimental loading-unloading curve and the residual dent profile are com-

pared with the FE predictions in Figures (6.22) and (6.23) for SP2. Figures (6.24) and (6.25) show results obtained for SP3. It is seen here that as the dent depth increases, the denting load also increases until it reaches maximum. Once the prescribed depth of the dent was achieved, the indenter started to move upwards in small steps until no contact occurred. Once the indenter was removed, the internal pressure was released. Subsequently the residual profile of the dent along the pipe length was measured. The corresponding plots are shown in Figure (6.23) and in Figure (6.25) for SP2, and SP3, respectively.

The comparison between the FE and experimental results is reasonable. The difference in maximum denting load is 18.3% for SP2 and it is 15.0% for SP3. The residual profile of the dent was measured experimentally by using linear gauge transducer as shown in Figure (6.15) and in Figure (6.16). The measured profiles were of the same shape and of the same trend as predicted by FE. The only problem which needs to be investigated is the discrepancy at the beginning of loading. This is to be addressed in Section (6.5.3), as it has already been mentioned. Reduction in wall thickness at the dent centre was measured for both SP2, and SP3 and the values were compared with the FE predictions. The results showed that for the corresponding dent's depth equal to, $(\frac{\delta}{D_o})_{max} = 0.23$, and with internal pressure equal to $p = 11.2\ MPa$, there was $\cong 5.2\%$ reduction in wall thickness.

6.5.2 Denting of pressurised pipes with surface defect

Test specimens, SP4, with a single axial gouge, and SP5 with two axial gouges, and SP6 with a large axial gouge were tested under internal pressure equal to, $p = 5.6\ MPa$. Assumed dent depths was, $(\frac{\delta}{D_o})_{max} \cong 0.16$. Some preliminarily calculations have shown that SP4, SP5, and SP6 may not survive denting and bending if they were to be pressurised to design level, p =11.2 MPa. On the other hand, pressure p = 5.6 MPa, looked to secure their integrity throughout denting and bending. Hence, the adopted level of pressure loading. Denting procedure was the same as for specimens, SP2, and SP3. The residual depth of the dent after releasing of the internal pressure for specimens SP4, SP5, and SP6 is shown in Figure (6.26), Figure (6.27) and Figure (6.28).

Experimental and FE results are compared in Table (6.16). Figure (6.29), and Figure (6.30) show comparison between experiment and FE for SP4. Figure (6.31), and (6.32) show comparison between experiment and FE for SP5. Figure (6.33), and Figure (6.34) show comparison between experiment and FE for SP6. The maximum difference in denting load is 10%, 9%, and 6%, respectively - see Table (6.16). Figure (6.30), Figure (6.32) and Figure (6.34) compare experimental measurements of dent's profile with FE prediction for pipes SP4, SP5, and SP6. The results show good agreement in terms of residual dent depth and dent shape.

6.5.3 The initial load-displacement curve

Figure (6.13), (6.22), (6.24), (6.29), (6.31), and Figure (6.33) show small differences between FE and experiment in the first portion of the loading curve. Two specimens were used, SP1 for empty pipe and SP2 for pressurised pipe to investigate these differences. It is seen from the above mentioned figures that there is a systematic error during the initial loading, on the load-deflection curves. One possibility could be associated with non-uniform wall thickness. Three steps were carried out to understand this issue and they were as follows:

For SP2, three FE models were constructed with different thicknesses: $t = 2.0\ mm$, $t = 2.10\ mm$, and $t = 2.19\ mm$. The results showed small drop in the denting load as the thickness decreased but there was no noticeable change in the slope at the beginning of the denting process - see Figure (6.35).

Next, the effect of pipe ovalisation was checked. This was done by constructing three separate FE models with different diameters. Three elliptical shapes with different diameters were used as sketched in Figure (6.36). In vertical direction the diameters were: $D_o = 82.82\ mm$, $D_o = 83.10\ mm$, and $D_o = 83.47\ mm$. In horizontal direction they were: $D_o = 83.82\ mm$, $D_o = 84.10\ mm$ $D_o = 84.47\ mm$. FE results showed decrease in denting load as the pipe's horizontal width increased but there was no difference in the initial slope - see Figure (6.37).

Finally, attention turned to validity of the rigid support. Instead of rigid support, it was decided to use a set of spring elements along the pipe length to model the wooden support. This was done by using nonlinear springs between pipe nodes

and ground in X and Y direction. Before calculation could proceed one needs to know values of stiffness of wood which was used for the support. A compression test was carried out to find stiffness of the wood. This was done by testing a piece of pine wood with dimensions 25.8 $mm \times 26.1\ mmm \times 25\ mm$. The piece was tested in compression by using Instron machine. The results obtained are plotted in Figure (6.38). At the end of the test the piece started to crack. The zoomed area of the global, load-displacement curve, was used to model the spring stiffness for the FE models. Computations have shown that the initial values of wood stiffness played important role in bringing better correlation of experimental and FE results.

A set of stiffness values extracted from the load-displacement curve were input into the nonlinear springs. The results were excellent for empty pipe, SP1, Figure (6.39). Good results were also obtained for pressurised pipe, SP2, Figure (6.40). This confirms that the rigid model of the support did not account for elastic behaviour of wooden support.

6.6 Repeatability of test results

Specimens, SP2, and SP3 were subjected to the same denting. Their material properties were slightly different as they were from different batches of pipes. The change in yield stress was, $(\frac{332-316}{332}) \times 100 = 4.8\ \%$. Their nominal dimensions were close - see Table (6.13). Loading/unloading versus depth of the dent is shown in Figure (6.41). Profile of residual dent in both pipes is shown in Figure (6.42). Results shown in Figures (6.41) and in Figure (6.42) are very close. This in turn confirm good repeatability of testing on denting.

6.6.1 Initial pressurisation

Details about strain gauges, i.e., locations and directions on pipe's surface are shown in Figures (C.9), (C.10), (C.11), (C.12), and Figure (C.13) in Appendix (C). Specimens, SP2 and SP3, were pressurised to the design level $p = 11.2\ MPa$. The axial strain obtained at the end of this pressurisation step was averaged for all strain gauges and they were compared with the FE prediction. The average axial strain for SP2 was

257 $\mu\varepsilon$, and 233 $\mu\varepsilon$ for SP3. The FE prediction was 220 $\mu\varepsilon$ for both, SP2, and SP3. The average hoop strain was 848 $\mu\varepsilon$ for both, SP2, and SP3, and the corresponding FE prediction was 898 $\mu\varepsilon$.

Specimens SP4, SP5 and SP6 were pressurised to the half of the design level, i.e., $p = 5.6\ MPa$. The gauges were placed close to edges of the gouges. The average axial strain from strain gauges was 120 $\mu\varepsilon$ for SP4, 123 $\mu\varepsilon$ for SP5, and 119 $\mu\varepsilon$ for SP6. The FE predictions were 116 $\mu\varepsilon$ for SP4, 112 $\mu\varepsilon$ for SP5 and 88.3 $\mu\varepsilon$ for SP6. The average hoop strain from strain gauges was 460 $\mu\varepsilon$ for SP4, and 70 $\mu\varepsilon$ for SP6. The FE values were 412 $\mu\varepsilon$ for SP4 and 98 $\mu\varepsilon$ for SP6, (there was no hoop strain gauge for SP5). The difference in the hoop strain values might be due to the presence of the gouges and the fact that strain gauges were close to edges of gouges.

Also, values of the FE strain were obtained as average values at nodes. This could overestimate the strain values at the surface due to the extrapolation of the results. And generally it can be concluded that the strain gauges gave reasonable results when compared to the finite element prediction for pressurisation step.

6.6.2 Denting

Once the pressurisation was completed, the denting process started and the same strain gauges were used to record any change in the strain distribution during this part of the experiment. Typical plot of experimental strain and FE-strain is shown in Figure (6.43), and in Figure (6.44) for SP4. The axial strain distribution for, SP2, is shown in Figure (6.45) for both gauges G02 and G04. Both gauges were on axial axis as sketched inside the Figure (the dashed line indicates the indenter's outline). The magnitude of axial strain increased as the dent depth, δ, increased. All axial strains were tensile. The hoop strain distribution for the same specimen is shown in Figure (6.46).

Distribution of axial strain for, SP3, is shown in Figure (6.47) for gauges G02, G04, and G06. Position of these gauges was shifted 60° in hoop direction - as sketched inside the Figure. Results showed tensile strains and their magnitude increased as the dent depth increased - as shown in Figure (6.48). The hoop strains are tensile at the beginning of the indentation and they change to compression as the dent depth

increases (especially for gauge, G05).

The hoop strain distribution for SP4 is shown in Figure (6.49) for gauges G07 and G02. The hoop strains were compressive and their magnitude increased with the increase of thedent's depth. Distribution of the hoop strain for gauges G03 and G05 is shown in Figure (6.50). The hoop strain distribution was tensile and the magnitude increased with the increase of the dent's depth. The axial strain distribution, for gauges G01, G06 and G08, is shown in Figure (6.51). It is seen that magnitude of tensile strain increases as the dent's depth increases (especially for gauges closer to the gouge tip).

For specimen SP5 with double axial gouges, the axial strain distribution obtained from gauges G04 and G05 is shown in Figure (6.52). The axial strain was a tensile strain at the beginning of the indentation procedure and it changed to compressive strain as the dent's depth increased. Figure (6.53) shows axial strain distribution for gauges G01, G02, and G03 which were located on central axis of the pipe - as sketched inside the figure. Magnitude of the axial strain increased with the increase of the dent's depth, and maximum strains were recorded by gauges closer to the dent vicinity or closer to the gouge tip.

Distribution of the axial strain for, SP6 and from gauges G01, G02, and G03 is plotted in Figure (6.54). The axial strain was tensile at the beginning and changed to compressive as the dent's depth increased. The magnitude was larger for gauges closer to the dent, as well as, gouge vicinity or gouge tip. In addition, the axial strain distribution for gauges G01, G02, and G03 positioned on the central axis is given in Figure (6.55). The axial strain was a tensile strain and it is magnitude increased as the dent's depth increased. Also, its magnitude was larger for gauges closer to the gouge tip. Most of the strain gauges were located close to the dent region to capture the change in the strain distribution around dent and gouge vicinity.

6.7 Contact area

The contact area described in Chapter (3) was confirmed here experimentally for one sample. The experimental test was carried out on specimen, SP3, by using a thin pressure sensitive membrane called $PressureX^R$ (SENSOR Product Inc., USA).

This sheet of film was put between the hemispherical indenter and the pipe during denting. As depth of the dent increased the contact area changed. This change of the contact area was mapped onto the film. Once the denting procedure was completed the film was sent to the manufacturer for processing. Results are depicted in Figure (6.56a), and in Figure (6.56b), for 2D, and 3D, respectively. The result is re-plotted in Figure (6.56c) which also shows the outer perimeter of the indenter. These contours can be compared with results obtained from ABAQUS in Figure (6.56d). The contact area measured experimentally for half circle is $A_{expt} = 286\ mm^2$ and from FE, the contact area is $A_{FE} = 235\ mm^2$. The difference in the contact area is 17.8% which is reasonable for this sensitive test. This test also confirms that the contact surface between indenter and shell is not a total contact. There are areas where these two surfaces do not interact. This is a very interesting observation: firstly the FE based, and then verified experimentally.

6.8 Observations

During experimental tests carried out on specimens SP1 to SP6 the following observations can be made:

- The presence of internal pressure stiffens the pipe hence there is an increased magnitude of denting load when compared to non pressurised pipes.
- No failure has occurred during pressurisation or during indentation for all specimens (whether empty or pressurised).
- Shapes of dents were smooth and there were no signs of any scratches or any surface defects.
- The presence of axial gouges had a small effect on the load-displacement path and on springback.
- The internal pressure was monitored and it was always constant. Small variation in the pressure was compensated by pressure accumulator.
- Reduction in wall thickness at the dent centre was measured for, SP2, and SP3, and it was compared with the FE prediction. The results showed that for dent

depth equal to $(\frac{\delta}{D_o})_{max} = 0.23$, with internal pressure equal to $p = 11.2\ MPa$, there was $\cong 5.2\%$ reduction in wall thickness.

- Strains measured by gauges gave results which compared reasonably well with the FE predictions for the pressurisation step.

6.9 Summary

- Gouges were introduced into surfaces of plain pipe using electrical discharge machine or high speed milling machine.
- The ground support for pipes in the form of a wooden saddle was used. The indenter was hemispherical and it was machined from a solid mild steel bar.
- Tensile tests were carried out in order to obtain material properties of tested pipes.
- The experimental model used a saddle support made from pine wood. Stiffness of this wooden support was measured experimentally. The measured stiffness was subsequently used in the FE model with nonlinear springs. This approach gave very good results, i.e., numerical and experimental results agreed very well.
- Repeatability of experimental tests was checked, and good results were obtained (the case of SP2 and SP3).
- Strain gauges were used during denting of specimens SP2 to SP6 in order to predict the axial and hoop strain distribution around vicinity of the dent.
- Contact area and its shape was measured experimentally. It compared well with the FE prediction. This test confirmed that there is no continuous contact between indenter and pipe during denting.

	Part 'P1'				Part 'P2'							Part 'P3'				
location	1	2	3	4	5	6	7	Centre	1	2	3	4	5	6	7	Average
1	2.12	2.13	2.12	2.11	2.10	2.07	2.03	2.03	2.02	2.01	1.98	2.16	2.17	2.17	2.15	2.11
2	2.12	2.13	2.13	2.11	2.14	2.13	2.12	2.12	2.06	2.04	2.05	2.17	2.17	2.16	2.16	2.13
3	2.11	2.13	2.13	2.11	2.17	2.16	2.13	2.12	2.08	2.09	2.11	2.19	2.18	2.14	2.15	2.13
4	2.10	2.11	2.11	2.10	2.14	2.14	2.11	2.10	2.10	2.13	2.13	2.18	2.17	2.14	2.15	2.13
5	2.11	2.13	2.12	2.09	2.09	2.10	2.09	2.11	2.12	2.12	2.14	2.18	2.18	2.16	2.16	2.12
6	2.12	2.13	2.14	2.11	2.05	2.03	2.03	2.08	2.09	2.11	2.12	2.19	2.19	2.16	2.16	2.11
7	2.10	2.11	2.12	2.10	2.02	2.04	2.06	2.06	2.06	2.08	2.11	2.18	2.18	2.15	2.15	2.10
8	2.11	2.13	2.12	2.08	2.05	2.07	2.04	2.04	2.02	2.04	2.03	2.17	2.18	2.14	2.15	2.10
Average	2.11	2.13	2.12	2.10	2.10	2.09	2.08	2.08	2.07	2.08	2.08	2.18	2.18	2.15	2.15	2.11

Table 6.1: The wall thickness of SP2, $(\frac{2L}{D_o}) = 6.0$. Data is in (mm). Note: there are 15, equally spared, measuring points along full length of the pipe.

	Part 'P1'				Part 'P2'							Part 'P3'				
loc.	1	2	3	4	5	6	7	Cen.	1	2	3	4	5	6	7	Ave.
1-5	84.16	84.21	84.32	84.25	84.13	84.08	84.02	84.13	84.01	83.98	84.01	83.93	83.95	84.02	84.07	84.08
3-7	84.17	84.12	84.03	83.82	83.93	83.98	84.01	84.23	84.06	84.08	84.18	84.39	84.47	84.37	84.31	84.14
2-6	84.14	84.16	84.27	84.13	84.09	84.03	84.01	84.13	84.04	84.04	84.06	84.05	84.21	84.18	84.14	84.11
4-8	84.20	84.16	84.04	83.83	83.94	84.01	84.01	84.24	84.05	84.06	84.12	84.19	84.16	84.22	84.23	84.10
Ave.	84.17	84.16	84.17	84.01	84.02	84.02	84.01	84.18	84.04	84.04	84.09	84.14	84.20	84.20	84.19	84.11

Table 6.2: The outside diameter of SP2, $(\frac{2L}{D_o}) = 6.0$. Data is in (mm).

Specimen	*P1*	*P2*	*P3*	*Exten.(1)*	*Exten.(2)*
SP1	–	255	–	–	–
SP2	130	255	130	255	255
SP3	128	254	128	255	255
SP4	132	255	132	255	255
SP5	140	255	140	252	252
SP6	124	254	124	250	250

Extension (1) with end closed and Extension (2)with oil inlet.

Table 6.3: Axial length of different parts, i.e., P1, P2, and P3 after machining. Length of two extensions (1) and (2) is also included. Data is in (mm).

Specimen	$D_o\ (mm)$	ΔD_o	% variance	$t\ (mm)$	Δt	% variance
SP1	84.20	0.012	0.140	2.07	0.0030	0.15
SP2	84.10	0.016	0.020	2.10	0.0043	0.20
SP3	84.06	0.012	0.015	2.09	0.0030	0.14
SP4	84.08	0.056	0.066	2.08	0.0027	0.13
SP5	83.94	0.027	0.030	2.08	0.0019	0.09
SP6	83.97	0.019	0.023	2.05	0.0042	0.20

Table 6.4: Values of the average wall thickness, and of the outside diameter, (within parts P1, P2, and P3) for all test specimens.

location	Width $(2w)$	Depth (e)	Length $(2c)$
1	0.97	1.07	21.0
2	0.99	1.05	21.0
3	0.99	1.05	21.0
4	0.99	1.05	21.0
5	0.97	1.06	21.0
6	0.95	1.06	21.0
Average	0.98	1.06	21.0

Table 6.5: Dimension of gouges obtained from measurements of acrylic mould for SP4. Data is in (mm).

location	Before use (mm)	After use (mm)
1	1.0	0.96
2	1.0	0.96
3	1.0	0.96
4	1.0	0.96
Average	1.0	0.96

Table 6.6: The measurements of the electrode's thickness before and after being used for mid-span gouge in, SP4. Length of electrode is $2c = 21.0\ mm$. Data is in (mm).

location	Width $(2w)$	Depth (e)	Length $(2c)$
1	1.08	0.96	21.0
2	1.06	0.94	21.0
3	1.06	0.98	21.0
4	1.06	0.94	21.0
5	1.08	0.94	21.0
Average	1.07	0.95	21.0

Table 6.7: Dimensions of gouge obtained from measurements of acrylic mould for SP5. Off-centre gouge, (slot A). Gouge length is $2c = 21.0\ mm$. Data is in (mm).

location	Width $(2w)$	Depth (e)	Length $(2c)$
1	1.02	0.98	21.0
2	1.04	0.98	21.0
3	1.06	0.98	21.0
4	1.08	0.98	21.0
5	1.06	0.98	21.0
Average	1.05	0.98	21.0

Table 6.8: Dimensions of gouge obtained from measurements of acrylic mould for SP5. Off-centre gouge, (slot B). Gouge length is $2c = 21.0\ mm$. Data is in (mm).

location	Before use (mm)	After use (mm)
1	1.0	0.960
2	1.0	0.960
3	1.0	0.960
4	1.0	0.960
Average	1.0	0.960

Table 6.9: The measurements of the electrode thickness before and after being used for the off-centre gouge, SP5, (slot A). The electrode length is $2c = 21.0\ mm$. Data is in (mm).

location	Before use (mm)	After use (mm)
1	1.0	0.960
2	1.0	0.960
3	1.0	0.960
4	1.0	0.960
Average	1.0	0.960

Table 6.10: The measurements of the electrode thickness before and after being used for off-centre gouge, SP5, (slot B). The electrode length is $2c = 21.0\ mm$. Data is in (mm).

location	Width ($2w$)	Depth (e)	Length ($2c$)
1	2.48	0.42	68.0
2	2.52	0.44	68.0
3	2.46	0.50	68.0
4	2.52	0.50	68.0
5	2.56	0.46	68.0
6	2.54	0.50	68.0
7	2.46	0.50	68.0
8	2.46	0.50	68.0
Average	2.50	0.48	68.0

Table 6.11: Dimensions of gouge obtained from measurements of acrylic mould, for SP6. Gouge length is $2c = 68.0\ mm$. Data is in (mm).

Specimen ↓	$\left(\frac{e}{t}\right)$	$\left(\frac{2w}{t}\right)$	$\left(\frac{2c}{D_o}\right)$
SP4	0.470	0.50	0.25
SP5	0.464	0.51	0.25
SP6	0.230	1.20	0.81

Table 6.12: Summary of normalised dimensions for depth, width and length of gouges. These dimensions were used to construct the FE models.

No:↓	D_o (mm)	t (mm)	L (mm)	e/t (%)	$2c/D_o$ (%)	$2w/t$ (%)	$p_{denting}$ (MPa)	Gouged	Bent
SP1	84.20	2.07	505.2	-	-		0.0	NO	NO
SP2	84.10	2.10	504.6	-	-	-	11.2	NO	YES
SP3	84.08	2.08	504.5	-	-	-	11.2	NO	YES
SP4	84.06	2.09	504.4	47	24.98	47.85	5.6	YES	YES
SP5	84.08	2.08	504.5	47	24.98	48.08 ⋆	5.6	YES	YES
SP6	83.97	2.08	503.8	23	81.0	120.2	5.6	YES	YES

Table 6.13: Geometry of six mild steel pipes. Models SP1, SP2, and SP3 had plain dents in them whilst models SP4, SP5, and SP6 were gouged. Note: ⋆ model no. SP5 had two axial gouges of the same geometry and placed symmetrically with respect to mid-length.

Specimen ↓	$(t)\ (mm)$	$\Delta t\ (mm)$	$(w)\ (mm)$	$\Delta w\ (mm)$	$A\ (mm^2)$
1	2.31	0.00222	20.03	0.0035	46.25
2	2.38	0.00682	12.34	0.0042	29.60
3	2.37	0.00115	20.01	0.0012	47.51
4	2.37	0.00106	12.01	0.0024	28.45

Table 6.14: The average wall thickness and width of tensile test specimens with the corresponding standard deviations. A is the cross-section area.

E (GPa)	σ_{yp} (MPa)	σ_{UTS} (MPa)	ν	Applicable to models
210.0	316.0	460.0	0.30	SP1, SP2 (Fig. 3.7b)
205.0	332.0	459.0	0.284	SP3, SP4, SP5, SP6 (Fig. 6.12)

Table 6.15: Average material properties of tested pipes obtained from uni-axial tests on flat coupons.

	F_{max} (kN)		$(\delta/D_o)_{max}$ (%)		$(\delta/D_o)_R$ (%)	
No:↓	**Expt**	**FE**	**Expt**	**FE**	**Expt**	**FE**
SP1	11.7	12.1	16.0	16.0	11.91	12.3
SP2	37.0	45.0	23.0	23.0	11.99	13.4
SP3	39.0	46.0	23.0	23.0	11.77	12.3
SP4	20.0	22.0	15.0	15.0	9.20	10.7
SP5	21.5	23.9	16.6	16.6	10.10	11.5
SP6	21.0	22.4	16.0	16.0	10.20	11.8

Table 6.16: Comparison of experimental and computed results for denting of plain and gouged pipes.

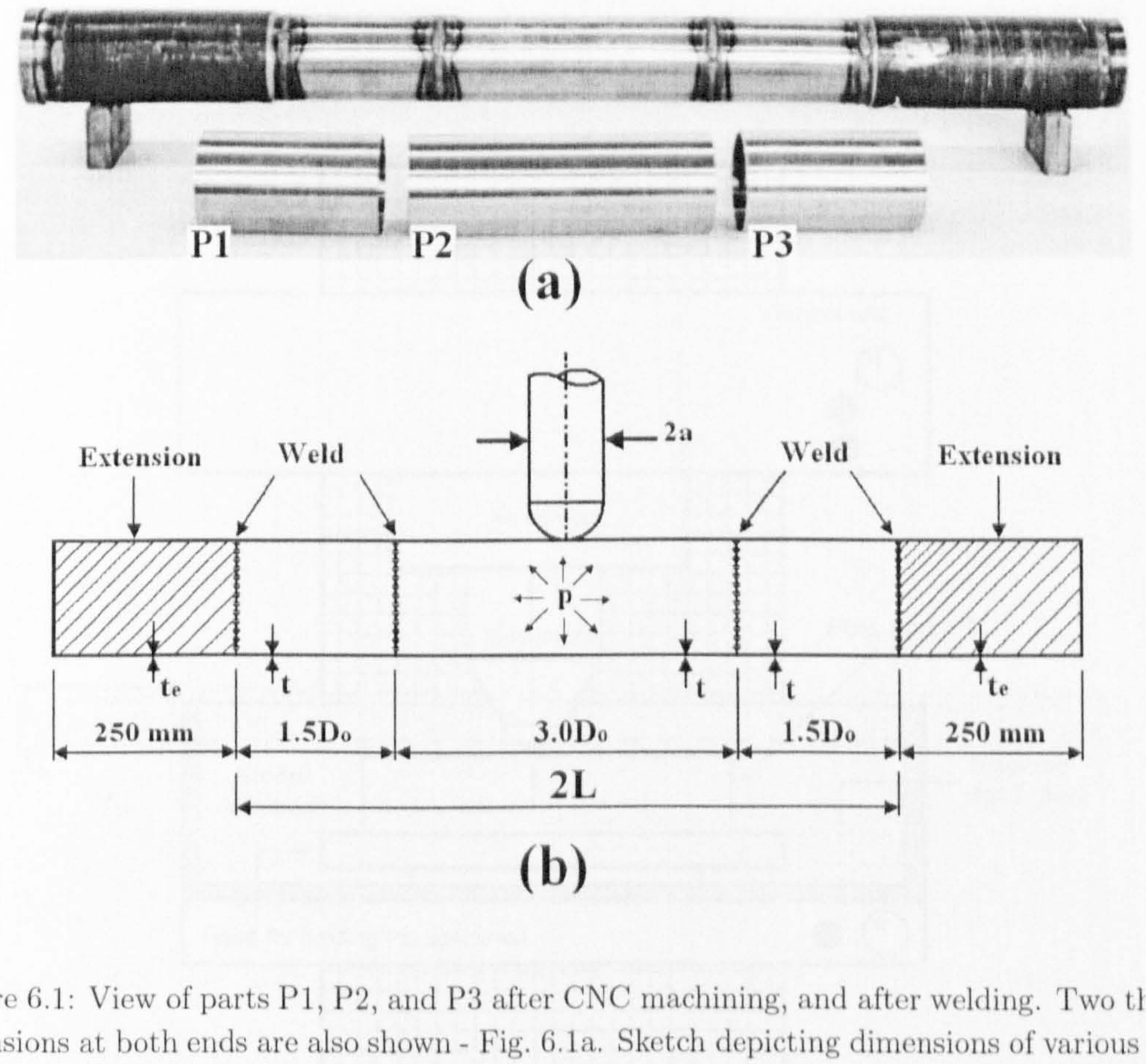

Figure 6.1: View of parts P1, P2, and P3 after CNC machining, and after welding. Two thicker extensions at both ends are also shown - Fig. 6.1a. Sketch depicting dimensions of various parts together with a vertical indenter - Fig. 6.1b.

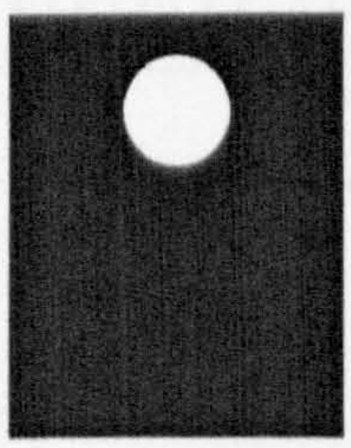

Figure 6.2: Machined electrode to be used in the electrical discharge machine (electrode made from Erodex material).

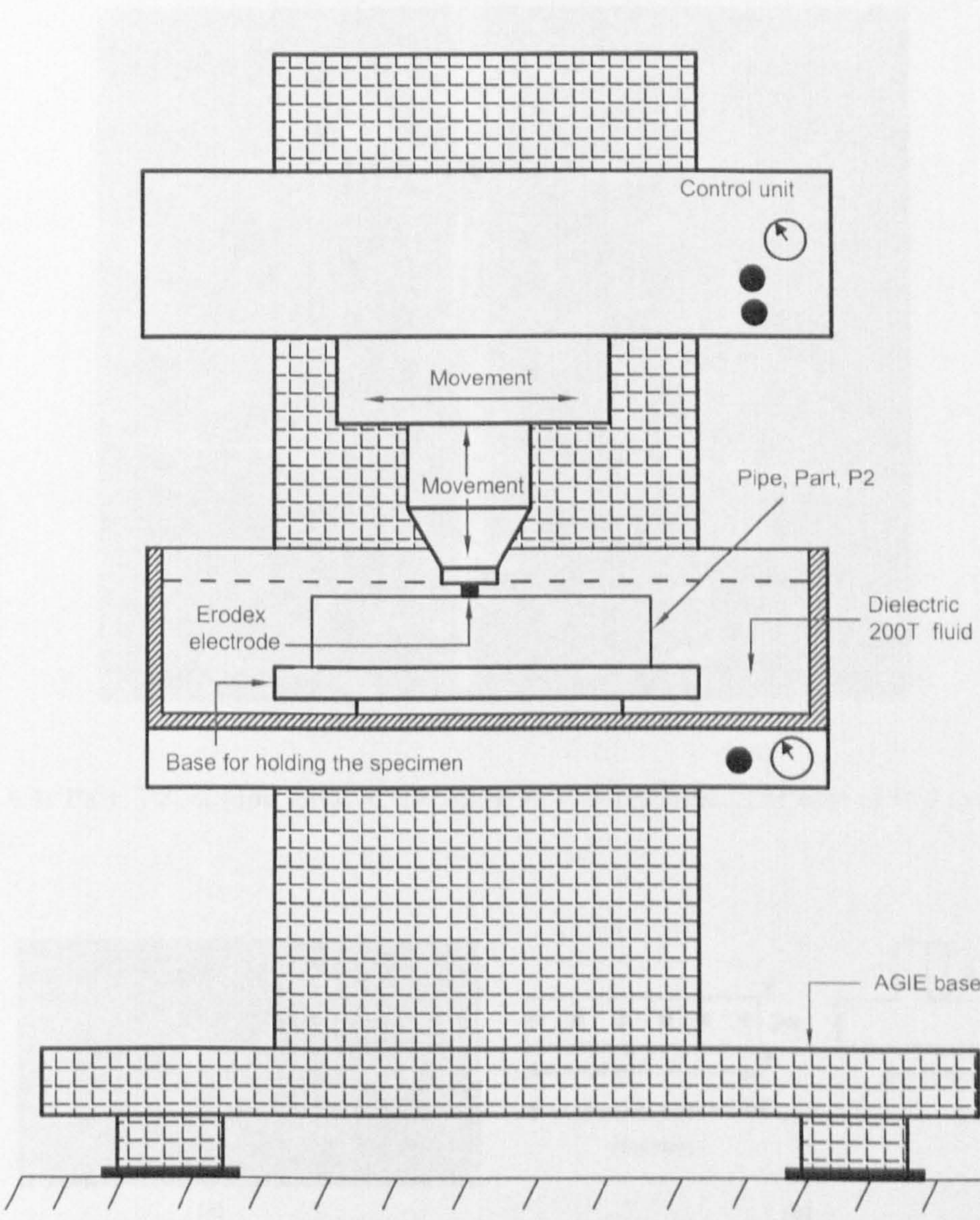

Figure 6.3: Sketch of the electrical discharge machine used for manufacturing of axial gouges.

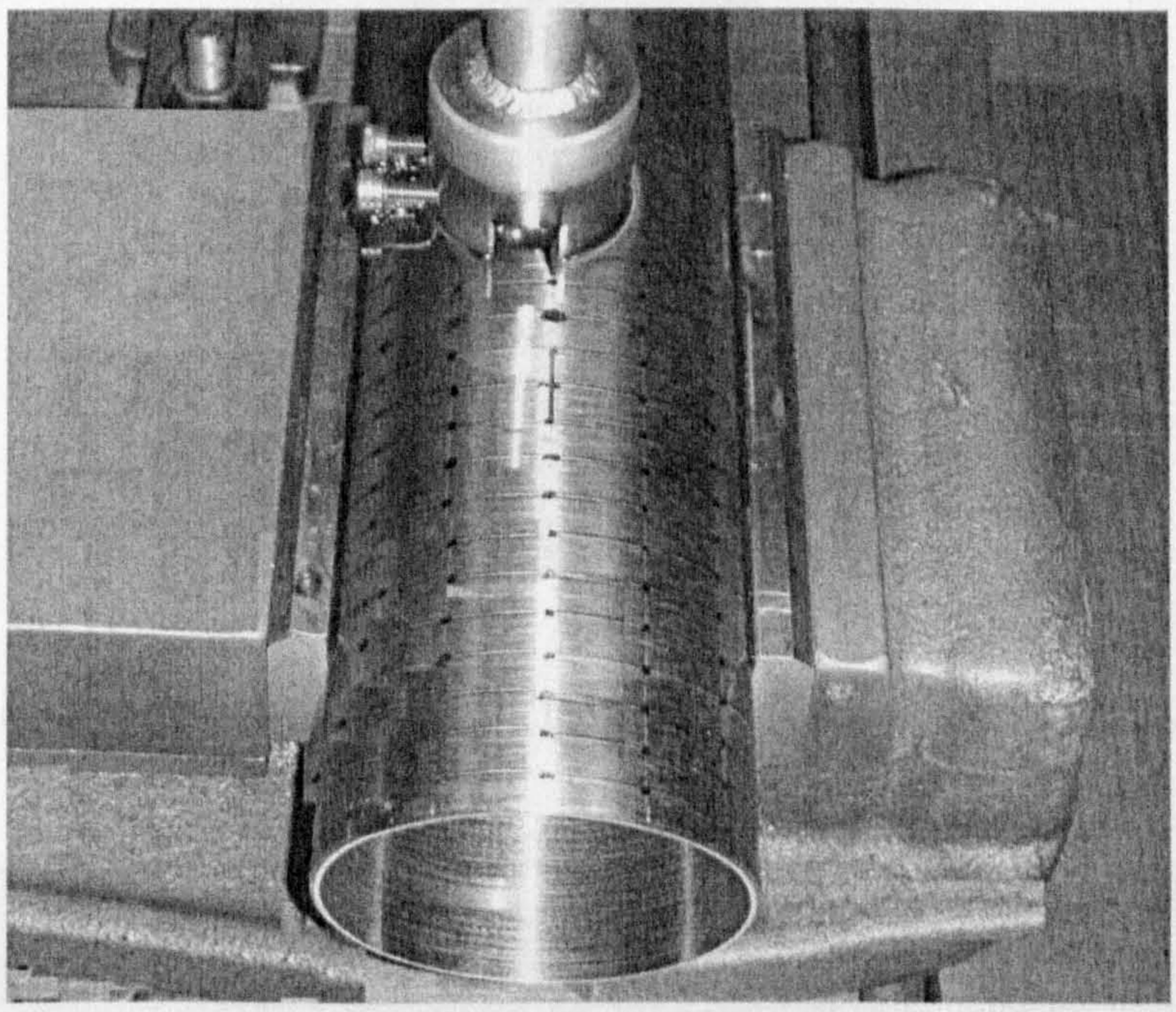

Figure 6.4: Part, P2, of pipe, SP5, in the spark erosion machine. The case of two axial gouges is shown.

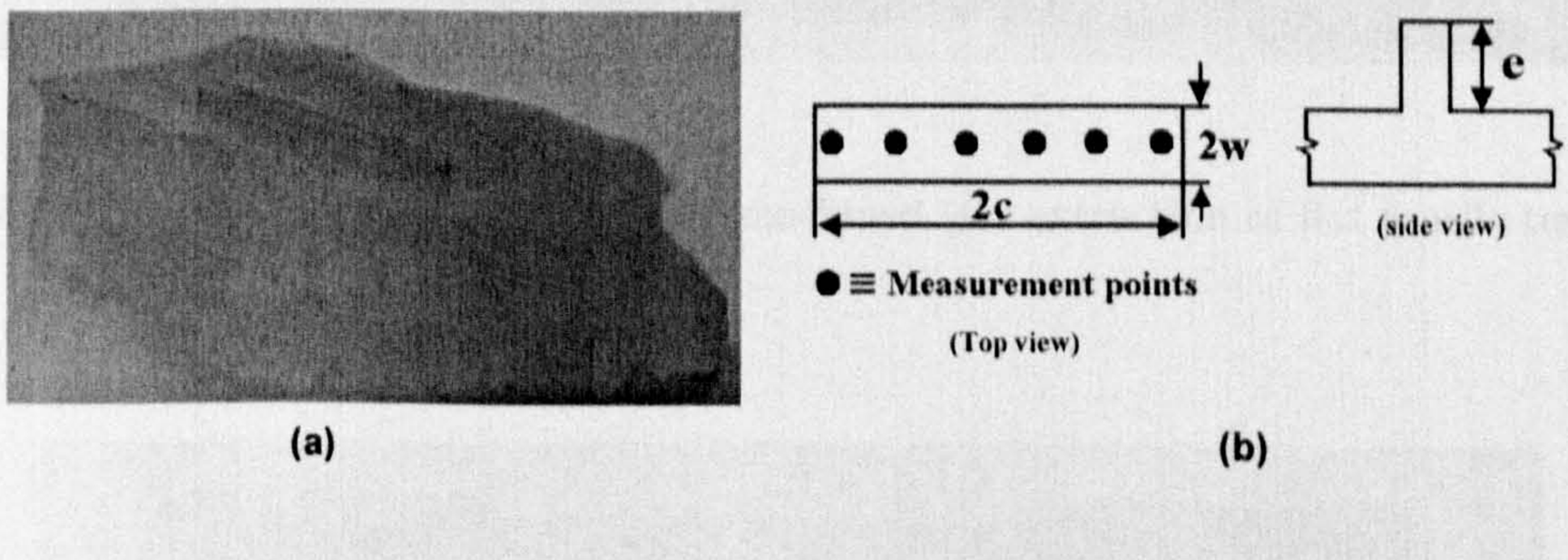

Figure 6.5: The male mold, in acrylic, of a narrow axial gouge, Figure (6.5a); sketch showing position of measuring points on the male mould, Figure (6.5b).

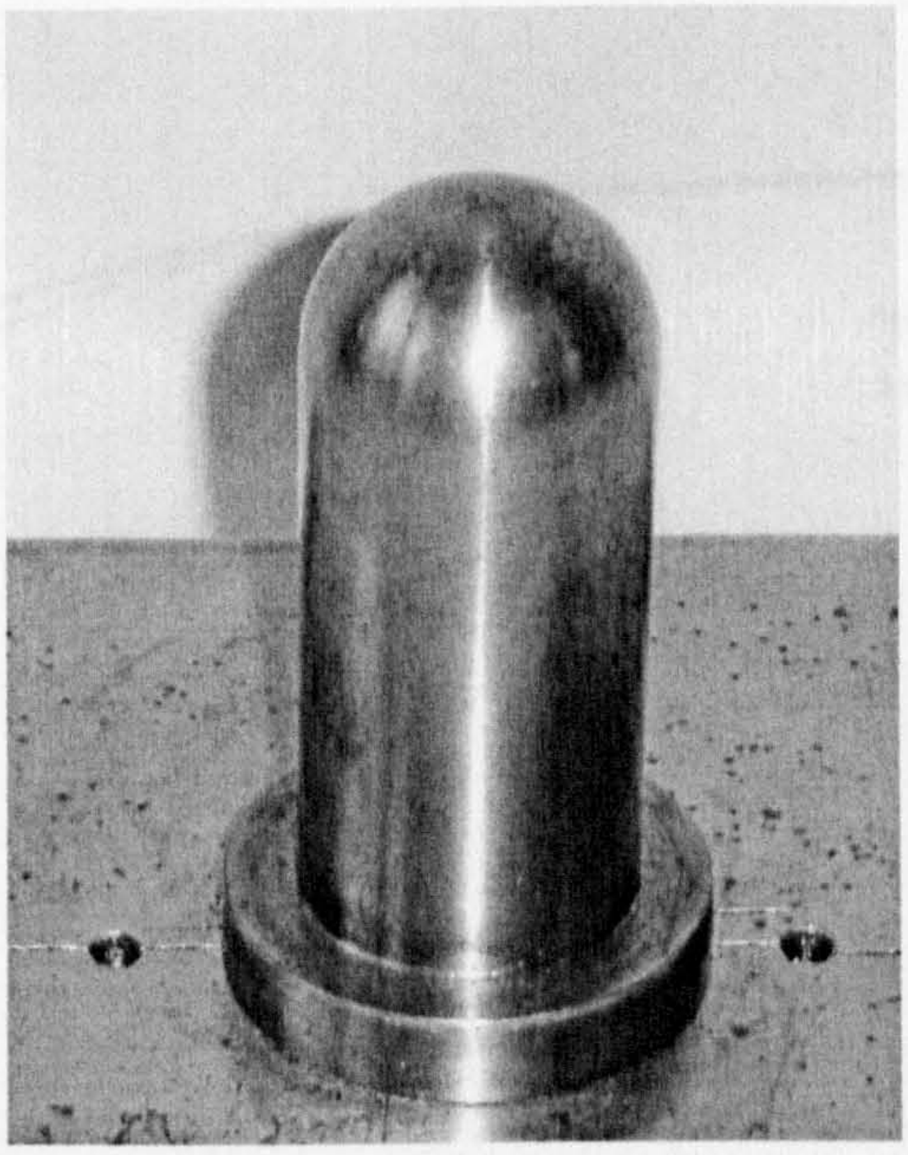

Figure 6.6: View of hemispherical indenter ($D_{indenter} = 34.7\ mm$, and $H_{indenter} = 80.0\ mm$).

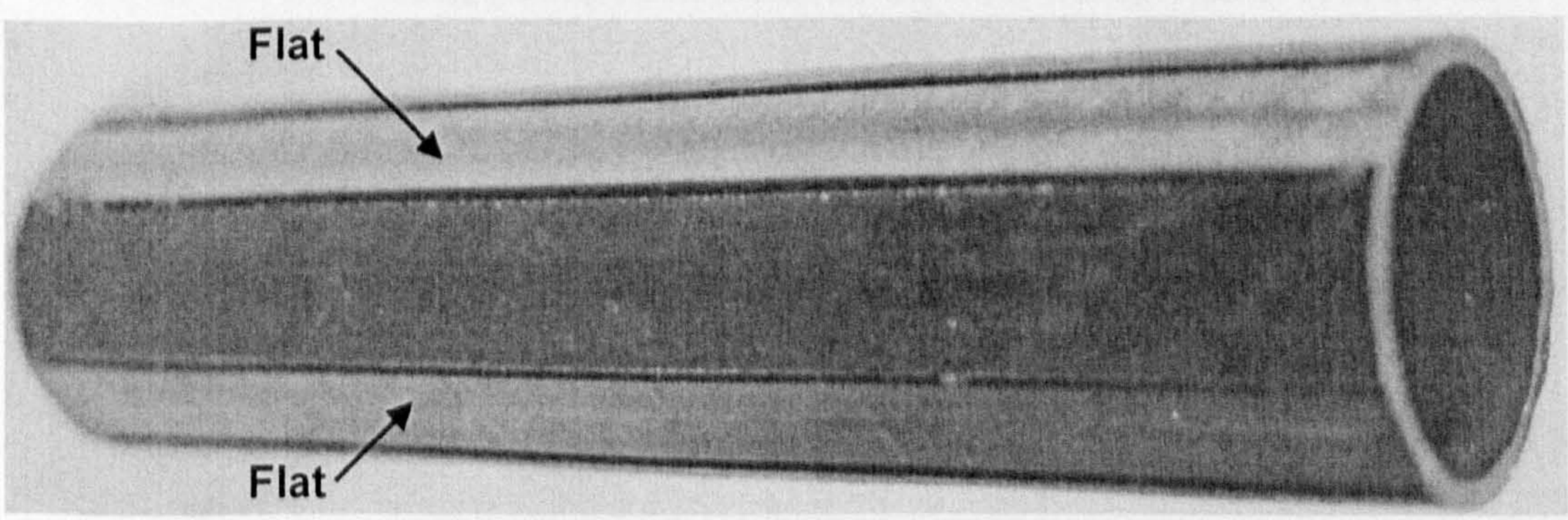

Figure 6.7: View of the pipe being partially machined (for extraction of flat tensile test specimens).

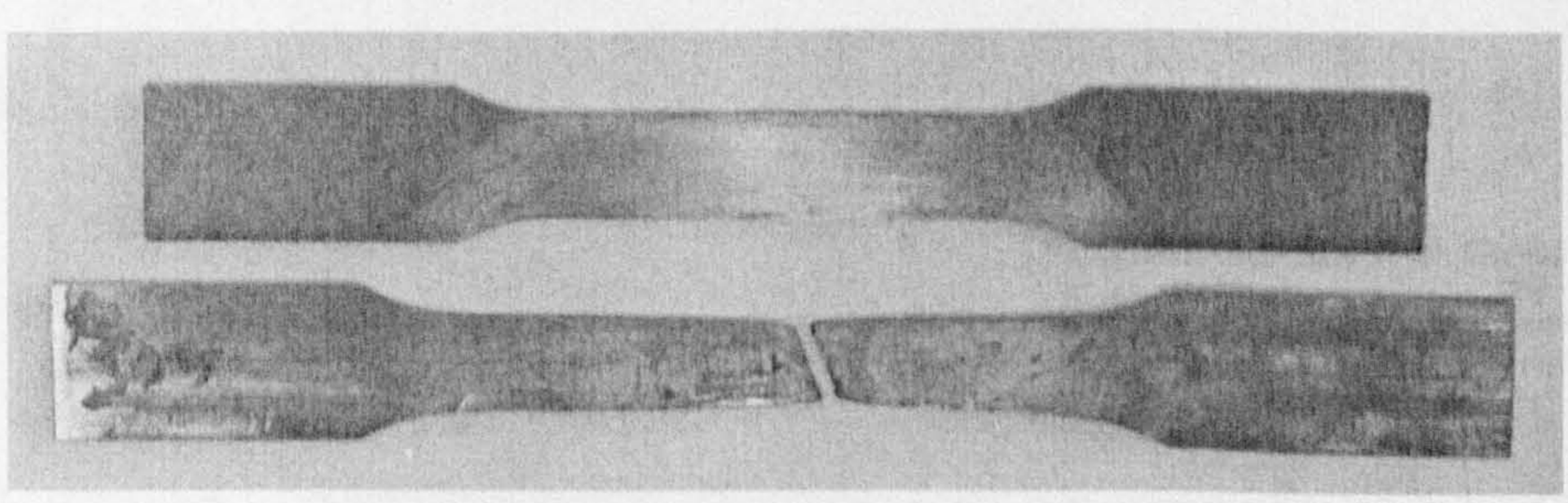

Figure 6.8: The tensile test specimen before and after being tested.

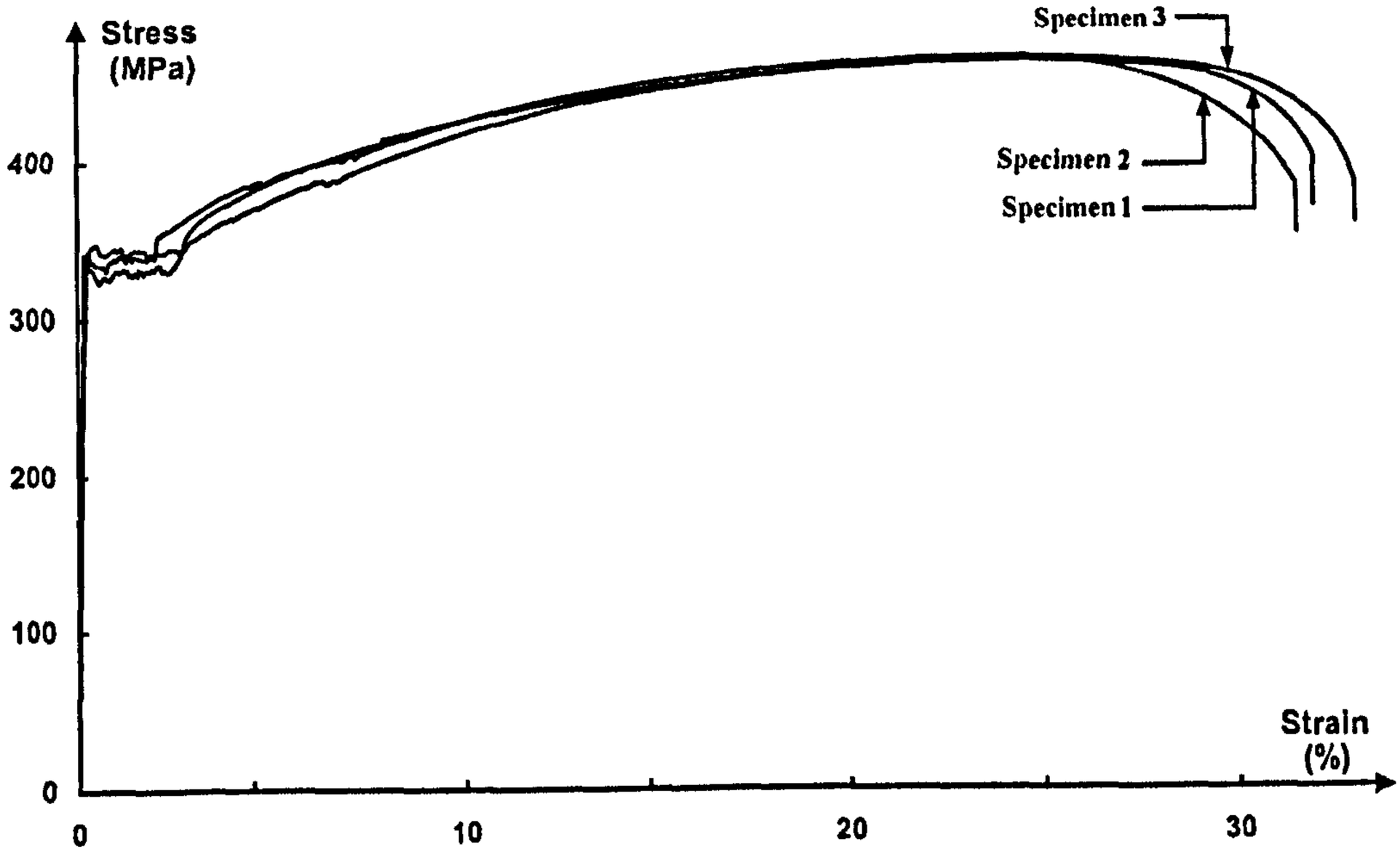

Figure 6.9: Plot of engineering stress-strain obtained for flat specimens 1, 2, and 3.

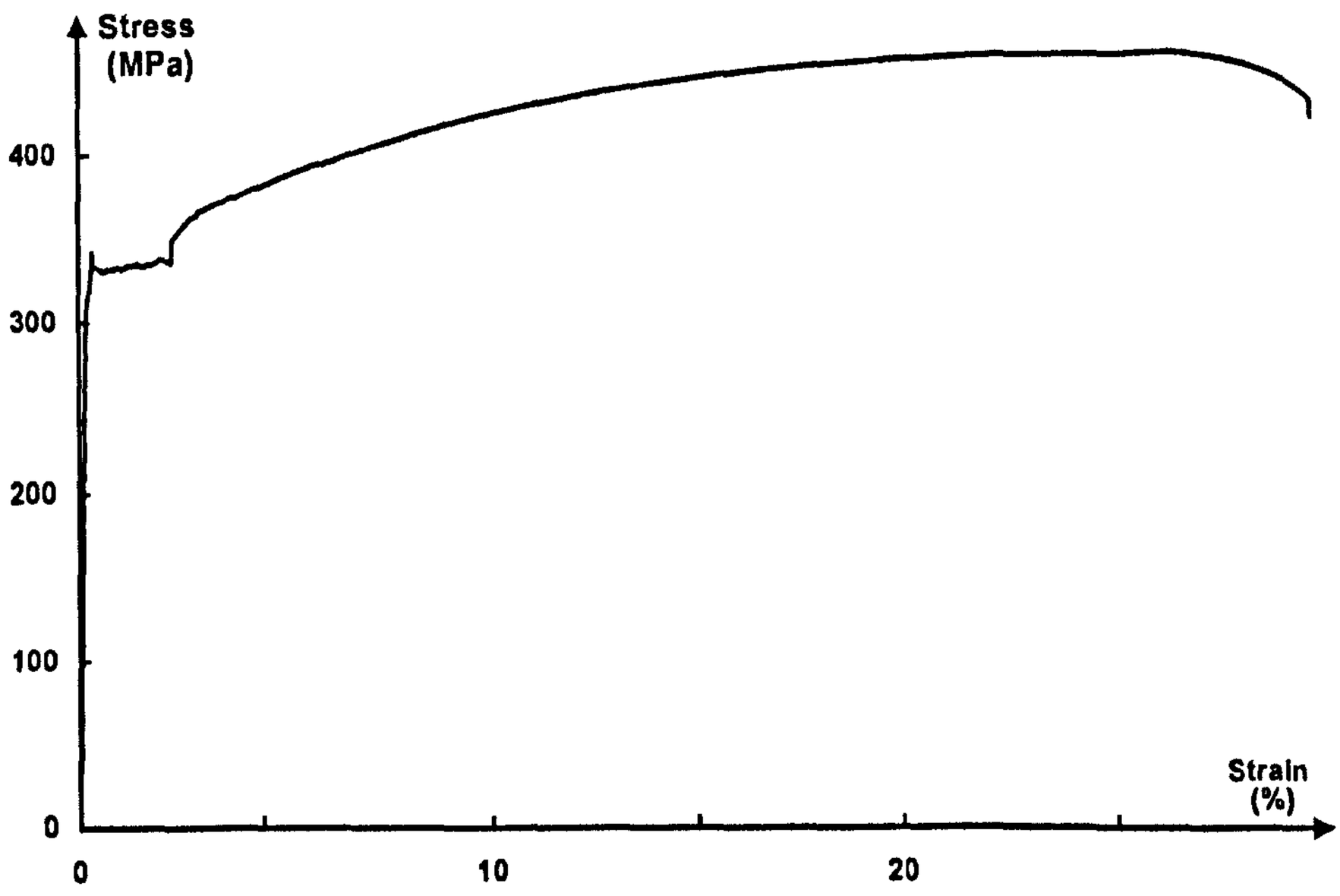

Figure 6.10: Plot of engineering stress-strain (averaged results from specimens 1, 2, and 3).

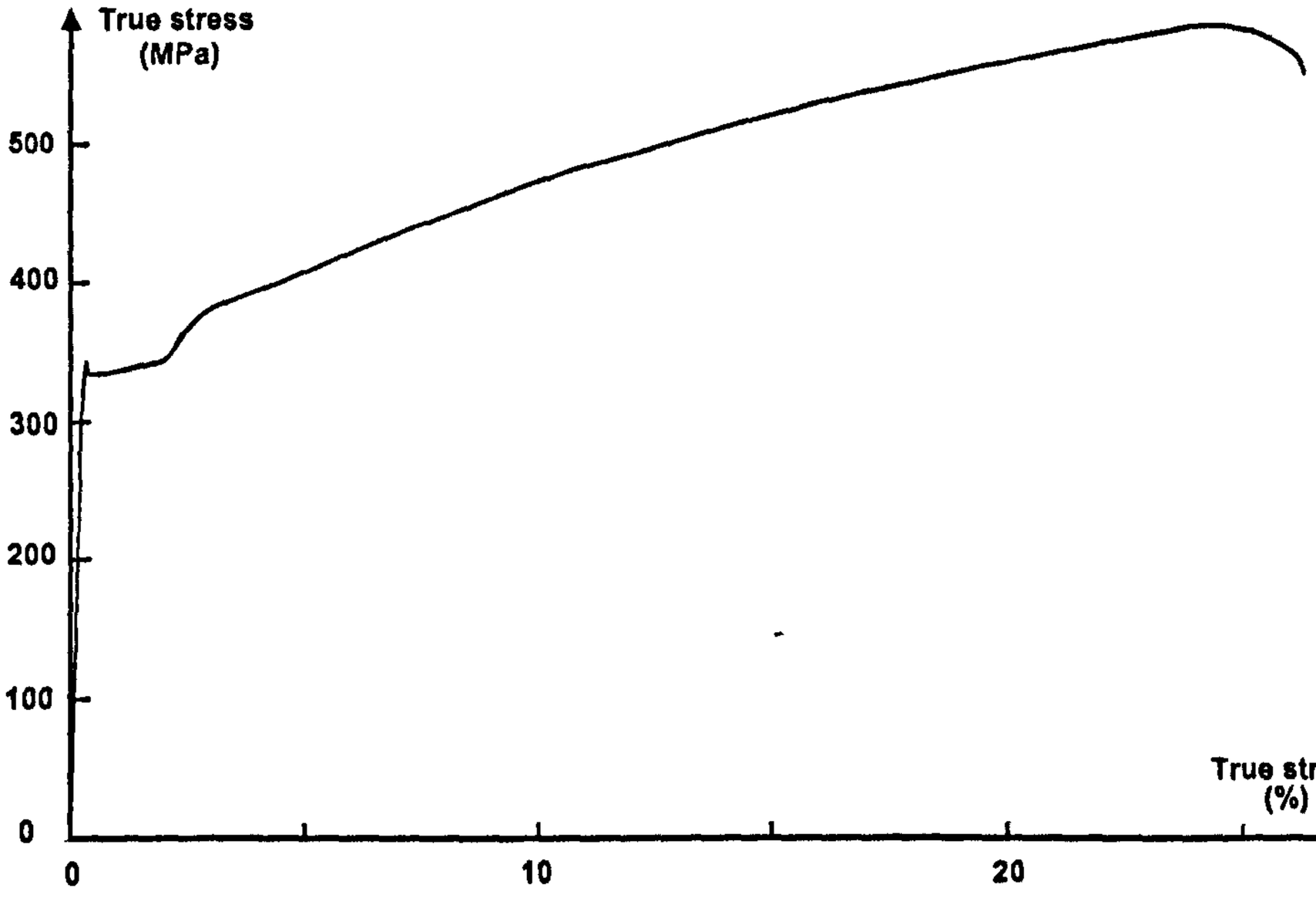

Figure 6.11: Plot of true stress-strain curve (based on average stress-strain curve, Figure (6.10)).

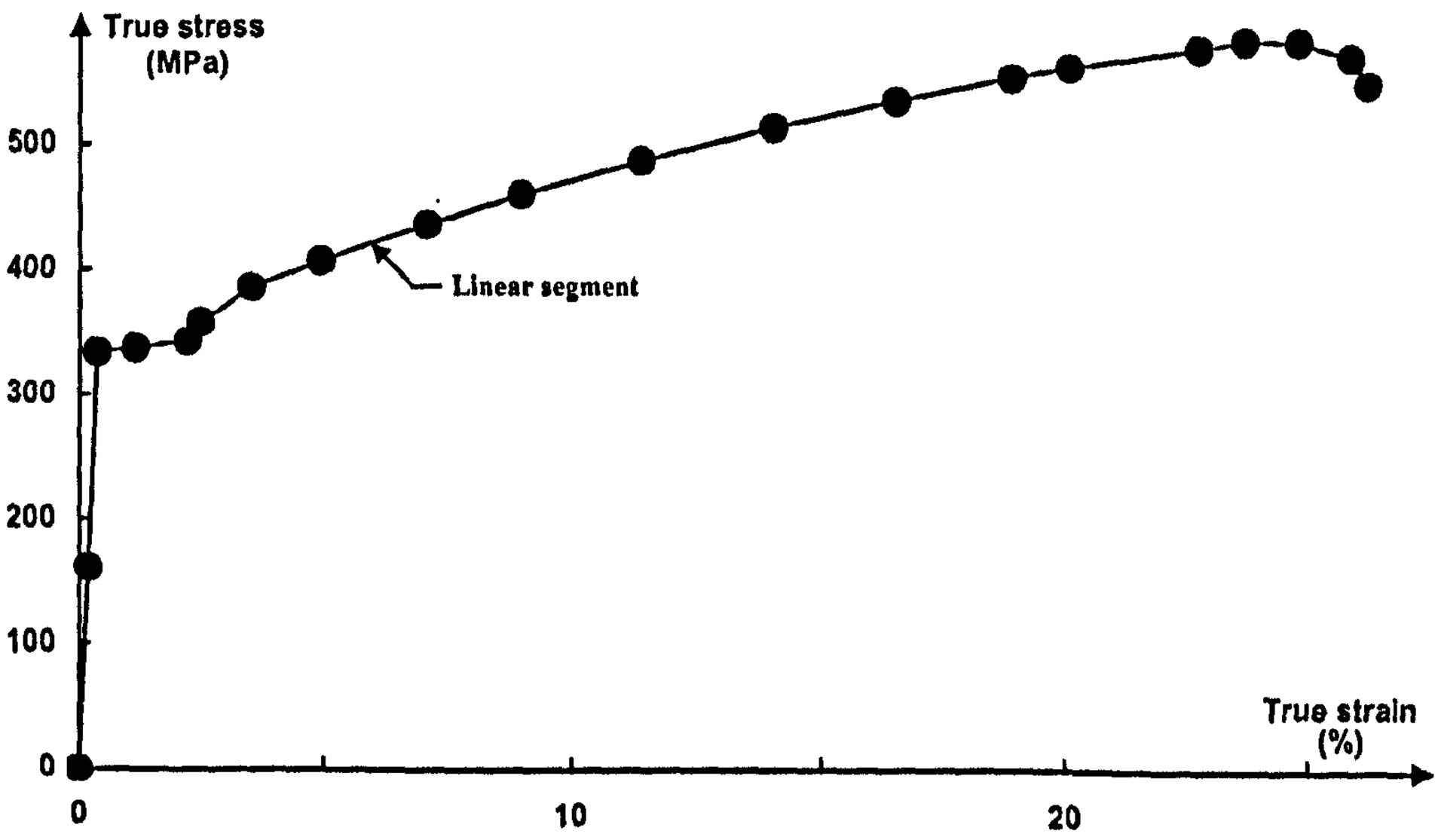

Figure 6.12: Nineteen linear segments of the true stress-strain curve used in the FE models.

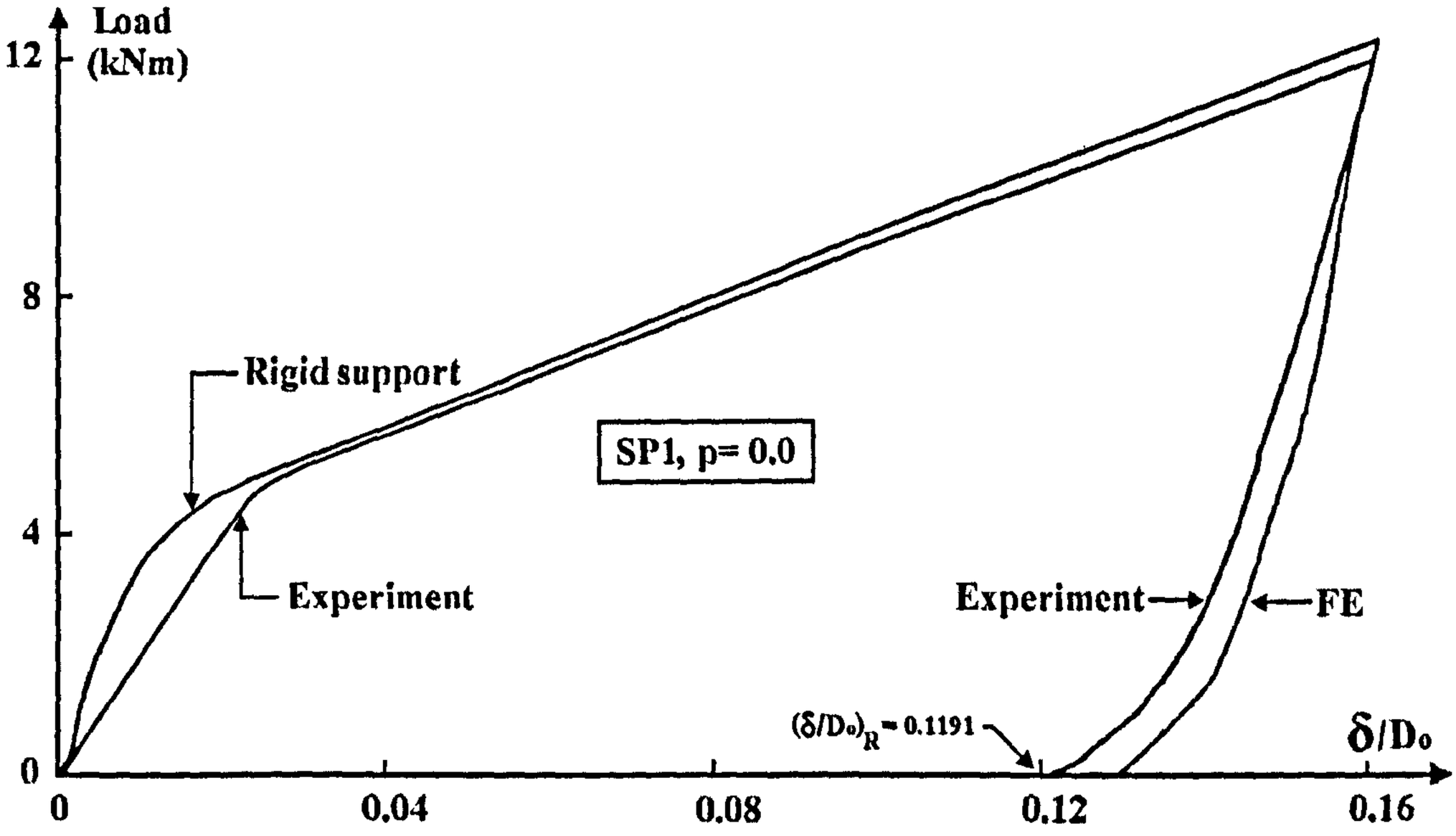

Figure 6.13: Plot of the experimental and FE loading-unloading curves versus depth of the dent for specimen, SP1. The specimen had no surface defect. Also, $\frac{a}{b} = 1.0$, $\frac{2L}{D_o} = 3.0$, $(\frac{\delta}{D_o})_{max} = 0.16$, $p = 0.0$, and $(\frac{\delta}{D_o})_R = 0.1191$.

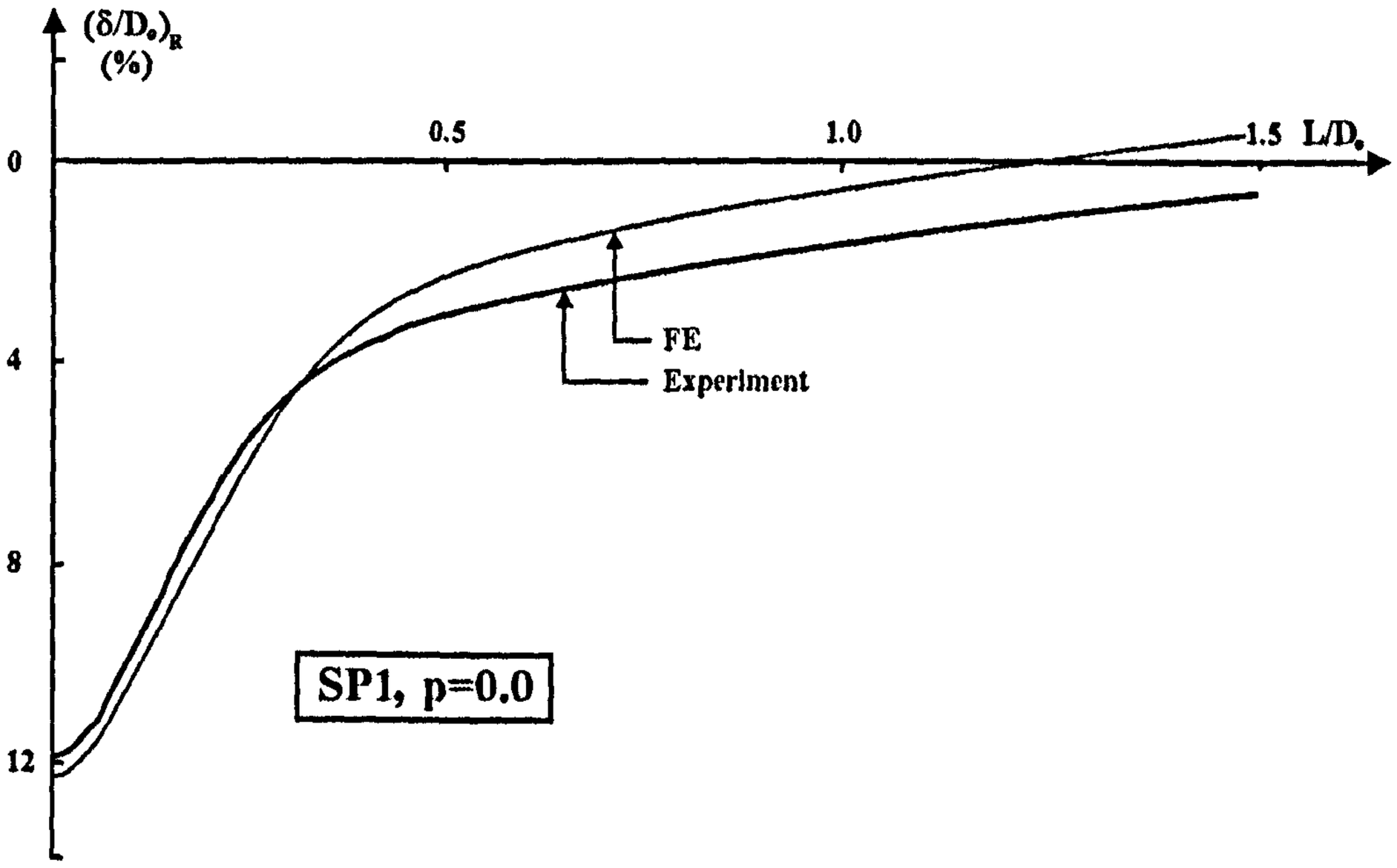

Figure 6.14: Comparison of the residual dent profile along pipe's length for specimen, SP1. The specimen had no surface defect. Also, $\frac{a}{b} = 1.0$, $\frac{2L}{D_o} = 3.0$, $(\frac{\delta}{D_o})_{max} = 0.16$, $p = 0.0$, $(\frac{\delta}{D_o})_R = 0.1191$.

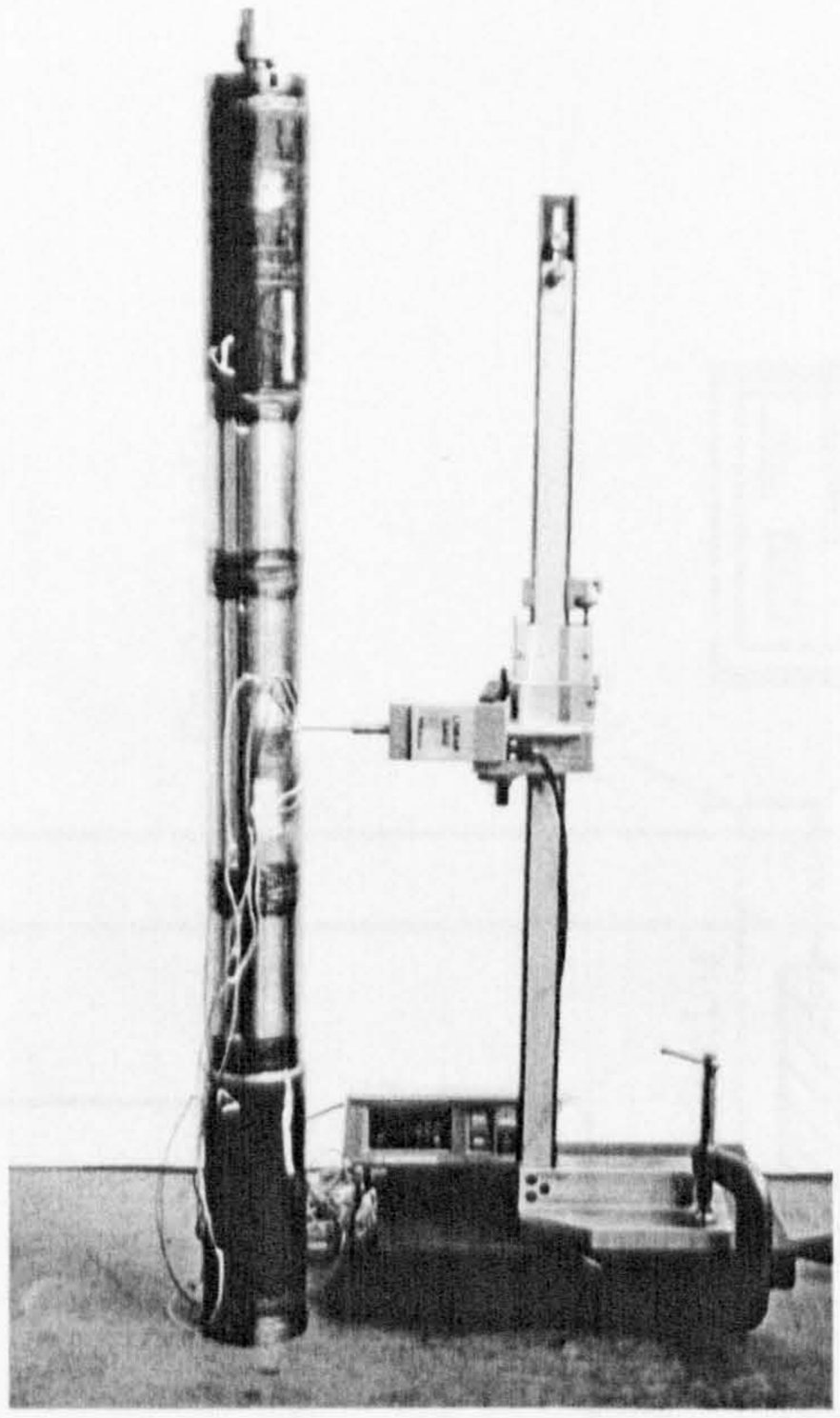

Figure 6.15: The Mitutoyo linear gauge transducer used for measurements of dent profile along the pipe's length for model SP3.

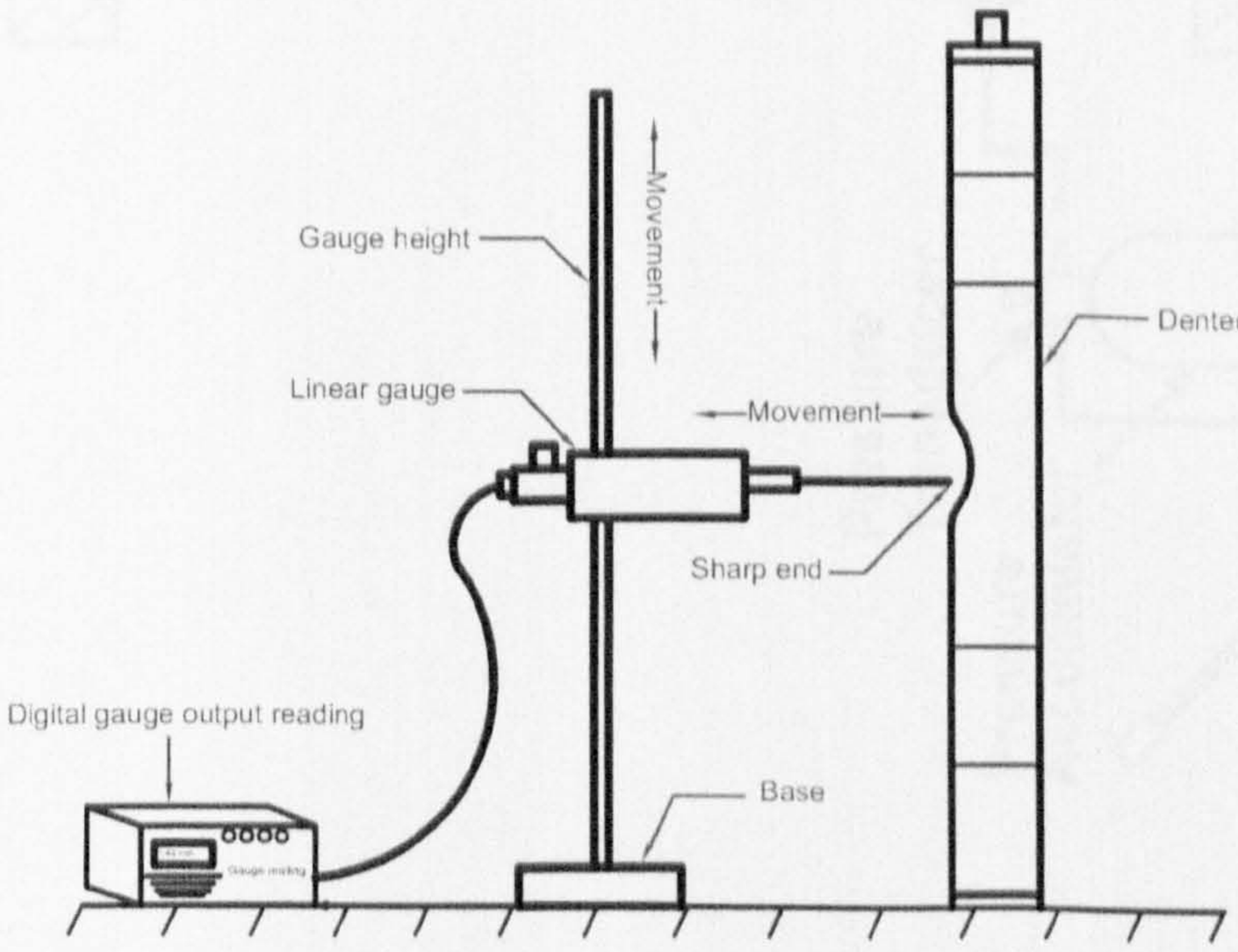

Figure 6.16: Sketch of the experimental setup used to obtain the dent's profile.

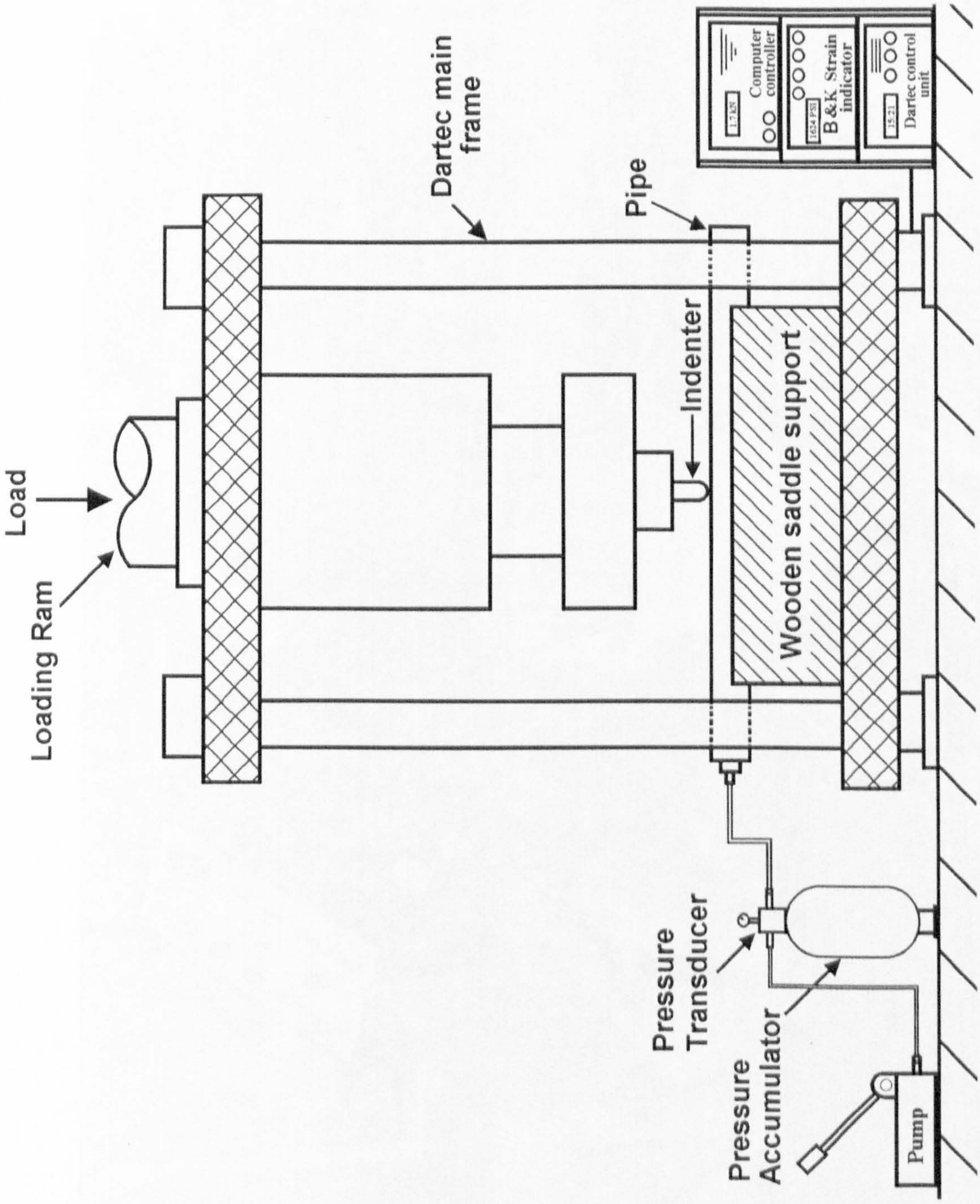

Figure 6.17: Sketch showing the experimental set up for pipe denting.

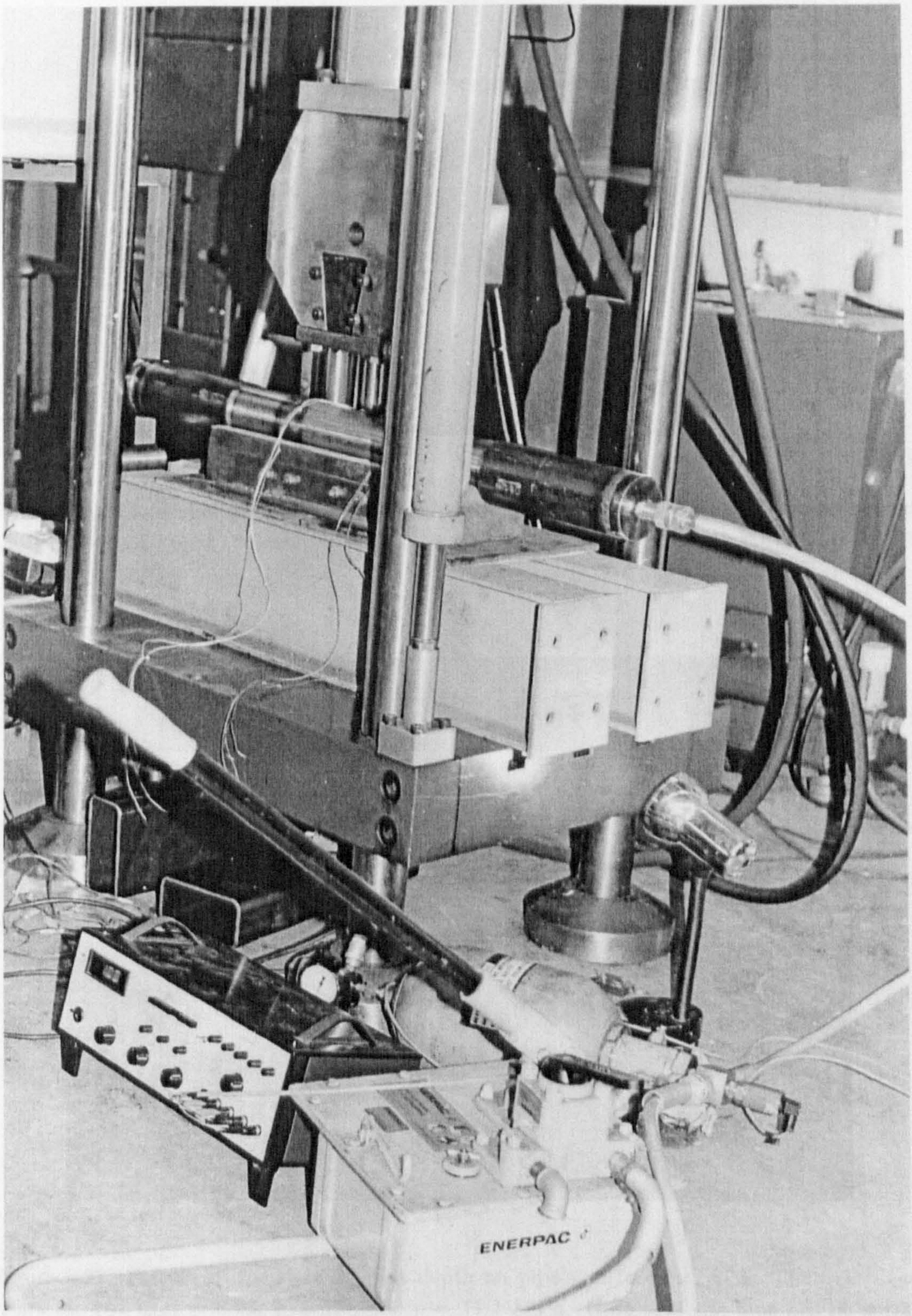

Figure 6.18: The experimental set up for denting a pipe. Also, arrangements for pressurising the pipe.

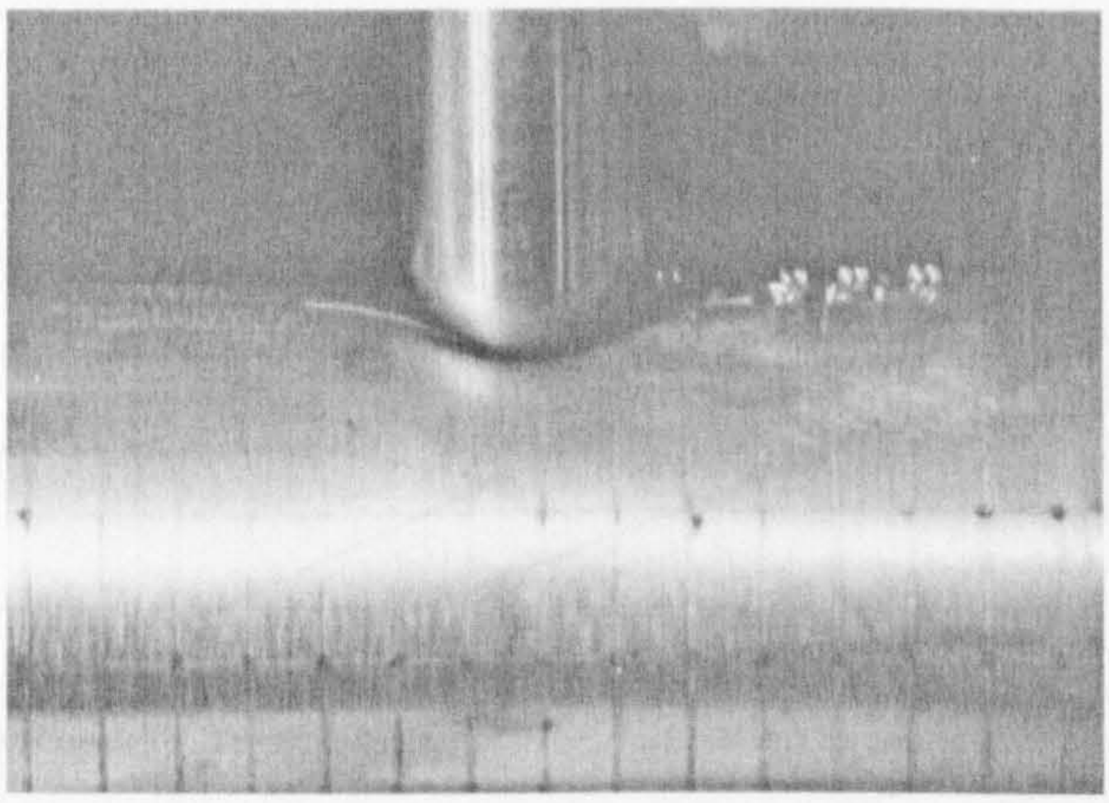

Figure 6.19: Close view of pipe, with double axial gouges, in contact with hemispherical indenter. Photograph shows the case: $(\frac{\delta}{D_o})_{max} = 0.166$, $\frac{a}{b} = 1.0$, $\frac{2c}{D_o} = 0.25$, $\frac{e}{t} = 0.47$, $\frac{2w}{t} = 0.4808$, and $p = 5.6\ MPa$.

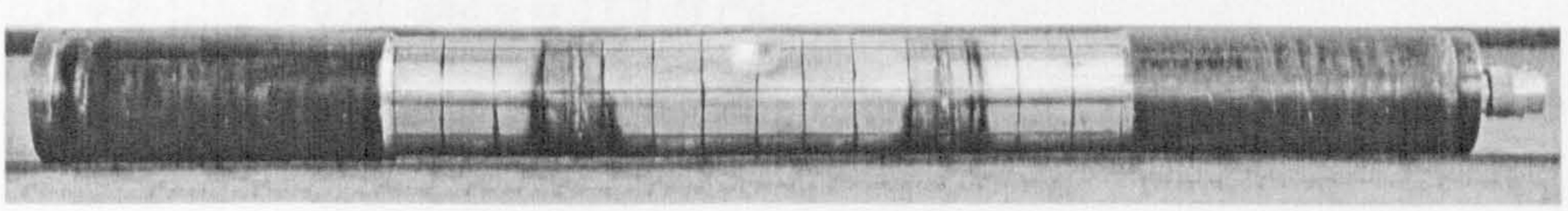

Figure 6.20: View of the residual dent depth on pipe's surface for, SP2. The case shown is for: $(\frac{\delta}{D_o})_{max} = 0.23$, $\frac{a}{b} = 1.0$, and $p = 11.2\ MPa$.

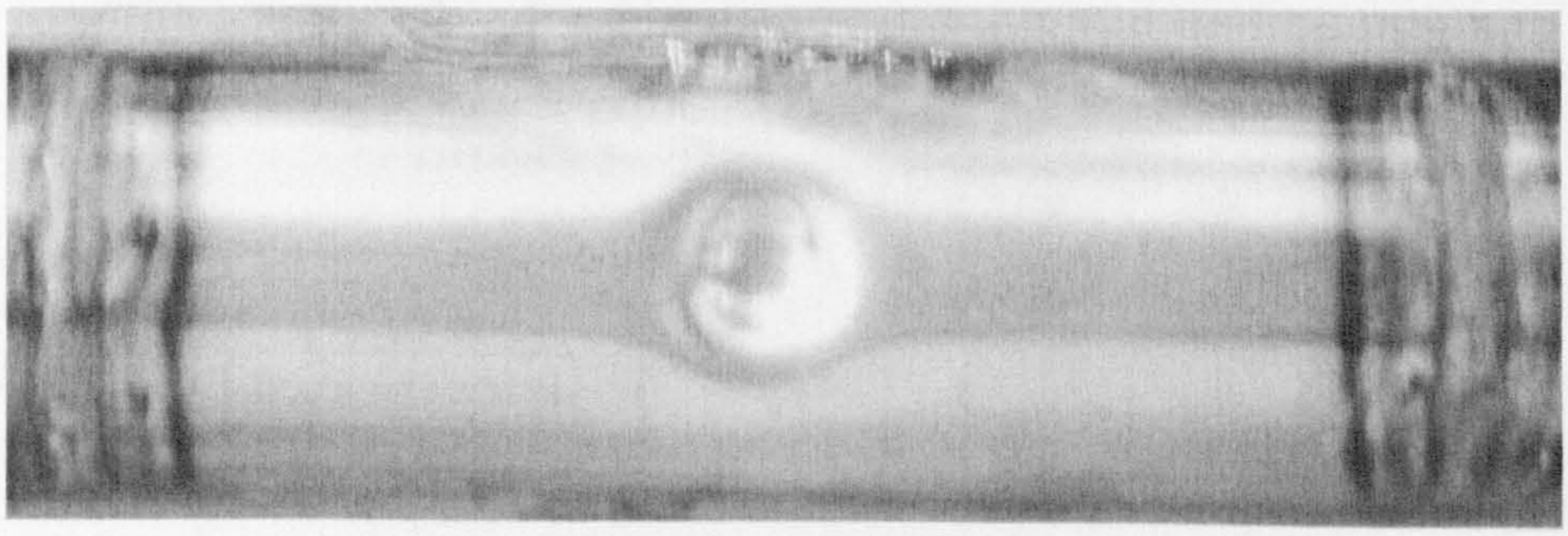

Figure 6.21: Picture of the residual dent depth on pipe's surface for, SP3. The case shown refers to: $(\frac{\delta}{D_o})_{max} = 0.23$, $\frac{a}{b} = 1.0$, and $p = 11.2\ MPa$. Note that the pipe has no surface gouges.

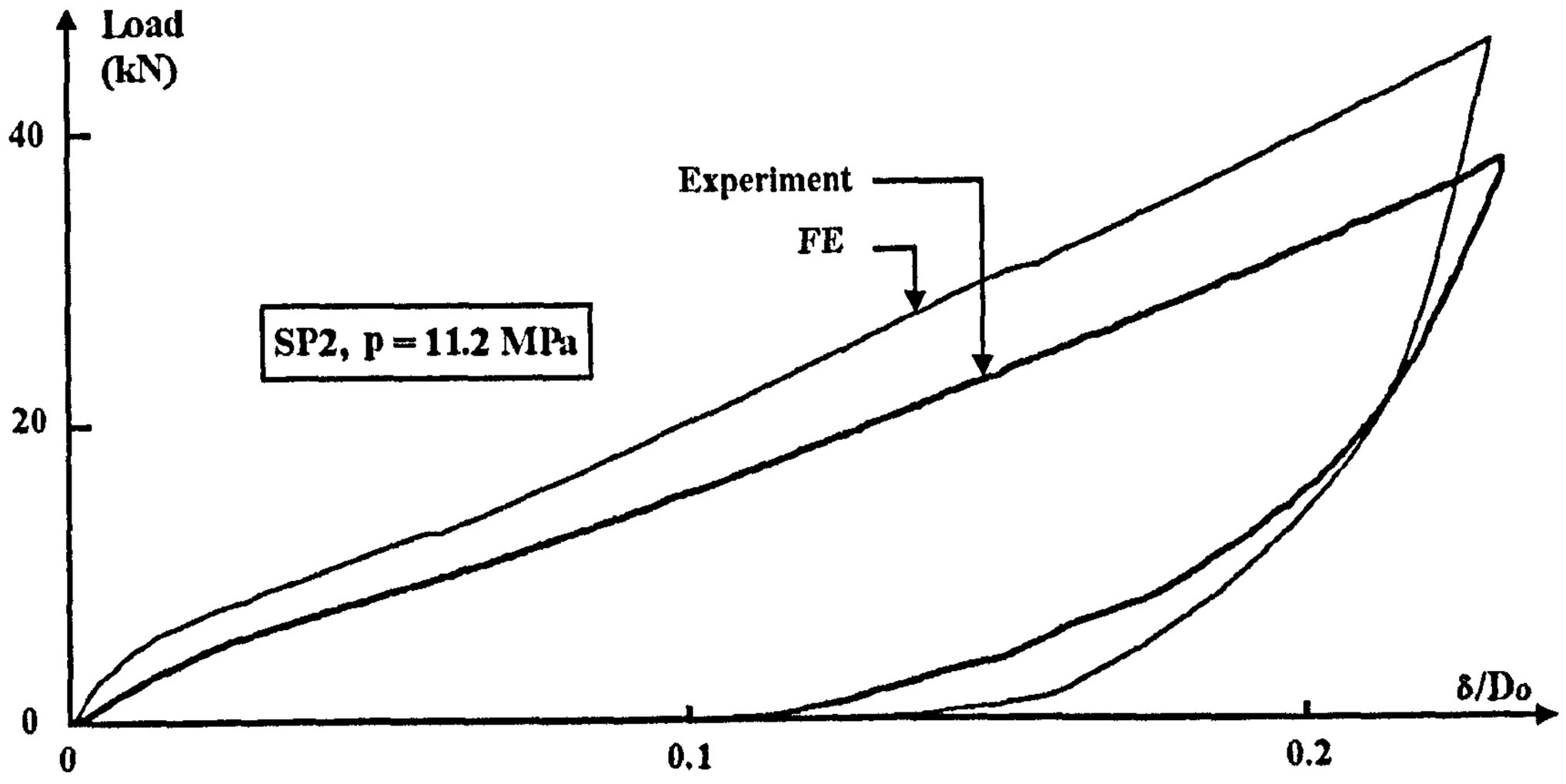

Figure 6.22: Plot of experimental and FE denting load versus depth of the dent, $\frac{\delta}{D_o}$ for, SP2. The specimen has no surface defect and the indenter was hemispherical, $\frac{a}{b} = 1.0$. Also, $\frac{2L}{D_o} = 6.0$, $(\frac{\delta}{D_o})_{max} = 0.23$, and $p = 11.2\ MPa$.

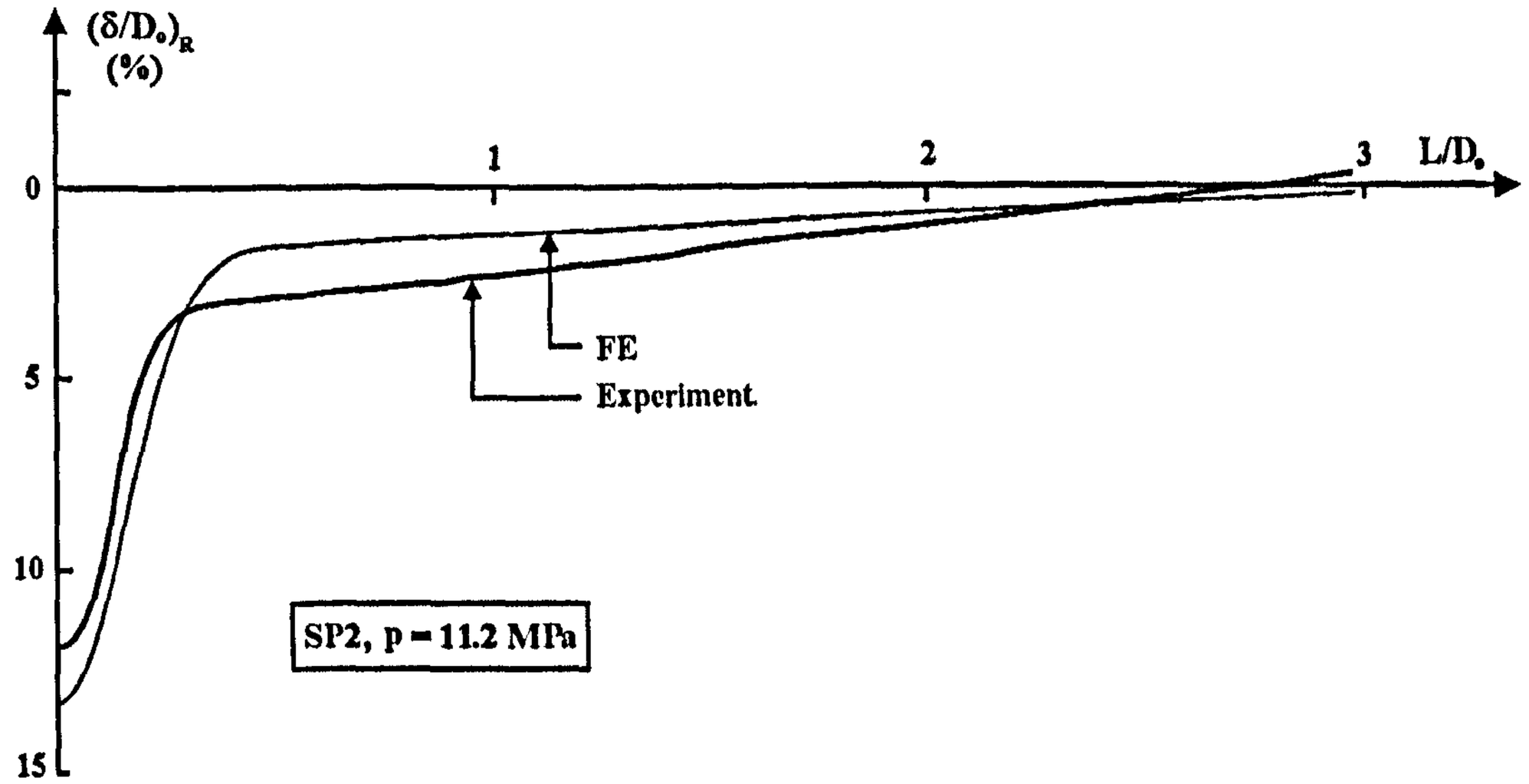

Figure 6.23: Comparison of the residual dent profile along pipe's length for specimen, SP2 after releasing internal pressure. The specimen was without surface defect. The indenter was hemispherical, $\frac{a}{b} = 1.0$. Also, $\frac{2L}{D_o} = 6.0$, $(\frac{\delta}{D_o})_{max} = 0.23$, and $p = 11.2\ MPa$.

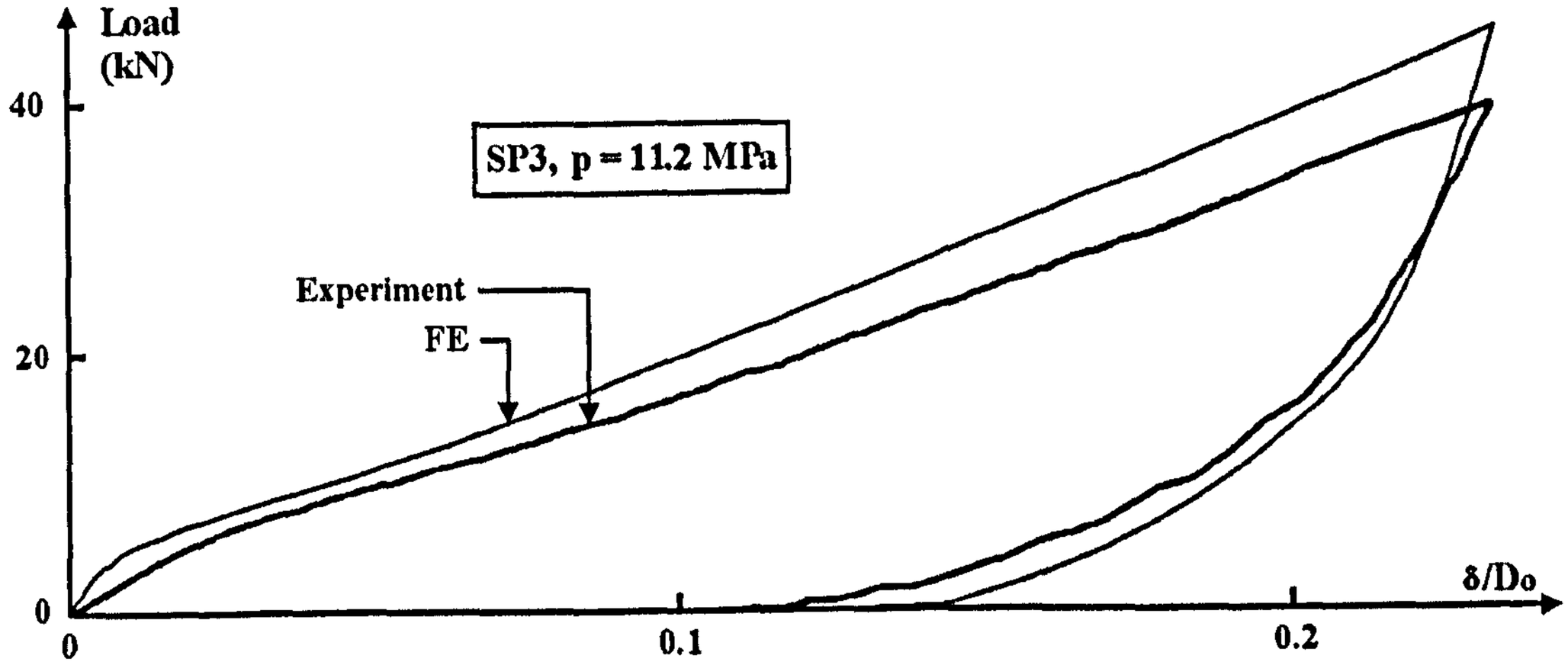

Figure 6.24: Plot of experimental and FE denting load versus depth of the dent, $\frac{\delta}{D_o}$ for, SP3. The specimen has no surface defect. Also, $\frac{a}{b} = 1.0$, $\frac{2L}{D_o} = 6.0$, $(\frac{\delta}{D_o})_{max} = 0.23$, and $p = 11.2\ MPa$.

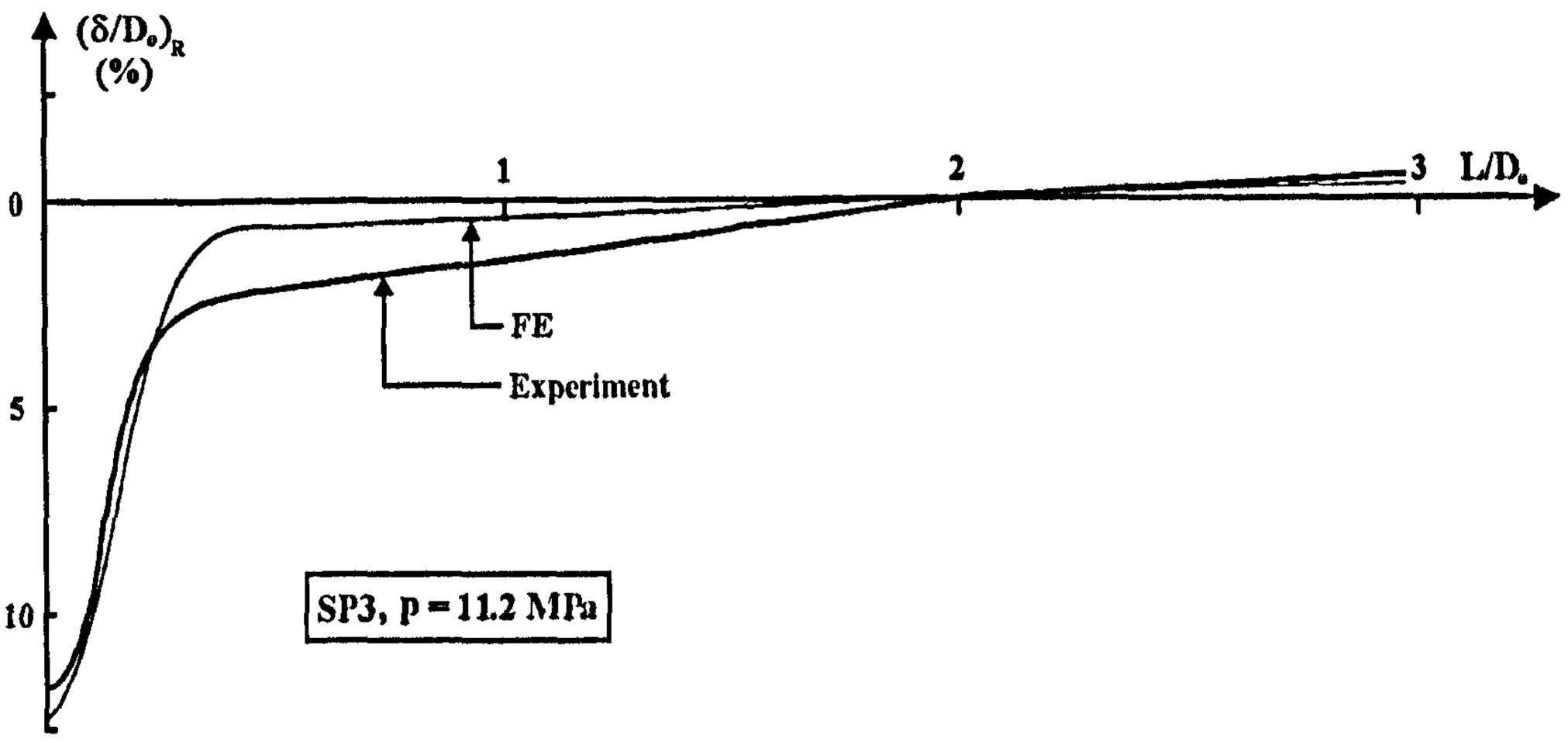

Figure 6.25: Comparison of the residual dent profile along pipe's length for specimen, SP3. The specimen had no surface defect. Also, $\frac{a}{b} = 1.0$, $\frac{2L}{D_o} = 6.0$, $(\frac{\delta}{D_o})_{max} = 0.23$, and $p = 11.2\ MPa$.

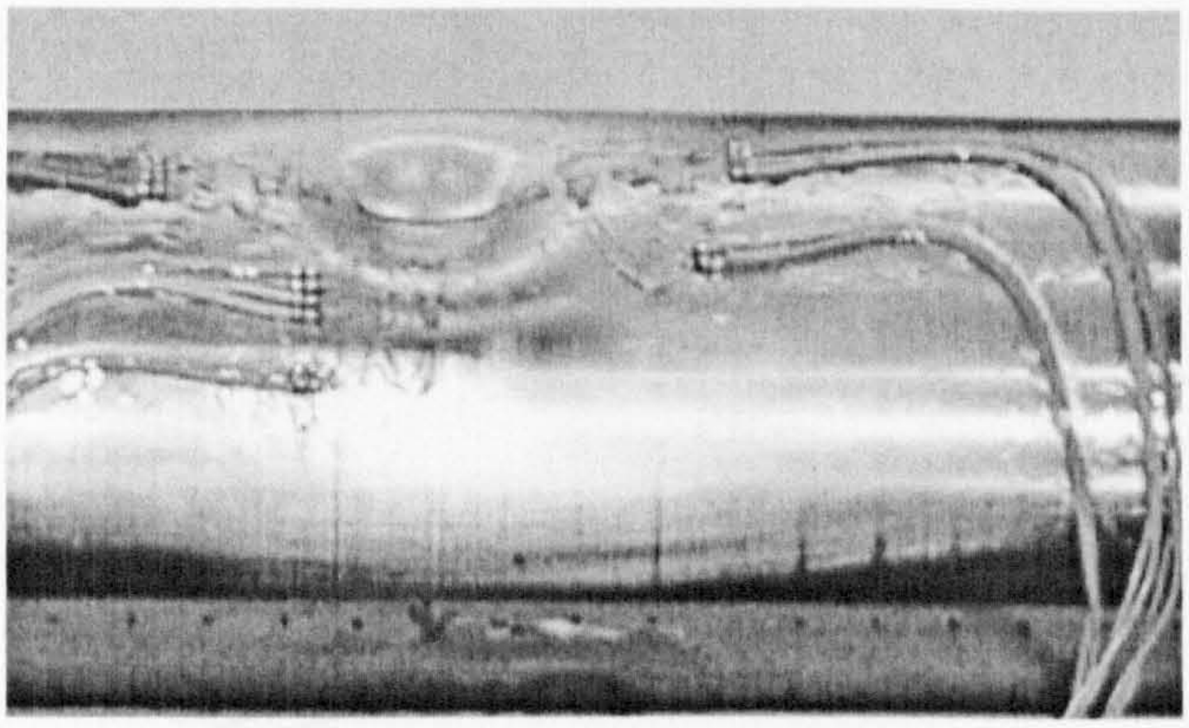

Figure 6.26: View of the pipe with mid-span gouge after being dented, (SP4 model). Also, $(\frac{\delta}{D_o})_{max} = 0.15$, $\frac{a}{b} = 1.0$, $\frac{2c}{D_o} = 0.25$, $\frac{e}{t} = 0.47$, $\frac{2w}{t} = 0.4785$, and $p = 5.6\ MPa$.

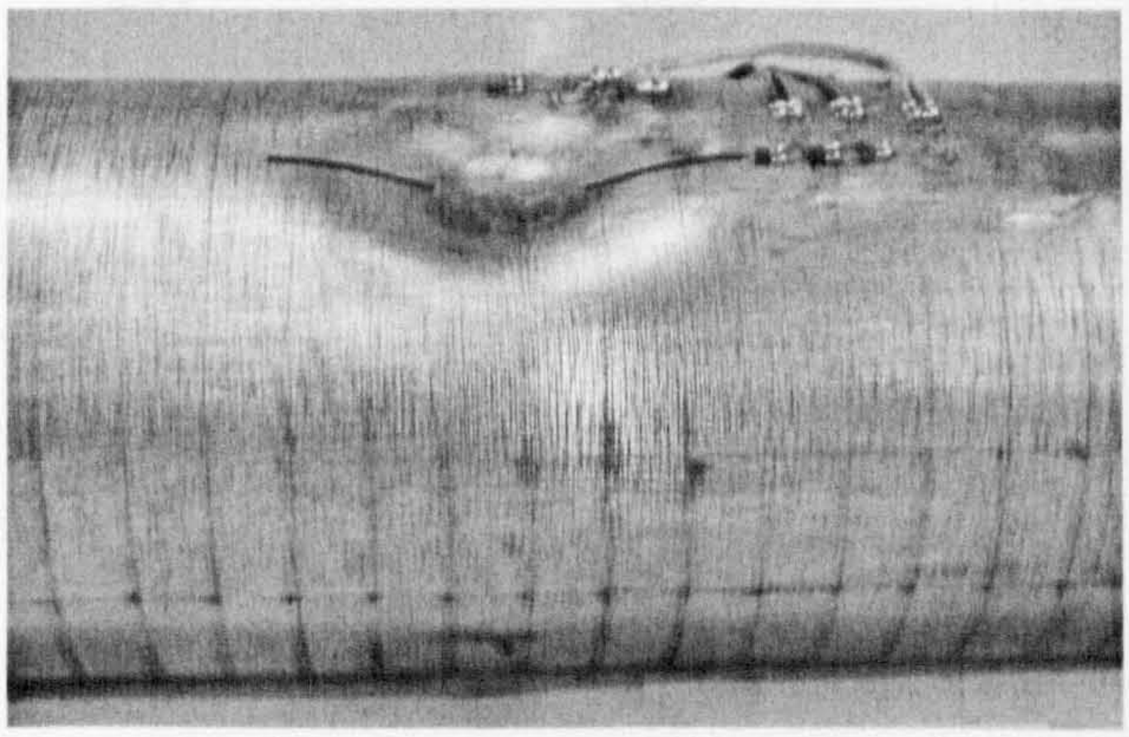

Figure 6.27: Laboratory scale pipe with two gouges after being dented, SP5. Variables were: $(\frac{\delta}{D_o})_{max} = 0.166$, $\frac{a}{b} = 1.0$, $\frac{2c}{D_o} = 0.25$, $\frac{e}{t} = 0.47$, $\frac{2w}{t} = 0.4808$, and $p = 5.6\ MPa$.

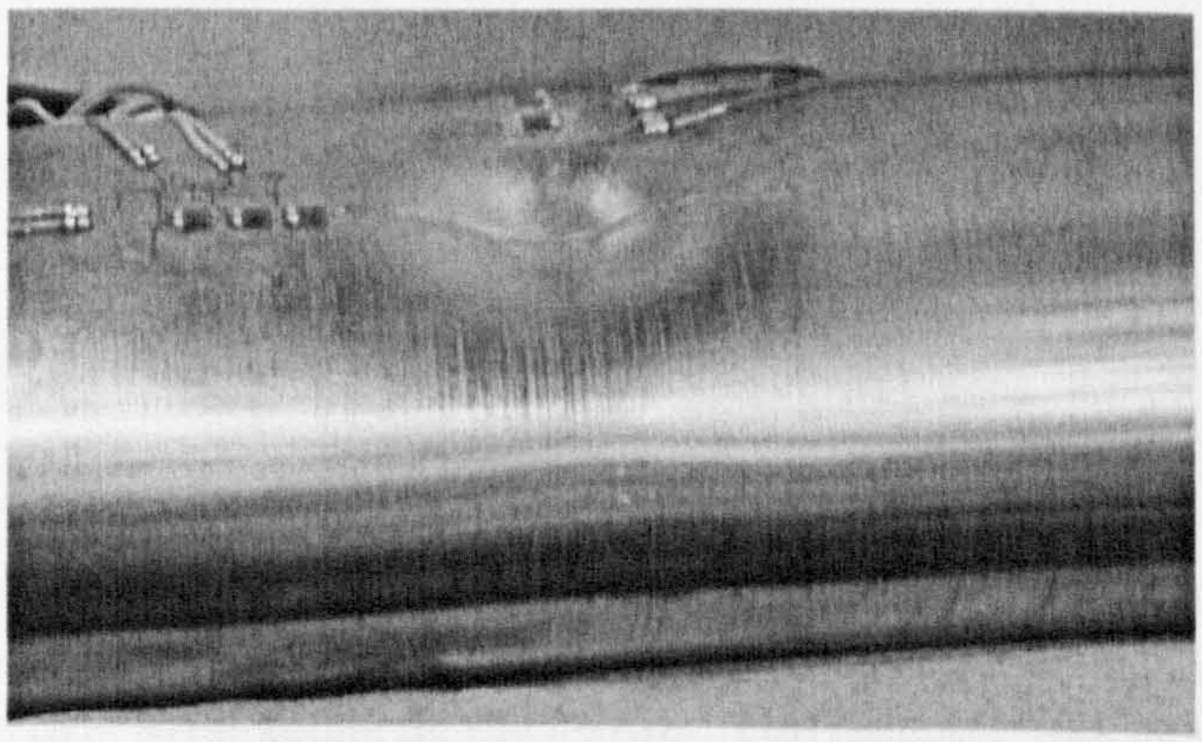

Figure 6.28: Laboratory scale pipe with large gouge after being dented, SP6. Variables were: $(\frac{\delta}{D_o})_{max} = 0.16$, $\frac{a}{b} = 1.0$, $\frac{2c}{D_o} = 0.81$, $\frac{e}{t} = 0.23$, $\frac{2w}{t} = 1.20$, and $p = 5.6\ MPa$.

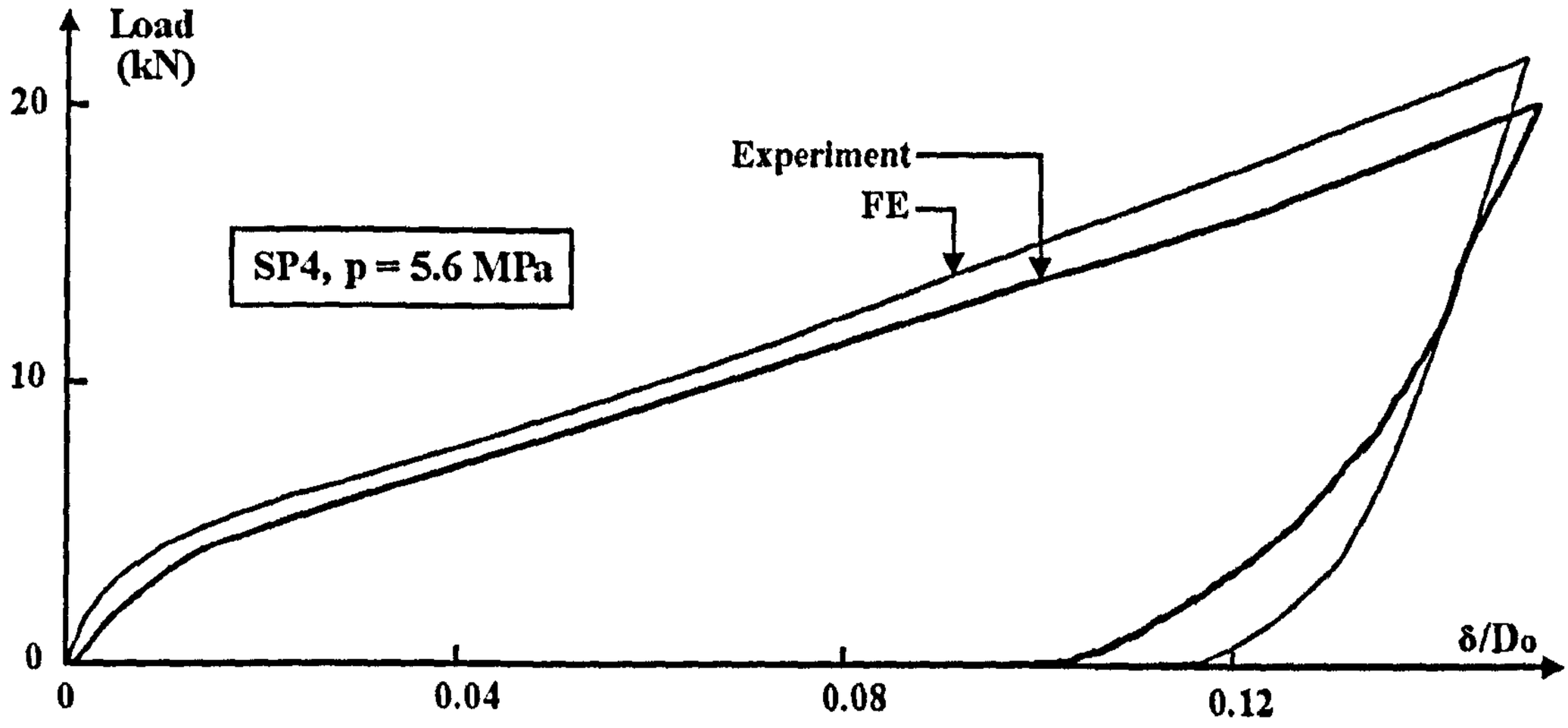

Figure 6.29: Experimental and FE denting loading-unloading versus depth of the dent, (SP4 model). The specimen has a single gouge at mid-span. Also, $\frac{a}{b} = 1.0$, $\frac{2L}{D_o} = 6.0$, $(\frac{\delta}{D_o})_{max} = 0.15$, and $p = 5.6\ MPa$.

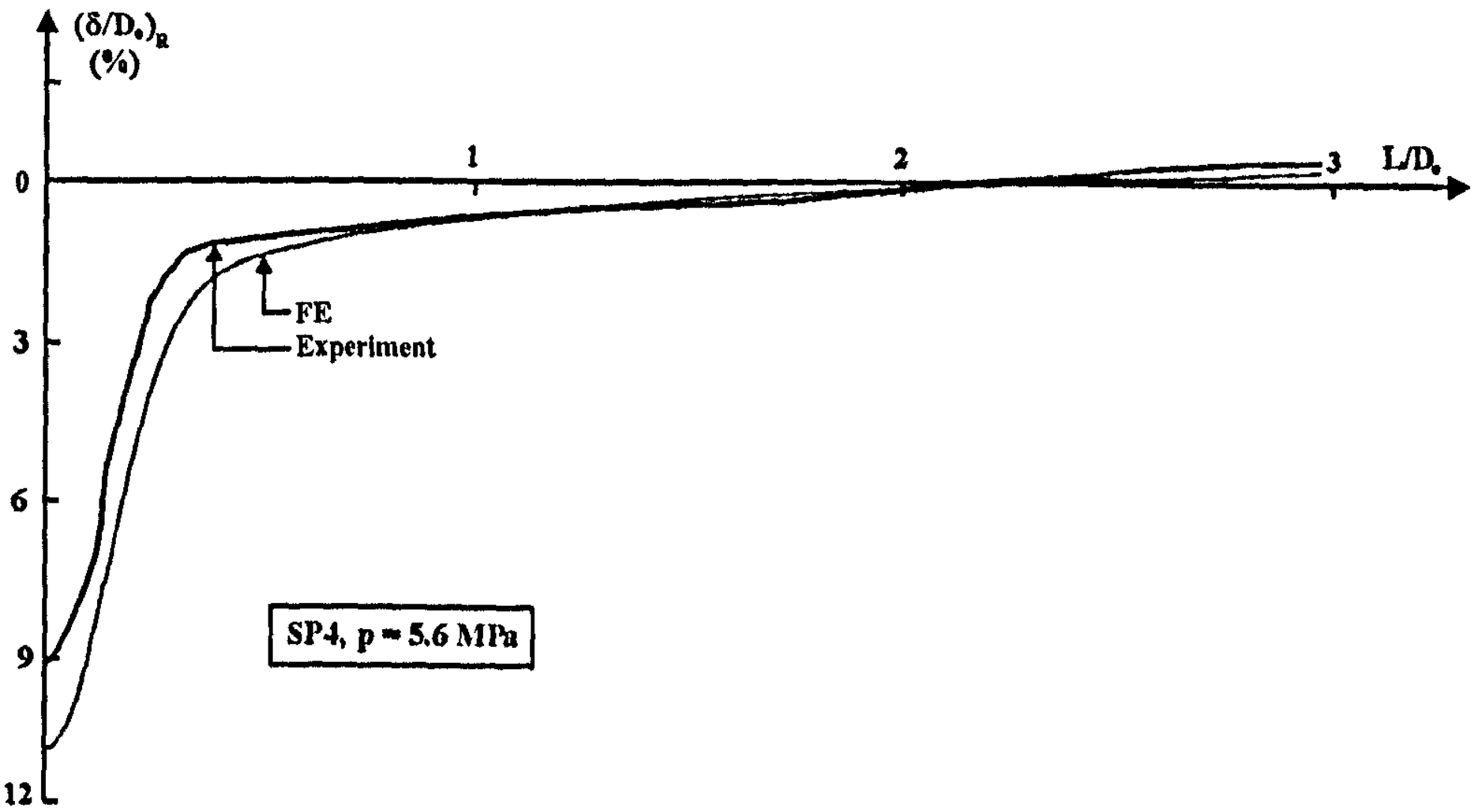

Figure 6.30: Comparison of the residual dent profile along pipe's length for specimen, SP4. The specimen had single axial gouge at the centre. The indenter was hemispherical, $\frac{a}{b} = 1.0$, $p = 5.6\ MPa$, $\frac{2L}{D_o} = 6.0$, and $p = 5.6\ MPa$.

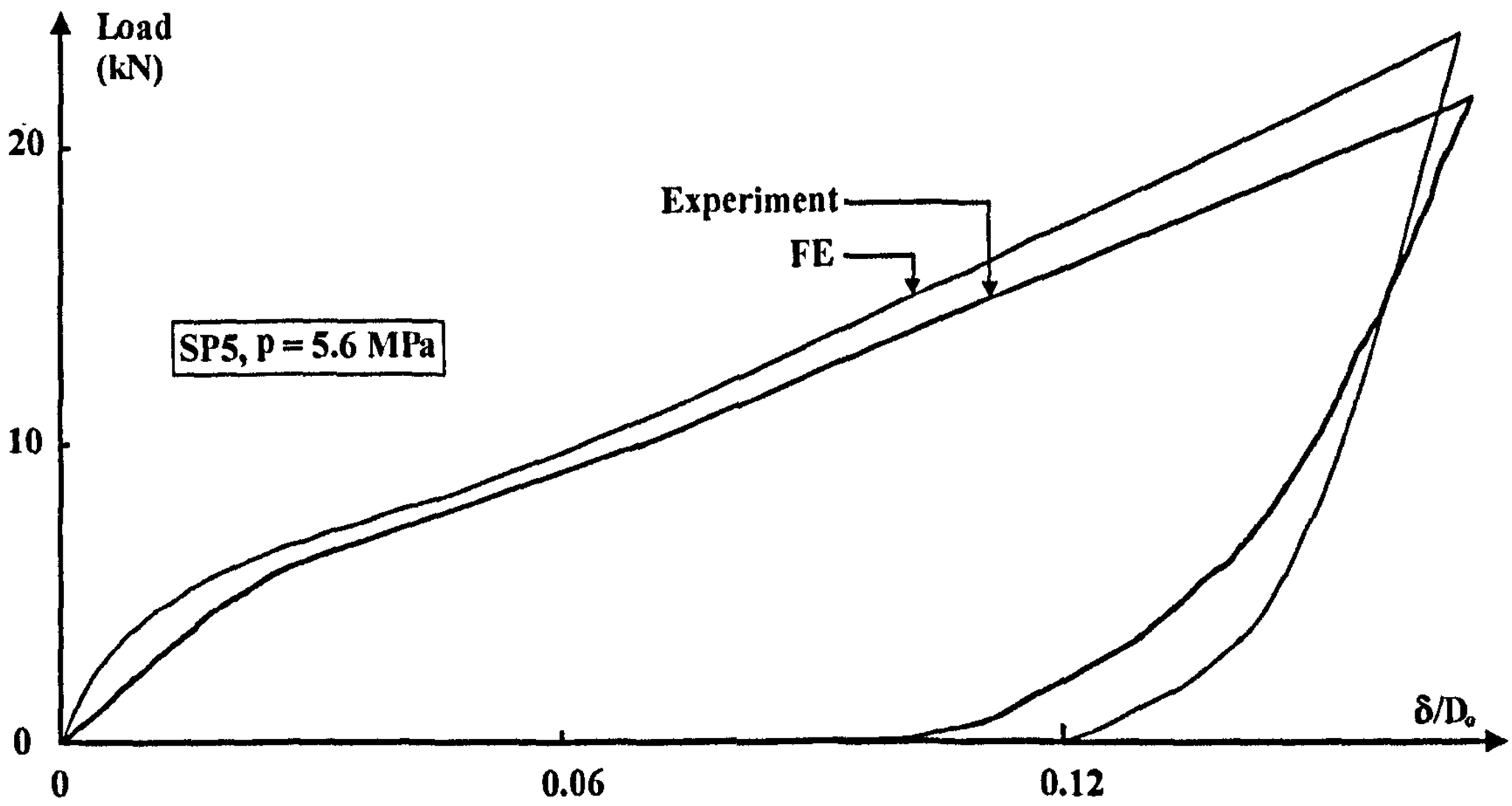

Figure 6.31: Plot of experimental and FE loading-unloading versus depth of the dent for specimen, SP5. The specimen had two gouges at the centre. Also, $\frac{a}{b} = 1.0$, $\frac{2L}{D_o} = 6.0$, $(\frac{\delta}{D_o})_{max} = 0.166$, and $p = 5.6\ MPa$.

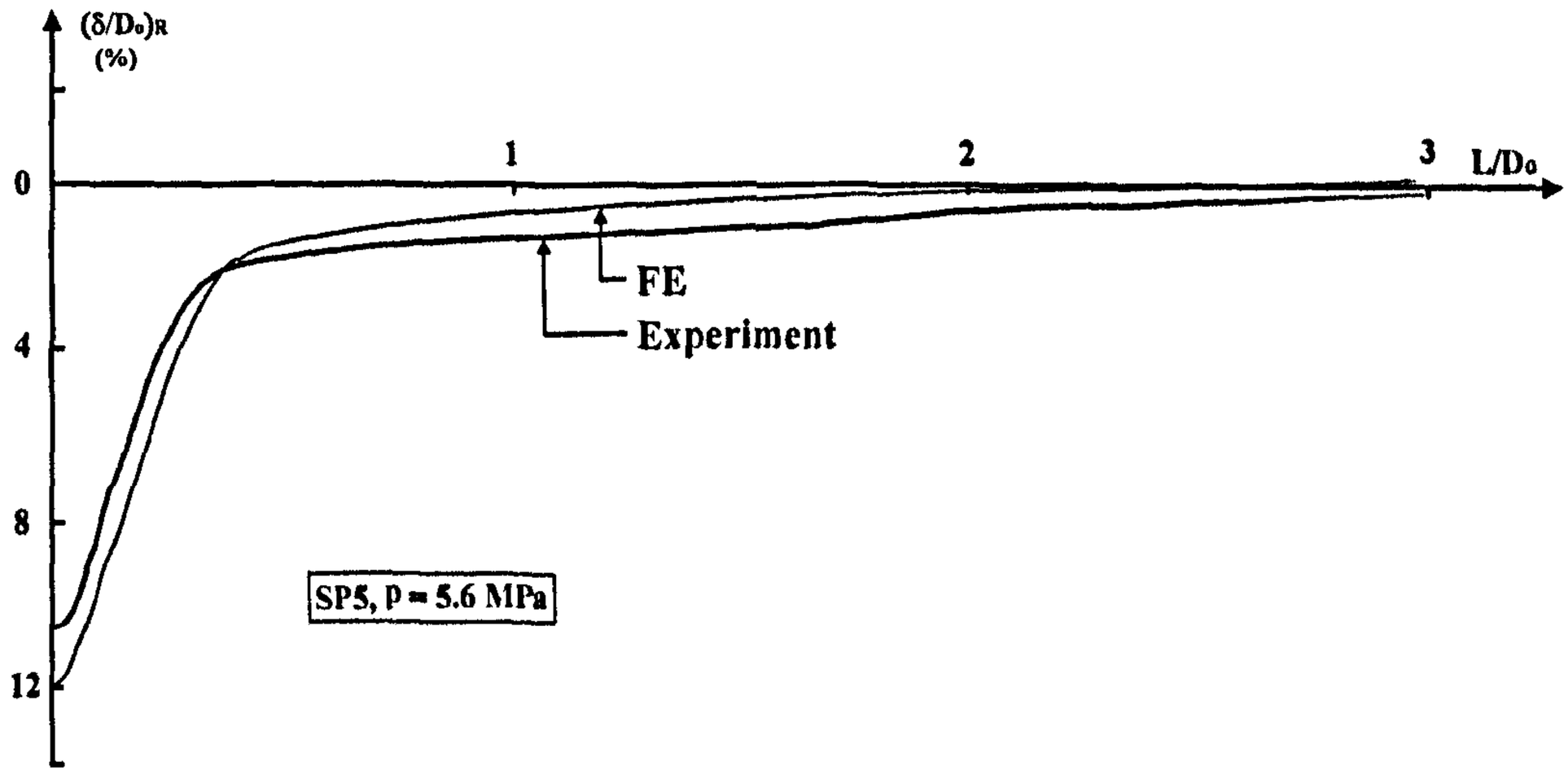

Figure 6.32: Comparison of the residual dent profile along pipe's length for specimen, SP5. The specimen had two gouges at the centre. Also, $\frac{a}{b} = 1.0$, $\frac{2L}{D_o} = 6.0$, $(\frac{\delta}{D_o})_{max} = 0.166$, and $p = 5.6\ MPa$.

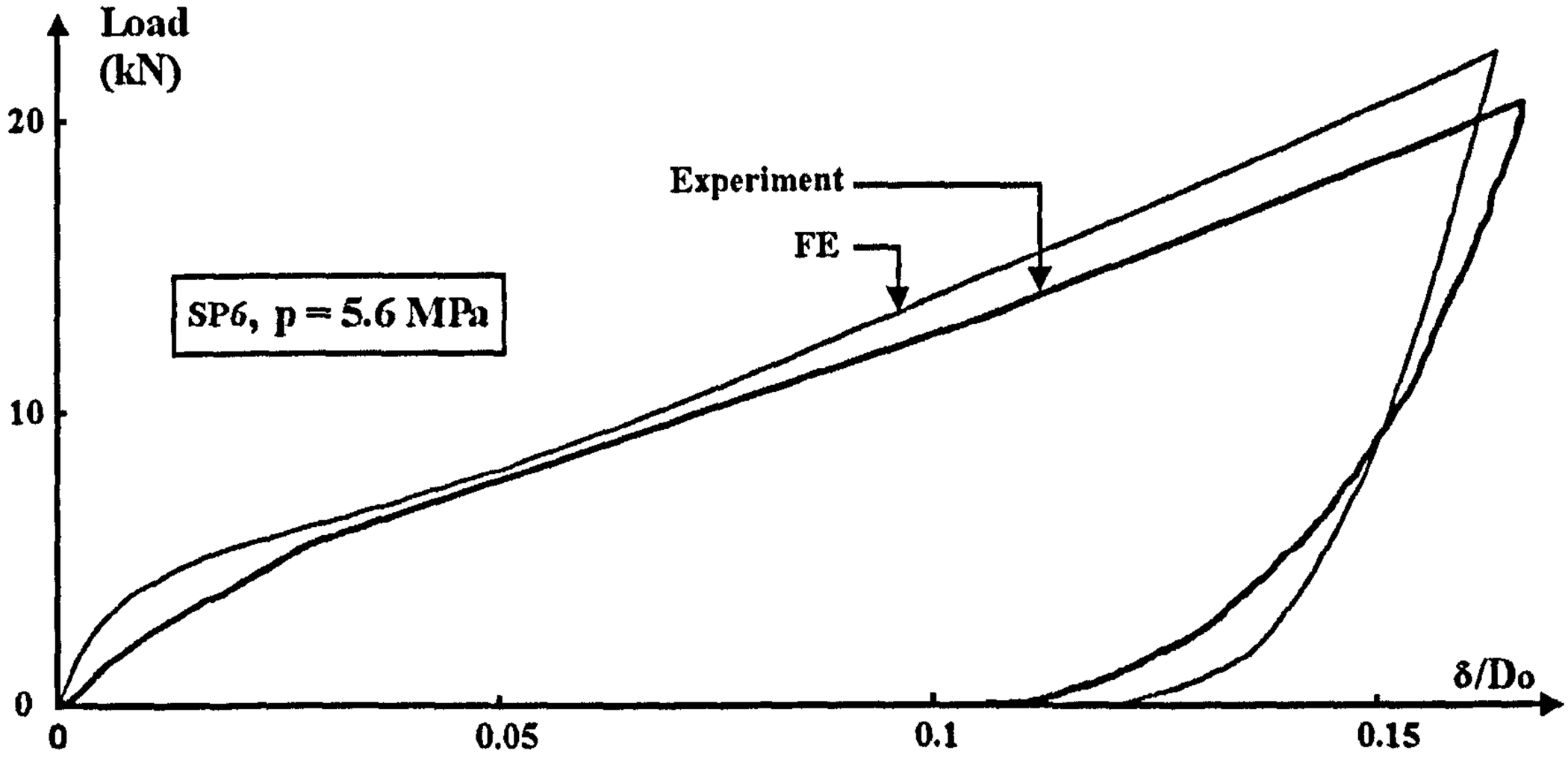

Figure 6.33: Plot of experimental and FE loading-unloading versus depth of dent for specimen, SP6. The specimen had a large gouge at the centre. Also, $\frac{a}{b} = 1.0$, $\frac{2L}{D_o} = 6.0$, $(\frac{\delta}{D_o})_{max} = 0.16$, and $p = 5.6\ MPa$.

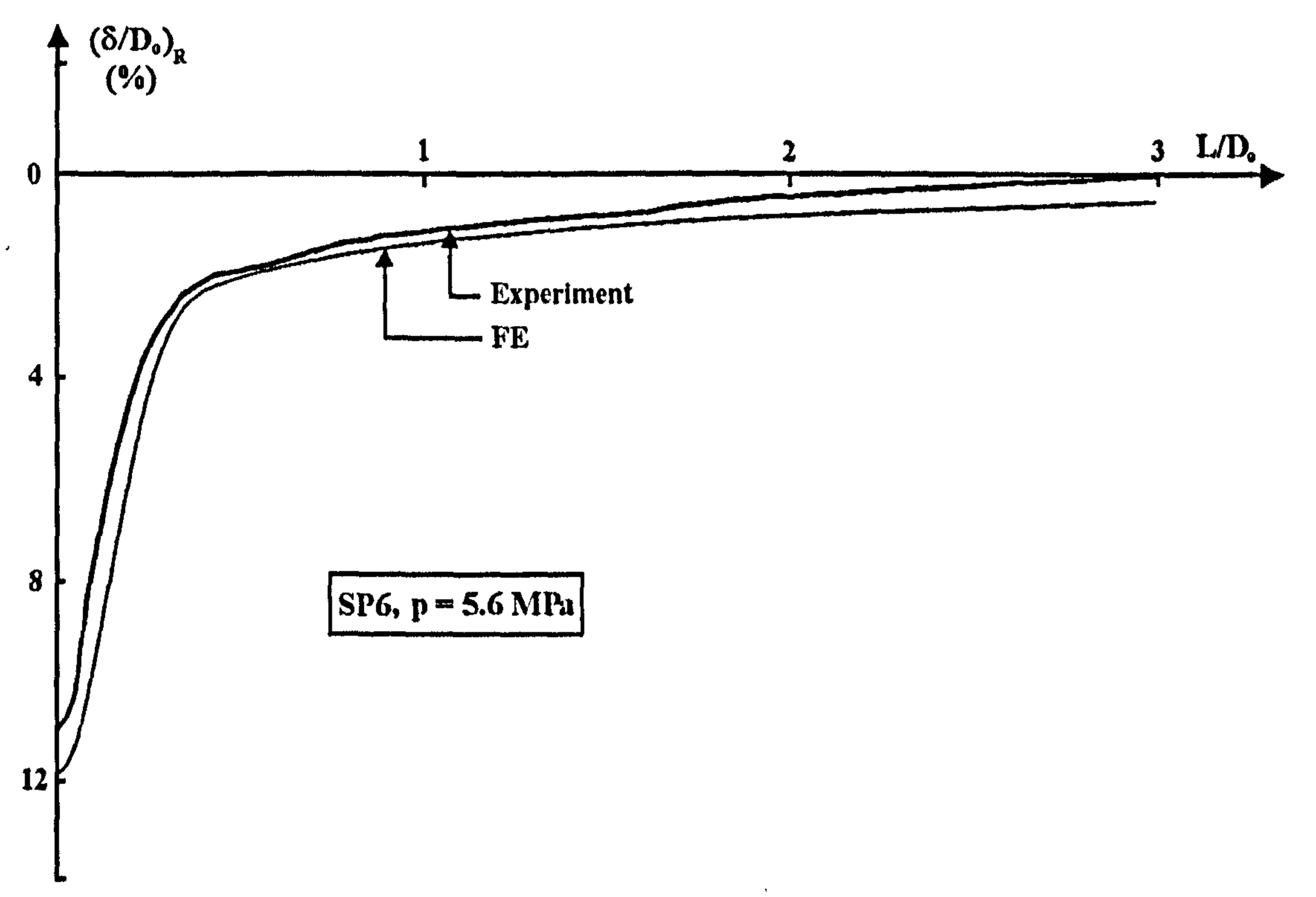

Figure 6.34: Comparison of the residual dent profile along pipe's length for specimen, SP6. The specimen had a large axial gouge at the centre. Also, $\frac{a}{b} = 1.0$, $p = 5.6\ MPa$, $\frac{2L}{D_o} = 6.0$, $(\frac{\delta}{D_o})_{max} = 0.16$, and $p = 5.6\ MPa$.

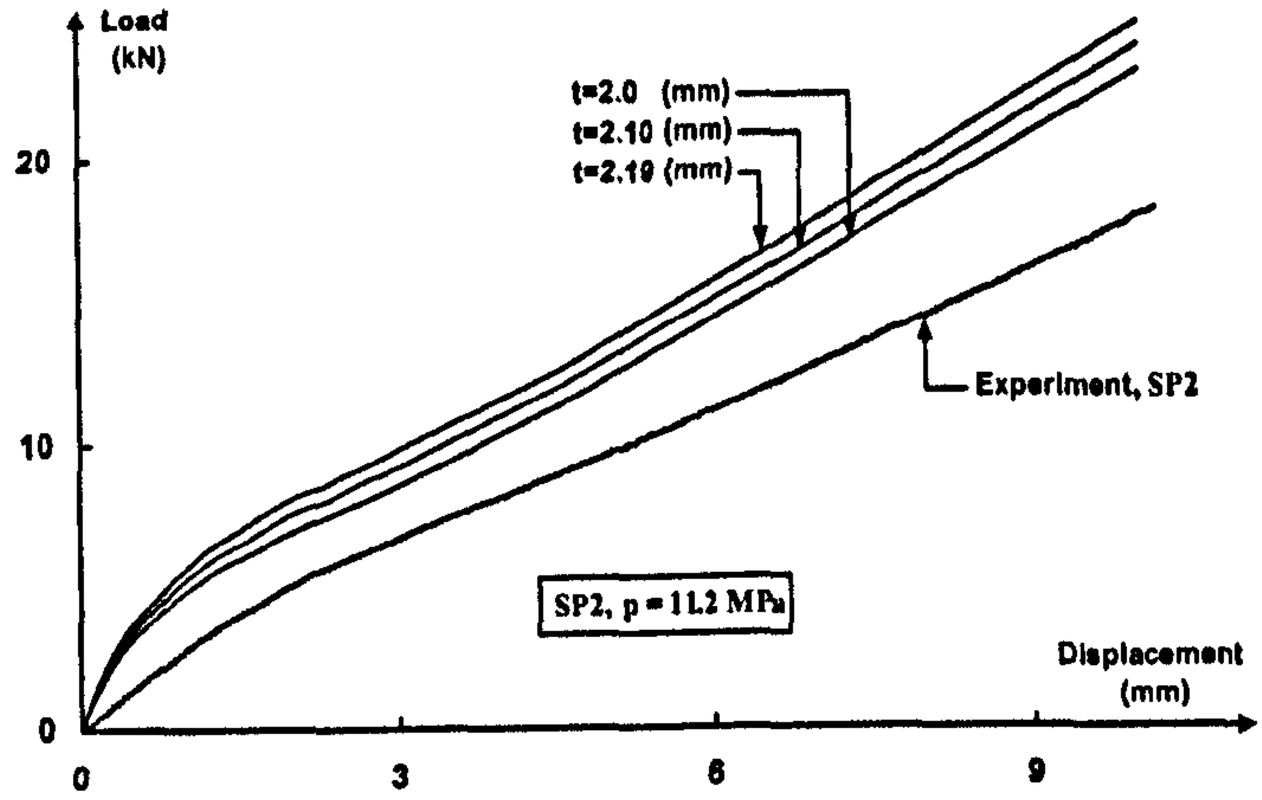

Figure 6.35: Denting load versus displacement for both experiment and FE analyses. FE results with different values of thickness are plotted. Also, $\frac{2L}{D_o} = 6.0$, $\frac{a}{b} = 1.0$, and $p = 11.2\ MPa$.

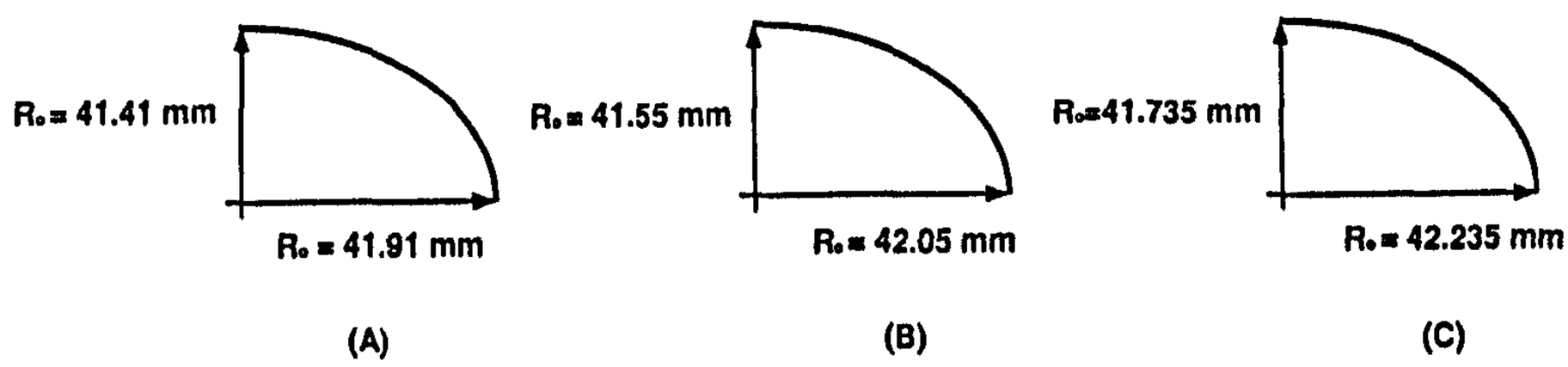

Figure 6.36: Shapes simulating ovalisation of pipe's cross-section to be modelled in the FE calculation.

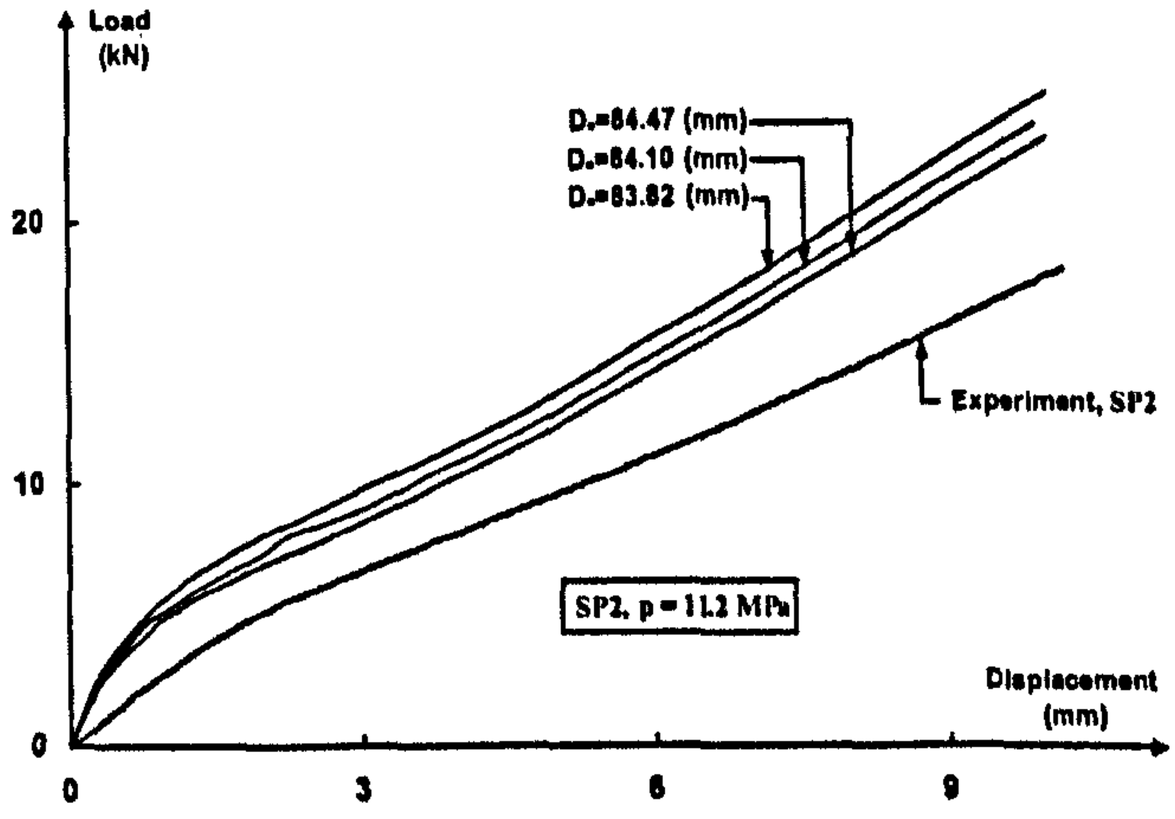

Figure 6.37: Plots of denting load versus displacement for different magnitudes of pipe ovalisation. Also, $\frac{2L}{D_o} = 6.0$, $\frac{a}{b} = 1.0$, and $p = 11.2\ MPa$.

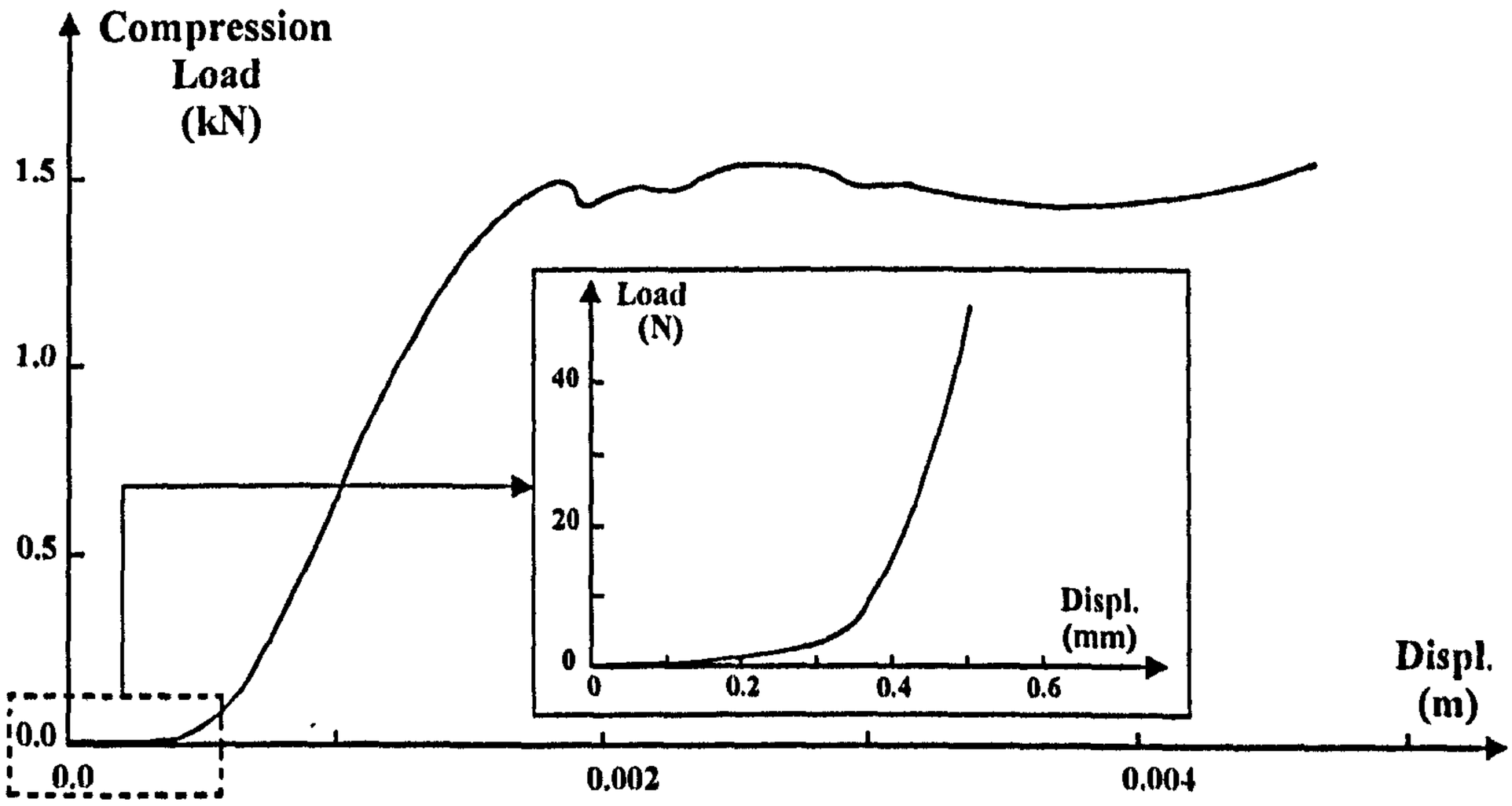

Figure 6.38: Compression test of the pine wood.

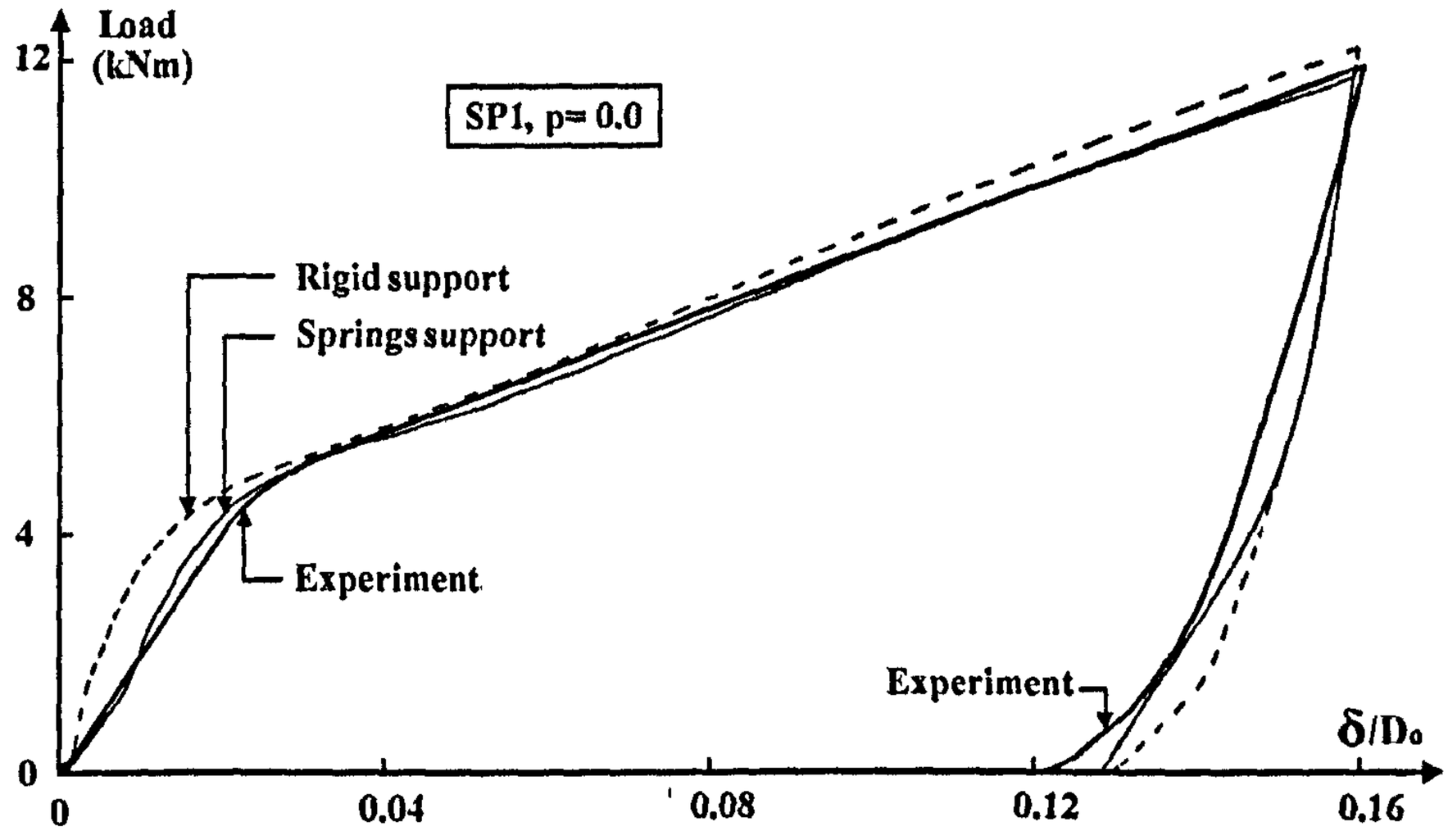

Figure 6.39: Comparison of denting loading-unloading versus displacement for specimen, SP1 being differently supported. Three types of support were used: rigid saddle, wooden saddle and a set of nonlinear springs. Also, $\frac{a}{b} = 1.0$, $\frac{2L}{D_o} = 6.0$, $p = 0.0$, and $(\frac{\delta}{D_o})_{max} = 0.16$.

Figure 6.40: Comparison of denting loading-unloading versus displacement for specimen SP2 being differently supported. Three types of support were used: rigid saddle, wooden saddle and a set of nonlinear springs. Also, $\frac{a}{b} = 1.0$, $\frac{2L}{D_o} = 6.0$, $p = 11.2\ MPa$, and $(\frac{\delta}{D_o})_{max} = 0.23$.

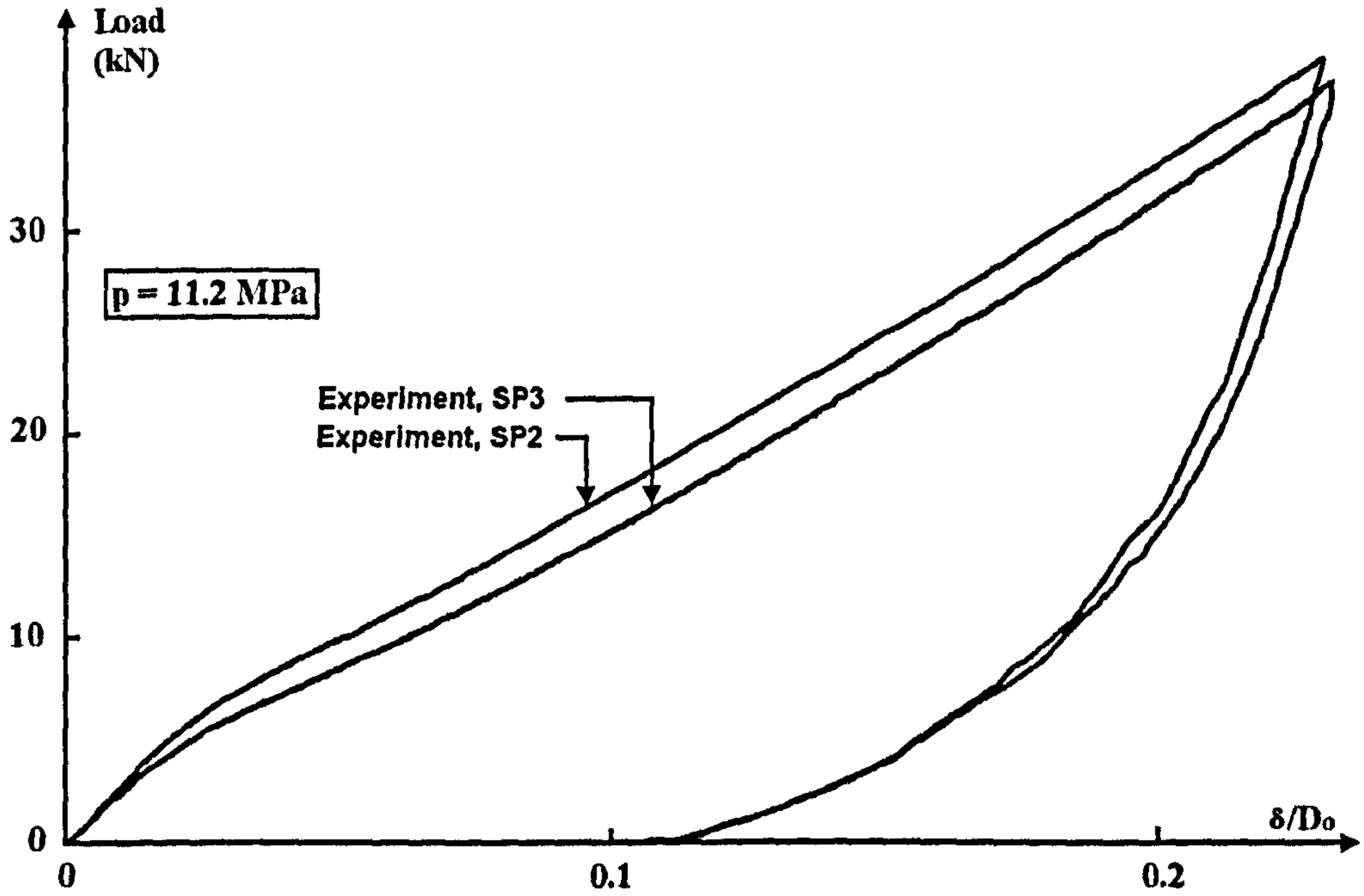

Figure 6.41: Plot of experimental loading-unloading curve versus dent's depth for specimens SP2 and SP3. Also, the indenter was hemispherical, $\frac{a}{b} = 1.0$, $\frac{2L}{D_o} = 6.0$, $p = 11.2\ MPa$, and $(\frac{\delta}{D_o})_{max} = 0.23$.

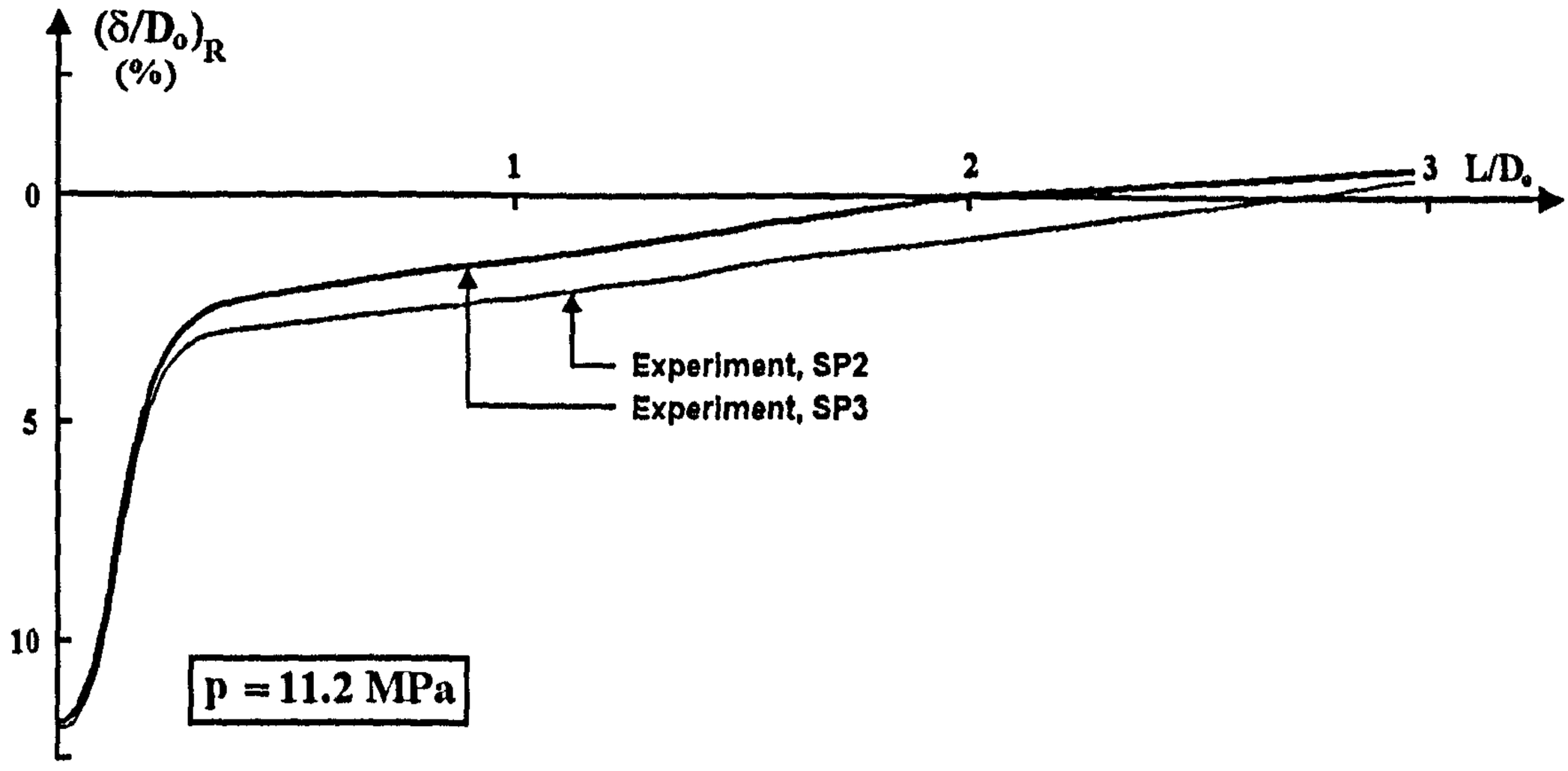

Figure 6.42: Plot of the residual dent profile along pipe's length for specimens SP2 and SP3 after releasing the internal pressure. The indenter was hemispherical, $\frac{a}{b} = 1.0$, $\frac{2L}{D_o} = 6.0$, and $(\frac{\delta}{D_o})_{max} = 0.23$.

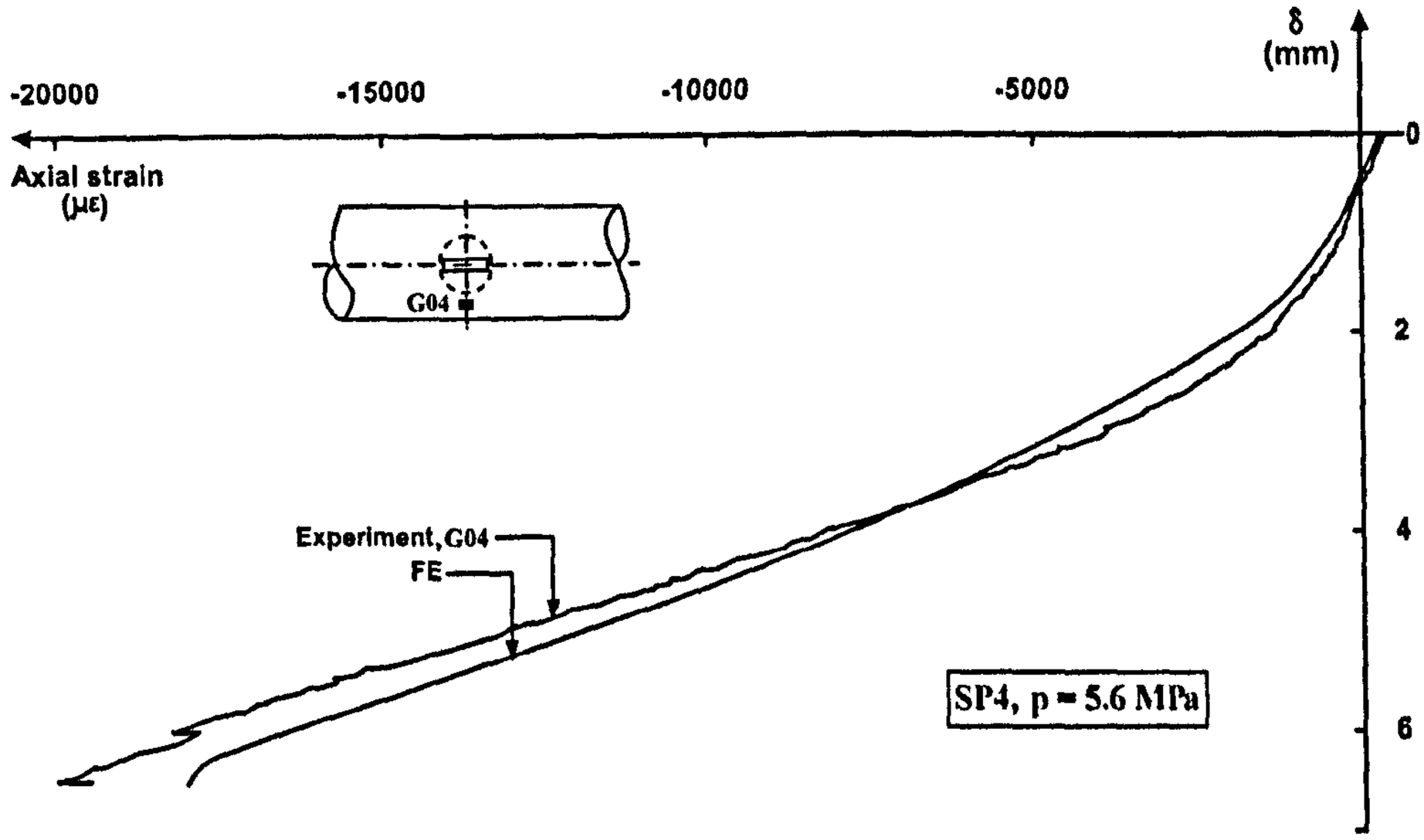

Figure 6.43: Axial strain versus dent depth, δ, for gauge number G04. The specimen, SP4, has a single axial gouge at the centre. Also, $p = 5.6\ MPa$, $\frac{a}{b} = 1.0$, $\frac{2L}{D_o} = 6.0$, and $(\frac{\delta}{D_o})_{max} = 0.15$.

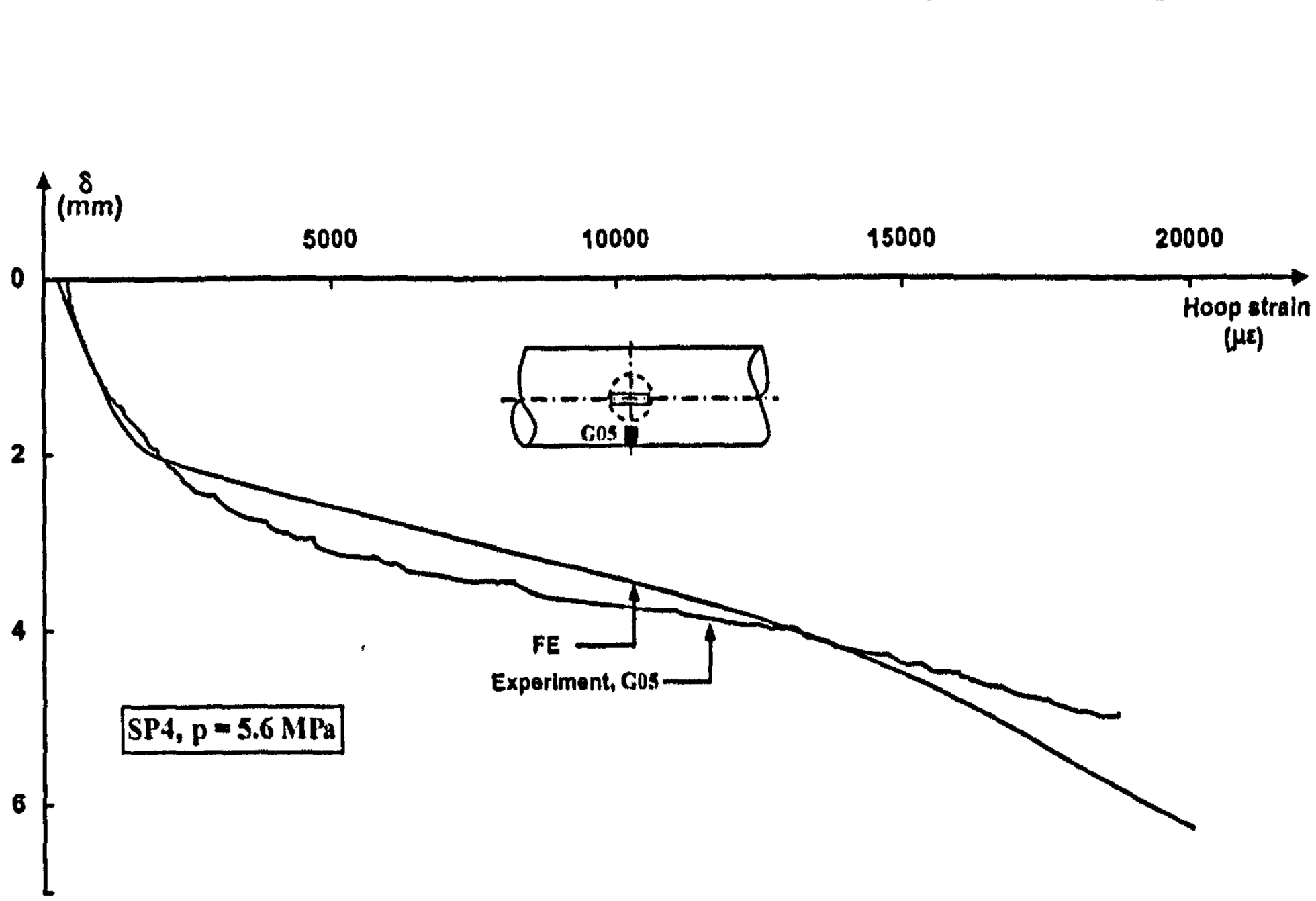

Figure 6.44: Hoop strain versus dent depth, δ, for gauge number G05. The specimen SP4 has a single axial gouge at the centre. Also, $p = 5.6\ MPa$, $\frac{a}{b} = 1.0$, $\frac{2L}{D_o} = 6.0$, and $(\frac{\delta}{D_o})_{max} = 0.15$.

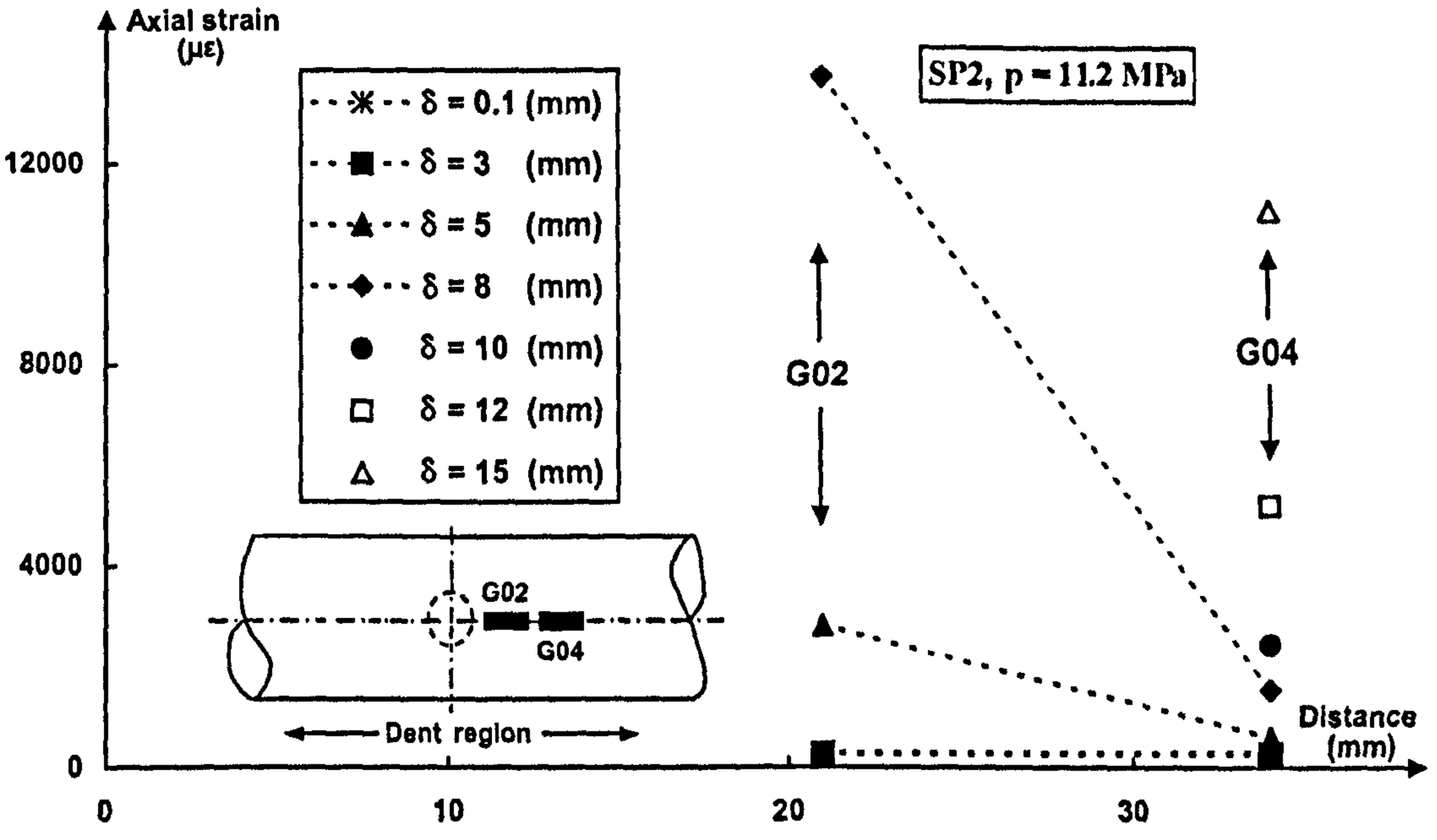

Figure 6.45: Distribution of axial strain in specimen SP2 (gauges G02 and G04). Both gauges were off-centre as sketched in the figure. Dashed circle indicates the indenter's location, (top view of the specimen).

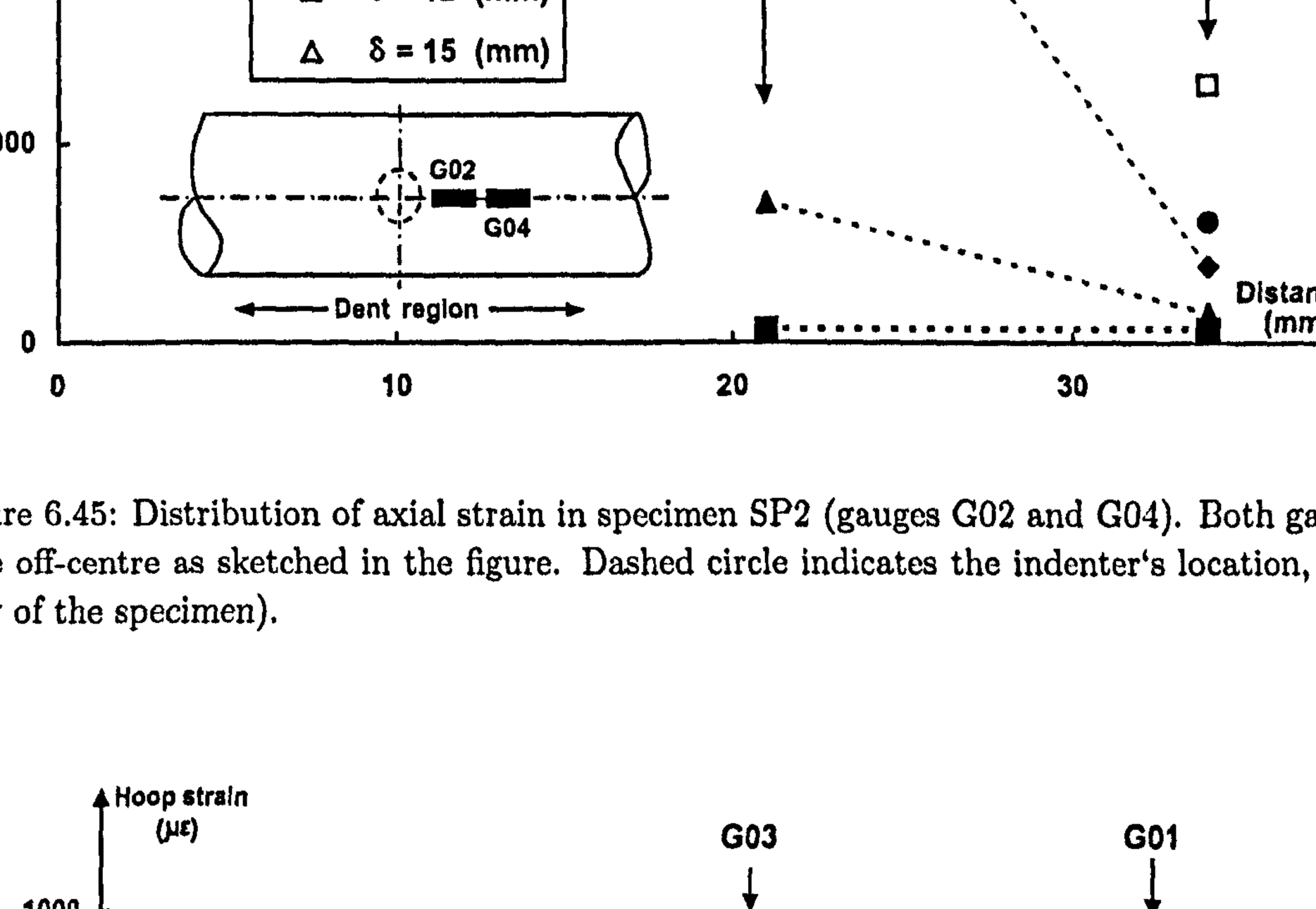

Figure 6.46: Distribution of hoop strain in specimen SP2 (gauges G01 and G03). Both gauges were off-centre as sketched in the figure. The dashed circle indicates the indenter's location, (top view of the specimen).

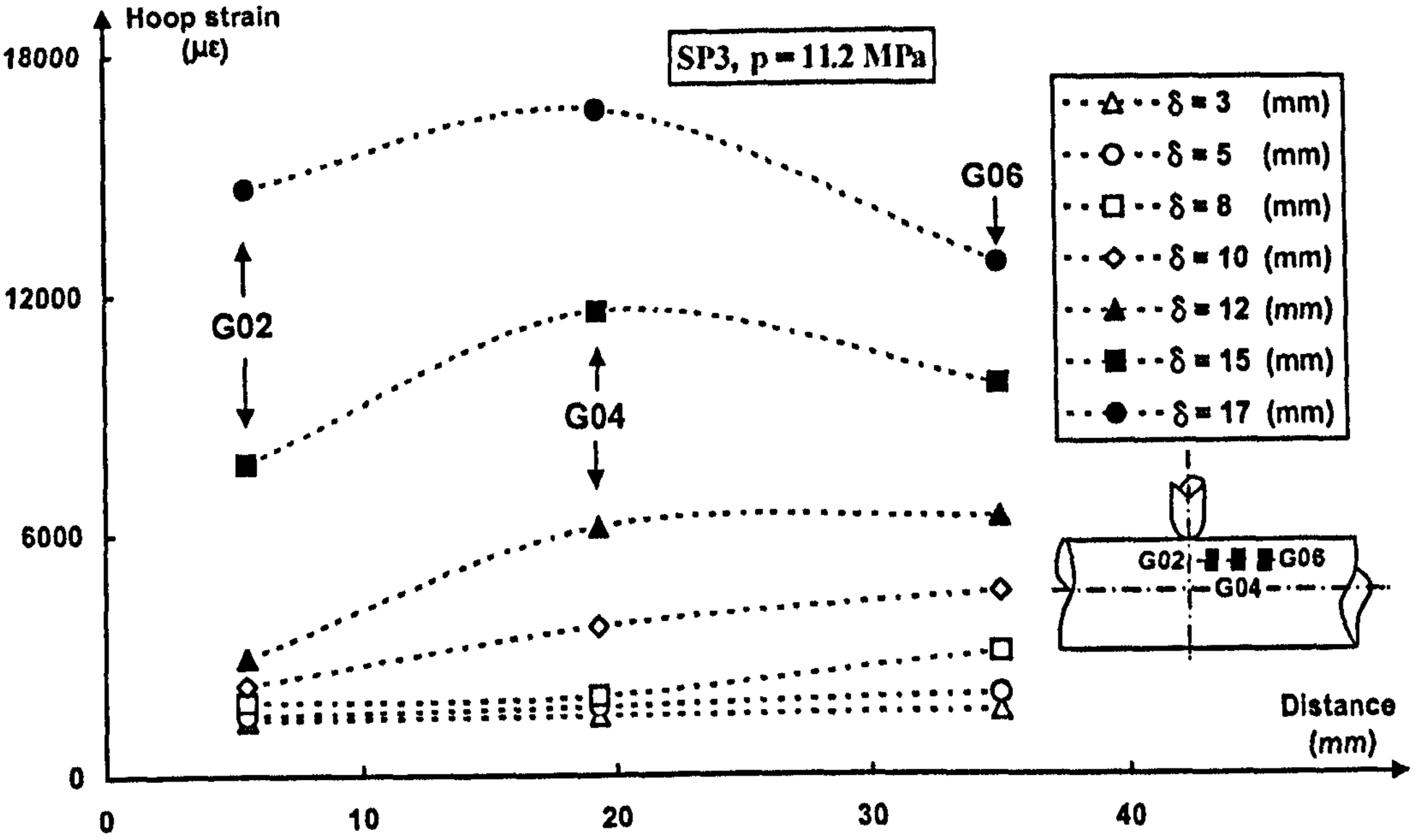

Figure 6.47: Distribution of hoop strain in specimen SP3 (gauges G02, G04, and G06). All gauges were off-centre as sketched in the figure, (side view of the specimen).

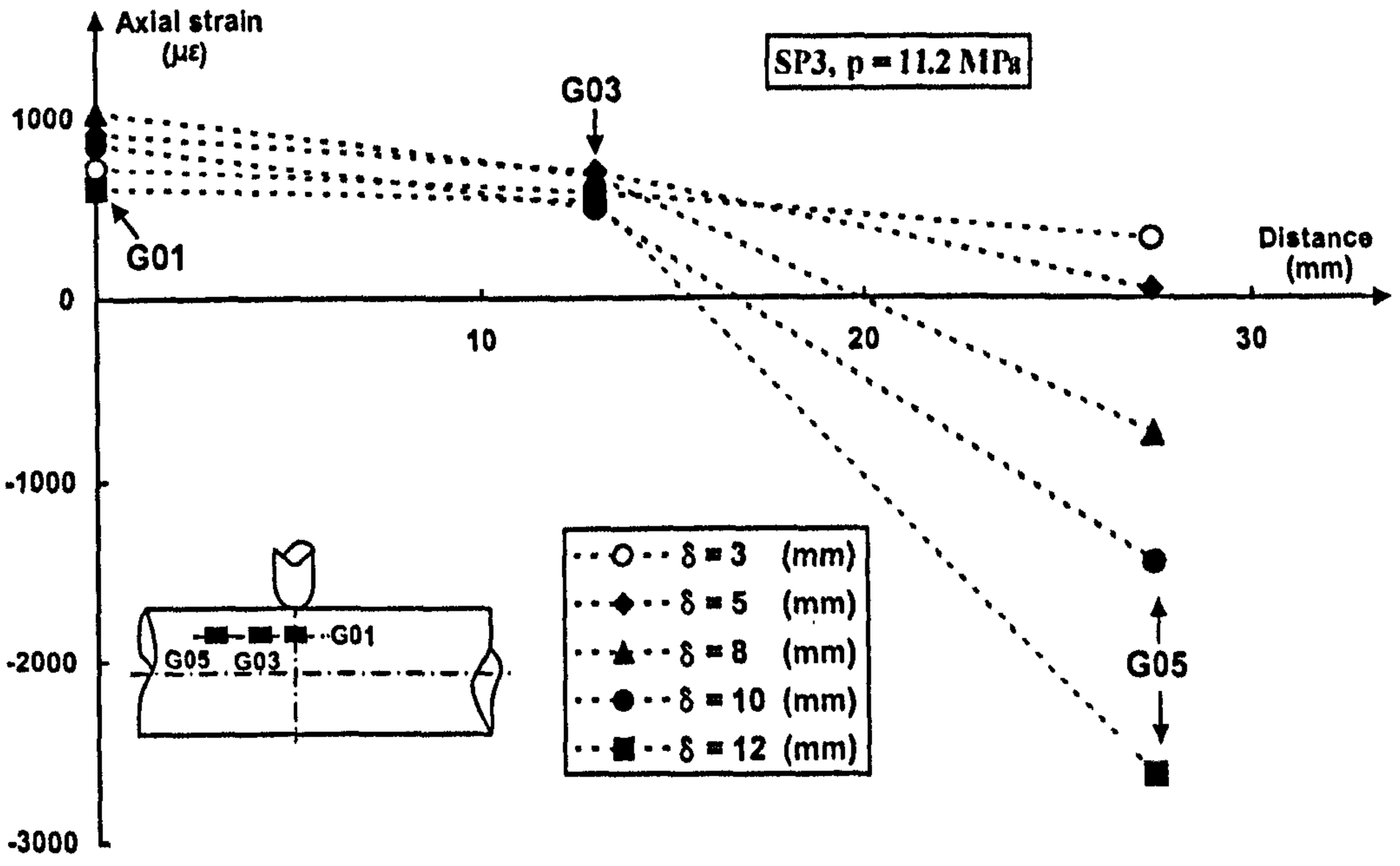

Figure 6.48: Distribution of axial strain in specimen SP3 (gauges G01, G03, and G05). All gauges were off-centre as sketched in the figure, (side view of the specimen).

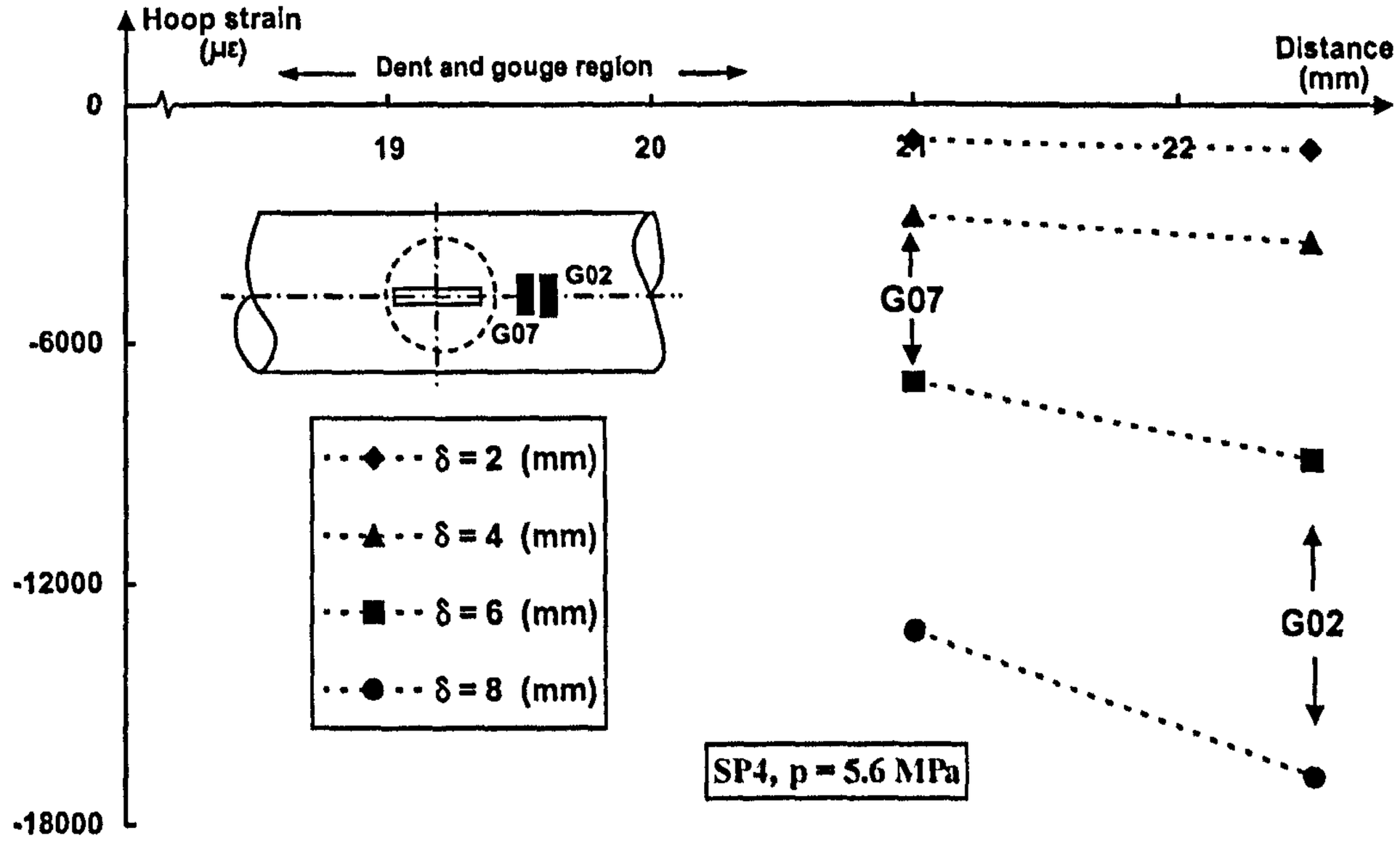

Figure 6.49: Distribution of hoop strain in specimen SP4 (gauges G02 and G07). Both gauges were off-centre as sketched in the figure. Dashed circle indicates indenter's location, (top view of the specimen).

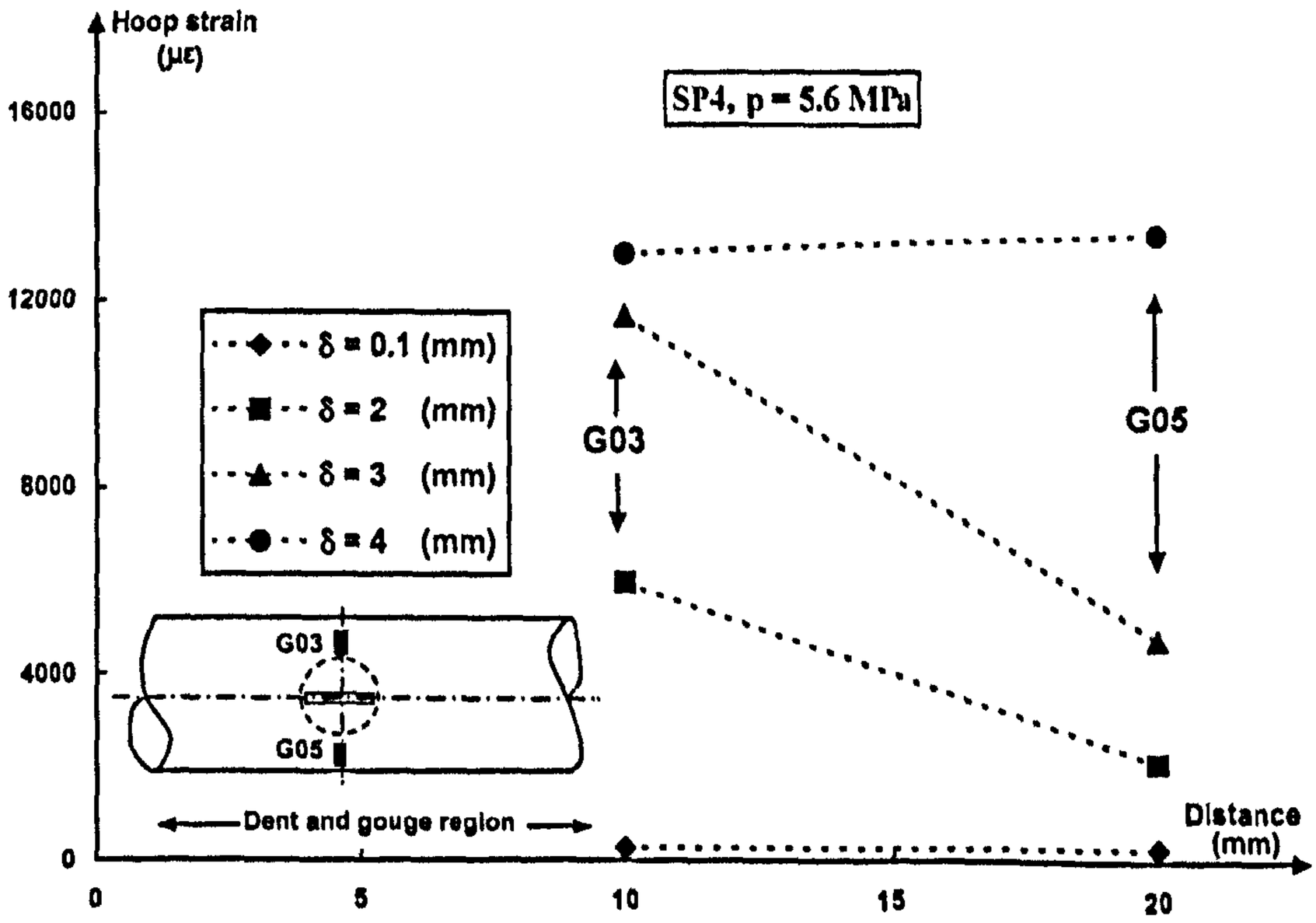

Figure 6.50: Distribution of hoop strain in specimen SP4 (gauges G03 and G05). Both gauges were off-centre as sketched in the figure. The dashed circle indicates indenter's location, (top view of the specimen).

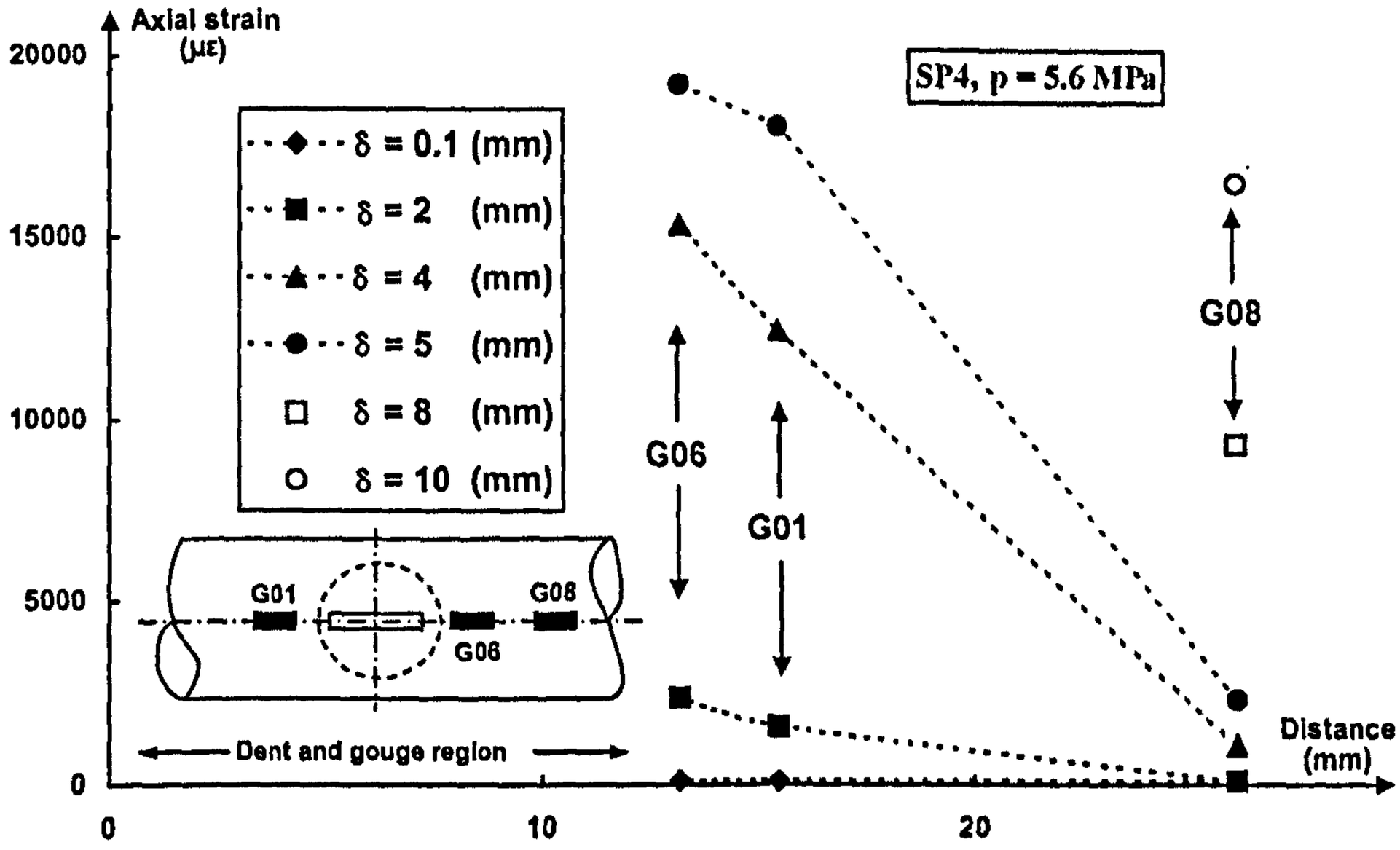

Figure 6.51: Distribution of axial strain in specimen SP4 (gauges G01, G06, and G08). All gauges were off-centre as sketched in the figure. The dashed circle indicates indenter's location, (top view of the specimen).

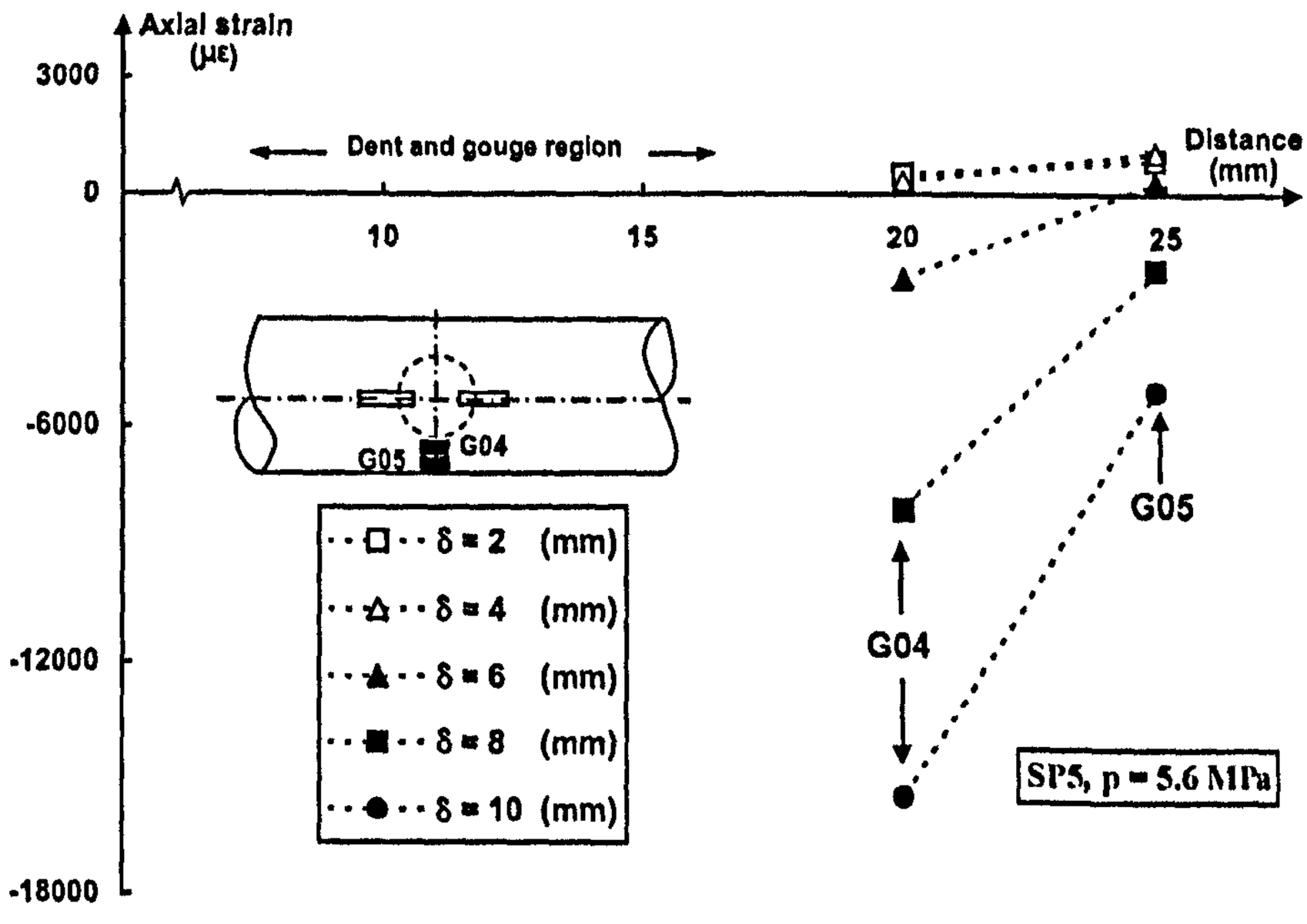

Figure 6.52: Distribution of axial strain in hoop direction for specimen SP5 (gauges G04 and G05). All gauges were off-centre as sketched in the figure. The dashed circle indicates indenter's location, (top view of the specimen).

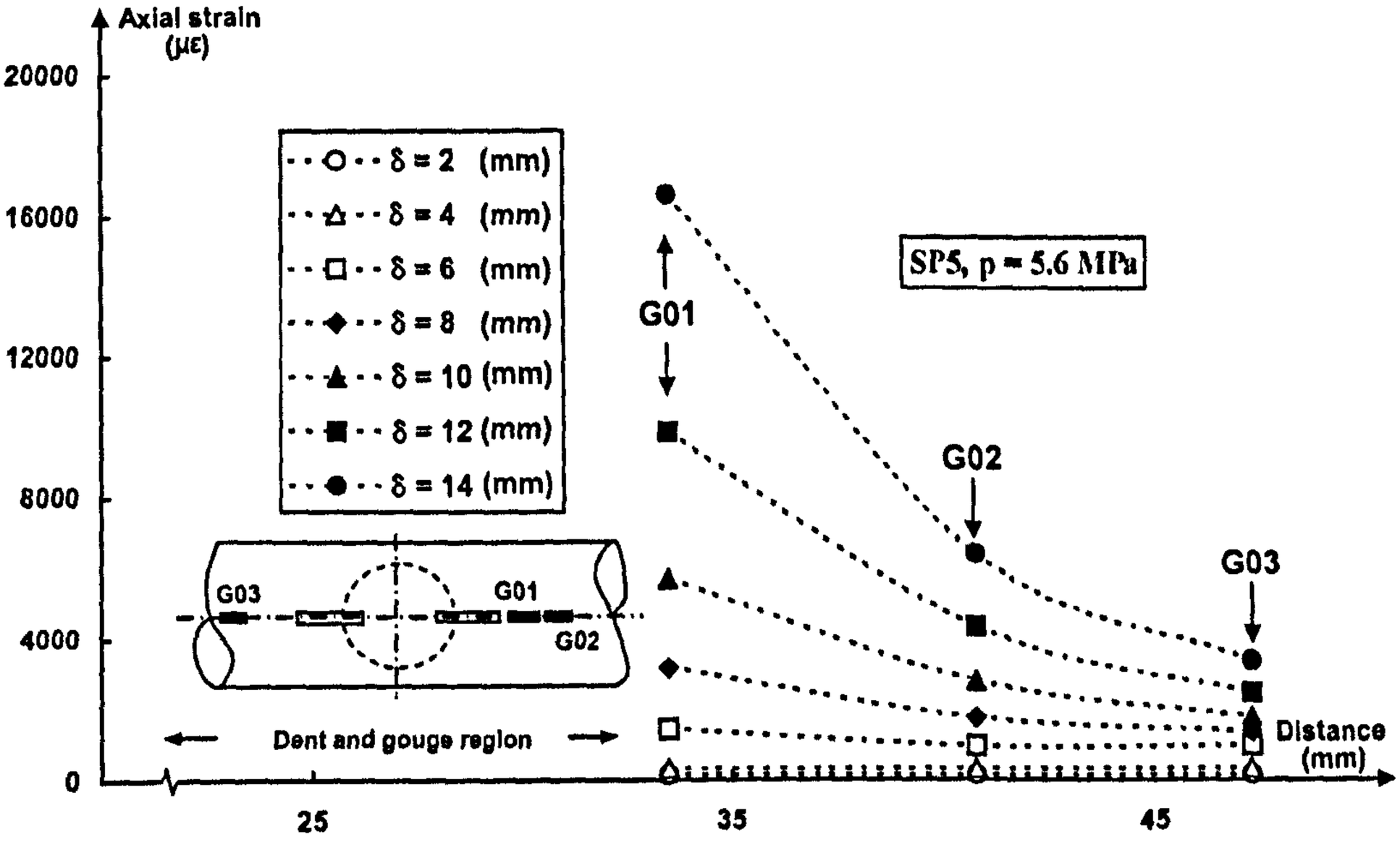

Figure 6.53: Distribution of axial strain in axial direction in specimen SP5 (gauges G01, G02, and G03). All gauges were off-centre as sketched in the figure. The dashed circle indicates indenter's location, (top view of the specimen).

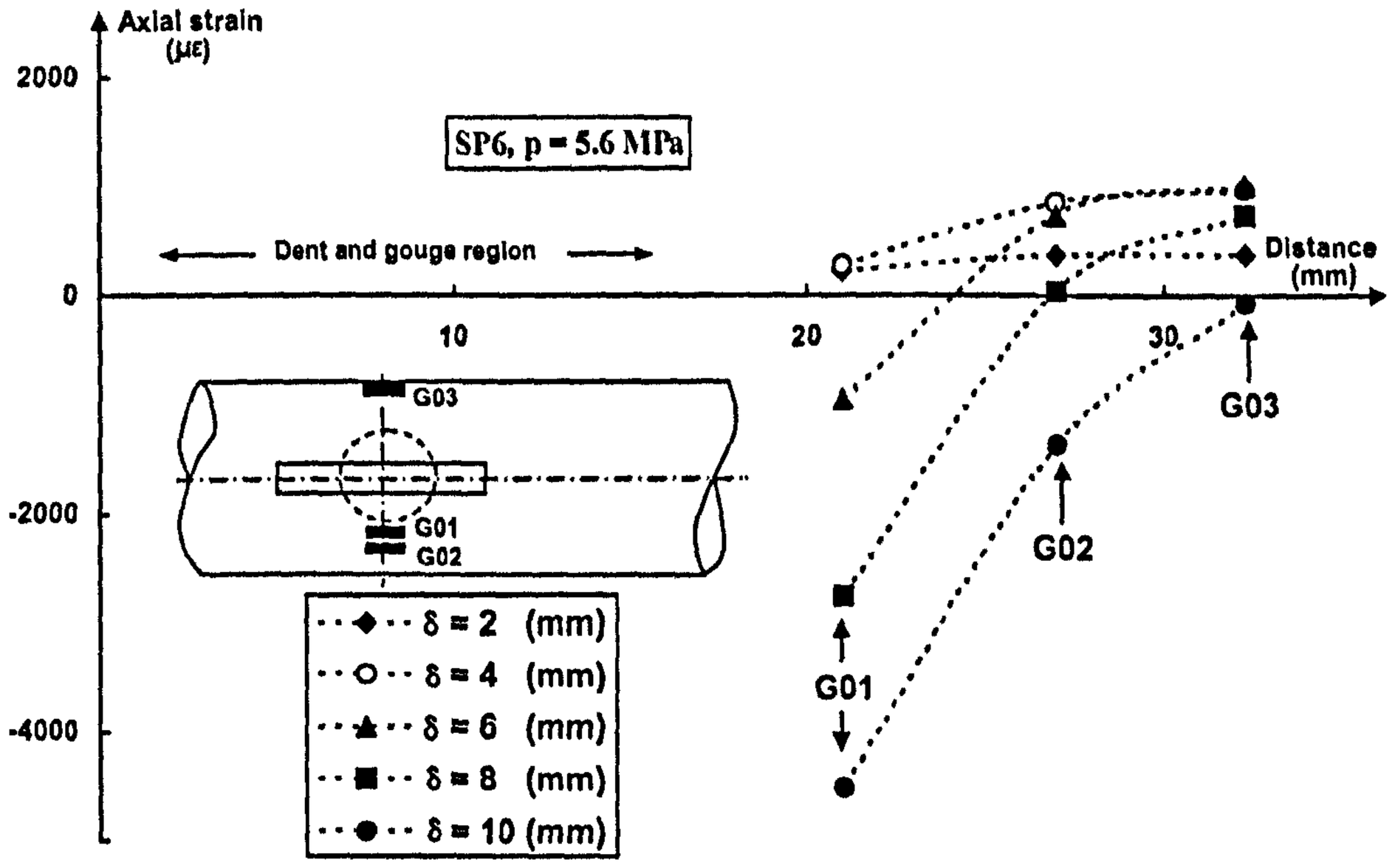

Figure 6.54: Distribution of axial strain in hoop direction in specimen SP6 (gauges G01, G02, and G03). All gauges were off-centre as sketched in the figure. The dashed circle indicates indenter's location, (top view of the specimen).

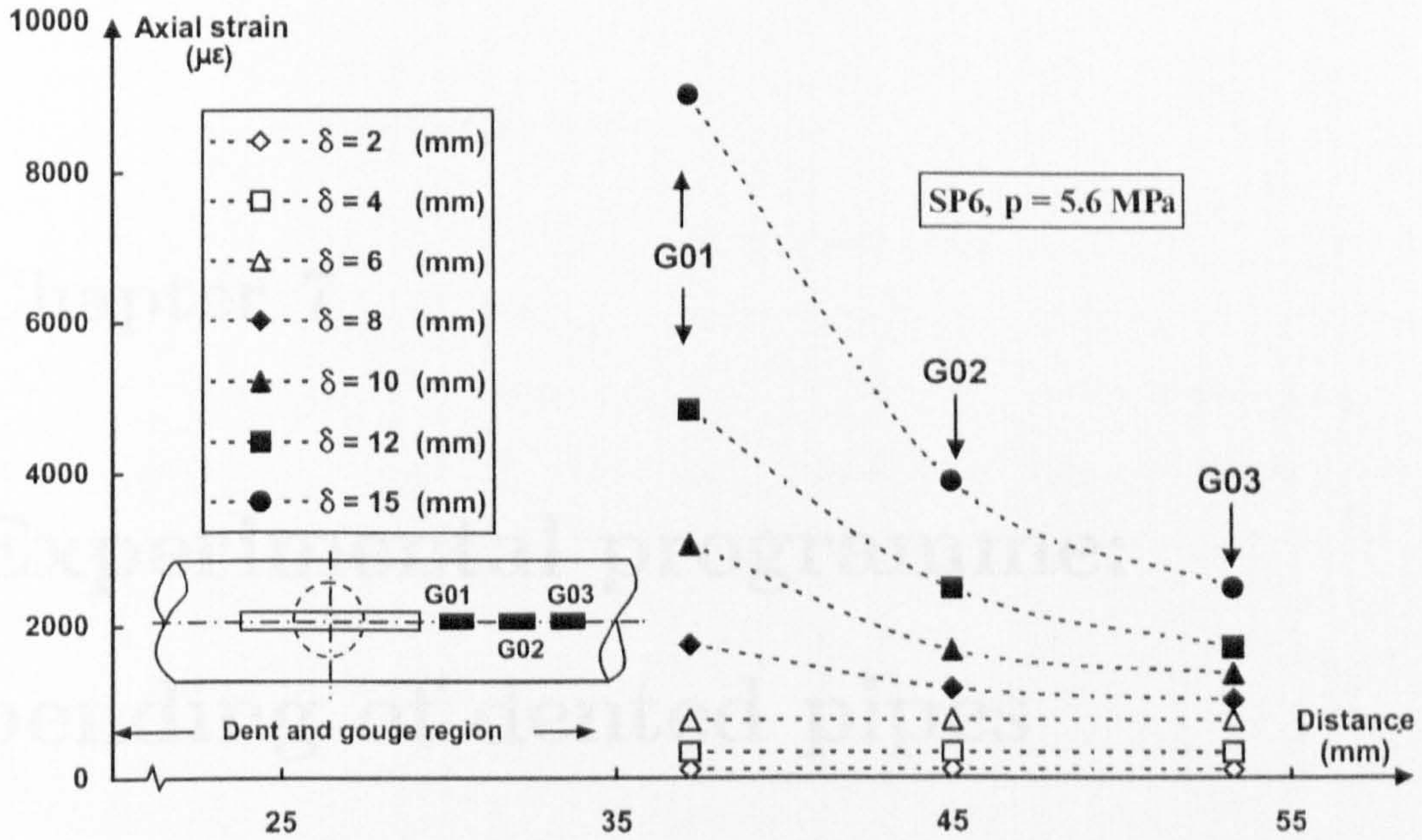

Figure 6.55: Distribution of axial strain in specimen SP6 (gauges G01, G02, and G03). All gauges were off-centre as sketched in the figure. The dashed circle indicates indenter's location, (top view of the specimen).

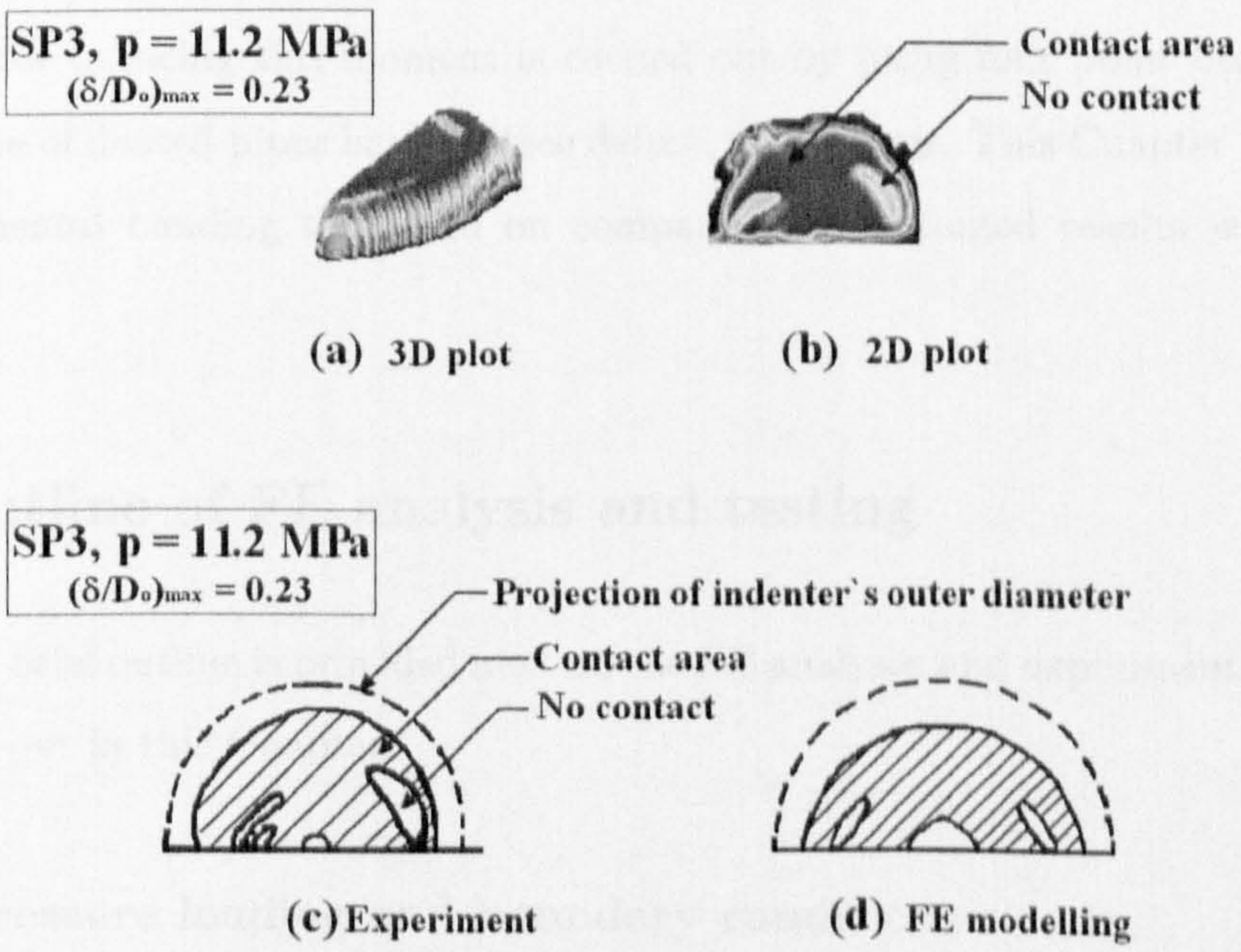

Figure 6.56: Contact area between indenter and pipe. Contact for half circle is shown due to symmetry. Also, $(\frac{\delta}{D_o})_{max} = 0.23$, $\frac{a}{b} = 1.0$, and $\frac{2L}{D_o} = 6.0$, and $p = 11.2\ MPa$.

Chapter 7

Experimental programme: bending of dented pipes

7.1 Introduction

The combined effect of pressure and bending on the behaviour of a dented pipe is addressed in this Chapter. The bending moment is applied to dented pipes. Procedure for inducing this moment is carried out by using four point bending technique. Some of dented pipes have surface defect, i.e., gouges. This Chapter is focussing on experimental bending tests and on comparison of obtained results with the FE predictions.

7.2 Outline of FE analysis and testing

A brief outline is provided next on the FE analyses and experimentation which are carried out in this Chapter.

7.2.1 Pressure loading and boundary conditions

Loading by internal pressure is the same as mentioned in Chapters (3), and (4). The magnitude of pressure during bending is different from pressure applied during denting of SP2, and SP3. The FE boundary conditions applied to bent models are the

same as detailed explicitly in Table (3.2) (see Figure (3.5)).

7.2.2 Post-denting assessments

Once denting was completed for specimens, SP2 to SP6, the pressure was released. Measurements of residual dent profile, straightness, and circularity of the pipe took place. After end of the denting all pipes showed no sign of any external cracks. Shape of dents was smooth for all specimens and all specimens had no scratches or any other external visible defects. Also, all dented specimens had residual strains and stresses due to pressurisation and denting.

7.2.3 Strain gauges

The strain gauges used during denting were checked for any damage. Some new gauges were added. Details about strain gauges are provided in Figures (D.1) to Figure (D.5), in Appendix (D).

7.3 Experimental set-up

7.3.1 Four point bending test

The test specimens which already have been dented, i.e., SP2, SP3, SP4, SP5, and SP6 are subjected to bending moment using four point bending approach. The objective is to apply a constant moment to the dented pipe. This moment can be in either direction towards opening or closing the dent - see Figure (4.1). A feature of this test is that the bending moment M is uniform over the central portion of the pipe and there is no shear force over this portion as shown in Figure (7.1). New arrangement for bending was designed, (four points bending test), as shown in Figure (7.2). The Dartec head was 'divided' to two-point loading. Rolled solid bar allows the test specimen to move or deform easily when subjected to vertical displacement. The bending moment test consists of the following steps:

- Test specimen is placed horizontally in Dartec machine as sketched in Figure

(7.3).

- All measuring instruments, i.e., measuring diameter growth, measuring system for angle rotation and pressure transducer are installed.

- Next, the dented pipes is pressurised to the required pressure level, $p = 5.6MPa$. The dented specimens are connected to pressure accumulator to compensate any change in pressure during the test. Figure (7.4) shows a typical plot of pressure versus centre node displacement for, SP2, during pressurisation.

- Vertical displacement using Dartec machine is applied in steps equal to 0.1 mm. As the displacement increases the angle of rotation starts to increase. Figure (7.5) shows loading-unloading curve for specimens, SP2, during bending test.

- The test specimen is subjected to Dartec displacement until buckling/bulging occurs.

7.3.2 Measuring of angular rotation

The arrangement for measuring and recording the angle of rotation is shown schematically in Figure (7.6). Photograph depicting actual pipe being bent is shown in Figure (7.7). The system was designed by using two bars which were attached to the dented pipe. These measuring arms were tack welded onto the test specimen. In unloaded state the measuring arms were parallel as can be seen in Figure (7.6). Two displacement transducers were then attached between these two bars, identified as transducer (1) and transducer (2). Both transducers could only move in horizontal direction. The distance between both arms was kept constant and equal to $\cong 3D_o$ (in order to eliminate recording of local deformations). Assuming that the rotation of the dented pipe was small one can assume that transducers were horizontal. Figure (7.8) shows displacement of the transducers versus time of the test (for specimen SP2). Both curves, from transducers (1) and (2), are similar to each other. The difference between them is the magnitude of transducer extension. This is expected since extension of transducer (2) is larger then that of transducer (1). The angular rotation was calculated using equation (7.2) (schematically explained in Figure (7.9)):

$$Sin\frac{\theta}{2} = \frac{X}{Y} = \frac{\delta ab - \delta cd}{2Y} \tag{7.1}$$

$$\theta = 2\ sin^{-1}\left(\frac{\delta ab - \delta cd}{2Y}\right) \tag{7.2}$$

where δab is the extension of line AB for transducer (1), δcd is the extension of line CD for transducer (2), and Y is the vertical distance between transducers before denting, and this equals 250 mm. The diameter growth was also measured for all test specimens using diameter growth gauge.

7.4 Application of bending moment

7.4.1 Dented pipes with no gouges (opening bending moment)-SP2 & SP3

The dented specimens, SP2, and SP3 which have no surface, gouges, were subjected to opening bending moment with internal pressure equal to, $p = 5.6\ MPa$. The pressure was constant during the bending test - see Table (7.1) for other details. The opening bending moment was applied in a such way that the dent was located on the tension side of the specimen - see Figure (4.1). Results obtained from four point bending fixture were post-processed, and plots of applied moment versus angle of rotation were obtained for both SP2, and SP3. Experimental results were compared with the FE prediction. Comparison is shown in Figure (7.10) for SP2, and in Figure (7.11) for SP3. As can be seen from both figures, there is a good agreement between both sets of data for up to 0.1 rad (about $\cong$ 6°), after which both curves diverge. The first portion of the curve is adequate for the limit analysis since twice elastic slope and five times elastic slope can be applied. The ultimate bending moment with its corresponding angular rotation for both experiment and FE are given in Table (7.2).

7.4.2 Dented pipes with gouge(s) (opening bending moment)-SP5 & SP6

The dented specimens SP5 and SP6 which have surface defects were subjected to opening bending moment with internal pressure $p = 5.6\ MPa$. This pressure was constant during the bending test. The moment was applied by using four point bending test facility. The results obtained from recording instruments were post-processed and they are shown in Figure (7.12) for SP5, and in Figure (7.13) for SP6. Plots of moment versus angle of rotation obtained from the FE analysis are also shown in these figures. As can be seen from both figures, there is a good agreement between both sets of results for up to 0.1 *rad* (about $\cong$ 6°), after which gap increases between FE and experiment. The ultimate bending moment with the corresponding angular rotation is also given in Table (7.2).

7.4.3 Dented pipe with a single gouge (closing bending moment)-SP4

The dented specimens, SP4, was subjected to closing bending moment with internal pressure equal to $p = 5.6\ MPa$. This pressure was constant during the bending test - see Table (7.1). The closing bending moment was applied in a such way that the dent was located on the compression side of the specimen - see Figure (4.1). The moment was applied by using the same four point bending test facility which was described previously.

The resulting moment versus angular rotation for SP4 is plotted in Figure (7.14). Again, the FE results are added to this figure as can be seen from this figure, there is a good agreement between both methods for up to 0.065 *rad* (about $\cong$ 3.5°), after which gap increases between FE and experiment. This difference is due to the fact that the closing bending moment accelerates the dent thus causing quicker buckling/bulging. The ultimate bending moment with its corresponding angular rotation is given in Table (7.2). For pipe, SP4, the ultimate bending moment is 5.16 kNm. This value is compared with the FE results, 4.2 kNm. This gives the percentage difference of 18.6%.

7.5 Buckling/bulging of bent pipes

The experimental bending tests were stopped once buckling/bulging appeared. As an example, a general view of the dented pipe, SP3, is shown in Figure (7.15). The combination of opening bending moment and internal pressure pushed out the dent, and a closer view of this case is shown in Figure (7.16) for SP2. Figure (7.17), on the other hand, shows different stages of the experiment, starting from manufacturing the pipe's defect through denting and than bending (for SP5 and SP6). For closing bending moment bulges appeared on both sides of the dent as shown in Figure (7.18a) for SP4. In the case of opening bending moment buckles/bulging appear on the opposite side of the dent around the welding region (Figure (7.18b) for SP5). In the FE results, for opening bending moment, the buckles occurred at the pipe's end. Therefore, further investigation was carried out here. The welding rings were included the new FE model by giving stiffer material for the ring and the results are seen in Figure (7.19). In this case bulges 'returned' to both ends - exactly as in the experiment. The ultimate bending moment was also computed for model with and without welding rings. Several points, 'b', 'c', 'd', and 'e' were checked along the opening moment curve - see Figure (7.20). Deformed profiles corresponding to points 'b', 'c', 'd', and 'e' are shown in Figure (7.21). It is seen here how inclusion of 'welding rings' into the FE model affects location of pipe failure.

Similar examination of the closing moment versus end rotation plot has been done for model SP4 - see Figure (7.22). A section through the pipe at various stages of loading, i.e., at points: 'b', 'c', and 'd' has been extracted. Shapes corresponding to these points are sketched in Figure (7.23). Bent configurations at the collapsing moment are shown in Figure (7.24) (for SP5), and in Figure (7.25) (for SP4). Both of these FE-generated shapes closely resemble photographs shown in Figure (7.18).

7.5.1 Repeatability of experiments (SP2, SP3)

It is seen from Table (6.13) that models SP2, and SP3 are nominally identical. They had no surface defects and after being dented to the same depth, $(\frac{\delta}{D_o})_{max} = 0.23$, with the same internal pressure, they were subjected to the same bending moment.

Both specimens have the same conditions in terms of dent depth, inside pressure and dimensions. The results obtained for moment loading versus angular rotation can be seen in Figure (7.26). The results compare well. Small discrepancy at larger rotation could be due to a small differences in the material properties. The percentage difference in the ultimate bending moment is $(\frac{6.15-6.0}{6.15}) = 2.44$ % and the percentage difference in the angular rotation is $(\frac{0.214-0.20}{0.214}) = 6.5$ %. It could be concluded here that both tests gave near the same results.

7.6 Strain gauge results

Strain gauges were used to record any change in strain distribution in and around the dent and gouge vicinity during bending. Details about positions of strain gauges for specimens SP2, SP3, SP4, SP5, and SP6 are provided in Appendix (D). A sample of the data obtained from the strain gauge reading as a function of the opening bending moment is given Figures (7.27) and (7.28). These figures show tension and compression for axial strain. These strains increase with the increase of the bending moment. The strain data was collected up to ultimate bending moment. The results are presented separately for each specimen and they are as follows:

- Distribution of the axial strain for SP2 is shown in Figure (7.29) for gauges G01, G02, G03 and G04. These gauges were located on axial axis as sketched inside the figure. The dashed line indicates the dent area. The axial strain increases as the opening bending moment increases and it is a tensile strain for gauge G01 and other gauges give compression strain. The maximum axial strain was predicted by gauge G01 which was closer to the dent centre. Distribution of the axial strain seems to be very sensitive in the dent region. Distribution of the hoop strain for gauges G09, G10, G11, and G12 is shown in Figure (7.30). This figure shows increase in the hoop strain as the opening bending moment increases. Also, hoop strain increases as it moves away from the dent centre. This confirms the high stress region (two stationary crescent-shaped regions of high external strains at the axial extremities of the dent were predicted by Lancaster et al. [68] for dented pipes).

Figure (7.31) shows distribution of axial strain for gauges G13, G14, and G16 in SP2. The axial strain increases as the moment loading increases. The maximum axial strain increases away from dent centre. The maximum is at the dent rim. This maximum, predicted by gauge G16, is located within the high strain region as predicted by Lancaster et al. [68]. In addition, Figure (7.32) shows hoop strain distribution in circumferential direction. The hoop strain increases as the opening bending moment increases for G06 to G08. This increase is smaller for gauge G05. Gauge G08 gives compression hoop strain as the opening bending moment increases.

- For specimen SP3, the strain gauges were located off-centre by angle equal to 60° as shown in appendix (D), Figure (D.2). Distribution of the axial strain increases as the opening bending moment increases. This strain increases significantly for G05 as shown in Figure (7.33) (as there are in high tension region). The hoop strain is compressive and it increases as the opening bending moment increases - see Figure (7.34).

- Distribution of the axial strain for SP4, which has an axial gouge at the dent centre, is shown in Figure (7.35) for gauges G01, and G06. The axial strain increases as the opening bending moment increases and changes from tensile strain to compression strain. This figure shows also maximum strain at the dent rim. The hoop strain distribution in for gauges G02 and G07 is shown in Figure (7.36). Both tensile strain and hoop strain increase as the closing bending moment increases. Figure (7.37) shows hoop strain distribution in circumferential direction for gauges G03, G04, and G05. The hoop strain increases with the increase of closing bending moment for gauge G03.

- Distribution of axial strain for SP5, which has two axial gouges, is shown in Figure (7.38) for gauges G01, G02, and G03. The results show compressive axial strain closer to the gouge edge for gauge G01. There is tensile stress away from the the gouge edge (from gauges G02, and G03). Distribution of the axial strain is shown in Figure (7.39). This figure shows increase in axial strain as the opening bending moment increases (for gauges located closer to the dent region).

- Distribution of the axial strain for SP6, which has a large axial gouge is shown

in Figure (7.40) for gauges G04, G05, and G06. The results show compressive axial strain close to the gouge edge (for gauge G04). Tensile stress was recorded away from the the gouge edge by gauges G05, and G06. Strain distribution in circumferential direction is presented in Figure (7.41). This figure shows increase of strain as the opening bending moment increases.

7.7 Burst tests

Once the four point test was completed on a dented pipe, the internal pressure was released. The test specimens were then taken to special pressure chamber facility for burst test. Figure (7.42) shows a sketch of the test arrangement.

The test specimen was filled with oil and pressurisation started in steps using hand pump until failure was reached. The burst pressures are summarised in Table (7.1). The burst pressures for specimens SP2 and SP3 which had no gouges were 23.6 MPa and 24.3 MPa, (2.8%). The burst pressure for SP4, which has single gouge at the centre, was 25 MPa.

The lowest failure pressure was 17.7 MPa. This was for SP5, which has two axial gouges. This was followed by 22 MPa for the wider axial gouge for SP6. A sample photograph of failed pipe, SP5, is shown in Figure (7.43) for two axial gouges. Figure (7.44) is for model SP6, and Figure (7.45) is for model, SP2.

7.7.1 Comparisons of burst pressure

The results obtained from experimental burst was compared to the results obtained from equations of burst for plain and gouged pipes but without dents or bending. The first equation (Eq. 7.3) was introduced by Ref. [53] for burst pressure of gouged pipe and the results were given in Table (7.3). Note that the first three values of pressure of this column was high since there is no gouge. These values were similar to values obtained for perfect pipe. The second equation (Eq. 7.4) was introduced by Ref. [30] for burst pressure of perfect pipe and the results were given in Table (7.3). The last equation (Eq. 7.5) is obtained from ASME code [17] for failure pressure of perfect pipe when pressurised internally. The results were given in Table (7.3). It is

seen that the presence of dents and gouges decrease the burst pressure significantly.

$$p_f = \sigma_f \left(\frac{t}{R_o}\right) \tag{7.3}$$

where: $\frac{\sigma_f}{\sigma} = \frac{1-(\frac{e}{t})}{1-((\frac{e}{t})(\frac{1}{M})}$, and $M = \sqrt{1 + 0.26\left(\frac{2c}{\sqrt{R_o t}}\right)^2}$

$$p_b = \overline{\sigma}\left(\frac{t}{R_o}\right) \qquad where\ \ \overline{\sigma} = \frac{(\sigma_{yp} + \sigma_{UTS})}{2} \tag{7.4}$$

$$p_f = \left(\frac{K-1}{0.6K+0.4}\right)\sigma_{UTS} \qquad for\ \ K \leq 1.5,\ \ and\ \ K = \frac{R_o}{R_i} \tag{7.5}$$

7.8 Observations

- The presence of internal pressure stiffen the pipe geometry hence it increases the bending load when compared to empty pipes.
- Buckling/bulging occurred in all opening bending tests. These were located away from the dent vicinity by $\cong 1.5D_o$ on the compression side of the pipe. For closing bending moment test bucking/bulging occurred in the dent vicinity on the compression side of the specimen.
- No failure has occurred during bending moment tests for all specimens.
- The presence of the axial gouges has small effect on the bending moment-rotation curve.
- The bending moment-rotation curve for all specimens, had similar trends. The bending moment increases with the increase of the angular rotation. All specimens had similar magnitude of the ultimate bending moment.

7.9 Summary

The measuring system for angular rotation proved to be adequate. It was able to measure large rotations. Good repeatability of tests was demonstrated for specimens

SP2 and SP3. None of the bent specimens failed during the tests. The experimental results agreed well with the FE predictions.

	D_o	t	e/t	$2w/t$	$2c/D_o$	$p_{bending}$	p_{burst}	**Bending type**
No:↓	(mm)	(mm)	(%)	(%)	(%)	(MPa)	(MPa)	
SP1	84.20	2.07	-	-	-	-	24.55	not bent
SP2	84.10	2.10	-	-	-	5.6	23.6	Opening
SP3	84.08	2.08	-	-	-	5.6	24.3	Opening
SP4	84.06	2.09	50	24.98	47.85	5.6	25.2	Closing
SP5	84.08	2.08	50	24.98	48.08*	5.6	17.7	Opening
SP6	83.97	2.08	25	80.98	120.2	5.6	22.0	Opening

Table 7.1: Details about pipes subjected to bending. Models SP2, and SP3 had plain dents in them. Models SP4, SP5, and SP6 were gouged. Note:⋆ model no. SP5 had two axial gouges of the same geometry and placed symmetrically with respect to the mid-length. SP1 was dented but not bent.

	$(BM)_{max}$ (kNm)		$(Rot.)_{max}$ (rad)	
No:↓	**Experiment**	**FE**	**Experiment**	**FE**
SP2	6.15	5.0	0.200	0.220
SP3	6.0	4.96	0.214	0.220
SP4	5.16	4.20	0.216	0.055
SP5	5.79	4.60	0.176	0.206
SP6	5.85	4.90	0.200	0.230

Table 7.2: Comparison of experimental and computed results for bending of dented plain and gouged, pipes. Note: $(BM)_{max} \equiv$ maximum bending moment, i.e., at the collapse, and $(Rot.)_{max} \equiv$ maximum end rotation, i.e., at collapse.

	Exp. (gouged & bent pipes)	**Num. (gouged pipe)**	**Num. (perfect pipe)**	
No:↓	p_{burst}	p_f $EQ.(7.3)$	p_{burst} $EQ.(7.4)$	p_f $EQ.(7.5)$
SP1	24.6	28.6⋆	22.6	29.1
SP2	23.6	29.0⋆	23.0	29.6
SP3	24.3	28.8⋆	23.1	29.3
SP4	25.2	21.3	23.3	29.4
SP5	17.7	21.4	23.2	29.3
SP6	22.0	23.1	23.2	29.3

$p_f \equiv$ failure pressure, $\star \equiv$ no gouge , Num. $\equiv$ numerical analysis, and Exp.$\equiv$ experiment

Table 7.3: Comparison of the burst test obtained from experiment with the calculated burst and failure pressure for plain and for gouged pipe. Results are in (MPa).

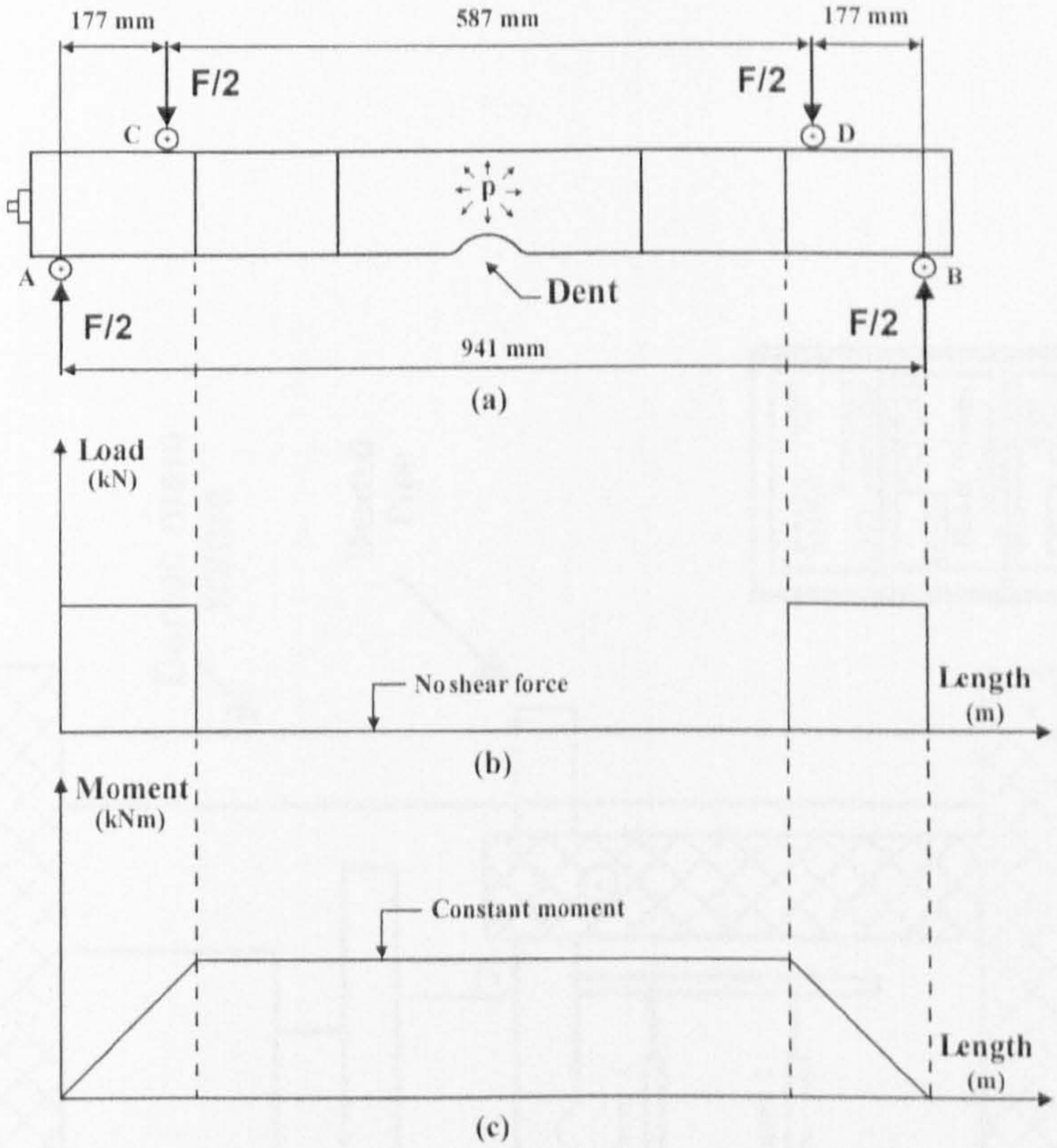

Figure 7.1: The shear force and bending moment diagrams for four point bending test.

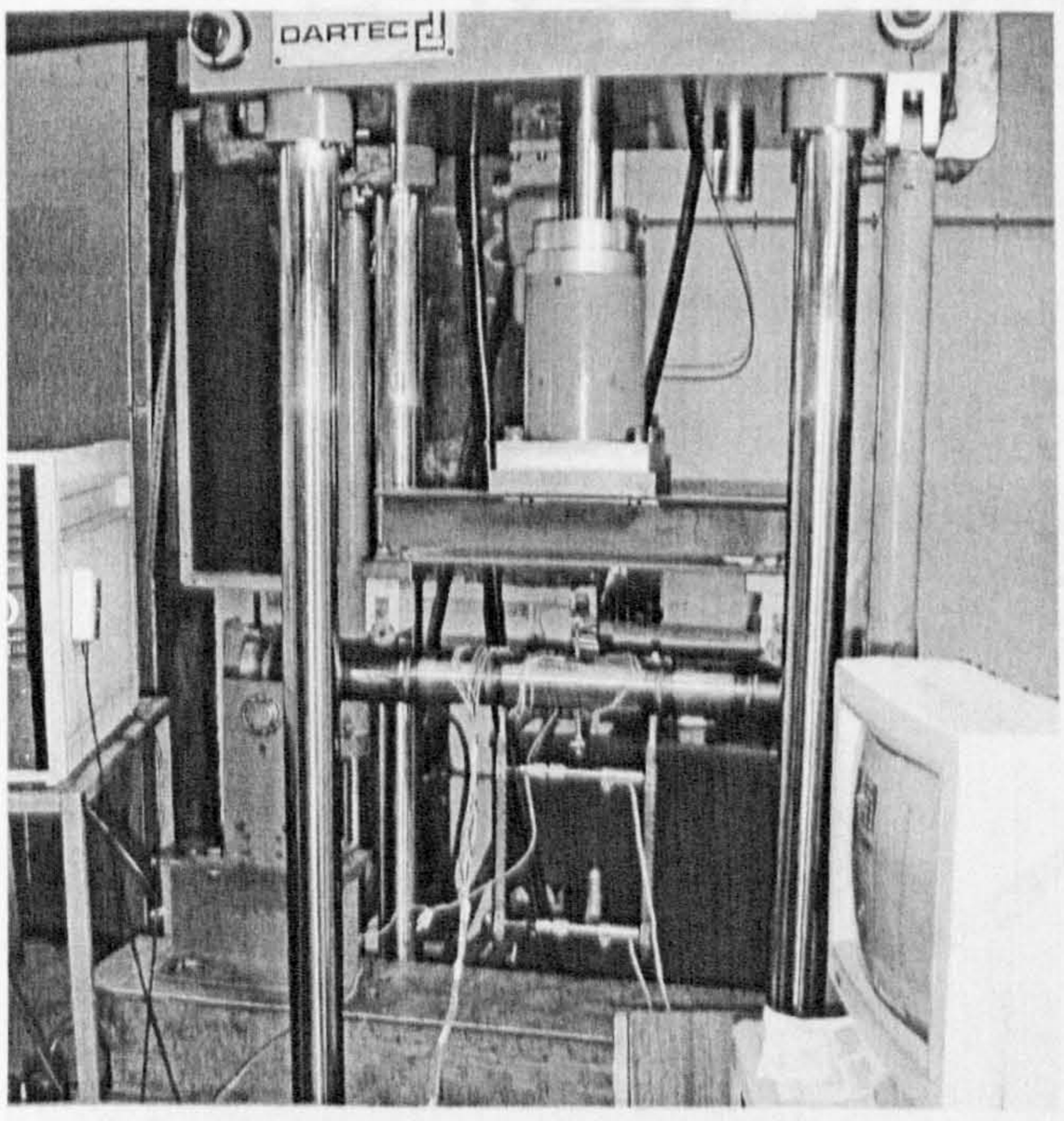

Figure 7.2: The four point bending test arrangement. Note two horizontal transducers measuring pipe's rotation.

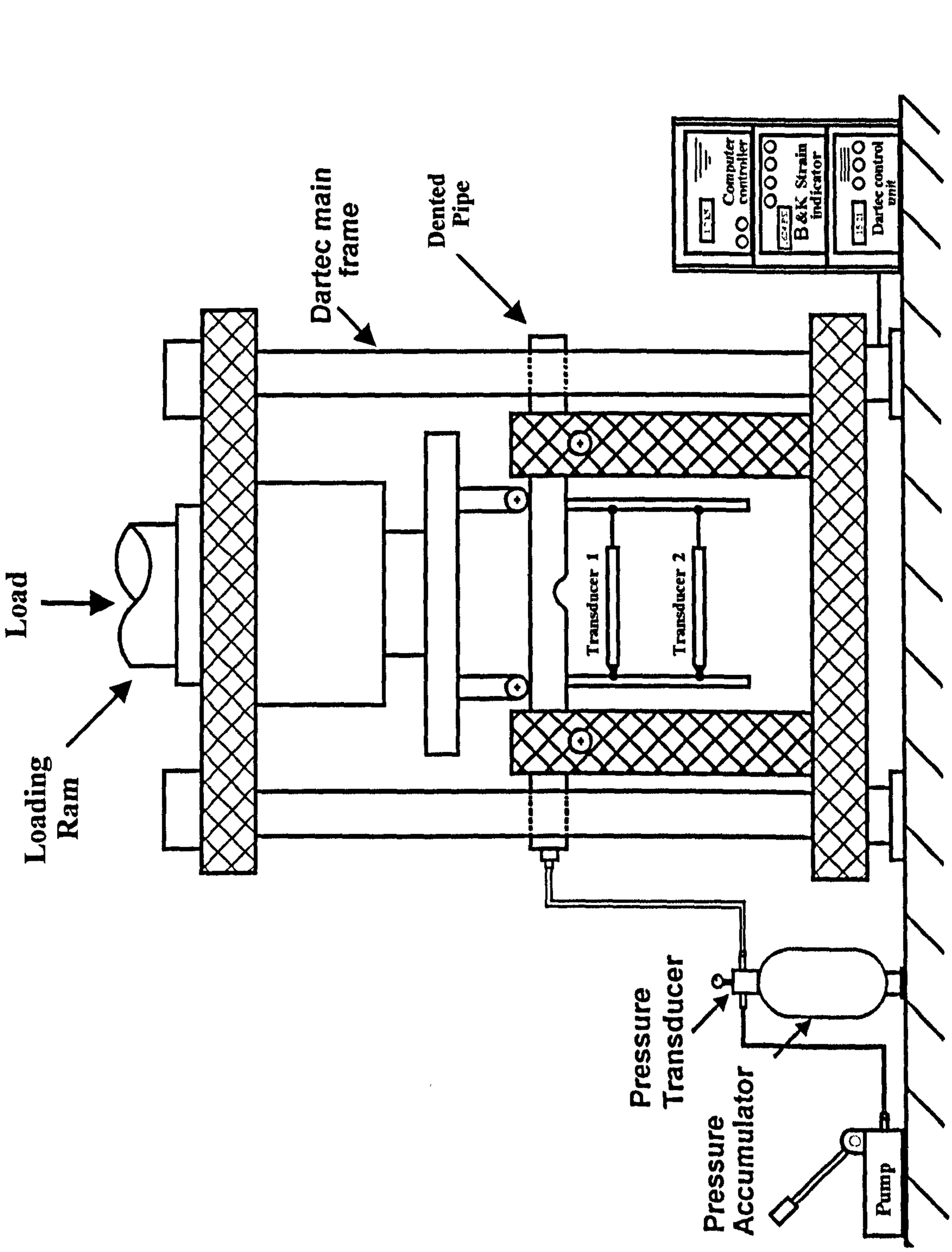

Figure 7.3: Sketch of the four point bending test and all of its measuring equipment (case of opening bending moment is sketched).

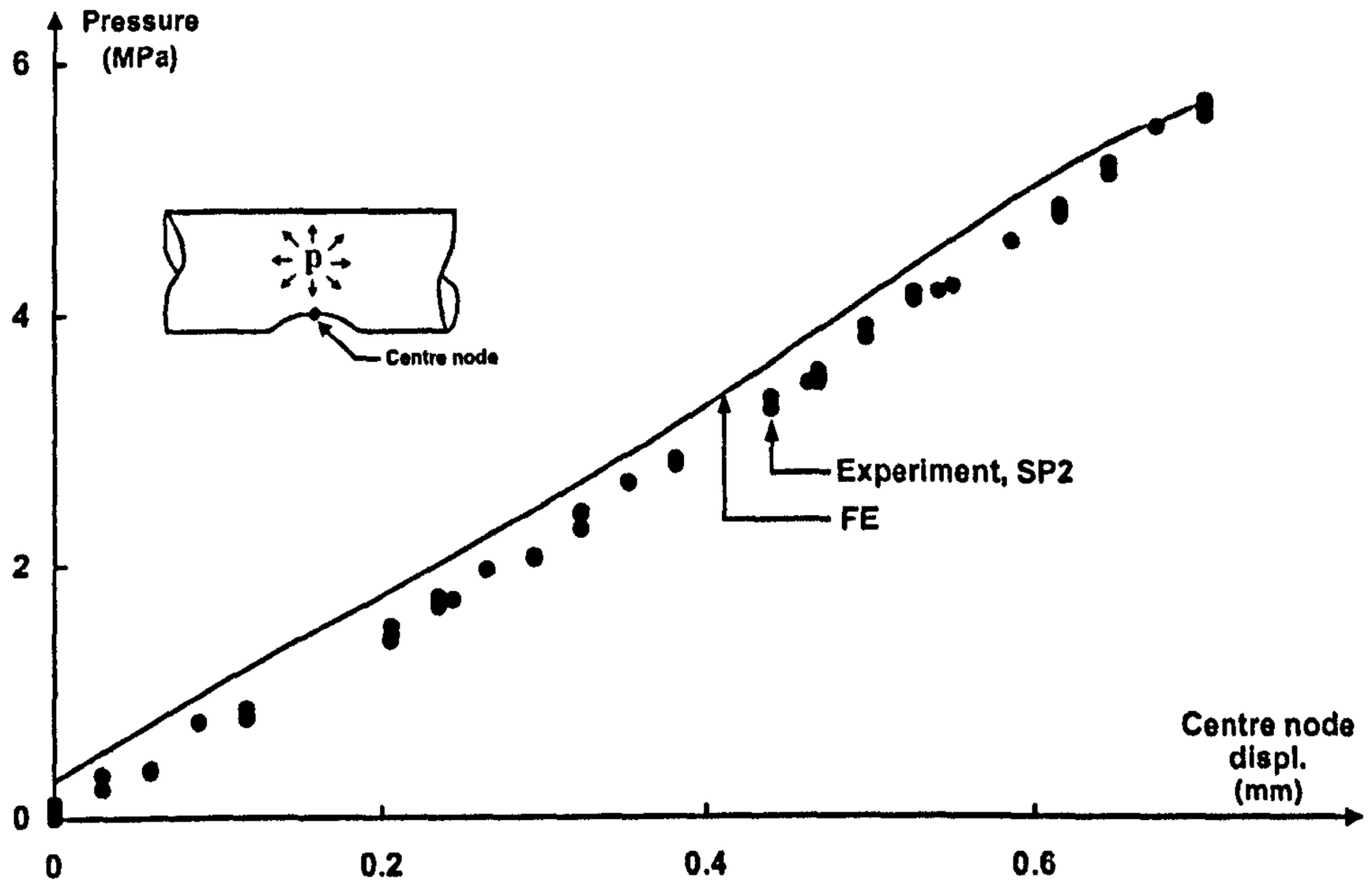

Figure 7.4: Pressure versus displacement of dented pipe - during pre-bending pressurisation, SP2. Also, $(\frac{\delta}{D_o})_R = 0.12$, and $\frac{2L}{D_o} = 6.0$.

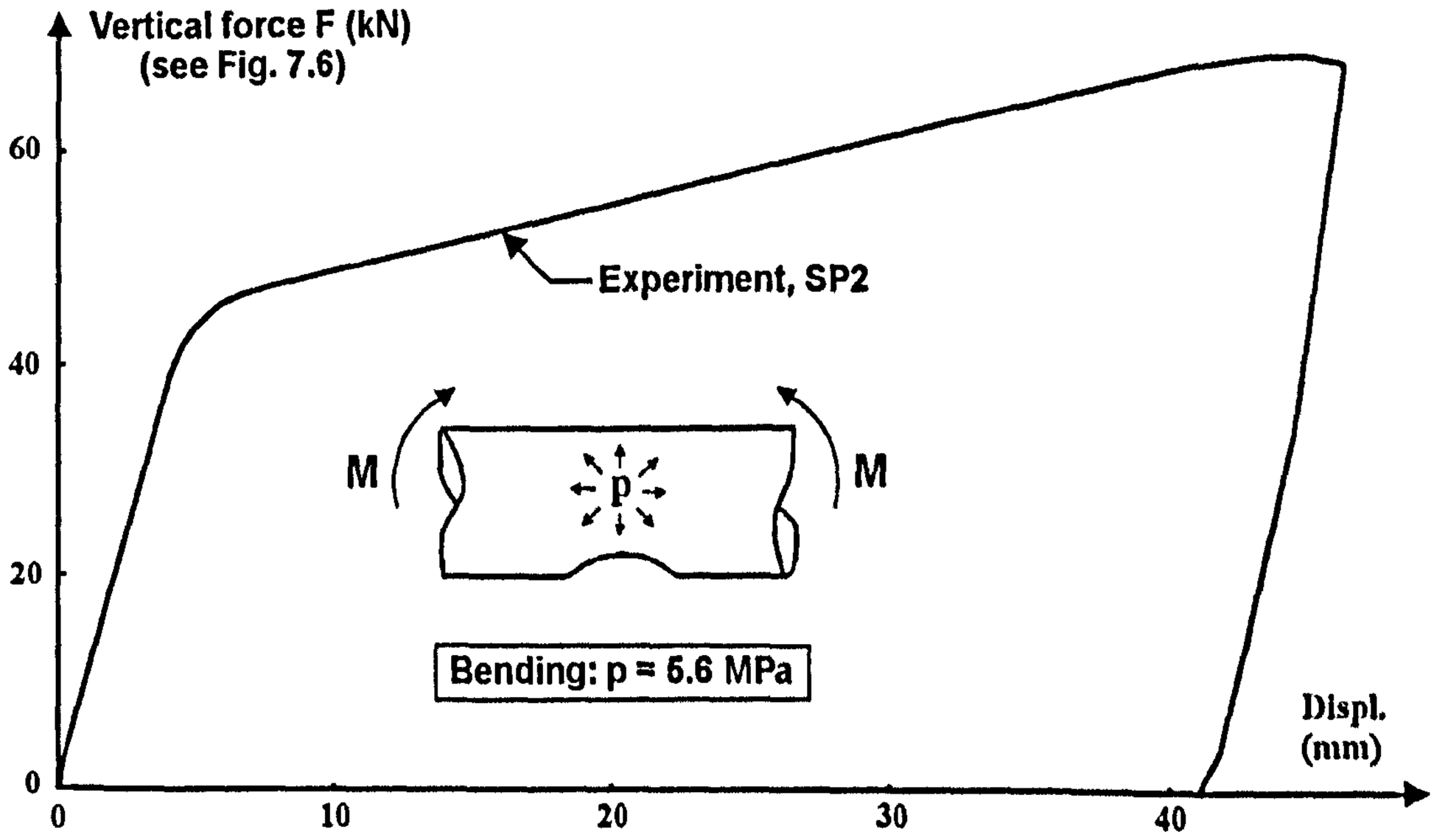

Figure 7.5: Dartec loading-unloading path applied to dented pipe, SP2 - through four point bending rig.

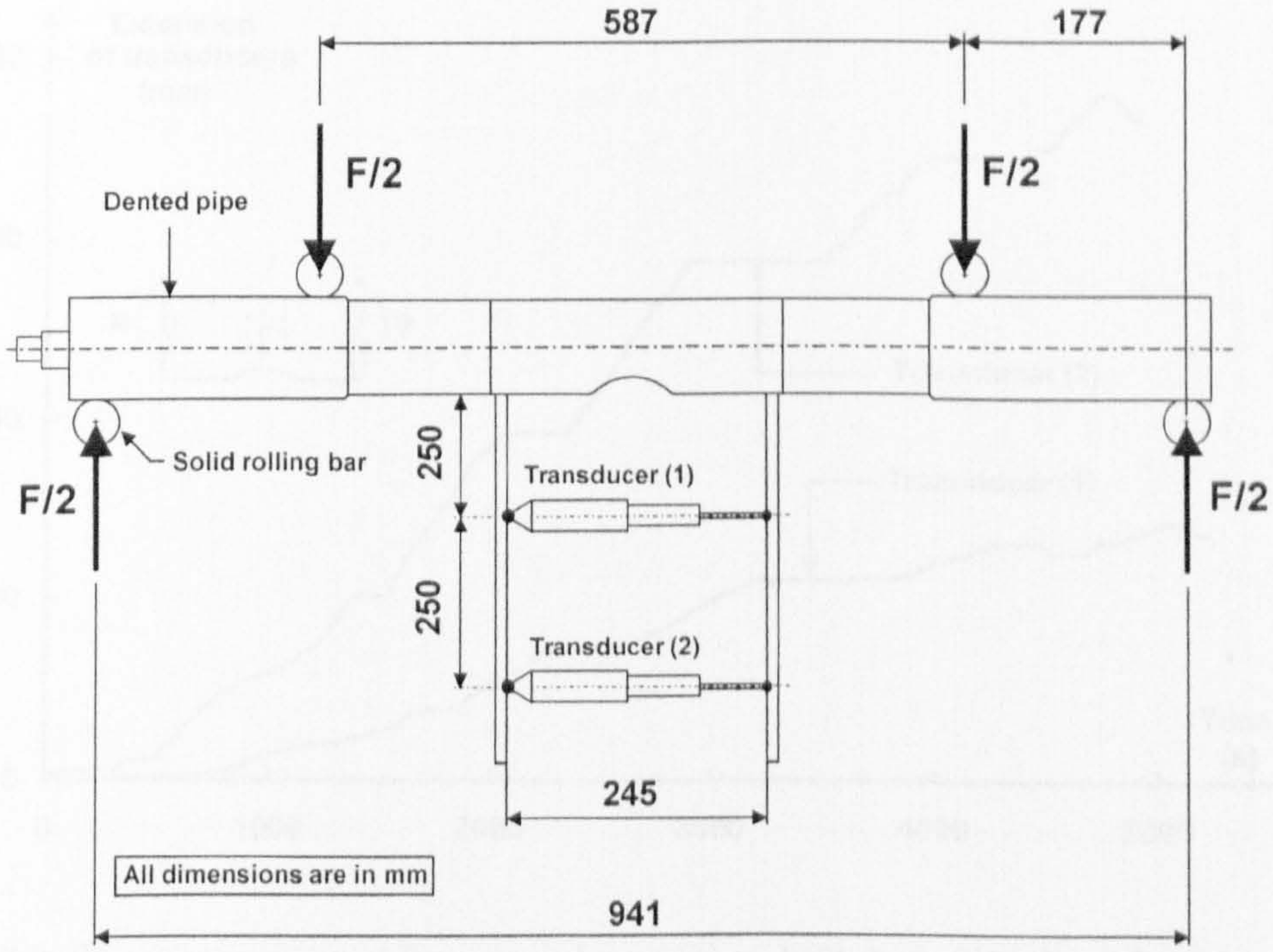

Figure 7.6: Sketch of experimental arrangements for measuring angle of rotation using two displacement transducers.

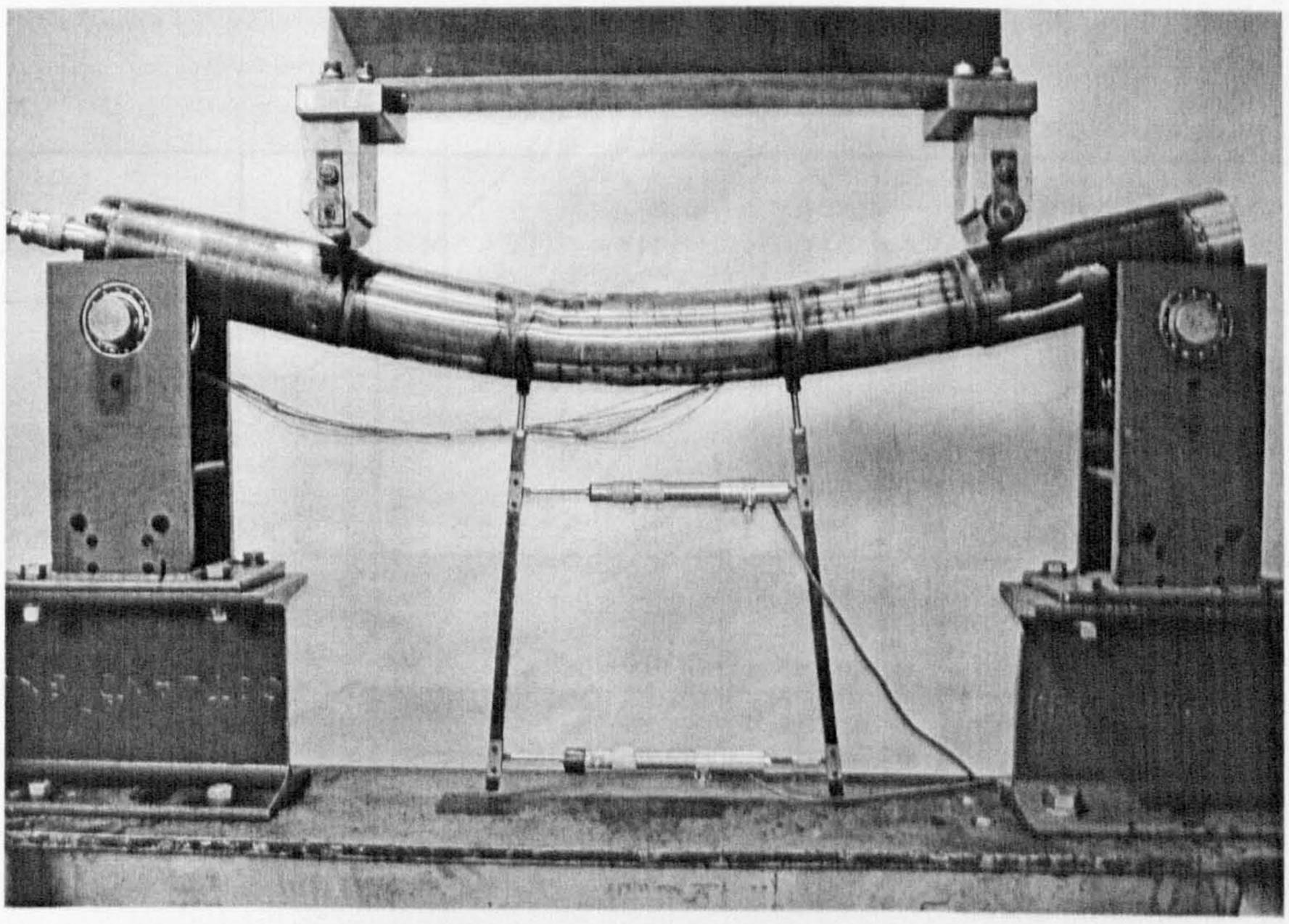

Figure 7.7: View of a pipe being bent.

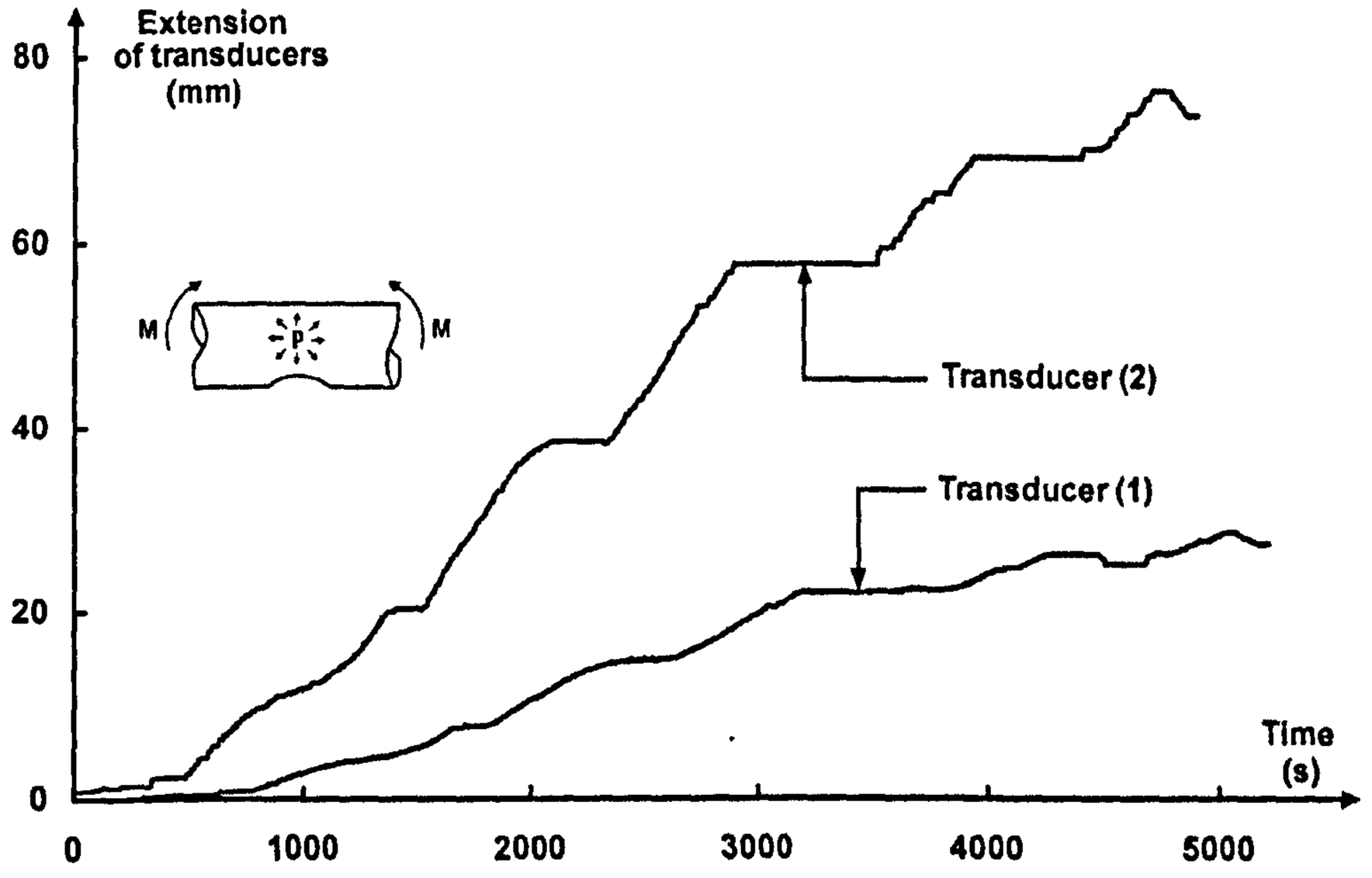

Figure 7.8: The response curves from transducers (1) and (2) during bending of specimen, SP2.

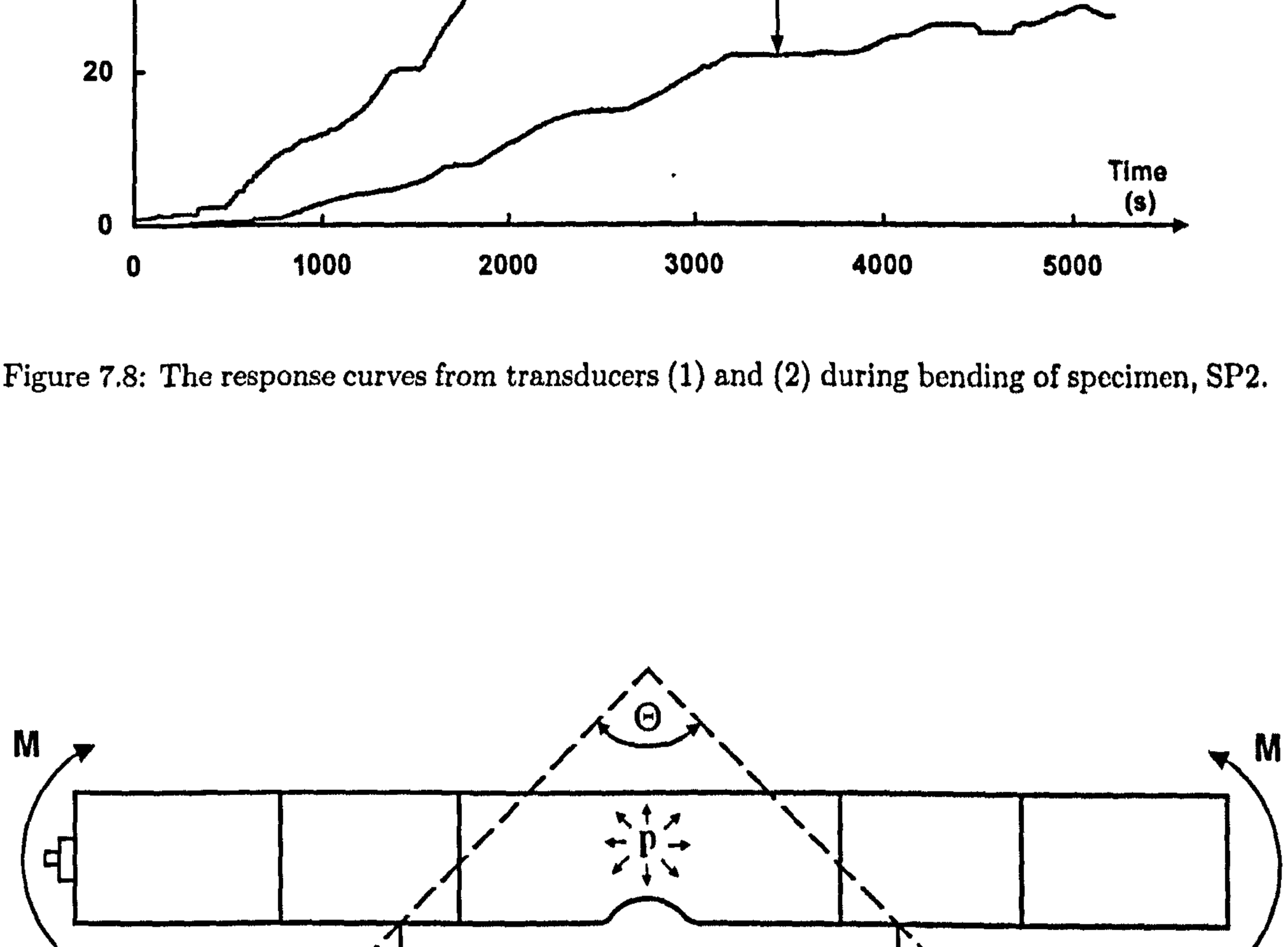

Figure 7.9: Sketch of the angular rotation.

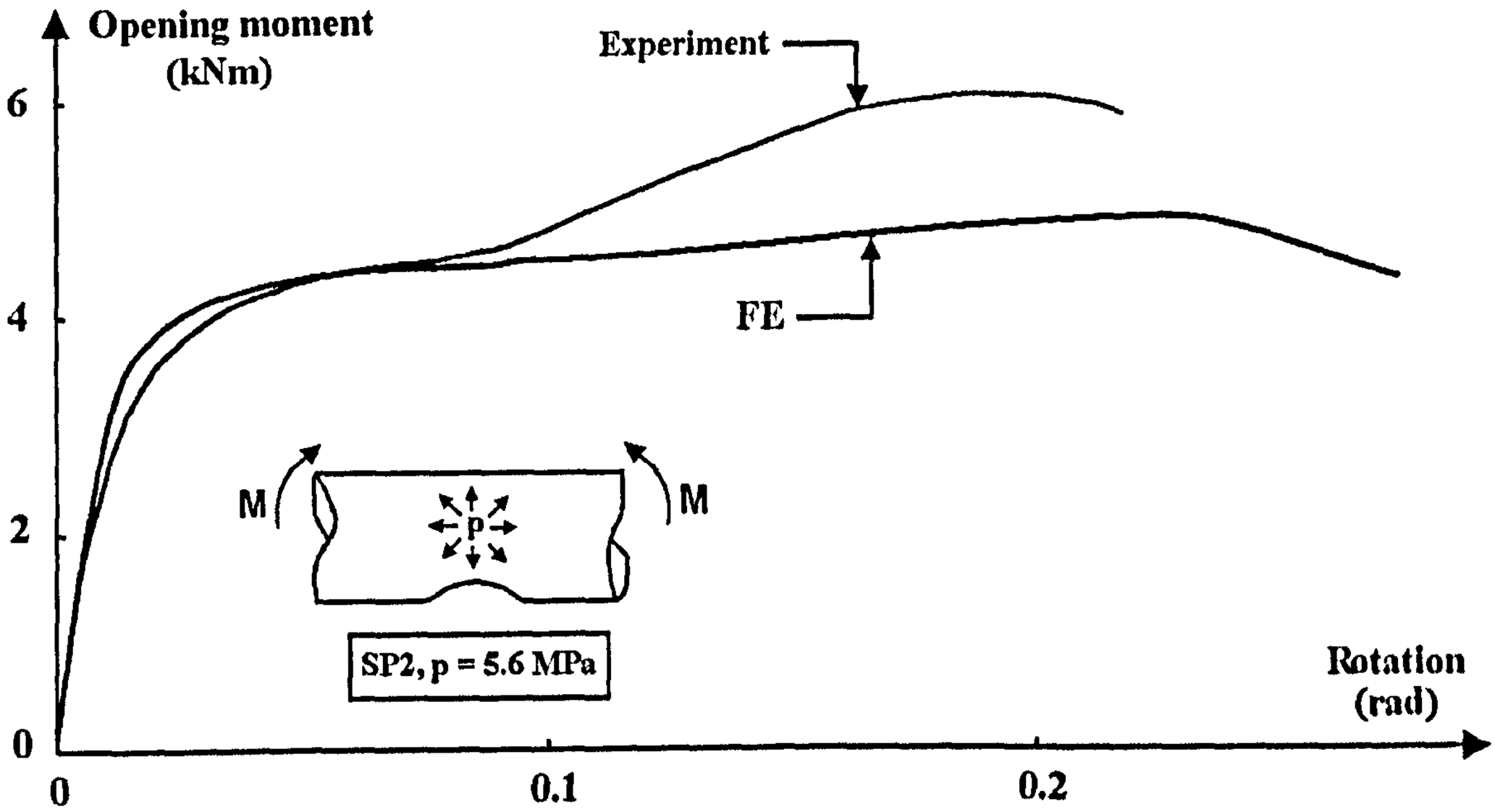

Figure 7.10: A comparison of results between FE and experiment for opening bending moment versus rotation curves (for SP2, no surface defect). The internal pressure was $p = 5.6\ MPa$, $(\frac{\delta}{D_o})_R = 0.1199$, and $\frac{2L}{D_o} = 6.0$.

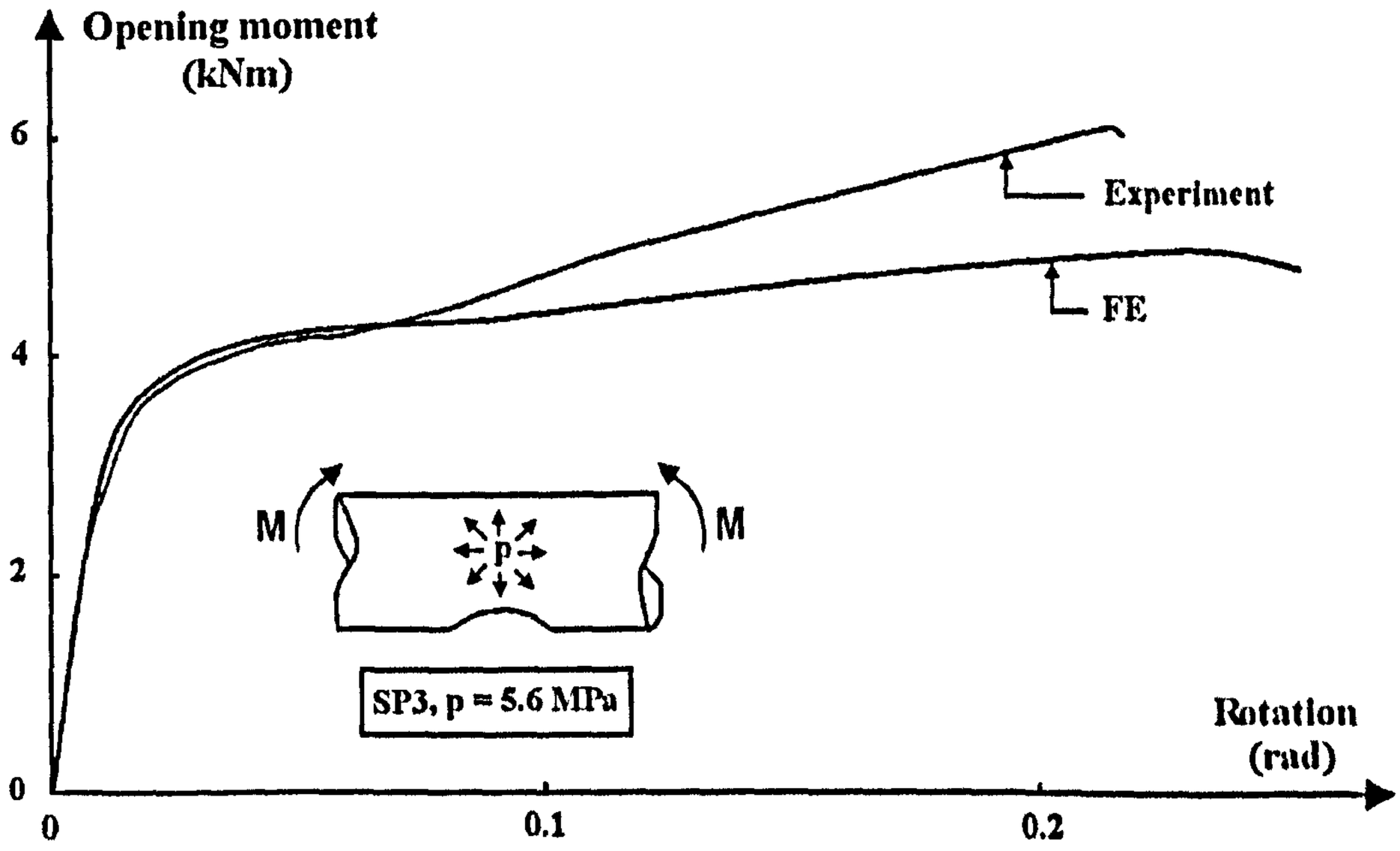

Figure 7.11: A comparison of results between FE and experiment for opening bending moment versus rotation curves (for SP3, no surface defect). The internal pressure was $p = 5.6\ MPa$, $(\frac{\delta}{D_o})_R = 0.1177$, and $\frac{2L}{D_o} = 6.0$.

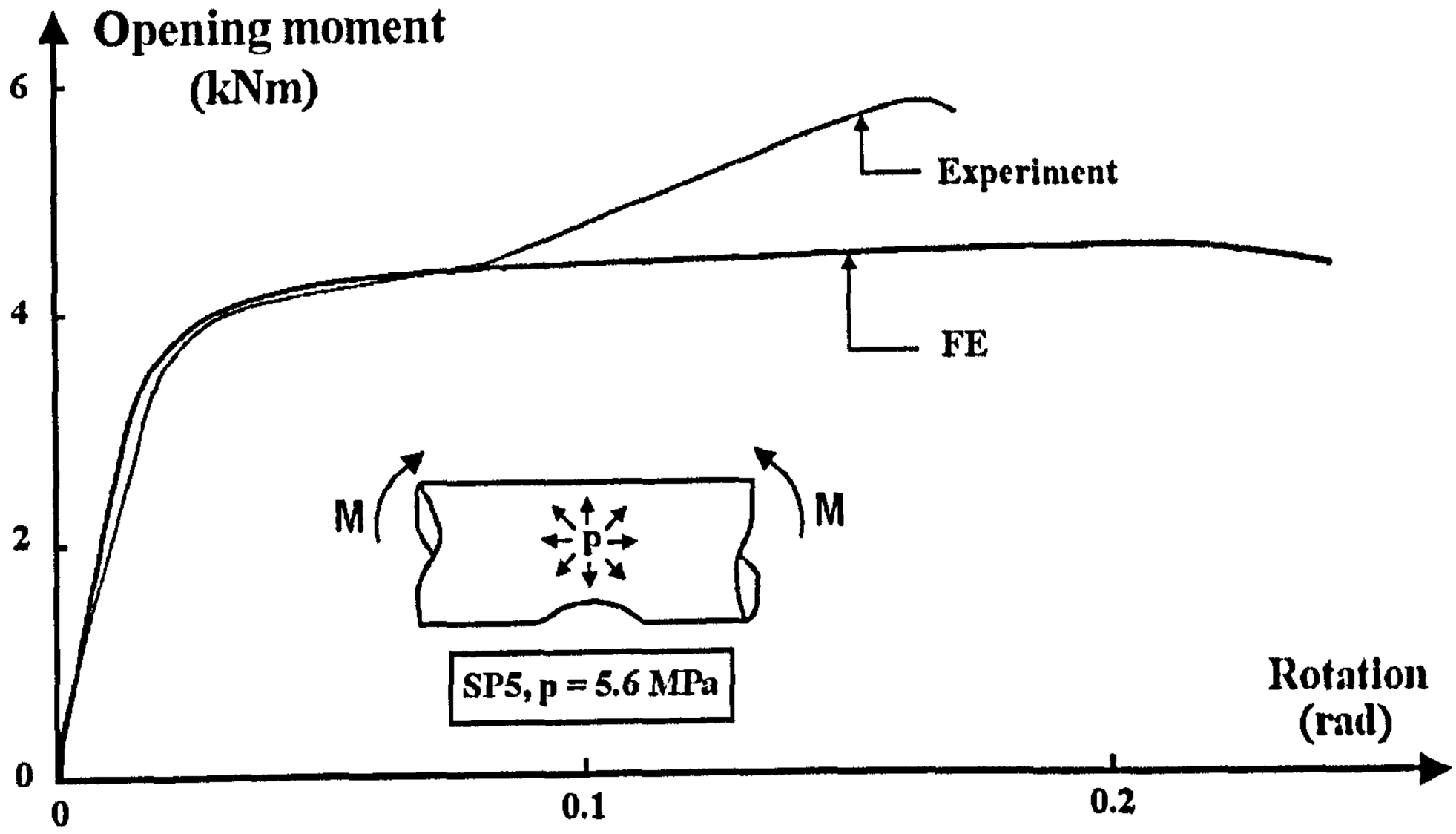

Figure 7.12: A comparison of results between FE and experiment for opening bending moment versus rotation curves (for SP5, with two axial gouges). Also, $p = 5.6\ MPa$, $(\frac{\delta}{D_o})_R = 0.101$, and $\frac{2L}{D_o} = 6.0$.

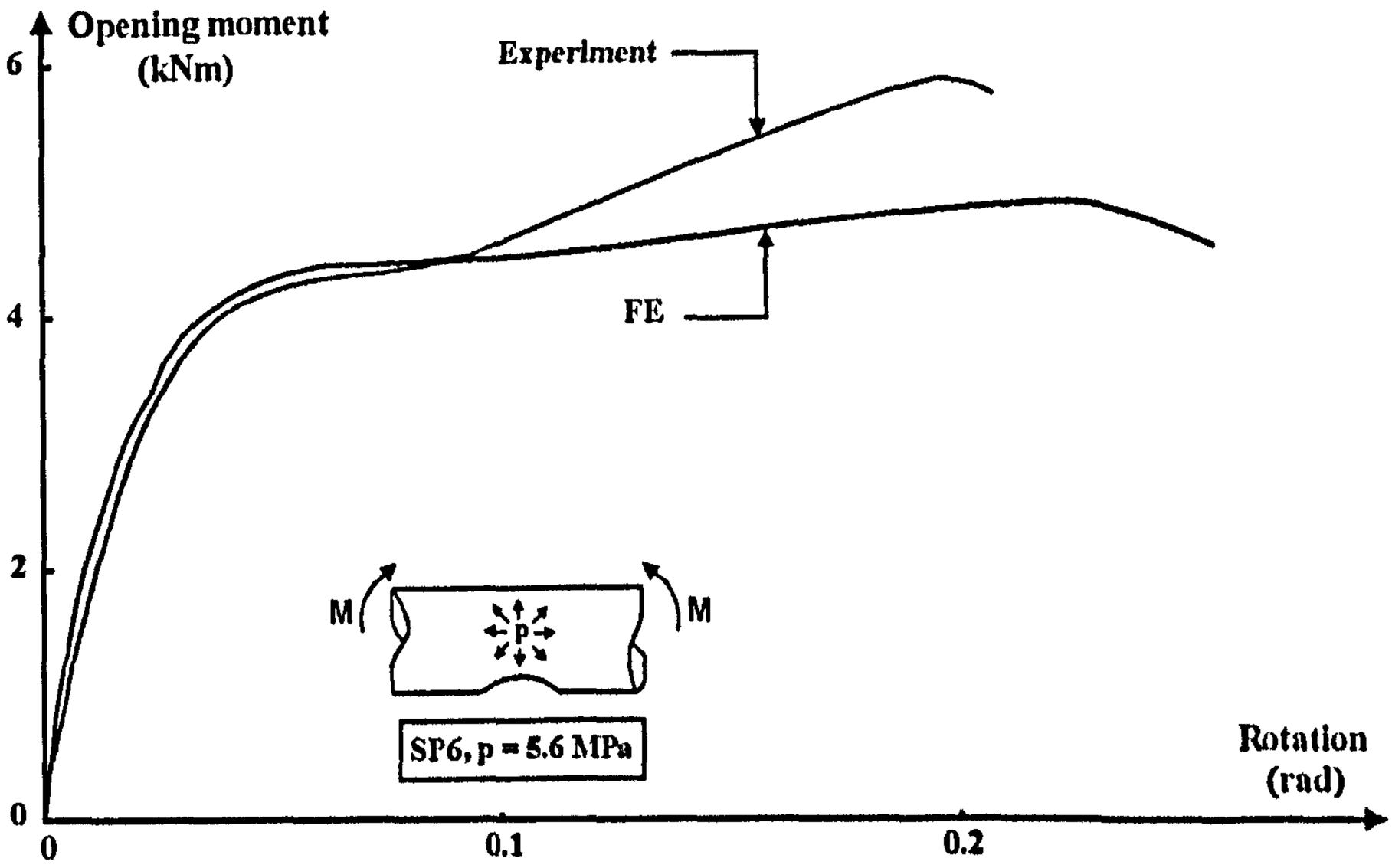

Figure 7.13: A comparison of results between FE and experiment for opening bending moment versus rotation curves (for SP6, with large axial gouge defect). The internal pressure was $p = 5.6\ MPa$, $(\frac{\delta}{D_o})_R = 0.102$, and $\frac{2L}{D_o} = 6.0$.

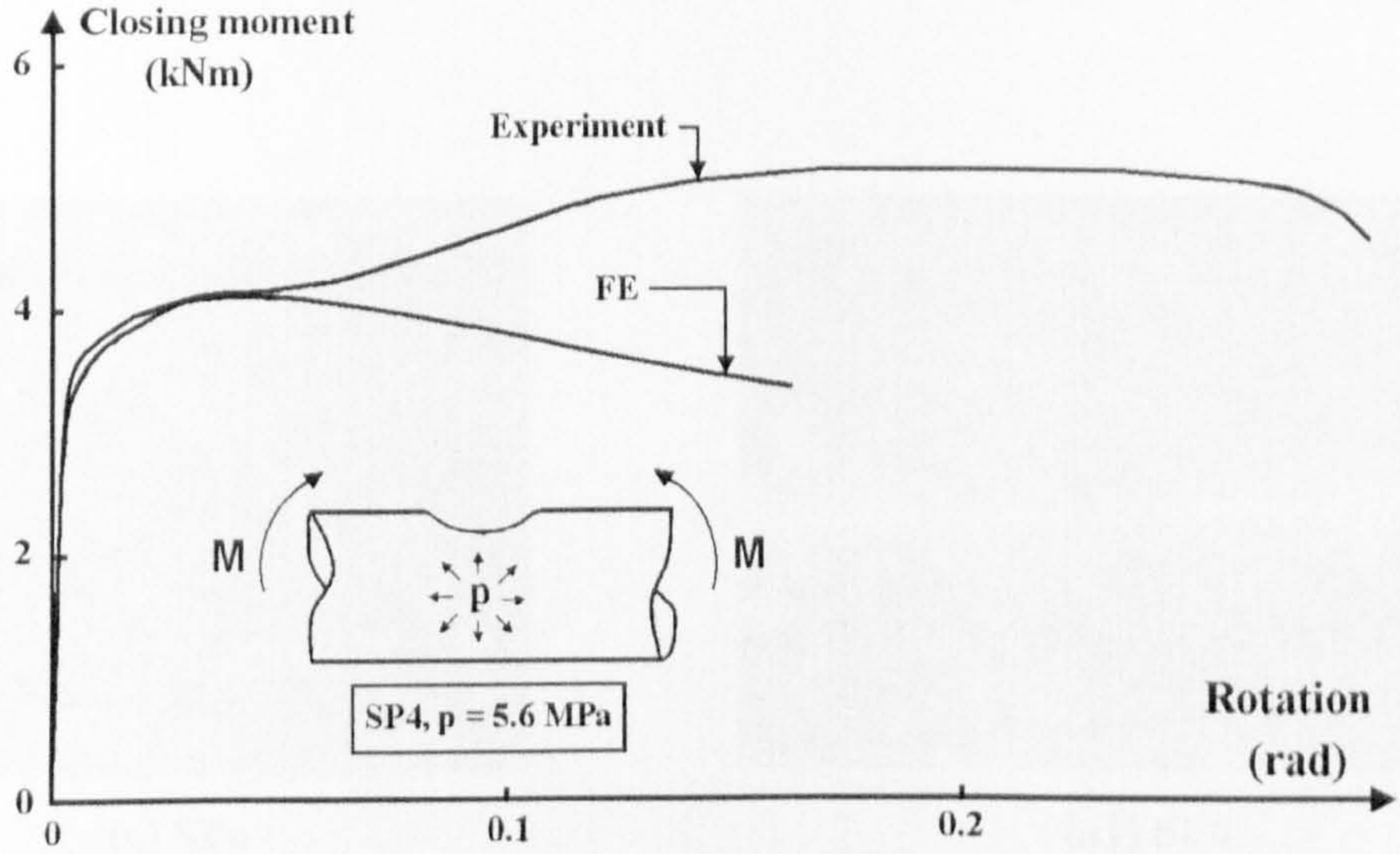

Figure 7.14: A comparison of results between FE and experiment for closing bending moment versus rotation curves (for SP4, with single axial gouge). Also, $p = 5.6\ MPa$, $(\frac{\delta}{D_o})_R = 0.092$, and $\frac{2L}{D_o} = 6.0$.

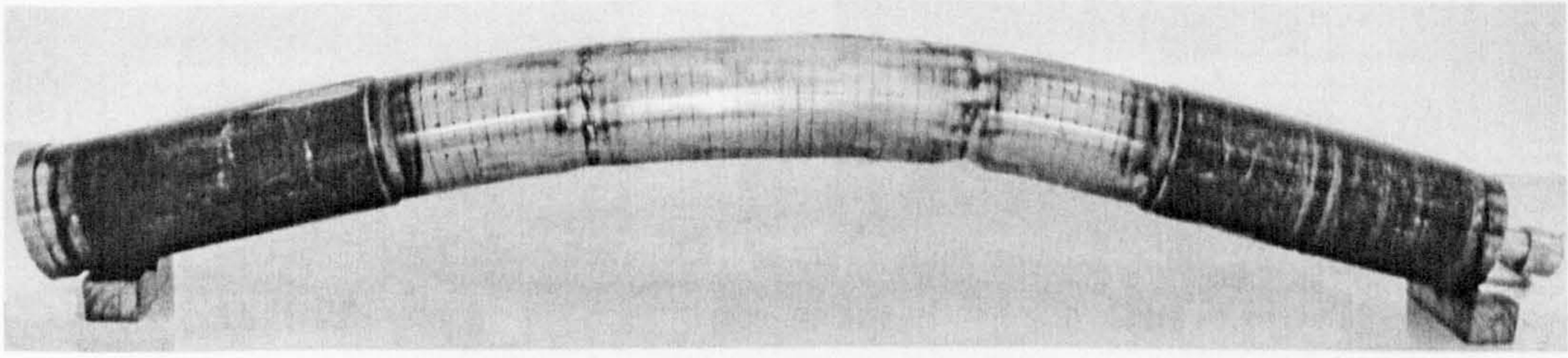

Figure 7.15: View of bent pipe after being subjected to opening bending moment, (SP3 model).

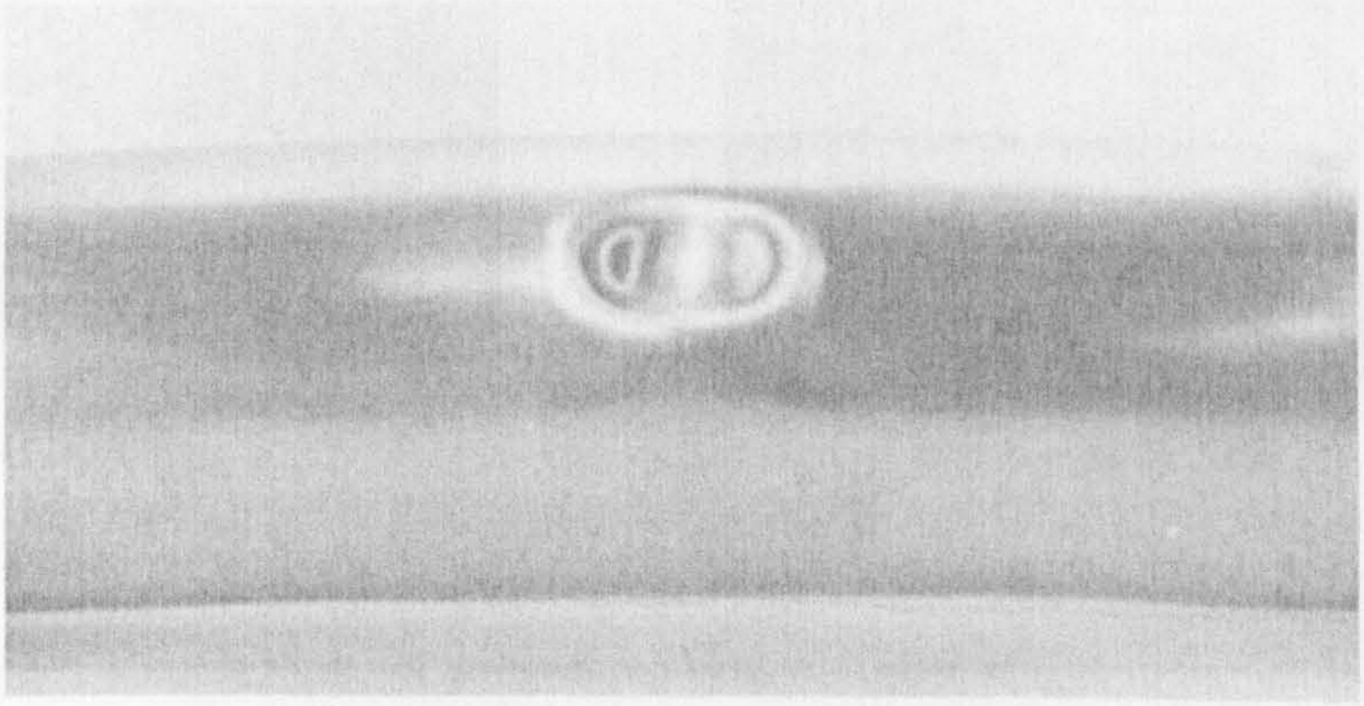

Figure 7.16: Closer view of bent pipe at the end of loading by opening bending moment.

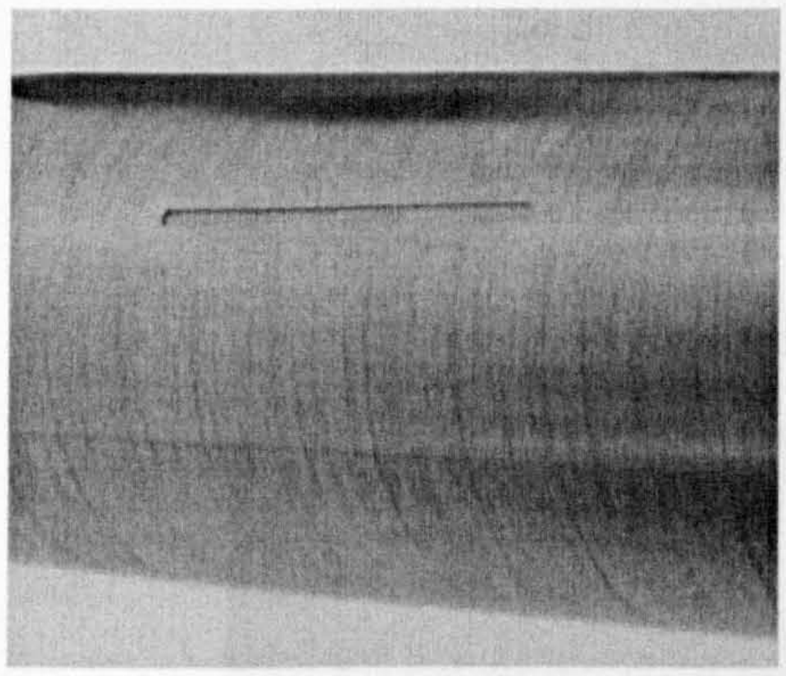

(a) SP6

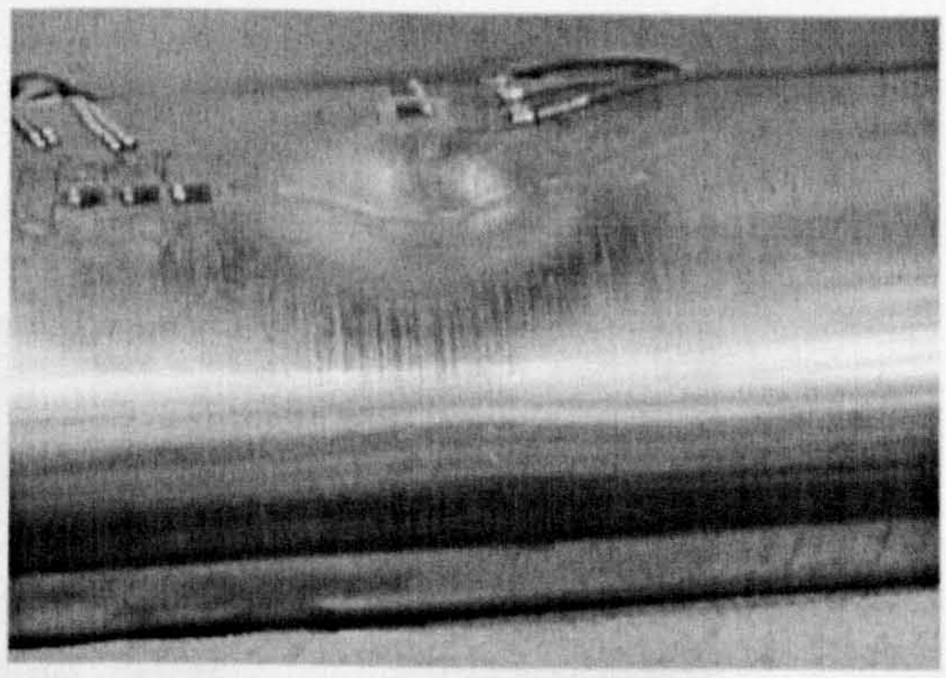

(a1) SP6

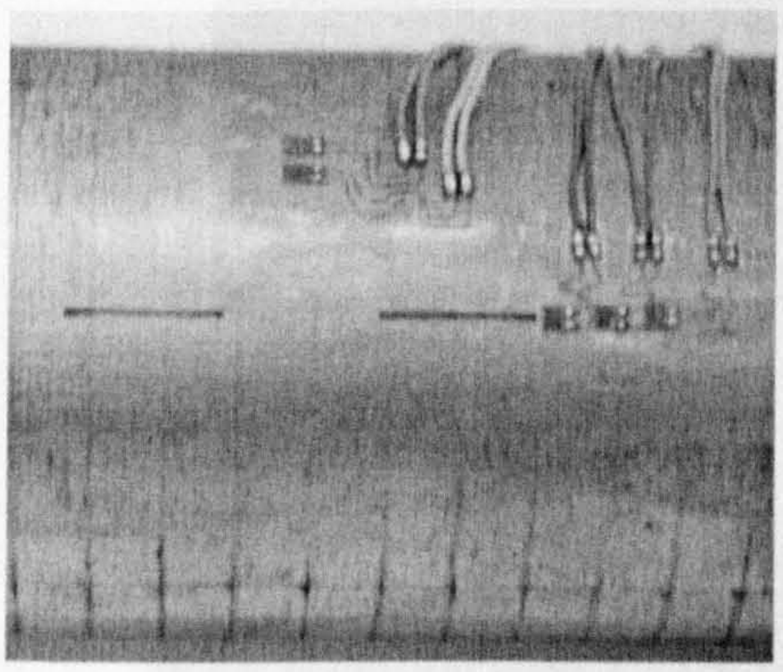

(b) SP5

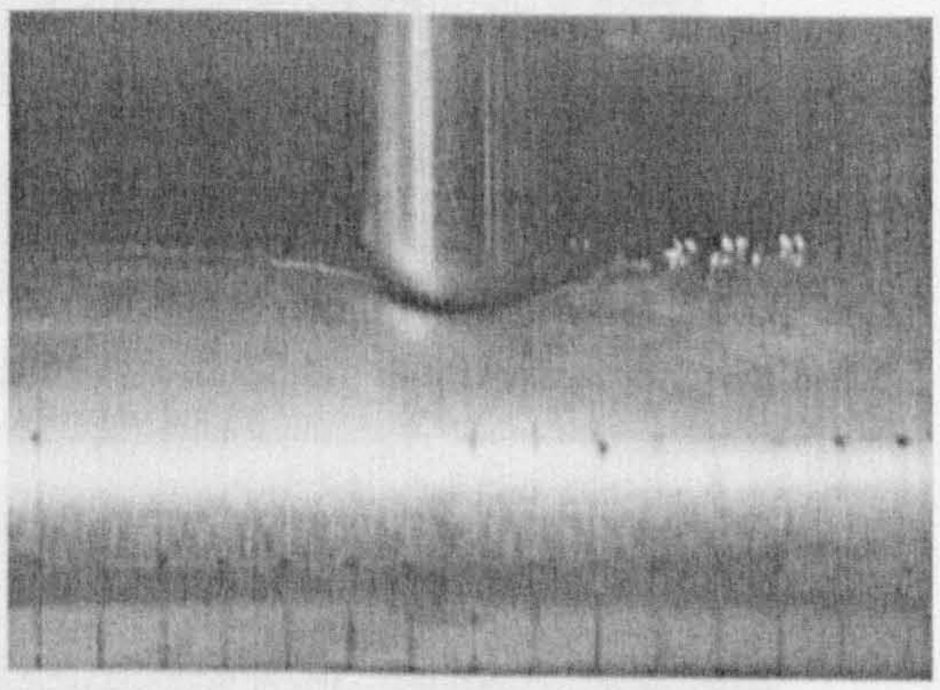

(b1) SP5

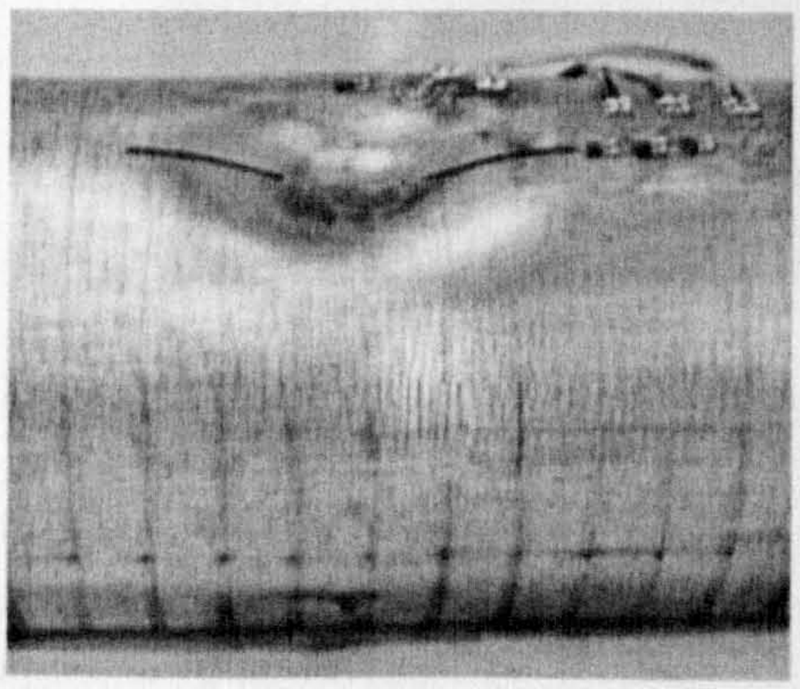

(c) SP5

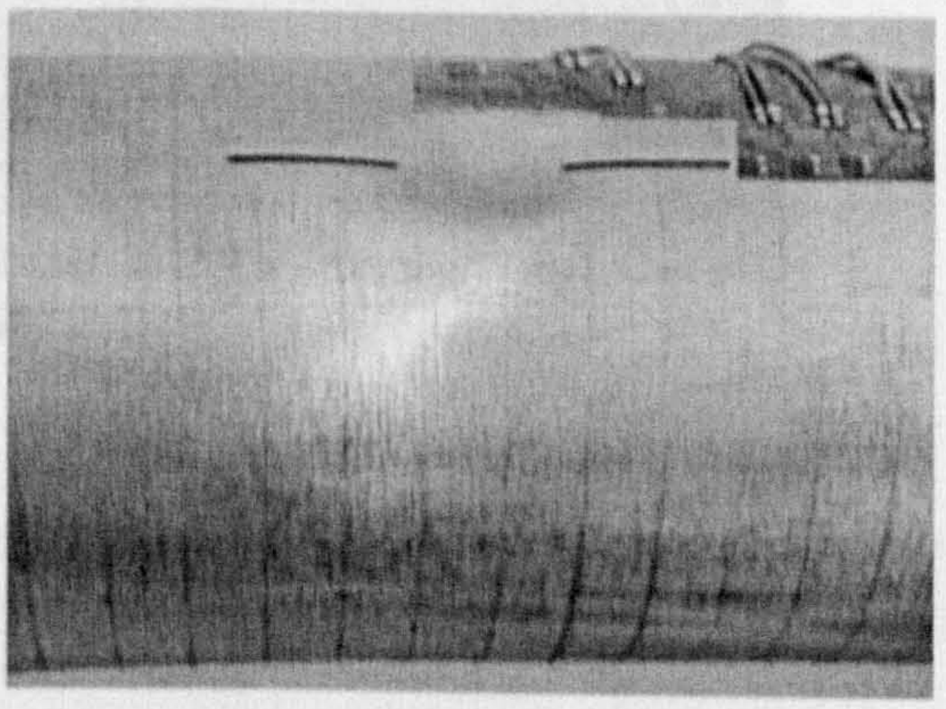

(c1) SP5

Figure 7.17: Photographs of gouged pipes at different stages of experimentation.

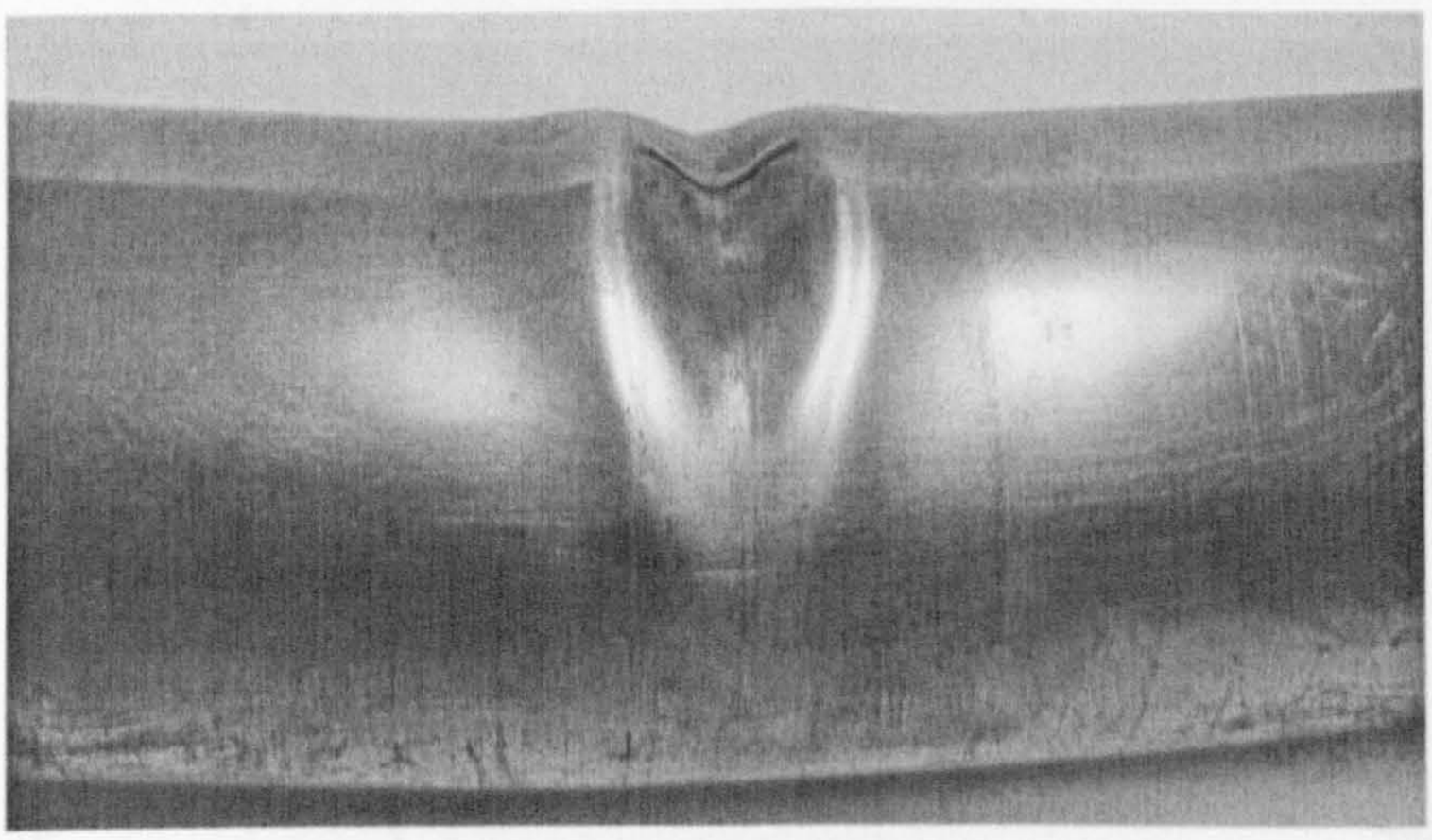

(a) SP4

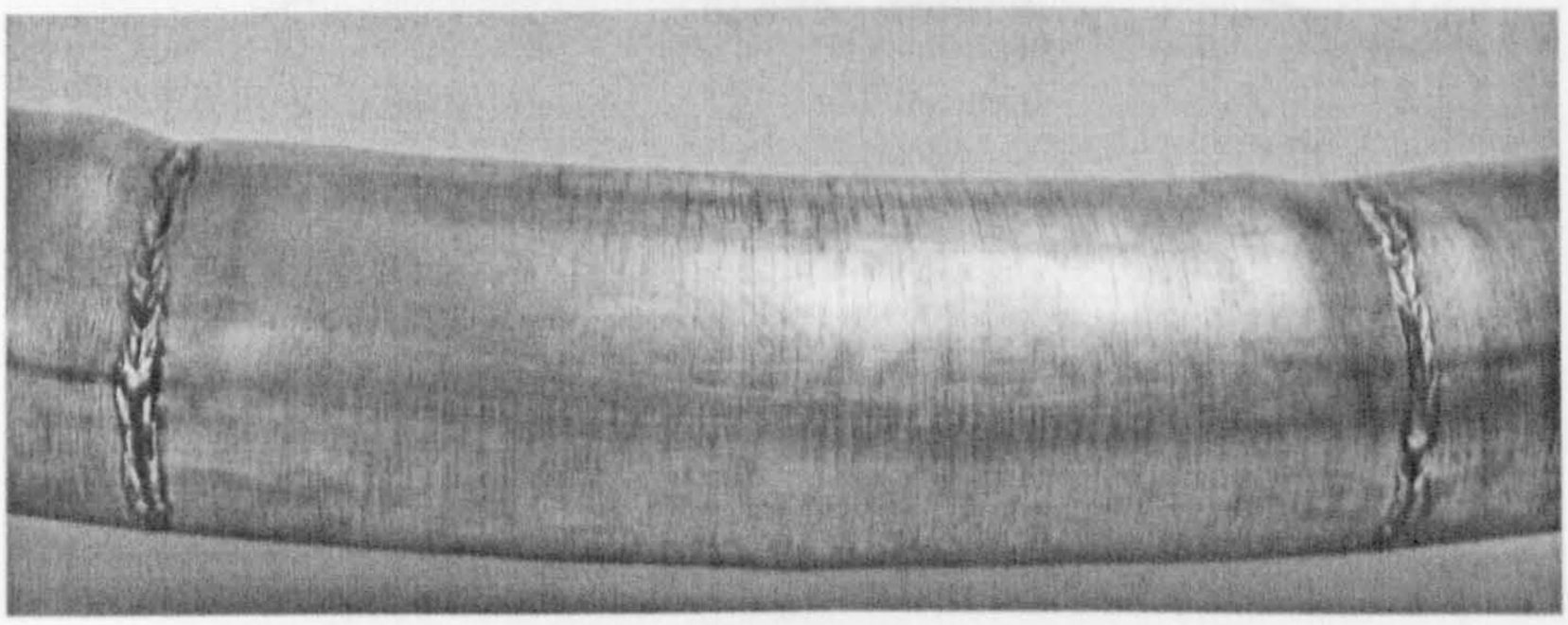

(b) SP5

Figure 7.18: Photographs depicting bulges in pipes at the maximum, collapsing bending moments for cases of: closing bending moment - Fig. (7.18a), and for collapsing opening bending moment - Fig. (7.18b).

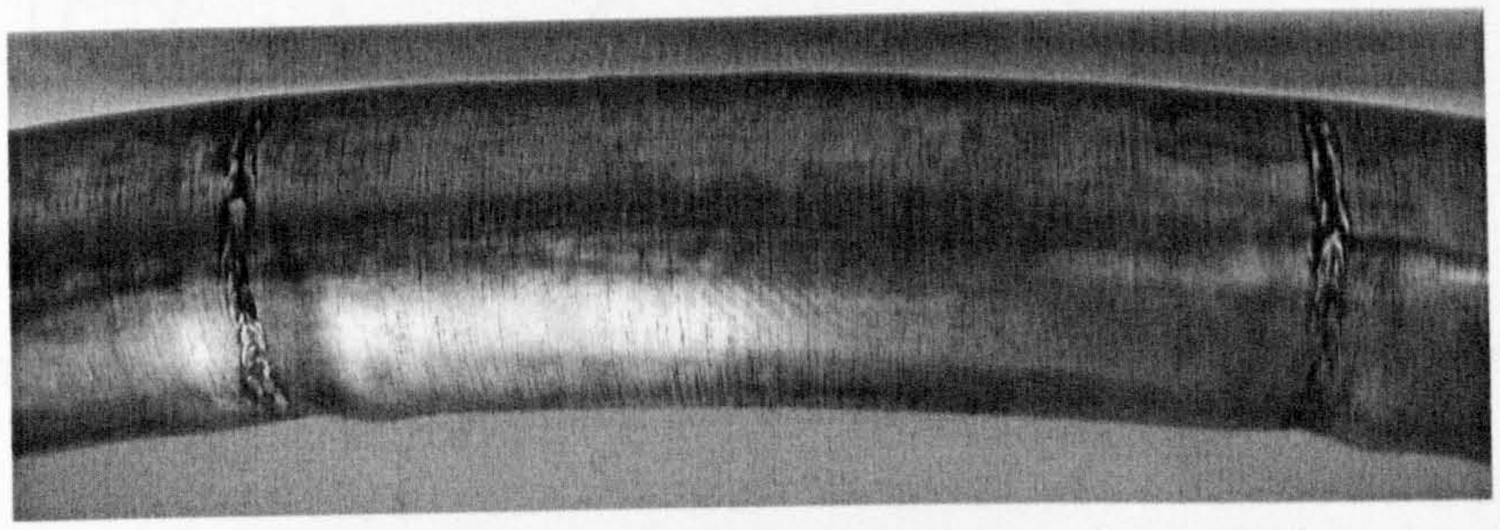

(a) SP5

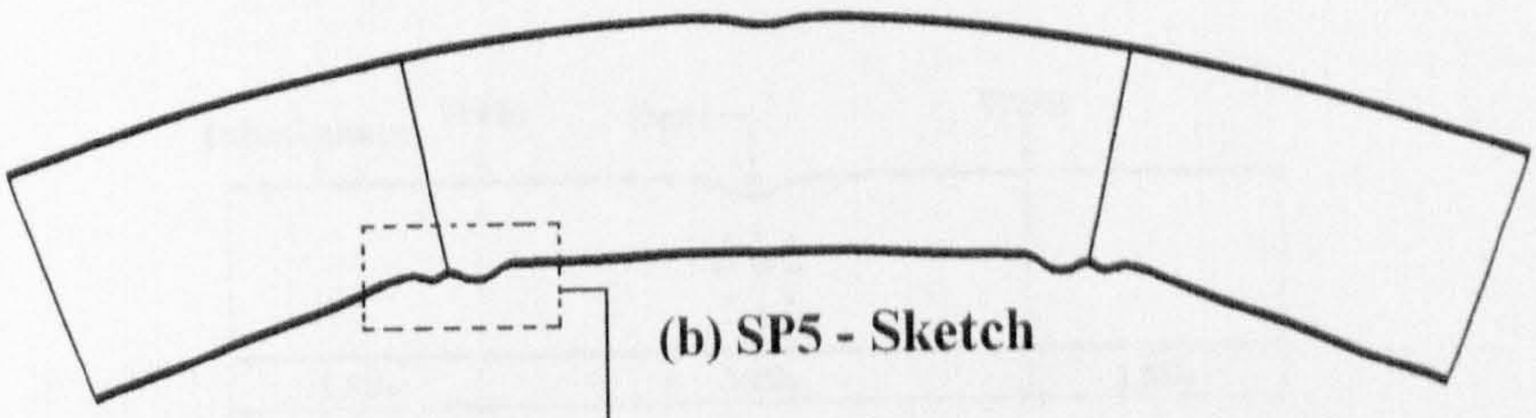

(b) SP5 - Sketch

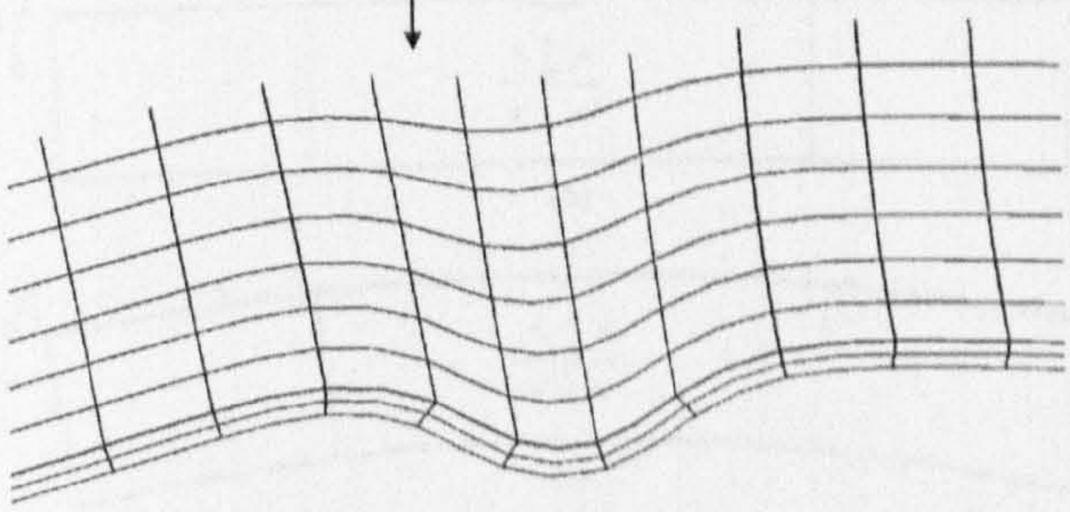

(c) FE

Figure 7.19: Comparison of the experimental and FE buckling/bulging modes at the collapsing bending moment.

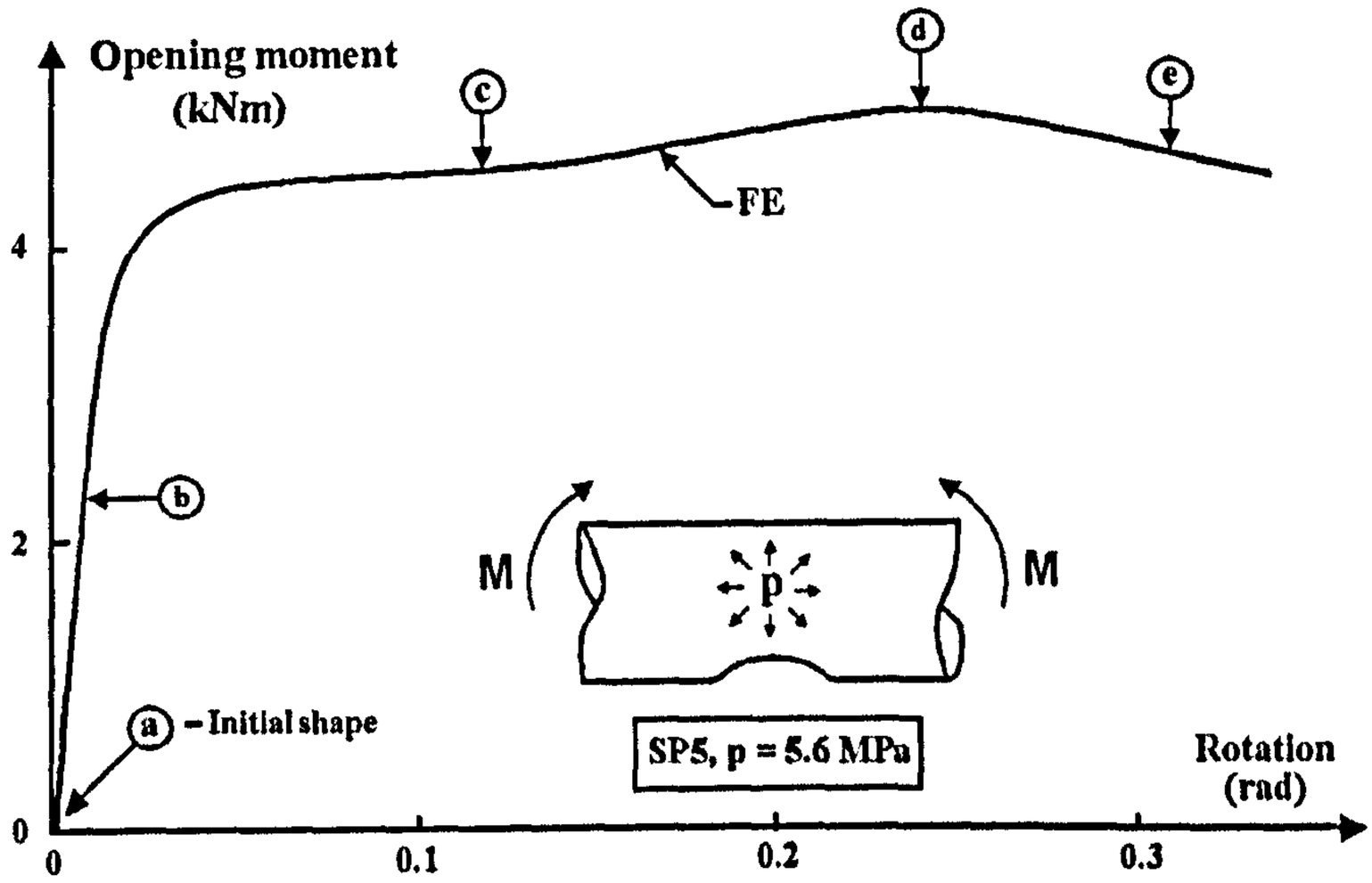

Figure 7.20: The bending moment versus pipe's end rotation for SP5. Also, $p = 5.6\ MPa$, $\frac{2L}{D_o} = 6.0$, and $(\frac{\delta}{D_o})_R = 0.1199$

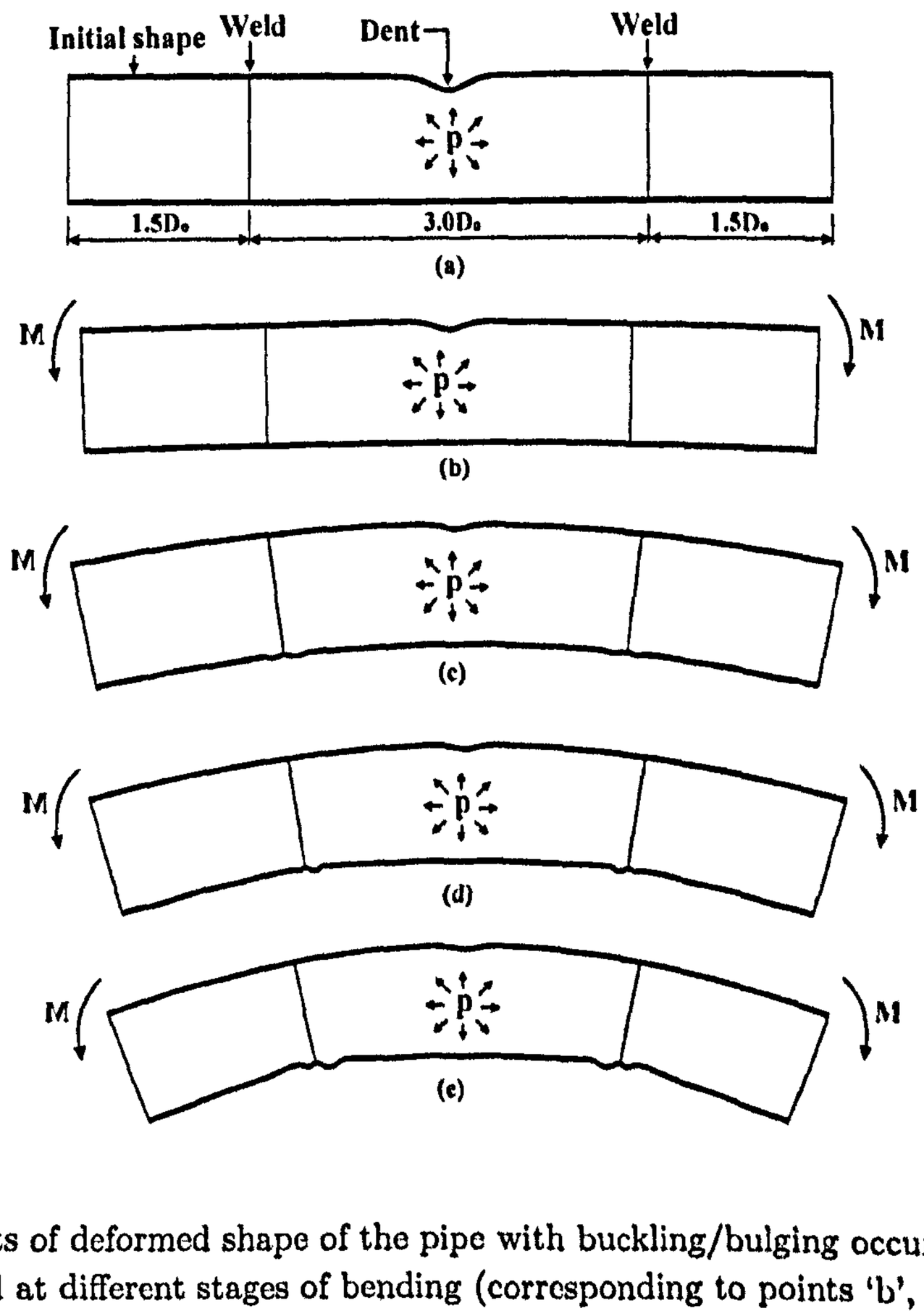

Figure 7.21: Plots of deformed shape of the pipe with buckling/bulging occurring on the compression side and at different stages of bending (corresponding to points 'b', 'c', 'd', and 'e' in Fig. (7.20)).

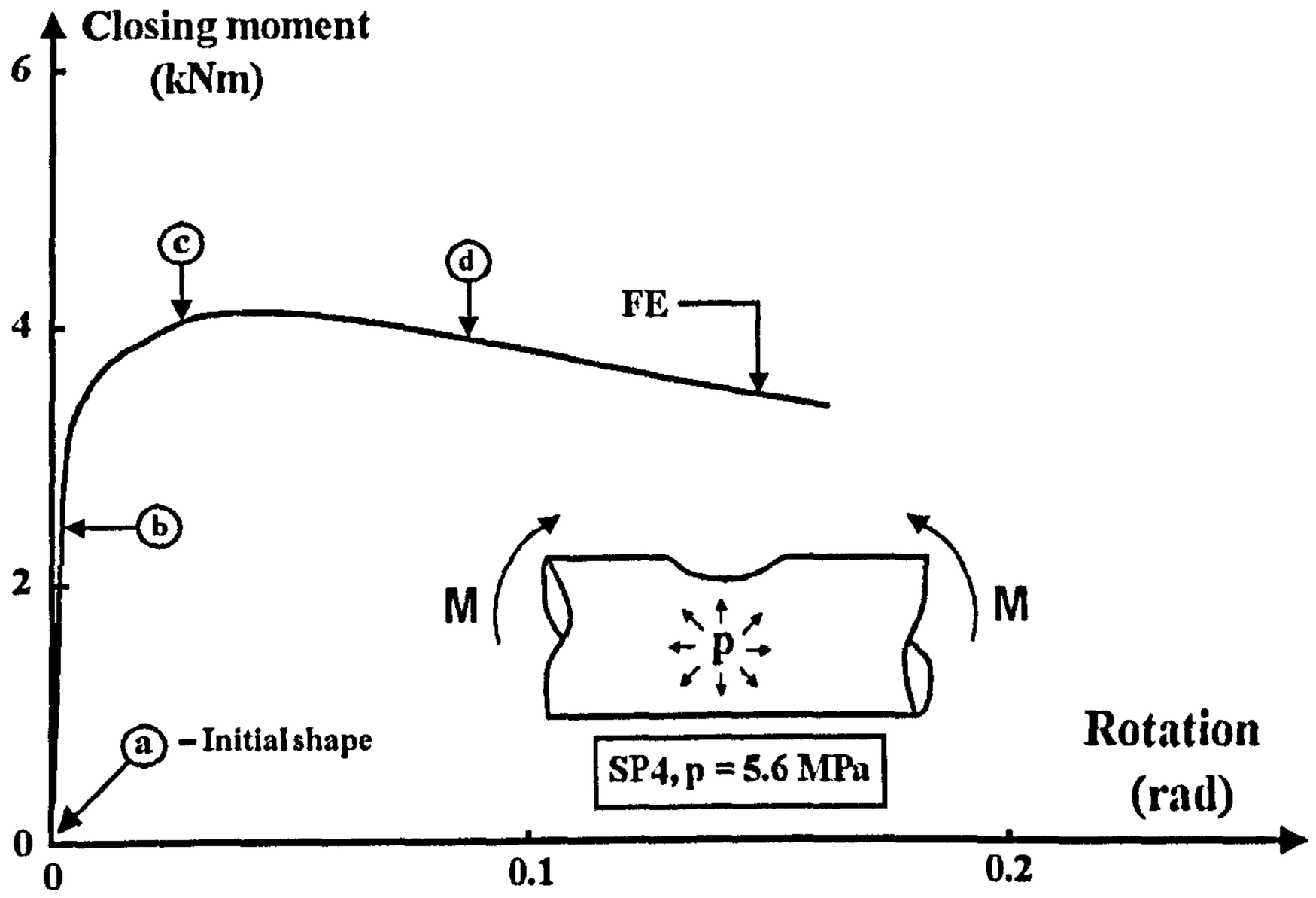

Figure 7.22: Plot of closing bending moment versus pipe's end rotation for SP4. Also, $p = 5.6\ MPa$, $\frac{2L}{D_o} = 6.0$, and $(\frac{\delta}{D_o})_R = 0.092$.

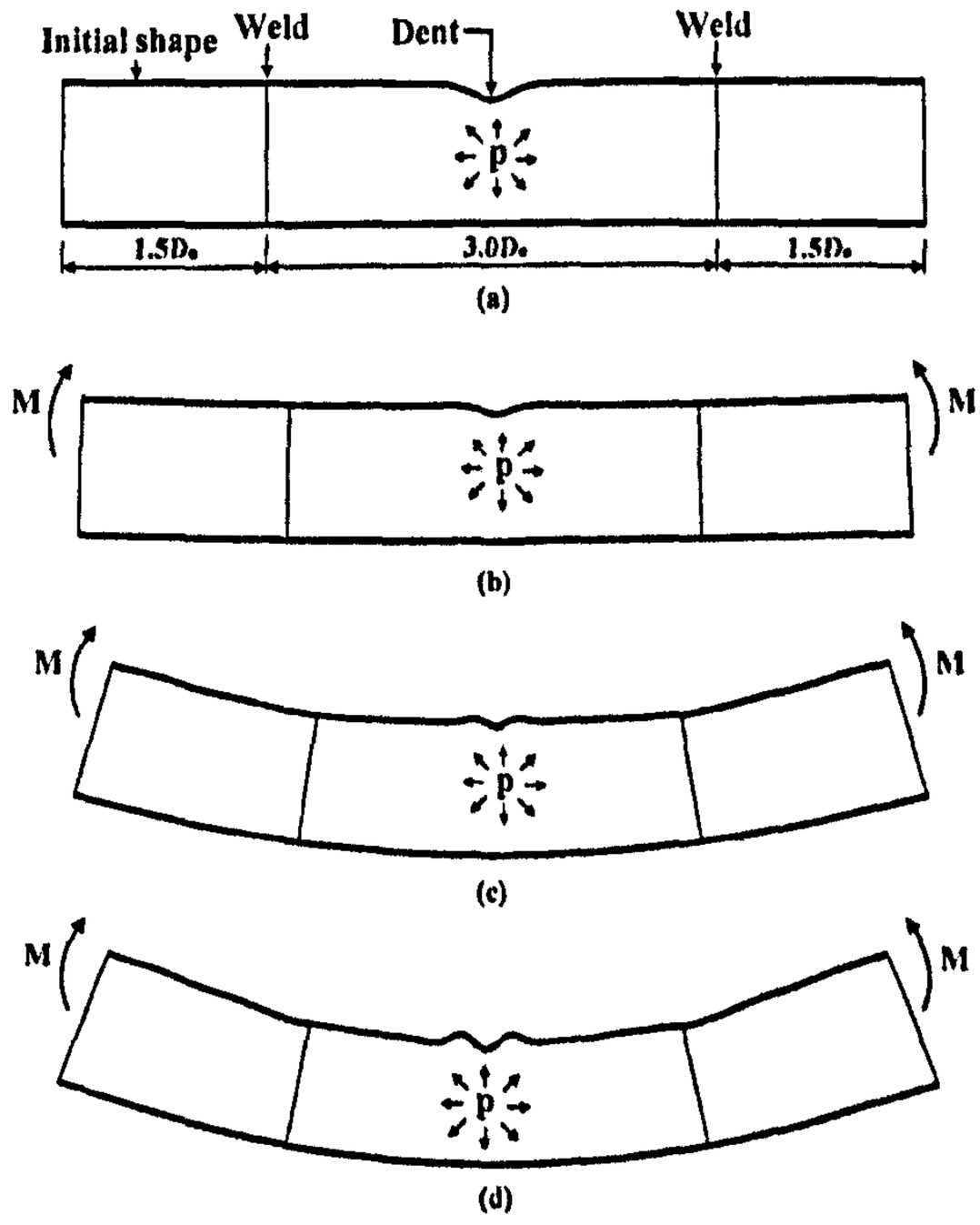

Figure 7.23: Plots of deformed shape of the pipe with buckling/bulging occurring on the compression side, and at different stages of closing bending corresponding to points 'b', 'c', and 'd' in Fig. (7.22).

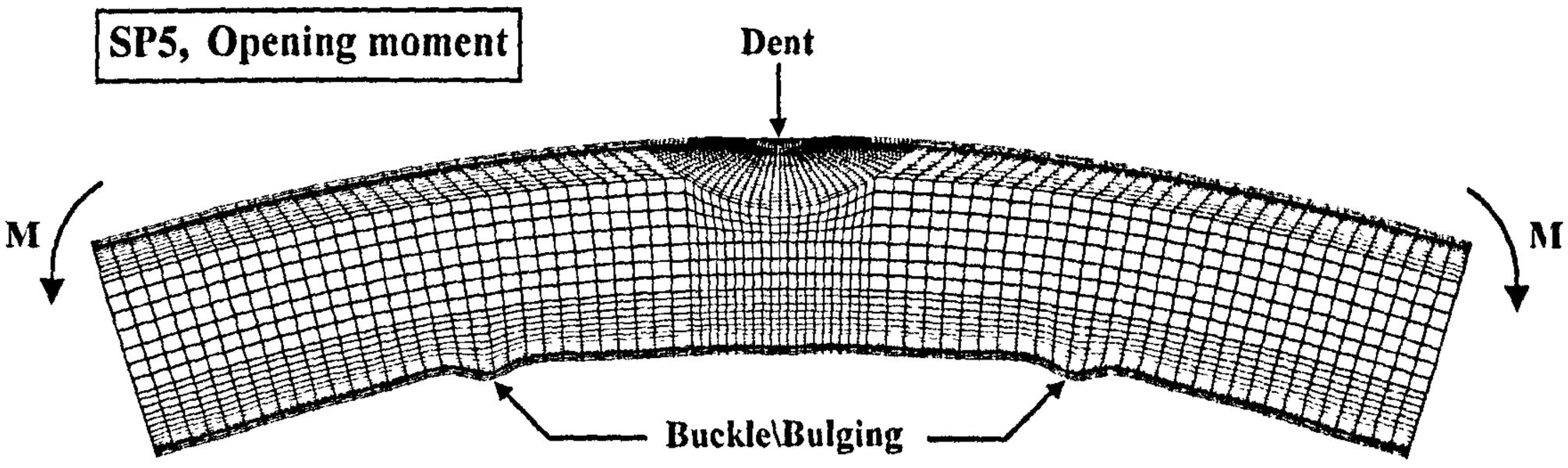

Figure 7.24: View of the bent pipe. FE shape shows buckling/bulging occurring on the compression side of the pipe when subjected to opening bending moment - see photograph in Figure (7.18b).

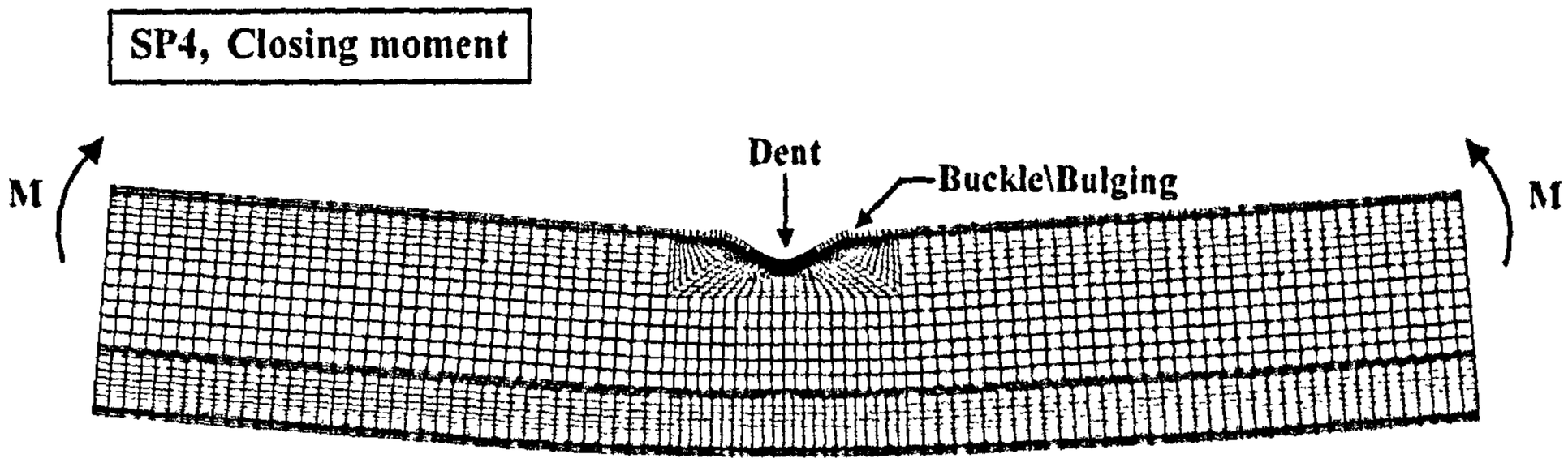

Figure 7.25: View of the bent pipe. FE shape shows buckling/bulging occurring on the compression side of the pipe when subjected to closing bending moment - see photograph in Figure (7.18a).

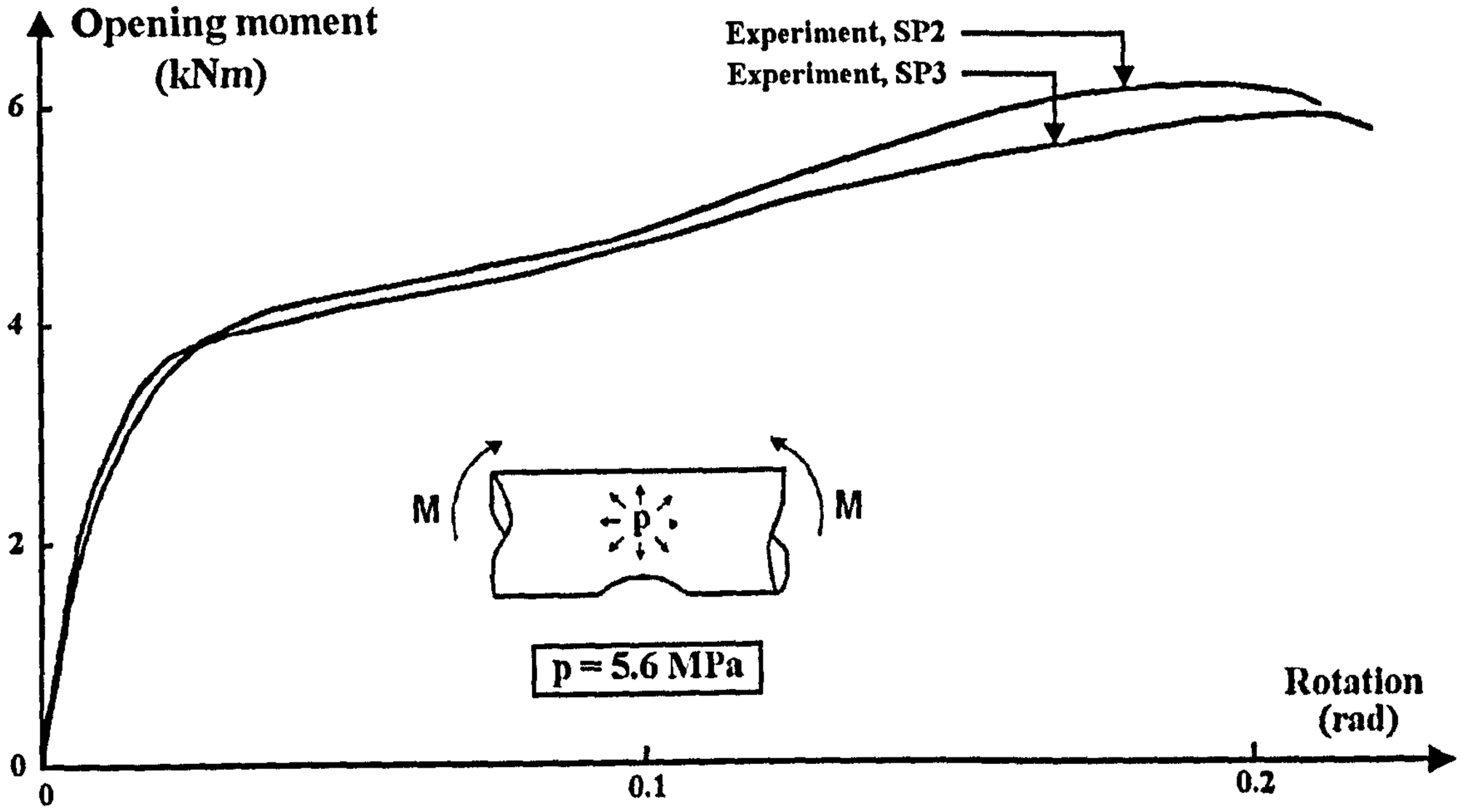

Figure 7.26: The repeatability of the test for SP2 and SP3. Also, $(\frac{\delta}{D_o})_R = 0.1199$ for SP2, and $(\frac{\delta}{D_o})_R = 0.1177$ for SP3. The internal pressure during bending was $p = 5.6\ MPa$, and $\frac{2L}{D_o} = 6.0$.

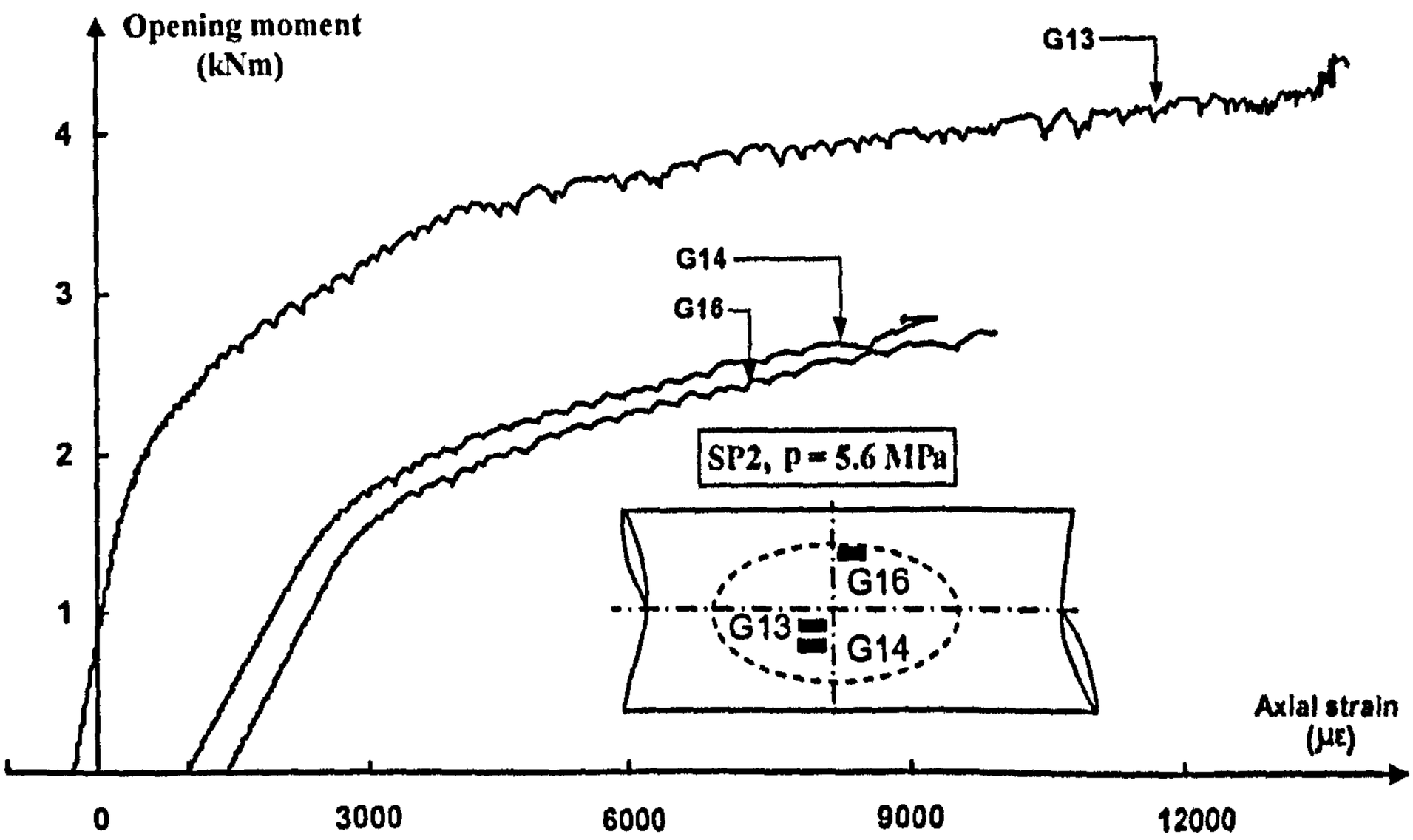

Figure 7.27: Opening bending moment versus axial strain in SP2 (gauges G13, G14, and G16). Also, $\frac{2L}{D_o} = 6.0$, and $p = 5.6\ MPa$.

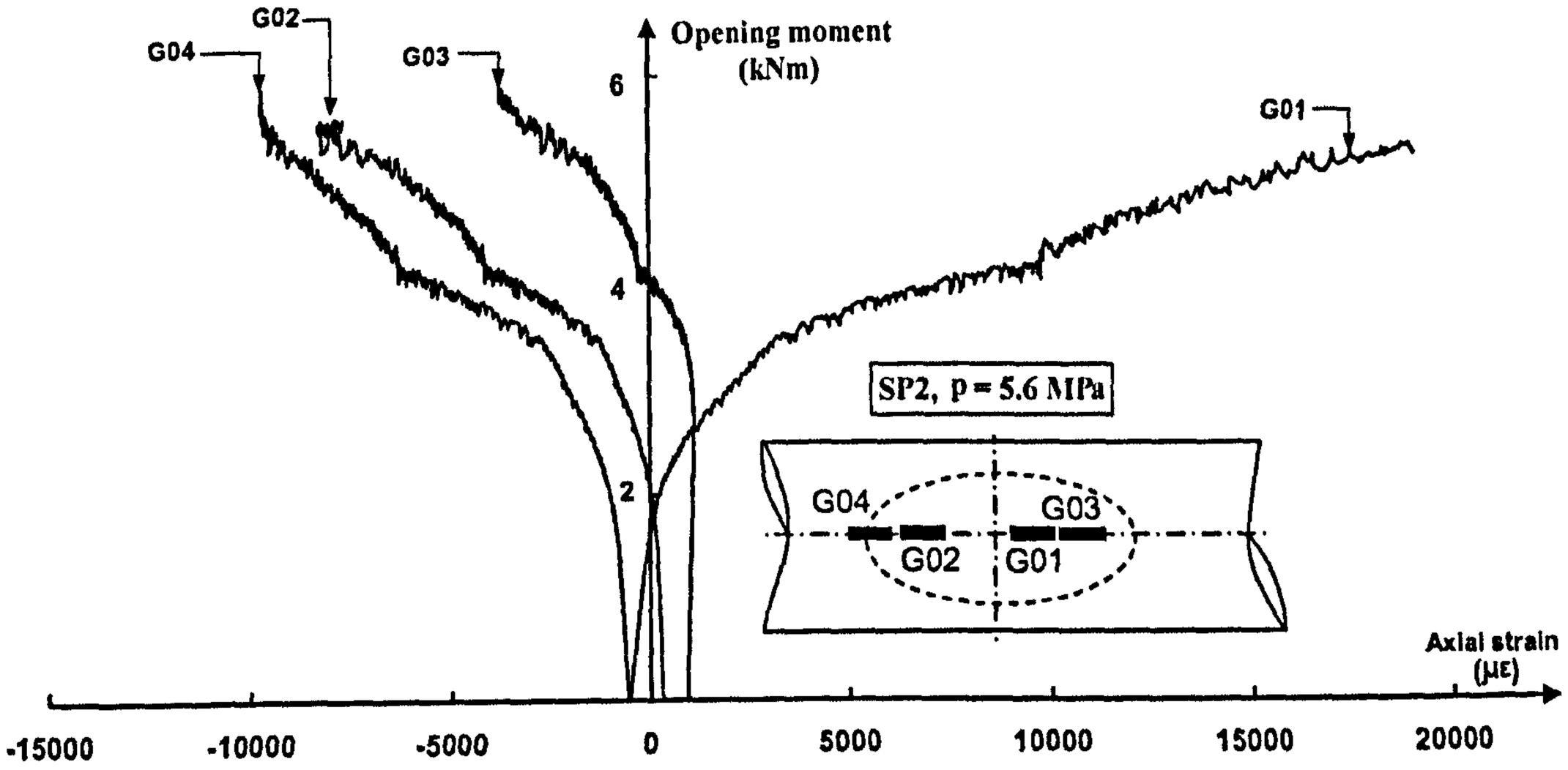

Figure 7.28: Open bending moment versus axial strain in SP2 (gauges G01, G02, G03, and G04). Also, $\frac{2L}{D_o} = 6.0$, and $p = 5.6\ MPa$.

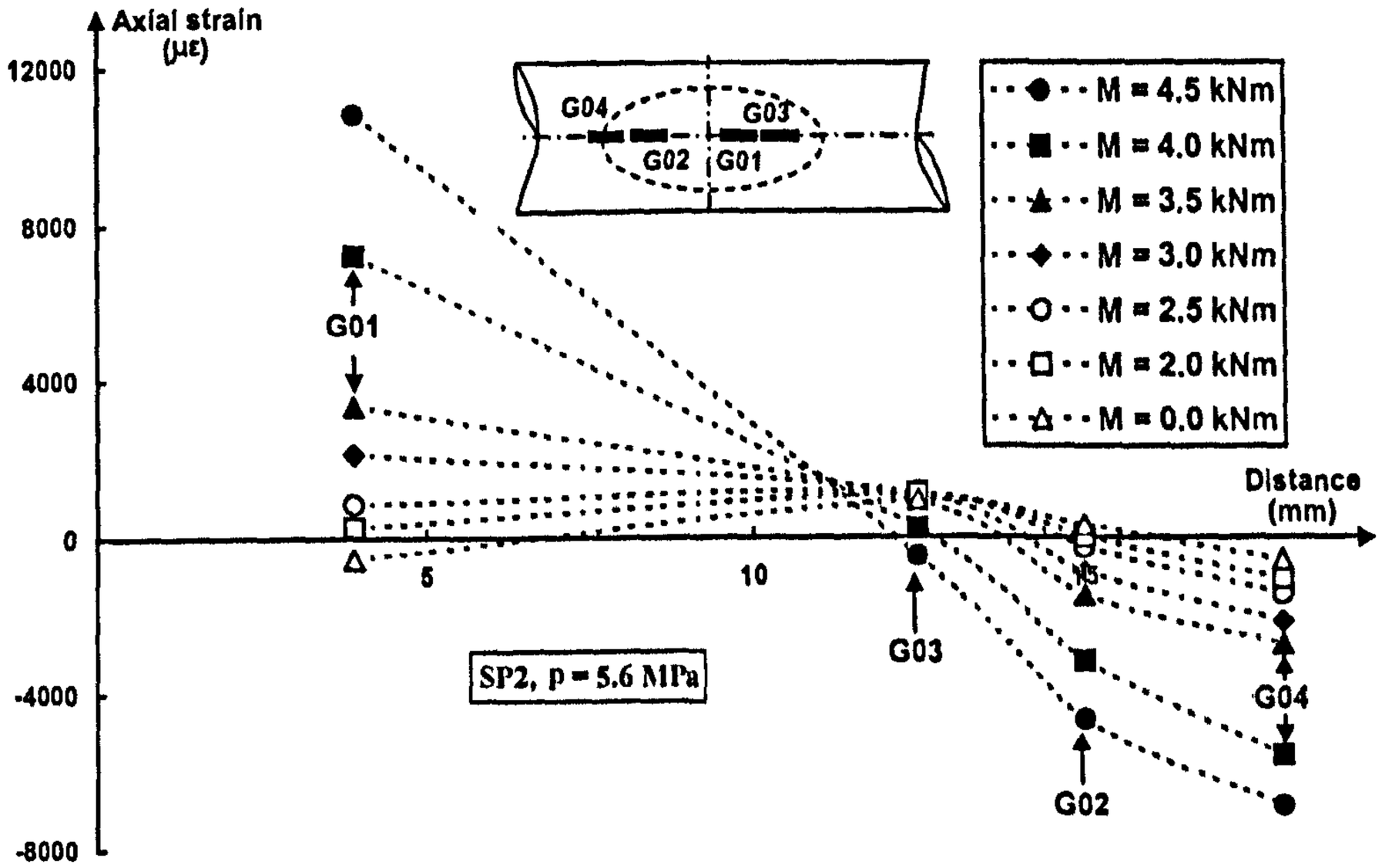

Figure 7.29: Distribution of axial strain in dented specimen, SP2, as sketched in the figure. The specimen has no gouge and the dashed line is the dented region. Also, $(\frac{\delta}{D_o})_R = 0.1199$, $p = 5.6\ MPa$, and $\frac{2L}{D_o} = 6.0$.

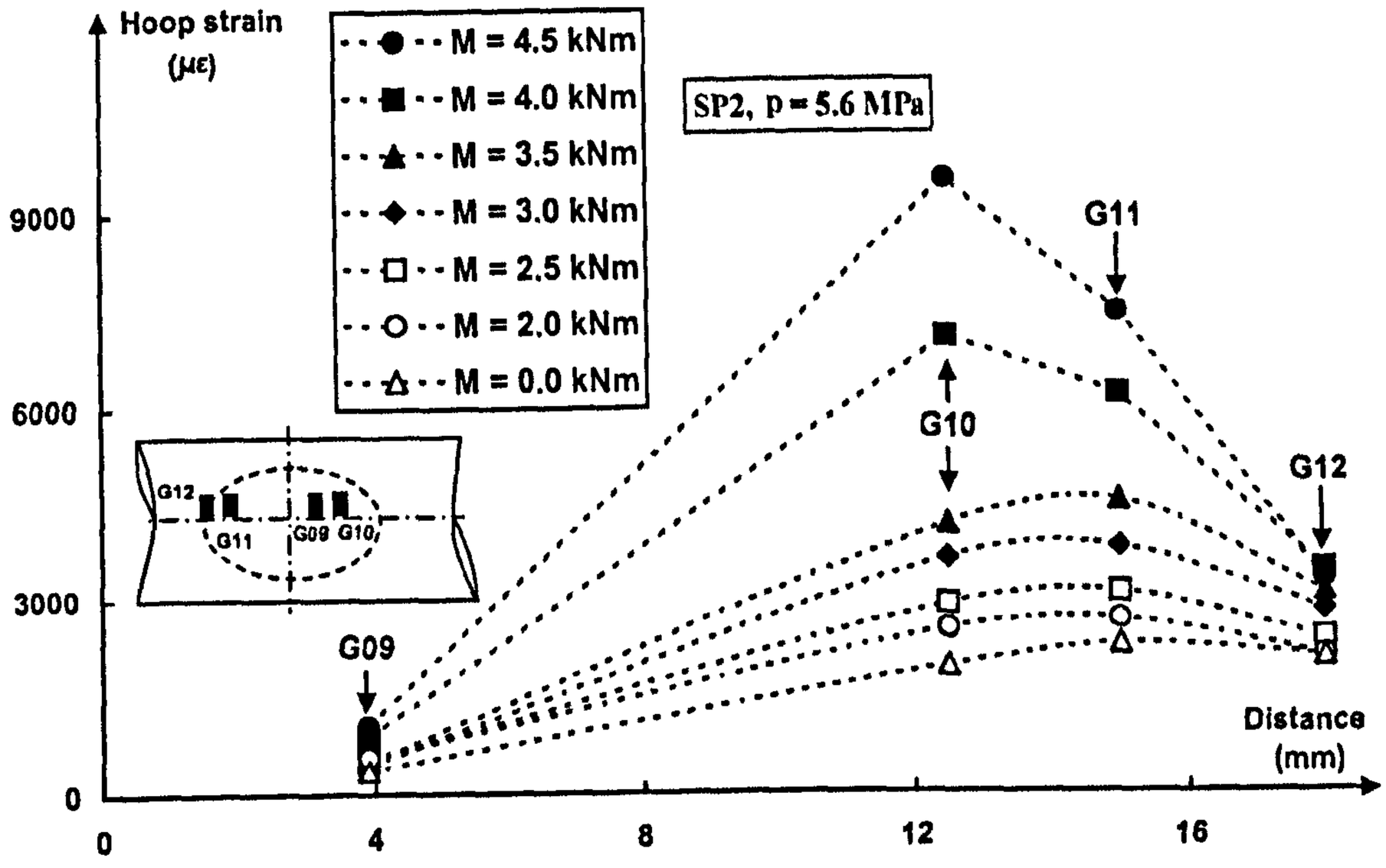

Figure 7.30: Distribution of hoop strain in dented specimen, SP2, as sketched in the figure. The specimen has no gouge and the dashed line is the dented region. Also, $(\frac{\delta}{D_o})_R = 0.1199$, $p = 5.6\ MPa$, and $\frac{2L}{D_o} = 6.0$.

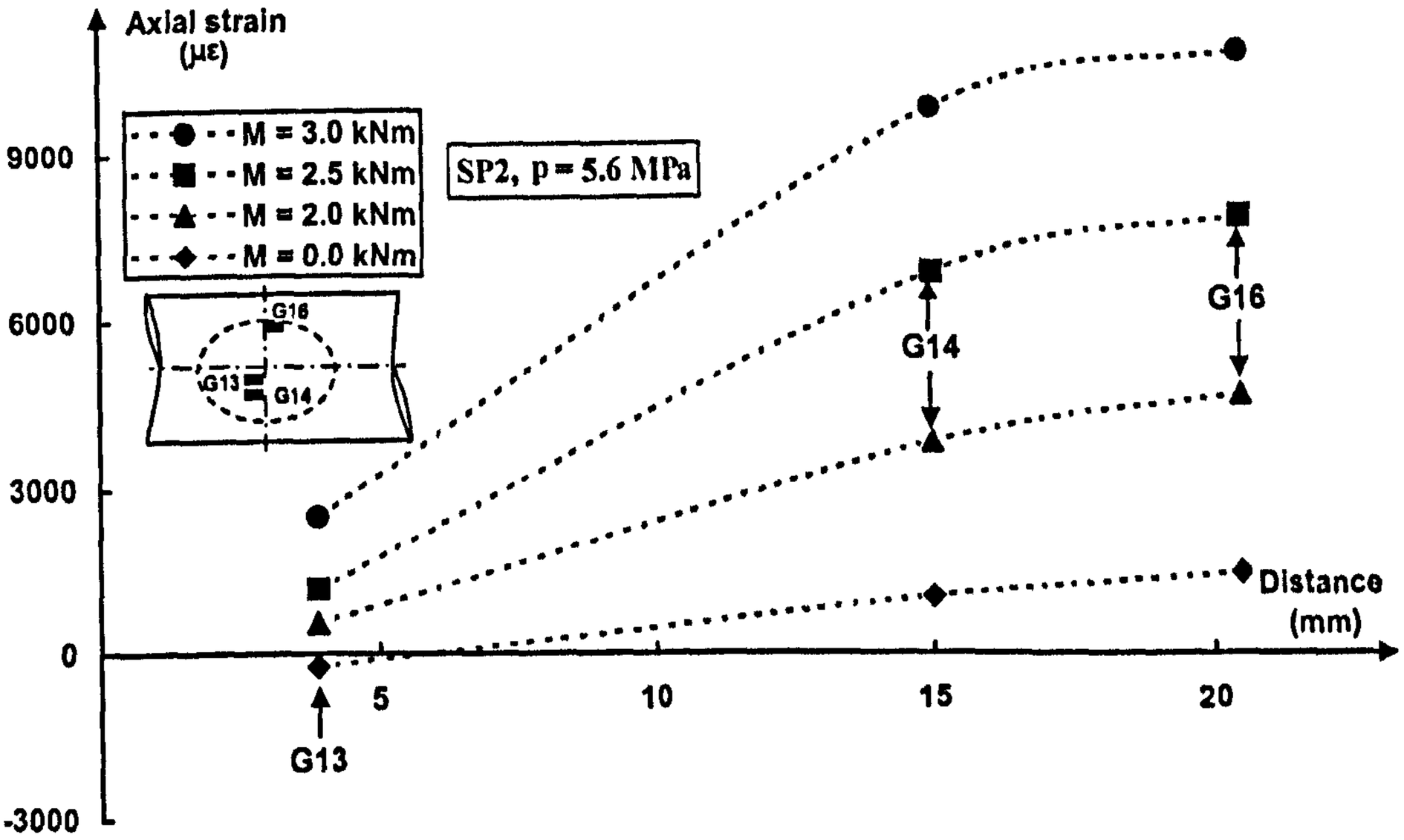

Figure 7.31: Distribution of axial strain in circumferential direction in dented specimen, SP2, as sketched in the figure. The specimen has no gouge and the dashed line is the dented region. Also, $(\frac{\delta}{D_o})_R = 0.1199$, $p = 5.6\ MPa$, and $\frac{2L}{D_o} = 6.0$.

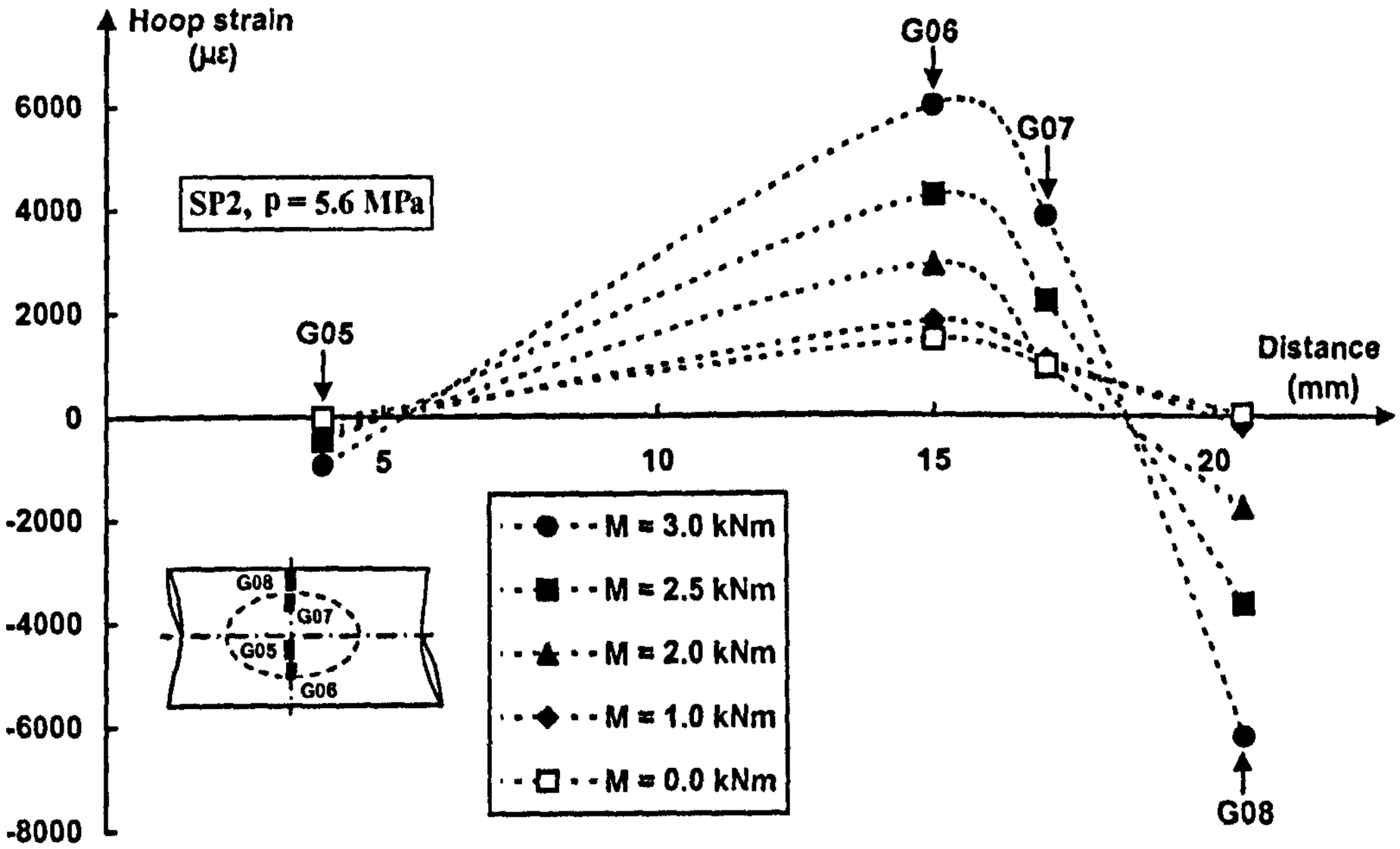

Figure 7.32: Distribution of hoop strain in circumferential direction in dented specimen, SP2, as sketched in the figure. The specimen has no gouge and the dashed line is the dented region. Also, $(\frac{\delta}{D_o})_R = 0.1199$, $p = 5.6\ MPa$, and $\frac{2L}{D_o} = 6.0$.

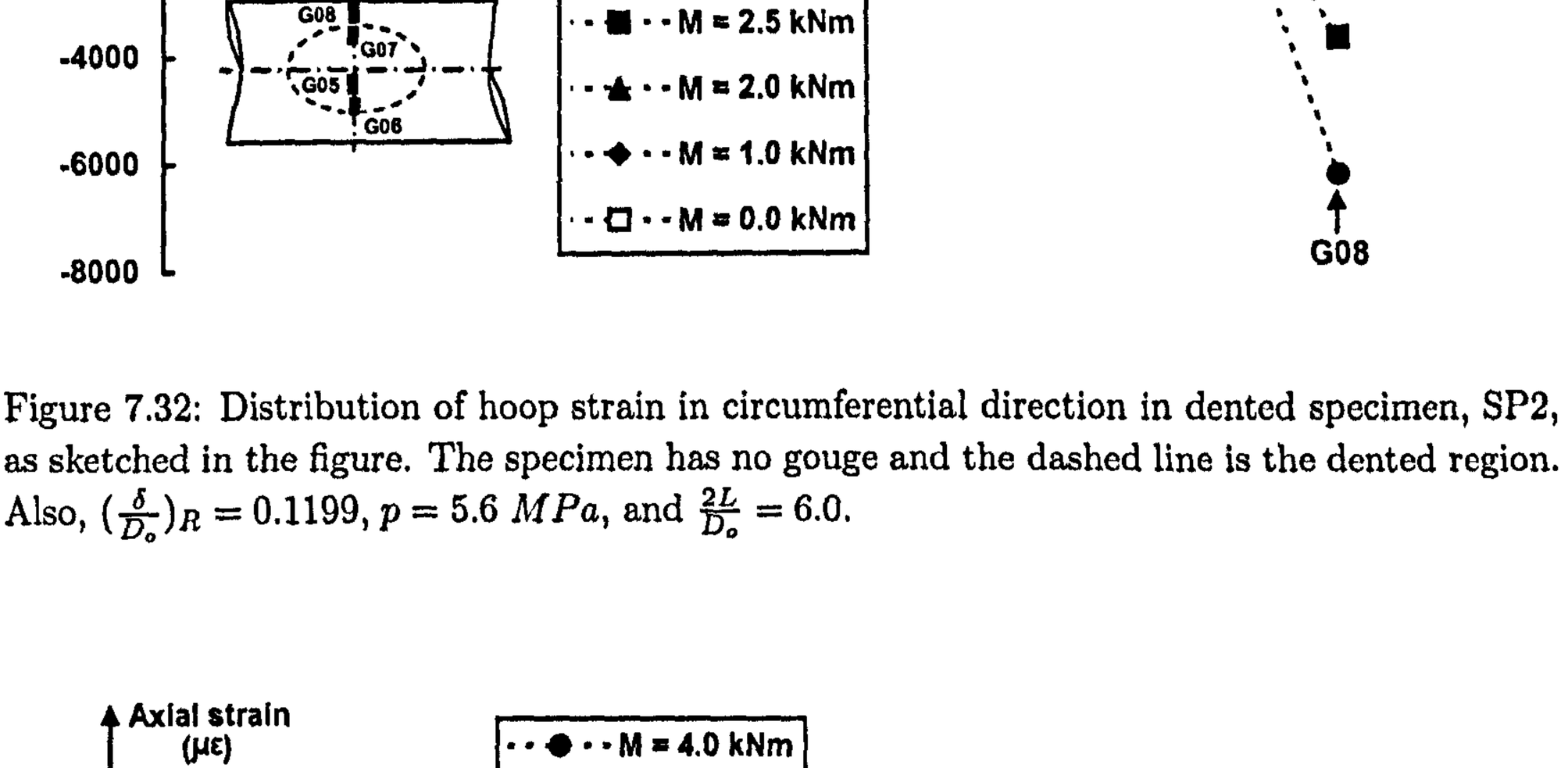

Figure 7.33: Distribution of axial strain in dented specimen, SP3, as sketched in the figure. The specimen has no gouge and the dashed line is the dented region. Also, $(\frac{\delta}{D_o})_R = 0.1177$, $p = 5.6\ MPa$, and $\frac{2L}{D_o} = 6.0$.

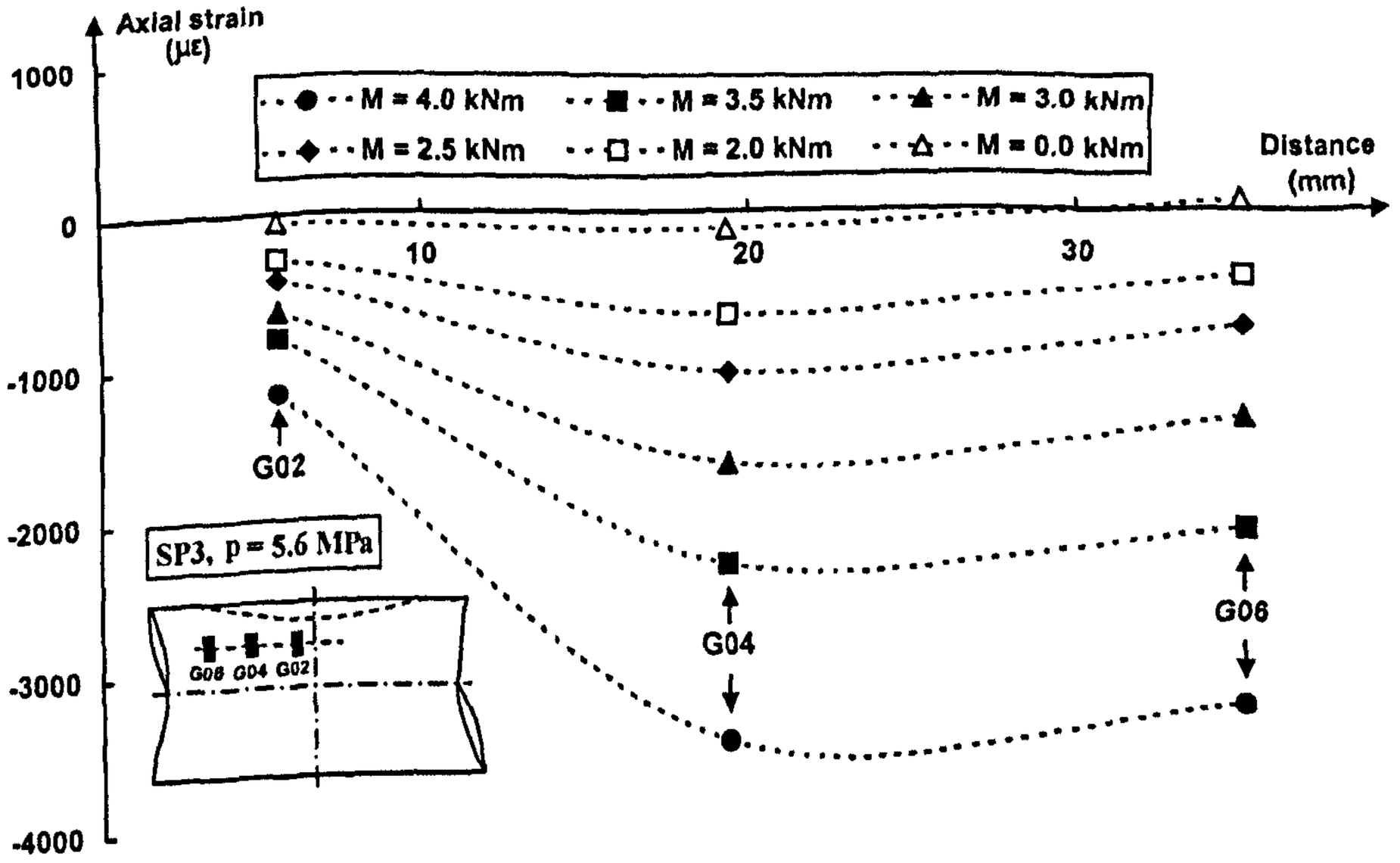

Figure 7.34: Distribution of hoop strain in dented specimen, SP3, as sketched in the figure. The specimen has no gouge and the dashed line is the dented region. Also, $(\frac{\delta}{D_o})_R = 0.1177$, $p = 5.6\ MPa$ and $\frac{2L}{D_o} = 6.0$.

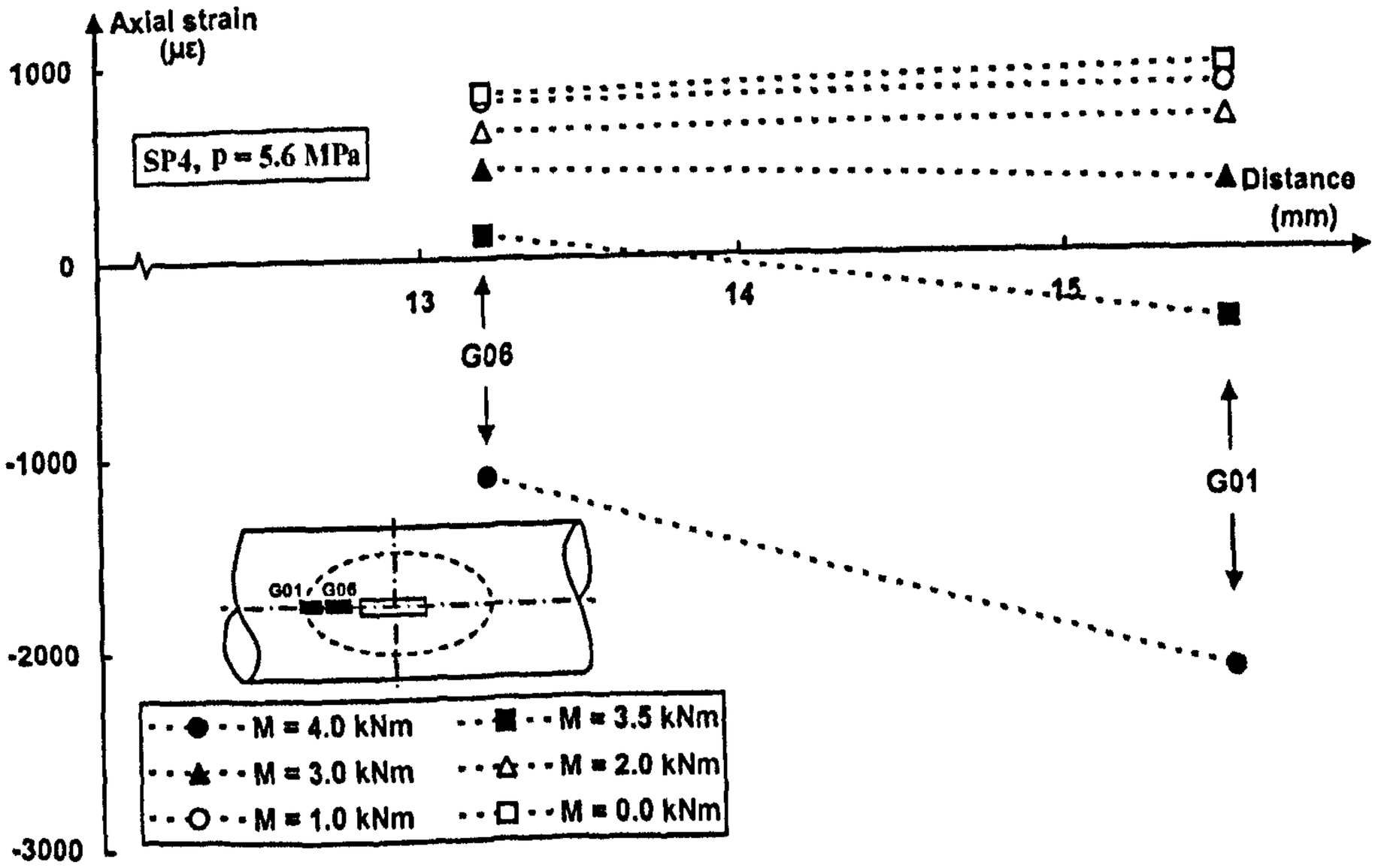

Figure 7.35: Distribution of axial strain in dented specimen, SP4, as sketched in the figure. The specimen has mid-span gouge and the dashed line is the dented region. Also, $(\frac{\delta}{D_o})_R = 0.092$, $p = 5.6\ MPa$, and $\frac{2L}{D_o} = 6.0$.

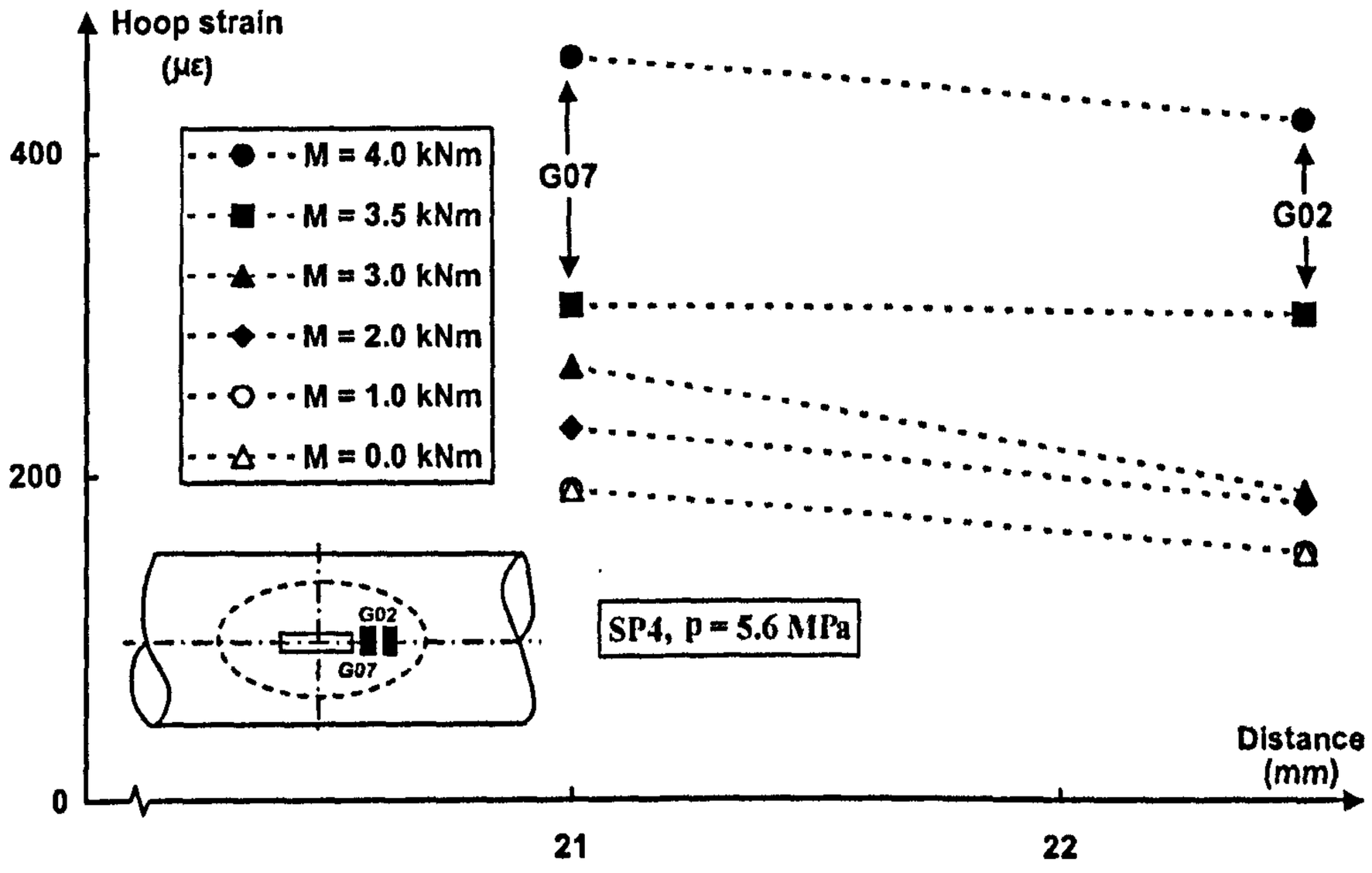

Figure 7.36: Distribution of hoop strain in hoop direction in dented specimen, SP4, as sketched in the figure. The specimen has mid-span gouge and the dashed line is the dented region. Also, $(\frac{\delta}{D_o})_R = 0.092$, $p = 5.6\ MPa$, and $\frac{2L}{D_o} = 6.0$.

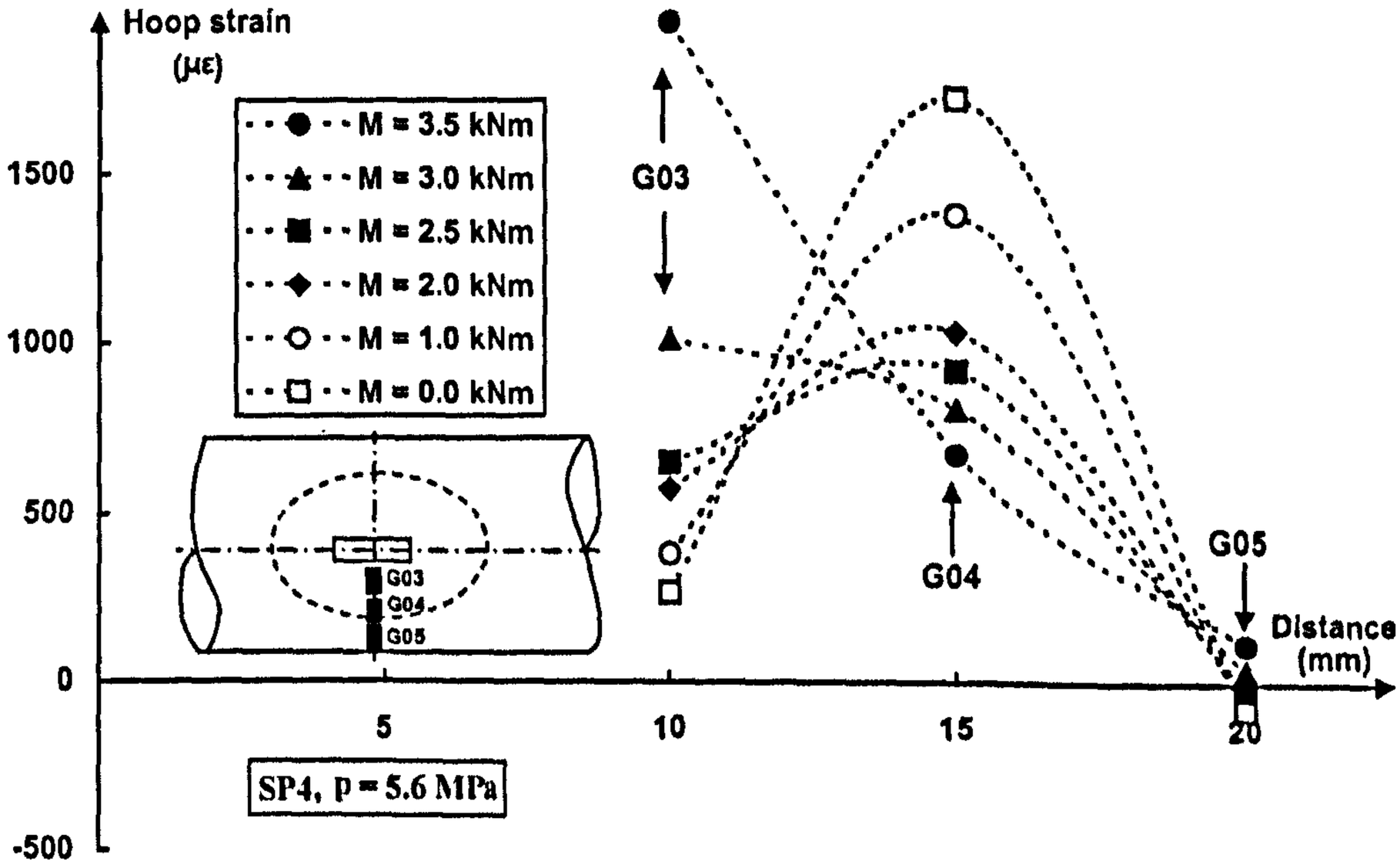

Figure 7.37: Distribution of hoop strain distribution in dented specimen, SP4, as sketched in the figure. The specimen has mid-span gouge and the dashed line is the dented region. Also, $(\frac{\delta}{D_o})_R = 0.092$, $p = 5.6\ MPa$, and $\frac{2L}{D_o} = 6.0$.

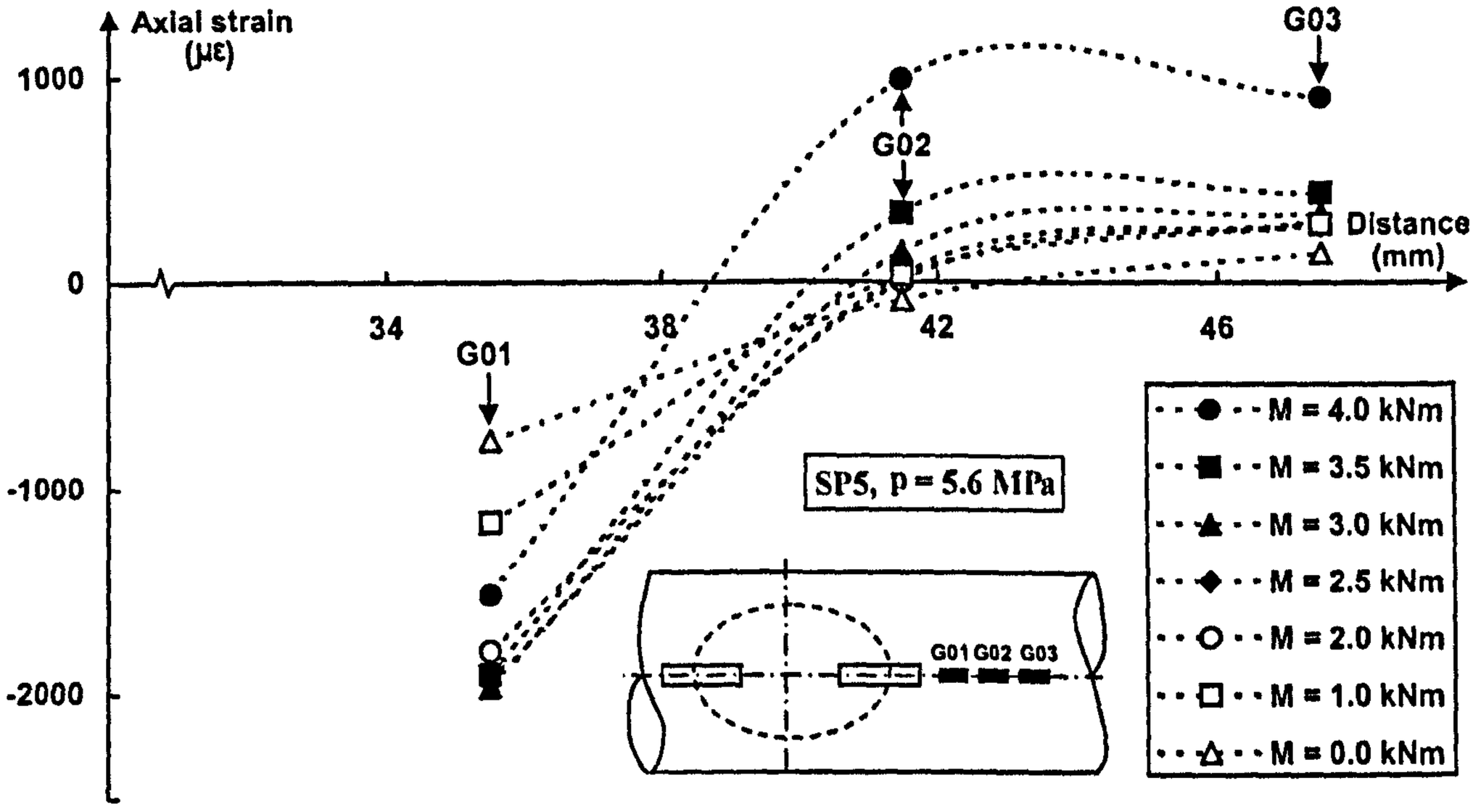

Figure 7.38: Distribution of axial strain in dented specimen, SP5, as sketched in the figure. The specimen has two axial gouges at the centre, the dashed line is the dented region. Also, $(\frac{\delta}{D_o})_R = 0.101$, $p = 5.6\ MPa$, and $\frac{2L}{D_o} = 6.0$.

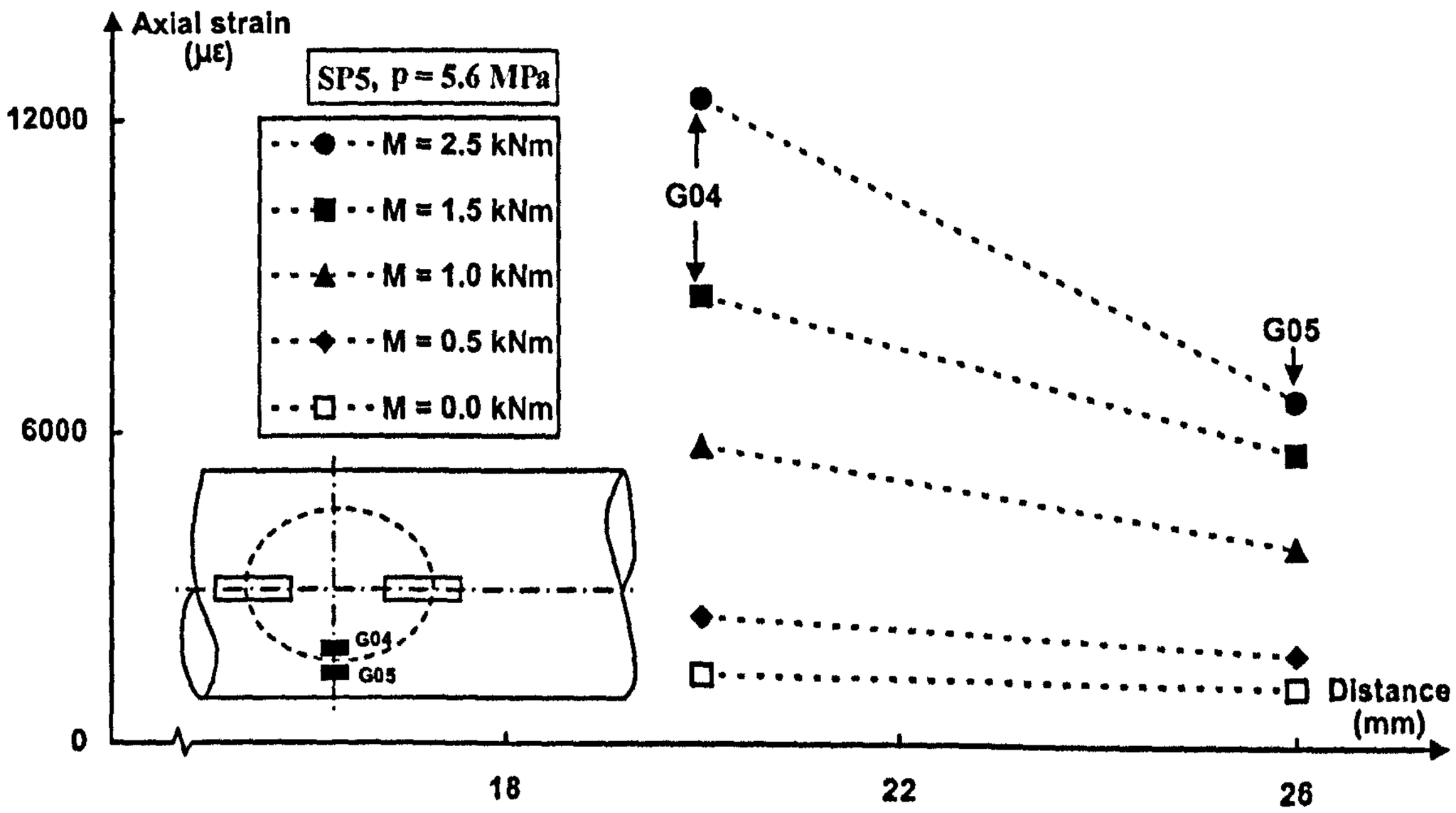

Figure 7.39: Distribution of axial strain in dented specimen, SP5, as sketched in the figure. The specimen has two axial gouges at the centre, the dashed line is the dented region, $(\frac{\delta}{D_o})_R = 0.101$, $p = 5.6\ MPa$, and $\frac{2L}{D_o} = 6.0$.

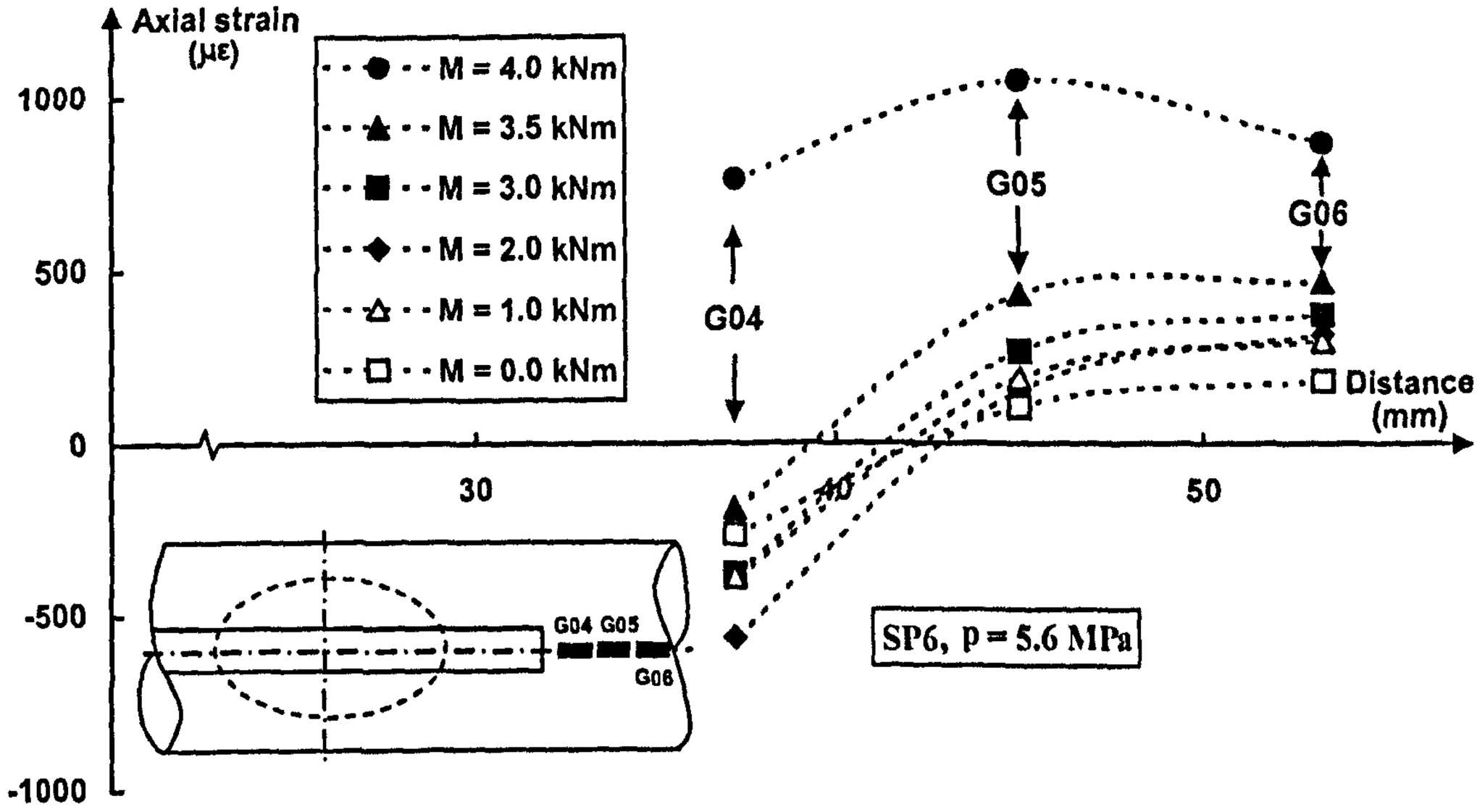

Figure 7.40: Distribution of axial strain in dented specimen, SP6, as sketched in the figure. The specimen has wider mid-span gouge, and the dashed line is the dented region. Also, $(\frac{\delta}{D_o})_R = 0.102, p = 5.6\ MPa$,and $\frac{2L}{D_o} = 6.0$.

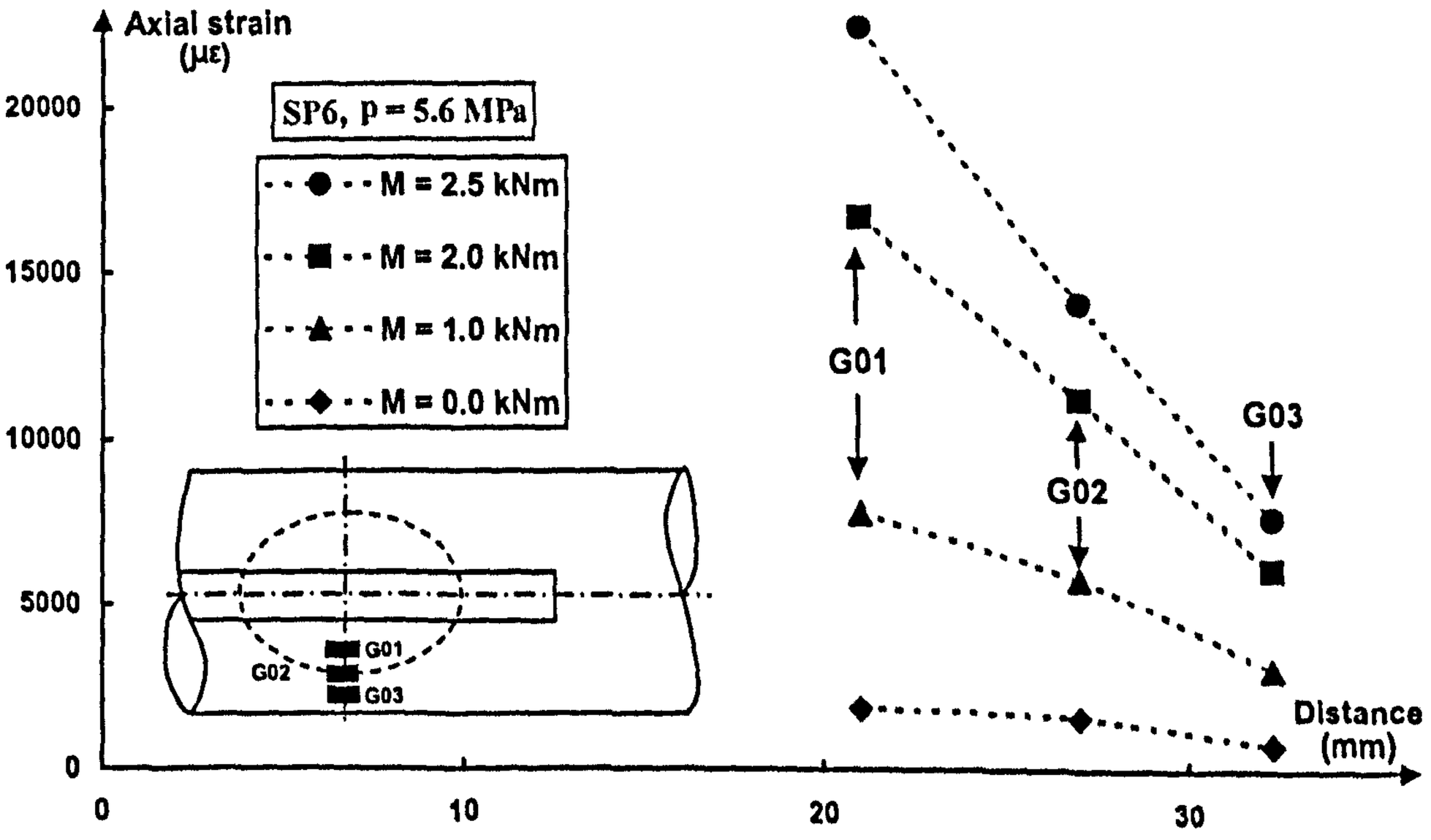

Figure 7.41: Distribution of axial strain in hoop direction in dented specimen, SP6, as sketched in the figure. The specimen has wider mid-span gouge, and the dashed line is the dented region. Also, $(\frac{\delta}{D_o})_R = 0.102, p = 5.6\ MPa$,and $\frac{2L}{D_o} = 6.0$.

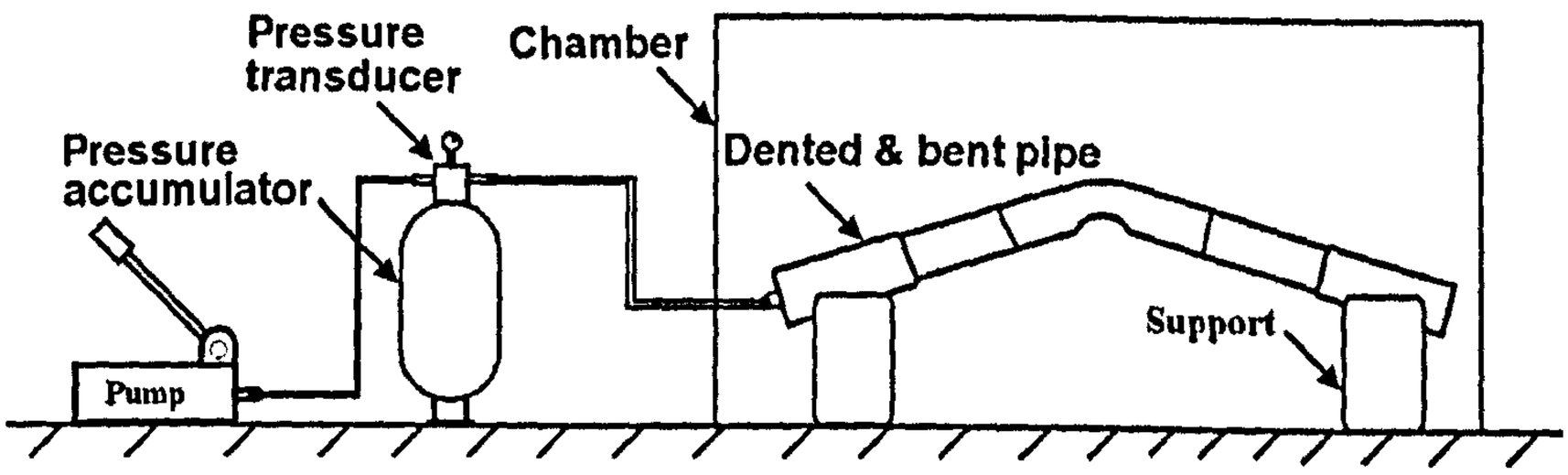

Figure 7.42: Arrangements for experimental burst test.

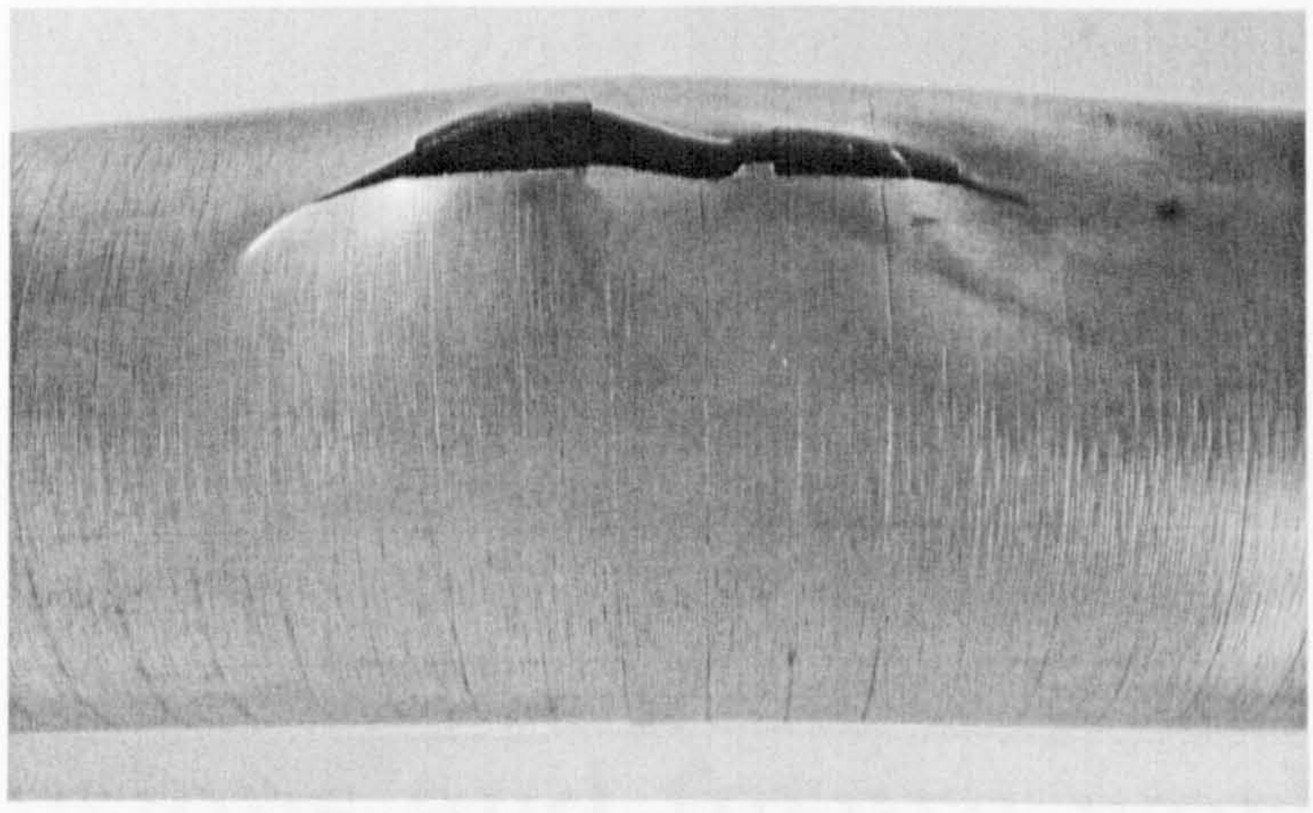

Figure 7.43: Photograph of dented and bent specimen, with two axial gouges - SP5, after burst. Burst occurred at the vicinity of gouges.

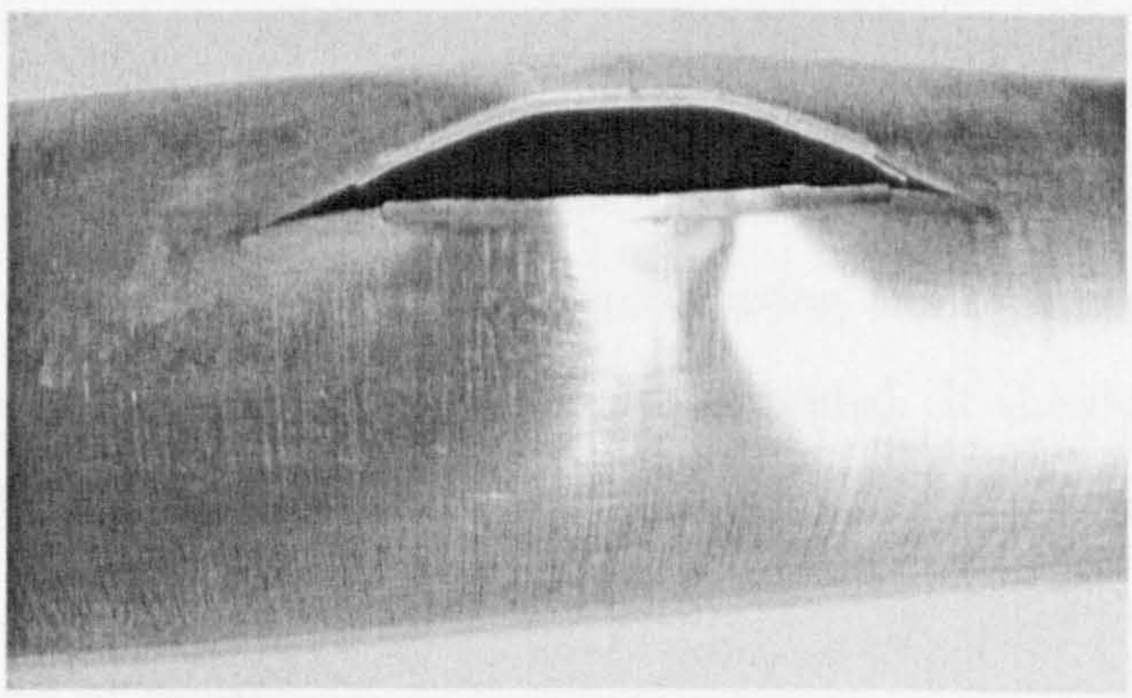

Figure 7.44: Photograph of dented and bent specimen, with a large axial gouge - SP6, after burst. Burst occurred at the vicinity of gouges.

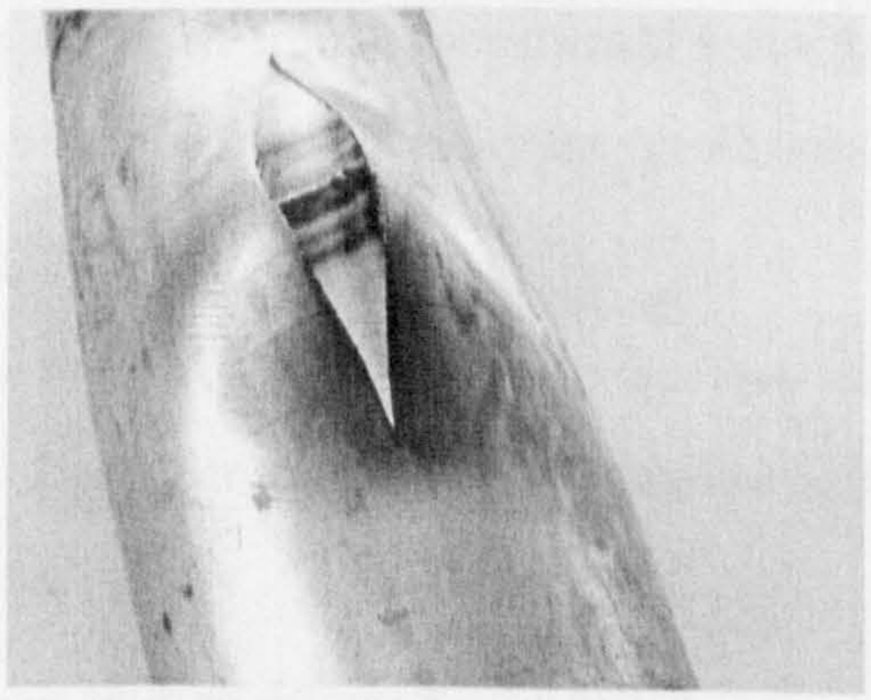

Figure 7.45: Photograph of dented and bent specimen, without gouge - SP2, after burst test. Damage propagated away from the dent vicinity.

Chapter 8

Conclusions and future work

8.1 General

This Chapter summaries significant observations and conclusions from the previous Chapters which need to be considered during the risk assessment investigations. Recommendations for future work are also provided. It should be noted that the conclusions presented herein are based solely upon the geometries investigated.

8.1.1 Literature survey

Major points from the literature survey are given here to highlight the current state of knowledge. They are as follows:

- Despite much data obtained from experimental tests, there is still need for the finite element analysis to be used specially for combined defects such as dents and gouges.
- Pipeline with dents of up to, $\frac{\delta}{D_o} = 24\%$, can survive and operate under normal operating pressure. Dents can be removed by pressurisation which leaves residual ripples in short dents.
- Most experiments on denting of small and full size pipes were carried for empty pipes. The failure pressure for combined dents and gouges are lower then for pipes with dents or gouges occurring separately.

- It appears that no work has been published on the effect of bending moment and pressure loading on dented/gouged pipes.

8.1.2 The finite element analysis

Due to the symmetry of the problem it was sufficient to use a quarter FE model. Throughout this study $3D$ solid reduced brick elements, C3D20R were used. This type of element was used successfully to model dents, gouges and cracks. Shell elements were excluded from the analysis since they are not suitable for modelling surface defects such as gouges. In all finite element calculations, it was essential to use the full-stress-strain curve rather than the elastic / perfectly plastic modelling of material.

8.1.3 The denting procedure without surface defects

- The finite element packages $ABAQUS$ 6.3 was successfully used to simulate the denting process for empty and for pressurised pipes. The load-displacement curves obtained from the FE analysis were similar to those obtained from experiments.

- A numerical study of a pipe subjected to transverse denting revealed the following features:

1. For a pressure free pipe, there is not much difference in the response curves corresponding to different shapes of indenters, e.g., hemispherical or elliptical.

2. For pressurised pipe, the magnitude of denting force can be several times higher and its actual value is strongly affected by shape of the indenter, i.e., whether it is of prolate or of oblate elliptical profile.

3. Pipes are likely to withstand deeper dents when they remain pressure free. On the other hand, depth of dents can be about 50.0 % smaller when the internal pressure is kept equal to the design level.

4. Permanent distortion of pipe's circular cross-section will propagate along pipe's length. This distance can be as high as ten times pipe diameter. At the same

time the cross-section area underneath the indenter can be reduced by as much as 18.0 %.

5. Growth of contact area between rigid indenter and pipe varies linearly with dent's depth. Contact area can change shape and some parts which were in contact may become contact free during denting. This has subsequently been confirmed experimentally.

6. Contact area between pipe and rigid saddle support not only changes its shape but drifts axially during denting process.

8.1.4 Denting of pipes with surface defects

- Modelling of axial defects such as gouges and cracks was achieved successfully. The gouges were modelled by removing part of the wall material whilst the cracks were modelled using node release method. The surface defects in all FE models had rectangular shape. Wide parameter study was carried out for gouged and cracked dents in pipes. Results of this study can be summarised as follows:

  1. For denting of empty pipes, the denting load decreases as the gouge depth and length increase.
  2. For cracked models, the denting load was nearly constant.
  3. The gouge width, $\frac{2w}{t}$, has little effect on denting of empty pipes.
  4. For denting of pressurised pipes, the denting load increases with presence of internal pressure. Also, springback is larger for pressurised pipe than for empty pipes.
  5. Cracks and gouges deeper than 50% of the wall thickness cannot sustain denting to the depth of $(\frac{\delta}{D_o})_{max} = 0.36$ with pipe's pressure equal to the design level.
  6. The amount of springback and distortion of the pipe's circular cross section remain unaffected by presence of variatious of defects, depth and their axial length when compared to the springback of non-defected pipes.

8.1.5 Bending of dented/gouged pipes

Main findings of this phase of computing are as follows:

1. Behaviour of dented pipes under moment loading is only dependent on whether the dent is on the compression (closing bending), or tension, (opening bending), side of the pipe. Dented pipes are stronger under opening bending than under closing bending.

2. Plastic load interaction diagrams for combined internal pressure and moment loading have been computed for both opening and closing bending moments. When pressure was applied first, the interaction diagrams were of essentially circular form whereas, when bending moment was applied first, the interactions were linear in form.

3. The presence of axial defects such as gouges and cracks did not affect the global moment-angular rotation to any great extend.

8.2 Experimental work

8.2.1 Manufacturing of test specimens

Various aspects of setting-up experiments have been successful. This includes the following tasks:

1. Specimens were successfully machined and welded.

2. Saddle support, machined from pine wood, performed well in all tests.

3. Axial gouges were successfully introduced to the pipe's surface using both electrical discharge machine, and milling machine.

4. Tensile tests on flat samples cut-out from the pipe were prepared and tested. This provided reliable material data for the FE analyses.

8.2.2 Experimental denting and comparison with the FE results

Major conclusions for experimental denting and the corresponding FE computing can be summarised as follows:

1. The denting was successful for (empty and pressurised pipes). Experimental loading-unloading curves, residual dent depths and dent's profiles were compared with prediction of the FE method. Results given by both methods agreed well.

2. Repeatability of experimental tests was carried out and good results were obtained for SP2 and SP3.

3. Strain gauges were used during denting and pressurisation process for specimens SP2 to SP6 to predict the axial and hoop strain distribution around the dent. The strain gauges gave reasonable results when compared with the FE predictions for pressurisation. During denting the strains increased as the dent depth increased. The maximum strain occurred on the dent rim as predicted by Lancaster [50] and [31].

4. In FE analyses the rigid support of the pipe gave higher slope than obtained from experiment. The use of a set of springs, with stiffness corresponding to wood closed the disparity between the experiment and FE.

5. The presence of axial gouges had little effect on the load-displacement curve and on springback.

6. Reduction in wall thickness at the dent centre amounted to $\cong 5.2\%$ (SP2, $(\frac{\delta}{D_o})_{max} = 0.23$).

8.2.3 Experimental bending and comparison with the FE results

Main conclusions from this part of experimentation and computing are as follows:

1. The measuring system for angular rotation proved to be adequate.

2. Repeatability of tests was good (SP2, and SP3).

3. All bent specimens, although pressurised, did not fail during bending.

4. Bending moment versus rotation curves had similar shape for all specimens.

5. The presence of gouges decreases the ultimate moment values.

6. Experimental and computed curves of bending moment versus rotation compared well for the initial rotation. Both curves diverged for rotation larger than about $\cong 6°$.

8.2.4 Burst tests

Major observations from this part of experimentation are as follows:

1. Two pipes, SP2, and SP3, have undergone the same denting and moment loading. Their burst pressures were 23.6 MPa, and 24.3 MPa. This can be regarded as confirmation of good repeatability of tests.

2. Pipes having axial gouges and subjected to opening bending moment burst at 17.7 MPa, and 22.0 MPa which illustrates detrimental role of gouges in dents (SP5, and SP6).

3. A single model with an axial gouge, SP4, and subjected to a closing bending moment failed at 25.2 MPa (which is higher than burst pressures for dented and dented/gouged pipes SP2, SP3, SP5, and SP6).

8.3 Recommendations for future work

In view of gained insight into the performance of dented, gouged, bent and burst models, it appears that the following problems should be addressed in the future:

1. Consider plain dents with circumferential gouges.

2. Experiments on pipes with combined dents and gouges need to considered for other geometries, e.g. $\frac{D}{t}$, and for other type of materials.

3. Contact between various components should be explored further using a thin film to identify processes between contacting surfaces. This appears to be very interesting avenue for research.

4. Further experimental work is also needed for bending of dented and gouged pipes. There is simply not enough experimental data in this important area from practical point of view.

5. Sequencing of surface defects is an open issue. Is the introduction of surface gouge to perfect pipe, followed by denting the same, as the introduction of gouges in already dented pipes?. Some of the FE results give confidence in the method, perhaps some preliminarily FE computing could provide a tentative answer first.

References

[1] C. Malacarne, "Transmission", presented at the 22nd World Gas Conference, Keynote address (KA-1-2), Tokyo, Japan, (ed.), K. Anzai, 2003, pp. 1-11, (*www.cgoa.cz/new/WOC4Report.doc*).

[2] R. J. Eiber, W. A. Maxey, C. W. Bert, G. M. McClure, "The effects of dents on the failure characteristics of line pipe", Battelle Columbus Laboratories, NG-18, Report No.125, Columbus, Ohio 43201, USA, 1981, pp. 1-38.

[3] D. G. Jones, "The significance of mechanical damage in pipeline", 3R International, 21 Jahrgan, Heft 7, 1982, 347-354.

[4] Procedures for inspection and repair of damaged steel pipelines designed to operate at pressures above 7 bar", TRANSCO Field Guide, BGC/PS/P11, UK, pp. 1-53.

[5] ASME B31 Code for Pressure Piping, Section 4 (B31.4), Liquid Petroleum Transportation Pipelines, and Section 8 (B31.8), Gas Transmission and Distribution Piping Systems, ASME, NY, 1995, (ISBN: 0791823733).

[6] B. Phil, "World-class pipeline safety", Gas Engineering and Management, Vol. 44, 2004, 32, (ISSN: 1465-7058).

[7] R. Bolt, "Database reflects recent trends in european gas-pipeline failures", Oil & Journal, Vol. 99, 2001, 48-52.

[8] National Transportation Safety Board, "Natural gas pipeline rupture and fire", Pipeline Accident Report NTIS No. PB2003-916501, D.C. 20594, Near Carlsbad, New Mexico, 2000, pp. 1-14, (www.ntsb.gov).

References

[9] National Transportation Safety Board, "Texas Eastern Gas Pipeline Explosion", Pipeline Accident Report NTSB number PAR-95-01, D.C. 20594, Edison NJ, 1994, pp. 1-8, (www.ntsb.gov).

[10] Recommendations on transmission and distribution practice", IGE/TD/1, Edition 3-Steel Pipeline for High Pressure Gas Transmission, Inst. Gas Engineers, 1993, pp. 1-163 .

[11] T. E. Zimmerman, P. Hopkins, N. Sanderson, "Can limit state design be used to design a pipeline above 80% SMYS?, in 'Proc. of the 17th International Conf. Offshore Mechanics and Arctic Engineering, OMAE98, Lisbon, Portugal,(ed.), C.G. Soares, ASME, NY, Vol. 1, 1998, pp. 1-20, (CD-ROM ISBN: 0791819523).

[12] A. Cosham and Phil Hopkins. A new industry document detailing best practices in pipeline defect assessment. *Penspen Integrity (APA), Newcastle Upon Tyne, NE6, 2001, UK, pp. 1-43.*

[13] A. Cosham, M. Kirkwood, "Best practice in pipeline defect assessment", in 'Proc. of the International Pipeline Conf.', IPC2000-0205, Alberta, Canada, (ed.), M. Mohitpour, ASME, NY, Vol. 1, 2000, pp. 1-11, (ISBN: 0791816664).

[14] A. Cosham, P. Hopkins, "The pipeline defect assessment manual", in 'Proc. of the 4th International Pipeline Conf.', IPC2002-27067, Alberta, Canada, (ed.), AL Edgeworth, Part B, ASME, NY, Vol. 2, 2002, pp. 1565-1581, (ISBN: 0791836207).

[15] A. Cosham, P. Hopkins, "The effect of dents in pipelines-guildance in the pipeline defect assessment manual", in 'Proc. of the Tenth International Conf. on Pressure Vessel Technology', ICPVT-10, Vienna, Austria, (ed.), J. L. Zeman, ÖGS, Austria, Vol. 1, 2003, pp. 111-119, (ISBN: 3-9501528-1-4).

[16] J. C. Gerdeen, "A Critical evaluation of plastic behaviour data and a united definition of plastic loads for pressure components", Welding Research Council Bulletin, Vol. 254, 1979, 1-63.

[17] ASME Boiler and Pressure Vessel Code, Section III, Division 1, Subsection NB 3213, Class1 Components, ASME, NY, 1998.

[18] MSC PATRAN 2001 r2a, PDA Engineering Softwer Product Division, Santa Ana, CA 92705, USA.

[19] Hibbitt, Karlsson and Sorenson Inc., "ABAQUS standard Users Manual", Version 6.4, Providence, Rhode Island, Pawtucket, RI-02860-4847, 2004, USA.

[20] C. J. Trench, "The U.S. oil pipeline industry's safety performance", The Association of Oil Pipe lines and the American Petroleum Institute, Allegro Engineering Consulting, NewYork, 2003, pp. 1-4.

[21] J. Eiber, J. Jones, G. Kramer, "Outside force causes most natural gas pipeline failure", Oil & Gas Journal, Vol. 85, 1987, 52-57.

[22] T. A. Bubenik, J. B. Nestleroth, R. J. Davis, H. Haines, "Multiple Magnetization level MFL for pipeline mechanical damage characterization", in 'Proc. of the 2000 Int. Pipeline Conf.', Calgary, Canada, (ed.), J. R. Ellwood, Vol. 2, ASME, NY, 2000, pp. 1511-1516, (ISBN: 0-7918-1666-4).

[23] C. R. Alexander, "Review of experimental and analytical investigations of dented pipelines", in 'Proc. of Pressure Vessels and Piping Conf.', Operations, Applications, and Components, NewYork, USA, ASME, NY, (eds) I. T Kisisiel, I. Ezekoye, R. K. Lewis, B. M. Lory, O. B. Shirani, J. Sinnapan, PVP-Vol. 395, 1999, pp. 197-209, (ISBN: 079181629X) .

[24] A. J. Rinehart, P. B. Keating, "Length effects on fatigue behavior of longitudinal pipeline dents", in 'Proc. of the 4th International Pipeline Conference', IPC02-27244, Calgary, Canada, (ed.), AL Edgeworth, ASME, NY, Part-B, 2002, pp. 1849-1858, (ISBN: 0-7918-3620-7).

[25] M. Beller, C. Mattheck, J. Zimmermann, "Stress concentrations in pipelines due to presence of dents", in 'Proc. of the 1st International Offshore and Polar Engineering Conf.', UK, (ed.), J.S. Chung, J. Wardenier, R.M.W. Frederking, W. Koterayama, ISOPE, CA, Vol. 2, 1991, pp. 421-424, (ISBN: 0962610453).

[26] C. R. Alexander, "Analysis of dented pipelines considering constrained and unconstrained dent configrations", in 'Proc. of the 1999 Energy Sources Technology

Conf.', ASME-99, Texas, USA, ASME, NY, 1999, pp. 1-13, (CD-ROM ISBN: 0791819558).

[27] C. R. Alexander, L. M. Connelly, "Analytical recreation of a dent profile considering varied soil, operating, and boundary conditions", in 'Proc. of the 1998 Energy Sources Technology Conf.', ASME-98, Texas, USA, Vol. 1, 1998, pp. 1-7, (CD-Rom ISBN: 0791812472).

[28] P. Hopkins, D. G. Jones, A. J. Clyne, "The significance of dents and defects in transmission pipelines", Journal of the IMech, Part E, 1989, 137-145.

[29] S. P. Belonos, R. S. Ryan, "Dents in pipeline", Oil & Gas Journal, Vol. 36, 1958, 155-161.

[30] L. S. Ong, A. K. Soh, J.H. Ong, "Experimental and finite element investigation of a local dent on a pressurised pipe", Journal of Strain Analysis, Vol. 27, 1992, 177-185.

[31] E. R. Lancaster, S. C. Palmer, "Experimental study of strains caused by pressurisation of pipes with dents", in 'Proc. of The 4th International Offshore and Polar Engineering. Conf.', ISOPE-94, (eds) J.S. Chung, Maeda Hisaaki, Naito Shigeru, Ikeda Yoshiho, Osaka, Japan, ISOPE, Colorado, Vol. 2, 1994, pp. 110-117, (ISBN: 1-880653-10-9).

[32] T. D. Park, S. Kyriakides, "On the collapse of dented cylinders under external pressure", International Journal of Mechanical Sciences, Vol. 38, 1996, 557-578.

[33] M. J. Rosenfeld, "Investigations of dent rerounding behaviour", in 'Proc. of the International Pipeline Conf.', Calgary, Canada, ASME, NY, Vol. 1, 1998, pp. 299-307, (ISBN: 0791815803).

[34] B. N. Leis, R. B. Francini, R. Mohan, D. L. Rudland, R. J. Olson, "Pressure-displacement behaviour of transmission pipelines under outside forces–towards a serviceability criterion for mechanical damage", in 'Proc. of the Eighth Int. Offshore and Polar Engineering Conf.', Montreal, Canada, (ed.), J.S. Chung, J. Wardenier, R.M.W. Frederking, W. Koterayama, ISOPE, CA, Vol. 2, 1998, pp. 60-67, (ISBN: 1-880653-36-2).

[35] B. Pal, V. Y. Salpekar, "Stress analysis of damaged submarine pipeline using finite element method", in 'Proc. of the Ninth International Offshore and Polar Engineering Conf.', Brest, France, (ed.), J.S. Chung, J. Wardenier, R.M.W. Frederking, W. Koterayama, ISOPE, CA, Vol. 2, 1999, pp. 153-159, (ISBN: 1-880653-41-9).

[36] D. C. Brooker, "Denting of pressurised pipelines under localised radial loading", International Journal of Mechanical Sciences, Vol. 46, 2004, 1783-1805.

[37] A. Dinovitzer, R. B. Lazor, R. Walker, C. Bayley, "A pipline dent assessment model", in 'Proc. of the 18th International Conference on Offshore Mechanics and arctic Engineering, OMAE99, Newfoundland, Canada, (ed.), C. G. Soares, ASME, NY, 1999, pp. 83-90, (CD-ROM ISBN: 0791819558).

[38] A. Dinovitzer, A. Bhatia, R. Walker, R. B. Lazor, "A pipeline dent assessment model considering localised effects", in 'Proc. of the ASME-2000 International Pipeline Conference', Alberta, Canada, (ed.), M. Mohitpour, ASME, NY, Vol. 2, 2000, pp. 735-742, (ISBN: 0791816664).

[39] A. Dinovitzer, R. B. Lazor, L. B. Carroll, J. Zhou, F. McCarver, S. Ironside, D. Raghu, K. Keith, "Geometric dent characterization", in 'Proc. of the 4th International Pipeline Conf.', IPC-2002-27076, Alberta, Canada, (ed.), AL Edgeworth, ASME, NY, Part-B, 2002, pp. 1589-1598, (ISBN: 0-7918-3620-7).

[40] T.H. Hyde, R. Luo, A.A. Becker, " Prediction of force-deflection behaviour of pressurised pipes subjected to axially long radial indentation", International Journal of Pressure Vessel & Piping, Vol. 82, 2005, 625-637.

[41] T.H. Hyde, R. Luo, A.A. Becker, " Elastic-plastic respone of unpressurised pipes subjected to axially-long radial indentation", International Journal of Mechanical Sciences & Piping, Vol. 47, 2005, 1949-1971.

[42] O. L. Seng, "Derivation of stresses associated with a long axial dent in a pressurized cylinder", International Journal of Mechanical Sciences, Vol. 33, 1991, 115-123.

[43] W. A. Maxey, "Defect behavior. 1.analysis made of outside-force damage to pipelines", Oil & Gas Journal, Vol. 85, 1987, 33-38 .

References

[44] W. A. Maxey, "Outside force defect behavior", Linepipe Research Supervisory Committee, Battelle Columbus Laboratories, AGA, NG-18, Report No. 162, Columbus, Ohio 43201, USA, 1986, pp. 1-30 .

[45] J. R. Fowler, "Criteria for dent acceptability in offshore pipeline", in 'Proc. of the 25th Annual Offshore Technology Conf.', Texas, USA, OTC-7311, Vol. 4, 1993, pp. 481-493, (ISBN: 9993013560).

[46] A. D. Hope, "The work hardening and fracture behaviour of linepipe steels", PhD Thesis, Cambridge University, UK, 1991.

[47] M. J. Rosenfeld, D. J. Warman, R. C. McGregor, "Toward an acceptance criterion for shallow dents affecting girth welds in gas transmission pipelines", ASME Pressure Vessel and Piping Codes and Standards (PVP), Orlando, USA, (ed.), D. P. Jones, ASME, NY, Vol. 1, 1997, pp. 373-383, (ISBN: 0791815706).

[48] G. Mannucci, M. Guagnelli, O. Vittori, C. Spinelli, "An experimental approach to evaluate the resistance of gas pipeline to dent and gouge by an excavator", in 'Proc. of the 4th International Pipeline Conf.', IPC-2002-27069, Alberta, Canada, (ed.), AL Edgeworth, ASME, NY, Part-B, 2002, pp. 1583-1587, (ISBN: 0-7918-3620-7).

[49] W. R. Tyson, K. C. Wang, "Effects of external damage (gouges and dents) on performance of linepipe: A review of work at Materials Technology Laboratories (MTL)", Report: MTL-34(OP), InL, CANMENT, ON, K1A 0G1, Canada, 1988, pp. 1-14.

[50] E. R. Lancaster, S. C. Palmer, "Strain concentration in pressurized dented pipes", Proc. Instn. Mech. Engrs, Part E, Vol. 210, 1996, 29-38.

[51] E. R. Lancaster, S. C. Palmer, "Model testing of mechanically damaged pipes containing dents and gouges", in 'Proc. of Pressure Vessels and Piping Conf.', Design and Analysis of Pressure Vessels, Piping, and Components, Louisiana, USA, ASME, NY, (ed.), C. Becht, Vol. 235, 1992, pp. 143-148, (ISBN: 0791807762).

[52] J. Spiekhout, A. M. Gresnigt, C. Koning, H. Wildschut, "Calculation models for the evaluation of the resistance against mechanical damage of pipelines", 3R International, 25 Jahrgang, Heft 4, 1986, 198-203.

[53] J. F. Kiefner, W. A. Maxey, R. J. Eiber, A. R. Duffy, "Failure stress levels of flaws in pressurized cylinders", Progress in flaw growth and fracture toughness testing, ASTM STP536, American Society for Testing and Materials, 1973, pp. 461-481.

[54] R. Song, Y. Bai, "Burst reliability of dented pipes with cracks", in 'Proc. of the Eighth International Offshore and Polar Engineering Conf.', ISOPE-98, Montreal, Canada, (ed.), J.S. Chung, J. Wardenier, R.M.W. Frederking, W. Koterayama, ISOPE, CA, Vol. 5, 1998, pp. 428-438, (ISBN: 1-880653-38-9).

[55] A. M. Gresnigt, R. J. van Foeken, "Burst pressure of dented and buckled pipes", in 'Proc. of the 17th International Conf. Offshore Mechanics and Arctic Engineering', Lisbon, Portugal, OMAE98, (ed.), C.G. Soares, ASME, NY, Vol. 1, 1998, pp. 1-11, (CD-ROM ISBN: 0791819523).

[56] E. R. Lancaster, S. C. Palmer, "Assessment of mechanically damaged pipes containing dents and gouges", in 'Proc. of Pressure Vessels and Piping Conf.', Service Experience and Life Management: Nuclear, Fossil, and Petrochemical Plants, ASME-93, Colorado, USA, (ed.), W. H. Bamford, Vol. 261, 1993, pp. 61-68, (ISBN: 0791809889).

[57] E. R. Lancaster, S. C. Palmer, "Burst pressures of pipes containing dents and gouges", Proc. Instn. Mech. Engrs, Part E, Vol. 210, 1996, pp. 19-27.

[58] T. G. Munting, C. Koning, "Varification of external damage models by burst tests on pipe sections", in 'Proc. of the 2nd International Pipeline Technology Conf.', Ostende, Belgium, (ed.), R. Denys, ASME, NY, Vol. 1, 1999, pp. 13-32, (ISBN: 0-444-82197X).

[59] J. F. Kiefner, C. R. Alexander, J. R. Fowler, "Repair of dents containing minor scratches", in 'Proc. of the Ninth Symposium on Pipeline Research', Technology for Energy Pipelines, PR No. 189-9322, 1996, pp. 51-521.

[60] R. G. Driver, T.E. Zimmerman, "A limit states approach to the design of pipelines for mechanical damage", in 'Proc. of the 17th International Conf. on Offshore Mechanics and Artic Engineering', OMAE98, Lisbon, Portugal, (ed.), C.G. Soares, ASME, NY, Vol. 1, 1998, pp. 1-14, (CD-ROM ISBN: 0791819523).

[61] D.C. Brooker, " Experimental puncture loads for external interference of pipelines by excavator equipment", International Journal of Pressure Vessel & Piping, Vol. 82, 2005, 825-832.

[62] D. C. Brooker, "Numerical modelling of pipeline puncture under excavator loading. Part I. Development and validation of a finite element material failure model for puncture simulation", International Journal of Pressure Vessels & Piping, Vol. 80, 2003, 715-725.

[63] D. C. Brooker, "Numerical modelling of pipeline puncture under excavator loading. Part II. Parametric study", International Journal of Pressure Vessels & Piping, Vol. 80, 2003, 727-735 .

[64] P. Roovers, R. Bood, M. Galli, U. Marewski, M. Steiner, M. Zarea, "EPRG methods for assessing the tolerance and resistance of pipelines to external damage", Pipeline Technology Conference, Brugge, Belgium, (ed.), R. M. Denys, ASME, NY, Vol. 2, 2000, pp. 405-425, (ISBN: 0-444-502718).

[65] M. A. Lynch, "Limit loads of piping branch junctions with cracks", PhD Thesis, The University of Liverpool, UK, 2001.

[66] G. K. Lee, "The influence of attachment size on the limit pressures of defective piping components", PhD Thesis, The University of Liverpool, UK, 2003.

[67] B. M. Das, "Principles of foundation engineering", PWS-Kent Publishing Company, Boston, 1990, Chapter 4, (ISBN:0534407528).

[68] E. R. Lancaster, "Behaviour of pressurised pipes containing dents and gouges", PhD Thesis, Cambridge University, UK, 1993.

[69] M. F. Hsieh, D. G. Moffat, J. Mistry, " Nozzles in knuckle region of a torispherical head: limit load interaction under combined pressure and piping loads", International Journal of Pressure Vessel & Piping, Vol. 77, 2000, 807-815.

[70] BS 5500: Specification for unfired fusion welded pressure vessels, Fig: E2 (A), British Standards Institute, London, UK, 1997, (ISBN: 0580270475).

[71] BS EN 10002-1:1990, Tensile testing of metallic materials, Part(1), Method of test, British Standards Institute, London, UK, 1990, (ISBN: 0580188051).

[72] G. E. Dieter, "Mechanical behaviour of mechanicals under tension.", Metals Handbook, 9th edition, 8. Mechanical testing, 1986, McGraw-Hill Science/Engineering/Math.

[73] O. H. Bjørnøy, O. Reng ård, S. Fredheim, P. Bruce, "Residual strength of dented pipelines, DNV test results", in 'Proc. of the Tenth Int. Offshore and Polar Engineering Conf.', ISOPE-2000, Seattle, USA, ((ed.), J.S. Chung, J. Wardenier, R.M.W. Frederking, W. Koterayama, ISOPE, CA, Vol. 2, 2000, pp. 182-188, (ISBN: 1-880653-48-6).

[74] T. Øberg, O. Rengård, T. Wiik, "Residual strength of dented pipelines and risers", DNV Report No.82-0567, Det Norske Veritas, Norway, 2000, pp. 1-10.

[75] N. Hagiwara, N. Oguchi, "Fatigure behavior of line pipes subjected to sever mechanical damage", Journal of Pressure Vessel Technology, Transactions of ASME, Vol. 121, 1999, 369-374.

Appendices

Appendix A

Known experiments on dents and gouges

No:	Ref.	Case	D_o (m)	L (m)	$\frac{D_o}{t}$	$\frac{\delta}{D_o}$ (%)	$\frac{2c}{D_o}$ (%)	$\frac{e}{t}$ (%)	p_i (MPa)	p_f (MPa)	σ_{yp} (MPa)	Indenter type	Comments
1	[73]	1	0.273	4;5	27.3	26	0.0	0.0	0.0	46	404;St	axial cyl.	plain dent;burst
2	[73]	2	0.273	4;5	27.3	28	0.0	0.0	0.0	34.7	404;St	axial cyl.	plain dent;burst
3	[73]	3	0.273	4;5	27.3	20	0.0	0.0	0.0	21.2	404;St	axial cyl.	plain dent;burst
4	[73]	4	0.273	4;5	27.3	12	0.0	0.0	0.0	42	404;St	axial cyl.	plain dent;burst
5	[73]	5	0.273	4;5	27.3	20	0.0	0.0	0.0	30	404;St	axial cyl.	plain dent;burst
6	[73]	6	0.814	4;5	40.7	18	99.5	10	0.0	4.5b	440;St	axial cyl.	notch;burst
7	[73]	7	0.814	4;5	40.7	18	99.5	10	0.0	7.4b	440;St	axial cyl.	notch;burst
8	[73]	8	0.814	4;5	40.7	18	99.5	10	0.0	23.6b	440;St	axial cyl.	notch;burst
9	[73]	9	0.814	4;5	40.7	18	99.5	10	0.0	27b	440;St	axial cyl.	notch;burst
10	[73]	10	0.814	4;5	40.7	12	99.5	10	0.0	7.4b	440;St	axial cyl.	notch;burst
11	[73]	11	0.814	4;5	40.7	5	99.5	10	0.0	16.2b	440;St	axial cyl.	notch;burst
12	[73]	12	0.814	4;5	40.7	12	99.5	30	0.0	6b	440;St	axial cyl.	notch;burst
13	[73]	13	0.814	4;5	40.7	12	42.5	70	0.0	7.7b	440;St	axial cyl.	notch;burst
14	[73]	14	0.814	4;5	40.7	12	42.5	50	0.0	6.8b	440;St	axial cyl.	notch;burst
15	[68]	4	0.100	0.338	54.1	4.9	25.4	14.1	0.0	3.68	163;Al	hemisph.	gouge;did not fail
16	[68]	5	0.100	0.338	54.1	4.3	25.4	31.7	0.0	7.11	163;Al	hemisph.	gouge;ruptured
17	[68]	6	0.100	0.338	54.1	6.4	25.4	47	0.0	5.86	163;Al	hemisph.	gouge;ruptured
18	[68]	7	0.100	0.338	54.1	9.7	25.4	0.0	0.0	4.25	163;Al	hemisph.	gouge;did not fail
19	[68]	8	0.100	0.338	54.1	10.8	25.4	15.2	0.0	3.63	163;Al	hemisph.	gouge;did not fail
20	[68]	9	0.100	0.338	54.1	10.2	25.4	30.3	0.0	7.12	163; Al	hemisph.	gouge;ruptured
21	[68]	10	0.100	0.338	54.1	10.6	25.4	45.4	0.0	5.49	163;Al	hemisph.	gouge;ruptured
22	[68]	11	0.100	0.338	54.1	15.8	25.4	0.0	0.0	4.37	163;Al	hemisph.	gouge;did not fail
23	[68]	12	0.100	0.338	54.1	15.1	25.4	15.3	0.0	3.63	163;Al	hemisph.	gouge;did not fail
24	[68]	13	0.100	0.338	54.1	15.2	25.4	29.7	0.0	7.52	163;Al	hemisph.	gouge;ruptured
25	[68]	14	0.100	0.338	54.1	15.3	25.4	45.5	0.0	5.21	163;Al	hemisph.	gouge;ruptured

Continued

No:	Ref.	Case	D_o	L	$\frac{D_o}{t}$	$\frac{\delta}{D_o}$	$\frac{2c}{D_o}$	$\frac{e}{t}$	p_i	p_f	σ_{yp}	Indenter type	Comments
			(m)			(%)			(MPa)				
26	[68]	1	0.100	0.338	54.1	7.20	25.4	44.3	1.386	6.15	163;Al	hemisph.	gouge;leaked
27	[68]	2	0.100	0.338	54.1	9.10	25.4	48.6	3.43	6.35	163;Al	hemisph.	gouge;leaked
28	[68]	4	0.100	0.338	54.1	6.40	25.4	47.0	0.0	5.86	163;Al	hemisph.	gouge;ruptured
29	[68]	5	0.100	0.338	54.1	10.6	25.4	45.4	0.0	5.49	163;Al	hemisph.	gouge;ruptured
30	[68]	6	0.100	0.338	54.1	15.3	25.4	45.5	0.0	5.21	163;Al	hemisph.	gouge;ruptured
31	[68]	1	0.100	0.338	54.1	11.7	25.4	45.0	0.0	6.72	163;Al	hemisph.	off-centre gouge;ruptured
32	[68]	1a	0.100	0.338	54.1	11.9	25.4	55.0	0.0	5.71	163;Al	hemisph.	off-centre gouge;ruptured
33	[68]	2	0.100	0.338	54.1	11.8	25.4	45.1	0.0	5.40	163;Al	hemisph.	off-centre gouge;ruptured
34	[68]	2a	0.100	0.338	54.1	13.0	25.4	56.2	0.0	3.15	163;Al	hemisph.	gouge;ruptured
35	[68]	3	0.100	0.338	54.1	12.0	25.4	46.6	0.0	6.72	163;Al	hemisph.	off-centre gouge;ruptured
36	[68]	4	0.100	0.338	54.1	12.1	25.4	43.9	0.0	7.08	163;Al	hemisph.	off-centre gouge;ruptured
37	[68]	5	0.100	0.338	54.1	12.3	25.4	48.2	0.0	3.47	163;Al	hemisph.	off-centre gouge;ruptured
38	[68]	6	0.100	0.338	54.1	11.9	25.4	46.0	0.0	6.29	163;Al	hemisph.	off-centre gouge;ruptured
39	[68]	9	0.100	0.338	54.1	15.3	25.4	45.5	0.0	5.21	163;Al	hemisph.	off-centre gouge;ruptured
40	[68]	7	0.100	0.338	54.1	13.2	50.8	44.4	0.0	5.15	163;Al	hemisph.	gouge;ruptured
41	[68]	10	0.100	0.338	54.1	14.9	50.8	45.4	0.0	4.14	163;Al	hemisph.	gouge;ruptured
42	[68]	8	0.100	0.338	54.1	12.1	280	31.8	0.0	2.69	163;Al	hemisph.	gouge;ruptured
43	[68]	11	0.100	0.338	54.1	6.8	25.4	0.0	0.0	7.59	163;Al	hemisph.	hoop gouge;did not fail
44	[68]	12	0.100	0.338	54.1	6.8	25.4	0.0	0.0	7.59	163;Al	hemisph.	hoop gouge;did not fail
45	[68]	13	0.100	0.338	54.1	7.37	25.4	0.0	0.0	7.59	163;Al	hemisph.	hoop gouge;did not fail
46	[68]	14	0.100	0.338	54.1	7.11	25.4	0.0	0.0	7.59	163;Al	hemisph.	hoop gouge;did not fail
47	[68]	15	0.100	0.338	54.1	12.0	25.4	0.0	0.0	not avail.	163;Al	hemisph.	hoop gouge;did not fail
48	[74]	1	1.067	not avail.	27.3	0.0	0.0	0.0	0.0	46.0	414;St	notch	burst
49	[74]	2	1.067	4; 5	27.3	28	0.0	0.0	0.0	34.7	414;St	notch	burst
50	[74]	3	1.067	4; 5	27.3	12	0.0	0.0	0.0	42.0	414;St	notch	burst

Continued

No:	Ref.	Case	D_o	L	$\frac{D_o}{t}$	$\frac{\delta}{D_o}$	$\frac{2c}{D_o}$	$\frac{e}{t}$	p_i	p_f	σ_{yp}	Indenter type	Comments
			(m)			(%)			(MPa)				
51	[74]	4	1.067	4; 5	45.3	18	76.0	3.0	0.0	7.40	414;St	notch	burst
52	[74]	5	1.067	4, 5	45.6	18	76.0	1.0	0.0	23.6	414;St	notch	burst
53	[74]	6	1.067	4, 5	47.0	18	76.0	0.0	0.0	27.0	414;St	notch	burst
54	[74]	7	1.067	4, 5	40.6	12	76.0	10.0	0.0	7.40	414;St	notch	burst
55	[74]	8	1.067	4, 5	40.6	5	76.0	10.0	0.0	16.20	414;St	notch	burst
56	[74]	9	1.067	4, 5	65.0	12	32.4	2.0	0.0	7.70	414;St	notch	burst
57	[74]	10	1.067	4, 5	65.0	12	32.4	2.0	0.0	6.80	414;St	notch	burst
58	[58]	1	0.305	not avail.	43.0	6.1	0.558	25	4.0	10.6	288;St	notch	burst
59	[58]	2	0.305	not avail.	43.0	9.3	0.558	27	4.0	9.90	288;St	notch	burst
60	[58]	1	0.305	not avail.	32.0	5.6	0.558	28	6.6	26.0	330;St	notch	burst
61	[58]	2	0.305	not avail.	32.0	8.8	0.558	24	6.6	24.1	330;St	notch	burst
62	[58]	1	0.305	not avail.	28.0	2.3	0.558	25	6.6	10.6	370;St	notch	burst
63	[58]	1	0.406	not avail.	30.0	1.8	0.418	23	6.6	10.6	338;St	notch	burst
64	[58]	1	0.457	not avail.	77.5	3.3	0.372	20	6.6	14.2	458;St	notch	burst
65	[58]	2	0.457	not avail.	77.5	2.0	0.372	19	8.0	13.7	458;St	notch	burst
66	[58]	2	0.508	not avail.	64.0	2.9	0.335	27	6.6	13.3	494;St	notch	burst
67	[58]	1	0.508	not avail.	64.0	2.3	0.335	28	8.0	14.7	494;St	notch	burst
68	[45]	A-1	0.324	9.14	18.6	15.0	0.0	0.0	8.0	14.7	380;Se	plate	no failure
69	[45]	A-2	0.324	9.14	19.0	15.0	0.0	0.0	$\star$	$\star\star$	454;Se	plate	no failure
70	[45]	B-1	0.324	9.14	40.9	20.0	0.0	0.0	$\star$	$\star\star$	366;Se	plate	plain dent;fatigue
71	[45]	C-2	0.324	9.14	51.0	20.0	0.0	0.0	$\star$	$\star\star$	395;Se	plate	plain dent;fatigue
72	[45]	H	0.324	9.14	24.8	18.3	0.0	0.0	$\star$	$\star\star$	359;Se	plate	plain dent;fatigue
73	[45]	E	0.324	9.14	31.8	17.0	0.0	0.0	$\star$	$\star\star$	353;Se	plate	plain dent;fatigue
74	[45]	F	0.324	9.14	31.8	17.2.0	0.0	0.0	$\star$	$\star\star$	353;Se	plate	plain dent;fatigue
75	[45]	G	0.324	9.14	50.3	17.2	0.0	0.0	$\star$	$\star\star$	579;Se	plate	plain dent;fatigue

Continued

No:	Ref.	Case	D_o (m)	L (m)	$\frac{D_o}{t}$	$\frac{\delta}{D_o}$ (%)	$\frac{2c}{D_o}$ (%)	$\frac{e}{t}$ (%)	p_i (MPa)	p_f (MPa)	σ_{yp} (MPa)	Indenter type	Comments
76	[45]	E	0.324	9.14	31.8	17.0	0.0	0.0	⋆	⋆⋆	353;Se	plate	plain dent;fatigue
77	[45]	F	0.324	9.14	31.8	17.2.0	0.0	0.0	⋆	⋆⋆	353;Se	plate	plain dent;fatigue
78	[45]	G	0.324	9.14	50.3	17.2	0.0	0.0	⋆	⋆⋆	579;Se	plate	plain dent;fatigue
79	[28]	BPU2	0.914	0.075	66.7	3.4	0.0	0.0	⋆	46.3	465;St	not avail.	plain dent;burst
80	[28]	BNO1	0.914	0.075	73.7	4.5	0.0	0.0	⋆	46.7	419;St	not avail.	plain dent;burst
81	[28]	BIE1	0.610	0.075	62.9	5.4	0.0	0.0	⋆	17.2	366;St	not avail.	plain dent;burst
82	[28]	BLV1	0.762	0.075	96.4	3.5	0.0	0.0	⋆	49.0	363;St	not avail.	plain dent;burst
83	[28]	EUY1	0.914	0.075	54.4	4.8	0.0	0.0	⋆	18.3	475;St	not avail.	plain dent;burst
84	[28]	FJB1	0.762	0.075	62.5	3.2	0.0	0.0	⋆	13.0	406;St	not avail.	plain dent;burst
85	[28]	FJB2	0.762	0.075	62.5	4.9	0.0	0.0	⋆	8.7	406;St	not avail.	plain dent;fatigue
86	[28]	FJK7	0.914	0.075	57.5	4.3	0.0	0.0	⋆	dnf	475;St	not avail.	plain dent;fatigue
87	[28]	FJK8	0.914	0.075	57.5	4.0	0.0	0.0	⋆	dnf	475;St	not avail.	plain dent;fatigue
88	[28]	FJK9	0.914	0.075	57.5	4.4	0.0	0.0	⋆	dnf	475;St	not avail.	plain dent;fatigue
89	[28]	BPU1	0.914	0.075	66.7	5.2	0.0	0.0	⋆	dnf	465;St	not avail.	plain dent;fatigue
90	[28]	BNO2	0.914	0.075	72.0	3.9	0.0	0.0	⋆	dnf	419;St	not avail.	plain dent;fatigue
91	[28]	BIE2	0.610	0.075	63.0	5.3	0.0	0.0	⋆	dnf	366;St	not avail.	plain dent;fatigue
92	[28]	BLV2	0.762	0.075	96.5	3.9	0.0	0.0	⋆	dnf	363;St	not avail.	plain dent;fatigue
93	[28]	EUY2	0.914	0.075	54.4	3.7	0.0	0.0	⋆	dnf	475;St	not avail.	plain dent;fatigue
94	[28]	FJB3	0.762	0.075	64.0	5.0	0.0	0.0	⋆	16500C	406;St	not avail.	plain dent;fatigue
95	[28]	FJB4	0.762	0.075	64.0	4.45	0.0	0.0	⋆	12300C	406;St	not avail.	plain dent;fatigue
96	[28]	EUY3	0.914	0.075	57.5	4.1	0.0	0.0	⋆	12700C	475;St	not avail.	plain dent;fatigue
97	[28]	EUY3	0.914	0.075	57.5	4.1	0.0	0.0	⋆	14600C	475;St	not avail.	plain dent;fatigue
98	[28]	BIE3	0.610	0.075	64.2	4.2	0.0	0.0	⋆	26100C	366;St	not avail.	plain dent;fatigue
99	[28]	BIE4	0.610	0.075	64.2	4.2	0.0	0.0	⋆	46500C	366;St	not avail.	plain dent;fatigue
100	[28]	BLX19	0.762	0.075	64.0	4.5	0.0	0.0	⋆	49700C	363;St	not avail.	plain dent;fatigue

Continued

No:	Ref.	Case	D_o (m)	L (m)	$\frac{D_o}{t}$	$\frac{\delta}{D_o}$ (%)	$\frac{2c}{D_o}$ (%)	$\frac{e}{t}$ (%)	p_i (MPa)	p_f (MPa)	σ_{yp} (MPa)	Indenter type	Comments
101	[28]	FJK2	0.914	0.075	57.5	4.1	0.0	0.0	⋆	5544C	475;St	not avail.	plain dent;fatigue
102	[28]	FJK6	0.914	0.075	57.5	4.2	0.0	0.0	⋆	3.920C	475;St	not avail.	plain dent;fatigue
103	[28]	FJK11	0.914	0.075	57.5	4.1	0.0	0.0	⋆	6930C	475;St	not avail.	plain dent;fatigue
104	[28]	FJK13	0.914	0.075	57.5	2.3	0.0	0.0	⋆	42242C	475;St	not avail.	plain dent;fatigue
105	[28]	FJK14	0.914	0.075	57.5	1.9	0.0	0.0	⋆	62000C	475;St	not avail.	plain dent;fatigue
106	[28]	FJK15	0.914	0.075	57.5	1.8	0.0	0.0	⋆	83311C	475;St	not avail.	plain dent;fatigue
107	[59]	B1-1N	0.324	not avail.	68.0	5.0	0.0	5.0	6.35	14.9	370;St	bar	notch;burst
108	[59]	B1-2G	0.324	not avail.	68.0	20.0	0.0	10.0	6.35	4.3	370;St	bar	notch;burst
109	[59]	B1-3N	0.324	not avail.	68.0	5.0	0.0	10.0	6.35	13.7	370;St	bar	notch;burst
110	[59]	B1-4G	0.324	not avail.	68.0	5.0	0.0	10.0	6.35	14.7	370;St	bar	notch;burst
111	[59]	B1-5D	0.324	not avail.	68.0	5.0	0.0	10.0	6.35	14.9	370;St	bar	notch;burst
112	[59]	B1-6N	0.324	not avail.	68.0	10.0	0.0	10.0	6.35	10.2	370;St	bar	notch;burst
113	[59]	B1-7N	0.324	not avail.	68.0	15.0	0.0	15.0	6.35	5.7	370;St	bar	notch;burst
114	[59]	B1-8N	0.324	not avail.	68.0	12.0	0.0	10.0	6.35	10.5	370;St	bar	notch;burst
115	[59]	B1-9G	0.324	not avail.	68.0	12.0	0.0	10.0	6.35	13.3	370;St	bar	notch;burst
116	[59]	B1-10G	0.324	not avail.	68.0	15.0	0.0	5.0	6.35	12.6	370;St	bar	notch;burst
117	[59]	B1-11N	0.324	not avail.	68.0	15.0	0.0	5.0	6.35	5.4	370;St	bar	notch;burst
118	[59]	B1-12G	0.324	not avail.	68.0	10.0	0.0	5.0	6.35	13.0	370;St	bar	notch;burst
119	[59]	B1-13N	0.324	not avail.	68.0	10.0	0.0	5.0	6.35	9.3	370;St	bar	notch;burst
120	[59]	B1-14G	0.324	not avail.	68.0	15.0	0.0	5.0	6.35	14.8	370;St	bar	notch;burst
121	[59]	B1-15N	0.324	not avail.	68.0	15.0	0.0	5.0	6.35	6.3	370;St	bar	notch;burst
122	[59]	F2-1N	0.324	not avail.	68.0	15.0	0.0	10.0	6.35	not avail.	370;St	bar	notch;fatigue
123	[59]	F2-2G	0.324	not avail.	68.0	15.0	0.0	10.0	6.35	not avail.	370;St	bar	notch;fatigue
124	[59]	F2-3G	0.324	not avail.	68.0	15.0	0.0	5.0	6.35	25427C	370;St	bar	notch;fatigue
125	[59]	F2-4N	0.324	not avail.	68.0	15.0	0.0	5.0	6.35	7267C	370;St	bar	notch;fatigue

Continued

No:	Ref.	Case	D_o	L	$\frac{D_o}{t}$	$\frac{\delta}{D_o}$	$\frac{2c}{D_o}$	$\frac{e}{t}$	p_i	p_f	σ_{yp}	Indenter type	Comments
			(m)			(%)			(MPa)				
126	[59]	F2-5G	0.324	not avail.	68.0	10.0	0.0	10.0	6.35	25427C	370;St	bar	notch;fatigue
127	[59]	F2-6N	0.324	not avail.	68.0	10.0	0.0	10.0	6.35	6582C	370;St	bar	notch;fatigue
128	[59]	F2-7G	0.324	not avail.	68.0	10.0	0.0	5.0	6.35	27790C	370;St	bar	notch;fatigue
129	[59]	F2-8N	0.324	not avail.	68.0	10.0	0.0	5.0	6.35	18093C	370;St	bar	notch;fatigue
130	[59]	F2-9G	0.324	not avail.	68.0	10.0	0.0	5.0	6.35	24970C	370;St	bar	notch;fatigue
131	[59]	F2-10N	0.324	not avail.	68.0	10.0	0.0	5.0	6.35	24970C	370;St	bar	notch;fatigue
132	[59]	F2-11G	0.324	not avail.	68.0	10.0	0.0	5.0	6.35	27479C	370;St	bar	notch;fatigue
133	[59]	F2-12N	0.324	not avail.	68.0	10.0	0.0	5.0	6.35	16316C	370;St	bar	notch;fatigue
134	[59]	PG-1	0.329	not avail.	68.0	not avail.	0.0	5.0	6.35	not avail.	375;St	bar	notch,fatigue
135	[59]	PG-2	0.329	not avail.	68.0	not avail.	0.0	5.0	6.35	not avail.	375;St	bar	notch;fatigue
136	[59]	PG-3	0.329	not avail.	68.0	not avail.	0.0	10.0	6.35	not avail.	375;St	bar	notch;fatigue
137	[59]	PG-4	0.329	not avail.	68.0	not avail.	0.0	10.0	6.35	not avail.	375;St	bar	notch;fatigue
138	[59]	PG-5	0.329	not avail.	68.0	not avail.	0.0	15.0	6.35	not avail.	375;St	bar	notch;fatigue
139	[2]	16	0.406	ring	64.0	1.8	0.0	0.0	0.0	9.31	383;St	hemisph.	plain dent;burst
140	[2]	9	0.762	ring	80.0	1.1	0.0	0.0	0.0	12.3	430;St	hemisph.	plain dent;burst
141	[2]	13	0.762	ring	80.0	1.7	0.0	0.0	0.0	10.2	430;St	hemisph.	plain dent;burst
142	[2]	16	0.406	ring	64.0	3.1	0.0	0.0	0.0	9.3	383;St	hemisph.	plain dent;burst
143	[2]	15	0.762	ring	80.0	1.7	0.0	0.0	0.0	2.76	430;St	hemisph.	plain dent;burst
144	[2]	10	0.762	ring	80.0	2.3	0.0	0.0	0.0	11.2	430;St	hemisph.	plain dent;burst
145	[2]	30	0.406	ring	64.0	5.6	0.0	0.0	0.0	13.8	383;St	hemisph.	plain dent;burst
146	[2]	13	0.762	ring	80.0	3.8	0.0	0.0	0.0	10.2	430;St	hemisph.	plain dent;burst
147	[2]	10	0.762	ring	80.0	4.2	0.0	0.0	0.0	11.7	430;St	hemisph.	plain dent;burst
148	[2]	6A	0.762	ring	80.0	1.3	0.0	0.0	0.0	6.5	430;St	hemisph.	plain dent;burst
149	[2]	15	0.762	ring	80.0	1.6	0.0	0.0	0.0	2.6	430;St	hemisph.	plain dent;burst
150	[2]	30	0.406	ring	64.0	4.1	0.0	0.0	0.0	13.8	383;St	hemisph.	plain dent;burst

Continued

No:	Ref.	Case	D_o (m)	L	$\frac{D_o}{t}$	$\frac{\delta}{D_o}$ (%)	$\frac{2c}{D_o}$	$\frac{e}{t}$	p_i (MPa)	p_f	σ_{yp}	Indenter type	Comments
151	[2]	6A	0.762	ring	80.0	2.4	0.0	0.0	0.0	6.5	430;St	hemisph.	plain dent;burst
152	[2]	9	0.762	ring	80.0	5.6	0.0	0.0	0.0	12.3	430;St	hemisph.	plain dent;burst
153	[2]	9	0.762	ring	80.0	1.3	0.0	0.0	0.0	12.3	430;St	hemisph.	plain dent;burst
154	[2]	6A	0.762	ring	80.0	1.3	0.0	0.0	0.0	6.5	430;St	hemisph.	plain dent;burst
155	[2]	15	0.762	ring	80.0	1.7	0.0	0.0	0.0	2.8	430;St	hemisph.	plain dent;burst
156	[2]	6A	0.762	ring	80.0	2.5	0.0	0.0	0.0	6.5	430;St	hemisph.	plain dent;burst
157	[2]	9	0.762	ring	80.0	5.6	0.0	0.0	0.0	12.3	430;St	hemisph.	plain dent;burst
158	[2]	10	0.762	ring	80.0	0.9	0.0	0.0	0.0	11.7	430;St	bar	plain dent;burst
159	[2]	11A	0.762	ring	80.0	5.5	0.0	0.0	0.0	11.7	430;St	bar	plain dent;burst
160	[2]	11A	0.762	ring	80.0	1.4	0.0	0.0	0.0	11.7	430;St	bar	plain dent;burst
161	[2]	11A	0.762	ring	80.0	5.5	0.0	0.0	0.0	11.7	430;St	bar	plain dent;burst
162	[2]	28	0.406	ring	64.0	4.2	0.0	0.0	0.0	17.0	383;St	bar	plain dent;burst
163	[2]	26	0.406	ring	64.0	7.7	0.0	0.0	0.0	17.6	383;St	bar	plain dent;burst
164	[2]	28	0.406	ring	64.0	3.8	0.0	0.0	0.0	17.0	383;St	bar	plain dent;burst
165	[2]	30	0.406	ring	64.0	6.0	0.0	0.0	0.0	13.8	383;St	bar	plain dent;burst
166	[2]	26	0.406	ring	64.0	7.0	0.0	0.0	0.0	17.6	383;St	bar	plain dent;burst
167	[2]	16	0.762	ring	80.0	2.3	0.0	0.0	0.0	9.3	430;St	bar	plain dent;burst
168	[2]	10	0.762	ring	80.0	1.1	0.0	0.0	0.0	11.7	430;St	bar	plain dent;burst
169	[2]	16	0.762	ring	80.0	3.7	0.0	0.0	0.0	9.3	430;St	bar	plain dent;burst
170	[2]	28	0.406	ring	64.0	8.1	0.0	0.0	0.0	17.0	383;St	bar	plain dent;burst
171	[2]	15	0.762	ring	80.0	3.0	0.0	0.0	0.0	2.8	430;St	bar	plain dent;burst
172	[2]	11A	0.762	ring	80.0	3.2	0.0	0.0	0.0	11.7	430;St	bar	plain dent;burst
173	[2]	25	0.762	ring	80.0	3.6	0.0	0.0	0.0	14.1	430;St	bar	plain dent;burst
174	[2]	30	0.406	ring	64.0	7.1	0.0	0.0	0.0	13.8	430;St	bar	plain dent;burst
175	[2]	28	0.406	ring	64.0	3.6	0.0	0.0	0.0	17.0	383;St	bar	plain dent;burst

Continued

No:	Ref.	Case	D_o (m)	L	$\frac{D_o}{t}$	$\frac{\delta}{D_o}$ (%)	$\frac{2c}{D_o}$ (%)	$\frac{e}{t}$ (%)	p_i (MPa)	p_f (MPa)	σ_{yp} (MPa)	Indenter type	Comments
176	[2]	26	0.406	ring	64.0	6.1	0.0	0.0	0.0	17.6	383;St	bar	plain dent;burst
177	[2]	30	0.406	ring	64.0	8.3	0.0	0.0	0.0	13.8	383;St	bar	plain dent;burst
178	[2]	49	0.610	ring	64.0	5.2	0.0	0.0	0.0	10.3	393;St	bar	plain dent;fatigue
179	[2]	50	0.610	ring	64.0	5.7	0.0	0.0	0.0	0.0	393;St	bar	plain dent;fatigue
180	[2]	40	0.406	ring	64.0	7.8	0.0	0.0	0.0	1.1	383;St	bar	plain dent;burst
181	[2]	41	0.406	ring	64.0	5.8	0.0	0.0	0.0	12.4	383;St	bar	plain dent;burst
182	[2]	43	0.762	ring	80.0	4.5	0.0	0.0	0.0	13.8	430;St	bar	plain dent;burst
183	[44]	1	0.762	2.1	77.0	2.67	70.0	24.3	not avail.	8.4	520;St	notch	rupture
184	[44]	2	0.762	2.1	74.0	2.90	65.0	13.61	not avail.	8.7	482;St	notch	rupture
185	[44]	3	0.762	2.1	74.0	3.37	72.5	7.92	not avail.	7.0	482;St	notch	rupture
186	[44]	4	0.762	2.1	74.0	2.27	24.0	12.4	not avail.	12.0	482;St	notch	rupture
187	[44]	5	0.762	2.1	74.0	2.60	50.0	7.92	not avail.	8.4	482;St	notch	rupture
188	[44]	6	0.762	2.1	100	3.20	26.7	16.7	not avail.	6.0	426;St	notch	rupture
189	[44]	7	0.762	2.1	101	3.53	52.5	25.4	not avail.	4.9	475;St	notch	rupture
190	[44]	8	0.762	2.1	67.0	5.25	49.0	11.7	not avail.	4.8	389;St	notch	rupture
191	[44]	9	0.762	2.1	67.0	3.50	36.0	20.0	not avail.	12.3	389;St	notch	rupture
192	[44]	10	0.762	2.1	52.0	2.70	100	26.3	not avail.	6.9	446;St	notch	rupture
193	[44]	11	0.762	2.1	52.0	1.70	49.5	25.7	not avail.	15.2	446;St	notch	rupture
194	[44]	12	0.762	2.1	67.0	2.20	35.0	23.3	not avail.	9.7	389;St	notch	rupture
195	[44]	13	0.762	2.1	52.0	2.25	45.0	11.6	not avail.	11.8	446;St	notch	rupture
196	[44]	14	0.762	2.1	67.0	3.80	42.0	13.3	not avail.	8.6	389;St	notch	rupture
197	[44]	15	0.762	2.1	92.0	1.83	36.9	10.5	not avail.	7.0	464;St	notch	rupture
198	[44]	16	0.762	2.1	92.0	1.43	36.9	5.90	not avail.	9.6	464;St	notch	rupture
199	[44]	17	0.762	2.1	92.0	1.98	22.4	10.9	not avail.	8.3	464;St	notch	rupture
200	[44]	1	0.762	2.1	77.0	3.0	30.8	10.23	not avail.	8.4	413,519;St	notch	rupture

Continued

No:	Ref.	Case	D_o (m)	L	$\frac{D_o}{t}$	$\frac{\delta}{D_o}$ (%)	$\frac{2c}{D_o}$ (%)	$\frac{e}{t}$ (%)	p_i (MPa)	p_f (MPa)	σ_{yp} (MPa)	Indenter type	Comments
201	[44]	2	0.762	2.1	77.0	2.0	35.0	3.84	not avail.	8.4	413,519;St	notch	burst
202	[44]	3	0.762	2.1	77.0	4.0	36.7	5.12	not avail.	8.6	413,519;St	notch	burst
203	[44]	4	0.762	2.1	77.0	3.2	55.0	5.12	not avail.	7.0	413;519;St	notch	burst
204	[44]	5	0.762	2.1	77.0	1.7	63.3	8.95	not avail.	7.0	413;519;St	notch	burst
205	[44]	6	0.762	2.1	77.0	2.3	70.0	11.5	not avail.	7.1	413;519;St	notch	burst
206	[44]	7	0.762	2.1	77.0	3.1	72.0	24.3	not avail.	7.1	413;519;St	notch	burst
207	[44]	8	0.762	2.1	77.0	3.1	70.0	20.5	not avail.	8.4	413;519;St	notch	burst
208	[44]	9	0.762	2.1	77.0	0.8	72.0	2.48	not avail.	8.7	413;519;St	notch	burst
209	[44]	11	0.762	2.1	74.3	0.8	78.3	4.95	8.6	not avail.	413;519;St	notch	burst
210	[44]	12	0.762	2.1	74.3	1.5	80.0	11.1	8.7	not avail.	413;519;St	notch	burst
211	[44]	13	0.762	2.1	74.3	1.5	70.8	2.48	7.1	not avail.	413;519;St	notch	burst
212	[44]	14	0.762	2.1	74.3	2.2	77.5	2.97	7.0	not avail.	413,519, st	notch	burst
213	[44]	15	0.762	2.1	74.3	2.9	75.0	5.69	7.0	not avail.	413;519;St	notch	burst
214	[44]	16	0.762	2.1	74.3	0.8	80.0	2.48	12.0	not avail.	413,519 ;St	notch	burst
215	[44]	17	0.762	2.1	74.3	1.6	76.7	4.21	12.0	not avail.	413;519;St	notch	burst
216	[44]	18	0.762	2.1	74.3	2.6	76.7	6.19	12.0	not avail.	413;519;St	notch	burst
217	[44]	19	0.762	2.1	100	2.0	80.8	6.0	5.96	not avail.	413;519;St	notch	burst
218	[44]	20	0.762	2.1	101	2.1	80.8	7.4	4.9	not avail.	413;519;St	notch	burst
219	[44]	21	0.762	2.1	101	2.8	81.7	8.5	4.9	not avail.	413;519;St	notch	burst
220	[44]	22	0.762	2.1	101	2.9	81.7	9.1	4.9	not avail.	413;519;St	notch	burst
221	[44]	23	0.508	2.1	66.7	1.8	120	8.3	4.8	not avail.	413;519;St	notch	burst
222	[44]	24	0.508	2.1	66.7	3.9	120	26.7	4.8	not avail.	413;519;St	notch	burst
223	[44]	25	0.508	2.1	66.7	3.9	120	33.3	4.8	not avail.	413;519;St	notch	burst
224	[44]	26	0.508	2.1	66.7	2.5	120	16.7	12.3	not avail.	413;519;St	notch	burst
225	[44]	27	0.508	2.1	52.5	2.0	120	15.8	6.9	not avail.	413;519;St	notch	burst

Continued

No:	Ref.	Case	D_o (m)	L	$\frac{D_o}{t}$	$\frac{\delta}{D_o}$ (%)	$\frac{2c}{D_o}$ (%)	$\frac{e}{t}$ (%)	p_i (MPa)	p_f (MPa)	σ_{yp} (MPa)	Indenter type	Comments
226	[44]	28	0.508	2.1	52.5	2.2	120	26.0	6.9	not avail.	413;519;St	notch	burst
227	[44]	29	0.508	2.1	52.5	1.4	120	13.1	15.1	not avail.	413;519;St	notch	burst
228	[44]	30	0.508	2.1	52.5	1.6	120	19.2	15.3	not avail.	413;519;St	notch	burst
229	[44]	31	0.508	2.1	52.5	0.7	115	21.5	11.8	not avail.	413;519;St	notch	burst
230	[44]	32	0.508	2.1	52.5	2.0	112	17.3	11.8	not avail.	413;519;St	notch	burst
231	[44]	33	0.508	2.1	67.0	1.8	97.5	5.7	8.6	not avail.	413;519;St	notch	burst
232	[44]	34	1.067	2.1	92.0	0.5	54.8	2.18	7.03	not avail.	413;519;St	notch	burst
233	[44]	35	1.067	2.1	92.0	1.0	54.8	2.40	7.03	not avail.	413;519;St	notch	burst
234	[44]	36	1.067	2.1	92.0	1.0	54.8	2.62	7.03	not avail.	413;519;St	notch	burst
235	[44]	37	1.067	2.1	92.0	1.2	52.4	3.50	7.03	not avail.	413;519;St	notch	burst
236	[44]	38	1.067	2.1	92.0	1.3	53.6	3.71	7.03	not avail.	413;519;St	notch	burst
237	[44]	39	1.067	2.1	92.0	1.5	54.8	6.77	7.03	not avail.	413;519;St	notch	burst
238	[44]	40	1.067	2.1	92.0	0.8	54.8	1.75	9.65	not avail.	413;519;St	notch	burst
239	[44]	41	1.067	2.1	92.0	0.9	54.8	4.80	9.65	not avail.	413;519;St	notch	burst
240	[44]	42	1.067	2.1	92.0	1.1	55.7	7.42	9.65	not avail.	413;519;St	notch	burst
241	[44]	43	1.067	2.1	92.0	0.7	56.2	5.46	7.03	not avail.	413;519;St	notch	burst
242	[44]	44	1.067	2.1	92.0	1.2	55.5	5.90	7.03	not avail.	413;519;St	notch	burst
243	[44]	45	1.067	2.1	92.0	1.2	54.8	6.55	7.03	not avail.	413;519;St	notch	burst
244	[44]	46	1.067	2.1	92.0	1.2	56.0	9.17	7.03	not avail.	413;519;St	notch	burst
245	[44]	47	1.067	2.1	92.0	1.6	56.7	13.1	7.03	not avail.	413;519;St	notch	burst
246	[44]	48	1.067	2.1	92.0	1.3	4.80	17.5	7.03	not avail.	413;519;St	notch	burst
247	[44]	49	1.067	2.1	92.0	1.3	45.2	5.46	7.03	not avail.	413;519;St	notch	burst
248	[44]	50	1.067	2.1	92.0	1.5	52.4	6.11	7.03	not avail.	413;519;St	notch	burst
249	[44]	51	1.067	2.1	92.0	0.7	54.3	2.84	7.03	not avail.	413;519;St	notch	burst
250	[44]	52	1.067	2.1	92.0	1.2	56.0	4.15	7.03	not avail.	413;519;St	notch	burst

Continued

No:	Ref.	Case	D_o	L	$\frac{D_o}{t}$	$\frac{\delta}{D_o}$	$\frac{2c}{D_o}$	$\frac{e}{t}$	p_i	p_f	σ_{yp}	Indenter type	Comments
			(m)			(%)			(MPa)				
251	[44]	53	1.067	2.1	92.0	1.3	56.0	7.21	7.03	not avail.	413;519;St	notch	burst
252	[44]	54	1.067	2.1	92.0	1.8	56.7	9.17	7.03	not avail.	413;519;St	notch	burst
253	[44]	55	0.508	2.1	101	1.6	80.0	8.4	6.7	not avail.	413;519;St	notch	burst
254	[44]	56	0.508	2.1	101	1.8	77.3	10.1	6.7	not avail.	413;519;St	notch	burst
255	[44]	57	0.508	2.1	101	2.5	79.3	16.8	6.7	not avail.	413;519;St	notch	burst
256	[44]	58	0.508	2.1	74.0	1.8	78.7	9.85	6.7	not avail.	413;519;St	notch	burst
257	[44]	59	0.508	2.1	74.0	2.1	80.0	12.3	6.7	not avail.	413;519;St	notch	burst
258	[44]	60	0.508	2.1	74.0	1.9	78.3	13.6	6.7	not avail.	413;519;St	notch	burst
259	[43]	78-1	0.508	2.1	86.0	3.1	17.0	10.3	not avail.	8.10	497;St	notch	burst
260	[43]	78-1	0.508	2.1	91.0	4.2	17.0	10.0	not avail.	13.9	509;St	notch	burst
261	[43]	48	0.610	2.1	63.0	3.0	11.0	39.5	not avail.	9.70	373;St	notch	burst
262	[43]	47	0.610	2.1	63.0	3.4	11.0	49.5	not avail.	8.83	373;St	notch	burst
263	[43]	44	0.610	2.1	63.0	3.3	11.0	49.5	not avail.	9.31	423;St	notch	burst
264	[43]	18-58	0.610	2.1	79.0	2.7	11.0	50.0	not avail.	6.76	387;St	notch	burst
265	[43]	18-60	0.762	2.1	79.0	2.7	11.0	50.5	not avail.	6.41	387;St	notch	burst
266	[43]	18-119	0.762	2.1	79.0	2.7	7.0	25.3	not avail.	9.83	371;St	notch	burst
267	[43]	18-120	0.762	2.1	79.0	2.7	7.0	25.0	not avail.	9.24	371;St	notch	burst
268	[43]	18-121	0.762	2.1	79.0	2.7	13.0	25.0	not avail.	6.93	371;St	notch	burst
269	[43]	69-17	0.762	2.1	91.0	3.2	33.0	10.0	not avail.	2.48	450;St	notch	burst
270	[43]	70-1	0.762	2.1	91.0	1.3	33.0	10.0	not avail.	9.48	450;St	notch	burst
271	[43]	70-2	0.762	2.1	91.0	1.3	33.0	51.0	not avail.	1.45	450;St	notch	burst
272	[43]	70-4	0.762	2.1	91.0	1.9	33.0	10.0	not avail.	5.0	491;St	notch	burst
273	[43]	70-5	0.762	2.1	91.0	1.3	33.0	20.0	not avail.	6.17	491;St	notch	burst
274	[43]	7-1	0.559	2.1	63.0	3.8	23.0	9.10	not avail.	9.60	279;St	notch	burst
275	[43]	7-2	0.559	2.1	63.0	3.8	45.0	10.0	not avail.	6.10	279;St	notch	burst

Continued

No:	Ref.	Case	D_o (m)	L	$\frac{D_o}{t}$	$\frac{\delta}{D_o}$ (%)	$\frac{2c}{D_o}$ (%)	$\frac{e}{t}$ (%)	p_i (MPa)	p_f (MPa)	σ_{yp} (MPa)	Indenter type	Comments
276	[43]	7-3	0.559	2.1	63.0	3.5	23.0	10.0	not avail.	8.10	279;St	notch	burst
277	[43]	7-4	0.559	2.1	63.0	3.9	23.0	10.0	not avail.	9.80	279;St	notch	burst
278	[43]	7-5	0.762	2.1	88.0	4.0	33.0	10.0	not avail.	11.2	509;St	notch	burst
279	[43]	7-6	0.406	2.1	59.3	5.1	31.0	10.0	not avail.	5.14	401;St	notch	burst
280	[43]	7-7	0.406	2.1	59.3	5.0	63.0	10.4	not avail.	1.40	401;St	notch	burst
281	[43]	7-8	1.067	2.1	108	4.3	24.0	10.3	not avail.	7.20	543;St	notch	burst
282	[43]	7-9	1.067	2.1	108	1.9	24.0	10.3	not avail.	9.10	543;St	notch	burst
283	[43]	7-10	1.067	2.1	108	1.9	12.0	10.3	not avail.	6.48	543;St	notch	burst
284	[43]	7-11	1.067	2.1	108	1.9	24.0	10.3	not avail.	4.06	523;St	notch	burst
285	[43]	7-12	0.406	2.1	59.0	5.7	31.0	11.0	not avail.	5.38	401;St	notch	burst
286	[43]	7-13	0.406	2.1	59.0	5.1	31.0	10.0	not avail.	5.79	401;St	notch	burst
287	[43]	7-14	1.067	2.1	108	2.1	24.0	5.10	not avail.	10.4	523;St	notch	burst
288	[43]	7-15	1.067	2.1	108	2.0	24.0	20.3	not avail.	2.50	523;St	notch	burst
289	[32]	1	0.0318	0.25	18.91	40.0	0.0	0.0	0.0	$0.804p_y$	262;Ss	hemisph.	plain dent;collapse
290	[32]	2	0.0317	0.25	18.26	40.0	0.0	0.0	0.0	$0.783p_y$	331;Ss	hemisph.	plain dent;collapse
291	[32]	3	0.0318	0.25	18.90	40.0	0.0	0.0	0.0	$0.652p_y$	262;Ss	hemisph.	plain dent;collapse
292	[32]	4	0.0318	0.25	18.90	40.0	0.0	0.0	0.0	$0.558p_y$	262;Ss	hemisph.	plain dent;collapse
293	[32]	5	0.0318	0.25	18.88	40.0	0.0	0.0	0.0	$0.473p_y$	262;Ss	hemisph.	plain dent;collapse
294	[32]	6	0.0318	0.25	18.90	40.0	0.0	0.0	0.0	$0.439p_y$	262;Ss	hemisph.	plain dent;collapse
295	[32]	7	0.0318	0.25	18.87	40.0	0.0	0.0	0.0	$0.393p_y$	262;Ss	hemisph.	plain dent;collapse
296	[32]	8	0.0318	0.25	18.92	40.0	0.0	0.0	0.0	$0.370p_y$	262;Ss	hemisph.	plain dent;collapse
297	[32]	9	0.0318	0.25	19.29	16.0	0.0	0.0	0.0	$0.753p_y$	231;Ss	hemisph.	plain dent;collapse
298	[32]	10	0.0317	0.25	19.27	16.0	0.0	0.0	0.0	$0.439p_y$	231;Ss	hemisph.	plain dent;collapse
299	[32]	11	0.0317	0.25	19.28	16.0	0.0	0.0	0.0	$0.331p_y$	231;Ss	hemisph.	plain dent;collapse
300	[32]	12	0.0316	0.25	24.7	40.0	0.0	0.0	0.0	$0.665p_y$	359;Ss	hemisph.	plain dent;collapse

Continued

No:	Ref.	Case	D_o (m)	L	$\frac{D_o}{t}$	$\frac{\delta}{D_o}$ (%)	$\frac{2c}{D_o}$	$\frac{e}{t}$	p_i (MPa)	p_f	σ_{yp}	Indenter type	Comments
301	[32]	13	0.0316	0.25	24.6	40.0	0.0	0.0	0.0	$0.677p_y$	343;Ss	hemisph.	plain dent;collapse
302	[32]	14	0.0316	0.25	24.7	40.0	0.0	0.0	0.0	$0.600p_y$	343;Ss	hemisph.	plain dent;collapse
303	[32]	15	0.0317	0.25	24.6	40.0	0.0	0.0	0.0	$0.539p_y$	372;Ss	hemisph.	plain dent;collapse
304	[32]	16	0.0317	0.25	24.4	40.0	0.0	0.0	0.0	$0.513p_y$	372;Ss	hemisph.	plain dent;collapse
305	[32]	17	0.0317	0.25	24.5	40.0	0.0	0.0	0.0	$0.462p_y$	372;Ss	hemisph.	plain dent;collapse
306	[32]	18	0.0317	0.25	24.4	40.0	0.0	0.0	0.0	$0.424p_y$	372;Ss	hemisph.	plain dent;collapse
307	[32]	19	0.0317	0.25	24.2	40.0	0.0	0.0	0.0	$0.401p_y$	372;Ss	hemisph.	plain dent;collapse
308	[32]	20	0.0316	0.25	24.9	40.0	0.0	0.0	0.0	$0.343p_y$	372;Ss	hemisph.	plain dent;collapse
309	[32]	21	0.0316	0.25	24.8	40.0	0.0	0.0	0.0	$0.305p_y$	372;Ss	hemisph.	plain dent;collapse
310	[32]	22	0.0316	0.25	24.9	40.0	0.0	0.0	0.0	$0.284p_y$	359;Ss	hemisph.	plain dent;collapse
311	[32]	23	0.0316	0.25	24.3	40.0	0.0	0.0	0.0	$0.266p_y$	359;Ss	hemisph.	plain dent;collapse
312	[32]	24	0.0318	0.25	24.7	16.0	0.0	0.0	0.0	$0.552p_y$	343;Ss	hemisph.	plain dent;collapse
313	[32]	25	0.0318	0.25	24.7	16.0	0.0	0.0	0.0	$0.325p_y$	331;Ss	hemisph.	plain dent;collapse
314	[32]	26	0.0318	0.25	24.8	16.0	0.0	0.0	0.0	$0.237p_y$	331;Ss	hemisph.	plain dent;collapse
315	[32]	27	0.0316	0.25	33.6	40.0	0.0	0.0	0.0	$0.934p_y$	331;Ss	hemisph.	plain dent;collapse
316	[32]	28	0.0317	0.25	33.6	40.0	0.0	0.0	0.0	$0.727p_y$	319;Ss	hemisph.	plain dent;collapse
317	[32]	29	0.0316	0.25	33.6	40.0	0.0	0.0	0.0	$0.592p_y$	331;Ss	hemisph.	plain dent;collapse
318	[32]	30	0.0317	0.25	33.6	40.0	0.0	0.0	0.0	$0.503p_y$	331;Ss	hemisph.	plain dent;collapse
319	[32]	31	0.0317	0.25	33.6	40.0	0.0	0.0	0.0	$0.462p_y$	319;Ss	hemisph.	plain dent;collapse
320	[32]	32	0.0317	0.25	33.6	40.0	0.0	0.0	0.0	$0.387p_y$	331;Ss	hemisph.	plain dent;collapse
321	[32]	33	0.0317	0.25	33.6	40.0	0.0	0.0	0.0	$0.346p_y$	331;Ss	hemisph.	plain dent;collapse
322	[32]	34	0.0317	0.25	33.6	40.0	0.0	0.0	0.0	$0.316p_y$	319;Ss	hemisph.	plain dent;collapse
323	[32]	35	0.0316	0.25	33.6	16.0	0.0	0.0	0.0	$0.727p_y$	319;Ss	hemisph.	plain dent;collapse
324	[32]	36	0.0318	0.25	33.6	16.0	0.0	0.0	0.0	$0.428p_y$	319;Ss	hemisph.	plain dent;collapse
325	[32]	37	0.0318	0.25	33.6	16.0	0.0	0.0	0.0	$0.294p_y$	319;Ss	hemisph.	plain dent;collapse

Continued

No:	Ref.	Case	D_o (m)	L	$\frac{D_o}{t}$	$\frac{\delta}{D_o}$ (%)	$\frac{2c}{D_o}$	$\frac{e}{t}$	p_i (MPa)	p_f	σ_{yp}	Indenter type	Comments
326	[3]	1	0.762	ring	60.0	3.06	not avail.	21.8	0.0	97.2;FS	414,427;St	explosive	gouge; burst
327	[3]	2	0.762	ring	60.0	4.69	not avail.	21.8	0.0	37.9;FS	414,427;St	explosive	gouge; burst
328	[3]	3	0.762	ring	60.0	1.18	not avail.	21.8	0.0	180;FS	414,427;St	explosive	gouge; burst
329	[3]	4	0.762	ring	60.0	1.75	not avail.	21.8	0.0	127.6;FS	414,427;St	explosive	gouge; burst
330	[3]	5	0.762	ring	60.0	3.64	not avail.	27.0	0.0	70.3;FS	414,427;St	explosive	gouge; burst
331	[3]	6	0.762	ring	60.0	6.02	not avail.	27.0	0.0	32.4;FS	414,427;St	explosive	gouge; burst
332	[3]	7	0.762	ring	60.0	3.25	not avail.	27.0	0.0	79.3;FS	414,427;St	explosive	gouge; burst
333	[3]	8	0.762	ring	60.0	2.07	not avail.	27.0	0.0	161.3;FS	414,427;St	explosive	gouge; burst
334	[3]	9	0.762	ring	60.0	6.98	not avail.	27.0	0.0	29.3;FS	414,427;St	explosive	gouge; burst
335	[3]	10	0.762	ring	60.0	1.25	not avail.	27.0	0.0	153.1;FS	414,427;St	explosive	gouge; burst
336	[3]	11	0.762	ring	60.0	1.68	not avail.	23.2	0.0	97.2;FS	414,427;St	explosive	gouge; burst
337	[3]	12	0.762	ring	60.0	1.79	not avail.	23.2	0.0	37.9;FS	414,427;St	explosive	gouge; burst
338	[3]	13	0.762	ring	60.0	1.63	not avail.	23.2	0.0	180;FS	414,427;St	explosive	gouge; burst
339	[3]	14	0.762	ring	60.0	1.48	not avail.	23.2	0.0	127.6;FS	414,427;St	explosive	gouge; burst
340	[3]	15	0.762	ring	60.0	1.87	not avail.	23.2	0.0	70.3;FS	414,427;St	explosive	gouge; burst
341	[3]	16	0.762	ring	60.0	1.28	not avail.	35.0	0.0	32.4;FS	414,427;St	explosive	gouge; burst
342	[3]	17	0.762	ring	60.0	1.63	not avail.	35.0	0.0	79.3;FS	414,427;St	explosive	gouge; burst
343	[3]	18	0.762	ring	60.0	1.90	not avail.	35.0	0.0	161.3;FS	414,427;St	explosive	gouge; burst
344	[3]	19	0.762	ring	60.0	1.40	not avail.	35.0	0.0	29.3;FS	414,427;St	explosive	gouge; burst
345	[3]	20	0.762	ring	60.0	1.60	not avail.	35.0	0.0	153.1;FS	414,427;St	explosive	gouge; burst
346	[3]	21	0.762	ring	60.0	2.43	not avail.	5.2	0.0	600.0;FS	414,427;St	explosive	gouge; burst
347	[3]	22	0.762	ring	60.0	2.03	not avail.	8.0	0.0	463.4.0;FS	414,427;St	explosive	gouge; burst
348	[3]	23	0.762	ring	60.0	2.38	not avail.	9.0	0.0	422.0;FS	414,427;St	explosive	gouge; burst
349	[3]	24	0.762	ring	60.0	2.50	not avail.	8.2	0.0	412.4;FS	414,427;St	explosive	gouge; burst
350	[3]	25	0.762	ring	60.0	2.42	not avail.	9.0	0.0	401.0;FS	414,427;St	explosive	gouge; burst

Continued

No:	Ref.	Case	D_o (m)	L	$\frac{D_o}{t}$	$\frac{\delta}{D_o}$ (%)	$\frac{2c}{D_o}$	$\frac{e}{t}$	p_i (MPa)	p_f	σ_{yp}	Indenter type	Comments
351	[3]	26	0.762	ring	60.0	2.42	not avail.	10.4	0.0	391.0;FS	414;427;St	explosive	gouge;burst
352	[3]	27	0.762	ring	60.0	2.52	not avail.	9.80	0.0	389.0;FS	414;427;St	explosive	gouge;burst
353	[3]	28	0.762	ring	60.0	6.71	not avail.	20.0	0.0	193.3;FS	414;427;St	explosive	gouge;burst
354	[3]	29	0.762	ring	60.0	6.90	not avail.	9.0	0.0	104.1;FS	414;427;St	explosive	gouge;burst
355	[3]	30	0.762	ring	60.0	6.97	not avail.	4.0	0.0	197.0.7;FS	414;427;St	explosive	gouge;burst
356	[3]	31	0.762	ring	60.0	6.97	not avail.	18.8	0.0	600.0;FS	414;427;St	explosive	gouge;burst
357	[3]	32	0.762	ring	60.0	7.62	not avail.	2.0	0.0	463.4.0;FS	414;427;St	explosive	gouge;burst
358	[3]	33	0.762	ring	60.0	7.67	not avail.	2.2	0.0	422.0;FS	414;427;St	explosive	gouge;burst
359	[3]	34	0.762	ring	60.0	8.82	not avail.	1.4	0.0	412.4;FS	414;427;St	explosive	gouge;burst
360	[3]	35	0.762	ring	60.0	1.47	not avail.	23.4	0.0	401.0;FS	414;427;St	explosive	gouge;burst
361	[3]	36	0.762	ring	60.0	2.03	not avail.	23.4	0.0	391.0;FS	414;427;St	explosive	gouge;burst
362	[3]	37	0.762	ring	60.0	2.40	not avail.	23.4	0.0	389.0;FS	414;427;St	explosive	gouge;burst
363	[3]	38	0.762	ring	60.0	2.57	not avail.	23.4	0.0	193.3;FS	414;427;St	explosive	gouge;burst
364	[3]	39	0.762	ring	60.0	3.23	not avail.	23.4	0.0	104.1;FS	414;427;St	explosive	gouge;burst
365	[3]	40	0.762	ring	60.0	1.67	not avail.	23.4	0.0	197.0;FS	414;427;St	explosive	gouge;burst
366	[3]	41	0.762	ring	60.0	2.70	not avail.	23.4	0.0	313.1;FS	414;427;St	explosive	gouge;burst
367	[3]	42	0.762	ring	60.0	2.20	not avail.	23.4	0.0	301.4;FS	414;427;St	explosive	gouge;burst
368	[3]	43	0.762	ring	60.0	2.40	not avail.	23.4	0.0	294.4;FS	414;427;St	explosive	gouge;burst
369	[3]	44	0.762	ring	60.0	2.60	not avail.	23.4	0.0	287.0;FS	414;427;St	explosive	gouge;burst
370	[3]	45	0.762	ring	60.0	3.10	not avail.	23.4	0.0	279.3;FS	414;427;St	explosive	gouge;burst
371	[3]	46	0.762	ring	60.0	3.53	not avail.	23.4	0.0	264.1;FS	414;427;St	explosive	gouge;burst
372	[3]	47	0.762	ring	60.0	1.53	not avail.	23.4	0.0	295.1;FS	414;427;St	explosive	gouge;burst
373	[3]	48	0.762	ring	60.0	2.03	not avail.	23.4	0.0	269.0;FS	414;427;St	explosive	gouge;burst
374	[3]	49	0.762	ring	60.0	1.43	not avail.	23.4	0.0	265.0;FS	414;427;St	explosive	gouge;burst
375	[3]	50	0.762	ring	60.0	1.93	not avail.	23.4	0.0	261.0;FS	414;427;St	explosive	gouge;burst

Continued

No:	Ref.	Case	D_o (m)	L	$\frac{D_o}{t}$	$\frac{\delta}{D_o}$ (%)	$\frac{2c}{D_o}$	$\frac{e}{t}$	p_i (MPa)	p_f	σ_{yp}	Indenter type	Comments
376	[3]	51	0.762	ring	60.0	2.47	not avail.	23.4	0.0	228.1;FS	414;427;St	explosive	gouge;burst
377	[3]	52	0.762	ring	60.0	2.83	not avail.	23.4	0.0	234.5;FS	414;427;St	explosive	gouge;burst
378	[3]	53	0.762	ring	60.0	4.07	not avail.	23.4	0.0	199.3;FS	414;427;St	explosive	gouge;burst
379	[3]	54	0.762	ring	60.0	3.30	not avail.	23.4	0.0	188.0;FS	414;427;St	explosive	gouge;burst
380	[3]	55	0.762	ring	60.0	3.97	not avail.	23.4	0.0	184.0;FS	414;427;St	explosive	gouge;burst
381	[3]	56	0.762	ring	60.0	4.47	not avail.	23.4	0.0	150.0;FS	414;427;St	explosive	gouge;burst
382	[3]	57	0.762	ring	60.0	5.37	not avail.	23.4	0.0	127.0;FS	414;427;St	explosive	gouge;burst
383	[30]	1	0.160	0.9	80.0	8.54	47.8	0.0	0.0	dnf	294;St	hemisph.	plain dent;burst
384	[30]	2	0.160	0.9	72.7	8.54	47.8	21.8	10.8	8.75	294;St	hemisph.	cracks;burst
385	[30]	3	0.162	0.9	99.4	10.0	47.8	44.3	7.90	4.80	294;St	hemisph.	cracks;burst
386	[30]	4	0.160	0.9	99.4	6.0	47.8	45.0	7.76	4.5	294;St	hemisph.	cracks;burst
387	[30]	5	0.162	0.9	99.4	6.0	47.8	40.8	11.4	7.5	294;St	hemisph.	cracks;burst
388	[30]	6	0.160	0.9	99.4	6.0	47.8	28.2	8.24	6.8	294;St	hemisph.	cracks;burst
389	[30]	7	0.162	0.9	99.4	10.0	47.8	10.4	11.2	12.0	294;St	hemisph.	cracks;burst
390	[30]	8	0.162	0.9	99.4	6.0	47.8	11.4	10.2	10.5	294;St	hemisph.	cracks;burst
391	[30]	9	0.162	0.9	99.4	2.0	47.8	45.0	7.76	4.75	294;St	hemisph.	cracks;burst
392	[30]	10	0.162	0.9	99.4	2.0	47.8	32.0	7.3	5.75	294;St	hemisph.	cracks;burst
393	[30]	11	0.162	0.9	99.4	2.0	47.8	10.9	10.7	11.0	294;St	hemisph.	cracks;burst
394	[30]	12	0.162	0.9	99.4	4.0	47.8	28.9	8.05	6.90	294;St	hemisph.	cracks;burst
395	[30]	13	0.162	0.9	99.4	4.0	47.8	12.9	9.02	10.5	294;St	hemisph.	cracks;burst
396	[30]	14	0.162	0.9	99.4	4.0	47.8	21.8	10.7	9.8	294;St	hemisph.	cracks;burst
397	[30]	15	0.162	0.9	99.4	4.0	47.8	36.0	9.7	6.5	294;St	hemisph.	cracks;burst
398	[30]	16	0.162	0.9	99.4	10.0	47.8	26	9.0	7.5	294;St	hemisph.	cracks;burst
399	[30]	17	0.162	0.9	99.4	8.0	47.8	11.4	10.2	9.2	294;St	hemisph.	cracks;burst
400	[30]	18	0.162	0.9	99.4	8.0	47.8	28.2	8.3	7.0	294;St	hemisph.	cracks;burst

Continued

No:	Ref.	Case	D_o	L	$\frac{D_o}{t}$	$\frac{\delta}{y}D_o$	$\frac{2c}{D_o}$	$\frac{e}{t}$	p_i	p_f	σ_{yp}	Indenter type	Comments
			(m)			(%)			(MPa)				
401	[75]	A-1	0.216	1.0	36.0	8.5	77.7	40.0	0.0	5076C	488;St	notch	fatigue
402	[75]	A-2	0.216	1.0	36.0	13.9	77.7	30.0	0.0	2515C	488;St	notch	fatigue
403	[75]	A-3	0.216	1.0	36.0	14.0	77.7	40.0	0.0	1552C	488;St	notch	fatigue
404	[75]	A-seam1	0.216	1.0	36.0	8.3	39.0	40.0	0.0	1C,fail	488;St	notch	fatigue
405	[75]	A-seam2	0.216	1.0	36.0	13.9	39.0	40.0	0.0	1C,fail	488;St	notch	fatigue
406	[75]	A-seams1	0.216	1.0	36.0	8.3	39.0	40.0	0.0	5076C	488;St	notch	fatigue
407	[75]	A-seams2	0.216	1.0	36.0	14.0	39.0	40.0	0.0	2515C	488;St	notch	fatigue
408	[75]	B-1	0.219	1.0	28.0	8.3	77.7	22.0	0.0	4247C	415;St	notch	fatigue
409	[75]	B-2	0.219	1.0	28.0	7.3	77.7	29.3	0.0	8322C	415;St	notch	fatigue
410	[75]	B-3	0.219	1.0	28.0	8.5	77.7	29.3	0.0	989C	415;St	notch	fatigue
411	[75]	B-4	0.219	1.0	28.0	13.7	77.7	22.0	0.0	4C,fail	415;St	notch	fatigue
412	[75]	B-5	0.219	1.0	28.0	13.7	77.7	29.3	0.0	1C,fail	415;St	notch	fatigue
413	[75]	C-1	0.216	1.0	26.0	8.3	77.7	22.0	0.0	4443C	539;St	notch	fatigue
414	[75]	C-2	0.216	1.0	26.0	8.3	77.7	29.3	0.0	2666C	539;St	notch	fatigue
415	[75]	C-3	0.216	1.0	26.0	8.3	77.7	29.3	0.0	36C	539;St	notch	fatigue
416	[75]	CSR-1	0.216	1.0	26.0	8.3	77.7	22.0	0.0	130C	539;St	notch	fatigue
417	[75]	CSR-2	0.216	1.0	26.0	8.3	77.7	29.3	0.0	18C	539;St	notch	fatigue
418	[75]	D-1	0.224	1.0	34.0	18.8	77.7	30.5	0.0	1491C	459;St	notch	fatigue
419	[75]	Dseam-1	0.224	1.0	34.0	18.8	77.7	33.7	0.0	1693C	459;St	notch	fatigue
420	[75]	Dseam-2	0.224	1.0	34.0	20.5	77.7	33.7	0.0	1470C	459;St	notch	fatigue

St ≡ mild steel, Al≡ Alminum, Se ≡ seamles steel, Ss ≡ stainless steel, cyl. ≡ cylinder, hemisph. ≡ hemispherical,

$\star$ ≡ subjected to cyclic loading, $\star\star$ ≡ failure pressure due to cyclic loading,

C ≡ cyclic to failure, FS ≡ failure stress, p_y ≡ yield pressure, p_i ≡ internal pressure, p_f ≡ failure pressure, σ_{yp} ≡ yield point of material, not avail. ≡ not available, dnf ≡ did not fail

Table A.1: Details about the existing experiments on dents, gouges, and combination of both.

Appendix B

PATRAN and ABAQUS files

Sample of the Patran journal file (*.db.jou) with the model data being truncated

```
$$ Creating journal file /tmp/ibrahim/journal.db.jou
uil_file_rebuild.start("/apps/patran2001/patran2001r2/template.db", @
"/tmp/ibrahim/journal.db")
$$---------- Global tolerance----------
$$
pref_geo_set_v1( 0, 0.0099999998, 3 )
pref_global_set_v2( TRUE, 3, "0.0003" )
pref_env_set_logical( "revert_enabled", FALSE )
$$
$$----------Creating points----------
$$
STRING asm_create_grid_xyz_created_ids[VIRTUAL]
asm_const_grid_xyz( "1", "[0.041 0 0]", "Coord 0",  @
asm_create_grid_xyz_created_ids )
$# 1 Point created: Point 1
asm_const_grid_xyz( "2", "[0.041 0.1288052988 0]", "Coord 0",  @
asm_create_grid_xyz_created_ids )
$# 1 Point created: Point 2
asm_const_grid_xyz( "3", "[0.041 0.1288052988 0.2523]", "Coord 0",  @
asm_create_grid_xyz_created_ids )
$# 1 Point created: Point 3
asm_const_grid_xyz( "4", "[0.041 0  0.2523]", "Coord 0",  @
asm_create_grid_xyz_created_ids )
$# 1 Point created: Point 4
asm_const_grid_xyz( "5", "[0.041 0.004  0.004]", "Coord 0",  @
asm_create_grid_xyz_created_ids )
--
--
--
asm_const_grid_xyz( "29", "[0.041 0.0858701992 0]", "Coord 0",  @
asm_create_grid_xyz_created_ids )
$# 1 Point created: Point 29
asm_const_grid_xyz( "30", "[0.041 0.083 0]", "Coord 0",  @
asm_create_grid_xyz_created_ids )
$# 1 Point created: Point 30
asm_const_grid_xyz( "31", "[0.041 0.0644026494 0]", "Coord 0",  @
asm_create_grid_xyz_created_ids )
$# 1 Point created: Point 31
asm_const_grid_xyz( "32", "[0.041 0.0644026494 0.2523]", "Coord 0",  @
asm_create_grid_xyz_created_ids )
$# 1 Point created: Point 32
asm_const_grid_xyz( "33", "[0.041  0.0644026494  0.035 ]", "Coord 0",  @
asm_create_grid_xyz_created_ids )
$# 1 Point created: Point 33
$$
$$----------Create curves----------
$$
STRING sgm_create_curve_2d_created_ids[VIRTUAL]
```

```
sgm_const_curve_2d_arc2point_v2( "1", 1, 0., FALSE, FALSE, 1, "Coord 0.1",  @
"Point 1", "Point 8", "Point 17", FALSE, sgm_create_curve_2d_created_ids )
$# 1 Curve Created: Curve 1
sgm_const_curve_2d_arc2point_v2( "2", 1, 0., FALSE, FALSE, 1, "Coord 0.1",  @
"Point 1", "Point 9", "Point 18", FALSE, sgm_create_curve_2d_created_ids )
$# 1 Curve Created: Curve 2
sgm_const_curve_2d_arc2point_v2( "3", 1, 0., FALSE, FALSE, 1, "Coord 0.1",  @
"Point 1", "Point 10", "Point 19", FALSE, sgm_create_curve_2d_created_ids )
$# 1 Curve Created: Curve 3
sgm_const_curve_2d_arc2point_v2( "4", 1, 0., FALSE, FALSE, 1, "Coord 0.1",  @
"Point 1", "Point 11", "Point 20", FALSE, sgm_create_curve_2d_created_ids )
$# 1 Curve Created: Curve 4
sgm_const_curve_2d_arc2point_v2( "5", 1, 0., FALSE, FALSE, 1, "Coord 0.1",  @
"Point 1", "Point 12", "Point 21", FALSE, sgm_create_curve_2d_created_ids )
$# 1 Curve Created: Curve 5
sgm_const_curve_2d_arc2point_v2( "6", 1, 0., FALSE, FALSE, 1, "Coord 0.1",  @
"Point 1", "Point 13", "Point 22", FALSE, sgm_create_curve_2d_created_ids )
$# 1 Curve Created: Curve 6
sgm_const_curve_2d_arc2point_v2( "7", 1, 0., FALSE, FALSE, 1, "Coord 0.1",  @
"Point 1", "Point 14", "Point 16", FALSE, sgm_create_curve_2d_created_ids )
$# 1 Curve Created: Curve 7
sgm_const_curve_2d_arc2point_v2( "8", 1, 0., FALSE, FALSE, 1, "Coord 0.1",  @
"Point 1", "Point 16", "Point 15", FALSE, sgm_create_curve_2d_created_ids )
--
--
--
asm_const_line_2point( "66", "Point 27", "Point 32", 0, "", 50., 1,  @
asm_line_2point_created_ids )
$# 1 Line created: Line 66
asm_const_line_2point( "67", "Point 32", "Point 23", 0, "", 50., 1,  @
asm_line_2point_created_ids )
$# 1 Line created: Line 67
asm_const_line_2point( "68", "Point 23", "Point 4", 0, "", 50., 1,  @
asm_line_2point_created_ids )
$# 1 Line created: Line 68
$$$
$$$
$$$----------------------Create surfaces-----------------------------------------------
$$$
STRING sgm_surface_4edge_created_ids[VIRTUAL]
sgm_const_surface_4edge( "1", "Curve 24", "Curve 23", "Curve 22", "Curve 21",  @
sgm_surface_4edge_created_ids )
$# 1 Surface Created: Surface 1
sgm_const_surface_4edge( "2", "Curve 19", "Curve 39", "Curve 24", "Curve 25",  @
sgm_surface_4edge_created_ids )
$# 1 Surface Created: Surface 2
sgm_const_surface_4edge( "3", "Curve 17", "Curve 40", "Curve 19", "Curve 26",  @
sgm_surface_4edge_created_ids )
$# 1 Surface Created: Surface 3
sgm_const_surface_4edge( "4", "Curve 15", "Curve 41", "Curve 17", "Curve 27",  @
```

```
sgm_surface_4edge_created_ids )
$# 1 Surface Created: Surface 4
sgm_const_surface_4edge( "5", "Curve 13", "Curve 42", "Curve 15", "Curve 28",  @
sgm_surface_4edge_created_ids )
--
--
--
sgm_const_surface_4edge( "21", "Curve 65", "Curve 53", "Curve 62", "Curve 55", @
 sgm_surface_4edge_created_ids )
$# 1 Surface Created: Surface 21
sgm_const_surface_4edge( "22", "Curve 62", "Curve 52", "Curve 48", "Curve 54", @
 sgm_surface_4edge_created_ids )
$# 1 Surface Created: Surface 22
sgm_const_surface_4edge( "23", "Curve 64", "Curve 51", "Curve 63", "Curve 53", @
 sgm_surface_4edge_created_ids )
$# 1 Surface Created: Surface 23
sgm_const_surface_4edge( "24", "Curve 63", "Curve 50", "Curve 49", "Curve 52", @
 sgm_surface_4edge_created_ids )
$# 1 Surface Created: Surface 24
$$
$$----------------------Create solids----------------------------------------------------
$$
STRING sgm_sweep_solid_ext_created_ids[VIRTUAL]\\
sgm_const_solid_extrude( "1", "<0.00105 0 0>", 1., 0., "[0 0 0]", "Coord 0",  @\\
"Surface 1:24", sgm_sweep_solid_ext_created_ids )\\
$# 24 Solids Created: Solids 1:24\\
sgm_const_solid_extrude( "25", "<-0.00105 0 0>", 1., 0., "[0 0 0]", "Coord 0", @\\
 "Surface 1:24", sgm_sweep_solid_ext_created_ids )\\
$# 24 Solids Created: Solids 25:48\\
$$
$$--------------Create boundary conditions----------------------------------------------
$$
loadsbcs_create2( "PLANEX", "Displacement", "Nodal", "", "Static", [ @\\
"Solid 23.1 26:30.1 36:38:2.1 1.2 16:48:32.2 2:6.3 12.3 14:47:33.3 24.4 25" // @\\
":40:15.4"], "Geometry", "Coord 0", "1.", ["< 1,,   >", "<    >"], ["", ""] )\\
$# Load/BC set "PLANEX" created.\\
loadsbcs_create2( "PLANEZ", "Displacement", "Nodal", "", "Static", [ @\\
"Solid 7:11.2 13.2 15.2 18:24:2.2 25.2 1.4 31:35.4 37.4 39.4 42:48:2.4"],  @\\
"Geometry", "Coord 0", "1.", ["<   >", "< ,1,  >"], ["", ""] )\\
$# Load/BC set "PLANEZ" created.\\
loadsbcs_create2( "NMPC", "Displacement", "Nodal", "", "Static", [ @\\
"Solid 40.1 41:47:2.1 16.3 17:23:2.3"], "Geometry", "Coord 0", "1.", ["<   >" @\\
, "< ,1,  >"], ["", ""] )\\
$# Load/BC set "NMPC" created.\\
$$
$$--------------Create pressure surface ------------------------------------------------
$$
loadsbcs_create2( "FACE", "Pressure", "Element Uniform", "3D", "Static", [ @\\
"Solid 40.1 41:47:2.1 16.3 17:23:2.3"], "Geometry", "", "1.", [" 1"], [""] )\\
*# Load/BC set "FACE" created.\\
```

```
loadsbcs_create2( "INSIDE", "Pressure", "Element Uniform", "3D", "Static", [ @\\
"Solid 25:48.6"], "Geometry", "", "1.", ["2"], [""] )\\
$# Load/BC set "INSIDE" created.\\
loadsbcs_create2( "GROUND", "Pressure", "Element Uniform", "3D", "Static", [ @\\
"Solid 23:24.6"], "Geometry", "", "1.", ["3"], [""] )\\
$# Load/BC set "GROUND" created.\\
loadsbcs_create2( "A1", "Pressure", "Element Uniform", "3D", "Static", [ @\\
"Solid 1.6 2:7:5.6"], "Geometry", "", "1.", ["0.1"], [""] )\\
--\\
--\\
loadsbcs_create2( "B4", "Pressure", "Element Uniform", "3D", "Static", [ @\\
"Solid 6:11:5.6"], "Geometry", "", "1.", ["0.5"], [""] )\\
$# Load/BC set "B4" created.\\
loadsbcs_create2( "B5", "Pressure", "Element Uniform", "3D", "Static", [ @\\
"Solid 12:13.6"], "Geometry", "", "1.", ["0.6"], [""] )\\
$# Load/BC set "B5" created.\\
loadsbcs_create2( "B6", "Pressure", "Element Uniform", "3D", "Static", [ @\\
"Solid 14:15.6"], "Geometry", "", "1.", ["0.7"], [""] )\\
$# Load/BC set "B6" created.\\
$$\\
$$----------Create mesh seed through thickness----------
$$
mesh_seed_create( "Solid 47.1.1", 1, 1, 0., 0., 0. )
mesh_seed_create( "Solid 23.1.1", 1, 1, 0., 0., 0. )
mesh_seed_create( "Solid 45.1.1", 1, 1, 0., 0., 0. )
mesh_seed_create( "Solid 21.1.1", 1, 1, 0., 0., 0. )
mesh_seed_create( "Solid 19.1.1", 1, 1, 0., 0., 0. )
mesh_seed_create( "Solid 43.1.1", 1, 1, 0., 0., 0. )
mesh_seed_create( "Solid 41.1.1", 1, 1, 0., 0., 0. )
mesh_seed_create( "Solid 17.1.1", 1, 1, 0., 0., 0. )
mesh_seed_create( "Solid 15.2.1", 1, 1, 0., 0., 0. )
mesh_seed_create( "Solid 15.2.3", 1, 1, 0., 0., 0. )
mesh_seed_create( "Solid 39.2.3", 1, 1, 0., 0., 0. )
mesh_seed_create( "Solid 37.2.3", 1, 1, 0., 0., 0. )
--
--
--
mesh_seed_create( "Solid 18.2.3", 1, 1, 0., 0., 0. )
mesh_seed_create( "Solid 1.1.3", 1, 1, 0., 0., 0. )
mesh_seed_create( "Solid 25.2.1", 1, 1, 0., 0., 0. )
$$
$$----------Create mesh seed for length ----------
$$
mesh_seed_create( "Curve 22", 1, 3, 0., 0., 0. )
mesh_seed_create( "Curve 23", 1, 3, 0., 0., 0. )
mesh_seed_create( "Curve 24", 1, 3, 0., 0., 0. )
mesh_seed_create( "Curve 21", 1, 3, 0., 0., 0. )
mesh_seed_create( "Curve 32", 1, 3, 0., 0., 0. )
mesh_seed_create( "Curve 39", 1, 3, 0., 0., 0. )
```

```
mesh_seed_create( "Curve 25", 1, 3, 0., 0., 0. )
mesh_seed_create( "Curve 20", 1, 7, 0., 0., 0. )
--
--
--
mesh_seed_create( "Curve 58", 1, 50, 0., 0., 0. )
mesh_seed_create( "Curve 57", 1, 50, 0., 0., 0. )
mesh_seed_create( "Curve 55", 1, 50, 0., 0., 0. )
mesh_seed_create( "Curve 53", 1, 50, 0., 0., 0. )
mesh_seed_create( "Curve 51", 1, 50, 0., 0., 0. )
$$
$$----------Create mesh----------
$$
INTEGER fem_create_mesh_solid_num_nodes
INTEGER fem_create_mesh_solid_num_elems
STRING fem_create_mesh_s_nodes_created[VIRTUAL]
STRING fem_create_mesh_s_elems_created[VIRTUAL]
fem_create_mesh_sol_5( "Solid 1:48", "IsoMesh", "Hex20", 1, ["0.00647372"],  @
49152, 0, 1, 0, 1, 0., "", "#", "#", "Coord 0", "Coord 0",  @
fem_create_mesh_solid_num_nodes, fem_create_mesh_solid_num_elems,  @
fem_create_mesh_s_nodes_created, fem_create_mesh_s_elems_created )
$$
$$----------Run the analysis----------
$$
```

APPENDIX B: PATRAN AND ABAQUS FILES

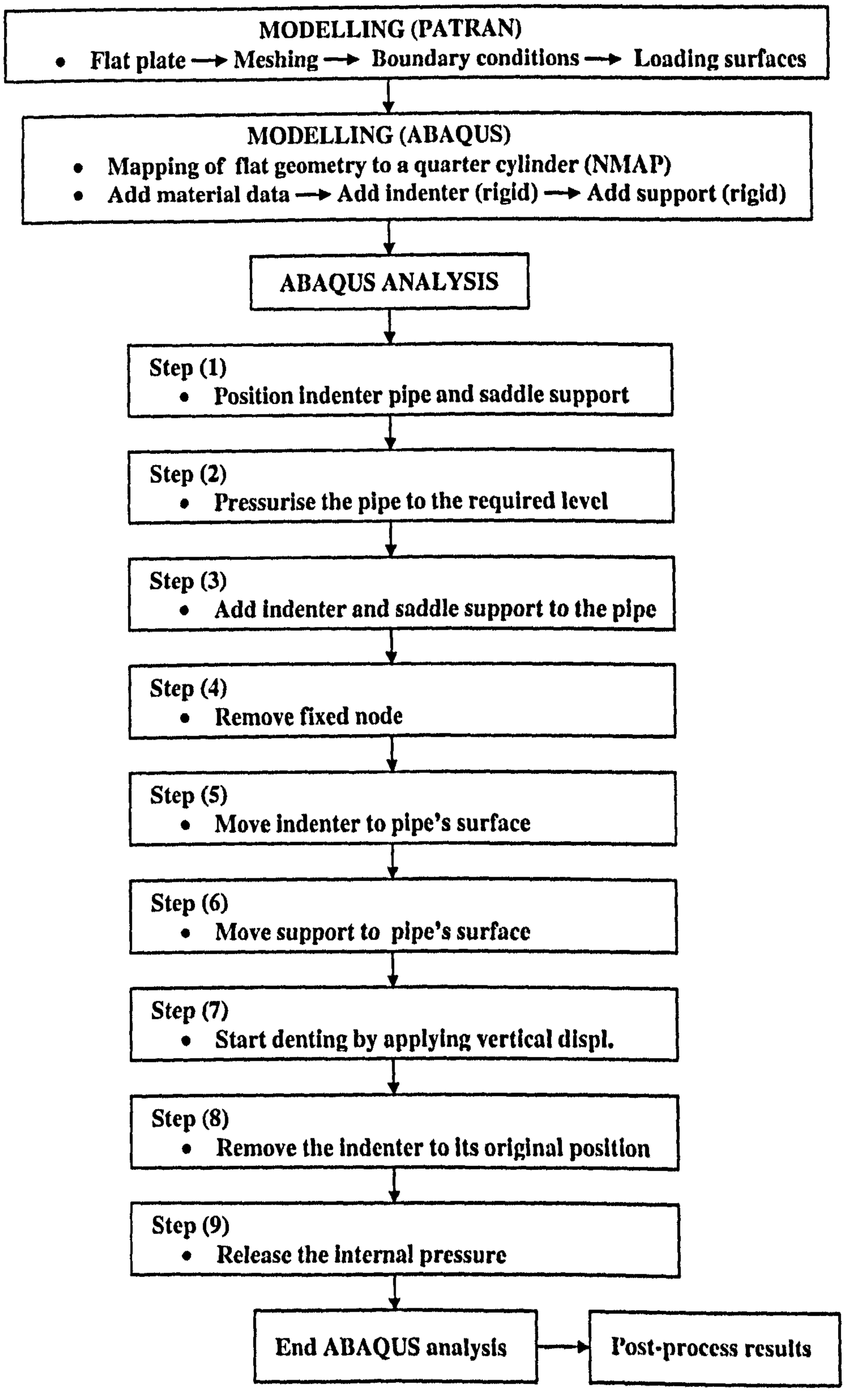

Figure B.1: The sequence of FE modelling and analyses steps.

APPENDIX B: PATRAN AND ABAQUS FILES

A sample of the input file used by ABAQUS with model data being truncated (model SP2).

```
**********************************************************************
*HEADING
*PREPRINT,MODEL=NO, HISTORY=NO, ECHO=NO
**********************************************************************
*NODE,NSET=MASTER                    (Master node for rotation of MPC)
555555, 0.0  ,0.0  , 0.253
*NODE,NSET=PUNCH
 70000,  0.0 ,  0.059495 ,0.0        (Reference node for indenter)
 60000 , -0.080,-0.080 ,-0.035       (Reference node for indenter)
**********************************************************************
*NODE, NSET=GEOM1
     1,      0.0421,          0.,      -0.005
     2,      0.0421,          0.,    -0.00375
     3,      0.0421,          0.,     -0.0025
     4,      0.0421,          0.,    -0.00125
     5,      0.0421,          0.
     6,      0.0421,     0.00125,      -0.005
     7,      0.0421,     0.00125,     -0.0025        Geometry
     8,      0.0421,     0.00125                    (Creating nodes)
     9,      0.0421,      0.0025,      -0.005
   --
   --
   --
 27344,     0.04003,   0.0258536,      -0.253
 27345,     0.04003,   0.0278423,      -0.253
 27346,     0.04003,   0.0298311,      -0.253
**********************************************************************
*ELEMENT, TYPE=C3D20R, ELSET=ALL
     1,    33,    35,    43,    41,    63,    65,    73,
    71,    34,    38,    42,    37,    64,    68,    72,
    67,    53,    54,    57,    56
     2,     3,     5,    13,    11,    33,    35,    43,
   --
   --                                                          Geometry
   --                                                          (Creating elements)
  3887,  7306,  7308,  7475,  7473,  9703,  9705,  9872,
  9870,  7307,  7418,  7474,  7417,  9704,  9815,  9871,
  9814,  9087,  9088,  9144,  9143
  3888, 14048, 14050,  7308,  7306, 14661, 14663,  9705,
  9703, 14049, 14160,  7307, 14159, 14662, 14773,  9704,
 14772, 14382, 14383,  9088,  9087
**********************************************************************
*NSET,NSET=GEOM
GEOM1,MASTER
*NSET,NSET=TOP
5, 70000
**********************************************************************
*ORIENTATION, NAME=ELE  ,SYSTEM=CYLINDRICAL
```

```
0.0,0.0,0.0,  0.0,0.0,0.1
3,0.0
*SOLID SECTION,ELSET=ALL , MATERIAL=STEEL,ORIENTATION=ELE
*MATERIAL,NAME=STEEL
*ELASTIC
210.0E09, 0.30
*PLASTIC
316.0E06 , 0.0
328.00E06 , 0.005120                    (Model section & Material properties)
--
--
--
598.44E06 , 0.327600
589.50E06 , 0.330110
**********************************************************************
*NSET, NSET=PLANEZ
    5,    8,   13,   16,   21,   24,   27,   30,
    --
    --
 21825, 21842, 21851, 21868, 21877, 21894, 21903, 21920,
 21929, 21946, 21955, 21972,  21981
*NSET, NSET=NMPC
  7306,  7417,  7473,  7584,  7640,  7751,  7807,  7918,
  7974,  8085,  8141,  8252,  8308,  8419,  8475,  8586,
  --
  --
 27334, 27335, 27336, 27337, 27338, 27339, 27340, 27341,
 27342, 27343, 27344, 27345,  27346
*ELSET, ELSET=FACE
  2969,  2970,  3055,  3056,  3137,  3138,  3215,  3216,
  3289,  3290,  3359,  3360,  3425,  3426,  3487,  3488
*ELSET, ELSET=FACE_1
  3507,  3508,  3563,  3564,  3581,  3582,  3631,  3632,          (BCs)
  --
  --
  3875,  3876,  3883,  3884,  3885,  3886,  3887,  3888
*NSET, NSET=PLANEX
    1,    2,    3,    4,    5,   22,   23,   24,
    --                                                          (BCs)
    --
 27114, 27123, 27140, 27149, 27166, 27175, 27192, 27201,
 27218, 27227, 27244, 27253, 27270, 27279, 27296, 27305,
 27322,  27331
*ELSET, ELSET=INDAREA
    2,    4,    6,    8,   10,   12,   15,   16,
    --
    --
   98,  100,  103,  104,  106,  108,  110,  112,    (Creating contact area)
  114,  116,  118,  120,  122,  124,  128,  129,
  130,  132,  135,  136,  138,  140,  161,  162
```

```
*ELSET, ELSET=INSIDE
   1,    3,    5,    7,    9,   11,   13,   14,
  17,   19,   21,   22,   25,   27,   29,   31,
  --                                                    (Define area of pressure)
  --
3857, 3859, 3861, 3863, 3864, 3865, 3869, 3871,
3873, 3875, 3877, 3879, 3880, 3883, 3885, 3886
*ELSET, ELSET=GROUND
 282,  286,  290,  294,  298,  302,  306,  310,
 316,  318,  364,  368,  372,  376,  380,  384,
 --                                                   (Creating contact area)
 --
3830, 3832, 3838, 3844, 3846, 3854, 3856, 3858,
3866, 3868, 3874, 3876, 3882, 3887
**********************************************************************
*NMAP,NSET=GEOM,TYPE=CYLINDRICAL  (Rotating the plate to pipe)
0.0, 0.0, 0.0,  0.0,0.0, -10.0
0.0,15.0 ,-10.0
1.0,1360.9448,1.0
**********************************************************************
*MPC
*BEAM,NMPC,555555
**********************************************************************
*SURFACE , TYPE=REVOLUTION, NAME=REVSURF
0.0, 0.059495, 0.0  , 0.0, 0.077, 0.0
START,0.01735,0.10
LINE,0.01735,0.0                                    (Creating Hemispherical indenter)
CIRCL,0.0,-0.01735,0.0,0.0
*RIGID BODY, ANALYTICAL SURFACE=REVSURF,  REF NODE=70000
*SURFACE ,NAME=CSURF
INDAREA,S1
*CONTACT PAIR,INTERACTION=ROUGH,SMALL SLIDING,ADJUST=0.0
CSURF,REVSURF
*SURFACE INTERACTION, NAME=ROUGH
*FRICTION
0.35
**********************************************************************
*SURFACE , TYPE=CYLINDER, NAME=RSURF
-0.080, -0.080, 0.0   ,   0.080,-0.080,0.0
-0.080,-0.080,-0.025
START,0.0, 0.07286
LINE,0.0194,0.07286
CIRCL,0.0435,0.05893 ,0.0194,0.045                  (Creating saddle support)
CIRCL,0.1165,0.05893, 0.08,0.080
CIRCL,0.14062,0.07286,    0.14062, 0.045
LINE,0.160  , 0.07286
*RIGID BODY, ANALYTICAL SURFACE=RSURF,  REF NODE=60000
*SURFACE ,NAME=GRSURF
GROUND,S1
*CONTACT PAIR,INTERACTION=SMOOTH,SMALL SLIDING,ADJUST=0.0
```

```
GRSURF,RSURF
*SURFACE INTERACTION,NAME=SMOOTH
*FRICTION
0.10
**********************************************************************
*BOUNDARY
21282,2,2
70000,1,1
70000,3,6                                    (BC)
60000,1,6
PLANEX,1,1
PLANEZ,3,3
**********************************************************************
*STEP,INC=10, NLGEOM        (Step 1,  separate rigid surfaces )
*STATIC
1.0,1.0
*MODEL CHANGE, TYPE=CONTACT PAIR, REMOVE
CSURF,REVSURF
GRSURF,RSURF
*END STEP
**********************************************************************
*STEP, INC=30, NLGEOM        (Step 2, Pressurisation)
*STATIC
0.1,1.0
*DLOAD
INSIDE, P2   , 11.175E06
FACE,  P5 , -106.8E06
FACE_1, P6 ,-106.8E06
*MONITOR,NODE=5 ,DOF=2
*NODE PRINT,NSET=TOP, FREQ=2
U1
*EL PRINT,ELSET=GAUGES, POSITION=AVERAGED AT NODES, FREQ=1
E
*RESTART,WRITE,FREQ=1
*END STEP
**********************************************************************
*STEP,INC=20,NLGEOM     ( Step 3, bring indenter and saddle surfaces to contact)
*STATIC
1.0,1.0
*MODEL CHANGE, TYPE=CONTACT PAIR, add
CSURF,REVSURF
GRSURF,RSURF
*END STEP
**********************************************************************
*STEP,INC=10, NLGEOM   (Step 4, release the fixed node)
*STATIC
1.0,1.0
*BOUNDARY
70000,1,1
70000,3,6
```

```
60000,1,6
PLANEX,1,1
PLANEZ,3,3
*END STEP
**********************************************************************
*STEP,INC=20, NLGEOM  (Step 5, adjusting indenter and pipe's surfaces )
**STEP2 INTERFERENCE FIT USING EXACT INTERFERENCE MAG.
*STATIC
0.1,1.0
*CONTACT INTERFERENCE
GRSURF,RSURF,0.20
*END STEP
**********************************************************************
*STEP,INC=20,NLGEOM  (Step 6, adjusting saddle and pipe's surfaces )
**STEP2 INTERFERENCE FIT USING EXACT INTERFERENCE MAG.
*STATIC
0.1,1.0
*CONTACT INTERFERENCE
CSURF,REVSURF,0.20
*END STEP
**********************************************************************
*STEP, INC=250,NLGEOM  (Step 7, denting )
*STATIC
0.1,1.0
*BOUNDARY
70000,2,2,-0.0196
*MONITOR,NODE=5 ,DOF=2
*NODE PRINT, NSET=TOP, FREQ=2
U,
RF
*EL PRINT,POSITION=AVERAGED AT NODES,SUMMARY=YES,
ELSET=GAUGES, FREQ=2
E
*OUTPUT, FIELD, VARIABLE=PRESELECT
*ELEMENT OUTPUT,ELSET=GAUGES
E
*OUTPUT, HISTORY
*NODE OUTPUT, NSET=TOP
U
RF
*RESTART,WRITE,FREQ=2
*END STEP
**********************************************************************
*STEP, INC=200, NLGEOM  (Step 8, remove indenter )
*STATIC
0.1,1.0
*BOUNDARY
70000,2,2,0.0
*MONITOR,NODE=5 ,DOF=2
*NODE PRINT, NSET=TOP, FREQ=2
```

```
U,
RF
*EL PRINT,POSITION=AVERAGED AT NODES,SUMMARY=YES,
ELSET=GAUGES, FREQ=2
E
*OUTPUT, FIELD, VARIABLE=PRESELECT
*ELEMENT OUTPUT,ELSET=GAUGES
E
*OUTPUT, HISTORY
*NODE OUTPUT, NSET=TOP
U
RF
*RESTART,WRITE,FREQ=2
*END STEP
**********************************************************************
*STEP, INC=120, NLGEOM  (Step 9, release the internal pressure )
*STATIC
0.1,1.0
*DLOAD
INSIDE, P2   , 0.0
FACE,  P5 , 0.0
FACE_1, P6 ,0.0
*MONITOR,NODE=5 ,DOF=2
*NODE PRINT, NSET=TOP, FREQ=2
U,
RF
*EL PRINT,POSITION=AVERAGED AT NODES,SUMMARY=YES,
ELSET=GAUGES, FREQ=2
E
*OUTPUT, FIELD, VARIABLE=PRESELECT
*ELEMENT OUTPUT,ELSET=GAUGES
E
*OUTPUT, HISTORY
*NODE OUTPUT, NSET=TOP
U, RF
*RESTART,WRITE,FREQ=2
*END STEP
```

Appendix C

The AutoCAD drawings for experimental denting

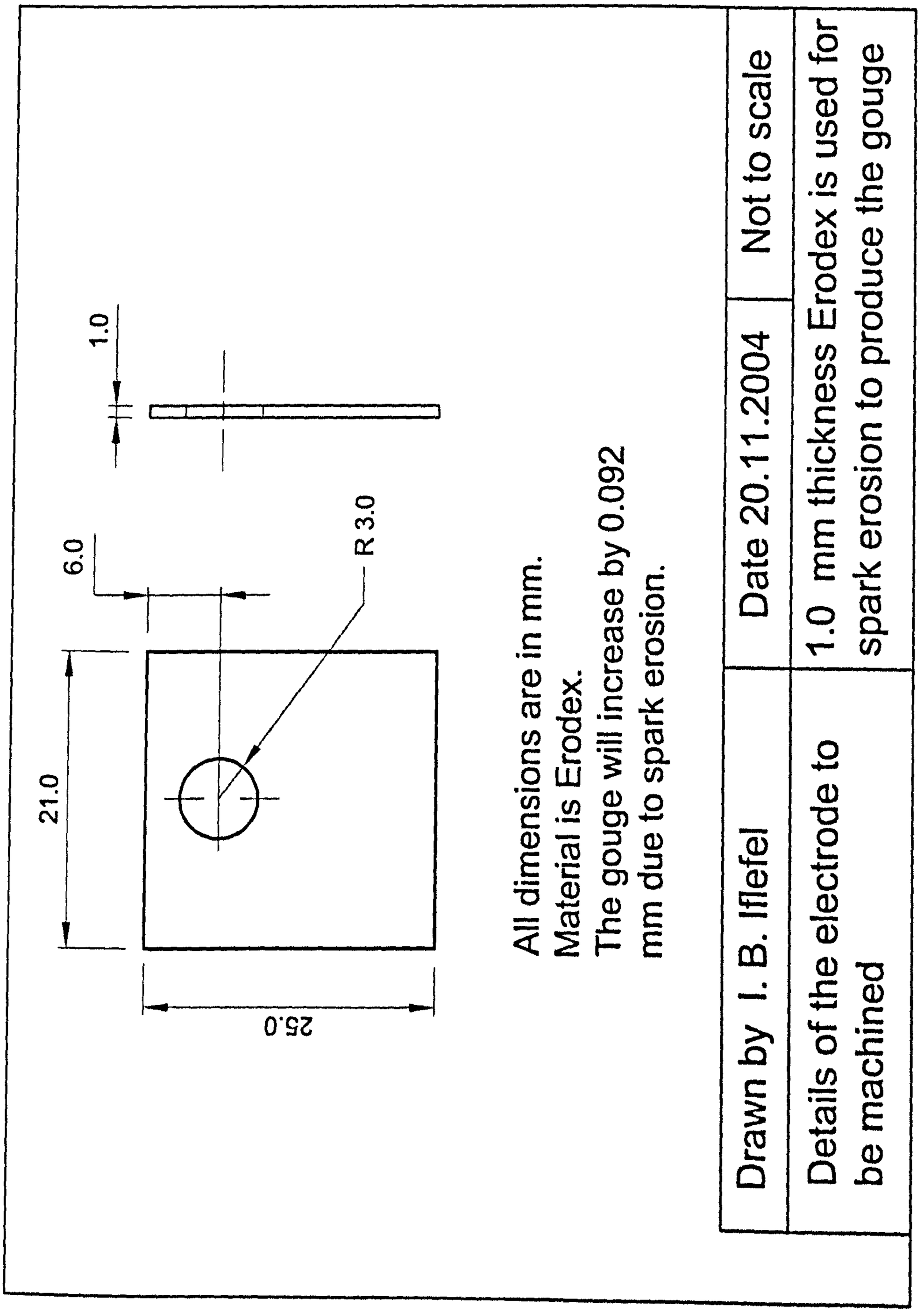

Figure C.1: Sketch showing details of Erodex electrode to be used for manufacturing axial gouge of length, $2c = 21.0\ mm$.

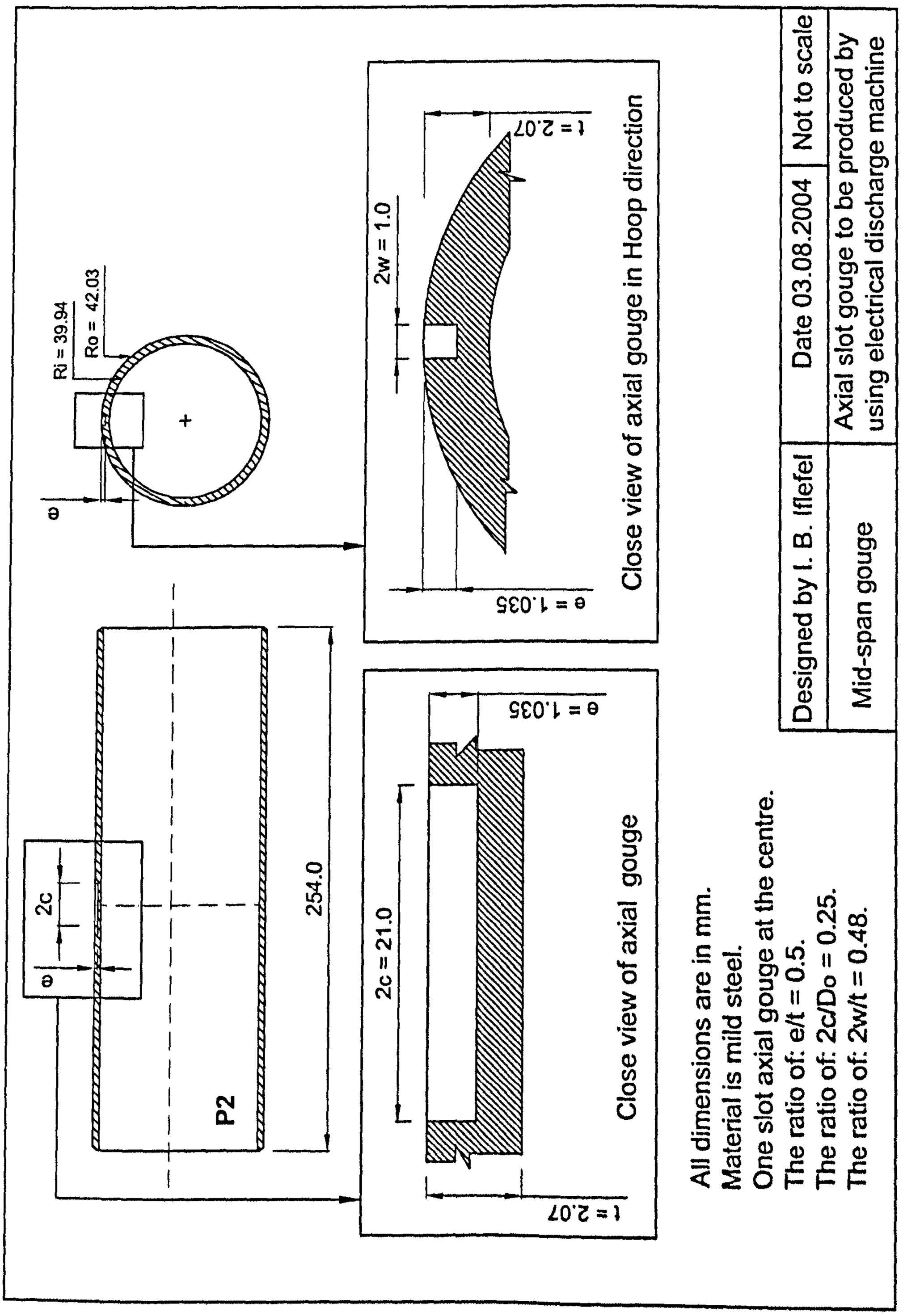

Figure C.2: Sketch of the machined axial gouge at mid-span to be created by using electrical discharge machine (in part P2 of model SP4).

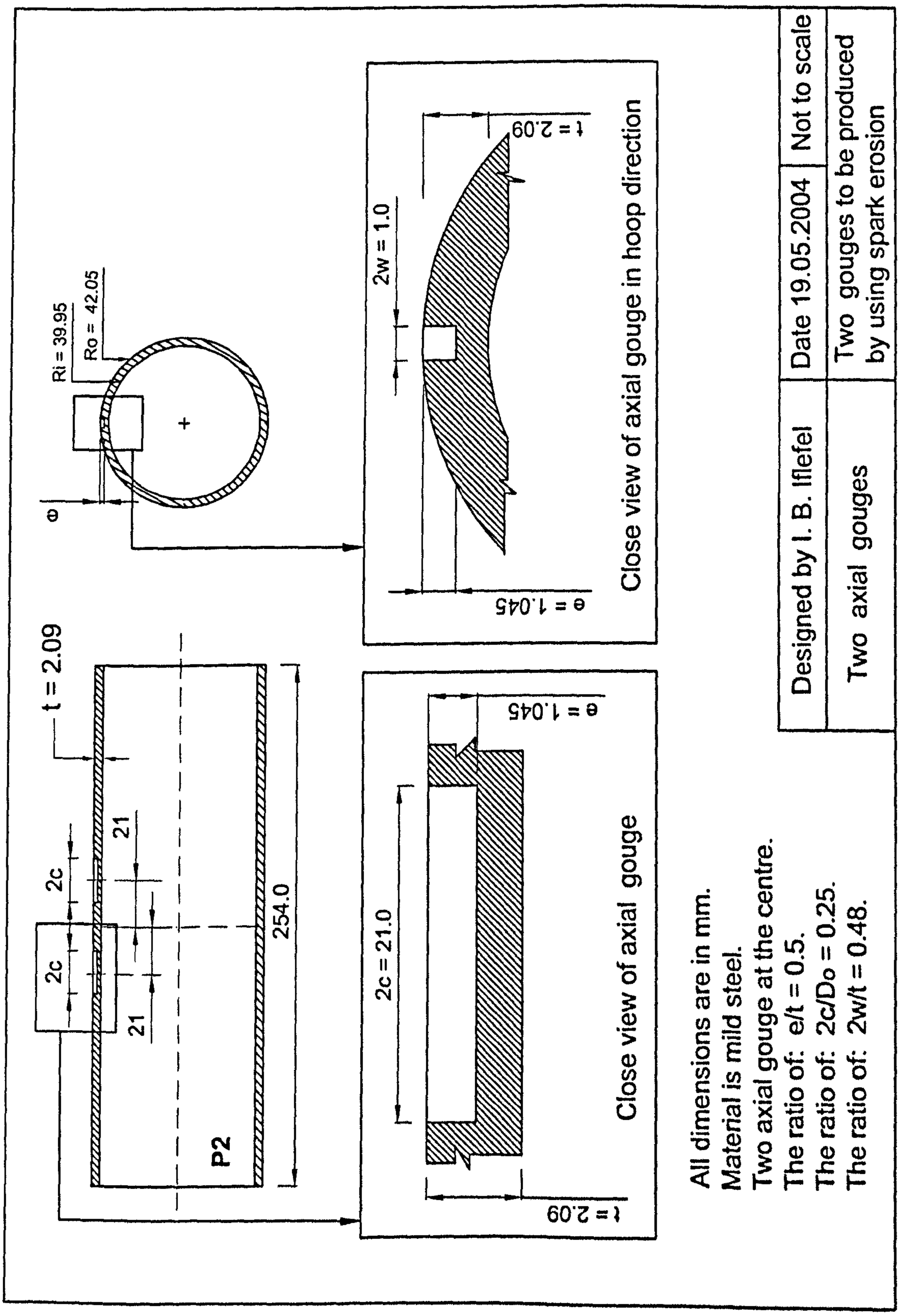

Figure C.3: Sketch of the machined two axial gouges at off-centre created by using electrical discharge machine (in part P2 of model SP5).

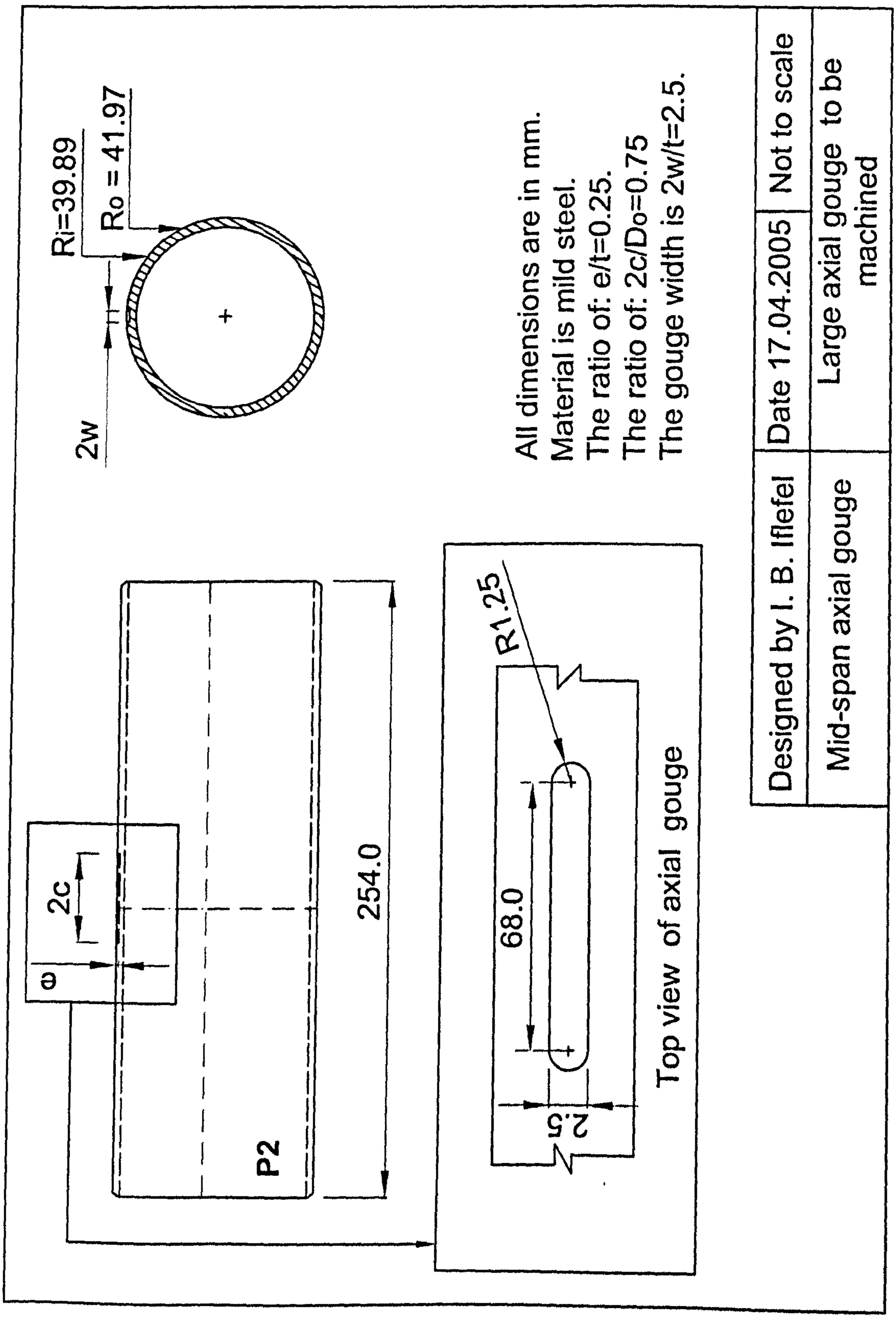

Figure C.4: Sketch of the machined axial gouge at mid-span created by using lathe machine (in part P2 of model SP6).

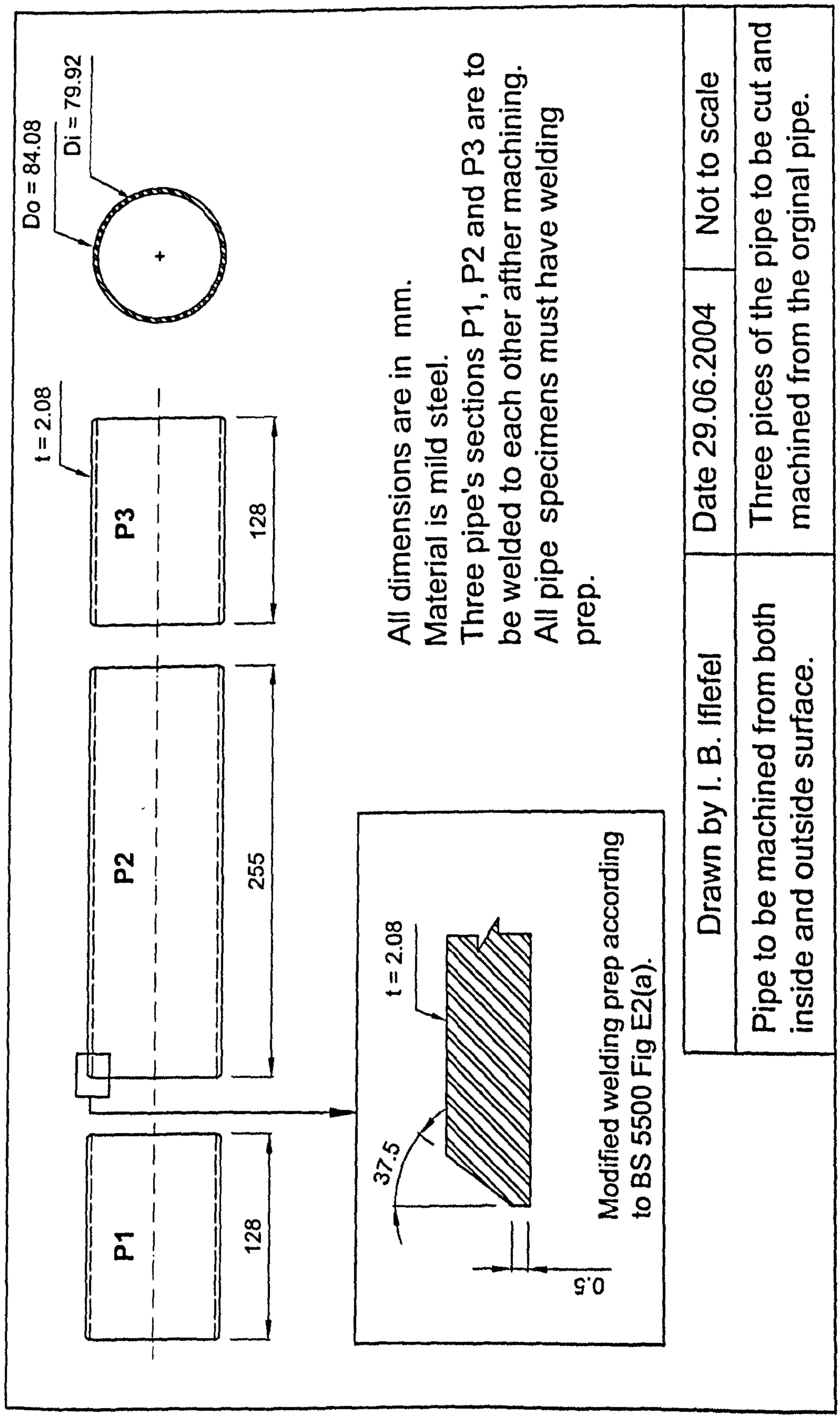

Figure C.5: Details of the machining of the test specimens with their welding prep, SP3.

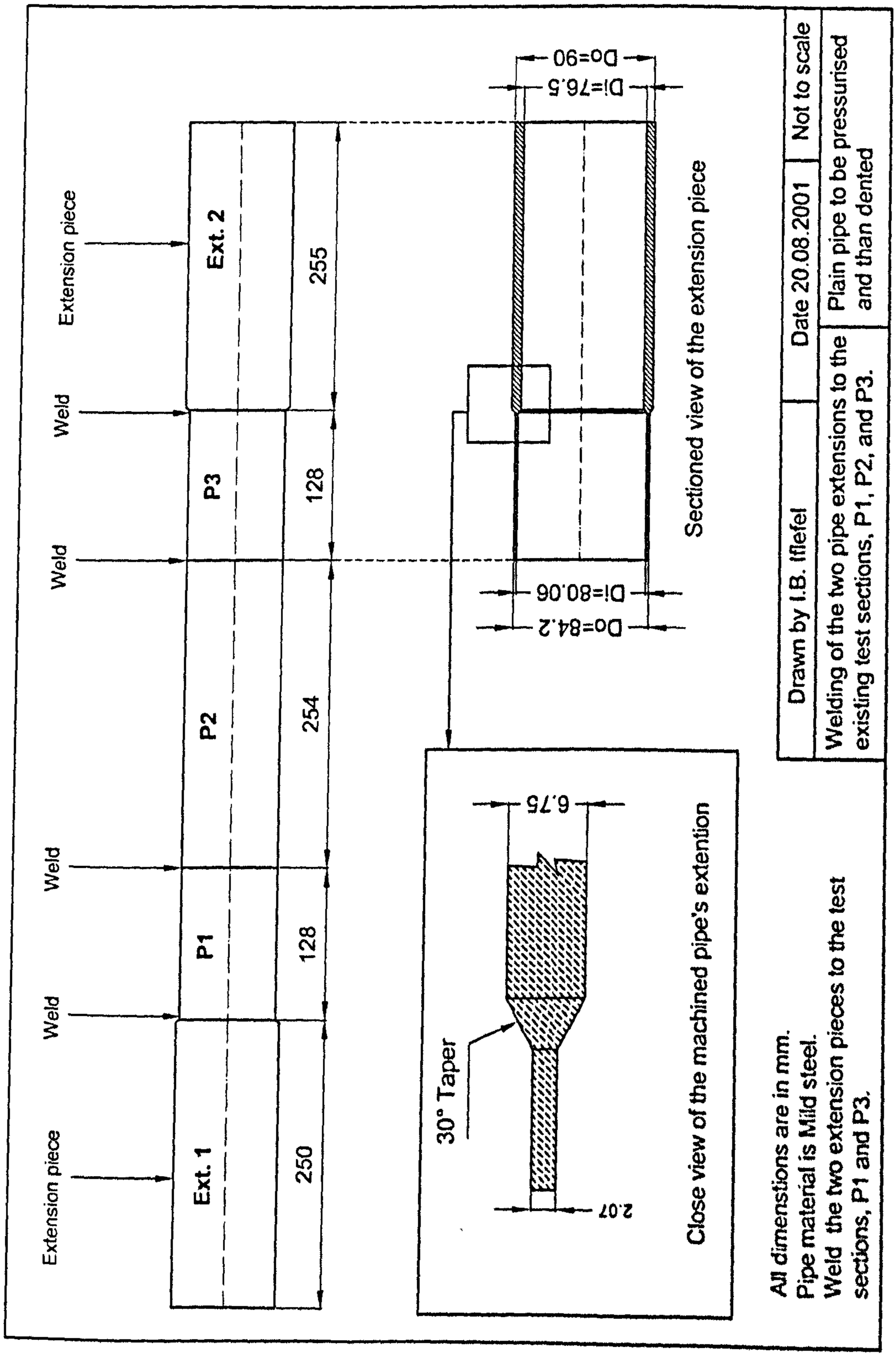

Figure C.6: Details about welding of test specimens P1, P2, P3, and extensions (according to modified BS 5500 Fig E2(a) [70]).

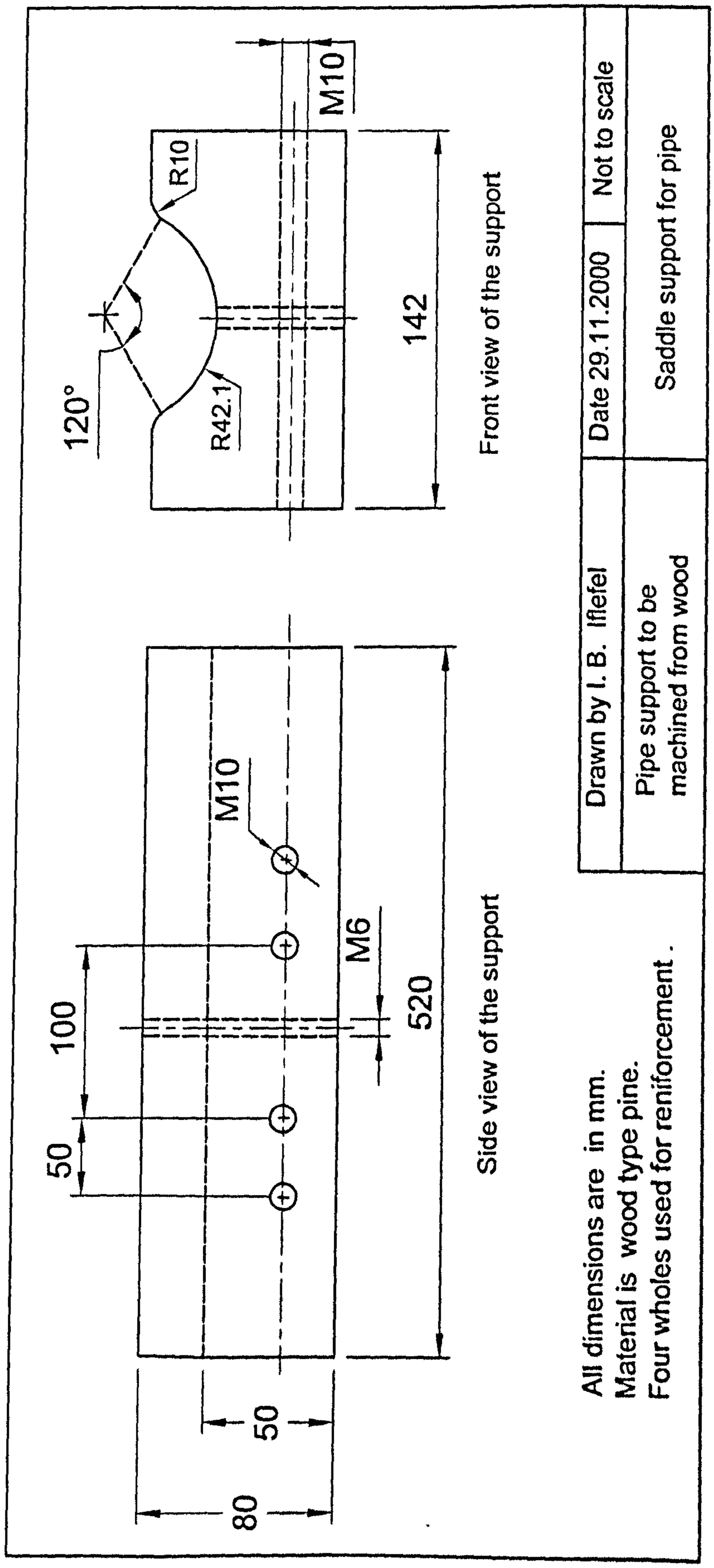

Figure C.7: Details of wooden saddle support to be used during denting.

Appendix C: The AutoCAD drawings for experimental denting

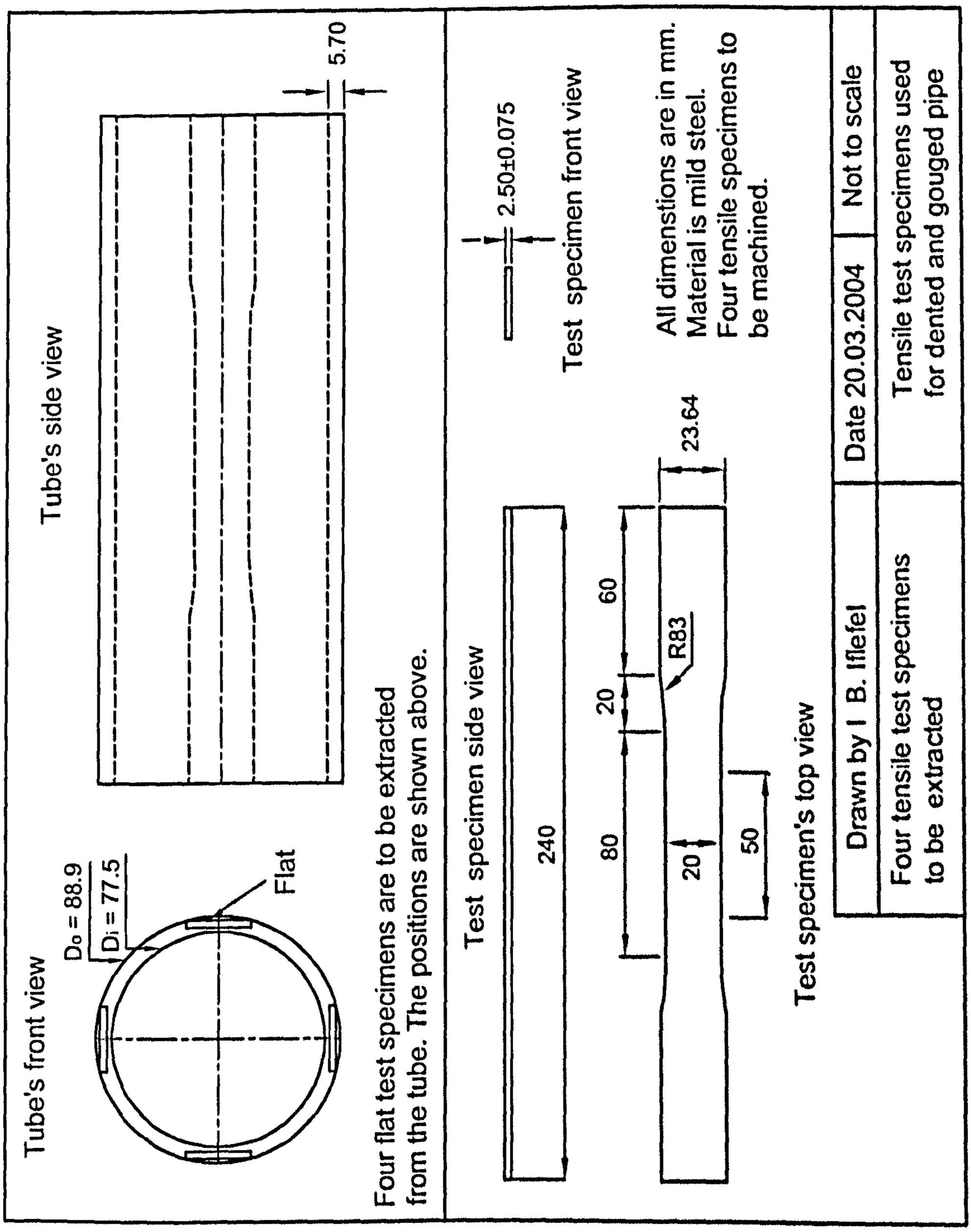

Figure C.8: Details of tensile test specimens according to *BS EN* 10002 – 1 : 1990 [71].

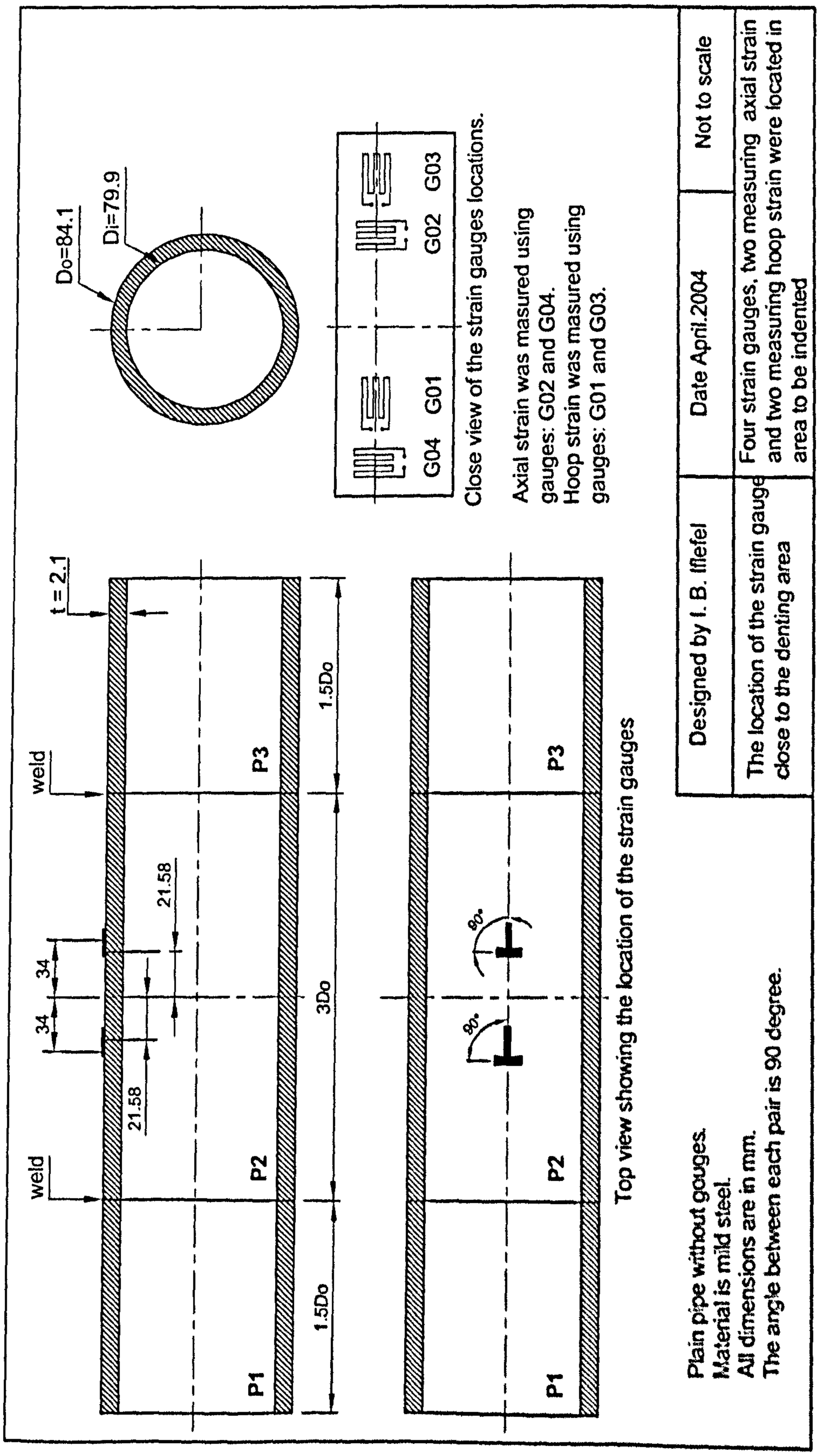

Figure C.9: Strain gauge locations and their directions for plain pipe without defect, SP2.

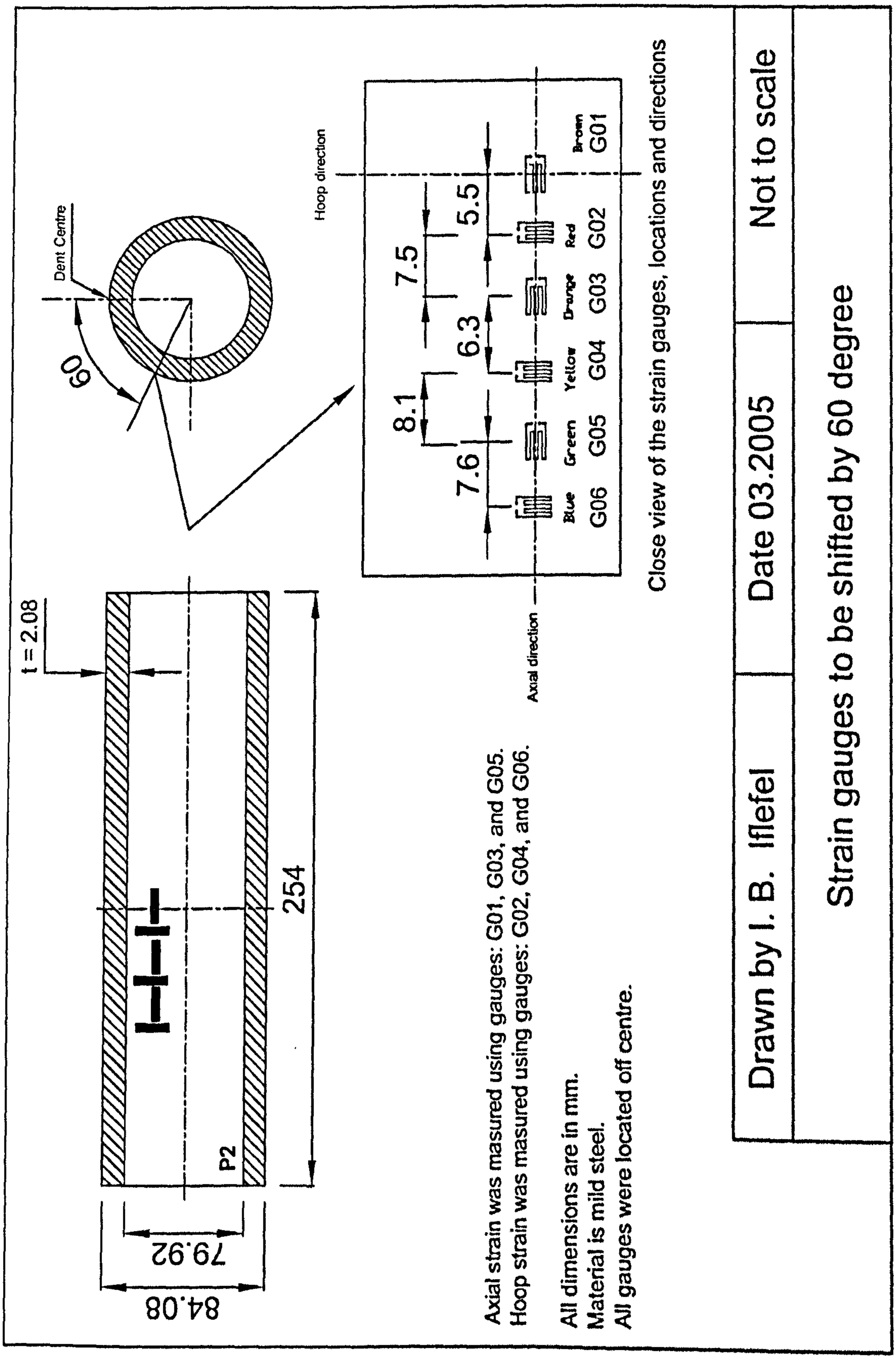

Figure C.10: Strain gauge locations and their directions for plain pipe. Note that strain gauges are shifted to one side (in part P2 of model SP3).

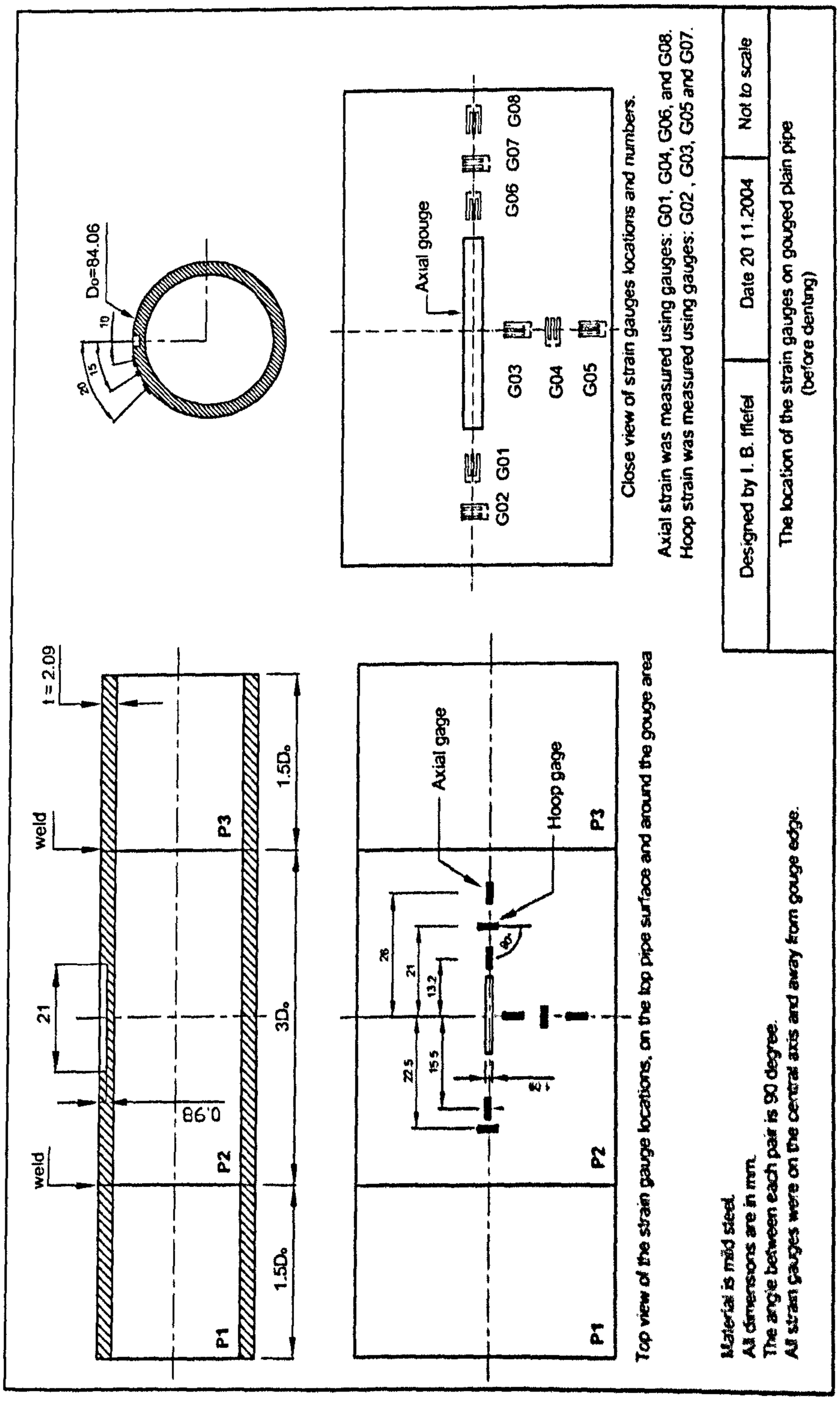

Figure C.11: Strain gauge locations and their directions for pipe with mid-span gouge (in part P2 of model SP4).

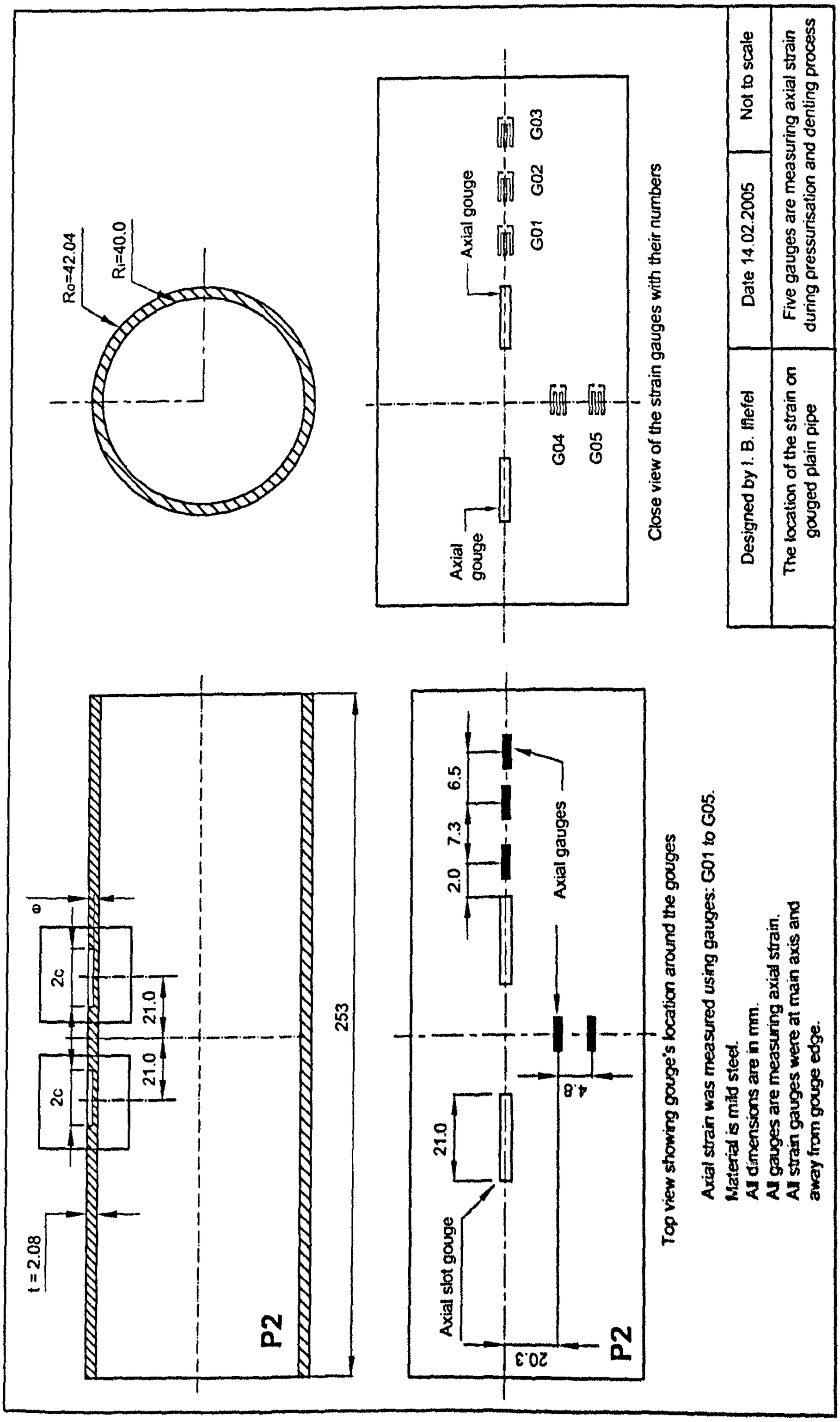

Figure C.12: Strain gauge locations and their directions for plain pipe with two axial gouges (in part P2 of model SP5).

Appendix D

The AutoCAD drawings for experimental bending

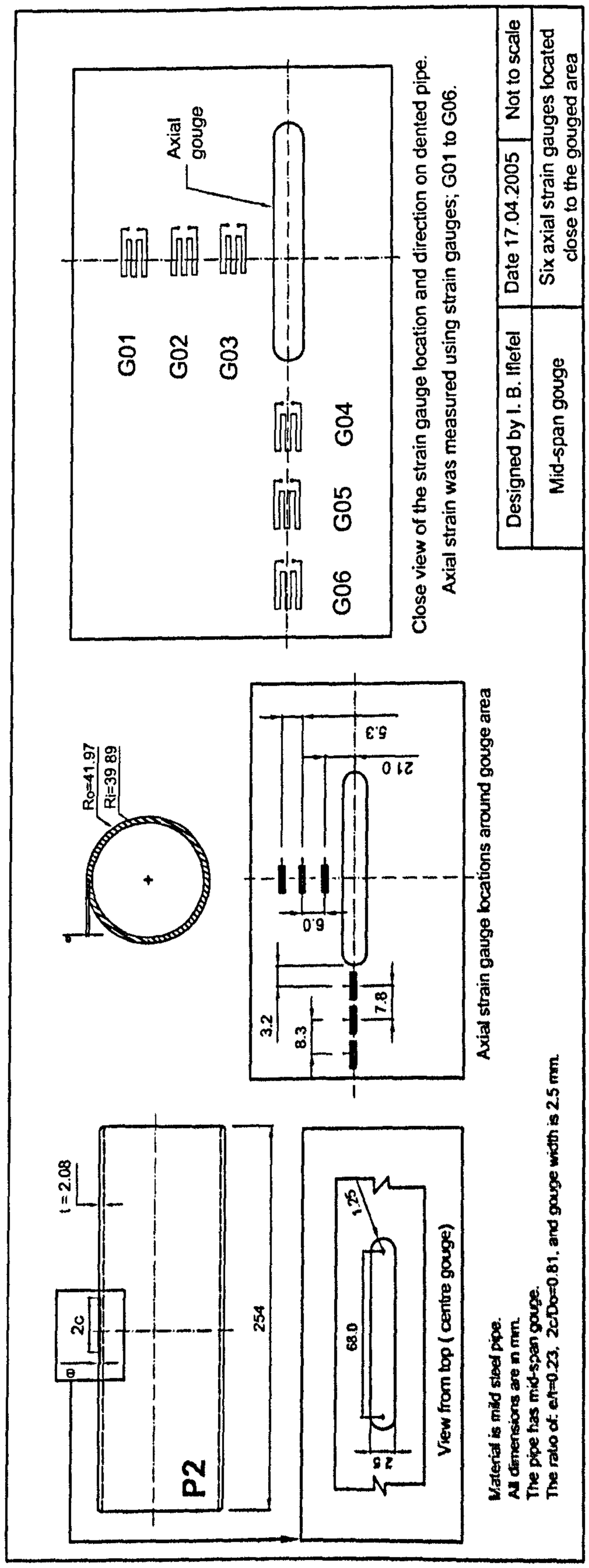

Figure C.13: Strain gauge locations and their directions for plain pipe with machined wider gouge (in part P2 of model SP6).

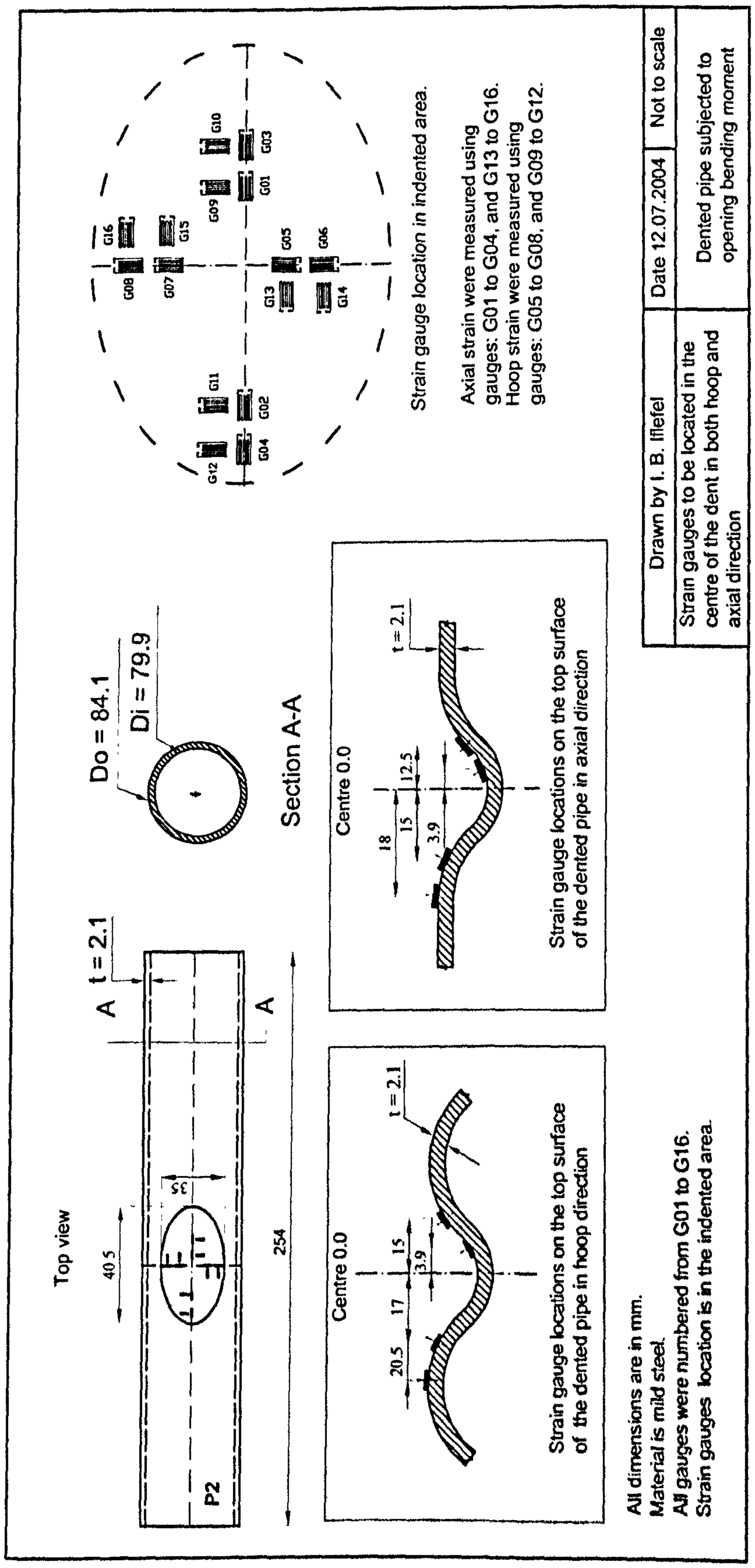

Figure D.1: Strain gauge locations and their directions for plain pipe (in part P2 of model SP2).

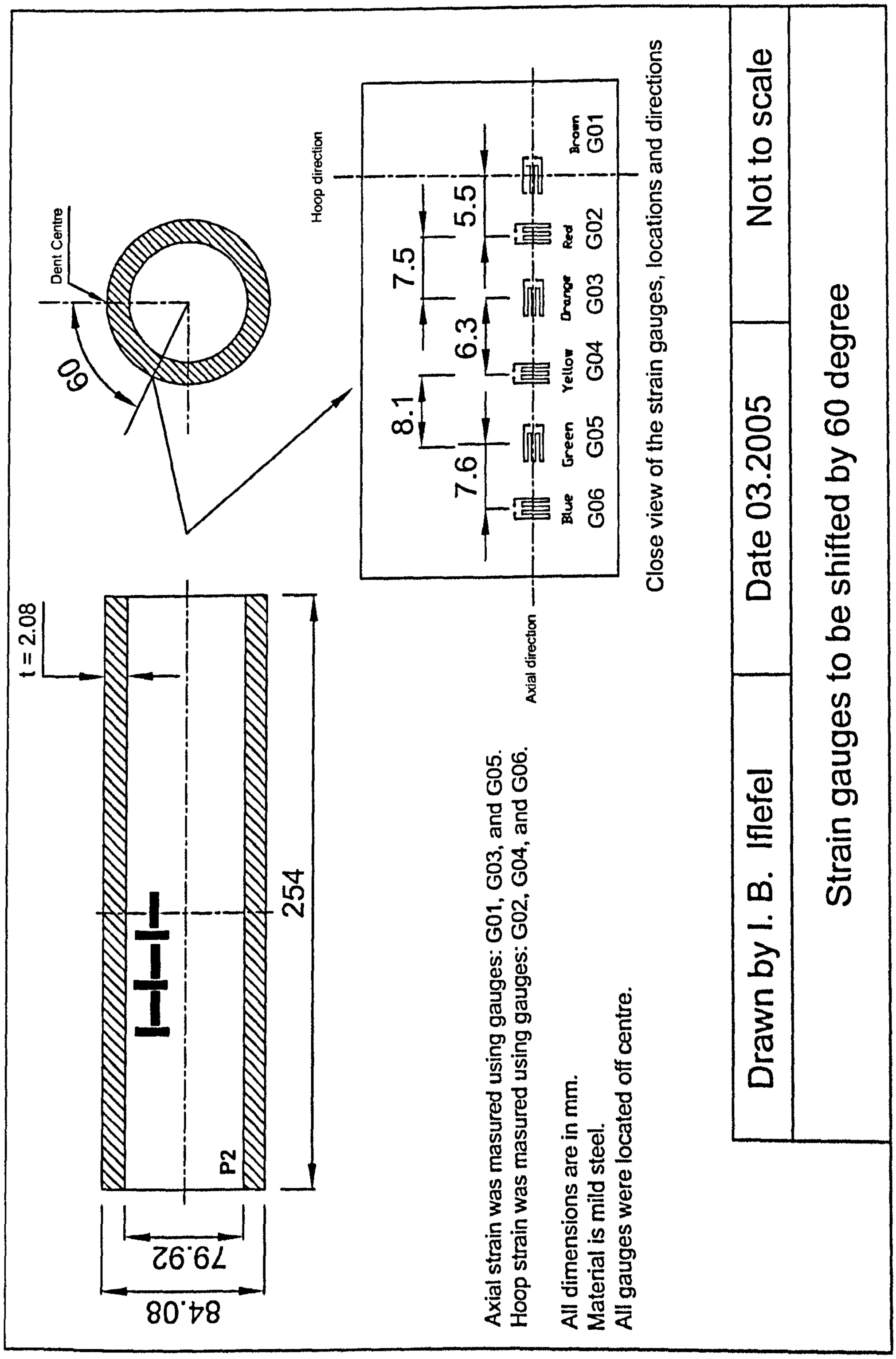

Figure D.2: Strain gauge locations and their directions for plain pipe (in part P2 of model SP3).

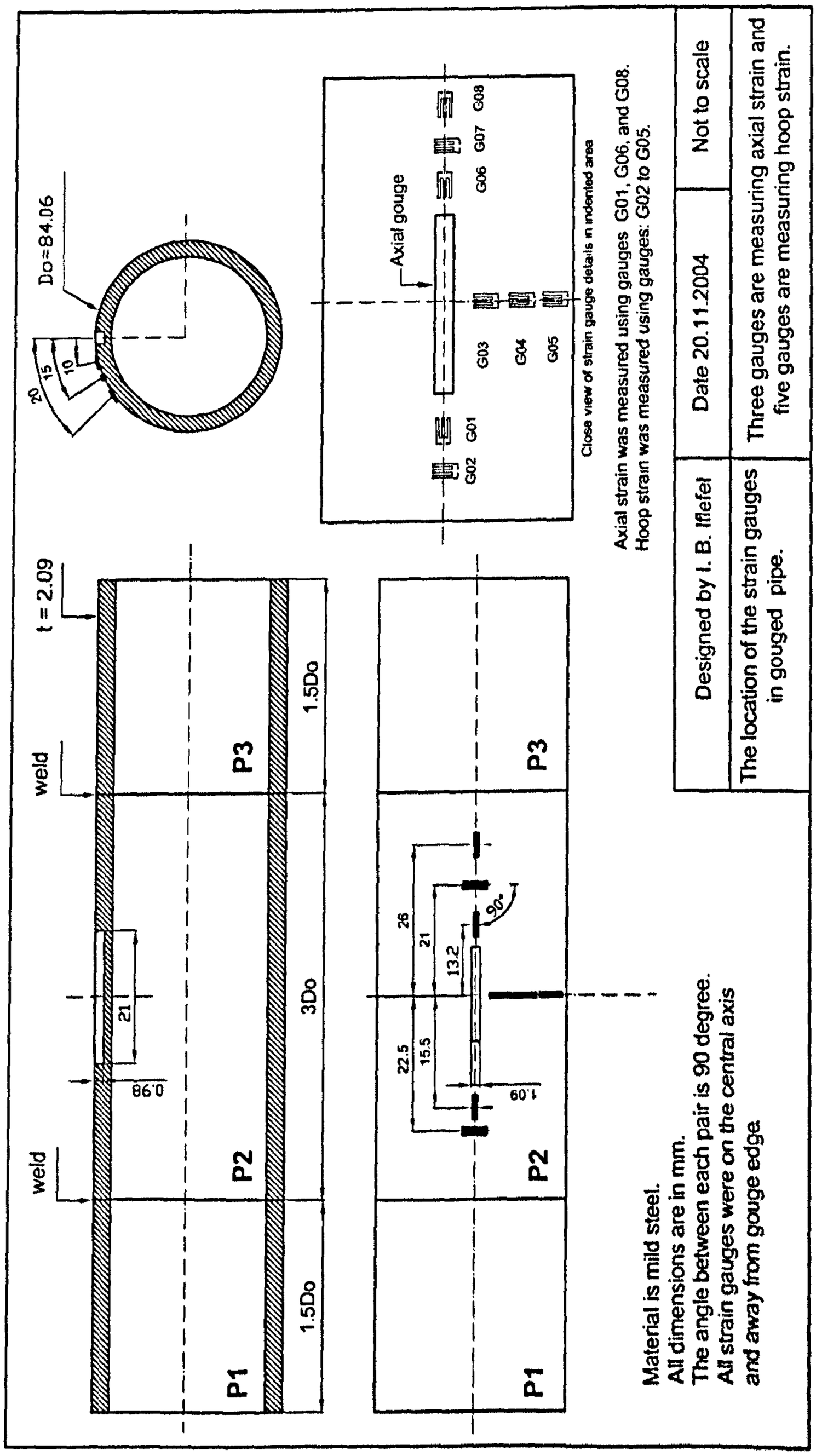

Figure D.3: Strain gauge locations and their direction for pipe with mid-span gouge (in part P2 of model SP4).

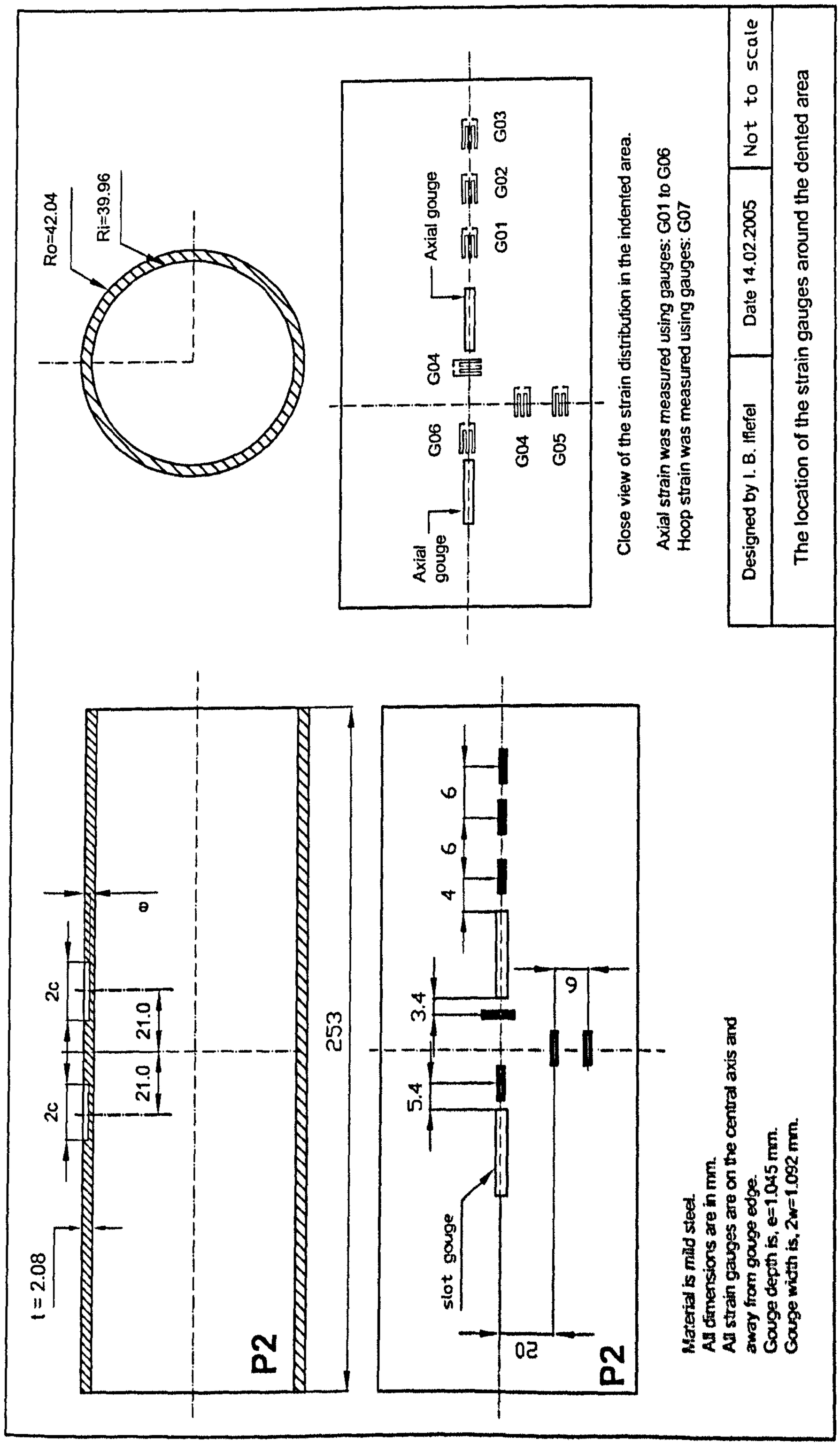

Figure D.4: Strain gauge locations and their directions for pipe with two axial gouges (in part P2 of model SP5).

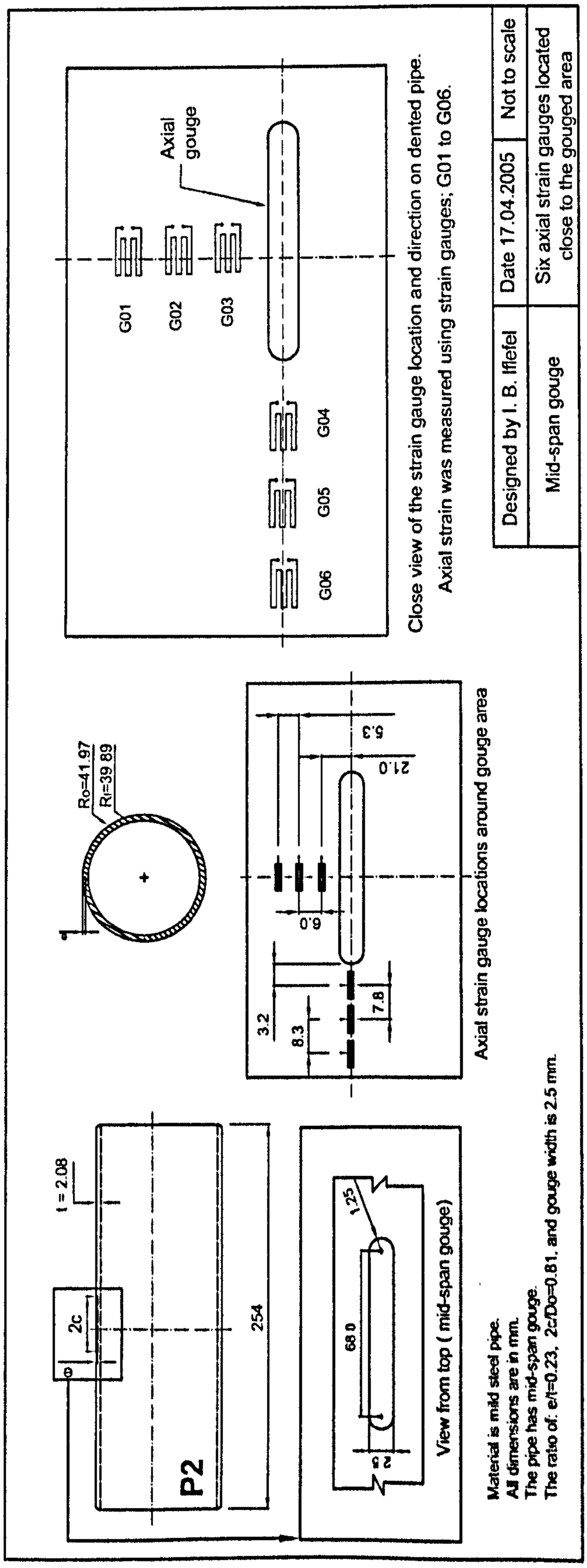

Figure D.5: Strain gauge locations and their directions for pipe with mid-span axial gouge (in part P2 of model SP6).